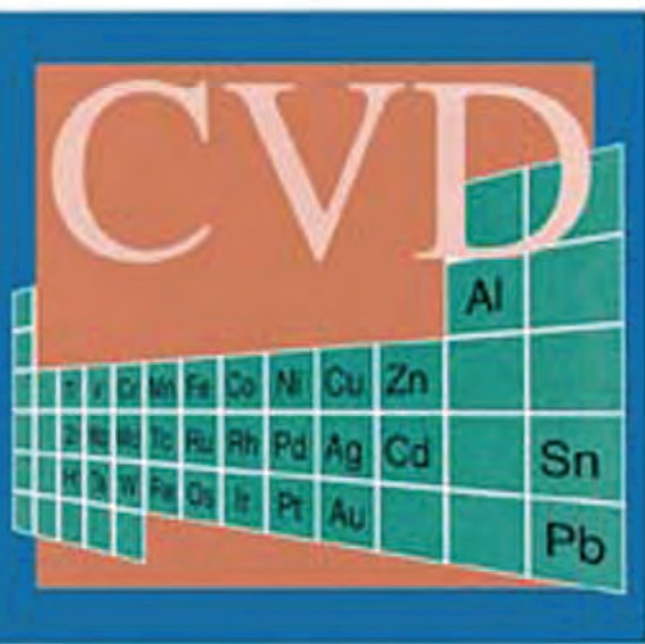


T. Kodas, M. Hampden-Smith

The Chemistry of Metal CVD




VCH

The Chemistry of Metal CVD

Edited by

Toivo T. Kodas and Mark J. Hampden-Smith



Weinheim · New York
Basel · Cambridge · Tokyo

This Page Intentionally Left Blank

The Chemistry of Metal CVD

Edited by

Toivo T. Kodas and Mark J. Hampden-Smith



© VCH Verlagsgesellschaft mbH, D-69451 Weinheim (Federal Republic of Germany), 1994

Distribution:

VCH, P.O. Box 10 11 61, D-69451 Weinheim, Federal Republic of Germany

Switzerland: VCH, P.O. Box, CH-4020 Basel, Switzerland

United Kingdom and Ireland: VCH, 8 Wellington Court, Cambridge CB1 1HZ, United Kingdom

USA and Canada: VCH, 220 East 23rd Street, New York, NY 10010-4606, USA

Japan: VCH. Eikow Building, 10-9 Hongo 1-chome, Bunkyo-ku, Tokyo 113, Japan

ISBN 3-527-29071-0

The Chemistry of Metal CVD

Edited by

Toivo T. Kodas and Mark J. Hampden-Smith



Weinheim · New York
Basel · Cambridge · Tokyo

Prof. Dr. Toivo T. Kodas
Department of Chemical Engineering
University of New Mexico
Albuquerque, NM 87131
USA

Prof. Dr. J. Mark Hampden-Smith
Department of Chemistry
University of New Mexico
Albuquerque, NM 87131
USA

This Book was carefully produced. Nevertheless, author and publisher do not warrant the information contained therein to be free of errors. Readers are advised to keep in mind that statements, data, illustrations, procedural details or other items may inadvertently be inaccurate.

Published jointly by
VCH Verlagsgesellschaft mbH, Weinheim (Federal Republic of Germany)
VCH Publishers Inc., New York, NY (USA)

Editorial Directors: Dr. Peter Gregory and Dr. Ute Anton
Technical Editor: Judith Binder
Production Manager: Hans Jörg Maier

Library of Congress Card No. applied for.

A catalogue record for this book is available from the British Library.

Deutsche Bibliothek Cataloguing-in-Publication Data

The chemistry of metal CVD / ed. by Toivo Kodas and Mark Hampden-Smith. – Weinheim ; New York ; Basel ; Cambridge ; Tokyo : VCH, 1994
ISBN 3-527-29071-0
NE: Kodas, Toivo [Hrsg.]

© VCH Verlagsgesellschaft mbH, D-69451 Weinheim (Federal Republic of Germany), 1994

Printed on acid-free and chlorine-free paper

All rights reserved (including those of translation into other languages). No part of this book may be reproduced in any form – by photoprinting, microfilm, or any other means – nor transmitted or translated into a machine language without written permission from the publishers. Registered names, trademarks, etc. used in this book, even when not specifically marked as such are not to be considered unprotected by law.

Composition: Richarz Publikations-Service, D-53757 Sankt Augustin. Printing: bek-druck, D-64291 Darmstadt. Bookbinding: IVB, D-64646 Heppenheim.

Printed in the Federal Republic of Germany

Preface

Chemical Vapor Deposition (CVD) has developed rapidly in recent years as a method to produce metal films for a variety of applications in the electronics and coatings industries. Originally, it was thought that CVD of all materials was limited by incorporation of carbon and, as a result, the primary applications of CVD would be in the coatings industry where purity is often not a major concern. However, advances in CVD of semiconductors showed that films with purities meeting or exceeding all other deposition techniques and with abrupt interfaces can be created.

Historically, the development of the CVD of metals has lagged behind CVD of compound semiconductors. However, because of the dramatic increase in effort in CVD of metals driven primarily by the microelectronics industry, this situation has improved and high-purity films of a wide variety of metals can now be deposited conformally at low temperatures. Success stories include CVD of tungsten and more recently of Al and Cu films, which are now of sufficient quality to be suitable for applications in the microelectronics industry.

The process of choosing the best precursor for a given application and then optimizing the deposition conditions has been hampered by the lack of communication between chemists, chemical engineers, materials scientists and electrical engineers. Typically, chemists have developed new precursors, chemical engineers have studied reactor behavior, materials scientists have examined film properties, and electrical engineers have incorporated metals into integrated circuits. To alleviate this problem, we have collected information about precursors, their behavior in CVD reactors, the use of the metals in integrated circuits, and film properties.

The major problems associated with CVD of metals have been the lack of suitable precursors that deposit high-purity metals at low temperatures and the poor understanding of the chemistry of CVD using existing precursors. In recent years, these problems have been addressed by studies of deposition chemistry and the development of a vast number of new precursors. For the benefit of researchers and students, we have summarized and discussed the properties of precursors to metal films and the chemistry of their CVD.

The Chemistry of Metal CVD is organized in the following manner, with an emphasis on microelectronics applications. Chapter 1, an introduction, discusses the applications of metal CVD as well as the types of processes used for metal deposition, and rationalizes which materials are used and why they are chosen. Chapters 2 through 8 discuss CVD of Al (2), W (3), Cu from Cu(II) precursors (4), Cu from Cu(I) precursors (5), Au and Ag (6), Pt, Pd, and Ni (7), and CVD of Ta, Cr, Mo, Fe, Co, Rh, Ir, and less-common metals (8). Chapter 9 summarizes the results from these chapters. Some fundamental physical and chemical phenomena that occur in CVD reactors are also discussed to provide a basis from which data in the literature can be interpreted. The goal of this work is to bring

together all aspects of the CVD of metals in a way that is useful for all those who work in this field.

Finally, the CVD of elemental material is, in principle, the simplest form of CVD. As a result, we believe this text will prove informative to those who are entering this field. In addition, certain aspects of this text can be incorporated into materials chemistry and engineering courses at the graduate and undergraduate levels.

March 1994

Toivo T. Kodas
Mark J. Hampden-Smith

Acknowledgments: Many individuals have worked tirelessly to develop this book. We would like to thank the authors of the chapters for their contributions of time and effort. We are grateful to the students and postdoctoral associates in our research groups who provided valuable comments for all of the chapters, especially Dr. Clive Chandler, Mr. Tom Corbitt, Mr. Steven Droes, Mr. Adrian Groenendyk, Mr. Abhijit Gurav, Mr. Ajay Jain, Ms. Teresa Powers, Dr. Christophe Roger; we are also indebted to the various reviewers who offered their guidance and support. We thank Ms. Judith Binder for her untiring and creative work in formatting, editing, and proofreading this book. Without her encouragement this book would not have been finished in a timely fashion. We are especially grateful to our families: for the understanding and support of our wives Cynthia Kodas and Tessa Hampden-Smith and for the love and patience of our children, Aidan Kodas, Emily Hampden-Smith and Harry Hampden-Smith.



Toivo T. Kodas, an Associate Professor in the Chemical and Nuclear Engineering Department at the University of New Mexico in Albuquerque, received his Ph.D. in Chemical Engineering from the University of California, Los Angeles, in 1986. He has worked on CVD processes at the IBM Almaden Research Center and on generation of particles by gas-phase processes at the ALCOA Technical Center. He is the recipient of a Presidential Young Investigator Award from the National Science Foundation, the Kenneth T. Whitby Award from the American Association of Aerosol Research, a College of Engineering Research Award, a Regents Lectureship, and an Outstanding Senior Teaching Excellence Award from the University of New Mexico. His research interests include gas-phase formation and processing of powders, laser deposition of materials, and chemical vapor deposition and etching of metals and metal oxides.



Mark J. Hampden-Smith is an Associate Professor and Regents Lecturer in Chemistry at the University of New Mexico. He received his Ph.D. from London University, Queen Mary/Westfield College in 1984 and held post-doctoral fellowships at the University of Guelph, Ontario, Canada (1984–1986) and Indiana University (1986–1988) conducting research on problems in synthetic and mechanistic inorganic and organometallic chemistry. His current research interests are in nanostructured inorganic materials, chemical vapor deposition and etching, and liquid-phase routes to metal oxides. He is a member of the American Chemical Society, Royal Society of Chemistry and Materials Research Society, and a recipient of a Camille and Henry Dreyfus Teacher-Scholar award.

This Page Intentionally Left Blank

Contents

List of Contributors	xix
Chemical Abbreviations	xxi
General Abbreviations	xxiii
1 Introduction	1
1.1 Introduction	4
1.2 Current Interconnect Schemes in Silicon Devices	8
1.2.1 Metal-Silicon Contacts	8
1.2.2 Diffusion Barrier Layers	9
1.2.2.1 Sacrificial Diffusion Barriers	10
1.2.2.2 Stuffed Diffusion Barriers	11
1.2.2.3 Passive Diffusion Barriers	12
1.2.2.4 Amorphous Diffusion Barriers	13
1.2.3 Contact Layers	14
1.2.3.1 Platinum Silicide (PtSi)	16
1.2.3.2 Titanium Silicide (TiSi ₂)	16
1.2.3.3 Cobalt Silicide (CoSi ₂)	17
1.2.3.4 Other Near Noble Silicides (NiSi, Pd ₂ Si, MoSi ₂)	17
1.2.4 Primary Interconnection	17
1.2.4.1 Aluminum Metallization	18
1.2.4.2 Tungsten Metallization	19
1.2.4.3 Copper Metallization	20
1.2.4.4 Gold Metallization	21
1.3 Metallization Requirements for the Year 2001 in Silicon-Based Technologies	22
1.3.1 Trends in Device and Process Architecture	22
1.3.2 CVD of Titanium	23
1.3.3 CVD of Metal Silicides	24
1.3.4 CVD of Metal Nitrides	25
1.3.5 CVD of Copper and Barrier Layers	25
1.3.6 Other Metallizations	27
1.4 Metal Deposition Techniques	28
1.4.1 Physical Vapor Deposition by Evaporation	28
1.4.2 Physical Vapor Deposition by Sputtering	29
1.4.2.1 Conventional Sputter Deposition Techniques	29
1.4.2.2 Magnetron-Based Sputter Deposition	29
1.4.3 Chemical Vapor Deposition	30

1.5	Manufacturing Issues in CVD Processes	33
1.6	Summary and Conclusions	37
	Acknowledgments	37
	References	38
2	Chemical Vapor Deposition of Aluminum	45
2.1	Applications of Aluminum Films	48
2.1.1	Microelectronics	48
2.1.2	Metallized Polymers	48
2.1.2.1	Gas Diffusion Barriers	49
2.1.2.2	Optical Properties	49
2.1.3	Adhesion	50
2.2	Comparison Between Physical Vapor Deposition (PVD) and Chemical Vapor Deposition (CVD) of Aluminum	51
2.3	Understanding the CVD Process	52
2.3.1	Surface Diffusion	52
2.3.2	Transport Phenomena	53
2.3.3	Gas-Phase Reactions	55
2.3.4	Surface Reactivity	56
2.3.5	Nucleation	56
2.3.6	Summary of Aluminum Precursors	57
2.4	CVD Using Triisobutylaluminum	58
2.4.1	Early Developments	58
2.4.2	Optimization of Aluminum CVD	60
2.4.2.1	Morphology of Aluminum Deposits	60
2.4.2.2	Alloys with Cu and Si	60
2.4.2.3	Nucleation Promoters	61
2.4.2.4	Aluminum Epitaxy on Si	62
2.4.3	Surface Decomposition Mechanism of TIBA	63
2.4.4	Patterning of Aluminum Films	66
2.5	Deposition of Aluminum from Trimethylaluminum	68
2.5.1	Thermal Activation of TMA	69
2.5.2	Plasma-Assisted Aluminum Deposition Using TMA	72
2.5.3	Laser-Assisted Aluminum Deposition from TMA	73
2.6	Deposition of Aluminum Films from Alane Precursors	74
2.6.1	Surface Reaction Mechanism of TMAA	77
2.6.2	Deposition in Cold-Wall Reactors Using TMAA	80
2.6.3	Deposition in Hot-Wall Reactors Using TMAA	81
2.6.4	Aluminum Deposition from TEAA	81
2.6.5	Aluminum Deposition from DMEAA	82
2.6.6	Selectivity of Deposition Using Alane Precursors	83

2.6.7	Aluminum Deposition Using Aluminaborane Precursors	84
2.6.8	Gas-Phase Aluminum Particle Formation From Amine Alanes	84
2.7	Alternative Aluminum Alkyl Sources	86
2.7.1	Triethylaluminum	86
2.7.2	Dimethylaluminum Hydride	88
2.7.3	Diethylaluminum Chloride	90
2.7.4	Aluminum Monochloride	91
2.8	Summary	92
	Acknowledgments	93
	References	93
3	Chemical Vapor Deposition of Tungsten	105
3.1	Introduction	108
3.2	Precursors - Synthesis - Properties	111
3.2.1	Historical Development	111
3.2.2	Tungsten Halides	112
3.2.3	Organometallic Precursors	115
3.2.3.1	Hexakis(trifluorophosphine)tungsten $[W(PF_3)_6]$	115
3.2.3.2	Hexacarbonyltungsten $[W(CO)_6]$	117
3.2.3.3	Bis(arene)tungsten Compounds	117
3.2.3.4	Tris(butadiene)tungsten $[W(\eta^4-C_4H_6)_3]$	118
3.2.3.5	Tetraallyltungsten $[W(\eta^3-C_3H_5)_4]$	118
3.2.3.6	Tris(methylvinylketone)tungsten $\{W[CH_3C(O)CH=CH_2]_3\}$	119
3.2.3.7	Cyclopentadienylmethyltricarbonyltungsten $[(\eta^5-C_5H_5)W(CO)_3CH_3]$	119
3.2.3.8	Bis(cyclopentadienyl)dihydridotungsten $[(\eta^5-C_5H_5)_2WH_2]$	119
3.2.3.9	Bis(methylcyclopentadienyl)dihydridotungsten $[(\eta^5-CH_3C_5H_4)WH_2]$	120
3.2.3.10	Cyclopentadienylhydridotricarbonyltungsten $[HW(\eta^5-C_5H_5)(CO)_3]$	120
3.2.3.11	Cycloheptatrienetetracarbonyltungsten $[(\eta^6-C_7H_8)W(CO)_3]$ and 1,5-Cyclooctadienetetracarbonyltungsten $[(1,5-COD)W(CO)_4]$..	120
3.3	Chemical Vapor Deposition (CVD)	121
3.3.1	Tungsten Halides as CVD Precursors	121
3.3.1.1	Tungsten Hexafluoride (WF_6)	121
3.3.1.2	Tungsten Hexachloride (WCl_6)	133
3.3.1.3	Tungsten Hexabromide (WBr_6)	138
3.3.2	Organometallic Compounds	138
3.3.2.1	Hexakis(trifluorophosphine)tungsten $[W(PF_3)_6]$	141

3.3.2.2	Hexacarbonyltungsten $[\text{W}(\text{CO})_6]$	141
3.3.2.3	Bis(benzene)tungsten $[\text{W}(\eta^6\text{-C}_6\text{H}_6)_2]$	143
3.3.2.4	Tris(butadiene)tungsten $[\text{W}(\eta^4\text{-C}_4\text{H}_6)_3]$	144
3.3.2.5	Tetraallyltungsten $[\text{W}(\eta^3\text{-C}_3\text{H}_5)_4]$	144
3.3.2.6	Tris(methylvinylketone)tungsten $\{\text{W}[\text{CH}_3\text{C}(\text{O})\text{CH}=\text{CH}_2]_3\}$	146
3.3.2.7	Cyclopentadienylmethyltricarbonyltungsten $[(\eta^5\text{-C}_5\text{H}_5)\text{W}(\text{CO})_3\text{CH}_3]$	146
3.3.2.8	Bis(cyclopentadienyl)dihydridotungsten $[(\eta^5\text{-C}_5\text{H}_5)_2\text{WH}_2]$	147
3.3.2.9	Bis(methylcyclopentadienyl)dihydridotungsten $[(\eta^5\text{-CH}_3\text{C}_5\text{H}_4)_2\text{WH}_2]$	148
3.3.2.10	Cyclopentadienylhydridotricarbonyltungsten $[\text{HW}(\eta^5\text{-C}_5\text{H}_5)(\text{CO})_3]$	149
3.3.2.11	Cycloheptatrienetricarbonyltungsten $[(\eta^6\text{-C}_7\text{H}_8)\text{W}(\text{CO})_3]$ and 1,5-Cyclooctadienetetracarbonyltungsten $[(1,5\text{-COD})\text{W}(\text{CO})_4]$...	149
3.4	In Situ Catalysis of Tungsten Deposition	150
3.5	Laser-Assisted Chemical Vapor Deposition (LCVD)	151
3.5.1	Hexacarbonyltungsten $\text{W}(\text{CO})_6$	152
3.5.1.1	Mechanistic Findings	152
3.5.1.2	Deposition Experiments	153
3.5.2	Tungsten Hexafluoride (WF_6)	155
3.5.2.1	Mechanistic and Kinetic Observations	155
3.5.2.2	Deposition Experiments	157
3.6	Plasma-Enhanced Chemical Vapor Deposition (PECVD)	160
3.7	Summary and Outlook	163
	Acknowledgments	164
	References	164
4	Chemical Vapor Deposition of Copper from Copper(II) Precursors	175
4.1	Introduction	178
4.2	Historical Review	179
4.3	Reactant Chemistry	182
4.3.1	Volatile $\text{Cu}(\text{II})$ Compounds	182
4.3.2	Reactant Geometry	185
4.3.3	Synthesis of $\text{Cu}(\text{II})$ Precursors	186
4.3.3.1	$\text{Cu}(\text{hfac})_2 \cdot n\text{H}_2\text{O}$ ($n = 0, 1, 2$)	186
4.3.3.2	Schiff-Base Complexes	187
4.3.4	Volatility	188
4.3.5	Reaction Stoichiometry	190
4.4	Adsorption Studies	191
4.4.1	Adsorption of $\text{Cu}(\text{II})$ Compounds	193
4.4.1.1	Molecular Adsorption	193

4.4.1.2	Dissociative Adsorption	193
4.4.1.3	Ligand Geometry	196
4.4.1.4	Reversibility	197
4.4.1.5	Non-Metallic Substrates	198
4.4.2	Adsorption of Cu(I) Compounds	199
4.4.3	Adsorption of H(hfac)	200
4.4.4	Ligand Decomposition	201
4.5	Growth Kinetics	202
4.5.1	Deposition Rates	202
4.5.2	Deposition Temperature	203
4.5.3	Reactant Concentration	204
4.5.4	Carrier Gas Effects	206
4.5.5	Substrate Selectivity	208
4.6	Film Properties	210
4.6.1	Purity	210
4.6.2	Resistivity	211
4.6.3	Microstructure	212
4.6.4	Other Properties	214
4.7	Reaction Mechanism	214
4.8	Rate Expression	216
4.8.1	Response Surface	216
4.8.2	Mechanism Fitting	217
4.9	Reactor Design	219
4.9.1	Transport Effects	220
4.9.2	Reactor Modeling	220
4.10	Plasma-Assisted CVD (PACVD)	222
4.10.1	Operating Variables	224
4.10.1.1	Reactor Configuration	224
4.10.1.2	Substrate Temperature	224
4.10.1.3	Power Density	225
4.10.1.4	Reactant Concentration	225
4.10.1.5	Carrier Gas	226
4.10.2	Reaction Mechanism	226
4.10.3	Film Properties	226
4.10.3.1	Purity	226
4.10.3.2	Resistivity	227
4.10.3.3	Morphology	227
4.10.3.4	Conformality	228
4.11	Laser-Assisted CVD (LCVD)	228
4.11.1	Operating Variables	229
4.11.1.1	Reactants	229

4.11.1.2 Growth Kinetics	229
4.11.1.3 Substrate Temperature	230
4.11.1.4 Laser Intensity	231
4.11.2 Film Properties	231
4.11.2.1 Purity	231
4.11.2.2 Resistivity	231
4.11.2.3 Morphology	231
4.11.3 Reaction Mechanism	232
4.11.3.1 Transport Effects	233
4.12 Summary	233
Acknowledgments	235
References	235
5 Chemical Vapor Deposition of Copper from Copper(I) Precursors	239
5.1 Introduction	242
5.2 Precursor Design	244
5.3 Synthesis and Characterization	249
5.4 Physical and Chemical Properties	251
5.4.1 Degree of Oligomerization	251
5.4.2 Vapor Pressures	254
5.5 Chemical Vapor Deposition	255
5.5.1 Reactor Types	255
5.5.2 Deposition Conditions	256
5.5.3 Physical Properties of Films	260
5.6 Reaction Stoichiometry, Kinetics, and Mechanisms	264
5.6.1 Reaction Pathways	264
5.6.1.1 Thermally-Induced Disproportionation	264
5.6.1.2 Thermally-Induced Decomposition	266
5.6.2 Reaction Kinetics	268
5.6.3 Surface Reaction Mechanisms	271
5.7 Selectivity	275
5.7.1 Factors Influencing Selectivity	275
5.7.2 Mechanism of Selectivity	281
5.7.3 Selective Deposition onto Patterned PTFE Substrates	286
5.8 Chemical Vapor Deposition of Copper Alloys	289
5.9 Etching	292
5.9.1 Comproportionation	293
5.9.2 Copper Oxide Formation and Removal	294
5.9.3 Formation of XCuL_2	295
5.10 Summary and Conclusions	295
Acknowledgments	296

References	296
6 Chemical Vapor Deposition of Gold and Silver	303
6.1 Introduction	305
6.2 Precursors for Gold CVD	306
6.2.1 Synthesis	306
6.2.2 Physical Properties	308
6.3 Precursors for Silver CVD	310
6.3.1 Synthesis	310
6.3.2 Physical Properties	313
6.4 Deposition Mechanisms and Surface Reactions During CVD of Gold	314
6.4.1 Thermal CVD	314
6.4.2 Photochemical Deposition	317
6.4.3 Plasma-Enhanced CVD	318
6.4.4 Ion and Eletron Beam Deposition	318
6.4.5 Deposition Rates	319
6.5 Applications for Au and Ag Deposition	321
6.5.1 Laser-Induced Circuit Repair	321
6.5.2 Laser Interconnection	322
6.5.3 Laser-Induced Deposition for Bonding	323
6.5.4 Photochemically Deposited Gold Films	323
6.6 Conclusions	324
Acknowledgments	324
References	325
7 Chemical Vapor Deposition of Platinum, Palladium and Nickel	329
7.1 Introduction	331
7.2 Platinum	331
7.3 Palladium	339
7.4 Nickel	340
7.5 Laser-Assisted CVD	342
7.5.1 Platinum	344
7.5.2 Palladium	347
7.5.3 Nickel	348
7.6 Ion-Assisted and Plasma-Assisted CVD	350
7.7 Outlook	351
Acknowledgments	352
References	352
8 Chemical Vapor Deposition of Assorted Metals	357
8.1 Introduction	360

8.2	Chemical and Physical Properties	367
8.2.1	Introduction	367
8.2.2	Precursor Characteristics	369
8.2.2.1	Metal Halides	369
8.2.2.2	Metal Alkyls	372
8.2.2.3	Complexes with Unsaturated Organic Ligands: Alkenes, Alkynes, Allyls, η^5 -Cyclopentadienyls, η^6 -Arenes and Related Complexes	374
8.2.2.4	Metal Carbonyls	378
8.2.2.5	Metal Trifluorophosphines	380
8.2.2.6	Metal β -diketonates	381
8.2.2.7	Metal Alkoxides	383
8.2.3	Vapor Pressures	383
8.3	Syntheses	385
8.4	Chemical Vapor Deposition	385
8.4.1	Deposition Characteristics	385
8.4.1.1	Introduction	385
8.4.1.2	Titanium	386
8.4.1.3	Zirconium	386
8.4.1.4	Hafnium	386
8.4.1.5	Vanadium	386
8.4.1.6	Niobium	387
8.4.1.7	Tantalum	388
8.4.1.8	Chromium	388
8.4.1.9	Molybdenum	390
8.4.1.10	Manganese	392
8.4.1.11	Technetium	392
8.4.1.12	Rhenium	392
8.4.1.13	Iron	393
8.4.1.14	Ruthenium	394
8.4.1.15	Osmium	395
8.4.1.16	Cobalt	395
8.4.1.17	Rhodium	397
8.4.1.18	Iridium	398
8.4.1.19	Zinc	400
8.4.1.20	Cadmium	400
8.4.1.21	Tin	400
8.4.1.22	Lead	400
8.4.1.23	Heterometallic Systems	401
8.4.2	Kinetics and Mechanisms	402
8.4.2.1	Metal Halides	402

8.4.2.2	Metal Alkyls	405
8.4.2.3	Complexes with Unsaturated Organic Ligands: Olefins, Alkynes, Allyls, Metallocenes, and Related Complexes ..	407
8.4.2.4	Metal Carbonyls	411
8.4.2.5	Trifluorosphosphines	413
8.4.2.6	Metal β -diketonates	413
8.4.2.7	Bi- and Multi-Nuclear Complexes	414
8.4.2.8	Heteronuclear Complexes	414
8.4.3	Selectivity	415
8.5	Summary and Conclusions	416
	Acknowledgments	417
	References	417
9	Overview of Metal CVD	429
9.1	Introduction	431
9.2	Classification of Precursors	431
9.3	Blanket Deposition: Reaction Pathways	437
9.3.1	Individual Precursors	437
9.3.2	Single-Source Precursors	439
9.4	Selective Deposition	441
9.4.1	Formation of Patterned Films	441
9.4.2	Summary of Selective CVD Methods	446
9.4.2.1	Intrinsic Difference in Reaction Rates	446
9.4.2.2	Sacrificial Solid-State Co-Reactant	447
9.4.2.3	Activation of Growth Surface	449
9.4.2.4	Photochemical Activation of Growth Surface	452
9.4.2.5	Passivation of Non-Growth Surface	453
9.4.2.6	Gettering or Removal of Nucleating Species from Non-Growth Surface	456
9.4.2.7	Physical Nucleation Barrier	456
9.5	Overall Reactor Behavior	458
9.6	Precursor Delivery	460
9.6.1	Bubblers and Direct Vaporization of Precursors	460
9.6.2	Liquid Delivery	461
9.6.3	Aerosol Delivery	463
9.7	Reactor Types: Hot-Wall and Cold-Wall	468
9.8	Boundary Layers; Feed-Rate-, Surface-Reaction-, and Diffusion-Limited Operation; and Temperature and Pressure Dependencies of Rate	469
9.8.1	Boundary Layers of Velocity, Temperature, and Reactant Concentration	470
9.8.2	Feed-Rate-, Surface-Reaction-, and Diffusion-Limited Deposition	475

9.8.2.1	Feed-Rate-Limited CVD	477
9.8.2.2	Diffusion- and Surface-Reaction-Limited CVD	478
9.8.3	Pressure and Temperature Dependencies of Rate	480
9.8.3.1	Reactant Partial Pressure Dependence of Rate	480
9.8.3.2	Temperature Dependence of Rate	481
9.9	Homogeneous Gas-Phase Reactions and Particle Formation	484
9.9.1	Particle Formation During CVD	484
9.9.2	Simultaneous Particle Deposition and CVD	486
9.10	Conclusions and Future Directions	489
	Acknowledgments	490
	References	490
Appendix 1:	Examples of Chemical Nomenclature	499
Appendix 2:	Definition of Terms	501
Index	515

This Page Intentionally Left Blank

List of Contributors

Thomas H. Baum
IBM Almaden Research Center
650 Harry Road
San Jose, CA, 95120, USA

Lutz Brandt
Department of Chemical Engineering
University of California
Los Angeles, CA 90024-1592, USA

Paul B. Comita
IBM Almaden Research Center
650 Harry Road
San Jose, CA, 95120, USA

Wayne L. Gladfelter
Department of Chemistry
University of Minnesota
Minneapolis, MN 55455, USA

Gregory L. Griffin
Department of Chemical Engineering
Louisiana State University
Baton Rouge, LA 70803, USA

Mark J. Hampden-Smith
Department of Chemistry
University of New Mexico
Albuquerque, NM 87131, USA

Robert F. Hicks
Department of Chemical Engineering
University of California
Los Angeles, CA 90024-1592, USA

Ajay Jain
Department of Chemical Engineering
University of New Mexico
Albuquerque, NM 87131, USA

Rahul Jairath
National Semiconductor Corporation
2900 Semiconductor Drive
Santa Clara, CA 95052, USA

Herbert D. Kaesz
Department of Chemistry and
Biochemistry
University of California
Los Angeles, CA 90024-1592, USA

Toivo T. Kodas
Department of Chemical Engineering
University of New Mexico
Albuquerque, NM 87131, USA

Andrew W. Maverick
Department of Chemistry
Louisiana State University
Baton Rouge, LA 70803, USA

Michael G. Simmonds
Department of Chemistry
University of Minnesota
Minneapolis, MN 55455, USA

Robert D. Tolles
SEMATECH
2706 Montopolis Drive
Austin, TX 78741, USA

Alfred A. Zinn
Department of Chemistry and
Biochemistry
University of California
Los Angeles, CA 90024-1569, USA

Chemical Abbreviations

BPSG	borophosphosilicate glass
BTMSA	bis(trimethylsilyl)acetylene
COD	1,5-cyclooctadiene
1,5-COD	1,5-cyclooctadiene
COT	cyclooctatetraene
Cp	cyclopentadienyl
DEACl	diethylaluminum chloride
DIBAH	diisobutylaluminum hydride
DMAH	dimethylaluminum hydride
DMEAA	dimethylethylaminealane
Et	ethyl
Hdpm	dipivaloylmethane
H(acac)	2,4-pentanedione or acetylacetone
acac	acetylacetonato
H(acim)	4-imino-2-pentanone
acim	4-imino-2-pentanato
H(dpm)	2,2,6,6-tetramethyl-3,5-heptanedione
dpm	2,2,6,6-tetramethyl-3,5-heptanedionato
H(fod)	6,6,7,7,8,8,8-heptafluoro-2,2-dimethyl-3,5-octanedione
fod	2,2-dimethyl-6,6,7,7,8,8,8-heptafluoro-3,5-octanedionato
H(hfac)	1,1,1,5,5,5-hexafluoro-2,4-pentanedione or 1,1,1,5,5,5-hexafluoroacetylacetone
hfac	1,1,1,5,5,5-hexafluoroacetylacetonato
H(nona-F)	1,1,1,5,5,5-hexafluoro-4-[(2,2,2-trifluoroethyl)imino]-2-pentanone
nona-F	1,1,1,5,5,5-hexafluoro-4-[(2,2,2-trifluoroethyl)imino]-2-pentadionato
H(ppm)	6,6,7,7,7-pentafluoro-2,2-dimethyl-3,5-heptanedione
ppm	6,6,7,7,7-pentafluoro-2,2-dimethyl-3,5-heptanedionato
H(tdf)	1,1,1,2,2,3,3,7,7,8,8,9,9,9-tetradecafluoro-4,6-nonanedione
tdf	1,1,1,2,2,3,3,7,7,8,8,9,9,9-tetradecafluoro-4,6-nonanedionato
H(tfac)	1,1,1-trifluoro-2,4-pentanedione or trifluoroacetylacetone
tfac	trifluoroacetylacetonato
H(tmhd)	2,2,6,6-tetramethyl-3,5-heptanedione
tmhd	2,2,6,6-tetramethyl-3,5-heptanedionato
H ₂ (acen)	4,4'-(1,2-ethanediyldinitrilo)bis(2-pentanone)
acen	4,4'-(1,2-ethanediyldinitrilo)bis(2-pentanedionato)
hfb	hexafluoro-2-butyne
HMDS	hexamethyldisilazane
<i>i</i> -Bu	isobutyl

<i>i</i> -Pr	isopropyl
Me	methyl
NBD	norbornadiene
Np	neopentyl
PTFE	poly(tetrafluoroethylene)
<i>t</i> -Bu	tertiary butyl
TEA	triethylaluminum
TEAA	triethylaminealane
TEOS	tetraethylorthosilicate
THF	tetrahydrofuran
TIBA	triisobutylaluminum
TMA	trimethylaluminum
TMAA	trimethylaminealane
TMVS	trimethylvinylsilane
VTMS	vinyltrimethylsilane
YIG	yttrium iron garnet

General Abbreviations

AES	Auger electron spectroscopy
ALE	atomic layer epitaxy
amu	atomic mass units
APCVD	atmospheric-pressure chemical vapor deposition
APOMVPE	atmospheric-pressure organometallic vapor-phase epitaxy
ASIC	application-specific integrated circuit
CBE	chemical beam epitaxy
CMOS	complimentary metal oxide semiconductor
CMP	chemical mechanical polishing
CVD	chemical vapor deposition
CW laser	continuous wave laser
dc	direct current
DRAM	dynamic random-access memory
DSC	differential scanning calorimetry
DTA	differential thermal analysis
ECR	electron cyclotron resonance
ED	electron diffraction
EDAX	energy dispersive analysis of X-rays
EDS	energy dispersive spectroscopy
ESCA	electron spectroscopy for chemical analysis
FET	field-effect transistor
FTIR	Fourier transform infrared (spectroscopy)
GC/MS	gas chromatography/mass spectroscopy
GSI	giga-scale integration
GTC-CVD	gas-temperature-controlled chemical vapor deposition
HREELS	high-resolution electron energy loss spectroscopy
HV	high vacuum
IC	integrated circuits
IR	infrared
LCVD	laser-assisted or laser-induced chemical vapor deposition
LEED	low-energy electron diffraction
LPCVD	low-pressure chemical vapor deposition
LPOMVPE	low-pressure organometallic vapor-phase epitaxy
LSI	large-scale integration
MBE	molecular beam epitaxy
MOCVD	metal-organic chemical vapor deposition
MOMBE	metal-organic molecular beam epitaxy
MOS	metal oxide semiconductor

MOSFET	metal-oxide semiconductor field-effect transistor
MOVPE	metal-organic vapor-phase epitaxy
MS	mass spectroscopy
Nd:YAG	neodymium-doped yttrium-aluminum-garnet
NMR	nuclear magnetic resonance (spectroscopy)
OMCVD	organometallic chemical vapor deposition
OMMBE	organometallic molecular beam epitaxy
OMVPE	organometallic vapor-phase epitaxy
PECVD	plasma-enhanced chemical vapor deposition
PVD	physical vapor deposition
RAIR	reflection-absorption infrared (spectroscopy)
RAM	random-access memory
RBS	Rutherford backscattering spectroscopy
RC	resistance capacitance
rf	radio frequency
RGA	residual gas analysis
RHEED	reflection high-energy electron diffraction
RIE	reactive ion etching
ROM	read only memory
RTCVD	rapid thermal chemical vapor deposition
SEM	scanning electron microscopy
SIMS	secondary ionization mass spectroscopy
SRAM	static random-access memory
TAB	tape automated bonding
TDS	thermal desorption spectroscopy
TED	transmission electron diffraction
TEM	transmission electron microscopy
TGA	thermogravimetric analysis
TOF	time-of-flight
TPD	temperature programmed desorption
UHV	ultra-high vacuum
ULSI	ultra-large-scale integration
UV	ultraviolet
VLSI	very-large-scale integration
VPE	vapor-phase epitaxy
XPS	X-ray photoelectron spectroscopy
XRD	X-ray diffraction
XRF	X-ray fluorescence (spectroscopy)

Element	Symbol	At. No.	mp	bp	Element	Symbol	At. No.	mp	bp	Element	Symbol	At. No.	mp	bp
Actinium	Ac	89	1050	3330	Actinium	Ac	89	1050	3330	Actinium	Ac	89	1050	3330
Aluminum	Al	13	660	2447	Helium	He	2	-272	4430	Promethium	Pm	61	1080	2727
Americium	Am	95	994	2600	Helium	He	2	-272	4430	Protactinium	Pa	91	1227	4027
Arsenic	As	51	631	2600	Hydrogen	H	1	-259	2600	Radium	Ra	88	700	1737
Astatine	At	18	-189	-185	Iodine	I	53	114	184	Radium	Ra	88	700	1737
Barium	Ba	83	302	334	Iodine	I	53	114	184	Radium	Ra	88	700	1737
Berkelium	Bk	97	1285	2970	Krypton	Kr	36	157	2872	Radium	Ra	88	700	1737
Beryllium	Be	4	1277	2484	Lanthanum	La	57	920	3470	Radium	Ra	88	700	1737
Bismuth	Bi	83	271	1579	Lanthanum	La	57	920	3470	Radium	Ra	88	700	1737
Boron	B	5	2177	3658	Lead	Pb	82	328	1751	Radium	Ra	88	700	1737
Bromine	Br	35	-7	59	Lead	Pb	82	328	1751	Radium	Ra	88	700	1737
Cadmium	Cd	48	321	767	Lithium	Li	3	181	1336	Radium	Ra	88	700	1737
Calcium	Ca	20	850	1487	Lithium	Li	3	181	1336	Radium	Ra	88	700	1737
Californium	Cf	98	—	—	Magnesium	Mg	12	650	1105	Radium	Ra	88	700	1737
Carbon	C	6	3730	4827	Magnesium	Mg	12	650	1105	Radium	Ra	88	700	1737
Cerium	Ce	58	795	3470	Manganese	Mn	25	1244	2120	Radium	Ra	88	700	1737
Cesium	Cs	55	29	679	Mendelevium	Md	101	—	—	Radium	Ra	88	700	1737
Chlorine	Cl	17	-101	-34	Mercury	Hg	80	-39	157	Radium	Ra	88	700	1737
Chromium	Cr	24	1857	2662	Molybdenum	Mo	42	-2610	4646	Radium	Ra	88	700	1737
Cobalt	Co	27	1494	2867	Nickel	Ni	60	1019	3111	Radium	Ra	88	700	1737
Copper	Cu	29	1085	2582	Nickel	Ni	60	1019	3111	Radium	Ra	88	700	1737
Curium	Cm	96	1083	2600	Niobium	Nb	41	2477	4863	Radium	Ra	88	700	1737
Dysprosium	Dy	66	1500	2600	Niobium	Nb	41	2477	4863	Radium	Ra	88	700	1737
Einsteinium	Es	99	—	—	Nitrogen	N	7	-210	-196	Radium	Ra	88	700	1737
Erbium	Er	68	1497	2390	Nitrogen	N	7	-210	-196	Radium	Ra	88	700	1737
Europium	Eu	63	826	1440	Oxygen	O	8	-219	-183	Radium	Ra	88	700	1737
Fermium	Fm	100	—	—	Phosphorus	P	15	44	280	Radium	Ra	88	700	1737
Fluorine	F	9	-220	-188	Phosphorus	P	15	44	280	Radium	Ra	88	700	1737
Francium	Fr	87	—	—	Plutonium	Pu	94	640	962	Radium	Ra	88	700	1737
Gadolinium	Gd	64	1306	3000	Plutonium	Pu	94	640	962	Radium	Ra	88	700	1737
Gallium	Ga	31	30	1980	Plutonium	Pu	94	640	962	Radium	Ra	88	700	1737
Germanium	Ge	32	940	2852	Plutonium	Pu	94	640	962	Radium	Ra	88	700	1737
Gold	Au	79	1064	2808	Plutonium	Pu	94	640	962	Radium	Ra	88	700	1737

Periodic Table Excluding Lanthanides and Actinides

[illegible]

Chapter 1

Introduction

**Rahul Jairath,^a Ajay Jain,^b
Robert D. Tolles,^c
Mark J. Hampden-Smith,^d and
Toivo T. Kudas^b**

**^aNational Semiconductor Corporation
2900 Semiconductor Drive
Santa Clara, CA 95052**

**^bDepartment of Chemical Engineering
University of New Mexico
Albuquerque, NM 87131**

**^cSEMATECH
2706 Montopolis Drive
Austin, TX 78741**

**^dDepartment of Chemistry
University of New Mexico
Albuquerque, NM 87131**

Abstract

The applications of chemical vapor deposition (CVD) metallization are discussed from the viewpoint of microelectronics strategies. The emphasis is on aluminum, tungsten, and copper and materials used in conjunction with these metals. This chapter begins with a discussion of sacrificial, stuffed, passive, and amorphous diffusion barrier layers such as Ti, Ti:W, TiN, and TaSiN used to separate metals and semiconductors. This is followed by a discussion of contact layers such as PtSi, TiSi₂, CoSi₂, and other silicides which are used to provide electrical contact to the semiconductor. The compatibility between the different metals, barrier layers, and contact layers is examined with emphasis on Al and Cu. Metallization requirements, deposition techniques, and manufacturing issues for CVD processes are then discussed.

Contents

1.1	Introduction	4
1.2	Current Interconnect Schemes in Silicon Devices	8
1.2.1	Metal-Silicon Contacts	8
1.2.2	Diffusion Barrier Layers	9
1.2.2.1	Sacrificial Diffusion Barriers	10
1.2.2.2	Stuffed Diffusion Barriers	11
1.2.2.3	Passive Diffusion Barriers	12
1.2.2.4	Amorphous Diffusion Barriers	13
1.2.3	Contact Layers	14
1.2.3.1	Platinum Silicide (PtSi)	16
1.2.3.2	Titanium Silicide (TiSi ₂)	16
1.2.3.3	Cobalt Silicide (CoSi ₂)	17
1.2.3.4	Other Near Noble Silicides (NiSi, Pd ₂ Si, MoSi ₂)	17
1.2.4	Primary Interconnection	17
1.2.4.1	Aluminum Metallization	18
1.2.4.2	Tungsten Metallization	19
1.2.4.3	Copper Metallization	20
1.2.4.4	Gold Metallization.....	21
1.3	Metallization Requirements for the Year 2001 in Silicon-Based Technologies	22
1.3.1	Trends in Device and Process Architecture	22
1.3.2	CVD of Titanium	23
1.3.3	CVD of Metal Silicides	24
1.3.4	CVD of Metal Nitrides	25
1.3.5	CVD of Copper and Barrier Layers	25
1.3.6	Other Metallizations	27
1.4	Metal Deposition Techniques	28
1.4.1	Physical Vapor Deposition by Evaporation	28
1.4.2	Physical Vapor Deposition by Sputtering	29
1.4.2.1	Conventional Sputter Deposition Techniques	29
1.4.2.2	Magnetron-Based Sputter Deposition	29
1.4.3	Chemical Vapor Deposition	30
1.5	Manufacturing Issues in CVD Processes	33
1.6	Summary and Conclusions	37
	Acknowledgments	37
	References	38

1.1 Introduction

Metallization is the term used for the formation of a metallic coating on a substrate. Metallic coatings are formed for a variety of applications that include oxidation-resistant, corrosion-resistant, abrasion-resistant, and reflective coatings; electrodes and electronic contacts (or interconnects); and others.¹ One of the most important uses of metallization is in microelectronic applications for which the metals of primary interest are W, Al, Cu, and Ti. Other metals used in specialized applications or as components of more complex materials such as metal silicides or metal alloys are Ni, Pd, Pt, Ag, and Au. This chapter describes the role of these metals in silicon-based microelectronic applications where chemical vapor deposition (CVD) is used to deposit blanket or surface-selective metal films. The applications of other metals (Mo, Ru, Co, Ir, Rh, Re, Ta, Cr, Fe, Cd, Sn, and Pb) are more varied and diverse in their scope and, although mentioned here briefly, are described in more detail in Chapter 8.

World-wide demand for consumer electronics has increased tremendously over the past decade and is expected to continue with the emergence of new markets in sophisticated personal computers, wireless communications, multimedia cable and telephone, personal workstations, and super computers. Equipment development will require cost-effective, high-performance integrated circuits (IC). Enhancement in the performance and speeds of these circuits can be achieved by reducing the device feature size²⁻⁴ and thereby the overall die size. Fortunately, die size reduction also leads to lower cost per device since more devices can be manufactured on each wafer. Metallic interconnects and other materials such as metal silicides, nitrides, and alloys are required at all levels of these microelectronic circuits in which they connect the various transistors, resistors, capacitors, and diodes to each other. These materials are also used to connect the circuitry on the silicon chip to the packages on which the chips are mounted; interconnects must also be scaled down as device sizes shrink.^{5,6} The important role of metallic interconnects, examples of the materials involved, and the complexity of these structures are shown in Figure 1-1.

The demand on performance of microelectronic devices has led to the use of complex multi-level structures. At the beginning of IC evolution, a single interconnect level was used because a relatively small number of devices had to be connected. As the number of devices on chips increased, primarily due to shrinking device size, the area occupied by the interconnect lines eventually exceeded the geometric area available on the chip.^{3,7} As a result, multilevel structures utilizing metal lines on two or more levels were implemented (Fig. 1-1). The motivation was not only to increase the packing density of the devices but also to carry out integration on larger chip areas. A multi-level structure offers much more flexibility for interconnect routing by increasing the effective surface area available for metallization. Typically, the first

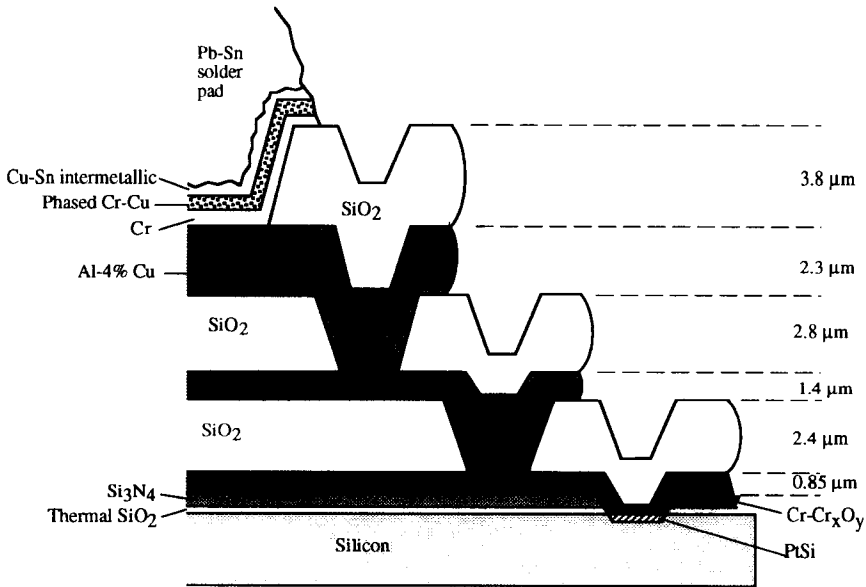


Figure 1-1. Schematic representation of role of metal interconnects in electronic circuitry.

level provides circuit interconnections while the higher levels provide power distribution. Multi-level schemes also reduce the area of the chip consumed by the power buses which is accompanied by a significant decrease in design time. Such metallization schemes greatly improve performance and simplify the chip layout. Figure 1-2 shows the benefits of increasing the number of interconnect layers in standard-cell ASIC (application specific integrated circuits) technology with $0.9\ \mu\text{m}$ and $0.5\ \mu\text{m}$ feature sizes. In both cases, an increase in the number of interconnect layers from two to three results in at least 40% improvement in packing density while simultaneously increasing performance by reducing interconnect delays.

At the same time as multilevel schemes have become increasingly complex, the minimum feature size for microelectronic devices has been shrinking rapidly. Manufacturing trends for DRAMs (dynamic random access memories) over the past decade are shown in Figure 1-3. Traditionally, ASIC-based designs have trailed the DRAM generation by about two years; however, in the recent past this gap has been reduced considerably and now stands at a little less than one year. Using current generation technology, ASIC designs with minimum feature sizes of $0.5\ \mu\text{m}$ have been integrated using four layers of metal. If current trends persist, devices with critical dimensions of $0.25\ \mu\text{m}$ will be wired with five or more interconnect layers by the year 2001.

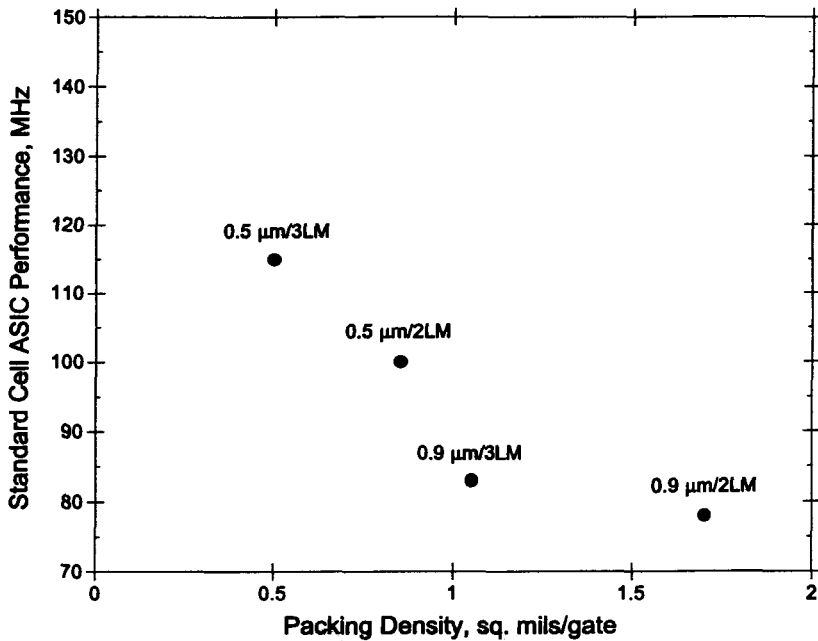


Figure 1-2. Advantages of increasing the number of interconnect layers in 0.9 μm and 0.5 μm based standard cell application-specific integrated circuits (ASIC) technology. (LM = levels of metallization, 1 mil = 25 μm).

The added complexities of multilevel architectures with small feature sizes have brought up new issues such as the manufacturability, reliability, and performance of the metal interconnect structures; thus, it is important to consider the parameters of metal interconnects which affect the performance of the overall integrated circuit. These include resistance capacitance (RC) delays⁵ associated with parasitic resistances and capacitances, IR (current resistance) voltage drops associated with current flows and resistances,⁵ power consumption,⁸ current carrying capability,⁹ and cross talk between adjacent lines. Both RC delays and IR voltage drops are directly proportional to the resistivities of the metal lines and are the driving force behind the use of lower resistivity metals such as Al and Cu. Cross talk between adjacent metal lines depends upon metal line width and spacing, both of which are determined by the packing density. The maximum packing density, in turn, depends on the ability of the metal lines to resist electromigration (movement of atoms due to flow of electrons) and hillock formation (the formation of mounds or piles of material on a feature) which depend on the properties of the specific metal chosen.¹⁰ Electromigration,^{11,12} hillock forma-

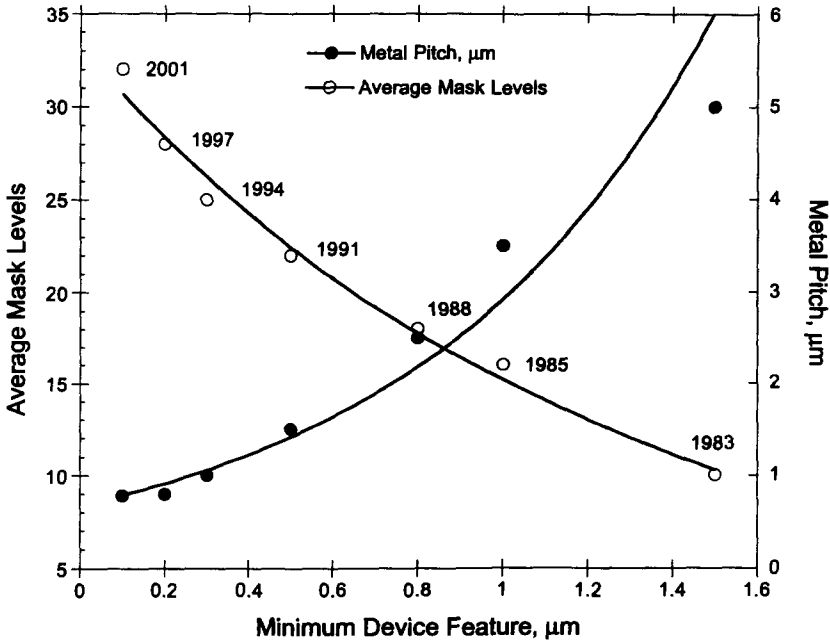


Figure 1-3. Manufacturing trends for DRAMs for the last decade. The metal pitch is the distance between the metal lines.

tion,^{13,14} and propagation delay of electrical signals through the interconnects⁵ are serious problems being addressed by new metallization materials and by changes in circuit design.

There are a variety of materials and processing issues associated with metallization in microelectronics which will be discussed. First, this chapter will cover metal-silicon contact layers and diffusion barriers that allow connections between various metals and silicon. The primary metals used in interconnects are then discussed followed by consideration of some of the challenges for metallization in the near future. A brief history of vapor deposition processes of metals provides some motivation for the use of CVD processes and background for other chapters in this book. The chapter concludes with a discussion of manufacturing issues faced in CVD processes and their implication for the design of CVD precursors. This last discussion has a direct bearing on the viability of CVD processes for any metals used in microelectronics applications.

1.2 Current Interconnect Schemes in Silicon Devices

Over the past decade, shrinking geometries have dictated modification or replacement of existing metallization technologies. With each technology generation, new interconnect schemes have evolved to meet the rapidly increasing performance demands. A current interconnect scheme for a typical complimentary metal oxide semiconductor (CMOS) device interconnected by three layers of metallization including Al, W, and Cu is shown in Figure 1-4. The increased importance of metals in this and related technologies will be covered in the following sections.

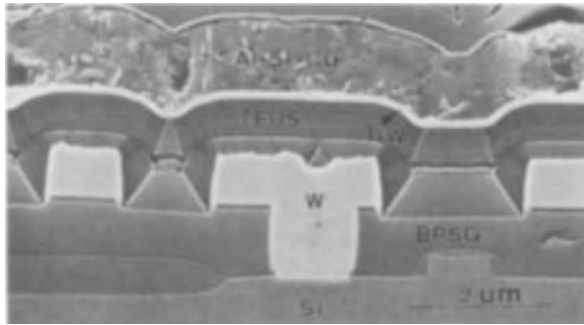


Figure 1-4. Current interconnect scheme for CMOS device with three layers of metallization.

1.2.1 Metal-Silicon Contacts

At the first interconnect level, contact is made between a metal and silicon, polysilicon, or materials such as GaAs. Depending upon its nature, the contact may be ohmic or rectifying. Inherently, all metal-semiconductor contacts are rectifying; they allow current to flow across the contact from semiconductor to metal under forward bias conditions but not under reverse bias.¹⁵ Although rectifying metal-silicon contacts find applications in Schottky diodes, ohmic contacts are desirable for the majority of IC applications. These can be fabricated by heavily doping the semiconductor material at concentrations greater than 10^{20} cm^{-3} which allows electrons to quantum-mechanically tunnel through the potential barrier of the metal-semiconductor interface in either

direction.^{16,17} As a result, current flow across the junction is independent of the voltage bias. Any contact layer must be compatible with this doped Si and the contact region must provide only a small resistance.

The resistance of an interface is expressed as specific contact resistivity, ρ_c . For a metal-silicon ohmic contact, ρ_c is typically of the order 10^{-6} - $10^{-8} \Omega\text{cm}^2$. On the other hand, ρ_c for metal-metal contacts is of the order of $10^{-9} \Omega\text{cm}^2$. In practice, contact resistance is a strong function of contact area and fabrication procedure. For example, contact resistance varies inversely as the square of the contact area. Also, the presence of native oxide or polymeric deposits at the contact interface significantly increases the contact resistance. Finally, any phases formed by reactions at typical processing temperatures must provide low resistance.

In addition to having a metal-silicon contact with good electrical properties, the chemical interaction between metal and silicon during subsequent thermal processing is of utmost importance because degradation of the properties of the silicon, for example, can occur. Chemical reaction can occur as a result of diffusion of silicon through the grain boundaries of the overlying polycrystalline metal film during thermal processing to either satisfy the solid solubility or to form a metal silicide. Although formation of certain metal silicides is desired for some applications, the high solid solubility of silicon in most interconnect metals is a serious problem which needs to be overcome.

Aluminum is the most common interconnect metal and is a good example of this difficulty. The solubility of aluminum in silicon is about 0.5 at.% at 450 °C and increases to about 1.65 at.% at 575 °C.¹⁸ The diffusion of silicon^{19,20} into aluminum as a result of this solubility results in rapid movement of aluminum atoms to fill the voids created by silicon. If, during thermal processing, the metal penetrates into the substrate deeper than the junction depth of the device, large leakage currents or electrically shorted junctions are created.^{21,22} After thermal processing, the solubility of silicon in the overlying aluminum decreases during the cooling cycle and results in preferential growth of epitaxial silicon at the contact edges as well as formation of silicon precipitates within the interconnect line.²³⁻²⁵ These precipitates cause large flux divergence of the current and result in early failure of the metal lines by electromigration.²⁶⁻²⁸ As a result, diffusion barrier layers are often needed to separate the metal from the silicon.

1.2.2 Diffusion Barrier Layers

Diffusion barrier layers are often introduced between the metal and semiconductor to suppress their interaction.¹⁰ Nicolet has discussed some of the characteristics necessary for diffusion barriers.²⁹

- * Good adhesion to adjacent materials
- * Easily dry etched in combination with metallic conductors
- * No excessive reaction with metals that would lead to large increases in resistance
- * Manufacturable deposition process
- * Good barrier properties with thicknesses < 200 nm
- * Low stress
- * No degradation of electromigration characteristics of interconnect.

Some of these requirements can be relaxed depending on the specific steps used to fabricate the IC and the materials involved.

The choice of the barrier material depends on the materials that must be separated. For the purpose of discussion, we will focus on the Al-Si system, although the concepts are applicable to other systems as well. Here, the purpose of the barrier layer is to keep the Si and Al separated during the overall thermal budget for a complete IC fabrication process and at the same time maintain the electrical integrity of the contact junction. The types of barriers such as sacrificial, stuffed, passive, and amorphous have been classified according to the mechanisms by which they suppress the chemical interaction of the separated materials.^{30,31} The discussion below highlights key characteristics of each of these barriers and the properties of some of the materials are summarized in Table 1-1.

Table 1-1 Barrier properties of commonly used materials [(N) = nitrogen stuffed]

Material	Barrier type	Resistivity ($\mu\Omega\text{cm}$)	Barrier thickness (\AA)	Maximum anneal cycle for stability of Al/barrier/Si contact
TiN	Passive	22	700	550°C/30 min
Ti	Sacrificial	41	500	400°C/30 min
TiW (pure)	Passive	65-75	1000	450°C/30 min
TiW (N)	Stuffed	200	1000	500-550°C/30 min
ZrN	Passive	136	800	550°C/30 min
RuO ₂	Passive	46	400	600°C/30 min

1.2.2.1 Sacrificial Diffusion Barriers

The purpose of a sacrificial barrier is to react with either or both of the overlying and underlying materials during thermal processing cycles. The barrier is generally thick enough not to be totally consumed by the end of these thermal cycles which helps to

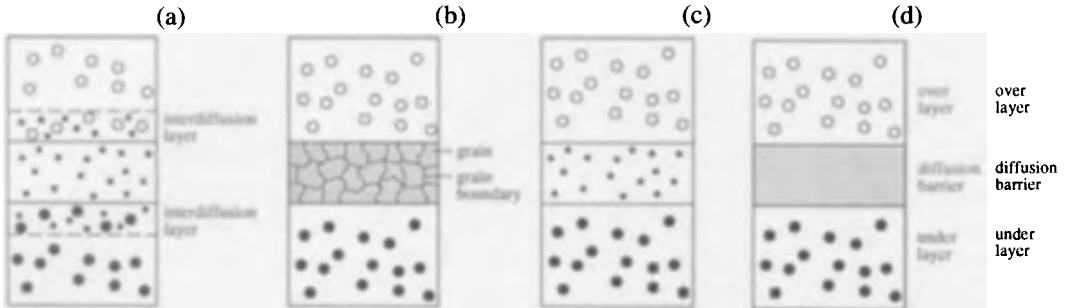


Figure 1-5. Schematic representation of various diffusion barriers, (a) sacrificial barrier, (b) stuffed barriers, (c) passive barriers, and (d) amorphous barriers.

maintain the separation between the two layers. Sacrificial barriers are commonly formed from pure metals and alloys and are depicted schematically in Figure 1-5a.

Many metals act as sacrificial diffusion barriers for aluminum. Typically, the metal reacts with aluminum at elevated temperatures to form metal aluminides which are not effective diffusion barriers.³² An example is titanium which acts as a sacrificial barrier between silicon and aluminum, but at 400 °C, reacts with aluminum to form TiAl_3 ^{33,34,35} which is not a diffusion barrier for silicon. Therefore, once the titanium is consumed by the reaction with aluminum, rapid interdiffusion of silicon and aluminum occurs and causes contact failure. A 1000 Å thick titanium layer diffusion barrier can withstand a thermal cycle of ~500 °C for approximately fifteen minutes before breaking down as a diffusion barrier.³⁶ Similarly, niobium acts as a sacrificial barrier for aluminum, but forms NbAl_3 which is not a diffusion barrier for Al.³⁷ Because sacrificial barriers have a finite lifetime, after which their barrier properties are no longer effective, they are not widely used. Some partially sacrificial barriers which rely on other mechanisms for their barrier properties are discussed below.

1.2.2.2 Stuffed Diffusion Barriers

In polycrystalline barrier films, the grain boundaries of the film act as diffusion pathways for atoms of the overlying and underlying layers. However, if the grain boundaries are blocked or filled with a foreign material during the deposition process, silicon diffusion through these boundaries can be reduced. This is referred to as "stuffing" of the grain boundaries and is shown schematically in Figure 1-5b. Approximately 1000 ppm of certain elements are required to minimize diffusion of silicon and metal atoms through the grain boundaries of the barrier material. Stuffed diffusion barriers have been formed primarily from nitrogen-stuffed metals.

Titanium-tungsten (Ti = 30 at.%, W = 70 at.%) films sputter deposited in a nitrogen-argon ambient are a common example of stuffed barrier layers.^{38,39} At 400-500 °C the titanium and tungsten in the Ti:W films react with aluminum to form TiAl_3 and WAl_{12} respectively while not reacting significantly with silicon. This helps to maintain contact stability. Nitrogen "stuffed" into the grain boundaries during the sputter deposition process serves to enhance the barrier properties of the Ti:W film.^{40,41} Often, these films are intentionally exposed to air before subsequent aluminum deposition to allow for further incorporation of nitrogen and oxygen atoms into the grain boundaries of the Ti:W film and thereby improve barrier performance. Sputter deposited Ti:W films typically exhibit good step coverage for contact dimensions of 1.0 μm and aspect ratios approaching 1:1.⁴² A drawback, however, is that films deposited on the reactor walls are often highly stressed and eventually start to flake off causing particulate contamination on the substrate.

1.2.2.3 Passive Diffusion Barriers

Passive diffusion barriers have a large negative free energy of formation and are, therefore, chemically inert, strongly bonded compounds; they do not interact with the overlying or underlying materials and generally have a low solid solubility for silicon and metals such as aluminum. As a result, these are preferred for barrier materials. Passive barriers, shown schematically in Figure 1-5c, are usually formed from metal nitrides. The most well-studied and most promising barrier layer is TiN.

Titanium nitride (TiN)⁴³⁻⁴⁷ acts as a passive barrier because it is chemically and thermodynamically stable. It acts as an impermeable barrier to silicon^{48,49} and has a high activation energy of diffusion for other metals.⁵⁰ Titanium nitride films can be deposited by (i) thermal nitridation of titanium films in nitrogen or ammonia ambients, (ii) reactive sputter deposition of titanium in a nitrogen environment, and (iii) chemical vapor deposition (CVD) using inorganic or metal-organic precursors. Titanium nitride films formed by thermal nitridation have limited barrier properties and are therefore not used widely in sub-half-micron-based technologies. Titanium nitride films formed using reactive sputter deposition techniques are stoichiometric and possess superior barrier properties. However, their use in sub-half-micron technologies is expected to be severely limited by the step coverage of the sputtered films. Collimating techniques during sputter deposition of materials have helped improve step coverage of reactively sputtered titanium nitride films for aspect ratios of more than 2:1 and contact sizes less than 0.5 μm . However, physical vapor deposition (PVD) techniques are inherently limited and may eventually yield to CVD of titanium nitride.

Other transition metal compounds such as carbides, borides, nitrides, and silicides also form strongly bonded compounds^{51,52} and can be used as passive diffusion barriers. Tungsten nitride,⁵³⁻⁵⁵ tantalum nitride,⁵⁶⁻⁶⁰ tin nitride,⁶¹ niobium nitride,^{60,62}

zirconium nitride,⁶³ vanadium nitride,⁶⁰ chromium nitride,⁶⁴ iron nitride,⁶⁵ and other metal nitrides have been deposited by CVD and are also potentially useful as diffusion barriers for Cu (as discussed in Section 1.3.4).

1.2.2.4 Amorphous Diffusion Barriers

Diffusion barrier layers generally break down due to the presence of grain boundaries in the films.¹⁰ Therefore, in order to eliminate grain boundaries, the films should be single crystal or amorphous. Deposition of single-crystal films is a difficult process from a manufacturing standpoint, and as a result, most research in microelectronics has focused on the development of amorphous barriers. Pure metals are generally deposited in polycrystalline form; however, depending upon the choice of metals used, metallic alloys can be deposited as amorphous phases. For example, the formation of an amorphous phase is favored if there are large differences between the alloying metals with respect to atomic size, crystalline structure, and electronegativity. In order for the resulting film to serve as an effective barrier, the alloy material must have a high crystallization temperature so that grain boundaries are not created during subsequent thermal annealing.⁶⁶ Also, if the film reacts with either the overlying or underlying material it might lower the crystallization temperature. The crystallization temperature and reaction temperature, therefore, characterize the barrier properties of the amorphous layer shown in Figure 1-5d.

Binary amorphous metallic alloys such as $\text{Ni}_{0.45}\text{Nb}_{0.55}$ and $\text{Fe}_{0.45}\text{W}_{0.55}$ usually consist of a near-noble metal and a refractory metal deposited by co-sputtering at room temperature.^{67,68} However, both are known to react with aluminum and silicon⁶⁹⁻⁷¹ and are, therefore, amorphous sacrificial barriers. Ternary systems such as Ta-Si-P and Ta-Si-N have also been investigated. Reactive rf (radio frequency) sputtering of a Ta-P and Ta-Si target in an Ar/N_2 plasma was used to deposit TaPN_2 ⁷² and $\text{Ta}_{36}\text{Si}_{14}\text{N}_{50}$ ⁶⁸ ternary amorphous phases. These phases have demonstrated superior diffusion barrier properties for copper and silicon at temperatures up to 700 and 900 °C, respectively, the primary failure mechanism being premature crystallization of the films at these temperatures. In addition, amorphous W_xN_y deposited using reactive sputter deposition techniques has been evaluated.^{73,74} Barrier properties of this film were similar to those of titanium nitride.⁷⁵ Although most of the amorphous barrier materials currently being evaluated have been deposited using PVD techniques, there is increased motivation for depositing amorphous barriers by CVD to permit conformal coating (uniform coating of non-planar surfaces) of trenches and vias (vertical connections).

As is evident from the above discussion, a barrier film may be kinetically stable or may be in thermodynamic equilibrium with the underlying and overlying materials. However, the diffusion rate through the barrier is very much dependent upon film microstructure and the presence of impurities in the grain boundaries. Therefore, in

reality, more than one mechanism often contributes to the effectiveness of a barrier material. For example, a passive barrier might also rely upon stuffed grain boundaries to decrease diffusion of overlying and underlying species, or a stuffed barrier layer might also have passive barrier properties to maintain its chemical integrity. These concepts are also applicable for GaAs integrated circuits.

1.2.3 Contact Layers

Although barrier materials can suppress silicon-metal interaction, they generally do not result in low contact resistance at the silicon-barrier interface.¹⁰ As a result, other materials such as metal silicides are used to form low-resistance, ohmic contact layers with silicon. Refractory metals such as Ta, Nb, Ti, Cr, Mo, and W, and noble and near noble metals including Fe, Co, Ni, Ru, Rh, Pd, Os, Ir, and Pt form silicides which have potential applications as contact layers.⁷⁶ However, these metal silicide films also act as sacrificial barriers by reacting with aluminum; for example, TiSi_2 reacts at 450 °C, CoSi_2 between 410 and 450 °C, NiSi_2 between 300 and 350 °C, and PtSi at about 250 °C. By themselves, they are not a complete solution to both the Al-Si interdiffusion and contact resistance problems. As a result these silicide contact layers are always used in conjunction with a barrier layer such as TiN to preserve the electrical integrity of the junction (Fig. 1-6).

The formation of the contact layer by Si-metal reaction offers an additional self-aligning capability (Fig. 1-6) by generating the metal silicide layer only in the contact window without the need for a masking step.⁷⁷ A thin layer of pure metal is deposited

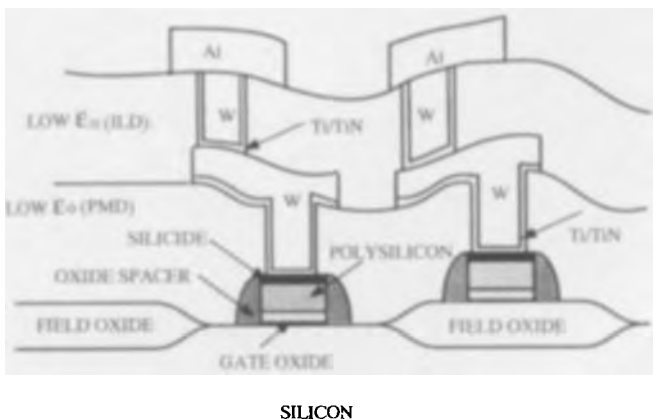


Figure 1-6. Schematic representation of a self-aligned contact structure with barrier layers (ILD = interlevel dielectric; PMD = polymetal dielectric).

by PVD or CVD and subsequently annealed to form the metal silicide at the interface with the silicon. The unreacted metal is then selectively etched away leaving metal silicide in the contact area. Since the reaction is in the solid phase, the reaction front remains relatively uniform. The uniform consumption of silicon by the contact metal to form silicide results in improved interfacial morphology and an intimate contact between the silicon and the metal silicide. This also results in formation of saturated chemical bonds at the interface. For these reasons, such contacts have excellent electrical characteristics.

Metal silicides also have other applications in semiconductor manufacture. Doped polysilicon was initially used as a gate electrode in metal oxide semiconductor (MOS) technology. However, the high resistivity of polysilicon ($\sim 1000 \mu\Omega\text{cm}$) results in unacceptably high RC time delays which limit device performance. An alternative is to deposit pure metal on top of the polysilicon and form the silicide by thermal annealing. This so-called polycide structure tends to retain most of the process advantages associated with polysilicon while offering a substantial reduction in resistivity. However, the one disadvantage of silicides is the need to use the well-characterized gate oxide/metal gate electrode interface. A stacked layer of metal silicide on polysilicon is an attractive alternative and has been successfully implemented in recent fabrication technology. Such an architecture retains the original gate oxide/electrode interface

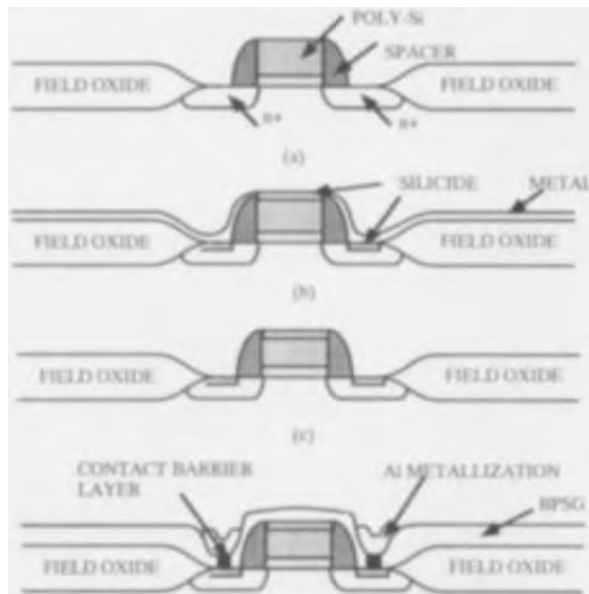


Figure 1-7. Salicide process for fabrication of advanced contact structures. (a) original device, (b) after depositing metal and heating to form silicides, (c) after removal of remaining metal, (d) after contact and barrier layer, Al and BPSG deposition.

while reducing the effective sheet resistance of the gate electrode by more than 80%. Because of their low resistivities, metal silicides are also used extensively as local interconnects, again, replacing polysilicon because of circuit time delay considerations. When the polycide structure for the gate is made at the same time as the silicide at the contact region, the process is called salicide formation.⁷⁸ Figure 1-7 shows the salicide process for fabrication of advanced contact structures.

The following discussion focuses on some of the silicides used commonly as contact layers in the microelectronics industry. Table 1-2 (p. 24) lists the resistivities of some common metal silicides. In principle, it is possible to form the silicide by CVD of the metal followed by annealing. Deposition of metal silicides directly by CVD using single-source precursors containing the metal and silicon has also been demonstrated (see heterometallic precursors in Ch. 8).

1.2.3.1 Platinum Silicide (PtSi)

Platinum silicide ($\rho_s \sim 30 \mu\Omega\text{cm}$) is used in the formation of Schottky diodes to increase the switching speed of bipolar transistors. It is formed by annealing a platinum-silicon stacked structure between 550 and 650 °C.^{78,79} The Pt can be deposited by PVD or CVD techniques (see Ch. 7). In this system, the Si diffuses through the newly formed PtSi and reacts at the PtSi-Pt interface. The PtSi-Si interface is buried beneath the original silicon surface resulting in a clean and intimate silicide-silicon contact. The unreacted platinum is then etched away in an aqua-regia bath.⁸⁰ Although PtSi was used extensively until the 1 Mb DRAM technology generation, lateral formation of PtSi at the contact window as well as agglomeration of PtSi above 800 °C have limited the use of PtSi as a contact material in advanced contact structures. Platinum silicide has been formed by reaction of Si with CVD Pt.⁸¹ The electrical properties have been studied⁸² and shown to be useful.

1.2.3.2 Titanium Silicide (TiSi₂)

Titanium silicide ($\rho_s \sim 15 \mu\Omega\text{cm}$) is the most popular metal silicide used for sub-micron contact applications. It is formed by annealing a titanium-silicon stacked structure at 600-900 °C in a nitrogen or argon ambient. Silicon is the diffusing species during the silicide formation. Lateral TiSi₂ formation is suppressed by using a nitrogen ambient which results in nitrogen stuffing of the grain boundaries and therefore reduces the diffusivity of silicon in titanium.^{83,84} Following the anneal, unreacted titanium is etched away in a sulfuric acid-hydrogen peroxide bath. Titanium silicide is thermally stable until about 550 °C for 30 min but is not an effective diffusion barrier against aluminum diffusion.^{85,86} An advantage of using TiSi₂ is that the salicide structure with TiSi₂ over polysilicon gates is more resistant to hot electron degradation compared to

conventional polysilicon gates.⁸⁷ Also, titanium is the only refractory metal that can reliably form a silicide during annealing with both polycrystalline and single-crystal silicon. As a result, it is possible to achieve simultaneous fabrication of self-aligned contact and gate structures. Titanium silicide films have been formed by CVD and exhibit good properties^{88,89} (see also Ch. 8).

1.2.3.3 Cobalt Silicide (CoSi₂)

Cobalt silicide has attracted wide attention for its applications as a contact and gate electrode material.⁹⁰ Similar to PtSi and TiSi₂, CoSi₂ is formed by annealing a cobalt-silicon stacked structure that can be obtained by PVD or CVD (see Ch. 8). The anneal is carried out between 400 and 900 °C in an argon-hydrogen ambient. In the formation of CoSi₂, cobalt is the diffusing species. As a result, CoSi₂ formation occurs without much lateral formation over the oxide spacer or without encroachment under the gate oxide. When using CoSi₂, contact resistance is low for both heavily doped n⁺ and p⁺ silicon junctions. In addition, the doping profiles in the junctions are essentially unchanged after the silicide formation. Studies have shown CoSi₂ to exhibit better properties than TiSi₂ for applications as both contact and gate electrode in the silicide process.⁹¹ Cobalt silicide has been formed by reaction of CVD Co with Si (see Ch. 8).

1.2.3.4 Other Near Noble Silicides (NiSi₂, Pd₂Si, MoSi₂)

Nickel,⁹² palladium,⁹³ and molybdenum^{94,97} form metal silicides by reaction with silicon at temperatures less than 600 °C; however, the resistivities of the silicide films are much higher than those for PtSi, TiSi₂, and CoSi₂. For example, the resistivity of NiSi₂ is about 50 μΩcm, Pd₂Si is ~30-35 μΩcm, and MoSi₂ is ~40-100 μΩcm.⁹⁸ In addition, MoSi₂ and NiSi₂ films suffer from high intrinsic stress which results in poor adhesion; therefore, these metal silicides have very limited applications for advanced IC fabrication. Table 1-2 (p. 24) lists the resistivities of some common metal silicides. Tungsten silicide has also been considered as a contact material which can be deposited by CVD⁹⁹⁻¹⁰¹ although its resistivity is 100 μΩcm. Tantalum silicide has a resistivity of 50 μΩcm and has also been formed by CVD.^{102,103}

1.2.4 Primary Interconnection

Once the contact and barrier layers have been formed, metal interconnects must be added. Aluminum, tungsten, and copper are the primary materials of interest along with gold in specialized applications such as contacts to GaAs. Since the primary reason for metallization is to provide a conductive interconnect path between the various circuit

components, it is essential that these interconnections do not interact with the materials which they contact. Due to its low resistivity ($\sim 2.7 \mu\Omega\text{cm}$), good adhesion to dielectrics, overall compatibility with semiconductor processing steps, and a great body of experience and information, the metal of choice has been aluminum. Currently, tungsten has some applications where only short distances are involved and the possible use of copper is also being explored.

1.2.4.1 Aluminum Metallization

Aluminum, the workhorse metal for the microelectronics industry (see Ch. 2), was initially used in direct contact with silicon but was later alloyed with silicon to reduce Si migration from the substrate into the aluminum lines. With the advent of shallow junctions ($\sim 1000 \text{ \AA}$) and smaller contact areas for VLSI devices, contact and barrier materials were introduced to prevent Si-Al interaction. In addition to Si-Al interactions, aluminum metallization also has other undesirable characteristics.

Aluminum is a light metal and is susceptible to electromigration under high current densities.^{104,105} Electromigration is the transport of metal atoms along grain boundaries driven by the force exerted by flowing electrons under high current densities. This results in voids on one end and extrusions on the other end of metal lines; Figure 1-8 shows an example of extrusions formed in aluminum lines. Electromigration can be reduced in two ways: first by reducing the surface area of grain boundaries by increasing the grain size, and second by stuffing the grain boundaries with an alloying element to reduce the rate of grain boundary diffusion. For this reason, aluminum interconnects are alloyed with about 4 wt.% Cu and 1.7 wt.% Si, well above their solid solubility in

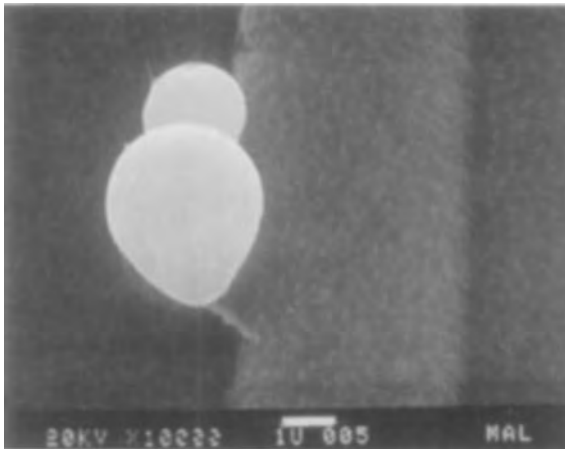


Figure 1-8. Micrograph of extrusion formed as a result of electromigration in an Al line.

aluminum at room temperature which causes the excess Cu and Si to precipitate out at the grain boundaries thereby decreasing grain boundary diffusion.^{104,105} Alloying aluminum with palladium is also attractive because Al-Pd is less susceptible to corrosion than Al-Cu.¹⁰⁵

Aluminum also has a much higher thermal expansion coefficient when compared to SiO₂ as well as excellent adhesion on SiO₂. This combination, however, can result in hillocks (aluminum protrusion from the film surface) which produce interlevel short circuits or low dielectric breakdown voltage between interconnect levels. As the pitch becomes more narrow, the lateral formation of hillocks may also result in short circuits caused by bridging of adjacent metal lines.

Aluminum metallization is currently accomplished by sputter deposition techniques. As a result, complete step coverage is difficult to obtain over highly rugged topography and filling of high-aspect ratio contact and via holes. It is possible to address this issue by using CVD techniques which offer the advantage of better step coverage than PVD techniques. However, CVD aluminum has not proven to be a manufacturable option (although some specialized applications exist) due to the roughness of the deposited films and an inability to reproducibly deposit aluminum alloyed with copper and silicon. Thus, as device dimensions have been scaled down into the submicron regime, designers have been forced to consider other materials, especially at the first interconnect level, which can be deposited by CVD and exhibit greater reliability under high current densities.

1.2.4.2 Tungsten Metallization

Tungsten has replaced aluminum in certain key areas of interconnect schemes. This metal has very high resistance to electromigration as well as resistance to hillock formation and can also be deposited by CVD with 100% step coverage (see Ch. 3). Chemical vapor deposition of tungsten is commonly effected by silane (SiH₄) or hydrogen (H₂) reduction of tungsten hexafluoride (WF₆) after a selective, self-limiting reduction by Si.¹⁰⁶⁻¹¹⁰

The main applications for tungsten are as contacts and vias (vertical connections) between interconnect levels. Contacts make connections between the device at the silicon level and the first layer of metal. Vias make connections between subsequent metal layers. Contact and via processing have a significant impact on the interconnect layout. For example, the minimum metal pitch at a given layer must be such that the contact or via openings at the top and bottom are completely enclosed by the overlying and underlying lines, respectively. If, due to manufacturing design, the contact or via is heavily sloped, the metal pitch at each layer is required to be higher than that for the preceding layer which severely limits the packing density of the device. When vertical contacts or vias are used there is not only significant saving in space but also an increase in packing density. When the design rules dictate use of contacts or vias with vertical

sidewalls, the problem of step coverage is solved by using CVD tungsten (see Ch. 3). In both cases, integration issues are similar to those outlined in the previous sections. At each level, Ti:W or titanium nitride is used to provide an adequate nucleation-adhesion layer for CVD tungsten. Tungsten deposited in the contact and via holes as a blanket film is generally of excellent step coverage. Selectively filling contact or via holes is an alternative where the need for etch back can be avoided by completely filling the shallower vias and partially filling the deeper vias. However, selective deposition of tungsten has not proven reliable and has not been aggressively pursued.

Tungsten deposited by blanket CVD has been used successfully as a first level interconnect and for filling high-aspect ratio contact and via holes. Although it has a higher resistivity ($\sim 5.7 \mu\Omega\text{cm}$) than aluminum, the interconnects do not necessarily limit the performance because of the short distances involved in the first level. Tungsten has also been used for making direct contact with silicon; its specific contact resistivity with n^+ Si can be very low and reasonably low for p^+ Si. Tungsten exhibits barrier properties for Si-Al interaction since aluminum does not react with tungsten below 500°C , and tungsten silicide formation at the W-Si interface occurs only at much higher temperatures. However, because tungsten is highly resistive, it is not a useful replacement for aluminum specifically when longer distances must be covered. For this reason copper interconnects are receiving more attention.

1.2.4.3 Copper Metallization

Copper may be a replacement for aluminum in portions of an interconnect scheme because it exhibits better electromigration resistance, better thermal expansion coefficient, and a lower tendency to form hillocks.¹¹¹ In addition, copper has 30-50% lower electrical resistivity ($\sim 1.7 \mu\Omega\text{cm}$) compared to Al alloy ($\sim 3\text{-}4 \mu\Omega\text{cm}$). Thus, copper interconnects laid down with the same design rules as for Al alloy could increase the operating frequency of devices as well as allow use of higher current densities.

Despite these advantages of copper over aluminum alloys, copper has been ignored in the past because of the lack of an anisotropic, low-temperature copper etch process.¹¹² Moreover, it is incompatible with some other materials used in IC fabrication schemes. For example, copper has a high diffusion coefficient in both silicon and silicon oxide. It acts as a "poison" to the active device area by forming deep acceptor level traps in the forbidden gap resulting in a reduction of the minority carrier lifetime. In addition, the lower heat of formation of copper oxide compared to Si/SiO₂ results in low thermal stability during annealing, planarization, and etch-back processes.

However, advances made in barrier technology, synthesis of new copper compounds for low-temperature selective CVD (Chs. 4 and 5), development of new low dielectric constant materials, and availability of new circuit designs may partially alleviate problems with manufacturability and incompatibility of copper with other fabrication materials.¹¹³ The fast diffusion can be curbed by encapsulating the metal lines with a

barrier material such as TiN (or other materials discussed in Section 1.3.5) which has a high activation energy for the diffusion of copper (4.4 eV).¹¹⁴ In addition, copper metallization could be coupled with new interlevel dielectric materials which are more resistant to copper diffusion. Copper could be deposited in a blanket mode in trenches with side walls covered with barrier layers followed by chemical-mechanical polishing to obtain a planarized trench fill for horizontal wiring.¹¹⁵ This would eliminate the need for dry etching. Finally, the use of multilayer circuit designs incorporating different metals at different levels could eliminate the problems of incompatibility with silicon and the lower heat of formation of copper oxide.

Implementation of this new metallization philosophy could extend the usefulness of current fabrication processes and buy time for the development of new interconnect materials. Aluminum metallization could be replaced by copper at the top interconnect level where the design rules are relaxed and then slowly become integrated into the intermediate level as more experience with fabrication and reliability is achieved. In this scheme various interconnect levels could be fabricated with different design rules and with different interconnect materials, each best suited for that metallization level with regard to overall circuit performance and reliability. The use of copper is discussed in more detail in Section 1.3.5.

1.2.4.4 Gold Metallization

Gold, a noble metal with high atomic weight, offers resistance to corrosion and has a low tendency for electromigration. Gold also has a lower resistivity ($\sim 2.2 \mu\Omega\text{cm}$) compared to aluminum. However, gold does not adhere to SiO_2 and has a very high diffusion coefficient in silicon and silicon oxide. These properties have discouraged the use of gold as an interconnect metal in silicon-based technologies. Nevertheless, gold interconnects are extensively used in the more expensive GaAs-based integrated circuits.¹⁰ The major problems in metal-GaAs interactions are that GaAs decomposes into Ga and As_2 (gas) at 580°C and that high temperatures near 850°C are needed to dope GaAs. Thus contacts must be stable against further processing at high temperatures. Most metals do not exhibit the required properties of high conductivity and compatibility with GaAs. The metal that has the best combination of properties is gold. However, a problem exists in that both Ga and As have appreciable solubility in gold. Fortunately, the compound AuGa_2 is thermodynamically more stable than all other compounds in the Ga-As-Au system. This suggests the need for CVD methods to deposit AuGa_2 and related materials as contact layers between Au and GaAs. Some progress has been made in this direction by using single-source CVD precursors for deposition of metal-gallium films (see heterometallic precursors in Ch. 8). Gold has been used as an interconnect material in contact with high- T_c superconductors.¹¹⁶ Sufficiently low contact resistivities have been obtained for actual interconnect applications.

1.3 Metallization Requirements for the Year 2001 in Silicon-Based Technologies

1.3.1 Trends in Device and Process Architecture

The past decade has witnessed major advances in device and process technology where innovation in architecture has resulted in greater integration of semiconductor devices on a single integrated circuit. Simple logic chips in large scale integration (LSI) have evolved into complex ICs with embedded memories in very large scale integration (VLSI). Each successive generation of ICs has integrated more of these devices, and this trend is expected to continue into ultra large scale integration (ULSI) and giga-scale integration (GSI).

As a result of the evolution from VLSI- to ULSI-based architecture, interconnects must improve their current carrying capabilities; however, Al-Cu alloy-based interconnect schemes are sensitive to high current densities and result in metal line failures due to electromigration as discussed above. With the increasing demand for improved current density capabilities, use of Al-Cu alloys in future multi-level metallization schemes is, therefore, doubtful. Metallic copper is more resistant to electromigration and promises to be a replacement for aluminum and aluminum alloy based metallizations.^{21,26}

Advances have also been made in interconnect architecture. A new approach is the use of Dual Damascene, a unique inlaid integrated interconnect technology developed and demonstrated by IBM.¹¹⁷ The Dual Damascene structure is a global planarization metal interconnect scheme consisting of self-aligned vertical metal plugs and horizontal metal wiring; both are deposited into grooves etched into the dielectric material. This architecture results in a dramatic reduction in defect density, reduces the number of process steps, improves interconnect performance, increases metallization options, and therefore provides significant manufacturing advantages. Integration of tungsten and copper metallization into this scheme is fairly easy due to the ability to deposit conformal films by CVD. However, aluminum metallization is difficult to work with in a Dual Damascene environment because of the limitations placed by the poor step coverage obtained using PVD processes.

A schematic representation of an interconnect scheme projected for the year 2001 is shown in Figure 1-9. The architecture is based upon Dual Damascene which uses low dielectric constant material as an insulator and copper as the primary interconnect material. The role of other metals in this architecture has been outlined in previous sections.

Giga-Scale Integration (GSI) interconnect schemes similar to that shown in Figure 1-9 are driven by the desire to integrate more devices to make more complex and faster

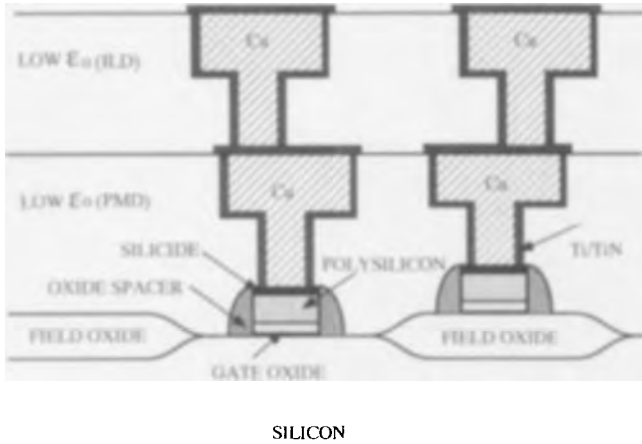


Figure 1-9. Interconnect scheme projected for the year 2001 (ILD = interlevel dielectric; PMD = polymetal dielectric).

circuits on a single chip, and the need to reduce costs. Extrapolating current trends, contact hole size for the 1 Gigabit DRAM generation is expected to be $0.15\ \mu\text{m}$. Clearly, at these dimensions, developing a metal contact fill with low resistivity is a serious challenge. The suitability of pursuing sputter deposition technology is a question that still remains to be answered. Chemical vapor deposition offers the possibility of high step coverage and contact-via fill at low cost. Therefore, a trend towards CVD of metals can be expected over the next decade. Based upon this trend, developments in metallization layers (discussed below) will be required.

1.3.2 CVD of Titanium

Titanium, commonly used at the contact level to form titanium silicide, also acts as an effective etch stop during etch-back of tungsten to form contact and via plugs. As contact sizes are reduced, there is no corresponding reduction in dielectric thickness, and the aspect ratio for the contact hole has been increasing with each generation. Since the resolution of sputter deposition technology is doubtful below $0.18\ \mu\text{m}$ sized contacts, CVD titanium technology is being pursued. However, CVD of high-quality titanium films has not been reported in the open literature (see Ch. 8). Inorganic routes to its deposition provide titanium metal but occur at unacceptably high substrate temperatures. For example, titanium iodide decomposes above $1000\ ^\circ\text{C}$ to form metallic titanium.¹¹⁸ It is possible that hydrogen reduction of titanium iodide may reduce this temperature somewhat. Organometallic precursors for titanium CVD have not yet yielded pure titanium films.¹¹⁹ The lack of a CVD titanium process is not currently

viewed as a serious technological limitation; however, a successful CVD titanium process would allow simplification of process tools and open new options for circuit design.

1.3.3 CVD of Metal Silicides

Silicides of titanium and tungsten are used routinely as local interconnects and as gate electrodes respectively. However, the decrease in device feature sizes requires consideration of new materials and processes. Table 1-2 lists typical resistivities for the relevant metal silicides. Silicides of cobalt, molybdenum and tantalum (see Ch. 8) are attractive choices to supplement polysilicon interconnection. Conventional techniques

Table 1-2. Resistivities of various silicide thin films.

Silicide	Formation technique	Sintering temperature (°C)	Resistivity ($\mu\Omega\text{cm}$)
TiSi ₂	Metal on poly Si	900	13-16
	Co-sputtered	900	25
ZrSi ₂	Metal on poly Si	900	35-40
HfSi ₂	Metal on poly Si	900	45-50
	Co-sputtered alloy		60-70
VSi ₂	Metal on poly Si	900	50-55
NbSi ₂	Metal on poly Si	900	50
TaSi ₂	Metal on poly Si	1000	35-45
	Co-sputtered alloy	1000	50-55
CrSi ₂	Metal on poly Si	700	~600
MoSi ₂	Metal on poly Si	1100	~90
	Co-sputtered alloy	1000	~100
WSi ₂	Co-sputtered alloy	1000	~70
FeSi ₂	Metal on poly Si	900	18-20
	Co-sputtered alloy	900	25
NiSi ₂	Metal on poly Si	900	~50
	Co-sputtered alloy	900	50-60
PtSi	Metal on poly Si	600-800	28-35
Pd ₂ Si	Metal on poly Si	400	30-35

to form silicides such as thermal reaction between metal and silicon are difficult to control, and there is a need to develop CVD processes for deposition of silicides.¹⁰⁷ Chemical vapor deposition of tungsten silicide is a fairly mature process at this time and is widely used in the manufacture of integrated circuits. Although CVD of titanium silicide using silane reduction of titanium tetrachloride at about 750 °C has been reported in the past, control of excessive silicon consumption by titanium tetrachloride during deposition must be addressed in manufacturing. Due to advantages in processing, cobalt silicide has recently received attention as a contact and gate electrode material (see Ch. 8). Other noble silicides such as nickel and palladium silicides can be formed at less than 600 °C. Both, however, have higher resistivities and do not offer significant advantages over current choices. Such critical issues will need to be addressed before CVD of metal silicides can be successfully integrated into current architectures.

1.3.4 CVD of Metal Nitrides

Titanium nitride is the most important metal nitride. Its deposition into sub-0.5 μm contact holes is currently achieved by collimated reactive sputter deposition of titanium in a nitrogen ambient. However, in the near future, there will be a need to develop CVD approaches. Integration of CVD titanium nitride films into sub-0.5 μm devices has recently been reported.¹²⁰ Film deposition was performed using a titanium tetrachloride-ammonia-hydrogen-based chemistry at 700-800 °C. Films obtained by this process have excellent quality and are highly conformal in nature. However, the deposition process using this chemical route is generally performed at more than 700 °C and is therefore incompatible with processes used on layers past the first level of metallization. Chemical vapor deposition of low resistivity titanium nitride films with low impurity levels has been reported recently using tetrakis(diethylamino)titanium and ammonia at ~450 °C.¹²¹ These films have adequate conformality for sub-0.5 μm technology requirements and have successfully been integrated with CVD tungsten based metallization schemes.¹²⁰ The barrier layer properties have also been demonstrated.^{122,123} The viability of CVD titanium nitride technology has clearly been demonstrated; whether the technology can be applied must now be addressed. Similarly, the successful use of other metal nitrides⁵¹⁻⁶⁵ in actual ICs must be demonstrated.

1.3.5 CVD of Copper and Barrier Layers

Of all metallization technologies to be developed in the next decade, CVD of copper is expected to provide the maximum leverage for circuit designers.¹¹² Due to its lower

resistivity when compared to aluminum, copper offers the distinct advantage of process architectures with short interconnect delay. Additionally, electromigration performance of copper-based metallization schemes is expected to be more than two orders of magnitude better than that of schemes based on aluminum alloy. Metallic copper has exhibited resistance to electromigration past the 1 Gamp/cm² level.^{21,26}

Chemical vapor deposition of high-quality copper has been reported using a variety of Cu(I) and Cu(II) precursors (Chs. 5 and 4, respectively). However, integration of copper into current architectures has been severely limited by the inability to effectively etch it in a manufacturing environment (Ch. 5). Typically, copper etch species such as CuCl exhibit low volatility below 250 °C, although progress has been made recently to lower this temperature.¹²⁴ Even at reduced temperatures, mask material stability is still an important issue.

The use of copper in integrated circuits provides several challenges for barrier and contact layers. These layers can potentially be deposited directly by CVD or can be formed by reaction of a metal deposited by CVD with the substrate. Copper is reactive towards most metals (Al, Au, Pd), metal silicides (CoSi₂, CrSi₂, TiSi₂), and silicon-based oxides.¹²⁵ Significant diffusion of copper into silicon dioxide has been reported when annealed at 400 °C for 30 minutes.¹²⁶ This seriously compromises the dielectric properties of the SiO₂. When copper contacts a polymer such as polyimide or other possible dielectrics, copper can diffuse into the polymer.¹²⁷ Copper exposed to ambient conditions forms Cu₂O and CuO, and no protective oxide layer is formed to prevent further oxidation.¹²⁸ In all cases, it is essential that all copper interconnects be completely encapsulated.

Significant progress has been made in developing diffusion barriers for separating Cu from Si and SiO₂. Tantalum and TiW are good diffusion barriers up to 500 °C.¹²⁹ Titanium metal is a barrier but is only effective up to 300 °C.^{129,130} Chromium is a possible diffusion barrier.¹³¹ Copper silicide formed by reaction of copper and silicon has been suggested as a diffusion barrier that functions at 600-800 °C.¹³² Tungsten nitride is an effective barrier at temperatures of 500 °C,¹³³ as is titanium nitride which is effective up to at least 450 °C against penetration into SiO₂ and Si.^{134,135} Chromium nitride^{125,136} and niobium nitride¹³⁷ have also demonstrated useful barrier layer properties.

Various schemes have been proposed to encapsulate copper and protect it from oxidation. Tantalum and Ti make excellent humidity-induced corrosion protectors, however, TiW is destroyed leading to formation of Cu₂O and Cu which makes Ta attractive because it is also an effective diffusion barrier.¹²⁹ Niobium is an effective passivating material for copper up to 400 °C for 30 min in dry oxygen.¹³⁷ Vanadium and tantalum are also effective but gave higher resistivities for the Cu/metal features.¹³⁷ Layered CrN/Cu/CrN/SiO₂ and TiN/Cu/TiN/SiO₂ structures were formed by a self-

aligning approach involving reaction of Ti and Cr with NH_3 at the surface of the Cu.^{134,136} The organic azole 1H-benzotriazole is an effective passivating agent for Cu.¹³⁸ Sputtered Si_3N_4 and PECVD SiO_xN_y behave as diffusion barriers for polyimide, a possible dielectric material in ICs.¹³⁹

In spite of these advances, however, passivation of copper and integration of this process into the overall interconnect architecture still remain serious issues.

1.3.6 Other Metallizations

The conductor metallization in printed wiring boards, including bonding pads to which IC chips as well as resistor and capacitor chips are attached, generally involves a variety of metals. Packages for chips also use a variety of metals which have been deposited by such methods as vacuum evaporation, sputtering, CVD, plating, and anodizing.¹⁴⁰⁻¹⁴⁸ At present, and as a result of the large feature sizes required, sputtering and vacuum evaporation are the mainstays of the industry. Examples of combinations of materials and construction used in hybrid thin-film metallization are shown in Figure 1-10. Gold and copper are the most common conductor materials while resistors have been fabricated from many materials, particularly NiCr, TaN, and Ta_2N . Adhesion layers often consist of titanium or chromium.

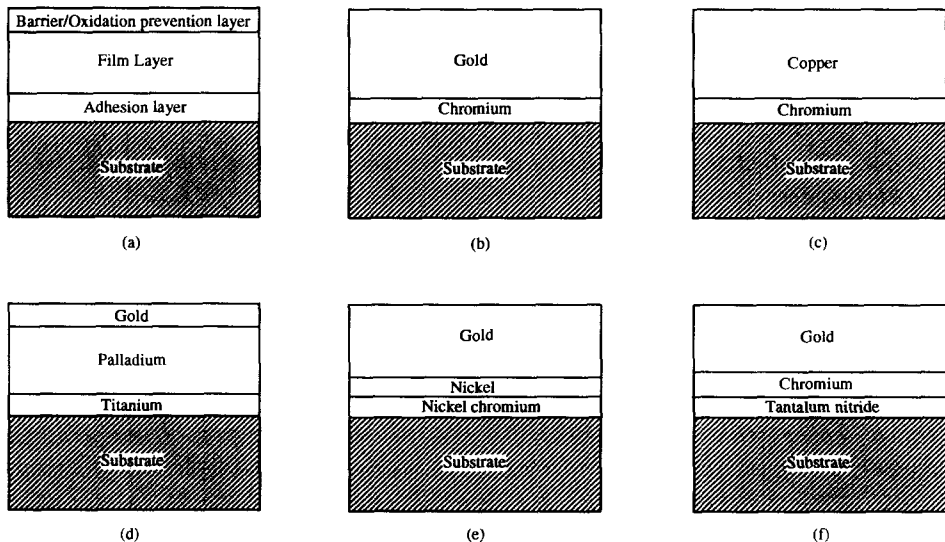


Figure 1-10. Hybrid thin film metallization showing different combinations of barrier, film, and adhesion layers.

1.4 Metal Deposition Techniques

Most film deposition processes can be divided into physical and chemical vapor deposition, and both processes are discussed briefly below. The reader is referred to other books for detailed discussions of these approaches.¹⁴⁰⁻¹⁴⁸ Other deposition techniques such as laser ablation-deposition and wet chemical or electrochemical deposition are not as commonly used in IC manufacture and therefore are not discussed here.

1.4.1 Physical Vapor Deposition by Evaporation

In an evaporation process, the material to be deposited is heated under high vacuum to vaporize the species which condense on the wafer surface.¹⁴⁰⁻¹⁴⁴ The base pressure in the chamber is generally better than 1×10^{-7} torr. At such low pressures, the mean free path of the evaporated species is long enough to allow it to condense on the wafer surface without collisions with the residual gas molecules. In the past, evaporation has been widely used for depositing aluminum, gold, and other metallic films for IC fabrication.

Most commonly, the material to be deposited is heated by an electron beam or induction. Electron-beam heating is achieved by directing a stream of high energy electrons at the target material to create a molten region at the surface. Thus, the hot region is separated from the cooled crucible allowing high-purity films to be deposited. However, e-beam heating of aluminum causes generation of X-rays which degrades the gate oxide characteristics in MOS devices. Inductive heating eliminates the generation of X-rays by using rf (radio frequency) coils around an insulator crucible to heat the material. The molten material, however, is in direct contact with the crucible which may contaminate the film.

Although evaporation of pure aluminum is a simple process, IC applications now demand use of aluminum alloyed with copper and silicon. Depositing alloy films using evaporation is difficult due to differences in vapor pressures of the various elements. This makes maintaining stoichiometry of both the target and the deposited films difficult because the target becomes richer in the less volatile species. Multiple source methods where each element is independently heated appear more promising but raise the issue of homogeneity in composition across the wafer surface. Also, since the evaporation process is inherently directional, films are deposited with poor step coverage. This is one of the major reasons for the increased interest in sputter deposition processes and CVD for VLSI fabrication.

1.4.2 Physical Vapor Deposition by Sputtering

1.4.2.1 Conventional Sputter Deposition Techniques

Sputtering is a process where the surface atoms of a target material are dislodged by bombardment of energetic ions generated in a glow discharge.¹⁴⁰⁻¹⁴⁴ The sputtered atoms are then ballistically transported to the substrate surface where they condense to deposit a film. There are basically two different configurations of glow discharges: (i) a direct current (dc) glow discharge and (ii) a radio-frequency (rf) glow discharge. Sputter processes are used to deposit both metal and insulator materials and, in some cases, to clean the wafer surface.

The dc plasma configuration is the simplest glow discharge with the target material as the cathode and the substrate as the anode. Ions are generated by the inelastic collisions of accelerating electrons with inert gas atoms. The ions are accelerated towards the cathode where they knock off atoms from the target material by momentum transfer. The sputtered atoms finally condense on the substrate and result in film deposition. A dc sputtering process, however, possesses certain limitations for depositing films for VLSI applications. For instance, it cannot be used to sputter deposit insulators as the glow discharge cannot be maintained if the electrodes are covered with an insulating material.

Application of ac voltage to the electrodes allows regeneration of the lost electrons and hence can sustain the discharge without the need for secondary electron emission from the target material. The rf discharge can also be used for dry etching; however, rf glow-discharges suffer from the same inefficiency of secondary electron utilization as dc discharges since most electrons emitted from the target are collected by the anode. The ionization events produced by the electrons are not significantly greater in number in an rf discharge than in a dc glow discharge. As a result, high deposition rates cannot be achieved for rf sputtering. This is the major motivation for the use of magnetron-based sputter deposition.

1.4.2.2 Magnetron-Based Sputter Deposition

Magnetrons are diode plasma devices which use a combination of electric and magnetic fields to provide a drift path for secondary electrons from the cathode that form a closed loop.¹⁴⁰⁻¹⁴⁴ By using these devices in a sputtering environment, it is possible to confine any electrons that might have strayed away from the cathode region of the plasma. The voltage in a magnetron is typically much lower than an rf diode at the same applied power. Current densities at the target are at least an order of magnitude higher than that for non-magnetron configurations. As a result, more ions are generated in the plasma which increases sputtering of the target material and also increases the deposition rate.

Inherently, the step coverage of sputter deposited films is very low. Bias sputtering is being used to enhance step coverage of sputter-deposited films. This is accomplished by resputtering material that is already deposited and redepositing it on the side wall of the contact or via hole. As the bias voltage is increased, ion bombardment of the substrate is increased and relatively more material is resputtered onto the side walls. In addition, the increased ion bombardment results in an increase in surface mobility of adsorbed target molecules on the substrate. As a result, step coverage is improved significantly. This approach is one of the main competitors with CVD processes.

1.4.3 Chemical Vapor Deposition

Chemical vapor deposition (CVD) is a process where one or more volatile inorganic, metal-organic, or organometallic precursors are transported in the vapor phase, often in a carrier gas, to the reactor chamber where they decompose on a heated substrate and subsequently deposit a solid film which results in elimination of volatile byproducts (Fig. 1-11). Only a short description is given here and the reader is referred to Chapter 9 and other texts for detailed discussion.¹⁴⁰⁻¹⁴⁸ Inert carrier gases such as Ar and N₂ are often used to enhance the rate of transport of solid or liquid phase precursors to the reactor chamber. However, other reactive carrier gases such as H₂, NH₃, and O₂ are also

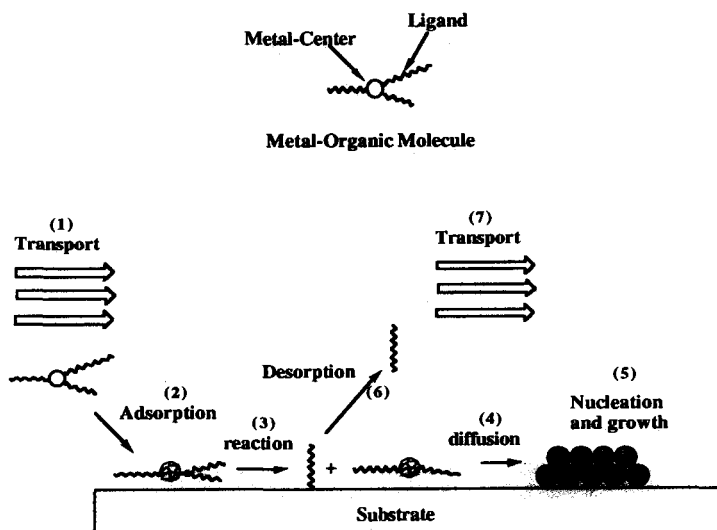


Figure 1-11. Illustration showing the fundamental steps involved in the CVD of a metal-organic molecule.

used which participate in the chemistry of film deposition by acting as reducing or oxidizing agents. Epitaxial, polycrystalline, and amorphous films can be deposited, dependent upon the deposition conditions and the material to be deposited.

Chemical reactions may also occur in the gas phase depending on the reactivity of the gas species and the pressure regime. These gas-phase homogeneous reactions are, however, often undesirable and can lead to nucleation of solid particles which can result in films containing impurities, defects, particulates, loss of selectivity, or poor adhesion. Depletion in precursor concentration before it reaches the substrate, resulting in lower deposition rates, may also occur. For such systems the distribution of source gases into the CVD reactor becomes a critical problem, and the gases are often allowed to mix only above the substrate surface in order to minimize gas-phase reactions. Lower operating pressures also tend to reduce gas-phase reactions due to longer mean free path and therefore reduction in the number of intermolecular collisions.

There are various steps involved in CVD. As the gas flows at sufficiently high pressure over the substrate, a boundary layer can be formed across which temperature, velocity, and concentration vary rapidly (Ch 9).¹⁴⁸ This boundary layer occurs primarily near atmospheric pressure conditions. The gaseous species have to diffuse through the boundary layer from the bulk gas flow in order to reach the surface. On reaching the surface, they chemisorb and undergo surface reactions to deposit a solid film with formation of volatile byproducts. The byproducts desorb from the surface, diffuse across the boundary layer, and are pumped out of the reaction chamber. The relative rates of these various processes are important because the slowest rate will limit the overall deposition rate.

Both gas-phase transport rates and surface reaction rates are important for CVD and any one of them can be rate-limiting. If the surface is at a sufficiently high temperature, the reaction can potentially proceed much more rapidly than the rate at which reactant gases are supplied to the substrate. This results in a mass-transport limited process. If the mass transport is also sufficiently fast, the deposition rate may then be limited by

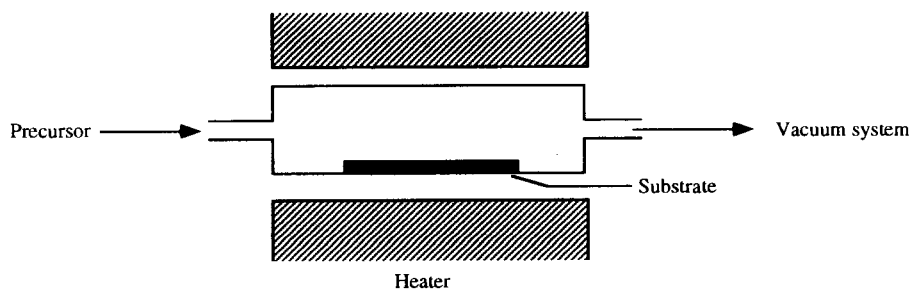


Figure 1-12. Hot-wall CVD reactor.

the rate at which the reactants are fed to the chamber. In such a case, the deposition is feed-rate limited. In both mass-transport and feed-rate limited conditions the deposition rate is relatively insensitive to temperature. On the other hand, in a surface reaction-controlled process, the rate increases exponentially with temperature according to the Arrhenius relationship. In actual processes, the temperature at which the deposition characteristics become surface reaction or mass transport limited is dependent on (i) apparent activation energy of the reaction, (ii) gas flow conditions in the reactor, and (iii) precursor delivery system. These considerations are discussed in depth elsewhere.^{147,148}

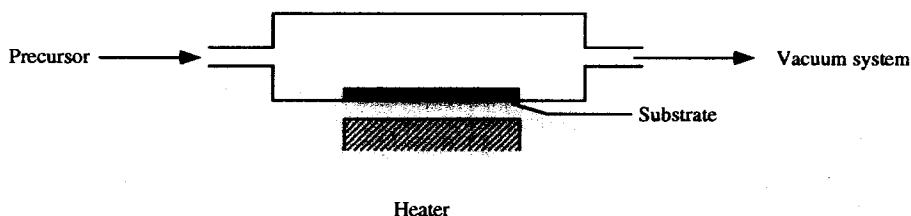


Figure 1-13. Cold-wall CVD reactor.

Chemical vapor deposition reactors are often differentiated by the method employed for heating the wafer and on the operating pressures. In a hot-wall reactor, the wafer as well as the reactor walls are heated via radiant heating (Fig. 1-12). Hot wall reactors are also often multi-wafer reactors allowing for high throughput. Because the reactor walls are also hot, deposition occurs there as well as on the substrate(s). As a result, the reactor is maintenance intensive. In cold-wall reactors, the wafer is heated to the process temperature and the walls of the reactor are kept at room temperature or just warm enough to prevent condensation of the reactant species (Fig. 1-13). Cold-wall reactor configurations are advantageous because they allow tailoring of the gas-flow directly over the wafer surface as well as suppressing precursor depletion because of the lack of deposition on the reactor walls. However, the throughput of cold-wall reactors is typically lower than for hot-wall reactors. The performance of these and other types of reactors has been discussed in detail elsewhere.^{147,148}

Another consideration in the design of CVD reactors is the operating pressure regime. For deposition at atmospheric pressure, the diffusion of gas species through the boundary layer to reach the wafer surface is often rate-limiting. A uniform concentration across the wafer surface is difficult to achieve because the flow dynamics are often poorly controlled. However, for reactors operating under low pressures, the diffusion coefficients of gaseous species are high because they increase with decreasing

pressure, and a well-defined boundary layer ceases to exist because of the long mean free paths of the gas species. Under these conditions, mass transport to the wafer no longer limits the deposition process and results in a uniform reactant concentration across the surface. It is, however, often difficult to control the temperature and therefore the thickness of the film across the wafer surface for low pressure CVD (LPCVD) processes where the deposition rate is surface-reaction limited because of the strong dependence of rate on temperature. These cases have been discussed extensively in several books.^{140,143,147,148}

For certain applications, a high substrate temperature is not desirable. An alternative is to transfer energy to the reactant gases in an rf glow discharge to make the species more reactive by the time they reach the wafer surface rather than by relying solely on thermal energy to initiate the chemical reaction. Additionally, bombardment of the surface by radicals and ions can modify the surface reaction pathways. Since the reactants can be in an excited state, the surface reaction can be initiated at a lower substrate temperature. This can be accomplished by plasma-enhanced CVD (PECVD). Both thermal and plasma-assisted CVD have been used for depositing metals, metal silicides, and metal nitrides, as well as for insulating films such as silicon oxide and silicon nitride for IC fabrication.^{140,142,143,147,148}

1.5 Manufacturing Issues in CVD Processes

A major consideration in using CVD processes in microelectronic applications is the cost of the process relative to alternatives such as PVD. As critical dimensions shrink beyond current generations, the level of complexity of all the processes involved in chip manufacture increases rapidly. As a frame of reference, a 0.5/0.35 μm -technology-based DRAM wafer fabrication facility costs approximately \$800 million, while a 0.35/0.25 μm -technology-based facility is expected to cost more than \$1 billion. The primary reason for this rapid increase in cost is the increased level of complexity in unit processes, such as CVD, which generally translates to more expensive equipment and a higher cost of ownership. Therefore, it is essential to develop CVD unit processes with a view towards providing cost-effective technological solutions. This section provides a brief introduction to this issue with emphasis on the roles of precursor cost and deposition rate in determining overall costs.

A cost of ownership (COO) model developed by SEMATECH has been used here to demonstrate the effect of various tool- (reactor) and process-related parameters on final cost per unit wafer. General trends in COO are similar for most CVD processes. Precursor utilization, deposition rate (tool throughput), defect density, tool maintenance, etc., may be modeled for a given unit process and tool. The example used here is for CVD of tungsten using a generic tool which costs \$1.5 million and with

performance characteristics of 200 hours mean time between coming on line and failure. Deposition was assumed to be effected using silane and tungsten hexafluoride chemistry. Figure 1-14 shows the effect of WF_6 usage on projected cost per wafer. As utilization increases from 0.5 gm/wafer to 2.0 gm/wafer, the cost increases from \$5.62 to \$6.87. Corresponding to this change, the contribution of consumables to total wafer cost increases from 8.73% to 25.3%. In a factory with 4000 wafer starts per week, this translates to about \$260,000 in increased production costs per year and emphasizes the role of precursor cost in CVD processes.

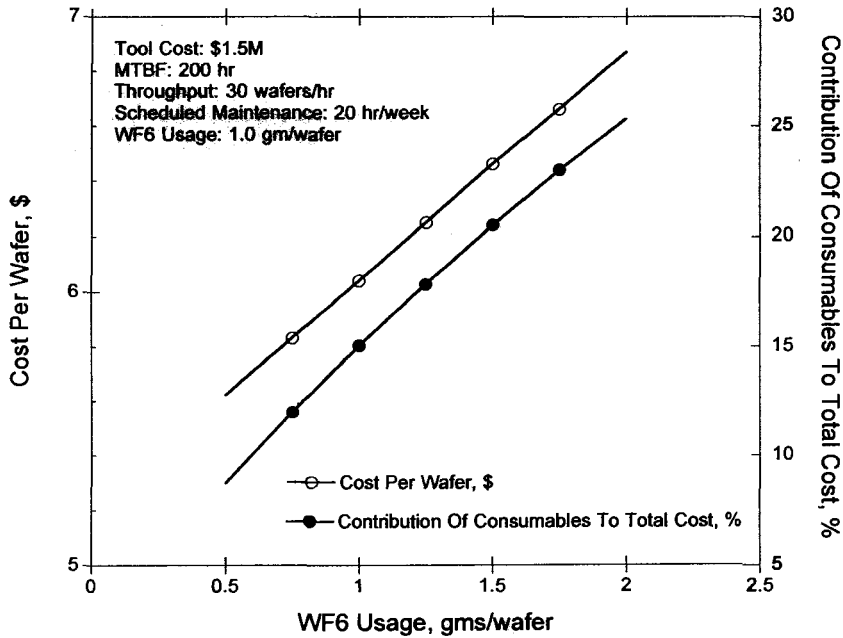


Figure 1-14. Effect of WF_6 usage on consumables cost and total cost/wafer.

Implementing defect prone processes in a production environment can prove even more detrimental. Figure 1-15 shows the effects of process defect density on wafer cost. The result of an increase in defect density from 0.10 cm^{-2} to 0.20 cm^{-2} is a wafer cost increase from \$9.87 to \$21.37. Add these changes to the contribution of scrap cost to total wafer cost and the increase is from 38.06% to 70.32%, representing almost \$2.4 million in increased production costs or more than \$5 million in lost revenue per year. These cost analyses emphasize the problem with complex CVD processes which are prone to contamination by gas-phase particulate formation or flaking of material from

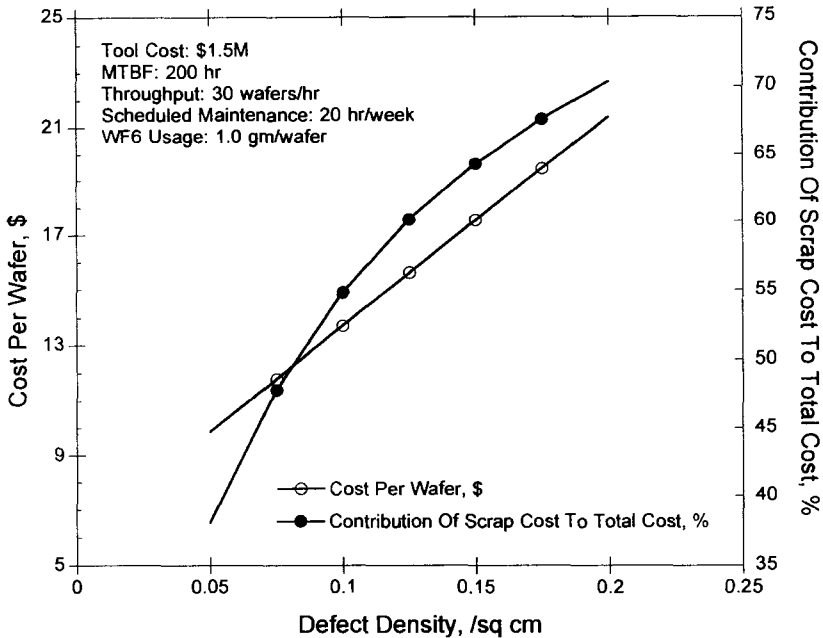


Figure 1-15. Effect of defect density on substrate scrap cost and total cost/wafer.

reactor walls and can result in increased defect density. Therefore, contamination control is receiving increased attention.

Parameters such as deposition rate and scheduled maintenance for CVD tools are critical factors in determining the overall cost of manufacturing wafers. For example, Figure 1-16 shows the effects of film deposition rate, and hence, tool throughput on wafer cost. An increase in throughput from 10 wafers/hour to 40 wafers/hour reduces wafer cost from \$16.49 to just \$4.73. What is equally important in this case is the corresponding increase in maximum wafer starts per week per tool from 1330 to 5340. The increase in production can reduce the number of tools required for a given factory and, at the same time, eliminate costs associated with owning an extra tool. Similarly, the effects of scheduled maintenance for the tool on wafer cost are shown in Figure 1-17. As scheduled maintenance requirements per tool increase from 10 hours/week to 40 hours/week, cost per wafer increases from \$5.67 to \$6.96. This corresponds to a decrease in maximum wafer starts per week per tool from 4290 to 3430, possibly resulting in the requirement of an extra tool. These results emphasize the need for high deposition rates (0.1-1 $\mu\text{m}/\text{min}$) in low-maintenance CVD processes.

A manufacturable CVD process is one which provides a low-cost solution to a technological challenge. Cost of ownership for a given CVD process takes into account

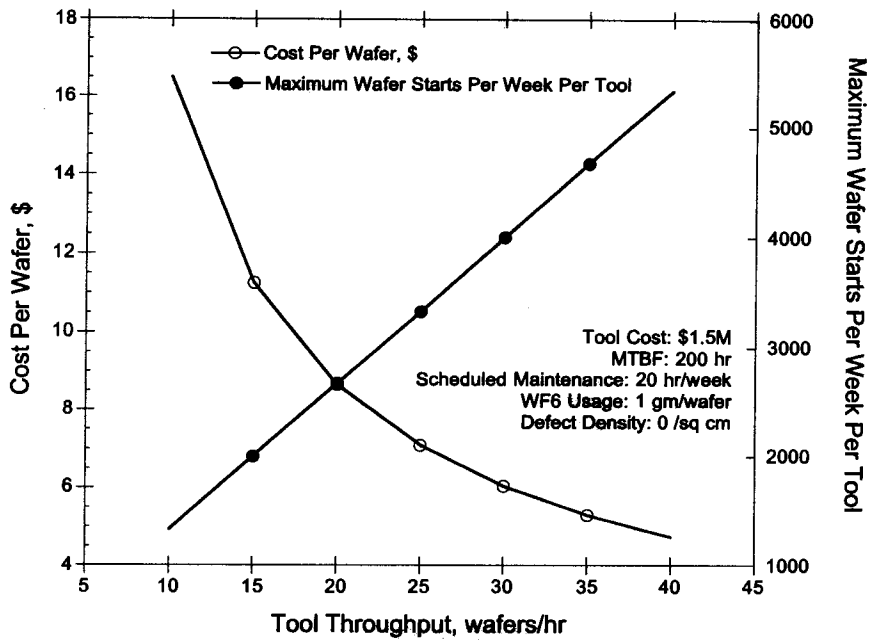


Figure 1-16. Effect of reactor throughput on maximum wafer starts/week and total cost/wafer.

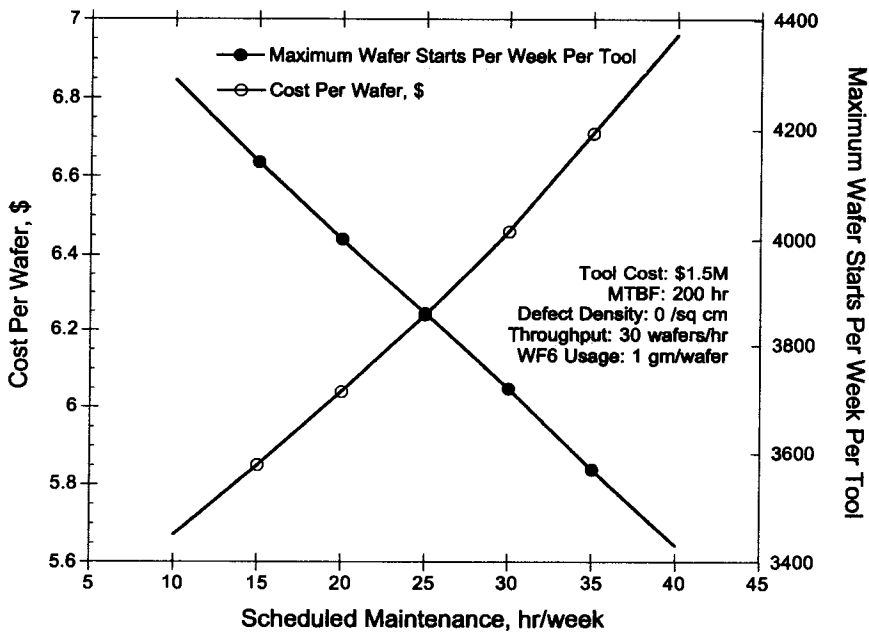


Figure 1-17. Effect of scheduled maintenance for reactor on maximum wafer starts/week and total cost/wafer.

various parameters such as tool cost, deposition rate, cost of precursors, process stability, propensity of the process to directly or indirectly generate defects, etc. In addition, there are other factors which make a process manufacturable, many whose effects are difficult to correlate with wafer cost. For example, the ability to restart a given process after a pause, time and effort required to perform a hard clean on a tool, and difficulty in temperature and temperature profile control are extremely important for the manufacturer. Consideration of these points at the developmental stage will allow fabrication of competitive products by way of improved manufacturability and eventually of non-intrusive reactors and processes.

1.6 Summary and Conclusions

A variety of challenges exist for further incorporation of metal CVD processes into microelectronic processing. High-purity metal films can be deposited at high rates by CVD. Aluminum is the most extensively used metal, but due to the difficulty in controlling film roughness for this metal, CVD is not the technique of choice. Instead, aluminum is deposited by physical vapor deposition processes. Tungsten CVD has limited applications as a first-level metallization, contact layer, and via fill because its resistivity is too high for most other applications. On the other hand, CVD of copper is being examined because of its low resistivity. The potential use of copper has raised other problems, however, especially the deposition of suitable diffusion barriers and contact layers. Overall there is a push towards CVD processes for metals, barrier layers, and contact layers in order to provide conformal coverage on surfaces with complex topographies. Thus, a large number of opportunities are available for the development of improved CVD processes for these materials.

Acknowledgments: The authors thank Abhijit Gurav, Steve Droes, and Tom Corbitt for their assistance. We also thank Judith Binder for her comments, attention to detail, hard work, and dedication in preparing the manuscript.

References

1. Kern, W. *Chemical Methods of Film Deposition in Thin Film Processes*, Vossen, J.L., Kern, W. (eds.), Academic, New York, 1978.
2. Moore, G.E. International Electron Devices Meeting, Washington, DC, Dec. 1975, p. 11..
3. Keyes, R.W. *IEEE Trans. Electron Devices* **1979**, ED-26, 271.
4. Dennard, R.H., Gaensslen, F.H., Yu, H., Rideout, V.L., Bassows, E., LeBlank, A.R. *IEEE J. Solid-State Circuits* **1974**, SC-9, 256.
5. Saraswatt, K.C., Mohammadi, F. *IEEE Trans. Electron Devices* **1982**, ED-29, 645.
6. Sze, S.M. *Physics of Semiconductor Devices*, 2nd Ed., John Wiley and Sons, New York, 1981.
7. Keyes, R.W. *Proc. IEEE* **1981**, 69, 267.
8. Brews, J.R. *IEEE Trans. Electron Devices* **1986**, ED-33, 1356.
9. Tripathi, V.K., Bucolo, R.J. *IEEE Trans. Electron Devices* **1987**, ED-34, 650.
10. Mayer, J.W., Lau, S.S., *Electronics Materials Science: For Integrated Circuits in Si and GaAs*, Macmillan, New York, 1990.
11. Skawpy, F. *Vrh. Bschr. Phys. Ges.* **1914**, 16, 156.
12. Penney, R.V. *J. Phys. Chem. Solids* **1964**, 25, 335.
13. Chaudary, P.J. *Appl. Phys.* **1974**, 45, 4339.
14. Thoma, M.J., Cochran, W.T., Harrus, A.S., Hey, H.P.W., Hills, G.W., Lawrence, C.W., Yeh, J.L. *Proc. 4th Inter. IEEE VMIC Multilevel Interconnection Conf.*, Santa Clara, CA, June, 1987, IEEE, New York, 1987, 20.
15. Bethe, H.A. Laboratory Report 43-12, Massachusetts Institute of Technology, Cambridge, MA, USA, 1942.
16. Chang, C.Y., Fang, Y.K., Sze, S.M. *Solid State Electron.* **1971**, 14, 541.
17. Conley, J.W., Duke, C.B., Mahan, G.D., Tiemann, J. *J. Phy. Rev.* **1966**, 150, 466.
18. Hansen, M., Anderko, A. *Constitution of Binary Alloys*, McGraw-Hill, New York, 1958.
19. Black, J.R. *Proc. IEEE* **1969**, 57, 1587.
20. Silikson, B. *Proc. IEEE* **1969**, 57, 1594.
21. Pramanik, D., Saxena, A.N. *Solid State Technology* **1983**, 26 (1), 127.
22. Reith, T.M. *Appl. Phys. Lett.* **1976**, 28, 3.
23. Schnable, G.L., Keen, R.S., Loewenstern, L.R., Rome Air Development Technical Rep. RADC-TR-67-331, Sep 67, 1967.
24. Schnable, G.L., Keen, R.S. *Annual Proc. Reliability Phys.* **1968**, 6, 170.
25. Reith, T.M., Schick, J.D. *Appl. Phys. Lett.* **1974**, 25, 524.
26. Pramanik, D., Saxena, A.N. *Solid State Tech.* **1983**, 26(3), 131.
27. Curry, J. Fitzgibbon, G., Guan, Y., Muollo, R., Nelson, G., Thomas, A. *Proc. International Reliability Physics*, Las Vegas, NV, April 1984, IEEE, New York, 1984, 6.
28. Flowers, D. *Proc. of 3rd IEEE VMIC Conference*, Santa Clara, CA, 78, 1984.

29. Nicolet, M.A. *Thin Solid Films* **1978**, 52, 415.
30. Nicolet, M.A., Gartner, M. *J. Vac. Sci. Tech.* **1981**, 19(3), 786.
31. Gupta, S., Sarg, J.-S., Ramachandran, V. *Semicond. Int.*, Oct. **1989**, 80.
32. Ball, R.K. Todd, A.G. *Thin Solid Films* **1987**, 149, 269.
33. Nakamura, K. Lau, S.S., Nicolet, M.A., Mayer, J.W. *Appl. Phys. Lett.* **1976**, 28, 277.
34. Bower, R.W. *Appl. Phys. Lett.* **1973**, 23, 99.
35. Farahani, M.M., Turner, T.E., Barnes, J.J. *J. Electrochem. Soc.* **1987**, 134(11), 2835.
36. Ting, C.Y., Crowder, B.L. *J. Electrochem. Soc.* **1982**, 129, 2590.
37. Farahani, M.M., Turner, T.E., Barnes, J.J. *J. Electrochem. Soc.* **1989**, 136(5), 1484.
38. Ghate, P.B., Blair, J.C., Fuller, C.R., McGuire, G.E. *Thin Solid Films* **1978**, 53, 117.
39. Nowiuki, R.S., Harris, J.M., Nicolet, M.-A., Mitchell, I.V. *Thin Solid Films* **1978**, 53, 195.
40. Canali, C., Fantini, F., Zanoni, E. *Thin Solid Films* **1982**, 88, 9.
41. Canali, C., Fantini, F., Zanoni, E. *Thin Solid Films* **1982**, 97, 325.
42. Saito, S., Matsuda, K., Nishizawa, K., Sakiyama, K. *Tungsten and other Refractory Metals for VLSI Applications II*, Material Research Society, Pittsburgh, PA, 1983, 319.
43. Goldschmidt, H.J. *Interstitial Alloys*, Plenum, New York, 1967.
44. Ting, C.Y., Wittmer, M. *Thin Solid Films* **1982**, 96(4), 327.
45. Kanamori, S. *Thin Solid Films* **1986**, 136(2), 195.
46. Delfino, M., Broadbent, E.K., Morgan, A.E., Barrow, B.J., Norcott, A.E. *IEEE Electron Device Lett.* **1985**, EDL-6, 591.
47. Kanamori, S., Matsumoto, T. *IEEE Trans. Electron Dev.* ED-33 **1986**, 402.
48. Krusin-Elbaum, L., Wittmer, M., Ting, C.Y., Cuomo, J.J. *Thin Solid Films* **1983**, 104, 81.
49. Wittmer, M. *J. Appl. Phys.* **1982**, 53, 1007.
50. Chamberlain, M.B. *Thin Solid Films* **1982**, 91, 155.
51. Galasso, F.S. *Chemical Vapor Deposited Materials*, CRC, Boca Raton, FL, 1991.
52. Pierson, H.O. *Handbook of Chemical Vapor Deposition*, Noyes, Park Ridge, NJ, 1992.
53. Chiu, H-T., Chuang, S-H. *J. Mater. Res.* **1993**, 18(6), 1353.
54. Nagai, M., Kishida, K. *Appl. Surf. Sci. B.* **1993**, 70-71, 759.
55. Nakajima, T., Watanabe, K., Watanabe, N. *J. Electrochem. Soc.* **1987**, 134(12), 3175.
56. Chiu, H-T., Chang, W-P. *J. Mater. Sci. Lett* **1992**, 11, 96.
57. Chiu, H-T., Chang, W-P. *J. Mater. Sci. Lett.* **1992**, 11(9), 560.
58. Chiu, H-T., Chang, W-P. *J. Mater. Sci. Lett.* **1992**, 11(2), 96.

59. Katz, A., Pearton, S.J., Nakahara, S., Baiocchi, F.A., Lane, E., Kovalchick, J. *J. Appl. Phys.* **1993**, 73(10), 5208.
60. Fix, R., Gordon, R.G., Hoffman, D.M. *Chem. Mater* **1993**, 5, 614.
61. Maya, L. *Inorg. Chem.* **1992**, 31(10), 1958.
62. Funakubo, H., Kieda, N., Mizutani, N., Kato, M. *Yogyo Kyokaishi* **1987**, 95(1), 55.
63. Wendel, H., Surh, H. *Appl. Phys. A* **1992**, 54(4), 389.
64. Schuster, F., Maury, F., Nowak, J.F., Bernard, C. *Surf. Coat. Technol.* **1991**, 46(3), 275.
65. Funakubo, H., Kieda, N., Kato, M., Mizutani, N., Tatsuno, T. *J. Mater. Sci.* **1990**, 25(12), 5303.
66. Donald, I.T., Davies, H.A. *J. Non-Cryst. Solids* **1978**, 30, 77.
67. Wiley, J.D., Percpezko, J.K.H., Nordonan, J.E., Gwo, K.-J. *IEEE Trans Ind. Electron.* **1982**, IE-29, 154.
68. Nicolet, M.-A., Suni, I., Finetti, M. *Solid State Tech.* **1983**, Dec., 129.
69. Hung, L.S., Saris, F.W., Wang, S.Q., Mayer, J.W. *J. Appl. Phys.* **1986**, 59, 2416.
70. Wang, S.Q., Mayer, J.W. *J. Appl. Phys.* **1989**, 65, 1957.
71. Reus, R. De. Thesis, University of Utrecht, The Netherlands, 1990.
72. Kolawa, E., Halperin, L.E., Pokelar, P., Vu, Q.T., Neith, C.W. *Mat. Res. Soc. Symp. Proc.* **1990**, 181, 33.
73. So, F.C.T., Kolawa, E., Kattelus, H.P., Zhao, H.-A., Nicolet, M.-A., Lien, C.-D. *J. Vac. Sci. Tech.* **1986**, A 4(6), 3078.
74. Kattelus, H.P., Kolawa, E., Attolter, K., Nicolet, M.-A. *J. Vac. Sci. Tech.* **1985**, A 3(6), 2246.
75. So, F.C.T., Kolawa, E., Zhao, A.-Y., Nicolet, M.-A. *Thin Solid Films* **1987**, 153, 507.
76. Bernard, C., Madar, R., Pauleau, Y. *Solid State Tech.* **1989**, 32, 79.
77. Ting, C.Y., Wittmer, M. *J. Appl. Phys.* **1983**, 54, 937.
78. Barggraaf, P. *Semicond. International* **1989**, A May, 293.
79. Hosack, H.H. *J. Appl. Phys.* **1973**, 44, 3476.
80. Merchant, P., Amano, J. *J. Vac. Sci. Tech.* **1983**, A 1(2), 459.
81. Rand, M.J. *J. Electrochem. Soc: Solid State Sci. and Tech.* **1975**, 122(6), 811.
82. Morabito, J.M., Rand, M.J. *Thin Solid Films* **1974**, 22, 293.
83. Haken, R.A. *J. Vac. Sci. Tech.* **1985**, B 3(6), 1657.
84. Fadjikan, R.M., Robenjl, R.P. *Electrochem. Soc. Meeting, Fall 1988, Ext. Abs.* 467, 686.
85. Ting, C.Y. *J. Vac. Sci. Tech.* **1982**, 20, 14.
86. Ting, C.Y., Wittmer, M. *J. Appl. Phys.* **1983**, 54, 937.
87. Chang, S.T., Chiu, R.Y. *IEEE Electron Device Letts.* **1986**, May, 244.
88. Ilderem, V., Reif, R. *Appl. Phys. Lett.* **1988**, 53(8), 687.
89. Ilderem, V., Reif, R. *J. Electrochem. Soc.* **1989**, 136(10), 2989.

90. Lucchiner, C.J. *Electrochem. Soc. Proc. First International Symp. VLSI Science and Technology* 82(7), Dell'Oca, C.J., Bullis, W. M. (eds.), Electrochem. Soc., Pennington, NJ. 1982, 232.
91. Wei, C.S., Raghavan, G., Dass, M.L.A., Frost, M., From, D. *Proc. 6th International IEEE VMIC Conf.* Santa Clara, CA **1989**, 241.
92. Hokeuk, E., Robinson, G.Y. *Thin Solid Films* **1978**, 53, 135.
93. Grinolds, H., Robinson, G.Y. *J. Vac. Sci. Tech.* **1977**, 14, 75.
94. Van Camp, G.J., Daams, J.L.C., Van Oastrom, A., Augustus, L.J.M., Tamminga, Y. *J. Appl. Phys.* **1979**, 50, 6915.
95. Van Camp, G.J., Reukers, W.M. *J. Appl. Phys.* **1979**, 50, 6923.
96. Inoue, S., Toyokura, N., Nakamura, T., Maeda, M., Takagi, M. *J. Electrochem. Soc.* **1983**, 130(7), 1603.
97. Gaczi, P.J., Reynolds, G.J. *J. Electrochem. Soc.* **1989**, 136(9), 2661.
98. Chow, T.P., Bower, D.H., Van Art, R.L., Katz, W. *J. Electrochem. Soc.* **1983**, 130(4), 952.
99. Brors, D.L., Fair, J.A., Monnig, K.A., Saraswat, K.C. *Solid State Tech.* April, 1983, 183.
100. Dobkin, D., Bartholomew, L., McDaniel, G., DeDontney, J. *J. Electrochem. Soc.* **1990**, 137(5), 1624.
101. Zhang, S-L., Buchta, R., Östling, M. *J. Mater. Res.* **1991**, 6(9), 1886.
102. Reynolds, G.J. *J. Electrochem. Soc.* **1988**, 135(6), 1483.
103. Wiczorek, C. *Thin Solid Films* **1985**, 126, 227.
104. Kwok, T. *Mat. Chem. Physics* **1993**, 33, 176.
105. Rodbell, K.P., Knorr, D.B., Mis, J.D. *J. Electronic Mat.* **1993**, 22(6), 597.
106. McConica, C.M., Krishnamani, K. *J. Electrochem. Soc.* **1986**, 133, 2542.
107. Sherman, A. *Chemical Vapor Deposition for Microelectronics*, Noyes, Park Ridge, NJ, 1987.
108. Singer, P.H. *Semicond. Int.* **1990**, March, 45.
109. Bradbury, D.R., Turner, J.E., Nauka, K., Chiu, K.Y. *IEDM* **1991**, 273.
110. Yu, M.L., Ahn, K.Y., Joshi, R.V. *IBM J. Research Develop.* **1990**, 34(6), 875.
111. Jain, A., Chi, K.M., Shin, H.K., Farkas, J., Kodas, T.T., Hampden-Smith, M.J. *Semicond. Int.* **1993**, June, 128.
112. Hampden-Smith, M.J., Kodas, T.T. *MRS Bull.* **1993**, 18, 39.
113. Murarka, S.P., Steigerwald, J., Gutmann, R.J. *MRS Bull.* **1993**, 18, 46.
114. Li, J., Mayer, J.W., *MRS Bull.* **1993**, 18, 52.
115. Steigerwald, J., Murarka, S.P., Gutmann, R.J. *Proc. Mat. Res. Soc. ULSI-VIII* **1993**, 99.
116. Ekin, J.W., Larson, T.M., Bergren, N.F., Nelson, A.J., Swartzlander, A.B., Kazmerski, L.L., Panson, A.J., Blankenship, B.A. *Appl. Phys. Lett.* **1988**, 52(21), 1819.
117. Kaanta, C.W., Bombardier, S.G., Cote, W.J., Hill, W.R., Kerszykowski, G.,

- Landis, H.S., Poindexter, D.J., Pollard, C.W., Ross, G.H., Ryan, J.G., Wolff, S., Cronin, J.E., VMIC Conf., June, 1991, 144.
118. Campbell, I.E., Jaffee, R.I., Blocher, J.M., Gurland, J., Gonser, B.W. *J. Electrochem Soc.* **1948**, 93(6), 271.
 119. Morancho, R., Petit, J., Debosi, F., Constant, G. *Proc. 7th Int. Conf. on CVD*, Sedgwich, T.O., Lydtin, H. (eds.), Electrochem. Soc., Pennington, NJ, 1979, 593.
 120. Travis, E.O., Paulson, W.M., Pintchovski, F., Bock, B., Parrillo, L.C., Kottke, M.L., Fa, K.-Y., Rice, M.J., Price, J.B. *Technical Digest*, IED Meeting 1990, 1990, 47.
 121. Fix, R., Gordon, R.G., Hoffman, D.M. *Chem. Mater.* **1991**, 3, 1138.
 122. Yokoyama, N., Hinode, K., Homma, Y., *J. Electrochem. Soc.* **1989**, 136(3), 882.
 123. Polignano, M.L., Circeli, N. *J. Appl. Phys.* **1990**, 68(4), 1869.
 124. Farkas, J., Chi, K.-M., Hampden-Smith, M.J., Kodas, T.T., Dubois, L. H. *J. Appl. Phys.* **1993**, 73, 1455.
 125. Li, J., Mayer, J.W. *MRS Bulletin* **1993**, 18(6), 52.
 126. Shacham-Diamand, Y., Dedhia, A., Hoffstetter, D., Oldham, W.G. *Proc. VIII VLSI Multilevel Intercon. Conf.* **1991**, 109.
 127. Green, P.F., Berger, L.L. *Thin Solid Films* **1993**, 224, 209.
 128. Li, J., Mayer, J.W. *Mater. Chem. Phys.* **1992**, 32, 1.
 129. Olowolafe, J.O., Mogab, C.J., Gregory, R.B. *Thin Solid Films* **1993**, 227, 37.
 130. Shacham-Diamand, Y., Dedhia, A., Hoffstetter, D., Oldham, W.G. *J. Electrochem. Soc.* **1993**, 140(8), 2427.
 131. Even, R., Palleau, J., Oberlin, J.C., Pantel, R., Laviale, D., Templier, F., Torres, J., Giustiniani, R., Cros, A. *Proc. Eur. Tech. Symp. 2nd*, Abadie, M.J.M., Sillion, B., (eds.), 1991, 407.
 132. Aboelfotoh, M.O., Krusin-Elbaum, L., Sun, Y.C. *Eur. Pat. Appl.* 472 804 A2, Mar. 1992.
 133. Charai, A., Hornstrom, E.S., Thomas, O., Fryer, P.M., Harper, J.M.E. *J. Vac. Sci. Technol.* **1989**, A7(3), 784.
 134. Li, J., Mayer, J.W., Shacham-Diamand, Y., Colgan, E.G. *Appl. Phys. Lett.* **1992**, 60(24), 2983.
 135. Shacham-Diamand, Y., Li, J. *Proc. Mat. Res. Soc. ULSI-VIII* **1993**, 123.
 136. Li, J., Chapman, P.F., Goodwin, F., Schacham-Diamand, Y., Mayer, J.W. *Proc. Mat. Res. Soc. ULSI-VIII* **1993**, 75.
 137. Itow, H., Nakasaki, Y., Minamihaba, G., Suguro, K., Okano, H. *Appl. Phys. Lett.* **1993**, 63(7), 934.
 138. Brusic, V., Frisch, M.A., Eldridge, B.N., Novak, F.P., Kaufman, F.B., Rush, B.M., Frankel, G.S. *J. Electrochem. Soc.* **1991**, 138(8), 2253.
 139. Adema, G., Hwang, L.T., Rinne, G.A., Turlik, I. *Proc. Electron. Compon. Technol. Conf. 42nd* **1992**, 776.

140. *Handbook of Thin Film Technology*, Maisel, L., Glang, E. (eds.), McGraw-Hill, New York, 1970.
141. Hill, R.J. *Physical Vapor Deposition*, Timescale, Berkeley, CA, 1976.
142. Chapman, B. *Glow Discharge Processing*, John Wiley & Sons, New York, 1980.
143. *Handbook of Thin Film Deposition Processes and Techniques*, Schuegraf, K.K. (ed.), Noyes, New York, 1988.
144. *Thin Film Processes II*, Vossen, J., Kern, W. (eds.), Academic, Orlando, FL, 1991.
145. Sze, S.M. *VLSI Technology, 2nd Edition*, McGraw Hill, New York, 1988.
146. Murarka, S.P., Peckerar, M.C. *Electronic Materials, Science and Technology*, Academic, Orlando, FL, 1989.
147. Hess, D.W., Jensen, K.F. *Microelectronics Processing*, American Chemical Society, New York, 1989.
148. Hitchman, M.L., Jensen, K.F. *Chemical Vapor Deposition*, Academic, New York, 1993.

This Page Intentionally Left Blank

Chapter 2

Chemical Vapor Deposition of Aluminum

**Michael G. Simmonds
Wayne L. Gladfelter**

**Department of Chemistry
University of Minnesota
Minneapolis, Minnesota 55455**

Abstract

Films of metallic aluminum are utilized widely in several industries. We will begin this chapter with a brief summary of these and focus on some of the critical physical properties required by these diverse applications. An association between these physical properties and the microstructure of the film will be made whenever possible. Following a general comparison between physical and chemical vapor deposition processes, we highlight some general features of CVD and their relationship to film structure. The majority of the chapter will summarize the literature describing the CVD of Al.

Contents

2.1	Applications of Aluminum Films	48
2.1.1	Microelectronics	48
2.1.2	Metallized Polymers	48
2.1.2.1	Gas Diffusion Barriers	49
2.1.2.2	Optical Properties	49
2.1.3	Adhesion	50
2.2	Comparison Between Physical Vapor Deposition (PVD) and Chemical Vapor Deposition (CVD) of Aluminum	51
2.3	Understanding the CVD Process	52
2.3.1	Surface Diffusion	52
2.3.2	Transport Phenomena	53
2.3.3	Gas-Phase Reactions	55
2.3.4	Surface Reactivity	56
2.3.5	Nucleation	56
2.3.6	Summary of Aluminum Precursors	57
2.4	CVD Using Triisobutylaluminum	58
2.4.1	Early Developments	58
2.4.2	Optimization of Aluminum CVD	60
2.4.2.1	Morphology of Aluminum Deposits	60
2.4.2.2	Alloys with Cu and Si	60
2.4.2.3	Nucleation Promoters	61
2.4.2.4	Aluminum Epitaxy on Si	62
2.4.3	Surface Decomposition Mechanism of TIBA	63
2.4.4	Patterning of Aluminum Films	66
2.5	Deposition of Aluminum from Trimethylaluminum	68
2.5.1	Thermal Activation of TMA	69
2.5.2	Plasma-Assisted Aluminum Deposition Using TMA	72
2.5.3	Laser-Assisted Aluminum Deposition From TMA	73
2.6	Deposition of Aluminum Films from Alane Precursors	74
2.6.1	Surface Reaction Mechanism of TMAA	77
2.6.2	Deposition in Cold-Wall Reactors Using TMAA	80
2.6.3	Deposition in Hot-Wall Reactors Using TMAA	81
2.6.4	Aluminum Deposition from TEAA	81
2.6.5	Aluminum Deposition from DMEAA	82
2.6.6	Selectivity of Deposition Using Alane Precursors	83
2.6.7	Aluminum Deposition Using Aluminaborane Precursors	84
2.6.8	Gas-Phase Aluminum Particle Formation From Amine Alanes	84

2.7	Alternative Aluminum Alkyl Sources	86
2.7.1	Triethylaluminum	86
2.7.2	Dimethylaluminum Hydride	88
2.7.3	Diethylaluminum Chloride	90
2.7.4	Aluminum Monochloride	91
2.8	Summary	92
	Acknowledgements	93
	References	93

2.1 Applications of Aluminum Films

2.1.1 Microelectronics

A combination of physical and chemical properties has rendered metallic Al films useful as interconnects in microelectronic devices.¹⁻¹⁰ The resistivity of bulk Al of $2.74 \mu\Omega\text{cm}$ is only slightly greater than that of silver ($1.61 \mu\Omega\text{cm}$) and copper ($1.70 \mu\Omega\text{cm}$). (See Chapters 1 and 8 for discussion of applications of these and other metals in microelectronics; Chapters 6, 5, and 4 discuss CVD of silver and copper from Cu(I) and (II) precursors, respectively.) Despite a surface oxide coating that protects the metal from corrosion, the ability to etch Al easily is an important aspect of its use in device manufacturing. Being amphoteric, Al can be dissolved in either strong acid or strong base. Smooth films of Al are required to create patterns using lithographic methods. One of the drawbacks of some of the Al films grown by CVD methods is their rough surface morphology.

An additional concern with using pure Al in microelectronic circuits stems from its susceptibility towards electromigration which involves the movement of atoms induced by electric fields, and becomes increasingly significant as the size of the interconnect lines decreases.¹¹ The impact that electromigration has on the lifetime of a device depends somewhat on the microstructure of the Al film.¹² Some efforts have focused on growing epitaxial films to reduce electromigration. Another method used to reduce the problem involves alloying the Al with small amounts of Cu and/or Si. The miscibility of these elements in Al limits their concentrations to a few percent.

A further aspect of the design of microcircuits depends on the solubility or reactivity of Al with semiconductors. Small amounts of Al will dissolve in Si and may cause problems at the interface between these two layers. Gallium arsenide and Al react at the interface to give AlAs (or an intermediate alloy) and Ga metal. To alleviate these problems, thin diffusion barriers of W or TiN are grown directly onto the semiconductor. For III-V semiconductors, alternative diffusion barriers include the metal aluminides, such as FeAl, which are thermodynamically stable in the presence of both GaAs and Al. These and other considerations are discussed in Chapter 1.

2.1.2 Metallized Polymers

There are a large number of applications of Al thin films on polymers; however, the majority of these focus on a few critical functions of the metal film. Evaporation and sputtering are the only methods used to grow these Al films. The relatively low melting points of polymers place severe restrictions on the substrate temperatures

accessible during the deposition. The development of CVD processes for growing Al films on polymers must focus on lowering the deposition temperature as much as possible.

2.1.2.1 Gas Diffusion Barriers

The performance of polymers such as polypropylene used in food packaging (potato chip bags, etc.) and other applications (party balloons) depends on their ability to prevent the diffusion of water, oxygen, and other gases through the membrane. Coating a polymer with Al substantially increases the effectiveness of the product. In some applications an Al film is deposited on the surface of a polymer which is then laminated with a second polymer to create a sandwiched structure. For obvious reasons, these films must be free from pinholes, and for the sake of appearance, they should be specularly reflective to visible light. A polycrystalline microstructure having a very small grain size is best suited to these requirements. Growth of films exhibiting this structure requires a high density of nucleation sites at the beginning of the growth process.

2.1.2.2 Optical Properties

The reflectivity of Al is second only to Ag, and many applications utilize this property. A high degree of specular reflectance is required in mirrors and in Al films applied for decorative purposes. Information storage on compact disks utilizes the

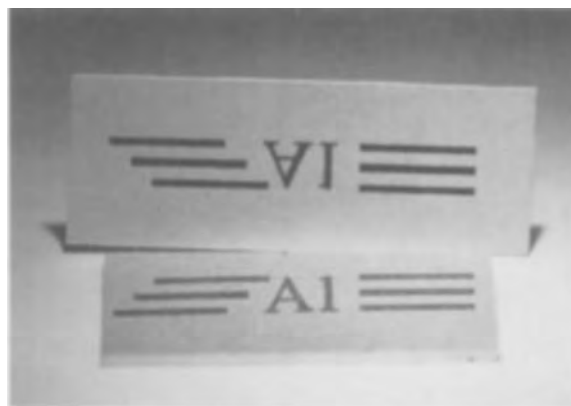


Figure 2-1 Photograph illustrating the reflectivity and smoothness of a CVD aluminum film grown from TMAA.¹³ The top image was printed on paper and is reflected off the Al film on the lower wafer. [Reprinted with permission from *Chem. Mater.* 1989, 1, 339. Copyright 1989 American Chemical Society]

reflectivity of Al films on polycarbonate. Specular reflectance is related to the fundamental reflectivity of a material and to its surface morphology. If the roughness of a surface, whether caused by a rough underlying substrate or by grain structure, approaches the wavelength of incident radiation, diffuse reflectance will result. Adjectives used to describe such films are milky, hazy, cloudy, and frosty. Specularly reflective films require smooth substrates. Except for epitaxial Al films grown on optically smooth Si at high temperatures, most mirror-like Al films are comprised of a large number of grains less than 200 nm in diameter. Figure 2-1 shows an example of such a film grown using trimethylamine alane, TMAA, in a CVD process.¹³

Some applications, such as tinted glass, utilize the absorptivity of very thin (10 nm) metal films to reduce the amount of light, especially in the infrared region, that is transmitted through a window. Related applications utilize thicker Al coatings on fibers to improve the thermal insulating properties of the product.

2.1.3 Adhesion

Although not an application in and of itself, strong adhesion of a metal layer to any type of different material such as a polymer, ceramic, or a semiconductor is critical to the performance and lifetime of the product. The situation is particularly aggravated with many polymer applications because of the flexibility of the substrate. At the microscopic level, adhesion can be attributed both to chemical bonds between the two surfaces and mechanical effects.¹⁴ The interaction between two atomically smooth surfaces can be attributed exclusively to the chemical bonds formed at the interface. These interactions can be due to van der Waals bonds, hydrogen bonds, dipolar attractions, ionic, and/or covalent bonds and are dependent on the chemical nature of the two surfaces. Real surfaces have a far more complex topology, and a good adhesive interface will involve a certain amount of conformal fitting between the two materials. Separation of the interfaces will not only require the surface chemical bonds to be severed, but it will also have to overcome the resistance to changing the shape of the materials located at the interface. This "microstructural Velcro effect" is controlled by the mechanical properties of the materials. Aluminum films generally adhere well to Si, SiO₂, other metals, and some polymers such as polyimide. Unfunctionalized polymers such as polyethylene often require surface pretreatment by, for example, a corona discharge to improve adhesion. Such treatments generally result in partial oxidation of the surface which leads to a stronger bond to Al.

2.2 Comparison Between Physical Vapor Deposition (PVD) and Chemical Vapor Deposition (CVD) of Aluminum

Evaporation and sputtering are the two methods by which most (if not all) commercial Al films are deposited.¹⁵⁻²⁰ These methods produce films of high purity on substrates that can be maintained at room temperature during deposition. The vast majority of Al films used in industry are polycrystalline, and the growth rates can exceed 10^3 nm/min in sputtering processes. Empirical, qualitative models (structure zone models) relating growth conditions to the microstructure of the film have been described for physical vapor depositions (PVD).²¹⁻²⁷ The reduced temperature (T/T_m), the growth temperature (in K) divided by the melting temperature (T_m) of the material being deposited, is one of the most important parameters in controlling the microstructure of the film. Other critical parameters include the flux of atoms to the surface, the surface and bulk diffusivity, the background pressure, and the film thickness.

In addition to the above parameters, chemical reactions are necessary to produce the thin film in a CVD process. Whereas high vacuum conditions are necessary for PVD processing, most CVD processes work in the range of 0.1 to 760 torr. The large values of the mean-free path and the high sticking coefficient of the atoms (or clusters) render PVD processes largely "line-of-sight" depositions. In CVD, the mean-free path of the molecules and their sticking coefficients are often reduced. This means that the "precursor" undergoes a large number of collisions upon entering the reactor before it collides with a surface. As a result of these collisions, the lower sticking coefficients of the molecules (compared to the atoms produced in PVD), and the surface diffusion of the molecules or fragments, CVD processing often gives a more conformal surface coverage.^{5,28} Because this allows numerous wafers or other substrates to be stacked in a reactor, the throughput of a CVD process can be higher. These advantages are partially offset by the high cost of the molecular precursors and the difficulty of maintaining a pure system. Some contaminants are present in the source of the molecular precursors while the molecular precursors themselves can undergo unwanted side reactions that generate impurities in the film. Because the molecular precursors must be stable enough to store for extended periods, depositions of thin films can require substrate temperatures that are higher than needed in PVD. Finally, because of the relative complexity of CVD, a greater effort is usually required to develop a successful process.

2.3 Understanding the CVD Process

The above discussion highlighted a few relationships between Al film microstructure and physical properties; some examples cited the importance of deposition parameters on the microstructure. This section provides a qualitative framework for discussing the critical relationships between deposition mechanisms and film microstructure. A portion of the discussion will address the role that nucleation plays in the formation of thin films. Chapter 1 also provides a short introduction to CVD technology.

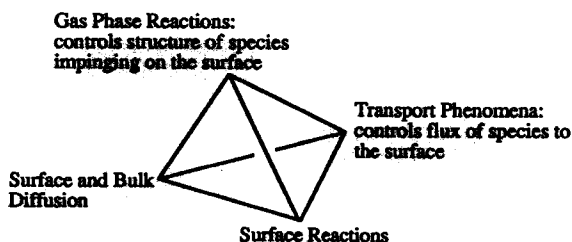


Figure 2-2 The relationships between the important processes involved in the growth of CVD thin films.

To design a process for depositing a particular film we must know the nature and number of the species impinging upon the growing surface, and we must understand what happens to these species once they arrive. Figure 2-2 shows the relationship of various phenomena that can be involved in the growth of a thin film. There is, unfortunately, no quantitative procedure to predict for every deposition which one (or more) of the four corners of the tetrahedron will be the most important in controlling a process. However, considering the chemistry of the precursors, the parameters of the deposition, and the design of the reactor can give a qualitative understanding of the process and its effect on film microstructure.²⁹

2.3.1 Surface Diffusion

As discussed in Section 2.2, substrate temperature greatly influences the mobility of atoms³⁰⁻³⁵ and molecules on the surface. It is not just the substrate temperature, however, that controls the microstructure of the film. It is the competition among the rates of surface and bulk diffusion, the flux of molecules to the surface, and the rates of

reactions that occur on the surface that combine to control the microstructure of the growing film.^{26,36-38}

A quantity that has been used to relate the effect of surface diffusion to the microstructure of thin films is the surface diffusion length³⁹⁻⁴¹ (Eq. 2.1). It defines the distance (l) an atom of Al is capable of moving in a period of time defined by the growth rate

$$l = [D \Omega^2 \Gamma \gamma / (k_B T v)]^{1/3} \quad (2.1)$$

where D = surface diffusivity (10^{-8} cm²/s estimated⁴² for Al^{43,44}), Ω = atomic volume (1.66×10^{-23} cm³), Γ = area density of atoms in the (111) surface (1.42×10^{15} cm⁻²), γ = surface tension (10^3 dyn/cm), k_B = Boltzmann constant, T = absolute temperature (423 K) and v = growth rate (1.67×10^{-7} cm/s). For the values given in parentheses, the diffusion length is $\sim 10^2$ nm. If the diffusion length is small compared to the initial roughness of the substrate, a columnar microstructure is likely to result because those high points on the surface will be exposed to a greater precursor flux.^{40,45-47} Larger values of l are capable of giving films in which the roughness of the original surface is smoothed and which exhibit larger grains. In addition to Al atoms migrating, adsorbed precursor molecules also have the possibility of diffusing. Virtually no data are available to evaluate this for Al or to establish its impact on the evolution of the microstructure. Limited data exist for a small number of other metal precursors.⁴⁸

A caveat that must accompany this discussion of surface diffusion is that the surface must be clean. Aluminum forms a coating of oxide upon exposure to the atmosphere which would alter surface diffusion of Al atoms. One of the most important requirements for growing single crystalline films (l must be large) is cleanliness of the reactor. Even under high vacuum conditions an impurity having a partial pressure of 10^{-6} torr will completely cover a surface in one second (providing the sticking coefficient is unity).

Finally, if a deposition is conducted at high temperature relative to the melting point, bulk diffusion can also effect the microstructure.⁴⁹

2.3.2 Transport Phenomena

Some deposition procedures are conducted under conditions which minimize the importance of hydrodynamics.⁵⁰ For instance, high vacuum methods such as molecular beam epitaxy (MBE) minimize the significance of both hydrodynamics and gas phase reactions because the size of the reactor itself is usually smaller than the mean-free path of the gases. Therefore, the precursors will not collide with each other before reaching the surface of the substrate. Motion of precursors in this molecular flow regime is

explained using the kinetic theory of gases. The majority of CVD processes, however, are conducted at higher pressures where the mean-free path is significantly smaller (<0.5 mm) than the dimensions of the reactor.

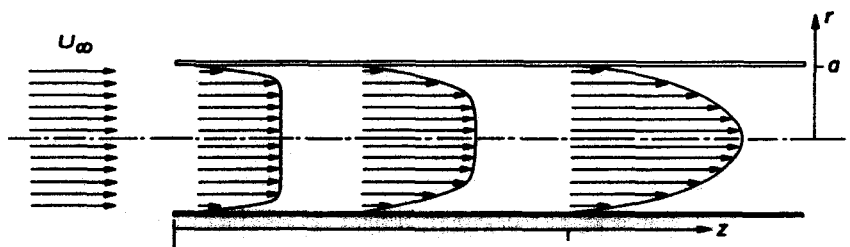


Figure 2-3 Evolution of the fully developed velocity profile for laminar flow in the entrance region of a tubular reactor.⁵² [Reprinted with permission from Springer-Verlag]

Under conditions of laminar flow through a tubular reactor, Figure 2-3 shows the evolution of the velocity field from a plug flow to a fully developed (parabolic) profile. Precisely at the vapor-solid interface the velocity of the vapor-gas mixture is zero. Due to the viscosity of the gas, this no-slip boundary condition gives rise to a transition zone in velocity (often incorrectly referred to as a "boundary layer") that eventually spreads over the whole reactor cross section. Similarly, there also exist transition regions from bulk-flow to interfacial values in temperature and concentrations. The latter are caused by diffusion of reactant from the fluid to the growth surface where the precursor is consumed, or by homogeneous gas phase reactions that set in as the vapor becomes heated by the susceptor. These effects are coupled; it is the synergism between them that governs the rate of mass transport.⁵¹⁻⁵⁵

Predicting the hydrodynamic behavior of real reactors is complex, but the results can be invaluable for designing the optimum reactor and growth conditions. Numerical methods have been developed to solve the partial differential equations defining the conservation of energy, mass (continuity equation), and momentum for a given system.^{56,57} Figure 2-4 shows the behavior of a typical inverted reactor for growing single crystal films of GaAs and other semiconductors. Temperature gradients existing between the incoming gases and the susceptor surface or the reactor wall cause recirculation cells to be established.⁵⁷ Precursor molecules trapped in these recirculation cells spend a much longer time within the reactor than predicted from the residence time as calculated from the flow rate. This often leads to unwanted side reactions that can generate impurities or particles that may have a detrimental effect on the performance of the thin film. A more detailed analysis of the problem in Figure 2-4

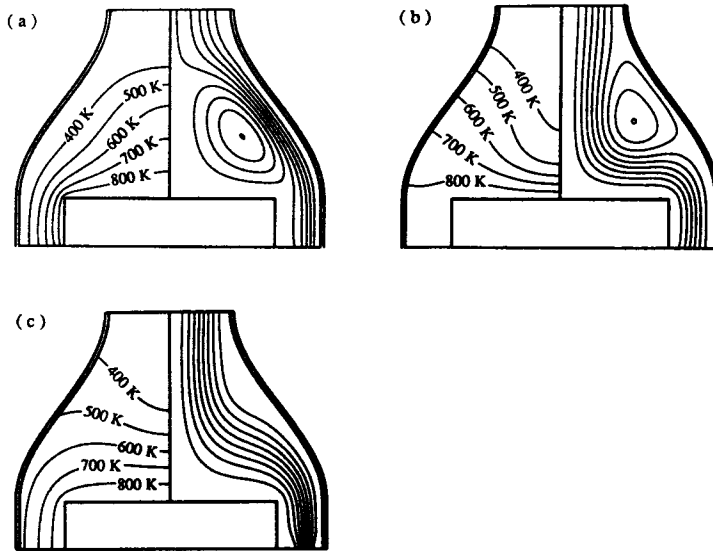


Figure 2-4 Theoretical effect of wall temperature boundary conditions on the streamlines and isotherms in a CVD system (a) idealized fixed wall temperature (300 K) (b) idealized insulated wall (c) non-idealized detailed model.⁵⁷ [Reprinted with permission from Elsevier Science Publishers]

leads to a forced convection dominated flow resulting in enhanced film uniformity. By incorporating rates of gas-phase and surface chemical reactions these models can simulate observed growth rates. True predictive capability is, unfortunately, hampered by the lack of knowledge of rate constants for many of the gas-phase and especially for the surface chemical reactions.

2.3.3 Gas-Phase Reactions

As the temperature of the molecular precursor increases the probability that it will undergo a chemical reaction also rises. In the reactor shown in Figure 2-4, isotherms illustrate the change of gas temperature as a function of distance from the substrate. In AI CVD processes unimolecular reactions may occur in the gas phase leading to highly reactive intermediates that can undergo one or more subsequent reactions.

2.3.4 Surface Reactivity

When the intact precursor or a partially reacted intermediate collides with and sticks to the growing surface, additional chemical reactions must occur that release the byproducts of the deposition. Although the flux of molecules to the surface will be constant, the sticking coefficient may change if the molecule hits the surface already covered with a layer of precursor. In addition, the reaction itself may change if the surface is coated with a partially reacted precursor.

Atoms at the surface of a material are less stable and therefore more reactive than atoms contained within the bulk of the solid. This can in part be understood by consideration of the coordination number of the atom. Aluminum is a face-centered cubic metal where the coordination number of each atom in the bulk is 12. The coordination number of each atom on the Al(111) surface is 9, and the coordination number of atoms exposed at steps or kinks in the surface can drop even lower.

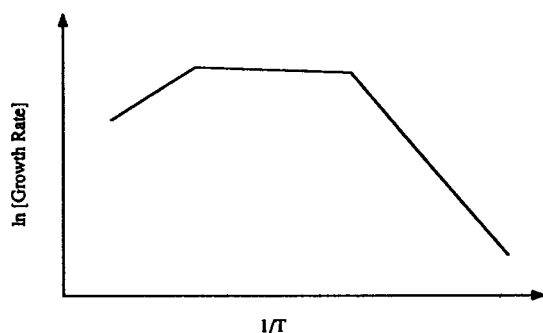


Figure 2-5 Dependence of CVD rate on the absolute temperature of a substrate.

Figure 2-5 illustrates the dependence of the rate of a deposition on temperature.^{58,59} The steep rise at low temperature is attributed to a surface reaction limiting regime, whereas the nearly flat region is the result of a mass transport limited deposition. At the high temperature limit of the deposition there may be a fall off in growth rate with increasing temperature. When observed, this has been attributed to the effect of temperature on the chemical equilibria involved in the growth process and to particle-formation in the gas phase (see Ch. 9).

2.3.5 Nucleation

The kinetic barrier towards steady state growth is usually lower than the barrier towards initial nucleation of the film.⁶⁰ The microstructure of a film depends largely on the rate of nucleation of the new phase, which will be sensitive to the same phenomena discussed above for steady-state growth. In addition, defects and impurities

on the substrate surface can play a dominant role in initiating nucleation. While much effort has been put forth to understand nucleation phenomena in physical vapor depositions, especially evaporation, little knowledge exists of its impact on chemical vapor depositions. As will be described later, numerous studies of Al depositions have included a surface pretreatment with TiCl_4 which, through a poorly understood mechanism, lowers the kinetic barrier of nucleation on surfaces such as SiO_2 and polymers. The smoother films which result from this pretreatment are desirable for many applications. Studies have shown that gas-phase nucleation induced by traces of H_2O can yield Al particles during the CVD process using dimethylethylamine alane.⁶¹

A potentially important future application of CVD involves selective area deposition. The basis for those examples described in the literature thus far results from different kinetic barriers towards nucleation on the two surfaces exposed to the same flux of the molecular precursor. In general, considerably more research must be completed for us to begin to understand the nucleation process for any given deposition system.

2.3.6 Summary of Aluminum Precursors

Table 2-1 Aluminum Precursors

Precursor (Abbreviation)	Vapor Pressure ^a	Growth Temp. ^b	Selectivity ^c
Trimethylaluminum (TMA)	11 (20)	300	none
Triethylaluminum (TEA)	0.1 (36)	160	_____
Triisobutylaluminum (TIBA)	0.1 (27)	250	Si, Metals
Diethylaluminum chloride (DEACl)	3 (60)	340	Si
Dimethylaluminum hydride (DMAH)	2 (25)	240	Si
Trimethylamine alane (TMAA)	1.1 (19)	100	Metals
Triethylamine alane (TEAA)	0.5 (25)	100	_____
Dimethylethylamine alane (DMEAA)	1.5 (25)	100	Metals
Trimethylamine aluminaborane (TMAAB)	_____	100	_____

^a Vapor pressure⁶² in torr with the temperature (°C) in parentheses.

^b Approximate lowest temperature (°C) reported for a thermal deposition.

^c Preference for growth on the material listed in the presence of other solids (usually SiO_2); does not include photo- or plasma-induced selectivity; blanks indicate no reports.

Table 2-1 lists most of the precursors that are discussed in this chapter. Drawings showing their molecular structures are included in their respective sections.

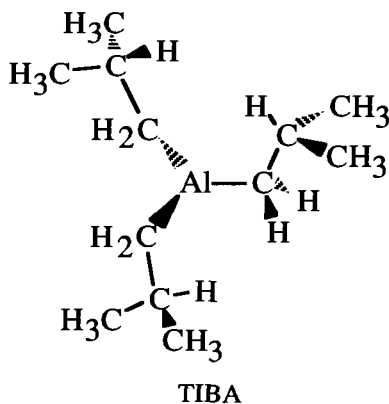
For detailed accounts, the reader is referred to three noteworthy publications describing the properties of Al compounds.⁶³⁻⁶⁵ A variety of brief summaries on Al CVD are also available.^{5,66-71}

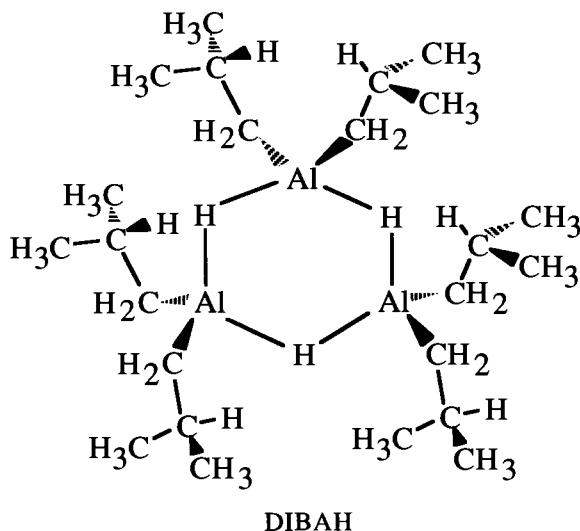
2.4 CVD Using Triisobutylaluminum

2.4.1 Early Developments

The precursor which has received the most attention to date for the deposition of high quality aluminum films is triisobutylaluminum (TIBA), a colorless and pyrophoric liquid having a vapor pressure at ambient temperatures of about 0.1 torr. It is known to be monomeric in the vapor phase.

During the latter half of the 1950s, TIBA was used to catalyze the polymerization of olefins, an application in which it continues to be widely utilized. During this same period, the pyrolysis of TIBA was found to produce high quality (> 99 atom %) Al deposits.^{66,72-74} This conversion is reversible under severe conditions. The mechanism responsible for the liberation of the isobutyl moieties is the well-known β -hydride elimination reaction. An early investigation of the gas phase decomposition kinetics corroborated some of these details.⁷⁵

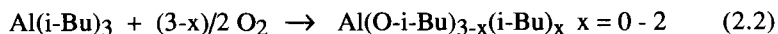




At temperatures above 50 °C TIBA loses one isobutyl ligand and forms diisobutylaluminum hydride (DIBAH) which has a substantially lower vapor pressure (0.01 torr at 40 °C) because it exists as a hydrogen bridged trimer. Typically, the precursor vessel and the associated gas lines through which TIBA is passed are heated to 40-50 °C and may lead to the formation of some DIBAH. Its formation has been associated with a reduction in the reflectivity of Al films;^{76,77} however, the reversibility of the β -hydrogen elimination can be used to suppress the dissociation by the addition of excess isobutene to the carrier gas.⁶⁶ The kinetic parameters for this step in the temperature range 107-173 °C were studied in an all-Teflon reaction vessel at pressures typically on the order of 100 torr.^{78,79} Under these conditions the homogeneous reaction had an activation energy (E_a) of 26.6 kcal/mol and a pre-exponential factor (A) of $1.6 \times 10^{11} \text{ s}^{-1}$.

Above approximately 200 °C DIBAH reacts to give Al. Although this decomposition does occur at temperatures below 200 °C most CVD studies employ a temperature in excess of this in order to obtain useful deposition rates. Aluminum can also be produced directly from TIBA without DIBAH formation.⁸⁰⁻⁸³

In addition to its propensity to form DIBAH, TIBA reacts with sources of oxygen to form alkoxides (Eq. 2.2). These alkoxides can be volatile and can therefore be a source of contamination in the films.^{84,85} The problem was alleviated by using a double distillation system upstream of the reaction zone.^{76,77}



Subsequent to the early reports, Al coatings were obtained from the pyrolysis of Al alkyls by a variety of authors.^{75,86,87}

2.4.2 Optimization of Aluminum CVD

It was not until the early 1980s that several groups demonstrated the usefulness of TIBA to very large scale integration (VLSI) applications in hot wall CVD reactors.⁸⁸⁻⁹¹ The reactors were of the horizontal, stainless steel type, containing stacked Si and SiO₂ substrate wafers. Typical deposition conditions included a furnace temperature of 200-300 °C and a precursor pressure of 0.2-0.5 torr. Under these conditions growth rates of 20-80 nm/min were achieved. These films exhibited excellent conformal coverage and had resistivities within 10% of the bulk value.

2.4.2.1 Morphology of Aluminum Deposits

Films grown on SiO₂ were polycrystalline with a propensity to orient in the (111) direction whereas those films grown on Si(100) surfaces showed a strong preference for the (100) orientation. Furthermore, the films had a rough surface morphology (10-15% of film thickness) giving them a frosty appearance at typical film thicknesses. The roughness of the films was believed to be a result of the slow rate of nucleation of Al on the surface of substrate wafers relative to the rate of Al growth. Because the growth of Al is autocatalytic, once nucleation has occurred, growth of Al takes place on the surface of the island more rapidly than the rate at which other islands are formed. Islands can nucleate throughout the deposition resulting in films that have an uneven distribution of grain sizes and may exhibit a columnar grain structure.

2.4.2.2 Alloys with Cu and Si

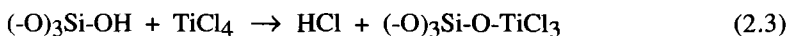
The short time to failure for the films of 9.1×10^4 h (due to high electromigration) did not compare favorably with the corresponding values for evaporated Al-Cu alloys (10^6 h).⁹⁰ An attempt has recently been made to incorporate Cu into Al films grown by CVD.⁹² The poor electromigration resistance exhibited by Al has also been alleviated somewhat by forming Al-Si alloys. A post-deposition alloying process inside a hot wall reactor has been described in which freshly deposited Al films were exposed to the vapors of silane (SiH₄) above 250 °C in a flow of H₂ carrier gas.⁸⁸ Silane decomposed on the Al surface and was subsequently absorbed by the film to form a solid solution up to the solid solubility limit at the temperature of the film. Dendritic silicon crystallites which protruded above the film surface were formed unless hydrogen was used during the alloying stage. The maximum temperature employed was 460 °C at which the solid

solubility limit is 0.5%. Films alloyed with Si at this temperature had a resistivity which was 20% higher than for bulk Al. Introducing disilane (Si_2H_6) directly into the TIBA feed gas prior to its introduction into the reaction chamber eliminated the need for a post-deposition stage.⁹³⁻⁹⁷ The resistivities of the Al-0.4% Si films were typically 10-15% higher than for bulk Al.

2.4.2.3 Nucleation Promoters

The relative kinetics of nucleating Al islands on substrates favors silicon over silicon oxide surfaces so that silicon substrates typically exhibit better uniformity of coverage.^{90,91,98,99} Nucleation promoters have been used to initiate film growth and to enhance the uniformity and smoothness of deposits. For example, dramatic differences in Al film uniformity are observed^{76,77,88,90,91} when silicon substrates are exposed in situ to TiCl_4 prior to Al deposition (the excess vapors being pumped out of the system before the reactor is exposed to TIBA).

The mechanism by which TiCl_4 functions is unknown although preliminary experiments have elucidated some interesting features of the pretreatment. The saturation coverage of Ti on SiO_2 substrates is consistent with a surface OH coverage of about 15-30% of a monolayer, and it has therefore been suggested that the incorporation of Ti onto SiO_2 occurs via a hydrolysis reaction between TiCl_4 and the surface hydroxyl groups (Eq. 2.3).¹⁰⁰⁻¹⁰³



Thermal desorption spectroscopy (TDS) studies in which SiO_2 was treated with TiCl_4 produced two desorption peaks occurring at -90°C and $+90^\circ\text{C}$.¹⁰⁴ The low temperature signal was attributed to the desorption of TiCl_4 multilayers, whereas the higher temperature peak resulted from desorption of the TiCl_4 bound to the substrate. Parallel studies of the surface composition using AES established that only half of the TiCl_4 desorbed at 90°C . Above this temperature the Cl:Ti ratio slowly dropped until by 600°C no Cl signal was visible. This change was attributed to slow loss of HCl from the surface. Qualitative experiments suggested that any TiCl_x present on the surface would promote nucleation.¹⁰⁴

A variety of metal catalysts have been shown to promote the decomposition of a host of metal alkyls.¹⁰⁵ These catalysts include TiCl_4 , TiH_2 , CrCl_3 , VCl_4 , and NbCl_5 . Not only have they been shown to hasten the decomposition reaction, but they also reduce the temperature of the decomposition. Seed layers of TiN, Cu¹⁰⁶, Au, Ni¹⁰⁷; and Cr^{88,89} can also be beneficial to film nucleation and growth and have been deposited by CVD (see Chs. 1,4,5,6,7, and 8). In a hot wall reactor at $230\text{--}270^\circ\text{C}$ under typical low pressure

conditions, films grown on SiO₂ coated in situ with sputtered TiN were smooth, highly reflective, conducting, and relatively free from pinholes, interfacial voids, and stress.

A novel, double wall CVD technique was used to grow smooth Al selectively on Si, metals (W, Mo, and Ti), and silicides (TiSi₂) in the presence of SiO₂ and Si₃N₄.⁹⁹ In this study, the substrate was positioned approximately midway between two heaters and was at a temperature typical for Al CVD. Gaseous TIBA was heated to a temperature higher than the substrate. It was conjectured that the gas impinging on the cooler substrate surface became highly supersaturated, generated a high density of nuclei, and therefore resulted in smoothing films.

Other advancements have been made to increase the smoothness of deposits; notably, preheating the gases before their arrival at the substrate surface⁹³ and introducing O₂ in low concentration⁶⁶ during a deposition have met with some success.

2.4.2.4 Aluminum Epitaxy on Si

With great care, epitaxial films of Al have been grown on the surface of Si(100) and Si(111) substrates using a technique referred to as gas-temperature-controlled CVD (GTC-CVD).^{93-97,108,109} In this technique, the precursor is preheated before its arrival at a heated substrate surface. It was proposed that the precursor formed reactive gas-phase intermediates which impinged on the substrate surface to promote the decomposition to Al. The procedure involved bubbling argon through TIBA (stored in a cylinder at 50 °C) into the reaction zone. The gases, at a total pressure of 2 torr, were then preheated to 230 °C in a copper cylinder. Upon exiting the cylinder, they came in contact with a silicon substrate. With a susceptor temperature of 400 °C, smooth epitaxial films of Al(111) were grown on Si(111) as evidenced by reflective high energy electron diffraction (RHEED). The typical growth rate at 400 °C was about 900 nm/min. Such films were highly reflective (> 90% specular between 310 and 600 nm) and had resistivities close to the bulk value of Al. Apart from the diffusion of 0.1% Si into the films, low levels of O, C, and H were detected (~20 ppm). An Arrhenius plot of the growth rate on Si(111) below 300 °C provided an activation energy for the surface reaction of 30 kcal/mol. Film growth was monitored with scanning electron microscopy (SEM) which indicated that Al islands with a low nucleation density grew initially on the silicon surface and coalesced at a film thickness of about 300 nm. Small changes in the temperature of the substrate had a dramatic effect on the film morphology so that below 400 °C the Al surface became rough and contained a mixture of the (111) and (100) orientations. Further work using transmission electron diffraction (TED) established that epitaxial Al(100) was formed on Si(100) at 380-400 °C using this deposition procedure. Near 400 °C the surface became rough again and the films were a mixed structure of Al(100) and (110). At higher temperatures films were (110) oriented although the grains were rotated 90° to each other. At temperatures below 380 °C the surface was rough and the films were polycrystalline. Overall, four

kinds of single crystalline epitaxial films on Si substrates were obtained: Al(001)/Si(001), Al(001)/Si(111), Al(111)/Si(111), and Al(110)/Si(115). The common epitaxial relationship in these films was Al[110]||Si[110] in the interfacial plane. Along this direction, four lattice spacings of Al matched three lattice spacings of Si.¹⁰⁹

The temperature sensitivity of Al growth on Si(111) has been researched independently using a set-up similar to that used in the above two studies, although the gases were not preheated prior to their arrival at the growth surface.¹¹⁰ With TED, epitaxial Al(100)/Si(111) with Al[110]||Si[112] was apparent at 380 °C whereas at around 420 °C a much smoother single crystal of Al(111)/Si(111) with Al[110]||Si[110] was grown. Films grown at 400 °C were polycrystalline with intermediate reflectivity and resistivity. The epitaxial relation appeared to be determined mainly at the initial stage of growth and was probably related to the interfacial energies between Al and Si at the different temperatures as opposed to a change in the CVD mechanism. Cross-sectional micrographs of the interface between Al and Si showed that the films deposited at 420 °C were comparatively dislocation free.

The ability to grow epitaxial films of Al on Si is, at first glance, curious considering the lattice mismatch of 25%. Films consistent with the above relationships have also been grown by physical vapor deposition techniques, however. The mismatch can be accommodated if one assumes a small displacement between Al and Si lattices at the interface over multiple unit cells. On one occasion, atomically resolved transmission electron micrographs (TEM) were used to investigate the lattice matching at the Al(111)/Si(111) interface, and four lattice planes of Al appeared to occupy the same distance as three lattice planes of Si.¹¹¹

2.4.3 Surface Decomposition Mechanism of TIBA

The surface chemistry of TIBA pyrolysis was investigated in a series of elegant studies in which a combination of effusive molecular beam scattering, TDS, Auger electron spectroscopy (AES), low-energy electron diffraction (LEED), high-resolution electron energy loss spectroscopy (HREELS), and SEM were used in ultra-high vacuum (UHV) compatible environments.⁸⁰⁻⁸³

The decomposition of TIBA on Al(100) and Al(111) surfaces took place at about 197 °C and resulted in the formation of carbon-free epitaxial Al, H₂ and isobutene.⁸² No DIBAH was detected. The studies also established that both hydrogen and isobutene readily desorb from Al at temperatures below that at which decomposition occurs indicating that product desorption is not rate limiting. Typical molecular beam scattering data illustrating these points are shown in Figure 2-6. The rate of formation

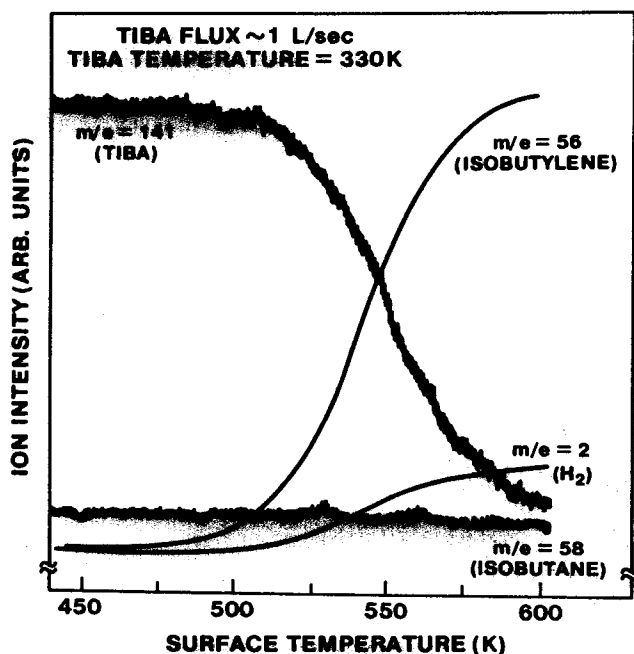


Figure 2-6 Data from molecular beam scattering experiments for TIBA on Al(100).⁸² The figure shows the scattered species as a function of substrate temperature. [Reprinted with permission from *J. Am. Chem. Soc.* 1989, *111*, 1634. Copyright 1989 American Chemical Society]

of isobutene was first order with respect to the flux of TIBA. Because all three isobutyl groups behaved identically, and because molecular TIBA desorption was never observed in the TDS study, it was suggested that the isobutyl groups become equivalent by diffusing over the Al surface following TIBA adsorption. Each of these isobutyl groups then participates in a rate-determining β -hydrogen elimination reaction to liberate isobutene and form a surface-bound hydrogen atom.^{112,113}

The rate of the surface limiting step is 2-5 times faster on Al(111) than on Al(100). The cause of this difference is unknown, although a tentative correlation has been made with the respective work functions of Al(111) and Al(100). It is interesting to note that the kinetic parameters for the β -hydride elimination of the isobutyl ligands on Al(111) are similar to the values obtained for the gas-phase elimination of one isobutyl group from TIBA.^{78,79} This may be interpreted as meaning that the transition state of the β -hydride elimination on Al(111) occurs on individual Al atoms.

Above 330 °C and 350 °C for Al(100) and Al(111) surfaces, respectively, carbon incorporation was evident consistent with a more highly activated β -methyl elimination

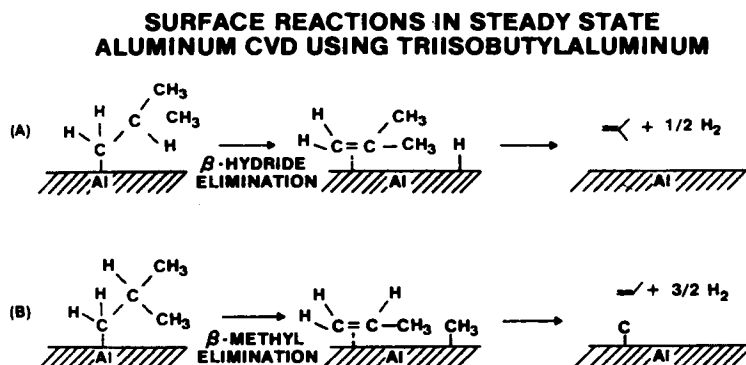


Figure 2-7 Proposed decomposition pathways for isobutene ligands on the surface of Al (A) below 600 K, (B) at higher temperatures.⁸² [Reprinted with permission from *J. Am. Chem. Soc.* 1989, *111*, 1634. Copyright 1989 American Chemical Society]

step of an isobutyl ligand. Figure 2-7 summarizes the proposed decomposition pathways during the steady state growth reaction.

A simple model predicted the steady state Al deposition rates based on the assumption that these are determined by the β -hydride surface reaction. By equating the rate of TIBA adsorption with the rate of isobutene evolution, the following expression (Eq. 2.4) was derived for the rate of Al deposition.

$$\text{Rate of Al Deposition} = \frac{A n_s \exp\left(-\frac{E_a}{RT}\right)}{\frac{A n_s}{\sigma s} \exp\left(-\frac{E_a}{RT}\right) + 1} \quad (2.4)$$

where n_s is the number of adsorbed TIBA per unit area at saturation coverage, σ is the flux of TIBA to the growth surface, s is the sticking probability of TIBA on Al, R is the gas constant, and T is the absolute temperature. The values $E_a=27.7$ kcal/mol, $A=3.8 \times 10^{11} \text{ s}^{-1}$ [Al(111)], and $E_a=32.6$ kcal/mol, $A=1.4 \times 10^{13} \text{ s}^{-1}$ [Al(100)] obtained from the thermal desorption studies were assumed to be independent of surface coverage. The model was verified at low pressures (10^{-6} torr) by assuming values for n_s and s (1.4×10^{14} and 1, respectively) and adjusting σ to give the best fit to the experimentally derived molecular beam scattering data points in the temperature range 130-380 °C. For

deposition at infinite TIBA flux, i.e., 1 torr, the model was compared to the Al deposition rates on SiO_2 .⁸⁸ The predictions for the kinetic parameters based on the UHV experiments were in reasonable agreement with the results obtained at orders of magnitude higher pressures in the hot-wall CVD system.

Aluminum deposition did not take place readily on the surface of silicon substrates unless the surfaces had been pretreated with TIBA at a temperature significantly above its decomposition temperature. This correlates with the work of others where it has been observed that the decomposition on the surface of silicon is a more highly activated process.

2.4.4 Patterning of Aluminum Films

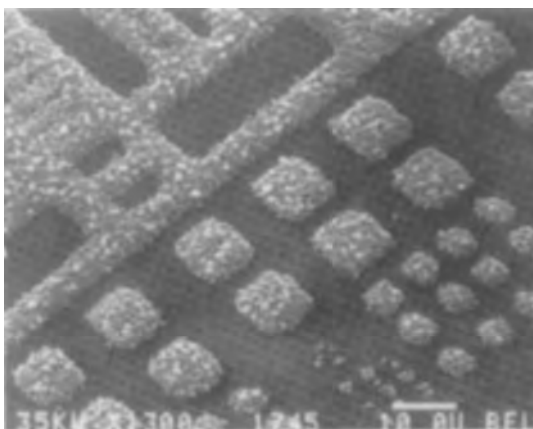
The reluctance shown by TIBA to deposit Al onto SiO_2 has been used to advantage to grow selectively on silicon and Al surfaces.^{89,98,99} The selectivity in such depositions is established at the nucleation stage of film growth. The mechanism behind selective area growth was investigated in a series of X-ray photoelectron spectroscopy (XPS) studies in a UHV compatible environment.¹¹⁴⁻¹¹⁶ The reason for the difference in the growth rates on the different surfaces was traced to the interaction of TIBA with oxygen in SiO_2 . Upon adsorption of TIBA on SiO_2 the first two isobutyl groups were readily lost, even at room temperature.¹¹⁴ The β -hydride elimination for the third isobutyl group, however, was suppressed, and the monoisobutylaluminum species inhibited film growth on SiO_2 by preventing further adsorption of TIBA.^{115,116} No decomposition of this last isobutyl group was observed *even when the surface of the substrate was sustained above typical growth temperatures (450 °C)*.

Ab initio molecular orbital calculations of the β -hydride elimination transition state for alkyl Al compounds in different environments suggested (1) promoting an electron from the occupied Al-C sigma bonding orbital to the empty π orbital on Al determines the energy of the transition state, and (2) the energy of this promotion is significantly increased when Al is bound to an electronegative atom such as oxygen.^{117,118} This may explain the reluctance of the last isobutyl group in TIBA to be removed from a SiO_2 surface. The second of the two results was evaluated by comparing the qualitative difference in the total energy for electron promotion to the π orbital in the 4-member transition state for a variety of radicals. The ease with which the elimination reaction is expected to occur on this basis, beginning with the lowest energy transition, is $(\text{AlH}_2)_2\text{Al} < \text{H}_2\text{Al} < (\text{CH}_3)_2\text{Al} < (\text{HO})_2\text{Al}$. Using the calculated values for these model systems, the estimated activation energy for the β -hydride reaction on Al is 21 kcal/mol (0.9 eV) and on $(\text{HO})_2\text{Al}$ (a model oxide surface) it is 92 kcal/mol (4 eV).

The ultraviolet (UV) laser irradiation of a substrate surface¹¹⁹ in the presence of an Al alkyl precursor has been shown to have a beneficial effect on the growth of Al films

deposited by conventional CVD methods. The principle behind this technique is to pre-nucleate a substrate surface with laser deposited Al so that subsequent thermal growth is promoted in specific regions of the substrate.^{120,121} Once a film has been nucleated, the laser is turned off and the passage of further TIBA vapors over the substrate results in the formation of an Al film only in the regions which had been exposed to the laser illumination. In this way, selective area film growth of Al has been implemented using both scanning and projection-masked, laser-assisted patterning techniques.^{107,120-127} The process has been demonstrated with a number of substrates such as Si, SiO₂, Al₂O₃, and GaAs where a significant barrier to thermal nucleation of

A



B

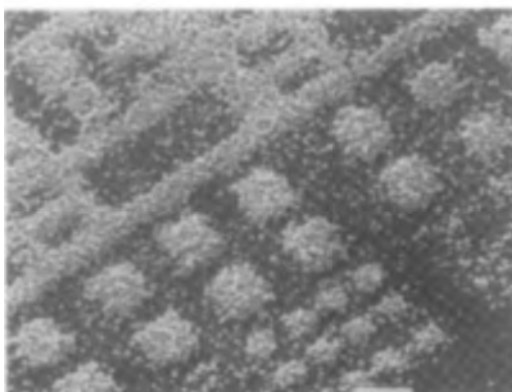


Figure 2-8 Scanning electron micrographs of Al lines pyrolytically grown from TIBA on glass at 250 °C after nucleation induced by laser irradiation at (A) 248 nm and (B) 193 nm.¹²³ [Reprinted with permission from the American Institute of Physics]

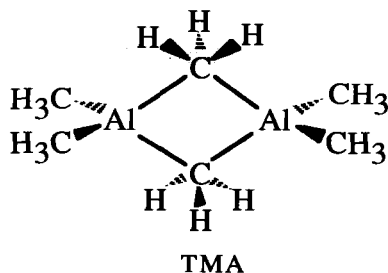
Al exists.¹²² Such films have resistivities of approximately $5 \mu\Omega\text{cm}$. With a 248 nm KrF excimer laser, a substrate temperature of 250 °C and an ambient TIBA pressure of approximately 0.1 torr, feature resolutions were dependent on the focusing of the UV radiation and not on gas phase diffusion lengths because the photoreactions were confined mainly to the surface adsorbate.^{107,122,124,125} When 193 nm radiation was used under identical conditions, control of spatial selectivity was severely impeded indicating that substantial photochemistry (and presumably nucleation) took place in the gas phase.^{123,128,129} This is illustrated in Figure 2-8.

The gas-phase photolysis products of TIBA (and other Al CVD precursors) were sensitive to the wavelength of the radiation.¹³⁰ The metal containing decomposition products monitored in the gas phase were Al atoms and AlH.¹³⁰⁻¹³⁴ A small but discernable increase in the yield of Al was detected at a photolysis wavelength of 193 nm over photolysis at 248 nm and may account for the loss of selectivity at the lower wavelength. In a similar study performed with trimethylaluminum (TMA), AlCH_3 , Al, and AlH were generated.¹³⁵⁻¹³⁸ The same products were observed for the surface-induced photolysis reactions on silicon and quartz.^{131,132}

The much higher abundance of AlH from TIBA can be rationalized by invoking the β -hydrogen elimination. A plausible mechanism for the surface photolysis of TIBA is similar to the one proposed for the surface pyrolysis reaction.^{117,126,128,139}

2.5 Deposition of Aluminum from Trimethylaluminum

Early studies of Al deposition, particularly by photolysis, involved the use of trimethylaluminum (TMA). This precursor is a liquid at room temperature with a vapor pressure of about 11 torr at 20 °C. It exists as a dimer in the gas phase at ambient temperatures and as a monomer at elevated temperatures ($\sim 200^\circ\text{C}$). The structure of the dimer given below shows that it contains both terminal and bridging methyl groups bound to Al. Each bridging methyl group attaches itself via a 3-centered 2-electron bond. The terminal methyls are bound by 2-centered 2-electron bonds.



This structure can be retained upon adsorption onto a substrate. Although somewhat counterintuitive, TMA has been shown to adsorb on the surface of silicon substrates up to ambient temperatures as the dimer with the *long axis of the molecule perpendicular* to the substrate surface.¹⁴⁰⁻¹⁴³

2.5.1 Thermal Activation of TMA

Deposition temperatures for TMA fall in the range 350-550 °C.¹⁴⁴ The mechanism for the decomposition of TMA both in the gas phase and on the surface of substrates is complex, and a number of studies have established that the path is strongly dependent on the conditions. There is no general agreement on the mechanism of aluminum deposition using TMA. The system is complicated by competing reactions which lead to the incorporation of relatively high concentrations of carbon into the films. The proposed mechanisms of TMA decomposition have invoked both the liberation of reactive radical species such as CH_3 ^{145,146} and stable molecular species such as CH_4 .^{143,147-151}

Data gathered using a combination of TDS, XPS, and EELS allowed a mechanism to be proposed in which monomeric TMA on the surface of a Si(100) substrate fragmented by an intramolecular pathway to eject CH_4 ^{143,147,149} (Fig. 2-9). Carbon incorporation was attributed to the presence of monomethylsilicon species formed on the substrate surface which subsequently decomposed to produce elemental carbon or C-H. Small amounts of CH_4 were evolved from a clean, polycrystalline Al surface following exposure to TMA.^{150,151} Large quantities of C, however, remained on the surface. In contrast, methyl radicals were detected by mass spectrometry when a beam of TMA was reacted with a variety of surfaces (Cu, Al, quartz, and GaAs) at temperatures ranging

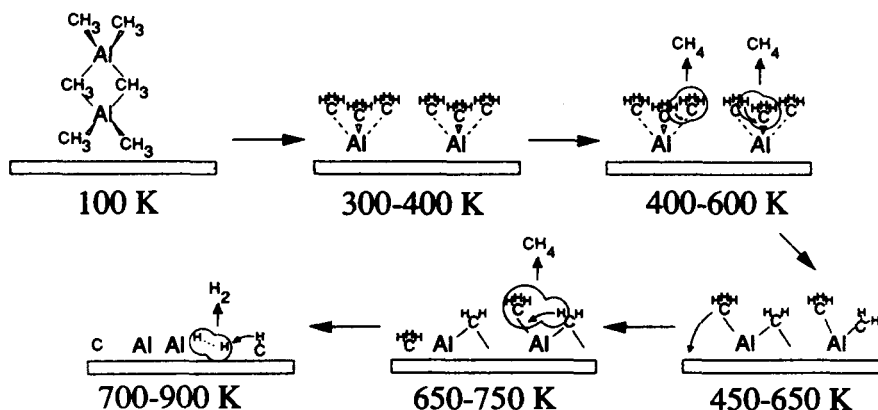


Figure 2-9 Mechanism proposed for TMA decomposition on Si(100).¹⁴³ [Reprinted with permission from *Chem. Mater.* 1989, 1, 406. Copyright 1989 American Chemical Society]

from 280-630 °C.^{145,146} The methyl radical signal increased in intensity as a function of increasing substrate temperature and was the only product detected. The observed activation energy for radical production was only about 13 kcal/mol despite the fact that the average Al-CH₃ bond energy is approximately 67 kcal/mol.⁶⁹ The following reaction in which a new Al-Al surface bond is formed (Eq. 2.5) was suggested to account for this discrepancy.



The formation of the Al-Al bond was theorized to compensate for the loss of at least

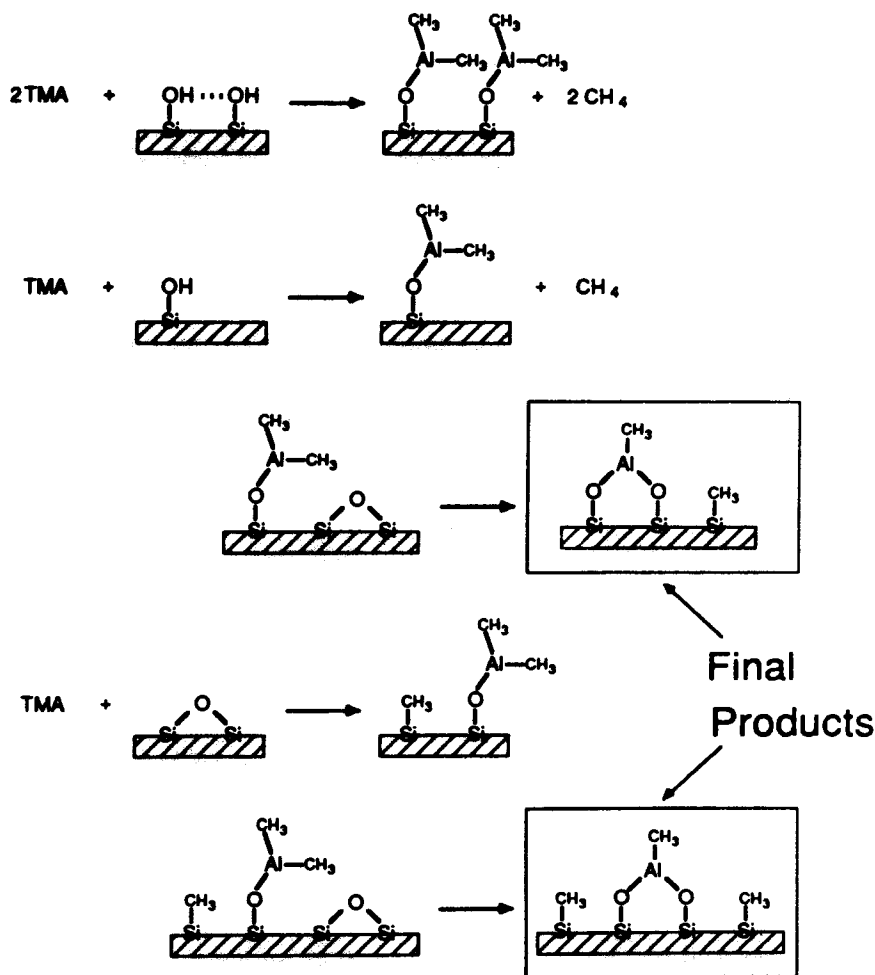
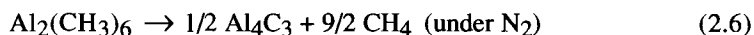


Figure 2-10 Reactions occurring on the various surface sites of silica after TMA adsorption.¹⁵² [Reprinted with permission from *J. Phys. Chem.* 1991, 95, 4453. Copyright 1989 American Chemical Society]

one Al-C bond. A number of researchers have investigated the mechanism for TMA chemisorption on SiO₂ and Al₂O₃ and have also found carbon to be a byproduct of the decomposition.¹⁵² A summary of the proposed reactions is outlined in Figure 2-10. It is intriguing to compare these results with those found for TMA adsorption on Ru(001).¹⁵³ The dominant desorption product in this case was H₂.

Aluminum films deposited by the pyrolytic decomposition of TMA contain high levels of carbon in the bulk of the film as well as at the substrate surface.^{73,154-157} Stoichiometries approaching Al₄C₃ have been observed. The formation of Al₄C₃ thin films is consistent with the assumed product from the thermal decomposition of TMA.¹⁵⁸ Fourier transform infrared spectroscopy was used to quantitatively observe the decomposition of TMA in a sealed stainless steel reactor heated to 150 °C and established that the reaction was first order in TMA and that the overall stoichiometry conformed to Equation 2.6.



Changing the atmosphere from N₂ to H₂ did not change the activation energy for the decomposition, although it did result in the formation of aluminum (Eq. 2.7).



In a pyrex cylinder at significantly higher TMA pressures (9.1- 85.5 torr) and temperatures (298-334 °C), the reaction products consisted largely of CH₄ and lesser amounts of ethane, ethylene, and H₂.¹⁵⁴ The observed kinetic order of 3/2 was rationalized by a sequence of radical chain reactions beginning with the dissociation of methyl radical from TMA and followed by methyl radical abstraction of a hydrogen atom from a second TMA. The activation energy for this homogeneous reaction was determined to be 45 kcal/mol, but in the presence of H₂ this was reduced. This value is notably different from the one obtained in the study described above. In both of these studies methyl radicals are proposed intermediates.

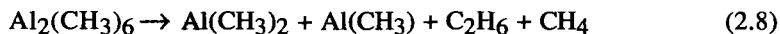
Thermodynamic calculations were used to predict the nature and relative amounts of equilibrium products following thermal decomposition of TMA.¹⁵⁹ For the heterogeneous decomposition at total pressures between 0.1-760 torr, Al₄C₃ was formed at 0-1250 °C and was accompanied by the formation of CH₄. Above ~100 °C the equilibrium between CH₄ and carbon and hydrogen became significant. The addition of H₂ shifted the CH₄ decomposition reaction to higher temperatures. In order to rationalize the formation of elemental Al,¹⁵⁵ it was necessary to invoke kinetic limitations on the decomposition reaction which bypass the formation of the most stable product, Al₄C₃. A useful conclusion based on this study is the probable

advantage gained from reacting TMA and H_2 prior to introducing TMA into the deposition region. Thermodynamics predict that the reaction at $200^\circ C$ results in the formation of AlH_3 and CH_4 . Aluminum trihydride (AlH_3) is unable to introduce carbon into the growing film and CH_4 decomposes very slowly except at relatively high temperatures. Hence, it may be possible to lower the level of carbon incorporation by this means. It will be seen in the next section that the use of precursor molecules containing AlH_3 is indeed able to reduce carbon levels in Al films to very low limits.

2.5.2 Plasma-Assisted Aluminum Deposition Using TMA

A radio frequency plasma caused TMA to react in the gas phase and to form $Al(CH_3)_2$ and $Al(CH_3)$ selectively.^{160,161} These latter species subsequently decomposed at the substrate surface (230 – $260^\circ C$) and gave rise to Al films which were free from carbon according to XPS analysis. Deposition rates of up to 30 nm/min were achieved by the reactions summarized in Equations 2.8 to 2.10.

Radio Frequency/ H_2 Plasma



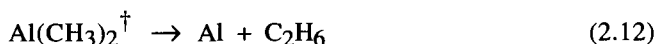
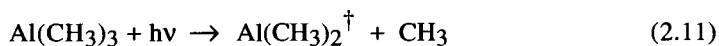
At the Substrate Surface



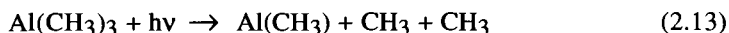
The as-deposited films were strongly $Al(100)$ oriented, reflective, and had resistivities as low as $2.7\ \mu\Omega\text{cm}$. An additional feature of interest was the ability to deposit the Al films selectively on a silicon surface in the presence of SiO_2 . A critical factor associated with the study was the need for a low plasma power. Higher power caused the TMA to decompose into more fragmented species and resulted in carbon incorporation.^{162,163} Specifically, films deposited using a TMA and H_2 mixture and a silicon substrate temperature below $100^\circ C$ had resistivities of about $3.8\ \mu\Omega\text{cm}$ and a carbon content of around 6%. In contrast to other studies, films deposited in this manner were smooth.

2.5.3 Laser-Assisted Aluminum Deposition From TMA

Laser-assisted techniques have been intensively investigated over the past ten years using methods similar to those described for TIBA. Much of the literature on TMA photolysis has been reviewed,^{69,71,164} and we therefore report only a brief summary of the salient features. In the far UV region (190-270 nm), TMA decomposes *in the gas phase* via two competing fragmentation pathways both of which involve a one-photon process for the monomer $\text{Al}(\text{CH}_3)_3$.¹⁶⁵ The Al-containing fragments from these photodecomposition reactions are Al and AlCH_3 ,^{133,135} and the ratio of these two species is wavelength dependent.¹³¹ Between 230-255 nm, atomic Al is produced in accordance with Equations 2.11 and 2.12 with little or no AlCH_3 . (In the equations below, † indicates that the species is in an excited state.)



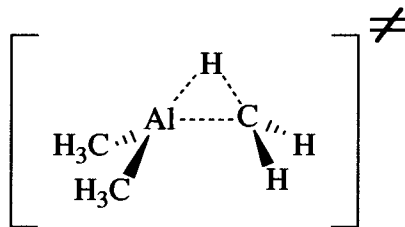
Only the monomer adsorbs light for wavelengths in excess of 220 nm. Below about 230 nm Eq. 2.13 becomes increasingly important and at 190 nm the product is almost exclusively AlCH_3 .



It is interesting that the production of Al atoms (Eq. 2.12) occurs at a longer wavelength than that required to produce AlCH_3 due to the rapid evolution of ethane in the latter case.¹³⁸

The reaction pathways *on the substrate surface*^{127,131,132,137,140-142,166-180} and in the gas phase^{131,133,135,137,138,154,158,165,181-188} were found to be sensitive to temperature, the chemical environment, the laser power, and the wavelength. For example, at low substrate temperatures CH_3 may not be readily desorbed leading to the incorporation of carbon into the film. Furthermore, rapid electronic relaxation of adsorbate molecules by the surface can make it difficult to remove carbon by a photolysis process alone.^{118,128} On the other hand, too high a substrate temperature facilitates alternative reaction pathways. These effects have resulted in Al films containing both occluded carbon and carbon directly bound to Al. The level of residual carbon is found to be sensitive to the presence of H_2 carrier which was thought to scavenge CH_3 and reactive radicals both from the gas phase and on substrate surfaces.^{175,176} The best films deposited from TMA employ a H_2 carrier and have

resistivities below $10\ \mu\Omega\text{cm}$ and carbon concentrations less than a few percent. In one case where 248 nm radiation was used to decompose TMA in the gas phase above a substrate heated to $200\ ^\circ\text{C}$, deposits with a resistivity of $9.2\ \mu\Omega\text{cm}$ were produced¹⁸¹ ($< 7\%$ C and $< 5\%$ O). In a separate study with low intensity 193 nm radiation focused onto Si(100) at ambient temperatures, Al with $< 1\%$ C content was deposited.¹⁷⁹ At relatively high laser powers $\text{AlH}(\text{CH}_3)_2$ has been detected in the gas phase and may be the result of a reaction channel involving an α -hydrogen elimination.¹⁸⁵



Finally, electron beam (6 kV) induced film growth has been reported using TMA in a high vacuum.¹⁸⁹ The films grown on a GaAs substrate heated up to $100\ ^\circ\text{C}$ contained substantial amounts of carbon.

In summary, the investigations of the decomposition of TMA both in the gas phase and on substrate surfaces suggest that this precursor is of questionable value for CVD applications due to the propensity for carbon to be incorporated into the films.

2.6 Deposition of Aluminum Films From Alane Precursors

Until recently, most CVD applications used Al alkyls because of their commercial availability. The preparation and properties of compounds containing the trihydride AlH_3 (alane) have been known for some time.⁶⁵ In the late 1960s patent literature, they were reported as being useful for plating Al films from the vapor phase and by electroless deposition to be used for diffusion barriers on a variety of metallic and non-metallic surfaces.¹⁹⁰⁻¹⁹² The films could be deposited at relatively low temperatures (100 - $200\ ^\circ\text{C}$) and had low oxygen and carbon contents. Despite these results, it is only of late that the Al metallization community has diverted attention to this class of precursor.

Alane itself is an unstable vapor at ambient temperatures which polymerizes to form a low vapor pressure solid containing bridging Al hydrogen bonds of the type Al-H-Al.⁶⁵ The coordination of the Lewis acid, AlH_3 , with a Lewis base, which donates a

single pair of valence electrons to the metal, gives rise to a relatively stable donor-acceptor complex. In this structure the Al atom possesses an octet of valence electrons which renders it stable with respect to polymerization. Among the commonly known basic donors are $(\text{CH}_3)_3\text{N}$, Et_3N , $(\text{CH}_3)_3\text{P}$, $(\text{CH}_3)_2\text{S}$, and THF.

Trimethylamine, triethylamine, and dimethylethylamine have been the focus of a number of recent publications where tertiary amine adducts have been utilized to grow Al films. These precursors are readily synthesized from one step reactions involving LiAlH_4 and the hydrochloride salt of the amine.¹⁹³ Several groups showed the potential of the precursor molecule trimethylamine alane, $[(\text{CH}_3)_3\text{N}]\text{AlH}_3$ (TMAA), for CVD applications.^{13,194-197} Pure aluminum films were deposited from this solid precursor at relatively high deposition rates and at temperatures below 100°C . Subsequent studies have involved the use of the liquid precursors triethylamine alane¹⁹⁸⁻²⁰⁰ (TEAA), the new compound dimethylethylamine alane^{201,202} (DMEAA), and $[(\text{CH}_3)_3\text{N}]\text{AlH}_2(\text{BH}_4)$.^{203,204} Alternative tertiary amine complexes of alane are known and some of these are liquids.¹⁹³ The thermal stability of the donor-acceptor complex is, however, sensitive to the steric bulk of the donor. For example, tri-*n*-butylamine alane is substantially less stable at room temperature than TMAA. These adducts of alane do not contain Al-C bonds, and the Al-N bond is easily cleaved. As a result, problems associated with carbon incorporation are minimized. In one study, carbon incorporation was below the background of secondary ion mass spectrometry²⁰⁵ (SIMS) ($\sim 2 \times 10^{18}$ atoms/cm³ or $10^{-3}\%$), and in a separate case the level of carbon was similar to that found in a device quality sputtered Al film.²⁰⁶ As a result of the promise exhibited by these compounds in the field of Al and Al related CVD processes (AlGaAs), they have begun to appear on the commercial market.

With trimethylamine, both the mono and the bis adducts are known and their structures are shown in Figure 2-11. These participate in a gas-phase equilibrium above

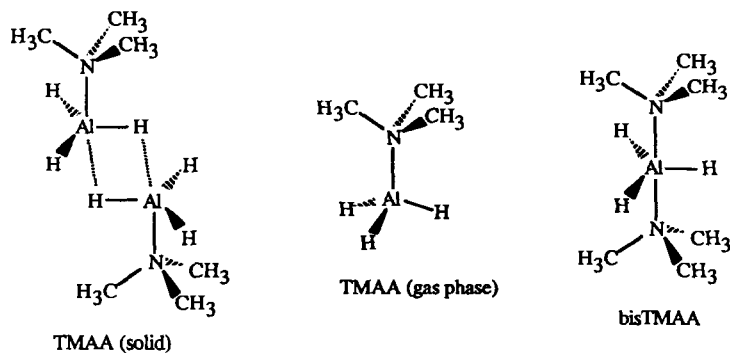


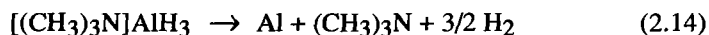
Figure 2-11 Structures formed by TMAA in the solid and gaseous phases.

the crystalline phase of the 2:1 complex.²⁰⁷ The 1:1 adduct is a monomer in the gas phase possessing C_{3v} symmetry.²⁰⁸⁻²¹⁰ In the condensed state, however, it exists as a dimer.²¹¹ The 2:1 adduct, on the other hand, is a monomer in both the condensed²¹² and gaseous phases.²⁰⁸ Triethylamine alane (TEAA) does not appear to exist as the bis adduct.⁶⁵ Dimethylethylamine alane was isolated as the 1:1 adduct in our work but the mass spectral evidence suggests that a small, but detectable, amount of the bis adduct is present.^{202,213} Furthermore, from the mass spectroscopic studies of the above adducts we have inferred the existence of some interesting clusters which include $[(R_3N)AlH_3]_2$ and $(R_3N)(AlH_3)_x$, where $R_3N = (CH_3)_2EtN$ or $(CH_3)_3N$, and $x \leq 4$.

Both the 1:1 and the 2:1 adducts of TMAA are colorless crystalline solids having vapor pressures at 25 °C of about 1 and 2 torr, respectively, whereas DMEAA and TEAA are clear colorless liquids with respective vapor pressures of 1.5 and 0.5 torr. Liquid precursors are desirable because they provide a constant, more easily reproducible flux of precursor into the reactor.

Although these precursors display sensitivity to atmospheric H_2O and O_2 they are significantly less air sensitive than the alkyl Al compounds and are not pyrophoric unless exposed to conditions of high humidity. In the atmosphere, the complexes decompose to give involatile Al oxides and hydroxides. This is fortuitous in the sense that the inevitable decomposition of the precursor which takes place inside storage vessels due to the presence of residual contaminants results in byproducts which are not readily transported to the deposition zone and therefore do not contribute to contamination in the films. In contrast, the Al alkyls react with traces of O_2 to form volatile alkoxides.^{84,85}

Studies have established that the pyrolysis of TMAA produces Al films at temperatures below 100 °C and liberates molecular hydrogen along with trimethylamine according to the stoichiometric reaction shown in Equation 2.14.



The adsorption and kinetics of film growth from TMAA²¹⁴ and TEAA²⁰⁰ have been investigated in a series of studies similar in nature to those performed with TIBA.⁸⁰⁻⁸³ Despite the similarities in the findings for the decomposition of these two alane precursors, there was also a striking difference in the kinetics which has been related to the subtle difference in the Al-N bond energy in changing the donor ligand from trimethylamine to the more sterically demanding triethylamine.

2.6.1 Surface Reaction Mechanism of TMAA

Trimethylamine alane was decomposed on Al(111), Al(100), and Si(111) single crystal surfaces as well as on Al_2O_3 .²¹⁴⁻²¹⁶ A distinction in the behavior of the decomposition on Al surfaces at temperatures below and above ambient was made. For Al(111) and Al(100) substrate temperatures in the range -190 to 10 °C the reactive

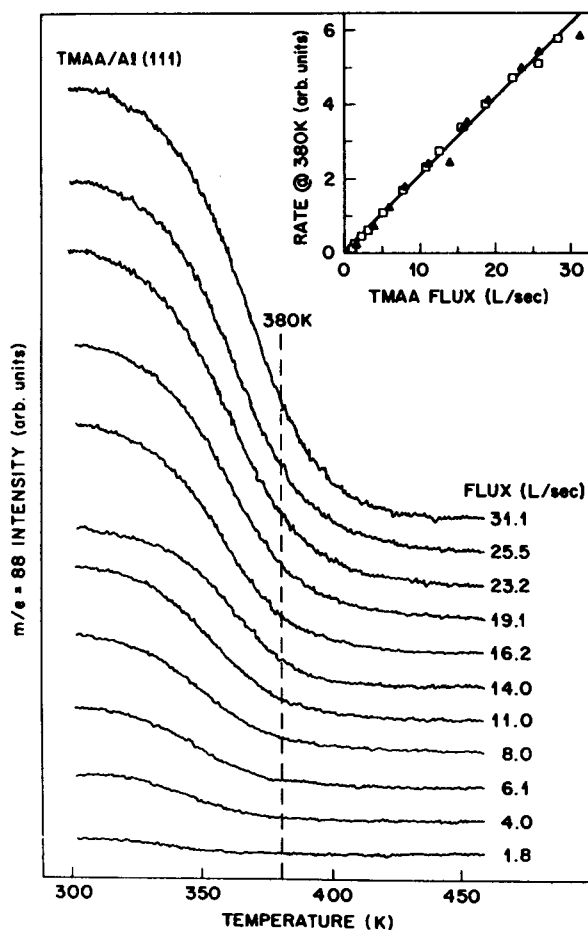


Figure 2-12 Molecular beam scattering profiles for TMAA incident on Al(111) as a function of surface temperature and TMAA flux. The inset (evaluated at 380 K) illustrates that the rate of TMAA disappearance is first-order in TMAA flux.²¹⁴ [Reprinted with permission from Elsevier Science Publishers]

sticking probabilities were equally low (< 0.01) with molecular desorption dominating the TDS studies. The small amounts of decomposition that were noted were attributed to defect sites.

Using molecular beam scattering it was established that above 30 °C growth of epitaxial Al took place with increasingly high efficiency (greater or equal to 0.5 at 30 °C) suggesting that a majority of the Al(100) and Al(111) sites were involved. Trimethylamine and H_2 were the observed desorption products. The Al films were highly reflective even for thicknesses above 1 μm and no C, N, or O were detected either in the bulk or on the surfaces of the films by AES. The decomposition of TMAA on Al was found to be first order with respect to the TMAA flux and occurred with equally high adsorbate conversions on the two crystal surfaces. The scattering profiles of TMAA from clean Al(111) are shown in Figure 2-12. The steady-state kinetics of the decomposition were modelled using the expression previously derived for TIBA. For temperatures up to 180 °C, the kinetic parameters for growth on both crystal faces of Al were identical and determined to be $3 \times 10^{12} s^{-1}$ and 17.8 kcal/mol for the preexponential factor and the activation energy, respectively (no preference for growth was found on different Al surfaces as was observed for TIBA). We compare this value to the activation energy of 13-15 kcal/mol calculated from an Arrhenius plot from results obtained in a cold-wall vertical reactor employing a H_2 flow at 0.6 torr total pressure.²⁰⁵ The E_a value for the gas-phase dissociation of the Al-N donor-acceptor bond has been determined to be 28 kcal/mol.²¹⁷

With TIBA, the ability to disperse the alkyl ligands over an Al surface facilitated the deposition. A similar scheme has been proposed for TMAA with the hydrogen atoms dispersing themselves over the Al surface. This behaviour of hydrogen is reflected in the TDS data for H_2 desorption from single crystal Al where a single H_2 desorption peak is observed at temperatures near 30 °C. It is interesting to note that the activation energy

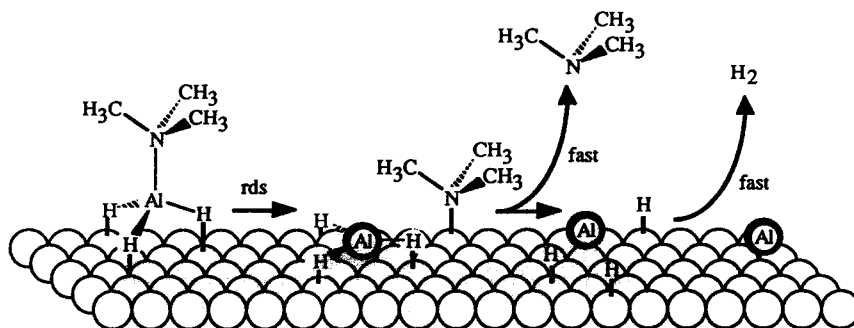


Figure 2-13 Decomposition mechanism of TMAA adsorbed on Al(111) and Al(100) surfaces.

for the elimination of H_2 from gaseous AlH_3 is approximately 42 kcal/mol²¹⁷ whereas the barrier to desorption of H_2 from a metallic surface of Al is about 16 kcal/mol.²¹⁸⁻²²⁰ Helium atom scattering studies conducted during aluminum deposition on an Al(111) surface suggested that above 670 °C growth proceeds by a step-flow mechanism.²²¹

Film growth on Al_2O_3 and Si(111) surfaces proved to be more difficult. Nucleation was more highly activated than the steady-state growth on Al with Si giving rise to the formation of polycrystalline Al which was textured in the (111) direction. On the basis of the surface studies and other data, the following decomposition pathway was proposed for the surface reaction under steady-state growth conditions (Fig. 2-13).

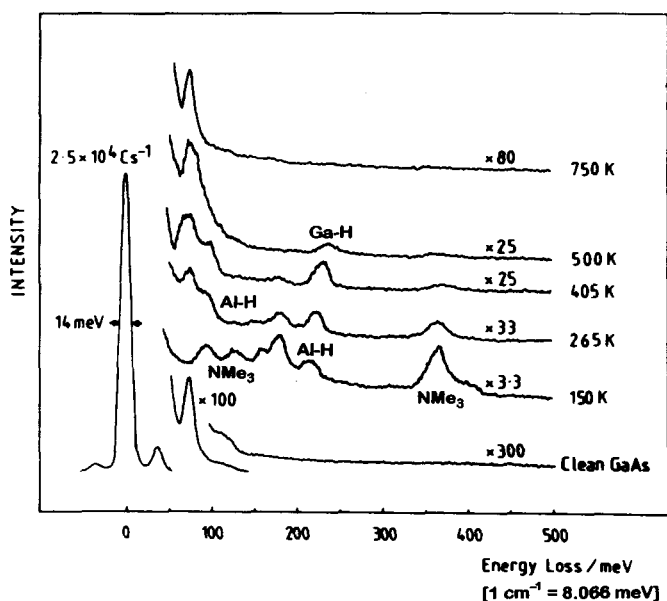
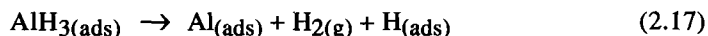
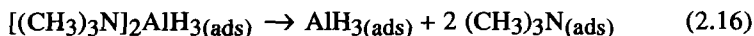
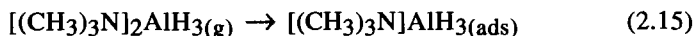


Figure 2-14 Vibrational spectra (HREELS) with changing temperature for bisTMAA adsorbed onto GaAs.²¹⁵ [Reprinted with permission from *Chemtronics* 1989, 4, 262. Copyright 1989 John Wiley & Sons, Ltd.]

The decomposition of bisTMAA on Al and the gallium-rich GaAs(100) surface has been investigated by others using molecular beam scattering, TDS and HREELS.^{215,216,222} For decomposition on GaAs(100), a similar reaction scheme was outlined (Eqs. 2.15 to 2.18) with respect to pyrolysis on the surface of Al.



In this scheme, TMAA dissociates on the GaAs surface below 130 °C liberating trimethylamine into the gas phase. A notable difference between the reactions on the surface of Al and GaAs was that hydrogen desorbed from the GaAs surface exposed to alane at two temperatures (500 and 600 °C) indicating that two adsorbed states were present. Similar results were obtained by dosing GaAs(100) surfaces with atomic hydrogen.²²³ This process was the most highly activated step in the overall conversion. Decomposition on the surface of metallic Al took place more readily than on the surface of GaAs. The vibrational spectrum (obtained using HREELS) at a series of temperatures established that the H₂ desorption occurring at higher temperature involved the recombination of H atoms bound to gallium. Below this temperature, it was proposed that hydrogen was desorbed from Al (Fig. 2-14).

2.6.2 Deposition in Cold-Wall Reactors Using TMAA

The film morphologies and the kinetics of Al growth have been investigated in cold-wall reactors by several groups.^{13,194-197,199,205,206} Nucleation difficulties, similar to those with TIBA, have been encountered during the growth of Al films from TMAA on the surface of Si and SiO₂. With TIBA, the approach taken to promote uniform nucleation was to pretreat the substrates with TiCl₄. The same protocol has been used with TMAA initially in hot-wall reactors^{13,196} and more recently in cold-wall systems.^{199,205,206} Once again, not only has this resulted in more uniform nucleation, it has also reduced the temperature at which Al can be grown. For example, Al films have been successfully grown on TiN, Cu, and TiCl₄-treated Si and SiO₂.^{199,206} Highly oriented polycrystalline (111) films were grown on TiCl₄-treated SiO₂ and TiN. On both TiCl₄-treated Si(100) and on Cu the films were randomly oriented, although the latter films did favor growth in the (100) direction. Films with a thickness up to 200-300 nm were highly reflective but at greater thicknesses the films developed a white haze which was attributed to an increase in surface roughness. Both grain size and crystal faceting increased with deposition temperature for all surfaces.

These depositions took place in the temperature range 200 to 350 °C and resulted in growth rates of up to 140 nm/min at TMAA pressures of 0.075 torr. Although typical depositions were carried out at 250 °C, growth on Cu substrates was possible at temperatures down to 85 °C. Higher growth rates (in excess of 1000 nm/min) have been observed below 200 °C.²⁰⁵ As stated earlier, growth rate can be substantially altered by the reactor design.

Little is known about the reaction between TMAA and TiCl₄.^{224,225} Alane, being a good hydride donor as well as a chloride acceptor, may form a Ti-H bond and H₂AlCl. This exchange can happen several times. The resulting titanium hydrides would need to reductively eliminate H₂; a process that should be facile.

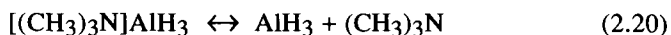
2.6.3 Deposition in Hot-Wall Reactors Using TMAA

Depositions conducted in hot-wall reactors are more likely to contain a contribution from chemistry occurring in the gas phase. For example, the dissociation of one of the trimethylamine ligands from [(CH₃)₃N]₂AlH₃ occurs in the gas phase at room temperature^{207,226} (Eq. 2.19).



An early estimate of the Al-N bond strength for the above reaction was 18 kcal/mol.²²⁶ Clearly, as the deposition of Al proceeds, the steady state concentration of (CH₃)₃N will perturb the above equilibrium.

The dissociation enthalpy of the second (CH₃)₃N (Eq. 2.20) in the gas phase has been estimated to be 26 kcal/mol.²¹⁷



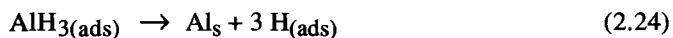
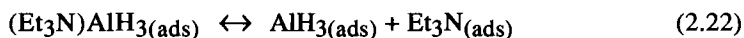
Because of the high reactivity of AlH₃, even the formation of very small quantities could be important, especially in the nucleation stage of film formation or in particle formation in the gas phase as discussed below. Direct determination of an accurate experimental value of this bond strength would be valuable. The dissociation enthalpies for several related donor-acceptor complexes of aluminum are known.²⁰⁰

2.6.4 Aluminum Deposition from TEAA

Aluminum films grown from TEAA had low impurity levels according to SIMS¹⁹⁸ (slightly above those in a sputtered Al film). Its lower vapor pressure resulted in

slower growth rates (still 2-4 times those of TIBA at 250 °C) although the film morphologies were similar at comparable temperatures and pressures. Films deposited on Ti without TiCl₄ pretreatment were randomly oriented.

The surface decomposition pathway in a UHV environment has also been studied.²⁰⁰ The structural similarity of TMAA and TEAA suggested that the overall decomposition mechanism for TEAA (Eqs. 2.21 to 2.25) should be similar to that for TMAA.



Experiments using TDS demonstrated that H₂ was the species which desorbed from the surface at the highest temperature leading the authors to propose H₂ desorption as the rate limiting step in the surface kinetics.

The kinetics of decomposition for TMAA and TEAA are controlled by the rate of Al-N bond cleavage and the rate of H₂ desorption, respectively. This difference between the proposed rate-determining steps is significant. Because H₂ desorption is an intrinsic step in the decomposition reaction of alane, the rate of TEAA decomposition defines the maximum rate of the surface reaction for this class of precursor. It follows that a further lowering of the barrier to cleavage of the Al-N bond on the surface will not alter the deposition rate or the temperature of deposition.

2.6.5 Aluminum Deposition From DMEAA

The most recently introduced member of the amine family of precursors is DMEAA. Its relatively high vapor pressure at room temperature (1.5 torr), its long shelf life, combined with the advantages of being a liquid have made it the precursor of choice for depositing Al films in our laboratory.^{201,202} At 170 °C the growth rate in a hot-wall reactor at a precursor partial pressure of 0.3 torr (total pressure with H₂ = 3.3 torr) on Cu substrates was 150 nm/min. The films were polycrystalline containing no detectable impurities as measured by AES. Faster growth rates have been obtained in our reactor using a higher flux of precursor; however, detailed kinetics studies have not been completed.

2.6.6 Selectivity of Deposition Using Alane Precursors

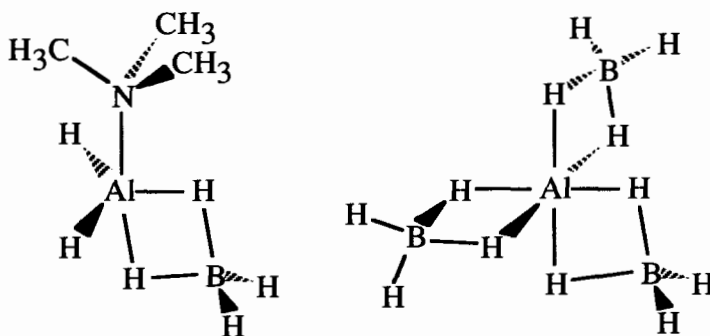
The so-called incubation period that is nominally encountered before Al growth is observed on Si and SiO₂ substrates from alane has been taken advantage of to grow Al films selectively on metallic surfaces.^{202,205} Aluminum has been deposited selectively on metals such as Au, Cu, and W in the presence of Si. These examples demonstrate the important influence that the substrate has on initiating film growth. In general, selectivity will be defined by events occurring during the nucleation of the new phase. Once the critical nucleus size²²⁷⁻²³⁰ is reached, steady state growth will continue regardless of the nature of the original substrate. A large number of factors could affect the formation of the critical nucleus. For example, a small sticking coefficient of the precursor on one of the surfaces could diminish the probability that a degree of supersaturation of the growth species necessary to induce nucleation is achieved. It is also possible that a surface sensitive chemical reaction must take place to generate the growth species.

As mentioned above, there is a large activation barrier for hydrogen elimination from isolated alane molecules. The selectivity for growth on metallic surfaces may be the result of their ability to catalyze the desorption of hydrogen. On surfaces such as SiO₂, TMAA was found to adsorb as an intact molecule.²³¹ Hydrogen desorption, however, may be slow until an Al cluster of some unknown size has formed allowing the growth to sustain itself. In support of this, it has already been mentioned that Al nucleation on Si and GaAs surfaces is slower than growth on Al. Both of these surfaces desorb H₂ at significantly higher temperatures than Al.^{215,216,232} Other factors such as the relative sticking coefficients of the reactants may also affect the nucleation rate.

Aluminum films have been selectively deposited from TMAA onto SiO₂ without heating the substrate using laser-assisted chemical vapor deposition and focused ion beam stimulated deposition techniques.^{194,195,197,233-235} The first of these two studies showed that Al films were deposited up to 97% pure with 3-5% of oxygen also being present. The second study used Ga⁺ to induce decomposition of the precursor, but high levels of C and N were incorporated into the Al films. Under conditions when the SiO₂ surface was sputtered with the Ga⁺ prior to introducing the TMAA uniform nucleation and deposition could be achieved. The effect of Ga⁺ was to increase the sticking coefficient of TMAA during the initial growth stage. An alternative pretreatment with the silane coupling agent aminopropyltriethoxysilane, H₂NCH₂CH₂CH₂Si(OEt)₃, also produced uniform deposits.²³³ The liquid precursor DMEAA has been used for laser (514 nm Ar⁺ laser) writing high-purity aluminum films. No carbon or oxygen was detected by Auger spectroscopy, and the resistivities averaged 3.6 μΩcm for films deposited above a laser power of 2.6 W.²³⁶

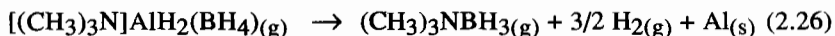
2.6.7 Aluminum Deposition Using Aluminaborane Precursors

Aluminaborane liquid precursors have been used to deposit thin films of Al, alumina and aluminum boride.^{203,204} All of the precursors are thermally stable, volatile, air-sensitive liquids. The precursor $[(CH_3)_3N]AlH_2(BH_4)$ was synthesized from $[(CH_3)_3N]AlH_2Cl$ and $LiBH_4$ and was reported to be stable indefinitely in an inert atmosphere at ambient temperatures.



Aluminaboranes

Polycrystalline Al films were grown from this complex on the substrates Si(100), GaAs(100), $SiO_2(100)$, Teflon and Mycor. Growth on SiO_2 and GaAs near 120 °C required that the surfaces were pretreated with $TiCl_4$. Film deposition was estimated to take place at rates of a few tens of nm/min on SiO_2 and at 0.8 nm/min on GaAs. The purity of the films was similar to that observed using other alane-based precursors. The overall chemical reaction involved in the deposition is shown in Equation 2.26, however, the mechanism of deposition is unknown.



Pyrolysis of the compound $Al(BH_4)_3$ produced films of aluminum boride rather than pure Al suggesting that the clean elimination of $(CH_3)_3NBH_3$ in Equation 2.26 is dependent on there being at least one terminal hydrogen atom attached to Al.

2.6.8 Gas-Phase Aluminum Particle Formation From Amine Alanes

As a result of chemical reactions occurring in the gas phase, particle formation can be problematic especially in cases where hot-wall reactors are used. Particles formed in the

gas phase can lead to the incorporation of micro or even macroscopic defects and reduce the device yield in the manufacturing process. Even more troublesome is the reduced lifetime of an initially working device. Particle formation has already been identified as a problem in the CVD of silicon²³⁷ as well as in other microelectronic processing systems.^{238,239} We have found that particles are formed in the gas phase of a low pressure, hot-wall CVD reactor used to deposit Al films from DMEAA.^{61,201}

Two methods of analyzing particles were interfaced to a LPCVD system. A laser light scattering particle counter detected large (> 200 nm) particles in real time and established that their appearance corresponded to the flow of precursor into the CVD reactor. An impaction system was used to collect particles (> 20 nm) for analysis using analytical electron microscopy and electron diffraction. This established that the particles were crystalline Al ranging in size from 20 nm to larger than 1000 nm depending on the growth conditions. For one case in which the reactor was at 170 °C, Al particles had a size range of 20-700 nm and a median size of about 85 nm. These were present in the gas phase at a number density of about 50 particles/cm³ and represent a small fraction of the total precursor passing into the reactor. A photograph illustrating the variety of Al particle morphologies which are typically obtained is shown in Figure 2-15.

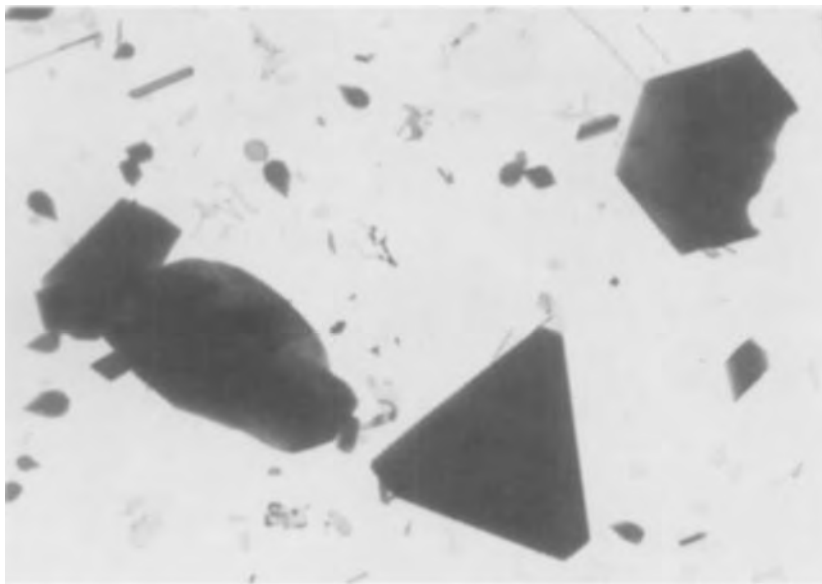


Figure 2-15 Typical Al particles collected during the CVD of Al at 170 °C using DMEAA.

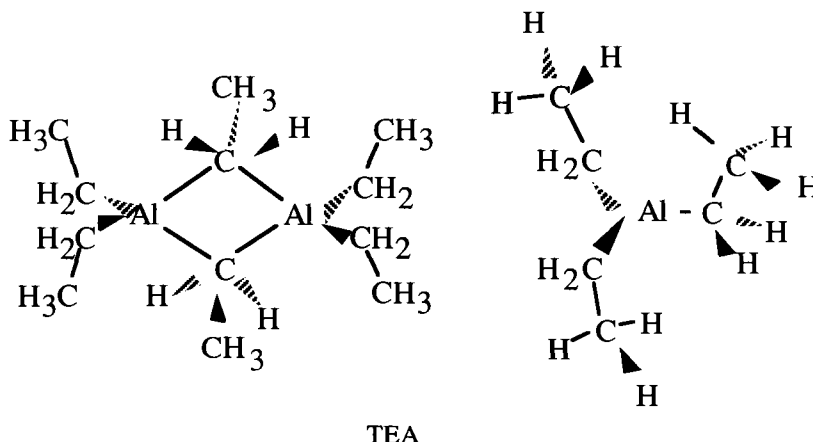
One possible source of particle nucleation is from gas phase impurities in the vacuum. Typically, this includes H_2O , CO , CO_2 , and N_2 as well as some hydrocarbons. We have been able to show that when trace amounts of H_2O , CO , and O_2 are leaked into the reactor during a deposition an increase in the number of particles occurs.⁶¹ For the cases of H_2O and CO larger numbers of Al particles are formed whereas O_2 causes the formation of significant numbers of Al oxide particles. These results strongly suggest that the nucleation of particles is induced by impurities in the gas phase, although we cannot rule out the possibility that they are also formed by other mechanisms.

2.7 Alternative Aluminum Alkyl Sources

Aside from the precursors which have already been described, other source compounds have been investigated, albeit to a lesser degree. This section attempts to summarize the salient features of the literature for the most important of these sources, the structural features of which are consistent with those of TMA, TIBA, and alane already described. It is reasonable to assume that structural similarities between the different sources will be reflected in their decomposition pathways. Fewer details exist for the compounds diethylaluminum chloride (DEACl) and AlCl . Characteristic of the Al alkyls, these compounds are pyrophoric and react vigorously with moisture. Additionally, they tend to exist in an associated state in the gas phase, particularly in the form of dimers.

2.7.1 Triethylaluminum

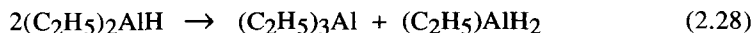
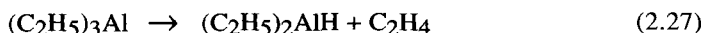
This source compound is a liquid at room temperature and has a vapor pressure of 0.1 torr at 36°C . The low ambient vapor pressure requires the precursor to be heated ($\geq 40^\circ\text{C}$), although decomposition has been detected at typical elevated bubbler temperatures.²⁴⁰ The kinetics of the thermal decomposition of gaseous TEA were reported in 1966 using a closed system in the temperature range $162\text{--}192^\circ\text{C}$ and a pressure of approximately 50 torr.²⁴¹ The data suggested that negligible amounts of the dimeric phase were present at temperatures in excess of 160°C . Other studies suggested that at 150°C , TEA is only 12% dimerized.²⁴²



Complete chemical analysis of the decomposition products alluded to the complexity of the reaction, the pathway of which was thought to involve concurrent molecular and free radical processes. The heterogeneous decomposition reaction was found to be first order with respect to TEA, and an Arrhenius plot gave a value for the activation energy of 29 kcal/mol and an A factor of $1.6 \times 10^8 \text{ s}^{-1}$. The entropy of activation at 180 °C based on this A factor was -24 eu, which was consistent with the highly ordered four-membered transition state of the β -hydride elimination reaction already outlined for TIBA.

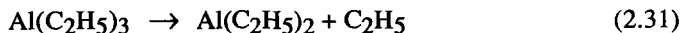
An independent study showed that films of Al deposited from gaseous TEA contained Al carbide as well as elemental carbon; the concentration of which increases with temperature.⁷⁵ Lower carbon incorporation was evident, however, relative to TMA.^{243,244} This fact probably reflects the importance of the β -hydride elimination and is a notable example of how the composition and the microstructure of a film are influenced by the structure of the molecular precursor.

The evidence is consistent with the following primary reactions (Eqs. 2.27 to 2.30).²⁴¹



Photofragmentation of gaseous TEA has been accomplished at 190 nm. Substantial quantities of atomic hydrogen were detected with time-of-flight mass

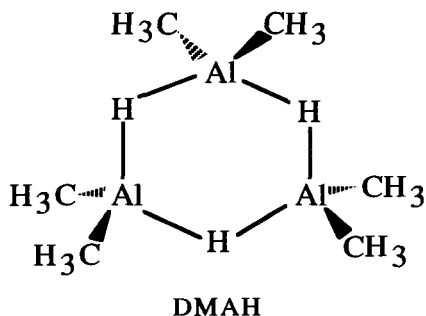
spectroscopy.^{245,246} Of the three possible dissociation pathways identified it appeared that a one-photon absorption mechanism was in operation whereby TEA forms an excited state which dissociates to produce C_2H_5 (Eq. 2.31). The ethyl radical goes on to form C_2H_4 and H without the absorption of a second photon (Eq. 2.32).



The authors point out that the presence of hydrogen radicals is important in other thin film deposition processes for scavenging carbon fragments by producing volatile hydrocarbons. Other studies performed at 193 and 248 nm on both gas phase and surface adsorbed TEA showed that AlH was produced in significant amounts along with Al and $AlCH_3$. In contrast, TMA had a strong tendency to form $AlCH_3$ and Al.^{130,131,133,134,137}

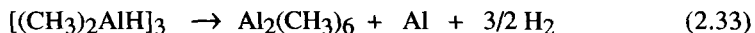
2.7.2 Dimethylaluminum Hydride

Dimethylaluminum hydride (DMAH) is a liquid at room temperature possessing a vapor pressure of 2 torr at 25 °C. In the pure liquid state it has a degree of association of at least three. In the vapor phase it is trimeric at low temperatures and becomes dimeric at around 160 °C. Unlike TMA and TEA which are alkyl bridged structures, the Al atoms in DMAH are straddled by hydrogen. The heat of association of 15-20 kcal/mol per H bridge is typically higher than for the CH_3 bridges in TMA having a value of about 10 kcal/mol per CH_3 .⁶⁴



Pyrolysis has typically been performed at temperatures from 230-280 °C in a hydrogen gas flow of a few torr where the partial pressure of DMAH was in the range of $0.2 \cdot 10^{-3}$ torr.^{240,247,248} Under these conditions and in cold-wall systems, film

growth rates of 500-1000 nm/min were achieved. The films had a rough surface and resistivities of 3 $\mu\Omega\text{cm}$. It was shown by SIMS analysis that for a film obtained at 280 °C carbon incorporation was at least as low as 0.05%.²⁴⁰ One possible explanation for the low carbon compared to depositions using TMA is the reaction shown in Eq. 2.33,¹⁵² which may proceed by the formation of alane (AlH_3) by a ligand redistribution reaction similar to the path described in Equations 2.27 to 2.30.



Selective growth of Al on Si in the presence of SiO_2 using DMAH has been observed.²⁴⁷⁻²⁴⁹ In one study an optimized temperature range of 235-245 °C was used.²⁴⁸ At 200 °C no deposit was found on either the Si or SiO_2 according to optical micrographs, while at 310 °C Al was deposited on both Si and SiO_2 with islands of Al appearing on the oxide surface. In a related report a temperature of 270 °C was used for selective growth.²⁴⁷ As a generalization, selectivity was possible on electrically conducting substrates like TiN and doped silicon but not on insulating materials such as SiO_2 and borophosphosilicate glass. Non-selective deposits could be obtained with the use of a radio frequency generated plasma above the sample surface.²⁴⁷ The plasma was used for one minute and was found to induce nucleation on SiO_2 . Once growth had been initiated, subsequent deposition took place on the prenucleated Al in the absence of the plasma.

Attention in this study was also focused on the epitaxial nature of the deposits as evidenced by RHEED patterns. Specifically, Al(100) and Al(111) were epitaxially grown on Si(111) and Si(100) faces, respectively. Films grown on SiO_2 on the other hand were (111) oriented. After 30 min annealing at 450 °C there were no indications of hillock formation.

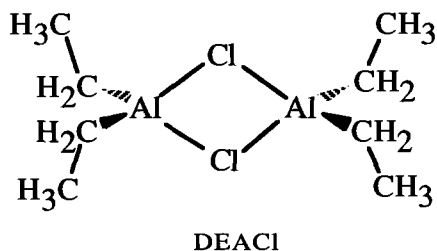
Photolytically generated Al deposits can be obtained from DMAH.²⁵⁰⁻²⁵⁵ Surface reactions of DMAH were induced with a deuterium lamp, an ArF laser, and an Ar ion laser. The best results utilized wavelengths below 200 nm on Si and SiO_2 substrates heated above ambient temperature.^{253,254} Under these circumstances nucleation occurred selectively on the substrate surface in the absence of gas phase reactions. For Si at temperatures of 170 and 270 °C a typical carbon content was 2-3%. Furthermore, at 270 °C in the presence of irradiation from a deuterium lamp, resistivities down to 6.2 $\mu\Omega\text{cm}$ were found. This result was compared with a resistivity of 140 $\mu\Omega\text{cm}$ for a film deposited at 260 °C without irradiation. Although photolysis appeared to enhance the quality of the deposits and lower the temperature of deposition, the latter value stands in marked contrast with the lower resistivities of other pyrolytically produced CVD films deposited in the presence of hydrogen at similar temperatures. Hydrogen may be making a notable contribution to the removal of carbon from these films. Evidence in these studies was also provided relating a decrease in the electrical resistivity of

deposits to an increase in substrate temperature. In a subsequent study the activation energy for aluminum growth on SiO_2 , induced by surface photolysis and pyrolysis, was measured *in situ*. The value was found to lie in the range 28-37 kcal/mol depending on the exact protocol.²⁵⁶

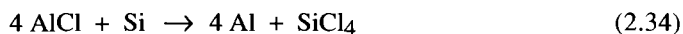
The influence of different photon wavelengths and the alkyl precursor structure on the photolytic decomposition of molecules present on a surface and in the gas phase was investigated using time-of-flight mass spectrometry.^{131,133,134,137} A series of Al alkyl precursor molecules were considered which included TMA, DMAH, and diethylaluminum chloride. For TMA, a high yield of $\text{Al}(\text{CH}_3)$ and Al was obtained at 193 nm along with small amounts of AlH . Replacing one methyl group on TMA with either Cl or H reduced the $\text{AlCH}_3:\text{Al}$ ratio by one order of magnitude for 193 nm photons and simultaneously increased the $\text{AlH}:\text{Al}$ ratio. Thus, replacing at least one of the methyl groups attached to Al with hydrogen may be a method to reduce carbon incorporation in films grown from trialkyl Al sources.

2.7.3 Diethylaluminum Chloride

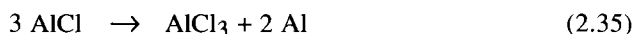
The final Al alkyl source molecule to be addressed here is diethylaluminum chloride (DEACl) which is also a liquid at ambient temperature.



Aluminum films have been grown from DEACl at 313-380 °C in a cold-wall system in a stream of hydrogen carrier gas.²⁵⁷ In the presence of $\text{Si}(100)$ and SiO_2 , the Al deposits were confined to the silicon surface. The precursor required heating to 60 °C in order to obtain a convenient vapor pressure. A film deposited on polycrystalline silicon at 338 °C was grown at a rate faster than 37 nm/min and had a resistivity of 5.1 $\mu\Omega\text{cm}$. Despite the faster deposition rates encountered on $\text{Si}(111)$, the activation energy on both $\text{Si}(111)$ and $\text{Si}(100)$ surfaces was 39 kcal/mol. With respect to the mechanism of film formation, the authors speculated that a pathway analogous to AlCl was involved.²⁵⁸ Together with their own observations they put forward the mechanism shown in Equation 2.34 in which the AlCl generated from DEACl was reduced by surface silicon.



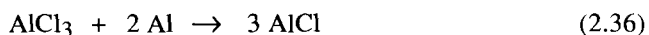
Fine grained Al nuclei grew on Ge and GaAs substrates, but continuous films were not obtained. In these cases a disproportionation reaction was considered to be responsible for film growth (Eq. 2.35).



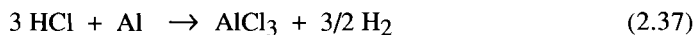
The nature of the surface reactions was probed by analyzing the gas-phase products using a quadrupole mass spectrometer. In a quartz tube containing H_2 and DEAlCl at 500°C , C_2H_6 and C_4H_{10} were produced in the initial stages of the decomposition, but C_2H_4 predominated at longer times. The effects of deposited Al were determined by repeating the experiment with a clean quartz tube containing Al wire. In this case C_2H_4 was detected from the beginning of the reaction conforming to the idea that following nucleation, deposition occurs via a β -hydride elimination.

2.7.4 Aluminum Monochloride

The vapor phase transport of Al by HCl has been used to grow thin films.²⁵⁸ Aluminum monochloride was generated by an in situ approach in which the vapors of AlCl_3 were passed over molten Al (Eq. 2.36).



Aluminum trichloride in Equation 2.36 was the product of an in situ reaction between HCl vapors and the molten Al (Eq. 2.37).



Both of these reactions took place over a bath of Al positioned inside the deposition furnace which was heated to $900\text{--}1000^\circ\text{C}$. Even under these conditions the equilibrium in Equation 2.36 lay predominantly to the left. Substrates (Si and SiO_2) were placed inside the tube in the steep temperature gradient ($150\text{--}550^\circ\text{C}$) at the downstream end of the furnace. In this lower temperature region the equilibrium (Eq. 2.36) shifted further to the left and deposited Al. The partial pressures of HCl and H_2 were 0.2 and 0.8 torr, respectively. In some cases Ti was vaporized from the upstream end of the furnace to activate the surface of substrates and to getter O_2 and H_2O . Typically, films grew at about 50 nm/min, were pure according to AES ($< 0.5\%$), and were comprised of randomly

oriented grains with a size of approximately 400 nm. Despite localized regions exhibiting a high degree of reflectivity, even the best films were marked by the presence of large voids. Film resistivities were in the range 3.4 to 3.7 $\mu\Omega\text{cm}$.

2.8 Summary

The chemical reaction mechanism of a deposition is determined by the molecular structure of the precursor and the substrate surface. With the exception of AlCl_3 , all of the precursors to Al thin films must be reduced from the +3 oxidation state. A feature that appears common to all of the organometallic precursors, except possibly TMA, is that the reduction is achieved by the elimination of molecular hydrogen. Although this reductive elimination is not favorable from the isolated gaseous precursors, the detailed studies of the surface reaction mechanisms established that it occurs readily on metallic Al, and in the case of TEAA, it is the rate limiting step. The rate determining steps in the deposition of Al using TIBA and TMAA are β -hydrogen elimination from a surface bound isobutyl ligand and Al-N bond cleavage on a surface bound TMAA molecule, respectively. The reasonable agreement between the kinetic models derived from the UHV studies and the growth rates under typical conditions suggests that the contribution of gas phase chemical reactions to the deposition is not large. Gas phase chemistry could, however, play a more significant role in the nucleation of Al films especially on insulating surfaces such as SiO_2 . The observation of small numbers of Al particles in the gas phase suggests that some chemistry does occur there. More research is needed to address this point.

The molecular structure of TMA is such that no facile route exists to either Al metal or a hydride. Formation of metallic films using TMA requires temperatures high enough to cleave the Al-C bonds or the use of lasers or RF plasmas to assist the deposition. Under these conditions, however, the tendency is to form the thermodynamically favored product, Al_4C_3 .

The composition of the thin film is critically dependent on the structure of the molecular precursor and its deposition mechanism. Although both TIBA and TMA are Al alkyls, the presence of the isobutyl groups allows for the more facile cleavage of the Al-C bond than is possible with TMA. The result includes far larger (up to stoichiometric) amounts of carbon incorporation into films grown using TMA. Carbon incorporation can be a problem using TIBA when the temperature of the deposition is raised above 330 $^\circ\text{C}$. At this point a new mechanism, β -methyl elimination, becomes competitive with β -hydrogen elimination. Because of the similarity between CH_3 and BH_3 , it is interesting to note that thin films grown using $\text{AlH}_3(\text{BH}_3)_3$ contain large amounts of boron.

Both the composition and microstructure will determine the physical and chemical properties of the films. The preceding paragraph outlines the relationship between

deposition mechanism and film composition. Comparing microstructures, however, of compositionally pure Al films grown from two different precursors, such as TIBA and TMAA, shows no obvious dependence on the growth mechanism. Further research comparing films grown in the same reactor under identical conditions is needed to address this important question.

Acknowledgements: The authors would like to thank the Center for Interfacial Engineering (a NSF-sponsored Engineering Research Center) at the University of Minnesota for funding and L. Dubois, J. Foord, M. Gross, T. Kobayashi, F. Rosenberger, and M. Stuke for preprints of their publications.

References

1. Learn, A.J. *J. Electrochem. Soc.* **1976**, 123, 994.
2. Pramanik, D., Saxena, A.N. *Solid State Technol.* **1983**, 26(3), 131.
3. Pramanik, D., Saxena, A.N. *Solid State Technol.* **1983**, 26(1), 127.
4. Garosshen, T.J., Stephenson, T.A., Slavin, T.P. *J. Metals* **1985**, 37(5), 55.
5. Levy, R.A., Green, M.L. *J. Electrochem. Soc.* **1987**, 134, 37C.
6. Pramanik, D., Saxena, A.N. *Solid State Technol.* **1990**, 33(3), 73.
7. Sequeda, F.O. *J. Metals* **1985**, 37(5), 43.
8. Green, M.L., Levy, R.A. *J. Metals* **1985**, 37(6), 63.
9. Nakamura, H. in *Extended Abstracts of the 19th Conference on Solid State Devices and Materials*, Jpn. Soc. *Appl. Phys.*, 1987, p 403.
10. Malik, F. *Thin Solid Films* **1991**, 206, 70.
11. Kwok, T., Ho, P.S. in *Diffusion Phenomena in Thin Films and Microelectronic Materials*, Gupta, D., Ho, P.S. (eds.), Noyes Publications, Park Ridge, NJ, 1988, p 369.
12. Vaidya, S., Sinha, A.K. *Thin Solid films* **1981**, 75, 253.
13. Gladfelter, W.L., Boyd, D.C., Jensen, K.F. *Chem. Mater.* **1989**, 1, 339.
14. Kinlock, A.J. *Adhesion and Adhesives*, Chapman and Hall, New York, 1987, p 441.
15. Graper, E.B. *J. Vac. Sci. Technol.* **1971**, 8, 333.
16. Hoffman, V. *Solid State Technol.* **1976**, 19(12), 57.
17. Vorous, T.V. *Solid State Technol.* **1976**, 19(12), 62.
18. Fuller, Ghate, P.B. *Thin Solid Films* **1979**, 64, 25.
19. Levy, R.A., Parrillo, L.C., Lecheler, L.J., Knoell, R.V. *J. Electrochem. Soc.* **1985**, 132, 159.
20. Yamada, I., Takagi, T. *IEEE Transactions on Electron Devices* **1987**, 34, 1018.

21. Movchan, B.A., Demchishin, A.V. *Phys. Met. Metallogr.* **1969**, 28(4), 83.
22. Thornton, J.A. *J. Vac. Sci. Technol.* **1974**, 11, 666.
23. Thornton, J.A. *Ann. Rev. Mater. Sci.* **1977**, 7, 239.
24. Messier, R., Giri, A.P., Roy, R.A. *J. Vac. Sci. Technol.* **1984**, A2, 500.
25. Messier, R., Yehoda, J.E. *J. Appl. Phys.* **1985**, 58, 3739.
26. Curran, J.E., Page, J.S., Pick, U. *Thin Solid Films* **1982**, 97, 259.
27. Wan, L.J., Chen, B.Q., Kuo, K.H. *J. Vac. Sci. Technol.* **1988**, A6, 3160.
28. Raupp, G.B., Cale, T.S. *Chem. Mater.* **1989**, 1, 207.
29. Jensen, K.F. in *Proceedings of the Ninth International Conference on Chemical Vapor Deposition*, Cincinnati, Ohio, Electrochem. Soc., Pennington, NJ, 1984, 3.
30. Binh, V.T. *Surface Mobilities on Solid Materials Vol. B86*, Plenum Press, NY, 1983, p 585.
31. Shustorovich, E. *Metal-Surface Reaction Energetics*, VCH Publishers, NY, **1991**, 232.
32. Levenson, L.L., Asano, M., Tanaka, T., Usui, H., Yamada, I., Takagi, T. *J. Vac. Sci. Technol.* **1988**, A6, 1552.
33. Russo, N., Toscano, M. *J. Vac. Sci. Technol.* **1988**, A6, 1559.
34. Levenson, L.L., Usui, H., Yamada, I., Takagi, T., Swartzlander, A. B. *J. Vac. Sci. Technol.* **1989**, A7, 1206.
35. Levenson, L.L., Swartzlander, A.B., Yahashi, A., Usui, H., Yamada, I. *J. Vac. Sci. Technol.* **1990**, A8, 1447.
36. Jansen, A.K., van den Brekel, C.H.J. *J. Cryst. Growth* **1978**, 43, 371.
37. Van den Brekel, C.H.J. *Philips Res. Repts.* **1977**, 32, 118.
38. Bales, G.S., Redfield, A.C., Zangwill, A. *Phys. Rev. Lett.* **1989**, 62, 776.
39. Mullins, W.W. *J. Appl. Phys.* **1957**, 28, 333.
40. Bales, G.S., Zangwill, A. *J. Vac. Sci. Technol.* **1991**, A9, 145.
41. Bai, P., McDonald, J.F., Lu, T.-M. *J. Vac. Sci. Technol.* **1991**, A9, 2113.
42. Gupta, D., Ho, P.S. *Thin Solid Films* **1980**, 72, 399.
43. Queirolo, G., Dellagiovanna, M., DeSanti, G. *J. Vac. Sci. Technol.* **1989**, A7, 651.
44. Feibelman, P.J. *Phys. Rev. Lett.* **1990**, 65, 729.
45. Shevchik, N.J. *J. Non-Cryst. Solids* **1973**, 12, 141.
46. Tang, C., Alexander, S., Bruinsma, R. *Phys. Rev. Lett.* **1990**, 64, 772.
47. Bales, G.S., Zangwill, A. *Phys. Rev. Lett.* **1989**, 63, 692.
48. Zeiger, H.J., Tsao, J.Y., Ehrlich, D.J. *J. Vac. Sci. Technol.* **1985**, B3, 1436.
49. Gupta, D. in *Diffusion Phenomena in Thin Films and Microelectronic Materials*, Gupta, D., Ho, P.S. (eds.), Noyes Publications, Park Ridge, NJ, 1988, p 1.
50. Jensen, K.F., Einset, E.O., Fotiadis, D.I. *Ann. Rev. Fluid Mech.* **1991**, 23, 197.
51. Rosenberger, F., personal communication.
52. Rosenberger, F. *Fundamentals of Crystal Growth*, Springer-Verlag, Berlin, **1979**, p 500.
53. Gillis, J.C., Hammond, M.L., Ramiller, C.L. in *Proceedings of the Ninth*

- International Conference on Chemical Vapor Deposition*, Cincinnati, Ohio, Electrochem Soc., Pennington, NJ, 1984, p 21.
54. Bird, R.B., Stewart, W.E., Lightfoot, E.N. *Transport Phenomena*, John Wiley and Sons, NY, 1960, p 780.
 55. De Croon, M.H.J.M., Giling, L.J. *J. Electrochem. Soc.* **1990**, 137, 2867.
 56. Moffat, H., Jensen, K.F. *J. Cryst. Growth* **1986**, 77, 108.
 57. Fotiadis, D.I., Kieda, S., Jensen, K.F. *J. Cryst. Growth* **1990**, 102, 441.
 58. Shaw, D.W. *J. Cryst. Growth* **1975**, 31, 130.
 59. Stringfellow, G.B. *Organometallic Vapor-Phase Epitaxy*, Academic Press, NY, 1989, p 398.
 60. Venables, J.A., Spiller, G.D.T., Hanbücken, M. *Rep. Prog. Phys.* **1984**, 47, 399.
 61. Simmonds, M.G., Gladfelter, W.L., Li, H., McMurtry, P.H. in *Chemical Perspectives of Microelectronic Materials III*, Abernathy, C.R., Bohling, D.A., Bates, Jr., C.W., Hobson, W.S. (eds.), Materials Research Society, Pittsburgh, PA, 1993, in press.
 62. Texas-Alkyls "Organometallics Product Information," 1988.
 63. Eisch, J.J. in *Comprehensive Organometallic Chemistry*, G. Wilkinson, Gordon, F., Stone, A., Abel, E.W. (eds.), Pergamon, Oxford, 1982, Vol. 1, p 555.
 64. Coates, G.E., Green, M.L.H., Wade, K. *The Main Group Elements*, Barnes and Noble, New York, 1967, Vol. 1, p 573.
 65. Wiberg, E., Amberger, E. *Hydrides of the Elements of Main Groups I–IV*, Elsevier, Amsterdam, 1971, p 785.
 66. Powell, C.F. in *Vapor Deposition*, Powell, C. F., Oxley, J.H., Blocher, Jr., J.M. (eds.), John Wiley and Sons, New York, 1966, p 277.
 67. Feist, W.M., Steele, S.R., Readey, D.W. in *Physics of Thin Films*, Hass, G. Thun, R.E. (eds.), Academic Press, New York, 1969, Vol. 5, p 237.
 68. Cooke, M.J. *Vacuum* **1985**, 35, 67.
 69. Herman, I.P. *Chem. Rev.* **1989**, 89, 1323.
 70. Jensen, K.F., Kern, W. in *Thin Film Processes II*, Vossen, J.L., Kern, W. (eds.), Academic Press, San Diego, 1991, p 283.
 71. Eden, J.G. in *Thin Film Processes II*, Vossen, J.L., Kern, W. (eds.), Academic Press, San Diego, 1991, p 443.
 72. Ziegler, K., Gellert, H.G. *Angew. Chem.* **1955**, 67, 424.
 73. Ziegler, K., Nagel, K., Pfohl, W. *Justus Liebigs Ann. Chem.* **1960**, 629, 210.
 74. Ziegler, K., Kroll, N.-R., Larbig, W., Steudel, O.-W. *Justus Liebigs Ann. Chem.* **1960**, 629, 53.
 75. Larikov, E.I., Zhigach, A.F., Popov, A.F., Kulikovskaya, T.N., Vladyskaya, N.V. *Khim. Prom.* **1964**, 3, 171 (Chem. Abstracts 61:7773).
 76. Kwakman, L.F.T., Sluijk, B.G., Piekaar, H., Granneman, E.H.A. in *Tungsten and Other Refractory Metals for VLSI Applications IV*, Blewer, R.S., McConica, C.M. (eds.), Materials Research Society, Pittsburgh, PA, 1989, p 315.

77. Piekaar, H.W., Kwakman, L.F.T., Granneman, E.H.A. in *Proceedings of the Sixth International IEEE VLSI Multilevel Interconnection (V-MIC) Conference*, Santa Clara, California, IEEE, Piscataway, NJ, 1989, p 122.
78. Egger, K.W. *J. Am. Chem. Soc.* **1968**, *91*, 2867.
79. Egger, K.W. *Intl. J. Chem. Kinetics* **1969**, *1*, 459.
80. Bent, B.E., Nuzzo, R.G., Dubois, L.H. *J. Vac. Sci. Technol.* **1988**, *A6*, 1920.
81. Bent, B.E., Nuzzo, R.G., Dubois, L.H. in *Laser and Particle-Beam Chemical Processing for Microelectronics*, Ehrlich, D.J., Higashi, V., Oprysko, M.M. (eds.), Materials Research Society, Pittsburgh, PA, 1988, p 177.
82. Bent, B.E., Nuzzo, R.G., Dubois, L.H. *J. Am. Chem. Soc.* **1989**, *111*, 1634.
83. Bent, B.E., Dubois, L.H., Nuzzo, R.G. in *Chemical Perspectives of Microelectronic Materials I*, Gross, M.E., Jasinski, J.M., Yates, Jr., J.T. (eds.), Materials Research Society, Pittsburgh, PA, 1989, p 327.
84. Terao, H., Sunakawa, H. *J. Cryst. Growth* **1984**, *68*, 157.
85. Frese, V., Regel, G.K., Hardtdegen, H., Brauers, A., Balk, P., Hostalek, M., Lokai, M., Pohl, L., Miklis, A., Werner, K. *J. Elect. Mater.* **1990**, *19*, 305.
86. Pierson, H.O. *Thin Solid Films* **1977**, *45*, 257.
87. Malazgirt, A., Evans, J.W. *Metall. Trans.* **1980**, *11B*, 225.
88. Cooke, M.J., Heinecke, R.A., Stern, R.C., Maes, J.W. *Solid State Technol.* **1982**, *25(12)*, 62.
89. Green, M.L., Levy, R.A., Nuzzo, R.G., Coleman, E. *Thin Solid Films* **1984**, *114*, 367.
90. Levy, R.A., Green, M.L., Gallagher, P.K. *J. Electrochem. Soc.* **1984**, *131*, 2175.
91. Levy, R.A., Green, M.L., Gallagher, P.K. in *Proceedings of the Ninth International Conference on Chemical Vapor Deposition*, Electrochem. Soc., Cincinnati, Ohio, Electrochem. Soc., Pennington, NJ, 1984, p 258.
92. Kwakman, L.F.T., Huibregtse, D., Piekaar, H.W., Granneman, E.H.A., Cheung, K.P., Case, C.J., Lai, W.Y.-C., Liu, R., Schutz, R.J., Wagner, R.S. in *1990 Proceedings of the Seventh International IEEE VLSI Multilevel Interconnection Conference*, Santa Clara, California, IEEE, Piscataway, NJ, 1990, p 282.
93. Sekiguchi, A., Kobayashi, T., Hosokawa, N., Asamaki, T. *Jpn. J. Appl. Phys.* **1988**, *27*, 364.
94. Kobayashi, T., Sekiguchi, A., Hosokawa, N., Asamaki, T. in *Chemical Perspectives of Microelectronic Materials I*, Gross, M.E., Jasinski, J.M., Yates, Jr., J.T. (eds.), Materials Research Society, Pittsburgh, PA, 1989, p 363.
95. Sekiguchi, A., Kobayashi, T., Hosokawa, N., Asamaki, T. in *Extended Abstracts of the 21st Conference on Solid State Devices and Materials*, Jpn. Soc. Appl. Phys., Tokyo, 1989, p 29.
96. Sekiguchi, A., Kobayashi, T., Hosokawa, N., Asamaki, T. *J. Vac. Sci. Technol.* **1990**, *A8*, 2976.
97. Sekiguchi, A., Kobayashi, T., Hosokawa, N., Asamaki, T. in *Tungsten and Other*

- Advanced Metals for VLSI/ULSI Applications V*, Wong, S.S., Furukawa, S. (eds.), Materials Research Society, Pittsburgh, PA, 1990, p 383.
98. Amazawa, T., Nakamura, H. in *Extended Abstracts of the 18th Conference on Solid State Devices and Materials*, Jpn. Soc. Appl. Phys., Tokyo, 1986, 755.
 99. Amazawa, T., Nakamura, H., Arita, Y. in *International Electron Devices Meeting (Technical Digest)*, San Francisco, CA, IEEE, New York, 1988, p 442.
 100. Hair, M.L., Hertl, W. *J. Phys. Chem.* **1973**, 77, 2070.
 101. Bakardjiev, I., Majdraganova, M., Bliznakov, G. *J. Non-Cryst. Solids* **1976**, 20, 349.
 102. Morrow, B.A., Hardin, A.H. *J. Phys. Chem.* **1979**, 83, 3135.
 103. Kinney, J.B., Staley, R. H. *J. Phys. Chem.* **1983**, 87, 3735.
 104. Wei, M.Y., Castro, T., Gladfelter, W.L., University of Minnesota, Minneapolis, unpublished results.
 105. Sakharovskaya, G.B., Korneev, N.N., Smirnov, N.N., Popov, A.F. *J. Gen. Chem. USSR* **1974**, 44, 560.
 106. Cheung, K.P., Case, C.J., Liu, R., Schutz, R.J., Wagner, R.S. in *Proceedings of the Seventh International IEEE VLSI Multilevel Interconnection Conference*, Santa Clara, CA, IEEE, Piscataway, NJ, 1990, p 303.
 107. Fleming, C.G., Blonder, G.E., Higashi, G.S. in *Laser and Particle-Beam Chemical Processing for Microelectronics*, Ehrlich, D.J., Higashi, G.S., Oprysko, M.M. (eds.), Materials Research Society, Pittsburgh, PA, 1988, Vol. 101, p 183.
 108. Kobayashi, T., Sekiguchi, A., Hosokawa, N., Asamaki, T. *Jpn J. Appl. Phys.* **1988**, 27, L1775.
 109. Kobayashi, T., Sekiguchi, A., Hosokawa, N., Asamaki, T. *J. Vac. Sci. Technol.* **1992**, A 10, 525.
 110. Nishikawa, S., Tani, K., Yamaji, T. *J. Mater. Res.* **1992**, 7, 345.
 111. Yamada, I., Usui, H., Tanaka, S., Dahmen, U., Westmacott, K.H. *J. Vac. Sci. Technol.* **1990**, A3, 1443.
 112. Bent, B.E., Nuzzo, R.G., Zegarski, B.R., Dubois, L.H. *J. Am. Chem. Soc.* **1991**, 113, 1143.
 113. Bent, B.E., Nuzzo, R.G., Zegarski, B.R., Dubois, L.H. *J. Am. Chem. Soc.* **1991**, 113, 1137.
 114. Mantell, D.A. *J. Vac. Sci. Technol.* **1991**, A9, 1045.
 115. Mantell, D.A. *J. Vac. Sci. Technol.* **1989**, A7, 630.
 116. Mantell, D.A. in *Chemical Perspectives of Microelectronic Materials I*, Gross, M.E., Jasinski J.M., and Yates, Jr., J.T. (eds.), Materials Research Society, Pittsburgh, PA, 1989, p 357.
 117. Higashi, G.S., Raghavachari, K., Steigerwald, M.L. *J. Vac. Sci. Technol.* **1990**, B8, 103.
 118. Higashi, G.S., Steigerwald, M.L. *Appl. Phys. Lett.* **1989**, 54, 81.
 119. Osgood, Jr., R.M. *Ann. Rev. Phys. Chem.* **1983**, 34, 77.

120. Tsao, J.Y., Ehrlich, D.J. *Appl. Phys. Lett.* **1984**, 45, 617.
121. Tsao, J.Y., Ehrlich, D.J. *J. Cryst. Growth* **1984**, 68, 176.
122. Higashi, G.S., Fleming, C.G. *Appl. Phys. Lett.* **1986**, 48, 1051.
123. Higashi, G.S., Blonder, G.E., Fleming, C.G., McCrary, V.R., Donnelly, V.M. *J. Vac. Sci. Technol.* **1987**, B5, 1441.
124. Blonder, G.E., Higashi, G.S., Fleming, C.G. *Appl. Phys. Lett.* **1987**, 50, 766.
125. Higashi, G.S., Blonder, G.E., Fleming, C.G. in *Photon, Beam, and Plasma Stimulated Chemical Processes at Surfaces*, Donnelly, V.M., Herman, I.P., Hirose, M. (eds.), Materials Research Society, Pittsburgh, PA, 1987, Vol. 75, p 117.
126. Mantell, D.A. *Appl. Phys. Lett.* **1988**, 53, 1387.
127. Higashi, G.S. *Chemtronics* **1989**, 4, 123.
128. Higashi, G.S. *Appl. Surf. Sci.* **1989**, 43, 6.
129. Wood, T.H., White, J.C., Thacker, B.A. *Appl. Phys. Lett.* **1983**, 42, 408.
130. Zhang, Y., Stuke, M. *Chem. Phys. Lett.* **1988**, 149, 310.
131. Zhang, Y., Stuke, M. *J. Cryst. Growth* **1988**, 93, 143.
132. Zhang, Y., Stuke, M. *J. Phys. Chem.* **1989**, 93, 4503.
133. Zhang, Y., Stuke, M. *Chemtronics* **1989**, 4, 71.
134. Zhang, Y., Stuke, M. in *Chemical Perspectives of Microelectronic Materials I*, Gross, M.E., Jasinski, J.M., Yates, Jr., J.T. (eds.), Materials Research Society, Pittsburgh, PA, 1989, Vol. 131, p 375.
135. Zhang, Y., Stuke, M. *Jpn. J. Appl. Phys.* **1988**, 27, L1349.
136. Zhang, Y., Stuke, M. *Chemtronics* **1988**, 3, 230.
137. Beuermann, T., Stuke, M. *Chemtronics* **1989**, 4, 189.
138. Beuermann, T., Stuke, M. *Chem. Phys. Lett.* **1991**, 178, 197.
139. Mantell, D.A., Orlowski, T.E. in *Laser and Particle-Beam Chemical Processing for Microelectronics*, Ehrlich, D.J., Higashi, V., Oprysko, M.M. (eds.), Materials Research Society, Pittsburgh, PA, 1988, Vol. 101, p 171.
140. Salaneck, W.R., Bergman, R., Sundgren, J., Rockett, A., Motooka, T., Greene, J.E. *Surf. Sci.* **1988**, 198, 461.
141. Motooka, T., Rockett, A., Fons, P., Greene, J.E., Salaneck, W.R., Bergman, R., Sundgren, J.-E. *J. Vac. Sci. Technol.* **1988**, A6, 3115.
142. Motooka, T., Fons, P., Greene, J.E. in *Chemical Perspectives of Microelectronic Materials I*, Gross, M.E., Jasinski, J.M., Yates, Jr., J.T. (eds.), Materials Research Society, Pittsburgh, PA, 1989, Vol. 131, p 345.
143. Gow, T.R., Lin, R., Cadwell, L.A., Lee, F., Backman, A.L., Masel, R.I. *Chem. Mater.* **1989**, 1, 406.
144. Biswas, D.R., Ghosh, C., Layman, R.L. *J. Electrochem. Soc.* **1983**, 130, 234.
145. Squire, D.W., Dulcey, C.S., Lin, M.C. *J. Vac. Sci. Technol.* **1985**, B3, 1513.
146. Squire, D.W., Dulcey, C.S., Lin, M.C. *Chem. Phys. Lett.* **1985**, 116, 525.
147. Lee, F., Gow, T.R., Lin, R., Backman, A.L., Lubben, D., Masel, R.I. in *Chemical Perspectives of Microelectronic Materials I*, Gross, M.E., Jasinski, J.M., Yates, Jr., J.T. (eds.), Materials Research Society, Pittsburgh, PA, 1989, p 339.

148. Wee, A., Murrell, A.J., French, C.L., Price, R.J., Jackman, R.B., Foord, J. S. in *Chemical Perspectives of Microelectronic Materials I*, Gross, M.E., Jasinski, J.M., Yates, Jr., J.T. (eds.), Materials Research Society, Pittsburgh, PA, 1989, p 351.
149. Gow, T.R., Lee, F., Lin, R., Backman, A.L., Masel, R.I. *Vacuum* **1990**, *41*, 951.
150. Strongin, D.R., Comita, P.B. in *In-Situ Patterning: Selective Deposition and Etching*, Bernhardt, A.F., Black, J.G., Rosenberg, R. (eds.), Materials Research Society, Pittsburgh, PA, 1990, Vol. 158, p 21.
151. Strongin, D.R., Comita, P.B. *J. Phys. Chem.* **1991**, *95*, 1329.
152. Bartram, M.E., Michalske, T.A., Rogers, Jr., J.W., *J. Phys. Chem.* **1991**, *95*, 4453.
153. Zhou, Y., Henderson, M.A., White, J.M. *Surf. Sci.* **1989**, *221*, 160.
154. Yeddanapalli, L.M., Schubert, C.C. *J. Chem. Phys.* **1945**, *14*, 1.
155. Rytz-Froidevaux, Y., Salathé, R.P., Gilgen, H.H. *Phys. Lett.* **1981**, *84A*, 216.
156. Leys, M.R. *Chemtronics* **1988**, *3*, 179.
157. Shanov, V., Ivanov, B., Popov, C. *Thin Solid Films* **1992**, *207*, 71.
158. Suzuki, N., Anayama, C., Masu, K., Tsubouchi, K., Mikoshiba, N. *Jpn. J. Appl. Phys.* **1986**, *25*, 1236.
159. Carlsson, J., Gorbatskin, S., Lubben, D., Greene, J.E. *J. Vac. Sci. Technol.* **1991**, *B9*, 2759.
160. Masu, K., Sakurai, J., Shigeeda, N., Tsubouchi, K., Mikoshiba, N., Takeuti, Y. in *Extended Abstracts of the 20th Conference on Solid State Devices and Materials*, Jpn. Soc. Appl. Phys., Tokyo, 1988, p 573.
161. Masu, K., Tsubouchi, K., Shigeeda, N., Matano, T., Mikoshiba, N. *Appl. Phys. Lett.* **1990**, *56*, 1543.
162. Kato, T., Ito, T., Ishikawa, H., Maeda, M. in *Extended Abstracts of the 18th Conference on Solid State Devices and Materials*, Jpn. Soc. Appl. Phys., Tokyo, 1986, p 495.
163. Kato, T., Ito, T., Maeda, M. *J. Electrochem. Soc.* **1988**, *135*, 455.
164. Flicstein, J. *Appl. Surf. Sci.* **1989**, *36*, 443.
165. Beuermann, T., Stuke, M. *Appl. Phys.* **1989**, *B49*, 145.
166. Ehrlich, D.J., Osgood, Jr., R.M. *Chem. Phys. Lett.* **1981**, *79*, 381.
167. Higashi, G.S., Rothberg, L.J. *Appl. Phys. Lett.* **1985**, *47*, 1288.
168. Higashi, G.S., Rothberg, L.J., Fleming, C.G. *Chem. Phys. Lett.* **1985**, *115*, 167.
169. Higashi, G.S., Rothberg, L.J. *J. Vac. Sci. Technol.* **1985**, *B3*, 1460.
170. Lubben, D., Motooka, T., Greene, J.E. *Phys. Rev.* **1989**, *B39*, 5245.
171. Lubben, D., Motooka, T., Greene, J.E., Wendelken, J.F., Sundgren, J., Salaneck, W.R. in *Laser and Particle-Beam Chemical Processing for Microelectronics*, Ehrlich, D.J., Higashi, V., Oprysko, M.M. (eds.), Materials Research Society, Pittsburgh, PA, 1988, Vol. 101, p 151.
172. Motooka, T. *Review of Laser Engineering* **1990**, *18*, 712.
173. Menon, M., Allen, R.E. *J. Vac. Sci. Technol.* **1989**, *B7*, 729.
174. Bouree, J.E., Flicstein, J., Nissim, Y.I. in *Photon, Beam, and Plasma Stimulated*

- Chemical Processes at Surfaces*, Donnelly, V.M., Herman, I.P., Hirose, M. (eds.), Pittsburgh, PA., Materials Research Society, 1987, Vol. 75, p 129.
175. Bouree, J.E., Flicstein, J. in *Laser and Particle-Beam Chemical Processing for Microelectronics*, Ehrlich, D.J., Higashi, V., Oprysko, M.M. (eds.), Materials Research Society, Pittsburgh, PA, 1988, Vol. 101, p 55.
 176. Flicstein, J., Bouree, J.E., Bresse, J.F., Pougnet, A.M. in *Laser and Particle-Beam Chemical Processing for Microelectronics*, Ehrlich, D.J., Higashi, V., Oprysko, M.M. (eds.), Materials Research Society, Pittsburgh, PA, 1988, Vol. 101, p 49.
 177. Bouree, J.E., Flicstein, J., Bresse, J.F., Rommeluere, J.F., Pougnet, A.M. in *Laser and Particle-Beam Chemical Processes on Surfaces*, Johnson, A.W., Loper, G.L., Sigmon, T.W. (eds.), Materials Research Society, Pittsburgh, PA, 1989, p 251.
 178. Bouree, J. E., Flicstein, J. *NATO ASI Ser., Ser. B* **1989**, 198, 33.
 179. Orlowski, T.E., Mantell, D.A. in *Laser and Particle-Beam Chemical Processing for Microelectronics*, Ehrlich, D.J., Higashi, V., Oprysko, M.M. (eds.), Materials Research Society, Pittsburgh, PA, 1988, Vol. 101, p 165.
 180. Oprysko, M.M., Beranek, M.W. *J. Vac. Sci. Technol.* **1987**, B5, 496.
 181. Solanki, R., Ritchie, W.H., Collins, G.J. *Appl. Phys. Lett.* **1983**, 43, 454.
 182. Motooka, T., Gorbatskin, S., Lubben, D., Greene, J.E. *J. Appl. Phys.* **1985**, 58, 4397.
 183. Motooka, T., Gorbatskin, S., Lubben, D., Eres, D., Greene, J.E. *J. Vac. Sci. Technol.* **1986**, A4, 3146.
 184. Eres, D., Motooka, T., Gorbatskin, S., Lubben, D., Green, J.E. *J. Vac. Sci. Technol.* **1987**, B5, 848.
 185. Brum, J.L., Tong, P., Koplitz, B. *Appl. Phys. Lett.* **1990**, 56, 695.
 186. Fischer, M., Lückerrath, R., Balk, P., Richter, W. *Chemtronics* **1988**, 3, 156.
 187. Okabe, H., Emadi-Babaki, M.K., McCrary, V.R. *J. Appl. Phys.* **1991**, 69, 1730.
 188. Yau, S., Saltz, D., Nayfeh, M.H. *Appl. Phys. Lett.* **1990**, 57, 2913.
 189. Ishibashi, A., Funato, K., Mori, Y. *J. Vac. Sci. Technol.* **1991**, B9, 169.
 190. Whaley, T.P., Norman, V. *US Patent* 3 209 326, 1965.
 191. Carley, D.R., Dunn, J.H. *US Patent* 3 375 129, 1968.
 192. Schmidt, D.L., Hellmann, R. *US Patent* 3 462 288, 1969.
 193. Ruff, J.K., Hawthorne, M.F. *J. Am. Chem. Soc.* **1960**, 82, 2141.
 194. Baum, T.H., Larson, C.E., Jackson, R.L. *Appl. Phys. Lett.* **1989**, 55, 1264.
 195. Baum, T.H., Larson, C.E., Jackson, R.L. in *Laser and Particle-Beam Chemical Processes on Surfaces*, Johnson, A.W., Loper, G.L., Sigmon, T.W. (eds.), Pittsburgh, PA, Materials Research Society, 1989, p 119.
 196. Beach, D.B., Blum, S.E., LeGoues, F.K. *J. Vac. Sci. Technol.* **1989**, A7, 3117.
 197. Baum, T.H. in *Laser/Optical Processing of Electronic Materials*, Santa Clara, California, SPIE-International Society for Optical Engineering, Bellingham, Washington, 1989, p 188.
 198. Gross, M.E., Fleming, C.G., Cheung, K.P., Heimbrook, L.A. *J. Appl. Phys.* **1991**, 69, 2589.

199. Gross, M.E., Dubois, L.H., Nuzzo, R.G., Cheung, K.P. in *Chemical Perspectives of Microelectronic Materials II*, Interrante, L.V., Jensen, K.F., Dubois, L. H., Gross, M.E. (eds.), Materials Research Society, Pittsburgh, PA, 1991, p 383.
200. Dubois, L.H., Zegarski, B.R., Gross, M.E., Nuzzo, R.G. *Surf. Sci.* **1991**, 244, 89.
201. Simmonds, M.G., Gladfelter, W.L., Nagaraja, R., Szymanski, W.W., Ahn, K.-H., McMurry, P.H. *J. Vac. Sci. Technol.* **1991**, A9, 2782.
202. Simmonds, M.G., Phillips, E.C., Hwang, J.-W., Gladfelter, W.L. *Chemtronics* **1991**, 5, 155.
203. Glass, J.A., Jr., Kher, S., Spencer, J.T. *Chem. Mater.* **1992**, 4, 530.
204. Glass, J.A., Jr., Kher, S., Spencer, J.T. *Thin Solid Films* **1992**, 207, 15.
205. Houlding, V.H., Coons, D.E. in *Tungsten and Other Advanced Metals for VLSI/ULSI Applications 1990*, Smith, G.C., Blumenthal, R. (eds.), Materials Research Society, Pittsburgh, PA, 1990, p 203.
206. Gross, M.E., Cheung, K.P., Fleming, C.G., Kovalchick, J., Heimbrook, L.A. *J. Vac. Sci. Technol.* **1991**, A9, 57.
207. Heitsch, C.W., Kniseley, R.N. *Spectrochim. Acta* **1963**, 19, 1385.
208. Fraser, G.W., Greenwood, N.N., Straughan, B.P. *J. Chem. Soc.* **1963**, 3742.
209. Almenningen, A., Gundersen, G., Haugen, T., Haaland, A. *Inorg. Chem.* **1968**, 7, 1575.
210. Almenningen, A., Gundersen, G., Haugen, T., Haaland, A. *Acta Chem. Scandinavica* **1972**, 26, 3928.
211. Atwood, J.L., Bennett, F.R., Elms, F.M., Jones, C., Raston, C.L., Robinson, K.D. *J. Am. Chem. Soc.* **1991**, 113, 8183.
212. Heitsch, C.W., Nordman, C.E., Parry, R.W. *Inorg. Chem.* **1963**, 2, 508.
213. Senzaki, Y., Gladfelter, W.L., University of Minnesota, Minneapolis, unpublished results.
214. Dubois, L.H., Zegarski, B.R., Kao, C.-T., Nuzzo, R.G. *Surf. Sci.* **1990**, 236, 77.
215. Foord, J.S., Murrell, A.J., O'Hare, D., Singh, N.K., Wee, A.T.S., Whitaker, T. J. *Chemtronics* **1989**, 4, 262.
216. Wee, A.T.S., Murrell, A.J., Singh, N.K., O'Hare, D., Foord, J.S. *J. Chem. Soc., Chem. Commun.* **1990**, 11.
217. Nechiporenko, G.N., Petukhova, L.B., Rozenberg, A.S. *Bull. Acad. Sci. USSR* **1975**, 24, 1584.
218. Mundenar, J.M., Murphy, R., Tsuei, K.D., Plummer, E.W. *Chem. Phys. Lett.* **1988**, 143, 593.
219. Paul, J., Hoffmann, F.M. *Surf. Sci.* **1988**, 194, 419.
220. Hara, M., Domen, K., Onishi, T., Nozoye, H., Nishihara, C., Kaise, Y., Shindo, H. *Surf. Sci.* **1991**, 242, 459.
221. Hinch, B.J., Doak, R.B., Dubois, L.H., submitted for publication in *J. Chem. Phys.* 1993.
222. Wee, A.T.S., Murrell, A.J., Singh, N.K., O'Hare, D.M., Foord, J.S. *Vacuum* **1990**, 41, 968.

223. Creighton, J.R. *J. Vac. Sci. Technol.* **1990**, A8, 3984.
224. Gavrilenko, V.V., Chekulaeva, L.A., Zakharkin, L.I. *Bull. Acad. Sci. USSR* **1977**, 26, 1131.
225. Kost, M.E., Golovanova, A.L. *Bull. Acad. Sci. USSR* **1975**, 24, 905.
226. Heitsch, C.W. *Nature* **1962**, 195, 995.
227. Hamilton, J.F., Logel, P.C. *J. Catal.* **1973**, 29, 253.
228. Lelental, M. *J. Electrochem. Soc.* **1973**, 120, 1650.
229. Jarrold, M.F., Bower, J.E. *J. Am. Chem. Soc.* **1988**, 110, 70.
230. Cox, D.M., Trevor, D.J., Whetten, R.L., Kaldor, A. *J. Phys. Chem.* **1988**, 92, 421.
231. Elms, F.M., Lamb, R.N., Pigram, P.J., Gardiner, M.G., Wood, B.J., Raston, C.L. *J. Chem. Soc., Chem. Commun.* **1992**, 1423.
232. Hirashita, N., Kinoshita, M., Aikawa, I., Ajioka, T. *Appl. Phys. Lett.* **1990**, 56, 451.
233. Gross, M.E., Harriott, L.R., Opila, Jr., R.L. *J. Appl. Phys.* **1990**, 68, 4820.
234. Lehmann, O., Stuke, M. *Appl. Phys. A* **1991**, 53, 343.
235. Foulon, F., Lehmann, O., Stuke, M. *Appl. Surf. Sci.* **1992**, in press.
236. Han, J., Senzaki, Y., Gladfelter, W.L., Jensen, K.F., *Chemical Perspectives of Microelectronic Materials III*, Abernathy, C.R., Bohling, D.A., Bates, Jr., C.W., Hobson, W.S. (eds.), Materials Research Society, Pittsburgh, PA, in press.
237. Murthy, T.U.M.S., Miyamoto, N., Shimbo, M., Nishizawa, J. *J. Cryst. Growth* **1976**, 33, 1.
238. Okuyama, K., Huang, D., Seinfeld, J., Tani, N., Kousaka, Y. *Chem. Eng. Sci.* **1991**, 46, 1545.
239. Okuyama, K., Huang, D.D., Seinfeld, J.H., Tani, N., Matsui, I. *Jpn. J. Appl. Phys.* **1992**, 31, 1.
240. Bhat, R., Koza, M.A., Chang, C.C., Schwarz, S.A. *J. Cryst. Growth* **1986**, 77, 7.
241. Smith, W.L., Wartik, T. *J. Inorg. Nucl. Chem.* **1967**, 29, 629.
242. Laubengayer, A.W., Gilliam, W.F. *J. Am. Chem. Soc.* **1941**, 63, 477.
243. Kobayashi, N., Fukui, T. *Elect. Lett.* **1984**, 20, 887.
244. Keuch, T.F., Veuhoff, E., Kuan, T.S., Deline, V., Potemski, R. *J. Cryst. Growth* **1986**, 77, 257.
245. Brum, J.L., Deshmukh, S., Koplitz, B. *J. Chem. Phys.* **1990**, 93, 7946.
246. Brum, J.L., Deshukh, S., Koplitz, B. *Chem. Phys. Lett.* **1990**, 165, 413.
247. Tsubouchi, K., Masu, K., Shigeeda, N., Matano, T., Hiura, Y., Mikoshiba, N. *Appl. Phys. Lett.* **1990**, 57, 1221.
248. Shinzawa, T., Sugai, K., Kishida, S., Okabayashi, H. in *Tungsten and Other Advanced Metals for VLSI/ULSI Applications*, Wong, S.S., Furukawa, S. (eds.), Materials Research Society, Pittsburgh, PA, 1990, p 377.
249. Tsubouchi, K., Masu, K. *J. Vac. Sci. Technol.* **1992**, A 10, 856.
250. Cacouris, T., Scelsi, G., Scarmozzino, R., Osgood, Jr., R.M., Krchnavek, R.R. in *Laser and Particle-Beam Chemical Processing for Microelectronics*, Ehrlich, D.J., Higashi, V., Oprysko, M.M. (eds.), Materials Research Society, Pittsburgh, PA, 1988, Vol. 101, p 43.

- 251. Cacouris, T., Scelsi, G., Shaw, P., Scarmozzino, R., Osgood, Jr., R.M. *Appl. Phys. Lett.* **1988**, 52, 1865.
- 252. Hanabusa, M., Hayakawa, K., Oikawa, A., Maeda, K. *Jpn. J. Appl. Phys.* **1988**, 27, L1392.
- 253. Hanabusa, M., Oikawa, A., Cai, P.Y. *J. Appl. Phys.* **1989**, 66, 3268.
- 254. Hanabusa, M., Ikeda, M. in *In-Situ Patterning: Selective Area Deposition and Etching*, Bernhardt, A.F., Black, J.G., Rosenberg, R. (eds.), Materials Research Society, Pittsburgh, PA, 1990, Vol. 158, p 135.
- 255. Zhu, N., Cacouris, T., Scarmozzino, R., Osgood, Jr., R.M. *J. Vac. Sci. Technol.* **1992**, B 10, 1167.
- 256. Scarmozzino, R., Cacouris, T., Osgood, Jr., R.M. in *In-Situ Patterning: Selective Area Deposition and Etching*, Bernhardt, A.F., Black, J.G., Rosenberg, R. (eds.), Materials Research Society, Pittsburgh, PA, 1990, Vol. 158, p 121.
- 257. Sasaoka, C., Mori, K., Kato, Y., Usui, A. *Appl. Phys. Lett.* **1989**, 55, 741.
- 258. Levy, R.A., Gallagher, P.K., Contolini, R., Schrey, F. *J. Electrochem. Soc.* **1985**, 132, 457.

This Page Intentionally Left Blank

Chapter 3

Chemical Vapor Deposition

of Tungsten

Alfred A. Zinn

**Department of Chemistry & Biochemistry
University of California, Los Angeles
405 Hilgard Avenue
Los Angeles, CA 90024-1569**

Abstract

This chapter presents an overview of chemical vapor deposition (CVD) of tungsten metal. The major applications of tungsten and its importance in microelectronics as related to electrical, mechanical, and chemical properties are described. In subsequent sections, a guide to precursors and their synthesis and properties is provided. The deposition kinetics, growth mechanisms, and selectivity are discussed. Methods for overcoming heteroatom impurities, which are still the major drawback of organometallic chemical vapor deposition (OMCVD), are examined. This is followed by discussion of laser-assisted CVD and plasma-enhanced CVD of tungsten. Finally, these results and theories are evaluated and problems as well as prospects for future developments are considered.

Contents

3.1	Introduction	108
3.2	Precursors - Synthesis - Properties	111
3.2.1	Historical Development	111
3.2.2	Tungsten Halides	112
3.2.3	Organometallic Precursors	115
3.2.3.1	Hexakis(trifluorophosphine)tungsten $[\text{W}(\text{PF}_3)_6]$	115
3.2.3.2	Hexacarbonyltungsten $[\text{W}(\text{CO})_6]$	117
3.2.3.3	Bis(arene)tungsten Compounds	117
3.2.3.4	Tris(butadiene)tungsten $[\text{W}(\eta^4\text{-C}_4\text{H}_6)_3]$	118
3.2.3.5	Tetraallyltungsten $[\text{W}(\eta^3\text{-C}_3\text{H}_5)_4]$	118
3.2.3.6	Tris(methylvinylketone)tungsten $\{\text{W}[\text{CH}_3\text{C}(\text{O})\text{CH}=\text{CH}_2]_3\}$	119
3.2.3.7	Cyclopentadienylmethyltricarbonyltungsten $[(\eta^5\text{-C}_5\text{H}_5)\text{W}(\text{CO})_3\text{CH}_3]$	119
3.2.3.8	Bis(cyclopentadienyl)dihydridotungsten $[(\eta^5\text{-C}_5\text{H}_5)_2\text{WH}_2]$	119
3.2.3.9	Bis(methylcyclopentadienyl)dihydridotungsten $[(\eta^5\text{-CH}_3\text{C}_5\text{H}_4)\text{WH}_2]$	120
3.2.3.10	Cyclopentadienylhydridotricarbonyltungsten $[\text{HW}(\eta^5\text{-C}_5\text{H}_5)(\text{CO})_3]$	120
3.2.3.11	Cycloheptatrienetetracarboxyltungsten $[(\eta^6\text{-C}_7\text{H}_8)\text{W}(\text{CO})_3]$ and 1,5-Cyclooctadienetetracarboxyltungsten $[(1,5\text{-COD})\text{W}(\text{CO})_4]$...	120
3.3	Chemical Vapor Deposition (CVD)	121
3.3.1	Tungsten Halides as CVD Precursors	121
3.3.1.1	Tungsten Hexafluoride (WF_6)	121
3.3.1.2	Tungsten Hexachloride (WCl_6)	133
3.3.1.3	Tungsten Hexabromide (WBr_6)	138
3.3.2	Organometallic Compounds	138
3.3.2.1	Hexakis(trifluorophosphine)tungsten $[\text{W}(\text{PF}_3)_6]$	141
3.3.2.2	Hexacarbonyltungsten $[\text{W}(\text{CO})_6]$	141
3.3.2.3	Bis(benzene)tungsten $[\text{W}(\eta^6\text{-C}_6\text{H}_6)_2]$	143
3.3.2.4	Tris(butadiene)tungsten $[\text{W}(\eta^4\text{-C}_4\text{H}_6)_3]$	144
3.3.2.5	Tetraallyltungsten $[\text{W}(\eta^3\text{-C}_3\text{H}_5)_4]$	144
3.3.2.6	Tris(methylvinylketone)tungsten $\{\text{W}[\text{CH}_3\text{C}(\text{O})\text{CH}=\text{CH}_2]_3\}$	146
3.3.2.7	Cyclopentadienylmethyltricarbonyltungsten $[(\eta^5\text{-C}_5\text{H}_5)\text{W}(\text{CO})_3\text{CH}_3]$	146
3.3.2.8	Bis(cyclopentadienyl)dihydridotungsten $[(\eta^5\text{-C}_5\text{H}_5)_2\text{WH}_2]$	147
3.3.2.9	Bis(methylcyclopentadienyl)dihydridotungsten $[(\eta^5\text{-CH}_3\text{C}_5\text{H}_4)_2\text{WH}_2]$	148

3.3.2.10	Cyclopentadienylhydridotricarbonyltungsten [HW(η^5 -C ₅ H ₅)(CO) ₃]	149
3.3.2.11	Cycloheptatrienetetracarboxyltungsten [(η^6 -C ₇ H ₈)W(CO) ₃] and 1,5-Cyclooctadienetetracarboxyltungsten [(1,5-COD)W(CO) ₄]	149
3.4	In Situ Catalysis of Tungsten Deposition	150
3.5	Laser-Assisted Chemical Vapor Deposition (LCVD)	151
3.5.1	Hexacarboxyltungsten W(CO) ₆	152
3.5.1.1	Mechanistic Findings	152
3.5.1.2	Deposition Experiments	153
3.5.2	Tungsten Hexafluoride (WF ₆)	155
3.5.2.1	Mechanistic and Kinetic Observations	155
3.5.2.2	Deposition Experiments	157
3.6	Plasma-Enhanced Chemical Vapor Deposition (PECVD)	160
3.7	Summary and Outlook	163
	Acknowledgments	164
	References	164

3.1 Introduction

The field of thin tungsten films and related materials has developed remarkably over the past decade. The number of papers published in this area is over 2000 and is increasing at the rate of about 100 per year. In addition, a workshop started in 1986 devoted to tungsten meets annually to discuss new developments.¹ Tungsten metal films have attracted this attention primarily because of their refractory characteristics and the wide range of applications from wear and corrosion protection to conducting layers and diffusion barriers in electronic devices.²

An important area of applications for thin tungsten films is wear and erosion protection for cutting and grinding tools, and for general corrosion protection of various materials.³ Tungsten is highly desirable for these applications because it is relatively hard and very stable against chemical attack even at high temperatures. The hardness and inert quality of tungsten phases can be enhanced by adding small amounts of carbon, nitrogen, or oxygen. This led to the discovery of a specific WC-phase German chemists call "Widiametall" (wie Diamant), which means diamond-like because this material is nearly as hard and chemically inert as diamond. Furthermore, tungsten shows the highest melting point of all metals (3410 °C) and maintains its hardness up to temperatures close to its melting point. This latter property is valuable for grinding and drilling tools where stability and hardness at high temperatures (3000-4000 °C) are necessary.

Other important applications for tungsten thin films are in micro-electronic and opto-electronic devices.⁴⁻⁹ Examples are source, drain, and gate metallization in transistors and diffusion barriers, ohmic contacts, and interconnections such as lines, vias, and plugs in integrated circuits (IC).^{7,8,10,11} The interest in tungsten for applications in IC metallization results from several favorable electrical, mechanical, and chemical properties and the availability of chemical vapor deposition (CVD) processing to deposit conformal films for via and plug filling. The most important aspects are discussed below.

Tungsten has a high activation barrier for self diffusion. As a result, tungsten has a high resistance to electromigration under high current densities.^{4-9,12} Tungsten also has a low thermal expansion coefficient which changes only marginally with temperature and has a good match to the thermal expansion coefficient of silicon. As a result, tungsten films do not suffer from hillock formation and also have low stress ($<5 \times 10^9$ dynes/cm²). Tungsten also forms ohmic contacts with silicon and III/V-semiconductors such as GaAs and InP. It is the only metal which does not interact with any major III/V-semiconductors (see Table 3-1).¹³ Tungsten does not react with GaAs (or other III/V-semiconductors) up to its decomposition temperature of 600-700 °C (depending on the conditions).¹⁴ Also, tungsten films do not form silicides such as WSi_2 or W_5Si_3 at temperatures below 600 °C when in contact with pure or n^+/p^+ doped silicon

Table 3-1. List of metals and intermetallic compounds thermodynamically stable with respect to III/V semiconductors. (From¹³, reprinted with permission).

III/V-Semiconductor	Stable Metals/Intermetallic Phases
AlP, AlAs, AlSb	ScAl ₂ , TiAl, TiAl ₃ , VAl, CrAl ₄ , MnAl, FeAl ₂ , FeAl ₃ , CoAl, NiAl, NiAl ₃ , CuAl ₂ , YAl ₂ , ZrAl, ZrAl ₂ , ZrAl ₃ , Zr ₂ Al ₃ , MoAl ₂ , MoAl ₃ , RuAl, RuAl ₂ , RhAl, PdAl, Pd ₂ Al ₃ , PdAl ₃ , LaAl ₂ , HfAl ₂ , HfAl ₃ , TaAl ₃ , WAl ₄ , ReAl ₂ , OsAl ₂ , IrAl, PtAl ₂ , Pt ₂ Al ₃ , PtAl ₃ , AuAl, CeAl ₂ , CeAl ₃ , SmAl ₂ , SmAl ₃ , ThAl ₂ , YbAl ₂ , YbAl ₃ , W.
GaP, GaAs, GaSb	Sc ₅ Ga ₃ , TiGa ₂ , TiGa ₃ , V ₂ Ga ₅ , CrGa, MnGa ₃ , FeGa ₃ , CoGa, CoGa ₃ , NiGa, Ni ₂ Ga ₃ , CuGa ₂ , YGa ₂ , ZrGa ₃ , Mo ₃ Ga, RuGa ₃ , RhGa ₂ , RhGa ₃ , PdGa, LaGa, LaGa ₂ , HfGa, HfGa ₂ , HfGa ₃ , TaGa ₃ , OsGa, IrGa ₂ , IrGa ₃ , PtGa, PtGa ₂ , Pt ₂ Ga ₃ , AuGa, AuGa ₂ , GdGa, GdGa ₂ , HoGa ₂ , PrGa ₂ , SmGa ₂ , TbGa ₂ , ThGa ₂ , CeGa ₂ ; (Pd ₂ Ga ₃ , PdGa ₃), W.
InP, InAs, InSb	Sc ₃ In, Ti ₃ In ₄ , CrIn ₃ , Mn ₃ In, CoIn, CoIn ₃ , NiIn, Ni ₂ In ₃ , Cu ₂ In, YIn ₃ , ZrIn ₃ , Mo, RuIn ₃ , RhIn, RhIn ₃ , PdIn, Pd ₂ In ₃ , PdIn ₃ , LaIn ₃ , Hf ₃ In ₄ , Ta, Re, Os, IrIn ₃ , PtIn ₂ , AuIn, AuIn ₂ , CeIn ₃ , NdIn ₃ , TbIn ₃ , Th ₂ In, YbIn ₂ , W.

layers.^{6,8,15} All of these factors make tungsten desirable for applications in microelectronic devices. However, the use of tungsten/silicon ohmic contacts has been limited by the poor adhesion of tungsten to the native silicon dioxide insulator surface layer. As a result, the use of an adhesion promoter such as titanium nitride (TiN) is required.

Tungsten (resistivity $\sim 5.6 \mu\Omega\text{cm}$) has been successfully used at the first interconnect level as a local interconnect to replace high resistivity ($\sim 500 \mu\Omega\text{cm}$) doped polycrystalline silicon. Tungsten is used because reliability issues demand a material which has a high resistance to electromigration under high current densities. Tungsten is also used for via and plug filling primarily because a CVD process is necessary for highly conformal fill of high-aspect-ratio structures.

Tungsten is an effective diffusion barrier for most commonly used semiconductors and aluminum metallization.¹⁵⁻²² Aluminum is the dominant material for interconnections in integrated circuits. However, aluminum has problems associated with its inability to form stable contacts in direct contact with most semiconductors.^{5,6,20} Extensive interdiffusion is frequently observed between aluminum and compound semiconductors as well as between aluminum and silicon. Tungsten plugs can suppress this interaction by acting as a diffusion barrier between semiconductors and aluminum.

Tungsten exists in three different phases: α -tungsten is the most common phase and is thermodynamically stable at all temperatures. It possesses the bcc model-type-A2 lattice.^{23,24} The α -phase is desirable for microelectronic applications because it exhibits the lowest resistivity of all crystalline phases. The β -tungsten phase is metastable below 630 °C and has a cubic, model-type-A15 lattice;^{23,25,26} however, annealing at temperatures above 700 °C transforms it into the α -phase. Small amounts of impurities such as oxygen, carbon, or halogens tend to stabilize the β -tungsten phase, and these have a strong influence on the lattice parameters.²⁷⁻³² Certain amounts of oxygen in tungsten also increase the resistance to silicide formation and chemical attack. The γ -tungsten phase (fcc, A1 type) has been observed only in sputtered films with

Table 3-2. Selected properties of tungsten metal.

Melting point	3680 K
Boiling point	5828 K
Density	19.32 g/cm ³
Knoop Hardness	485 kg/nm ²
Young's Modulus	410 GPa
Yield strength	4.0 GPa
Electrical conductivity:	
α -Tungsten	5.65 $\mu\Omega\text{cm}$ at 300 K
β -Tungsten	40 $\mu\Omega\text{cm}$ ⁴¹
	100-300 $\mu\Omega\text{cm}$ ^{42,43}
	300-1000 $\mu\Omega\text{cm}$ ¹¹
γ -Tungsten	unknown
Specific heat capacity	0.13 J/gK
Thermal expansion	4.6 x 10 ⁻⁶ °C (0-500 K)
coefficient	5.2 x 10 ⁻⁶ °C (600-1000 K)

thickness less than 2 μm formed at temperatures between 200 and 400 °C. It is transformed to the stable α -phase upon annealing at 700 °C.^{33,34}

It is important to determine which phase is present in tungsten thin films because these phases show significant differences in their resistivity (see Table 3-2). The α -phase has the lowest resistivity of 5.65 $\mu\Omega\text{cm}$ at 300 K. Several values have been published for the β -tungsten phase. The problem with obtaining reliable values is that the amounts of impurities (carbon, oxygen, halogens) and the α -phase strongly influence resistivity. Values as low as 40 $\mu\Omega\text{cm}$ have been reported for the β -phase.^{35,36} Other authors have reported values of 100-300 $\mu\Omega\text{cm}$.^{37,38} Petroff et al.³⁹ obtained very thin β -tungsten films (100-150 Å) with resistivities of 100-300 $\mu\Omega\text{cm}$ using rf sputtering techniques to avoid heteroatom impurities.

3.2 Precursors - Synthesis - Properties

3.2.1 Historical Development

The first tungsten deposition experiments were reported as early as 1855. Friedrich Wöhler used WCl_6 with hydrogen as a carrier gas to deposit tungsten metal.⁴⁰ He obtained dense and shiny tungsten mirrors on the walls of his tubular glass reactor by heating the deposition zone to about 800 °C. During the following years, several other groups investigated the use of WCl_6 as a tungsten CVD precursor to optimize the processing conditions. Low-pressure conditions and temperatures of up to 1500 °C were employed.

Almost a century later, in 1947, the next milestone in the CVD of tungsten was set by Lander and Germer^{41,42} in their pioneering work on tungsten and molybdenum deposition using the metal *hexacarbonyl* compounds. Like Wöhler, Lander and Germer also used hydrogen as a carrier gas. They investigated a wide range of low-pressure conditions and were able to lower the deposition temperature to 350-600 °C.

The only work on WBr_6 as a tungsten source for CVD was published by Caves in 1962.⁴³ He used a van Arkel/de Boer apparatus to synthesize the precursor in situ with subsequent deposition in the same apparatus. The films were essentially free of impurities. At that time, there was great interest in tungsten coatings because of their excellent corrosion and temperature resistance and because the bulk metal was expensive and difficult to process by other routes.

At present, the dominant tungsten CVD precursor is tungsten hexafluoride (WF_6) which is a gas at room temperature. The CVD chemistry using WF_6 has been extensively studied, is fairly well understood, and is used routinely in the microelectronics industry.

Reduction of WF_6 with either hydrogen or silane allows deposition of pure tungsten in the temperature range of 300-500 °C. It is also possible to reduce WF_6 by silicon to deposit tungsten selectively on a silicon surface. Furthermore, very high purity tungsten hexafluoride is currently available at low cost. For these reasons, WF_6 will probably continue to be the dominant precursor for W CVD for microelectronic applications.

There is also some interest in developing organometallic precursors for specialized applications such as low-temperature tungsten deposition for wear- and corrosion-resistant coatings. Organometallic compounds are promising because they can provide high vapor pressures and low decomposition temperatures. They can also be liquids at temperatures below 100 °C which facilitates processing. However, the main disadvantage of organometallic precursors is the possibility of carbon and oxygen contamination in the films. Only in the past 10 years have organometallic compounds drawn increasing attention as potential CVD precursors. This has been motivated by success with metals such as Ni, Pt,¹³ Cu, Rh, Ir, and others in which high-purity metal films have been obtained from organometallic precursors as described in this book.

The next section discusses the synthesis and properties of precursors used for CVD of W. The advantages and disadvantages of various WF_6 reduction chemistries will then be discussed.

3.2.2 Tungsten Halides

The tungsten halides WF_6 ,⁴⁴ WCl_6 ,⁴⁴ and WBr_6 ⁴⁴ are simple to synthesize (Table 3-3), readily available, and have sufficient vapor pressures to be used in CVD (Table 3-4). Beside thermal decomposition, which usually has to be carried out at relatively high temperatures, many reducing agents such as H_2 , SiH_4 , Si, Si_2H_6 , B_2H_6 , PH_3 ,^{45,46} SiH_2Cl_2 ,⁴⁷ and GeH_4 ^{48,49} have been used to obtain pure tungsten films. The most common reducing agents are H_2 and SiH_4 .

Tungsten hexafluoride (m.p.: 1.9 °C; b.p.: 17.1 °C) is a colorless gas at ambient temperature with a high vapor pressure (1 torr at 25 °C). Tungsten hexachloride is a dark blue solid at room temperature which melts at 275 °C and vaporizes at 346 °C (b.p.). It can be easily sublimed in vacuum (≤ 20 torr) at 150 °C and shows a vapor pressure of 7 torr at 200 °C. Tungsten hexabromide, like WCl_6 , is a dark blue salt at room temperature which melts at 232 °C under a bromine atmosphere. It is sensitive to reduction and starts to decompose under nitrogen or argon at 40 °C to yield WBr_5 and other sub-bromides. The most stable sub-bromides, WBr_5 and WBr_4 (both black), seem to be the active species in vapor deposition experiments. At elevated temperatures, WBr_6 is easily synthesized from the elements. In contrast to WF_6 and WCl_6 , SiH_4 and Si seem to be less convenient reducing agents for WBr_6 because the SiBr_4 generated is not

Table 3-3. Comparison of synthesis methods of precursors used for tungsten CVD.

Compound	Synthesis	Comments	Ref.
WF ₆	W + 3 F ₂ → WF ₆		44
WCl ₆	W + 3 Cl ₂ → WCl ₆		44
WBr ₆	W + 3 Br ₂ → WBr ₆		44
W(CO) ₆	WCl ₆ + 2 AlEt ₃ + CO (excess) → W(CO) ₆ + 2 AlCl ₃ + 3 C ₄ H ₁₀	50 °C, 70 bar CO	58
W(C ₆ H ₆) ₂	WCl ₆ + 2 Al/AICl ₃ + C ₆ H ₆ (excess) → W(C ₆ H ₆) ₂ + 3 AlCl ₃	yield: 1.8 %	63
	metal vapor condensation methods	yield: 30-40 %	64,65
W(PF ₃) ₆	WCl ₆ + 6 Cu + PF ₃ (excess) → W(PF ₃) ₆ + 6 CuCl	300 bar/250 °C	56
W(allyl) ₄	W(OPh) ₆ + 6 (C ₃ H ₅)MgBr → W(η ³ -allyl) ₄ + C ₆ H ₁₀ + 6 Mg(OPh)Br	THF, 60 °C, 60%	73
(C ₅ H ₅) ₂ WH ₂	WCl ₆ + 4 NaC ₅ H ₅ + 2 NaBH ₄ → (C ₅ H ₅) ₂ WH ₂ + (C ₅ H ₅) ₂ + B ₂ H ₆ + 6 NaCl	THF, 65-75%	80-83
[CH ₃ (C ₅ H ₄) ₂ WH ₂	WCl ₆ + 4 Na(C ₅ H ₄ CH ₃) + 2 NaBH ₄ → [CH ₃ (C ₅ H ₄) ₂ WH ₂ + (C ₅ H ₄ CH ₃) + B ₂ H ₆ + 6 NaCl	THF, 65-75%	80-83
(C ₅ H ₅)W(CO) ₃ (CH ₃)	(C ₅ H ₅)W(CO) ₃ Na + CH ₃ I (excess) → (C ₅ H ₅)W(CO) ₃ (CH ₃) + NaI	40 °C, THF	79
W(butadiene) ₃	WCl ₄ + 2 Mg + butadiene (excess) → W(C ₄ H ₆) ₃ + 2 MgCl ₂	-20 °C, 30%	69,70
	co-condensation of tungsten atoms with butadiene (molar ratio 1:100)	77 K, 50-60%	68
W(methylvinyl- ketone) ₃	(CH ₃ CN) ₃ W(CO) ₃ + CH ₃ C(O)CH=CH ₂ (excess) → W(CH ₃ C(O)CH=CH ₂) ₃ + 3 CO + 3 CH ₃ CN	hexane, 69 °C, 60%	77
(C ₅ H ₅)WH(CO) ₃	(C ₅ H ₅)W(CO) ₃ Na + CH ₃ COOH → (C ₅ H ₅)WH(CO) ₃ + CH ₃ COONa	THF	84
(C ₇ H ₈)W(CO) ₃	(CH ₃ CN) ₃ W(CO) ₃ + C ₇ H ₈ → (C ₇ H ₈)W(CO) ₃ + 3 CH ₃ CN	hexane, 69 °C	84
(C ₈ H ₁₂)W(CO) ₄	(CH ₃ CN) ₃ W(CO) ₃ + C ₈ H ₁₂ → (C ₈ H ₁₂)W(CO) ₄	hexane, 69 °C	84

Table 3-4. Selected properties of tungsten precursors.

Compound	Melting point (°C)	Boiling point (°C)	Vapor pressure (Torr/°C)	Decomp. temp. (°C)	Ref.
WF ₆	2.0	17	880/21	>750	12,85
WCl ₆	275	346	7/200	≈600	12
WBr ₆	232	decomp.	—	≈600	43
W(CO) ₆	subl.	decomp.	1/65	230	60,61
W(C ₆ H ₆) ₂	decomp.	—	0.0001/40	60-160 (see text)	67
W(PF ₃) ₆	214	decomp.	subl. in vacuum at 40 °C	320	56
W(allyl) ₄	95 decomp.	—	subl. in vacuum at 60 °C	≈95	74
(C ₅ H ₅) ₂ WH ₂	189-190 (subl.)	decomp.	1/146	280-300	83,156
[CH ₃ (C ₅ H ₄) ₂ WH ₂	93-94 (subl.)	decomp.	1/117	≈200	83
(C ₅ H ₅)W(CO) ₃ (CH ₃)	145	decomp.	1/109	(≈300)	156
W(butadiene) ₃	decomp.	—	subl. at 0.001/50	130-135	68,75
W(methylinvinyl- ketone) ₃	136-139 (decomp.)	—	subl. at 0.1/80	136-139	77
(C ₅ H ₅) ₂ WH(CO) ₃	66-68	—	~0.1/65	—	84
(C ₇ H ₈) ₂ W(CO) ₃	—	—	~0.01/65	130	84
(1,5-COD)W(CO) ₄	—	—	~0.01/65	150	84

as volatile (m.p.: 5.2 °C; b.p.: 152.8 °C) or as thermally stable as SiF₄ and SiCl₄ and might introduce impurities into the deposited tungsten films. The most convenient reducing agent for WBr₆ is hydrogen.

3.2.3 Organometallic Precursors

Organometallic compounds are potential tungsten sources for CVD due to several favorable properties (see also Table 3-4):

- (1) Organometallic compounds generally show a *significantly higher volatility* compared to inorganic metal salts (with the exception of unusually volatile species such as WF₆). In most cases ambient temperatures are sufficient for high growth rates and wafer throughput.
- (2) The *relatively low thermal stability* of organometallic compounds makes it possible to deposit films at temperatures as low as 100-200 °C compared to H₂ or SiH₄ reduction of WF₆ which occurs at higher temperatures.
- (3) The *benign chemical reactivity* obtained through liberation of non-corrosive products is an advantage over the tungsten halides, WF₆ and WCl₆, for certain applications.⁵⁰⁻⁵⁴

Furthermore, the decomposition reactions of organometallic compounds can be kinetically rather than thermodynamically controlled which allows formation of meta-stable phases such as the β-tungsten phase, which is not accessible by other methods.^{7,12} However, the major drawback of organometallic CVD is incorporation of heteroatoms in metal films. New reaction pathways have to be found that will allow reaction of organometallic precursors with clean removal of the ligands. The feasibility of methods to overcome this problem has been demonstrated. (See Section 3.5 and other chapters of this book.) The following sections (3.2.3.1 - 3.2.3.11) discuss the properties of organometallic precursors for W (Fig. 3-1).

3.2.3.1 Hexakis(trifluorophosphine)tungsten [W(PF₃)₆]

The inorganic complex W(PF₃)₆ is obtained in the form of colorless crystals which sublime at 40 °C/0.001 torr. Decomposition of the vapor begins at 320 °C. A drawback is the difficult synthesis of this species which involves high-temperature and high-pressure techniques (see Table 3-3).^{55,56} A favorable property of W(PF₃)₆ is its stability in air. Furthermore the absence of oxygen and carbon atoms in this precursor avoids such heteroatom impurities in the deposits. The high vapor pressure of the ligand itself [760 torr at -101.8 (b.p.)] and its high stability allow the ligand to desorb from

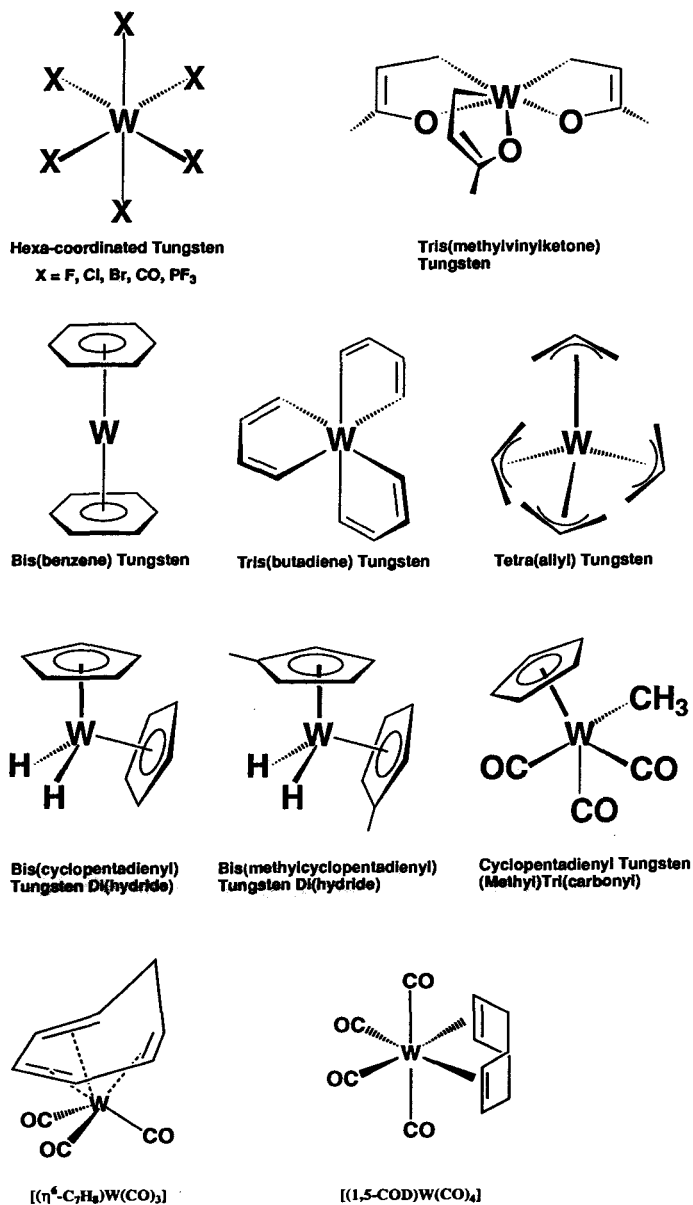
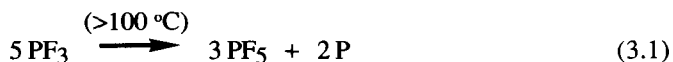
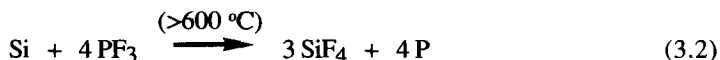


Figure 3-1. Structures of the tungsten complexes used for CVD.

the deposition surface without decomposition in some cases. However, free PF₃ can disproportionate before desorption according to Equation 3.1



which can lead to phosphorus impurities. This process is slow at 100 °C, but becomes important at higher temperatures. Another possible source for phosphorus contamination is the reaction of PF₃ with silicon:



This reaction becomes quantitative above 600 °C but at lower temperatures is slow. Nevertheless, even a small amount of phosphorus in the films^{57,58} is undesirable because it increases the resistivity of the deposited tungsten films.

3.2.3.2 Hexacarbonyltungsten [W(CO)₆]

Hexacarbonyltungsten is a white volatile solid whose vapor starts to decompose at about 230 °C and can be synthesized by reduction of the hexachloride with AlEt₃ in benzene while applying a CO pressure of 70 bar⁵⁹ (see Table 3-3). However, small amounts of impurities catalyze the decomposition at even low temperatures. At temperatures between 28 and 35 °C the vapor pressure follows the relation: $\log_{10}P = 12.094 - 4077/T$ (T in K, P in torr), and between 80 and 150 °C it follows the relation: $\log_{10}P = 11.523 - 3872/T$.^{41,42} Mass spectroscopic studies of the decomposition behavior of this precursor⁶⁰ revealed that the high impurity level found below 400 °C is due to the incomplete desorption of intermediate pyrolysis products from the substrate surface. At higher temperatures, the amount of carbon and oxygen impurities in the tungsten film decreases reaching a minimum at 600-700 °C. Above 700 °C the concentration of carbon and oxygen in the metal films depends on the CO decomposition reaction ($2 \text{ CO} \longrightarrow \text{CO}_2 + \text{C}$) and the interaction of CO and CO₂ with the film surface. This can lead to an increased impurity level in the metal films. Thermodynamic calculations confirmed these findings for the gas/surface interactions.^{61,62}

3.2.3.3 Bis(arene)tungsten Compounds

Bis-arene compounds of tungsten are green to dark green solids which are extremely oxygen and moisture sensitive and start to thermally decompose in vacuum at 60 °C forming metal mirrors. Solution synthesis gives extremely low yields (see Table 3-3).⁶³ However, a more effective synthesis is the co-condensation of metal vapor with an excess of arene at -196 °C.^{64,65} For W(η⁶-C₆H₆)₂, the relation of vapor pressure to temperature follows the equation $\log_{10}P = 14.41 - 6307.8/T$ (T in K; temperature range

40-110 °C), which gives a vapor pressure of 0.0001 torr at 60 °C and a ΔH_{subl} of 120.5 kJ/mol (see also Table 3-5). The presence of one alkyl substituent attached to the aromatic ligand, e.g., methyl, lowers the m.p. to almost room temperature (40-42 °C). This effect is independent of the nature of the alkyl group. The boiling points, however, do not change significantly compared to the unsubstituted bis-arene compounds.^{66,67}

Table 3-5. Comparison of vaporization energies of various bis-arene group six transition metal compounds and constants for vapor pressure determination.^{66,67}

$\log_{10} P = A - B/T$ (T in K; P in torr)				
Compound	A	B	ΔH_{subl} [kJ/mol]	ΔH_{vapor} [kJ/mol]
Cr(C ₆ H ₆) ₂	10.32	4265.7	81.6	—
Mo(C ₆ H ₆) ₂	11.68	4946.2	94.6	—
W(C ₆ H ₆) ₂	14.41	6307.8	120.5	—
Cr(C ₆ H ₆)(C ₆ H ₅ CH ₃)	10.09	3927.7	—	—
Mo(C ₆ H ₆)(C ₆ H ₅ CH ₃)	9.85	3919.0	—	—
W(C ₆ H ₆)(C ₆ H ₅ CH ₃)	9.40	3910.0	—	—
W(C ₆ H ₆)(C ₆ H ₅ -ethyl)	9.56	4034.4	—	77.0
W(C ₆ H ₅ -ethyl) ₂	9.92	4283.2	—	82.0
W(C ₆ H ₆)(C ₆ H ₅ -propyl)	9.76	4158.6	—	79.5
W(C ₆ H ₅ -propyl) ₂	10.27	4532.0	—	86.6

3.2.3.4 Tris(butadiene)tungsten [W(η^4 -C₄H₆)₃]

Tris(butadiene)tungsten is a white solid which decomposes at 135 °C via loss of all three ligands. It is air stable for more than one week and can be sublimed in vacuum at 0.001 torr and 50 °C. It is synthesized by reducing tungsten tetrachloride with magnesium in the presence of excess butadiene.⁶⁸⁻⁷¹

3.2.3.5 Tetraallyltungsten [W(η^3 -C₃H₅)₄]

Tetraallyltungsten is a white, moderately air sensitive, and volatile solid which can be easily sublimed in vacuum at 60 °C. An improvement over the original⁷² synthesis is given by Benn et al.⁷³ by reducing tungsten hexaphenolate with an allyl Grignard reagent (see Table 3-3). Thermogravimetric analysis (TGA) using a 5:95 mixture of hydrogen and argon showed a weight loss corresponding to loss of all allyl groups;

propane was identified by gas chromatography/mass spectroscopy (GC/MS) as the main volatile product. Incomplete loss of the ligands was observed under an atmosphere of nitrogen.⁷⁴⁻⁷⁶

3.2.3.6 Tris(methylvinylketone)tungsten $\{W[CH_3C(O)CH=CH_2]_3\}$

This compound is obtained in relatively low yield from the reaction of $(CH_3CN)_3W(CO)_3$ with methylvinylketone in boiling hexane solution (see Table 3-3) as a light yellow, *air stable*, and very volatile solid which can be easily sublimed in vacuum (0.1 torr) at 80 °C.⁷⁷ X-ray diffraction shows the molecule adopts a rare trigonal prismatic geometry. Mass spectroscopic investigations demonstrated the facile loss of one ligand as an initial process, whereas the further fragmentation is more complex.⁷⁸ The thermogravimetric analysis (TGA) revealed rapid decomposition at 140 °C with complete loss of all three ligands.⁷¹

3.2.3.7 Cyclopentadienylmethyltricarbonyltungsten [[η^5 -C₅H₅)W(CO)₃CH₃]

This precursor is a yellow, *air stable*, crystalline solid at room temperature and melts at 145 °C without decomposition. The compound is very soluble in all common organic solvents and may remain stable for several days. It is, however, insoluble in and unaffected by water but is attacked by acids and bases. The synthesis involves two steps (see Table 3-3) but is easily undertaken and is almost quantitative. The compound $(\eta^5\text{-C}_5\text{H}_5)\text{W(CO)}_3\text{CH}_3$ sublimes readily in vacuum at 25-50 °C. Showing a vapor pressure of 1 torr at 109 °C, the volatility of $(\eta^5\text{-C}_5\text{H}_5)\text{W(CO)}_3\text{CH}_3$ is about one order of magnitude lower than that of $W(CO)_6$. In the temperature range between 60 and 140 °C, the vapor pressure of $(\eta^5\text{-C}_5\text{H}_5)\text{W(CO)}_3\text{CH}_3$ follows the relation: $\log_{10}P = 10.861 - 4125.8/T$ (T in K, P in torr).⁷⁹

3.2.3.8 Bis(cyclopentadienyl)dihydridotungsten [[η^5 -C₅H₅)₂WH₂]

This compound is a very air sensitive, yellow crystalline solid. It melts at 189-190 °C in a closed capillary accompanied by sublimation (DSC data). The compound is extremely soluble in all common organic solvents, but insoluble in and unaffected by water. The synthesis involves several steps (see Table 3-3) and has to be carried out under inert atmospheric conditions.⁸⁰⁻⁸³ The compound $(\eta^5\text{-C}_5\text{H}_5)_2\text{WH}_2$ sublimes in vacuo at 100-120 °C. With a vapor pressure of 1 torr at 146 °C, its volatility is less than two orders of magnitude lower than that of $W(CO)_6$. At temperatures between 100 and 160 °C, the vapor pressure of $(\eta^5\text{-CH}_3\text{C}_5\text{H}_4)_2\text{WH}_2$ follows the relation: $\log_{10}P = 10.398 - 4335.9/T$ (T in K, P in torr).⁸³

3.2.3.9 Bis(methylcyclopentadienyl)dihydridotungsten $[(\eta^5\text{-CH}_3\text{C}_5\text{H}_4)_2\text{WH}_2]$

Like $(\eta^5\text{-C}_5\text{H}_5)_2\text{WH}_2$, this tungsten compound is also a pale yellow, air-sensitive, crystalline solid. It melts at 93-94 °C in a closed capillary accompanied by sublimation. Thermogravimetric analysis carried out under a stream of nitrogen showed that $(\eta^5\text{-CH}_3\text{C}_5\text{H}_4)_2\text{WH}_2$ starts to decompose at 195-200 °C. The residue consists of tungsten and carbon. While extremely soluble in all common organic solvents, $(\eta^5\text{-CH}_3\text{C}_5\text{H}_4)_2\text{WH}_2$ is insoluble in and unaffected by water. The synthesis involves several steps (see Table 3-3) and has to be carried out under inert atmospheric conditions. The compound $(\eta^5\text{-CH}_3\text{C}_5\text{H}_4)_2\text{WH}_2$ sublimes easily in vacuo at 80 °C and shows a vapor pressure of 1 torr at 117 °C. In the temperature range of 80 to 120 °C the vapor pressure of $(\eta^5\text{-CH}_3\text{C}_5\text{H}_4)_2\text{WH}_2$ follows the relation: $\log_{10}P = 11.720 - 4572/T$ (T in K, P in torr).⁸³

3.2.3.10 Cyclopentadienylhydridotricarbonyltungsten $[\text{HW}(\eta^5\text{-C}_5\text{H}_5)(\text{CO})_3]$

This precursor is a yellow, air sensitive, crystalline solid at room temperature and melts at 66-68 °C without decomposition. This compound sublimes readily in vacuum at about 60 °C. The volatility of $\text{HW}(\eta^5\text{-C}_5\text{H}_5)(\text{CO})_3$ is about one order of magnitude lower than that of $\text{W}(\text{CO})_6$. The synthesis has to be carried out under inert atmospheric conditions (see Table 3-3).^{79,84}

3.2.3.11 Cycloheptatrienetricarbonyltungsten $[(\eta^6\text{-C}_7\text{H}_8)\text{W}(\text{CO})_3]$ and 1,5-Cyclooctadienetetracarbonyltungsten $[(1,5\text{-COD})\text{W}(\text{CO})_4]$

The compounds $(\eta^6\text{-C}_7\text{H}_8)\text{W}(\text{CO})_3$ ($\text{C}_7\text{H}_8 = 1,3,5\text{-cycloheptatriene}$) and $(1,5\text{-COD})\text{W}(\text{CO})_4$ ($1,5\text{-COD} = 1,5\text{-cyclooctadiene}$) were obtained from the reactions of $(\text{CH}_3\text{CN})_3\text{W}(\text{CO})_3$ or $(\text{C}_2\text{H}_5\text{CN})_3\text{W}(\text{CO})_3$ with cycloheptatriene and cyclooctadiene, respectively, in refluxing hexane (see Table 3-3).⁸⁴ The compound $(\eta^6\text{-C}_7\text{H}_8)\text{W}(\text{CO})_3$ is a bright red, air-stable crystalline solid which sublimes readily in vacuum at 80 °C and decomposes at about 130 °C. The compound $(1,5\text{-COD})\text{W}(\text{CO})_4$ is a yellow, air-stable crystalline solid which sublimes readily in vacuum at 90 °C and decomposes at about 150 °C. The volatilities of these two precursors are about two orders of magnitude lower than that of $\text{W}(\text{CO})_6$.

3.3 Chemical Vapor Deposition (CVD)

3.3.1 Tungsten Halides as CVD Precursors

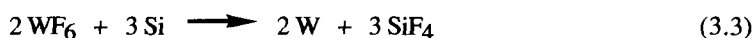
3.3.1.1 Tungsten Hexafluoride (WF₆)

Although thermal decomposition of WF₆ without any reducing agents can be achieved above 750 °C,⁸⁵ most methods of tungsten CVD involve reducing agents such as H₂, Si, SiH₄, Si₂H₆, B₂H₆, PH₃,^{45,46} SiH₂Cl₂,⁴⁷ and GeH₄^{48,49} to obtain much lower deposition temperatures. Among them, H₂, Si, and SiH₄ are the most common in IC metallization processes.

Mechanistic and Kinetic Observations

The WF₆/Si System

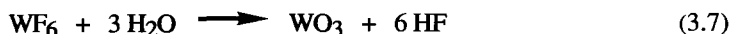
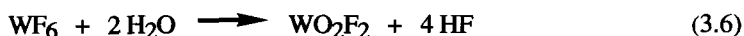
The reduction of WF₆ by a silicon substrate (displacement reaction⁸⁶) allows selective tungsten deposition in the exposed contact region of highly doped silicon without deposition on insulators such as SiO₂ or Si₃N₄. This reaction involves a solid-phase reactant and as a result is highly sensitive to the substrate pretreatment and the amount of native oxide on the silicon surface. It generates SiF₄ below 400 °C (Eq. 3.3) and SiF₂ above 400 °C (Eq. 3.4) thus consuming twice as much silicon as shown in Equation 3.3.⁸⁷⁻⁸⁹



These reactions are extremely fast and stop within a few seconds when a critical thickness of the deposited tungsten layer is reached. Surprisingly, the values reported in the literature for the critical thickness vary significantly. Values from 10 nm⁹⁰ to 15 μm⁹¹ have been reported. The mechanism of self-limitation is not fully understood because the reactor setup, the pre-treatment of the silicon surface, and the characteristics of the native surface oxide layer play critical roles in this process. One possible explanation is that tungsten is an excellent diffusion barrier for silicon; therefore, a continuous layer of tungsten of a certain thickness on the silicon substrate will inhibit silicon diffusion to the tungsten surface and stop penetration of WF₆ to the Si/W interface. Kuiper et al.⁸⁹ and Kobayashi et al.⁹¹ explained the discrepancy in critical thicknesses by noting that the thicker tungsten films are porous and have a density of

only $\approx 10 \text{ g/cm}^3$ (bulk tungsten: 19.3 g/cm^3 at 20°C) caused by extended formation of channels in the deposits and in the silicon substrate. Such channels prolong the diffusion process and therefore the tungsten deposition. The formation of these channels is enhanced by the reduction process because three to six Si atoms (Si: $12.1 \text{ cm}^3/\text{mol}$) on the surface are replaced by only two W atoms (W: $9.53 \text{ cm}^3/\text{mol}$) which leaves twice as much space as the generated tungsten atoms can fill. This makes the tungsten films look like "Swiss cheese" and permits silicon migration to the surface where deposition will take place preferentially forming the aforementioned channels or column-like structure.⁹² However, after a relatively short time, the channels become plugged and the process comes to a halt.

The closing of the channels and the formation of a continuous solid tungsten barrier against the silicon diffusion seems to be influenced by two effects: (1) If the silicon surface is not perfectly clean, WF_6 can penetrate a freshly built native oxide layer through pinholes and weak spots and tungsten will grow under the protective SiO_2 layer deep into the silicon films. This leads to the formation of thick tungsten films, much thicker than expected from a self-limiting process.⁹²⁻⁹⁷ Therefore, very thin and smooth tungsten layers are generated only if the silicon surface is very clean (no oxide layer) or is covered with a nearly perfect oxide layer with very few pinholes. Less clean conditions promote the formation of thicker films. (2) Hitchman et al.⁹⁴ and others^{31,92,95-97} point out that traces of water also influence the thickness of the tungsten deposits. Small amounts of water react instantly with WF_6 to form oxyhalides and HF:



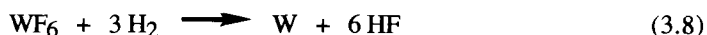
The HF generated can attack the SiO_2 and the tungsten layer leading to the formation of weak spots and pinholes and re-exposing the silicon surface. This causes encroachment problems where tungsten deposition starts to occur at the silicon-silicon dioxide interface. The generation of HF is also related to formation of deep channels in the silicon substrate. These processes cause rough interfaces and the formation of wormholes^{50,98-100} leading to high contact resistance and high junction leakage currents.

A possible solution to this problem could be the addition of SiF_4 to the system to drive reaction 3.3 to the left. However, this also reduces the growth rate significantly.⁹⁸ The encroachment and worm-hole formation problem has been solved by using silane reduction which prevents formation of HF by providing a different reaction pathway to

avoid the silicon reactions 3.3 and 3.4 almost completely (see following sections).^{48,88,101-106}

The WF₆/H₂ System

Tungsten hexafluoride can be reduced with hydrogen at temperatures between 300 and 800 °C, and this process has been used in the past for metallurgical coatings. This deposition route has attracted attention for microelectronic metallization because of the possibility of selective deposition. The hydrogen reduction of WF₆ is endothermic and is entropy driven. The overall reaction is described by Equation 3.8.^{86,107,108}



The reaction product HF can cause encroachment and worm-hole formation. For these reasons and because of the poor adhesion of tungsten on the native silicon dioxide present on Si, tungsten is not deposited directly on silicon. The highly doped regions of the source and drain are usually covered with a bilayer of material where one layer of material provides an ohmic contact with silicon and the other layer acts as an adhesion promoter for tungsten.

Deposition Rate Determinations for the WF₆/H₂ System

Although there are extensive reaction kinetic studies that cover a wide range of temperatures and pressures, few studies have examined the reaction mechanism of tungsten deposition. The reaction orders have been evaluated and are 0 and 1/2 for WF₆ and H₂, respectively.

$$\text{growth rate} \propto P(\text{WF}_6)^0 P(\text{H}_2)^{1/2} \quad (3.9)$$

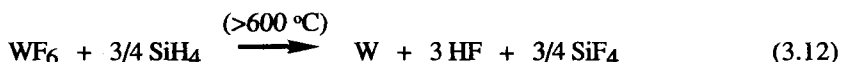
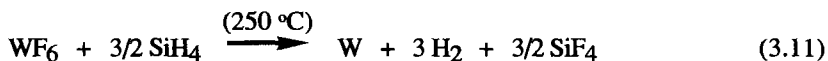
This reaction order has been verified by numerous workers for low-pressure CVD conditions where the growth rate is not transport-limited.^{86,109-111} This reaction has an apparent activation energy of ~16 kcal/mol.¹¹² However, a different reaction rate was observed for a hot-wall reactor where the feed gases were heated significantly by the substrate (Eq. 3.10). The reaction order was two for each reagent probably because of significant homogeneous gas-phase reactions. This kinetic regime has not been studied in detail.

$$\text{growth rate} \propto P(\text{WF}_6)^2 P(\text{H}_2)^2 \quad (3.10)$$

The WF₆/SiH₄ System

Tungsten deposition by silane reduction^{48,88,101-106} has attracted attention because of the higher deposition rates of up to ~ 1 $\mu\text{m}/\text{min}$. This approach prevents formation of wormholes and encroachment and suppresses silicon substrate consumption. Depending on the SiH₄/WF₆ ratio and deposition temperature, either tungsten or tungsten silicide can be deposited by CVD. The ratio is also critical in determining whether deposition is blanket or selective as well as the phase of the deposited tungsten film. For SiH₄/WF₆ ratios up to 1.6, tungsten deposition is selective while at higher ratios deposition is blanket. The α -tungsten phase is deposited for SiH₄/WF₆ ratios typically less than 1 while β -tungsten is deposited at the higher ratio of 1 to 3 (see Table 3-7). The amount of silicon incorporation increases with deposition temperature resulting in significantly higher film resistivities and eventual deposition of tungsten silicide.

There are a number of possible reaction pathways for tungsten deposition by silane reduction with the most probable pathways with SiF₄, H₂, and HF as byproducts represented in Equations 3.11 and 3.12.



Yu and Eldridge^{87,88} and Sivaram et al.¹¹³ studied the surface reactions of WF₆/SiH₄ and concluded that formation of H₂ is the dominant reaction pathway (Eq. 3.11) for tungsten deposition. The other reaction pathway leading to formation of HF was only observed at temperatures above 600 °C. This is contrary to the equilibrium calculations which suggest HF as the major reaction byproduct rather than hydrogen indicating that silane reduction takes place far from equilibrium. Yu and Eldridge also identified SiF₄ as another byproduct with very little SiF₂.

As mentioned before, the WF₆/H₂ reaction is relatively slow and is kinetically bypassed because the WF₆/SiH₄ reaction is faster. Studies of this process have been difficult because of the changes in composition of the deposited films over the pressure and temperature range investigated. In the system SiH₄/WF₆, two deposition processes (Si and W) compete with each other and the products vary with conditions. Schmitz et al. studied the growth rate of Si and W separately^{114,115} to achieve a reliable result. He and Rosler et al.¹⁰¹ found independently that the growth rate for the tungsten deposition for reactant ratios of 0.5-1.3 (SiH₄/WF₆) follows the rate law:

$$\text{growth rate} \propto P(\text{WF}_6)^0 P(\text{SiH}_4)^{1/2} \quad (3.13)$$

However, the reaction mechanism is much more complicated than suggested by this equation. Attempts to obtain an activation energy for this process did not give reliable results. The deposition rate had only a weak dependence on temperature suggesting that the deposition process is mass transport limited rather than kinetically controlled making it invalid for use of mechanistic determination.

Silane reduction has some advantages over hydrogen reduction. The most important advantage is a higher deposition rate by at least an order of magnitude up to $\sim 1 \mu\text{m}/\text{min}$ using cold-wall LPCVD. The films are also smoother for silane reduction compared to hydrogen reduction. Furthermore, the adhesion of tungsten deposited by silane reduction is good on Si, TiW, and TiN. However, it is difficult to control gas-phase reactions between WF_6 and SiH_4 due to their high reactivity even at room temperature. As a result, silane reduction is used only for a short duration to initiate tungsten nucleation followed by the hydrogen reduction process in the production of blanket tungsten films.

The use of disilane Si_2H_6 has also been explored for WF_6 reduction. Disilane reduces the tungsten deposition temperature to nearly 150°C . However, due to the higher reactivity of disilane with WF_6 , the deposited tungsten is not dense. The higher order silanes are even more reactive leading to discontinuous film deposition. A major processing difficulty using silane compounds as reducing agents is their violent reaction with WF_6 which can lead to tremendous explosions. This can be avoided by using a low total pressure, low partial pressure of the silane, and a relatively fast flow rate in the deposition experiments.^{101,114,115}

Mechanisms for Loss of Selectivity

Selective tungsten CVD is an attractive method for via filling. Use of selective CVD reduces the number of processing steps for via filling compared to etching strategies by eliminating patterning steps which are expensive and cumbersome. The origin of selective deposition on conductive surfaces versus silicon dioxide surfaces is partially due to the inability of SiO_2 to reduce WF_6 and partially due to the inability of H_2 to chemisorb on the SiO_2 surface.^{51,52,116-118}

The use of selective tungsten CVD, however, has not been widespread because of difficulties in reliably suppressing tungsten nucleation on the silicon dioxide surface in a manufacturing environment.¹¹⁹⁻¹²⁴ Both extrinsic and intrinsic reasons exist for the loss of selectivity. The extrinsic factors are material- and process-specific issues which are dependent on the reactor design and material selection. Intrinsic reasons are dependent on the CVD chemistry which cannot be easily controlled.

A material-specific issue is the purity of the feed gases; specifically, the purity of the feed gases at the point-of-use. Currently, very high-purity WF_6 (at least 99.999%) is

commercially available. However, the purity of the feed gases may be affected by the delivery system which can result in degraded selectivity. For this reason, the gas delivery system should minimize bends in the gas lines to avoid dead space, provide bakeable valves to remove water vapor, include point-of-use filtration to remove particles and water vapor, and an independent pump for the gas lines to prevent cross contamination.

The most important process specific issues are the removal of organic, inorganic, and metallic impurities from the silicon dioxide surface which are left during photoresist stripping after lithographic steps. Impurities on the silicon dioxide surface are potentially sites of tungsten nucleation and can contribute to loss of selectivity; therefore, an in situ plasma clean is desirable to decontaminate the silicon dioxide surface with minimum exposure to the ambient atmosphere before selective tungsten CVD.

The reactor design and choice of reactor material are also important for selective tungsten CVD. Although WF_6 and H_2 do not react in the gas phase at room temperature, WF_6 and SiH_4 undergo extensive gas-phase reactions, even at room temperature, that lead to formation of highly reactive reaction intermediates and particle formation. For this reason it is difficult to maintain selectivity with silane reduction compared to hydrogen reduction. This problem can be minimized by controlling the mixing of the two gases above the wafer surface. The use of cold-wall reactors and coating the reactor-walls with an inert material such as Teflon are also effective because they reduce the concentration of reaction intermediates and products (by suppressing reaction on the reactor walls) that can degrade selectivity.

The intrinsic reasons for loss of selectivity are the volatile products formed during tungsten CVD which can adsorb and decompose on the silicon dioxide surface to initiate tungsten nucleation. This is referred to as the "proximity effect" where the rate of nucleation of tungsten on the oxide surface is affected by the proximity of the tungsten surface. A number of species such as HF , SiF_4 , SiF_x ($x < 4$), and WF_x ($x < 6$) are possibly responsible for the loss of selectivity.

Hydrogen fluoride is the main reaction product in hydrogen reduction and has been studied as a possible candidate for loss of selectivity by introducing HF to the gas stream. However, all attempts to accelerate selectivity loss have been unfruitful, and it is believed that HF is not responsible for loss of selectivity.

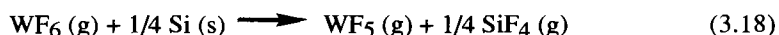
Tungsten subfluorides WF_x ($x < 6$) have been identified as the primary species responsible for loss of selectivity.^{119,120} Selectivity loss is initiated by formation of tungsten pentafluoride (WF_5) by reaction of WF_6 with the deposited tungsten (Eq. 3.14). The WF_5 can diffuse through the gas phase to neighboring silicon dioxide surfaces or to the reactor walls, or can be pumped out of the reactor. On the silicon dioxide surface, WF_5 disproportionates even at low temperatures to form WF_6 and non-volatile WF_4 (Eq. 3.16). The WF_4 undergoes further disproportionation (Eq. 3.17) above 200°C to form tungsten nuclei. The net result of these reactions is the transport of tungsten

atoms from the deposition surface to the silicon dioxide surface. This intrinsic tungsten transport is actually an etching reaction initiated by formation of WF_5 .



This mechanism for loss of selectivity cannot be controlled unless the reactivity of WF_5 with the silicon dioxide surface is suppressed. The dependence of the nature of the silicon dioxide surface on loss of selectivity has been studied. Of the various silicon dioxide surfaces, phosphorus-doped SiO_2 deposited by CVD showed significantly lower numbers of tungsten nuclei while metal nitrides showed greater numbers of nuclei.¹²¹⁻¹²³ The improved selectivity for doped SiO_2 was explained by the presence of phosphorus which interrupted nucleation by gettering "tungsten subfluorides." Wafer treatment with phosphoric acid has also been shown to improve selectivity on various insulator surfaces.¹²⁴

Selectivity loss in the presence of exposed silicon surfaces is worse than in the presence of tungsten surfaces. However, it is not understood whether this is due to the formation of silicon subfluorides which enhance the loss in selectivity or increased production of tungsten subfluorides in the presence of elemental silicon. Although introduction of silicon subfluorides during Si reduction leads to blanket tungsten deposition, it is unlikely that silicon subfluorides would be formed at typical CVD conditions which should result in complete formation of silicon tetrafluoride. Increased production of WF_5 directly at the silicon surface is represented in Equation 3.18 and is more plausible.



The loss of selectivity is then by the pathway described above. However, the species responsible for loss of selectivity has not been clearly identified for the case of silicon reduction.

Selective tungsten deposition using silane reduction has been studied by a number of groups but has been difficult to carry out reproducibly. The reasons for the loss of selectivity have not been studied for the silane process. The study is complicated because of the extensive gas-phase reaction between WF_6 and SiH_4 even at room temperature which can contribute to the loss of selectivity. The gas-phase reaction can be suppressed

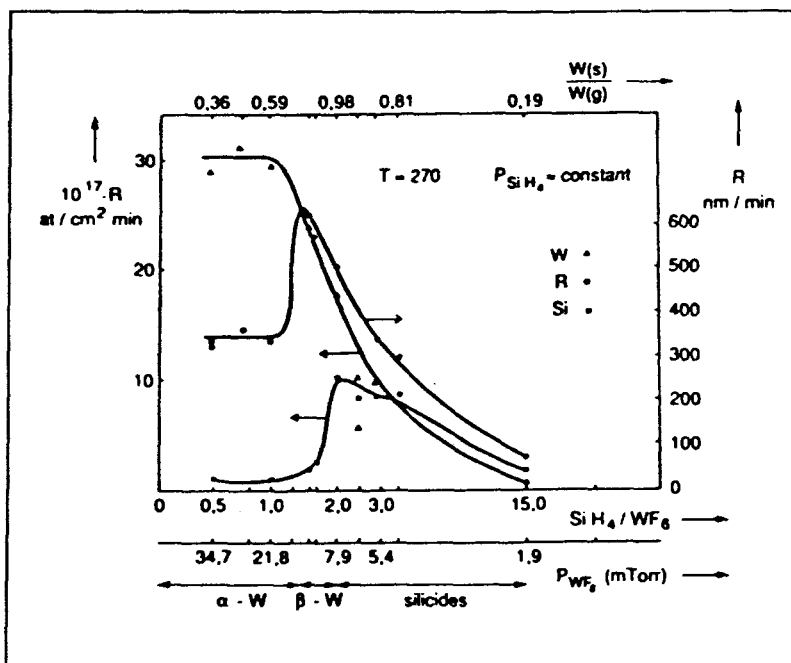


Figure 3-2. Film growth (R in nm/min) and W and Si deposition rate (in $\text{atoms}/\text{cm}^2 \text{sec.}$). $W(s)/W(g)$ is the conversion degree of WF_6 . (From¹¹⁴ reprinted with permission).

by using lower pressure, lower silane flow rates, and a relatively high overall flow rate (see Fig. 3-2).^{101,114,115}

Deposition Experiments

The System WF_6/Si and WF_6/H_2

Tungsten deposition using WF_6 has been summarized in Table 3-6. Dass et al.¹²⁵ used a commercial cold-wall batch reactor to deposit tungsten at rates of $540 \text{ \AA}/\text{min}$ at 400°C using a total pressure of 0.4 torr and WF_6 to H_2 flow rate ratio of 1:5. Beside the main α -tungsten phase, a second phase determined as $\text{WO}_{2.9}$ ($\text{W}_{20}\text{O}_{58}$) was evenly distributed throughout the film which had a resistivity of $\sim 8 \mu\Omega\text{cm}$.

Low-pressure CVD of tungsten on Si substrates was investigated by Saraswat et al.¹⁵ using a conventional hot-wall reactor (275 – 450°C deposition temperature, 0.25 – 0.5 torr total pressure). The deposited tungsten film was self-limiting with growth rates

Table 3-6. Comparison of deposition conditions (thermal) and film properties using WF₆ as precursors.

Growth Rate ($\mu\text{m}/\text{h}$)	Deposition Temperature ($^{\circ}\text{C}$)	Carrier gas	Reactor Pressure (torr)	Substrate	Film Resistivity and Purity	Ref.
---	420-800	H ₂ , Ar, He	1-10, 760	Si, SiO ₂ , Sapphire	6-15 $\mu\Omega\text{cm}$, α -W, 100% W	127
---	260-400	H ₂ /Ar	0.1-1	Si, SiO ₂ , TaSi ₂	10-15 $\mu\Omega\text{cm}$	97
---	288-403	WF ₆ :H ₂ , 1:15	0.2-10; 760	Si (100)	6 $\mu\Omega\text{cm}$	109
---	300	SiH ₄	UHV	Si (100)	30 $\mu\Omega\text{cm}$	87
90	250-550	SiH ₄	vacuum	Si (100)	7.5-15 $\mu\Omega\text{cm}$, low Si %	101
36	500-570	H ₂ /Ar	3.5	GaAs	50 $\mu\Omega\text{cm}$, 2% C, O	129
14	350-550	H ₂ /Ar	0.5-4.5	InP	55 $\mu\Omega\text{cm}$	130
---	<400	vacuum, GeH ₄	1.5	Si, SiO ₂	10-15% Ge, β -W, 200 $\mu\Omega\text{cm}$	105
---	>500	vacuum, GeH ₄	1.5	Si, SiO ₂	1% Ge, α -W, 10 $\mu\Omega\text{cm}$	105

independent of deposition time, temperature, and precursor concentration in the gas phase. The growth process stopped after only a few seconds. Tungsten was also selectively deposited on Si by hydrogen reduction at deposition rates of 30-40 Å/min which increased with temperature. The tungsten formed low-resistance ohmic contacts with both heavily doped n^+ and p^+ shallow (0.3 μm) junctions. The tungsten also provided an effective diffusion barrier between Si and Al. Schottky contacts on N-type silicon exhibited excellent I-V characteristics with a barrier height of 0.62 eV.

Metz et al.¹²⁶ used both Si and H_2 reduction processes to continue tungsten deposition on silicon substrates to overcome the Si/WF_6 self-limiting reaction. The experiments were carried out in a conventional hot-wall reactor at low pressure and 300 °C. In the first step (less than 1 min duration) the silicon substrate was exposed only to WF_6 resulting in formation of a 40 nm thick tungsten film. Hydrogen was then introduced into the gas stream to continue tungsten growth until a thickness of 1200 Å was reached. Conformal step coverage and excellent selectivity were achieved. Although, less than 1 at.% oxygen and no fluorine could be detected in the deposits, the resistivity was not lower than 18 $\mu\Omega\text{cm}$.

Further investigations^{29,52,86,92,107,109,110,127} of the WF_6/H_2 system in the pressure range of 0.0001 torr to 65 ktorr and at temperatures between 300 and 800 °C confirmed the results described above. Adjusting the deposition parameters (temperature, pressure, flow rate, H_2 to WF_6 ratio), depending on the type of reactor used, hot-wall or cold-wall (on silicon substrates), leads in most cases to pure tungsten films (94-100 at.% W) with low resistivities (8-18 $\mu\Omega\text{cm}$), conformal step coverage, and excellent selectivity. Normally α -tungsten is the main phase in these films. Under certain conditions, however, deposition of the high-resistivity β -tungsten phase was also observed.²⁹

The System WF_6/SiH_4

As shown in section 3.2.1, the chemistry of this system is complicated and was only used for blanket tungsten deposition at 400-500 °C¹²⁸ until several groups^{101,103} demonstrated selective tungsten deposition at temperatures as low as 270 °C. Foster et al.¹⁰² and Kusumato et al.¹⁰³ obtained high deposition rates of 0.5 - 1 $\mu\text{m}/\text{min}$ and were able to completely suppress encroachment processes.

Yu et al. and Yu and Eldridge reported the growth of mirror-like tungsten films at 0.05 torr and 300 °C using silane reduction.^{87,88} The films exhibited poor adhesion on silicon dioxide but adhesion was greatly improved by initial deposition at 500 °C (which resulted in deposition of tungsten silicide) followed by tungsten deposition at 300 °C. Thick tungsten films with resistivity of $\sim 30 \mu\Omega\text{cm}$ were deposited.

Since the silane reduction proceeds far from thermodynamic equilibrium, the composition and morphology of the films were highly dependent on the gas-phase

Table 3-7. Dependence of film properties on the SiH_4/WF_6 ratio in the gas phase.¹¹⁴

SiH_4/WF_6 ratio	Predicted W phase	Observed W phase	Film composition (at.%)			Film Resistivity ($\mu\Omega\text{cm}$)
			F	O	Si	
0.55	$\alpha\text{-W}$	$\alpha\text{-W}$	<1	3	3	94
1.1	$\alpha\text{-W}$	$\alpha\text{-W}$	<1	2	3	95
1.3	$\alpha\text{-W}$	$\alpha\text{-W}$	<1	2	3	93
1.5	$\alpha\text{-W}$	$\beta\text{-W} + \text{amorph.}$	<1	6	7	87
1.6	$\alpha\text{-W}$	$\beta\text{-W} + \text{amorph.}$	<1	9	9	82
2.0	$\text{W}_5\text{Si}_3 + \alpha\text{-W}$	$\alpha\text{-W} + \text{amorph.}$	<1	<1	35	63
2.5	$\text{W}_5\text{Si}_3 + \text{WSi}_2$	amorphous	<1	<1	45	53
3.0	$\text{W}_5\text{Si}_3 + \text{WSi}_2$	amorphous	<1	<1	47	51
3.8	$\text{WSi}_2 (+ \text{W}_5\text{Si}_3)$	amorphous	<1	<1	49	49
15.0	$\text{WSi}_2 + \text{Si}$	no reflections	<1	<1	55	43
						250

--- Not measured

Deposition temperature: 270 °C; total pressure: 2 torr; data compiled from reference¹¹⁴

composition. Schmitz et al.¹¹⁴ investigated this dependence at 270 °C at a total pressure of 0.2 torr over the SiH₄/WF₆ ratio of 0.55-15. The α -tungsten phase with resistivities of $\sim 19 \mu\Omega\text{cm}$ was deposited for SiH₄/WF₆ ratios of less than 1.3. For SiH₄/WF₆ ratios of 1.5-3.0, β -W (resistivity: 390-430 $\mu\Omega\text{cm}$) was deposited as the main phase (see Table 3-7; Fig. 3-2). At higher ratios, diffraction patterns started to weaken until a ratio of 15 where no more peaks were observed by X-ray diffraction (XRD). At this temperature (270 °C) only a microcrystalline silicide phase was observed. However, annealing under vacuum at 800 °C converted the metastable β -tungsten to α -W²⁷⁻³⁰ with appearance of the tungsten silicide phase W₅Si₃ on the XRD pattern. The elemental analysis of the tungsten films showed α -tungsten films with minor amounts of Si (3 at.%) and oxygen (2-3 at.%). Films with the β -W phase contained up to 9 at.% Si and oxygen. These impurities stabilize the β -phase as shown by several authors.^{31,32,35} In the range 3.0-15.0, oxygen was not detected while the Si content increased up to 55 at.%. Fluorine contamination was always below the detection limits (<1 at.%). Selectivity was obtained in a narrow temperature range of 270-320 °C. At lower temperatures no deposition occurred while above 350 °C selectivity was completely lost.

Tungsten Deposition on GaAs and InP Using Rapid Thermal Low-pressure Chemical Vapor Deposition

Despite the expected severe encroachment problem for the WF₆/H₂ system with respect to GaAs, successful deposition of tungsten on GaAs and InP was reported by Katz et al. in 1992.¹²⁹⁻¹³¹ To avoid long exposure times of the III/V-compound semiconductor substrates to the very corrosive WF₆/H₂ atmosphere, a new deposition technique, rapid thermal low-pressure chemical vapor deposition (RTCVD), was developed to deposit tungsten on GaAs and InP. The substrate was loaded at room temperature into the reactor and flushed with the reaction gas mixture for 2 min before it was flash-heated to the deposition temperature of 500-570 °C for 20 to 30 sec. The pressure in the system was kept at 4-5.5 torr and a ratio of the WF₆/H₂/Ar gas mixture of 1:30:1 was maintained. In the short deposition periods, 200 nm thick polycrystalline tungsten films were deposited with very fine grain structure, carbon and oxygen impurities of less than 2 at.%, and a resistivity of $\sim 560 \mu\Omega\text{cm}$. In situ annealing for 30 sec at 300-600 °C lowered the resistivity to $\sim 50 \mu\Omega\text{cm}$. The annealing led to an interface reaction which penetrated 500 Å into the GaAs substrate, but did not result in incorporation of Ga or As in the tungsten films. The films showed excellent morphologies with sharp interfaces. Under the same conditions, similar results were obtained for InP substrates.¹²⁹⁻¹³¹

The System WF₆/GeH₄

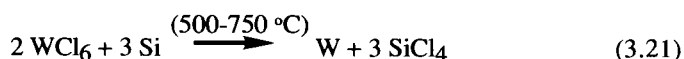
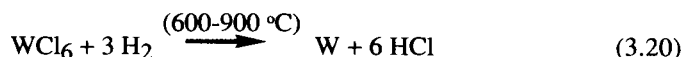
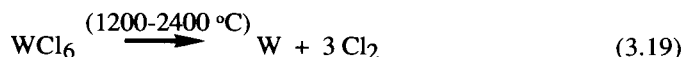
Van der Jeugd^{48,49} studied WF₆ reduction with GeH₄ at temperatures between 300 and 600 °C using a conventional cold-wall reactor. Thermodynamic calculations suggest

that tungsten deposition should be possible under similar conditions as those for the SiH_4/WF_6 reduction process.⁴⁸ Higher resistivity ($\sim 200 \mu\Omega\text{cm}$) β -tungsten was deposited at temperatures between 300 and 400 °C stabilized by a significant amount of Ge (10-15 at.%) incorporation. At higher temperatures (> 400 °C) the levels of Ge impurities and β -tungsten phase decreased leading to pure α -tungsten with resistivities of $\sim 10 \mu\Omega\text{cm}$ and less than 1 at.% Ge. High-resolution scanning electron micrographs (SEM) confirmed the absence of any encroachment or wormhole growth. The β -tungsten layers were thermally stable below 600 °C but could be converted into α -tungsten by annealing for 30 min at temperatures above 600 °C. In addition, the films showed good adhesion on both Si and SiO_2 . The β -tungsten phase was deposited selectively at temperatures below 350 °C, however, at higher temperatures selectivity was lost.

Low contact resistance of 5 ohm was obtained for submicron contact plugs filled with β -tungsten. The contact resistance to a $2 \times 2 \mu\text{m}^2$ $\{\text{n}^+\text{Si}\}/\{\text{p}^+\text{Si}\}$ region was as low as the contact resistance of an annealed Al (Al with 1 at.% Si) /Si reference sample. A low contact resistance is more important than lower resistivity of the tungsten phase because contact resistance contributes much more to the total resistance than the resistivity of the contact material. This is especially the case for the deposited β -tungsten films. Therefore, this process can be used to deposit a contact material in integrated circuits.⁴⁹

3.3.1.2 Tungsten Hexachloride (WCl_6)

Tungsten hexachloride can be reduced to tungsten metal with the same compounds which were employed for the reduction of WF_6 :



The reaction products Cl_2 and HCl show much weaker encroachment and corrosive effects on silicon and III/V semiconductors than F_2 and HF . This is a potential advantage for WCl_6 as a tungsten source despite the disadvantages of a much lower vapor pressure than that of WF_6 and the difficulties in controlling the processing parameters associated with the use of a solid precursor.

Early work on tungsten CVD using WCl_6 as a precursor was carried out by Powell et al.¹³² Tungsten deposition from WCl_6 at atmospheric pressure without a reducing agent is only achieved at temperatures between 1200 and 2400 °C. Powell showed it was possible to lower this deposition temperature to 600-900 °C by reducing the tungsten hexachloride with hydrogen. He also obtained good results using low pressure (5 torr) and temperatures between 700 and 900 °C.¹³³ (See also Table 3-8.)

In 1968 Mehalchick et al.¹³⁴ investigated the deposition behavior of the WCl_6/H_2 system at atmospheric pressure employing a hot-wall vapor-plating reactor. At low temperatures (< 450 °C) coarse, porous, and non-uniform deposits were obtained resulting from incomplete reduction of the precursor; between 550 and 650 °C dense, uniform films were deposited; above 700 °C, fine and particulate tungsten coatings were formed by homogeneous reaction. Contamination of the precursor with oxyhalides (WOCl_4 and WO_2Cl_2) led to highly porous and nonadherent deposits.

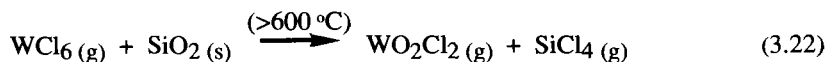
The use of WCl_6 as a precursor for tungsten deposition was investigated by Melliar-Smith et al.¹²⁷ The experiments were carried out in a cold-wall reactor with a 86:14 mixture of argon and hydrogen at 1 atm pressure, 550 to 950 °C substrate temperature, and 150 °C (± 5) source temperature. To prevent premature recrystallization in the reactor, the feed gas lines were also held at the source temperature of 150 °C. Bright, adherent, crystalline metal films were obtained at a growth rate of 100 nm/min. Pole figure X-ray measurements showed a slight (110) orientation and bcc structure of the tungsten deposited on SiO_2 . This preferred orientation was enhanced by annealing for 1 hour at 900 °C. No evidence was found for the presence of the β -W phase. The films were very pure (0.05-0.1 at.% chlorine) and showed resistivity values close to bulk tungsten (5.65 $\mu\Omega\text{cm}$ at 20 °C). A thickness of 2000 to 3000 Å was obtained in a few minutes and up to 6 μm in an hour. The contact resistance of W-Si structures was investigated to check the possible application of this deposition process for manufacturing microelectronic devices. Samples obtained from deposition using WCl_6 at temperatures between 600 and 800 °C had high, non-ohmic contact resistances. With increasing deposition temperature, the I-V characteristics of the contacts resembled more and more that of ohmic contacts; this was also accompanied by decreased contact resistance. Finally, temperatures as high as 850 °C gave ohmic contacts with low resistance. The authors explained this temperature dependence with the presence of a detrimental interfacial native oxide layer on the silicon substrate on which the tungsten film was actually deposited. At higher temperatures the thin oxide layer might not prevent contact formation due to rapid diffusion of tungsten and/or silicon through this layer. However, high temperatures enhance significantly the formation of WSi_2 which can result in nonadherent films.

The reaction mixtures WCl_6/Ar and WCl_6/H_2 were investigated by Hårsta and Carlsson^{54,135} at temperatures ranging from 475 to 750 °C, using a hot-wall reactor with a total pressure of 3.6 torr (WCl_6 partial pressure: 0.12-0.2 torr; H_2 partial

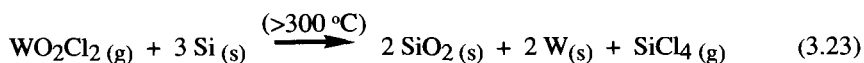
pressure: 0-2.4 torr) and a linear gas flow velocity of 41-66 cm/sec (deposition time, 10-60 min). Throughout the experiments only the α -W phase was grown and no silicides were detected up to deposition temperatures of 750 °C. The tungsten coatings exhibited slight (110) texture, but at higher temperatures the WCl_6/H_2 system gave strong (200) orientation. Excellent selective deposition was observed using patterned Si/SiO₂ wafers.

The WCl_6/Ar system:

Thermodynamic calculations were carried out for WCl_6 . The driving force values excluded deposition on SiO₂ (no deposition on the reactor glass walls can be observed). However, Hårsta and Carlsson⁵⁴ found severe silicon encroachment using an WCl_6/Ar mixture. This was explained by the following reactions

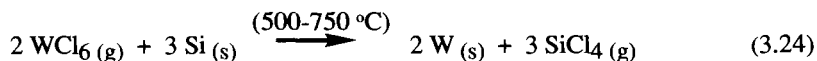


which can occur only in the absence of hydrogen. This can be followed by



and the reaction can sustain itself since the SiO₂ formed in the second step can initiate the first step (Eq. 3.22) again. According to these reactions, etching of SiO₂ is favored and increases with higher temperatures, lower total pressure, and higher WCl_6/Ar ratio.

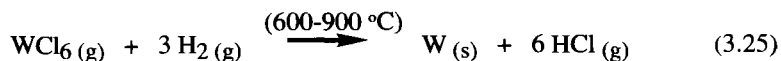
The predominant reaction with silicon is independent of temperature and total pressure:



It also follows that low temperatures, high total pressures, and high WCl_6/Ar ratios favor selectivity.

The WCl_6/H_2 system:

Deposition on both Si and SiO₂ is favored thermodynamically. In experiments carried out at temperatures above 575 °C, tungsten deposited on the silicon substrate as well as on the glass reactor walls. The main reaction is



Etching of SiO_2 can be excluded. The thermodynamically favored reaction on silicon is reduction of WCl_6 with silicon (Eq. 3.24). The process is favored by low temperature, high total pressure, and high WCl_6 concentration. These conditions also favor selectivity (derived from driving-force ratios).

A problem was the irreproducibility of the film thickness on silicon substrates; under identical conditions the thickness varied between 0.1 and 0.44 μm . This was traced to differences in the oxide layer thickness on the silicon substrates, which is formed by exposing the substrate to air for about 30 sec while loading into the reactor. An oxide layer is more difficult to remove by the WCl_6/Ar system because the latter etches SiO_2 more slowly than WF_6/Ar . Therefore, the chloride process is affected more by oxide layers on the substrate than is the fluoride process.

Ammerlaan et al.³⁶ used a cold-wall reactor and silicon substrates for their CVD experiments and reduced WCl_6 with hydrogen gas. The deposition at atmospheric pressure and temperatures ranging from 480 to 670 $^\circ\text{C}$ was limited by the feed rate of the metal source to the reactor. The films were non-uniform with rough surfaces. Smooth and very pure (less than 1% oxygen) tungsten films were obtained at low pressure (40 torr) at a rate of 10-110 nm/min (at low pressure, the growth rate was surface reaction controlled) and resistivities for α -W films were 8-17 $\mu\Omega\text{cm}$ and for β -W films were 41 $\mu\Omega\text{cm}$. These growth rates are significantly higher than those observed by Hårsta and Carlsson^{54,135} and are related to the higher H_2 pressure in this work. It is assumed that the finding in the WF_6/H_2 system for the growth rate dependence on the partial pressure of hydrogen (directly proportional) can also be applied to the WCl_6/H_2 system.^{86,109}

The reproducibility of film composition is usually poor. In most experiments the α -phase is formed but sometimes, under the same conditions, the β -W phase is observed. This is of great importance, since the two tungsten phases show significant differences in resistivity (α -W: 5.65 $\mu\Omega\text{cm}$; β -W: ≈ 40 $\mu\Omega\text{cm}$ and higher). In addition to Si, other surfaces (Mo, TiN, and W) can be coated with the WCl_6/H_2 system as well (growth rate: 6-10 nm/min at 540 $^\circ\text{C}$; 40-67 nm/min at 624 $^\circ\text{C}$). In the absence of hydrogen, tungsten substrates were etched by WCl_6 . Some of the tungsten films deposited on silicon showed loss of adhesion after exposure to air for several days due to reactions at the W/Si interface involving chlorinated species. This indicates chlorine contamination of the tungsten deposits. X-ray diffraction measurements of coatings deposited on W/Si substrates at 624 $^\circ\text{C}$ revealed WSi_2 formation at the interface. Pauleau and Lami¹¹¹ showed that tungsten silicide formation is prevented by high amounts of SiO_2 on the surface of silicon below 800 $^\circ\text{C}$. Formation of WSi_2 takes place at temperatures as low as 625 $^\circ\text{C}$ when only small amounts of oxygen are present at the interface.

Earlier work on WCl_6 as a tungsten CVD precursor¹³² employed low-pressures (< 20 torr), deposition temperatures between 600-1500 $^\circ\text{C}$, and evaporation temperatures for the precursor of 165-230 $^\circ\text{C}$. It was found that the presence of hydrogen did not assist

Table 3-8. Comparison of deposition conditions and film properties using WCl_6 and WBr_6 as precursors.

	Growth Rate ($\mu\text{m/h}$)	Deposition Temperature ($^{\circ}\text{C}$)	Carrier Gas (ratio)	Reactor Pressure (torr)	Substrate	Film Properties	Ref.
WCl_6	6-24	600-700	none; H_2	760	Cu	bright, adherent, nonporous	133
	—	450-700	H_2	760	Si, SiO_2	dense, coherent	134
	6	550-950	$\text{WCl}_6:\text{H}_2:\text{Ar}$ 1:10:60	760	Si, SiO_2 , sapphire	7-70 $\mu\Omega\text{cm}$, 99.9% W/0.1% Cl	127
	0.04-0.44	450-750	H_2/Ar	0.5-4.5	Si(100), SiO_2 , Mo	$\alpha\text{-W}$	54
	0.6-7	480-670	H_2, N_2	40, 760	Si, Mo, W, TiN	8-17 $\mu\Omega\text{cm}$, >1% O, $\alpha\text{-W}$	36
	—	≥ 380	H_2	760	tungsten	>99% W	43
WBr_6	60	1100-1500	vacuum	10^{-7}	tungsten	>99% W	43

the plating process. Pring and Fielding¹³⁶ obtained no deposition above 20 torr and deposition temperatures higher than 1000 °C. Best results were obtained at a pressure below 10 torr and at 1000 °C. The deposits were described as bright, adherent, non-porous, and with a thickness up to 5 µm. A crucial point seems to be the purity of the precursor, because it was observed that small amounts of oxychlorides or other volatile impurities in WCl_6 have deleterious effects upon adhesion and uniformity of the tungsten films.

3.3.1.3 Tungsten Hexabromide (WBr_6)

Caves⁴³ investigated WBr_6 as a possible tungsten source using a sealed glass reactor following the van Arkel/de Boer iodide process to avoid oxygen contamination. Prior to the deposition, the all-glass reaction system was pumped, flamed, and sealed at about 10^{-7} torr. The precursor was formed in situ at 480 °C, oxyhalide impurities were removed by sublimation (below 230 °C), and the precursor was then kept at 110-380 °C with an optimal temperature of 330 °C. The precursor reacted on tungsten wire at 1100-1500 °C to yield highly pure, very dense, and uniform tungsten films with a thickness up to 320 nm. At the optimal deposition temperature of 1300-1370 °C a growth rate of 60 µm/h was observed. The impurities detected were 2 ppm carbon, 4 ppm oxygen, 10 ppm sulfur, and traces of other elements, probably caused by impurities from the tungsten metal used to synthesize the precursor and/or the substrate. Tungsten could be deposited on any material, provided the substrate is stable under the deposition conditions. The hardness and purity of the obtained material compare favorably with that obtained from high-purity tungsten refined from electron-beam zone melting. Similar results can be obtained in a common horizontal flow reactor at temperatures as low as 380 °C, if hydrogen is employed as carrier gas and reducing agent. Without hydrogen, no deposition was observed below 1100 °C. An overview of tungsten CVD using the precursors WCl_6 and WBr_6 is given in Table 3-8.

3.3.2 Organometallic Compounds

Although it is not an organometallic compound, the inorganic complex $\text{W}(\text{PF}_3)_6$ is included in this section because it contains the transition metal in a low oxidation state similar to the organometallic compounds discussed herein. An overview of the deposition conditions of organometallic precursors is given in Table 3-9, and the properties of the tungsten films are summarized in Table 3-10.

Table 3-9. Deposition conditions of OMCVD experiments using organometallic tungsten precursors.

Compound	Evaporation Temperature (°C)	Deposition Rate (μm/h)	Deposition Temperature (°C)	Carrier Gas (ratio)	Reactor Pressure (torr)	Substrate	Ref.
W(CO) ₆	30	—	150-800	none, H ₂	0.03-760	not given	41,42
W(CO) ₆	30	0.8	200-550	H ₂ , Ar	0.001-0.01	Si, SiO ₂	139
W(CO) ₆	50-80	—	250-400	H ₂	150-300	Si, SiO ₂	142
W(CO) ₆	—	—	420	N ₂	760	Si, SiO ₂	140
W(CO) ₆	50-70	8.0	350-540	none	10 ⁻⁷	Si(100)	84
W(C ₆ H ₆) ₂	20-80	—	300-600	H ₂ , N ₂ , He, Ar	760	SiO ₂ , Al, Cu, Ag, steel	146
W(C ₆ H ₆) ₂	160-170	0.005-10	475-500	none	0.01-10	graphite	147
W(PF ₃) ₆	80	0.2	450	none, H ₂ , He, Ar	10 ⁻⁴ - 1	Si, SiO ₂ , ceramics	137
W(allyl) ₄	60 °	0.05-0.18	300-400	none, H ₂	0.01-0.02	Si, SiO ₂	75,149
(C ₅ H ₅) ₂ WH ₂	100-155	0.05-5	300-600	H ₂	760/0.1	Si, SiO ₂	83,155,156
[CH ₃ (C ₅ H ₄) ₂ WH ₂	90-100	—	300-600	H ₂	760/0.1	Si, SiO ₂	83
(C ₅ H ₅)W(CO) ₃ (CH ₃)	72-81	0.01-2.0	320-620	H ₂ /N ₂ ; (1:1)	1-2	Si(100)	154
W(butadiene) ₃	≈100	—	400-600	H ₂ or Ar	760	Si, SiO ₂	71,148
W(methylvinylketone) ₃	100	—	200-400	H ₂ or Ar	0.1	Pt, Cu, Si, SiO ₂ , TiN	71
(C ₅ H ₅)HW(CO) ₃	70-100	1.7-40	480-700	none	2.0-7.0	Si, SiO ₂	84
(C ₇ H ₈)W(CO) ₃	110-120	0.06	350-700	none	1.3	Si, SiO ₂	84
(1,5-COD)W(CO) ₄	110-120	0.06	350-700	none	1.5	Si	84

Table 3-10. Comparison of tungsten film properties obtained by OMCVD.

Compound	Substrate	Deposition System		Deposition Temp. (°C)	Growth Rate (μm/h)	Tungsten Film Properties			Ref.
		Carrier Gas	Reactor Pressure (torr)			Impurities (at. %)	Resistivity (μΩcm)	Adherence	
W(CO) ₆	Si, SiO ₂	H ₂	0.03-760	150-800	—	0-35 C	—	good	41,42
W(CO) ₆	Si, SiO ₂	H ₂ , Ar	0.001-0.01	200-550	0.8	<0.1 C	16	good	139
W(CO) ₆	Si, SiO ₂	H ₂	150-300	250-400	—	16-25 C, O	—	bad	142
W(CO) ₆	Si, SiO ₂	N ₂	760	420	—	10 C, O	6.6-12.5	good	140
W(CO) ₆	Si	none	10 ⁻⁷	350-540	8.0	4-30 C, 1-15 O	≥28	—	84
W(C ₆ H ₆) ₂	SiO ₂ /metals	H ₂ , He	760	300-600	—	low	good	very good	146
W(C ₆ H ₆) ₂	graphite	none	0.01-10	475-500	—	low C	good	very good	147
W(PF ₃) ₆	Si/SiO ₂	H ₂ , He	10 ⁻⁴ - 1	450	—	very pure	good	very good	137
W(allyl) ₄	Si/SiO ₂	H ₂	0.01-0.02	300-400	0.05-0.18	44 C, 10 O	>106	very good	75,149
(C ₅ H ₅) ₂ WH ₂	Si/SiO ₂	H ₂	760/0.1	300-600	0.05-5	25 C, 3.5 O	150-250	excellent	83,155, 156
[CH ₃ (C ₅ H ₄) ₂ WH ₂	Si/SiO ₂	H ₂	760/0.1	300-600	—	25 C, 3.5 O	150-250	excellent	80
(C ₅ H ₅)W(CO) ₃ (CH ₃)	Si	H ₂ /N ₂ (1:1)	1-2	320-620	0.01-2	5-10 C, 5-15 O	40-600	good	154
W(butadiene) ₃	Si/SiO ₂	H ₂ or Ar	760	400-600	—	very high C, O	—	good	71,148
W(methylvinylketone) ₃	Pt	H ₂ or Ar	0.1	300	—	high C, O	—	bad, cracks	71
W/Pt co-deposition (C ₅ H ₅) ₂ WH ₂ /	Si/SiO ₂	H ₂	760	350-400	0.02	5.3 C, 1.8 O	52±4	excellent	154
(C ₅ H ₅)Pt(CH ₃) ₃	Si	none	10 ⁻⁷	350-700	40	50-70 C, 1 O	very high	—	84
(C ₇ H ₈)W(CO) ₃	Si	none	10 ⁻⁷	350-700	—	60 C, 1 O	300-1500	—	84
(1,5-COD)W(CO) ₄	Si	none	10 ⁻⁷	350-700	—	—	300-1500	—	84

--- Not Measured

3.3.2.1 Hexakis(trifluorophosphine)tungsten $[\text{W}(\text{PF}_3)_6]$

Only two patents deal with the deposition of tungsten from this precursor,^{137,138} and very few details are given about experimental conditions. The tungsten films, obtained by a combination of a cold-wall reactor with a directly heated substrate at 450 °C and assisted by an additional selective area irradiation from a UV source from outside the reactor, are described as highly pure, heat resistant, uniform, and with good electrical conductance. The precursor is transported to the reactor at 80 °C by applying a dynamic vacuum (0.0001-1 torr) to the system in the direction of the deposition chamber or by using a carrier gas, such as hydrogen or a noble gas. Thermal dissociation is controlled so that thermal decomposition and deposition may take place in the regions of the substrate that are illuminated by the additional UV beam. With this setup, deposition was achieved on Si, SiO_2 , and ceramics. Films with a thickness of 0.1 μm can be grown in 30 min. The described combination of the two deposition methods allows for selective and epitaxial deposition of tungsten as well as other metals (e.g., V, Nb, Ta; Cr, Mo; Fe; Co; Ni).

3.3.2.2 Hexacarbonyltungsten $[\text{W}(\text{CO})_6]$

Early investigations of tungsten deposition using $\text{W}(\text{CO})_6$ as a tungsten source were summarized by Powell et al. in 1966.¹³² At atmospheric pressure, only higher temperatures (600-900 °C) gave pure metal deposits unless the metal carbonyl was fed into the reactor as an extremely dilute mixture. At lower temperatures (350-600 °C), highly pure films were obtained only at low pressure (0.1-0.01 torr) and a hydrogen to metal carbonyl ratio of 100:1. In these pioneering studies, the main emphasis was placed on the mechanical properties of refractory metal coatings for protection of bearing surfaces against wear.^{41,42}

Further investigations of the usefulness of $\text{W}(\text{CO})_6$ as a precursor to deposit tungsten for microelectronic devices were carried out by Kaplan and d'Heurle.¹³⁹ They assembled a vertical hot-wall reactor setup and tested the deposition behavior of $\text{W}(\text{CO})_6$ under dynamic vacuum (0.001-0.01 torr) at temperatures between 200 and 580 °C using argon and/or hydrogen as carrier gas. At deposition temperatures above 500 °C, 1.3 μm thick tungsten coatings (deposition rate 1.3 $\mu\text{m}/\text{h}$) with resistivity values around 11 $\mu\Omega\text{cm}$, low carbon content (250-4400 ppm), and good adherence were obtained only by introducing hydrogen into the reaction chamber. The resistivity of the films was directly proportional to the carbon content. Both increased with decreasing temperatures. However, no carbide formation could be detected in films grown at 300-450 °C (XRD investigations). Also, films deposited above 450 °C showed (100) orientation whereas at lower temperatures no preferred orientation was observed. The adhesion of these tungsten films was highly dependent on the deposition temperature.

Films formed above 500 °C showed good adhesion (Scotch-tape test) while adhesion became unsatisfactory at lower temperatures (< 400 °C). The addition of oxygen or water (1-2 torr partial pressure) to the carrier gas greatly improved the adhesion to silicon surfaces at temperatures as low as 325 °C; employing an initially low deposition rate to build up a film several hundred Å thick followed by normal conditions gave the same results. Attempts to improve the resistivity with low-temperature deposition (<400 °C) and adding H₂S, CO₂, and Ar to the carrier gas gave limited success.^{41,42} Further work¹⁴⁰⁻¹⁴³ confirmed these earlier results.

Diem et al.,¹⁴⁰ using a stainless steel hot-wall reactor at atmospheric pressure and N₂ carrier gas, obtained tungsten films contaminated with 10% carbon and 10% oxygen. Annealing the samples for 1 hour at 850 °C in vacuum or forming-gas atmosphere greatly improved the purity and resistivity of the tungsten films (up to 96 at.% W and 6.6-12.5 μΩcm resistivity). After annealing, however, the initially sharp W/Si interface became thicker and more diffuse.

Boyes¹⁴¹ studied the nucleation behavior and texture of tungsten during the deposition process from W(CO)₆ on molybdenum and platinum with a field-ion microscope. On molybdenum substrates, tungsten films exhibited (111) texture divided by a very low angle boundary close to the (001) zone line decoration. The films were also oriented with respect to the molybdenum substrate. The tungsten films on platinum were polycrystalline and showed a pronounced (211) texture. In this case, no epitaxial relationship was discovered.

Vogt¹⁴² tested the possible application of W(CO)₆ for coating microspheres in a fluidized-bed reactor at high pressure (20/40 kPa) with hydrogen as carrier gas. The coatings contained high heteroatom impurities, namely 16-25% each of oxygen and carbon. It was assumed that physical entrapment of chemisorbed CO molecules in the films was probably due to the slow desorption and removal of CO in the system.

The observations from various scientists reported earlier (see above) suggest that employing low pressure and highly diluted W(CO)₆/H₂ gas mixture (with Ar or He) should lead to much cleaner coatings with the fluidized-bed system.

Tungsten films were deposited on Si from W(CO)₆ in a cold-wall stainless steel reactor with a base pressure of 10⁻⁷ torr.⁵⁴ At 540 °C and 15 mtorr, a deposition rate of approximately 8 μm/h was achieved. The surfaces of the as-deposited films, which were analyzed by AES after transfer in vacuo, contained 20% carbon and 10% oxygen. The C (KLL) lineshape indicated that the carbon was predominantly carbidic. Depth profiling revealed that the bulk of the film contained >95 at.% tungsten, with only approximately 4 at.% carbon and 1 at.% oxygen. SEM images showed columnar growth and a grain size of 100-200 nm. Results from XRD indicated that as-deposited films were polycrystalline α-W with (100) orientation when deposited on Si(100). The resistivity was 28 μΩcm, substantially higher than that of bulk α-W, as a likely consequence of carbon and oxygen impurities. Films deposited at 375 °C and 15 mtorr had lower bulk

tungsten contents (around 70 at.%), and at steady state, the growth surface contained 30% carbon and 10-15% oxygen. These results suggest that at 375 °C CO dissociation competes more favorably with CO desorption from the growth surface. Consistent with the results of Diem et al.¹⁴¹ in vacuo annealing of films deposited at low temperatures was effective in reducing the impurity concentrations and resulted in polycrystalline α -W films.

Zaera¹⁴³ investigated the interaction and surface chemistry of $W(CO)_6$ with a Ni(100) surface under ultra-high-vacuum conditions (10^{-10} torr) at temperatures ranging from 85 to 1100 K. Tungsten hexacarbonyl chemisorbs at low temperatures (85-235 K) and decomposes into tungsten atoms and CO upon heating of the surface to temperatures of 250 K and above. Carbon monoxide is the main desorption product when the surface is not fully covered with a mono-layer of $W(CO)_6$. Molecular desorption is observed around 225 K when multilayer deposition takes place. The deposition step requires 12 ± 2 kcal/mol and follows zero-order kinetics (Karapet'yants¹⁴⁴ and Barnes¹⁴⁵ and their associates report 16-18 kcal/mol at 298 K). From XPS data all the metal-carbon bonds break around 250 K to form tungsten atoms and chemisorbed CO. Around 400 K 80% of the CO has desorbed and the remaining 20% is dissociated by the co-deposited tungsten. The latter is oxidized during this process (W^{2+} , W^{6+} were detected). Atomic C and O recombine around 600-700 K with subsequent desorption from the surface leaving behind pure zero-valence tungsten. Finally, at 1100 K, most of the tungsten migrates into the nickel (100) film.

These results are important for CVD processes of tungsten and possibly other metals. They suggest that in the presence of nickel it might be possible to obtain highly pure tungsten films at temperatures as low as 300 °C using $W(CO)_6$. This might be achieved by the co-deposition of tungsten and nickel from $W(CO)_6$ with small amounts of a nickel precursor such as $Ni(CO)_4$. The effect of co-deposition of tungsten with other metals on the quality of the obtained metal films is discussed in detail in Section 3.4.

3.3.2.3 Bis(benzene)tungsten [$W(\eta^6-C_6H_6)_2$]

Bis(benzene)tungsten and other bis(arene)tungsten compounds for CVD were discussed in a British patent issued in 1960.¹⁴⁶ The information, however, was vague. A hot-wall reactor was employed using low-pressure conditions and deposition temperatures between 300 and 600 °C. Higher deposition temperatures resulted in the decomposition of the ligand, generating carbon and/or polymerizable hydrocarbons such as ethylene and acetylene which usually led to contamination of the plated metal. With this method tungsten was deposited on substrates such as glass, glass wool, ceramics, plastics such as Nylon[®], Bakelite[®], and metals such as Al, Cu, Ag, and stainless steel. Carrier gases included H_2 , N_2 , He, and Ar. Generally the experiments were carried out at ambient pressure, but higher and lower pressures were explored as well. The metallic

coatings were bright and shiny with good adherence to the substrate and contained only a small number of heteroatoms. They exhibited desirable electrical conductance properties, furnished corrosion protection, and gave striking decorative effects (color).

Another patent¹⁴⁷ described the deposition of tungsten metal on graphitic material using bis(arene)tungsten compounds to protect this material against high temperatures and chemical attack. The inventors used a hot-wall reactor without a carrier gas and achieved the best results between 475 and 500 °C and pressures of 0.01-10 torr. The coatings were relatively pure and essentially free of carbides and oxides. A partial pressure of the precursor higher than 10 torr gave less adherent coatings. Tungsten films with a thickness of 0.01-50 μm were deposited in 3-6 hours. Similar high-quality tungsten coatings were obtained at significantly lower temperatures by using a combination of methods. One example was to employ UV radiation to initiate the deposition process in addition to heating the substrate just below or at the decomposition threshold (≈ 250 °C) of the precursor.

3.3.2.4 Tris(butadiene)tungsten [$\text{W}(\eta^4\text{-C}_4\text{H}_6)_3$]

Preliminary investigations of this precursor were carried out by Kaesz and Niemer.¹⁴⁸ The deposition was undertaken in a hot-wall short-path CVD reactor. All the experiments were performed at ambient pressure with hydrogen as a carrier gas. The precursor was warmed to 80 °C under a stream of H_2 (flow rate 15 mL/min) and transported to the substrate held at 280-450 °C. The minimum temperature for deposition was 280 °C. Flawless mirror-like films occurred on glass or on Si(100) wafers as well as on the wall of the reactor in the heating zone. The XPS analysis showed large amounts of oxygen and carbon (each 30-40%). After annealing under an atmosphere of hydrogen (650 °C, 2 h), the carbon and oxygen content could be decreased to 15-20 at.% each. Employing Ar as carrier gas and a deposition temperature of 550-600 °C led to the deposition of films with even poorer quality.

3.3.2.5 Tetraallyltungsten [$\text{W}(\eta^3\text{-C}_3\text{H}_5)_4$]

Chemical vapor deposition using tetraallyltungsten yields dark, reflective, adherent, amorphous, and insulating tungsten carbide films on glass (Pyrex®) and silicon substrates.⁷⁵ A hot-wall, short-path reactor was operated at a pressure of 0.01-0.02 torr and a substrate temperature between 300 and 400 °C. In some experiments hydrogen was introduced into the system through a needle valve while maintaining the low pressures given above. The growth rates of the films ranged from 0.05 to 0.18 $\mu\text{m/h}$. Auger electron spectroscopy measurements revealed a film composition of 40 at.% tungsten, 44 at.% carbon, 10 at.% oxygen and about 6 at.% silicon after sputtering through the surface layers. By analyzing the XPS spectra in the region of the $\text{W}(4f_{7/2})$ and $\text{W}(4f_{5/2})$ electrons, it was confirmed that the films contain a high percentage of the WC phase

(WC-sputtered: 31.7/33.9 eV; found: 31.69/33.78 eV). In addition, a small amount of graphitic carbon was observed in all films (at 285.0 eV). The deposits appeared to be resistant to aqua regia, a characteristic property of WC material. However, the observed high resistivity of $>10^6 \mu\Omega\text{cm}$ for the obtained deposits disagrees with the reported resistivity value of only $17 \mu\Omega\text{cm}$ for the WC phase. This suggests that the high resistivity is caused by the additional oxygen impurities (and probably interstitial carbon atoms) in the deposits. Analysis of the exiting volatile byproducts revealed that 95% of the products were propane and propene; only minor amounts of ethane, ethylene and benzene were detected and no changes in the composition were observed at temperatures between 350 and 450 °C.

Similar carbon-rich films have been reported for the deposition of ZnSe using $\text{Se}(\eta^1\text{-allyl})_2$ where a 2:1 ratio of propene to hexadiene was found for the volatile products.¹⁴⁹ In contrast to these findings, the allyl compounds of Pd, Cd, Hg, and Te gave essentially carbon-free Pd, CdTe, and HgTe films.¹⁴⁹⁻¹⁵² The dominant pyrolysis pathway for these materials was the formation of hexadiene resulting from bond homolysis which generated allyl radicals. These data suggest the formation of carbon-free films occurs only when bond homolysis becomes the main decomposition pathway and can be directly correlated to the formation of hexadiene.

Another important decomposition pathway of transition metal allyl complexes is thermal β -hydride elimination. This was demonstrated by heating $[\eta^5\text{-C}_5(\text{CH}_3)_5]_2\text{Ta}(\eta^3\text{-allyl})$ in a benzene solution which resulted in the formation of allene and propyne complexes.¹⁵³ This decomposition pathway might also occur for other metals leading to deposition of pure metal films. However, the high carbon content of the tungsten film deposits using $\text{W}(\eta^3\text{-allyl})_4$ implies formation of strong metal-carbon bonds during the decomposition. Reaction pathways with α -hydride elimination increase the metal-carbon bond order and might account for the high carbon content in these tungsten films. Because tungsten carbene, carbyne, alkylidene, and metallocycle complexes are relatively stable,⁵⁹ they are probable intermediates in the decomposition pathways. A possible reaction pathway for the decomposition of $\text{W}(\eta^3\text{-C}_3\text{H}_5)_4$ is shown below:



In this context, the decomposition behavior of $\text{W}(\eta^3\text{-allyl})_4$ using TGA techniques (Section 3.2.2.5) suggests that using CO or a hydrogen/CO-rich mixture as a carrier gas should lead to less carbon in the films. The use of CO as carrier gas revealed *hexadiene* as the main volatile product. As shown above, the formation of hexadiene was

correlated with a bond homolysis reaction pathway leading to complete removal of all allyl ligands and pure metal films. For further discussion of metal allyl compounds see Chapter 8.

3.3.2.6 Tris(methylvinylketone)tungsten $\{W[CH_3C(O)CH=CH_2]_3\}$

Kirss⁷¹ investigated this precursor containing tungsten in the zero valence state. The possible advantages over many other organometallic precursors are threefold: (1) The neutral π -donor ligands can desorb easily from the tungsten film surface without chemical reaction such as hydrogenation or cleavage of σ -bonds. (2) The metal is already in the zero valence state; so, no further reduction is necessary. (3) The activation of C-H which can cause carbon contamination is less likely to take place because of the absence of σ -carbon-metal bonds.

Experiments were carried out under low pressure (0.1 torr) in a hot-wall reactor using hydrogen or argon as carrier gas and deposition temperatures from 200 to 400 °C. The precursor was kept at 100 °C and at a pressure of 2 torr. Using hydrogen as carrier gas, at 200 °C most of the precursor passed the heating zone unchanged. Very thin tungsten films were obtained only on platinum, not on Si, SiO₂, Cu, and TiN. No carbon or oxygen could be detected by energy dispersive analysis of X-rays (EDAX) in the very smooth deposits. At 300 °C rapid film growth takes place on platinum substrates. At this temperature the deposition process consumes all the precursor fed into the reaction chamber. The films show many surface cracks and contain significant amounts of oxygen which increase with higher temperatures. No appreciable deposition on Si, SiO₂, Cu, and TiN was achieved below 400 °C. Gas chromatography/mass spectroscopy (GC/MS) analysis of the volatile by-products indicated small amounts of methylvinylketone and methylethylketone and a large amount of an unidentified species with a higher molecular weight.

3.3.2.7 Cyclopentadienylmethyltricarbonyltungsten $[(\eta^5-C_5H_5)W(CO)_3(CH_3)]$

This compound was investigated by Spee et al.¹⁵⁴ using a vertical hot-wall CVD reactor with a background pressure of 0.1 to 0.01 torr and a cold-wall stagnant flow reactor with 0.001 torr background pressure at temperatures between 320 and 620 °C. The experiments were carried out in a 1:1 mixture of hydrogen and nitrogen with a flow rate of 100 l/h for the hot-wall and 18 l/h for the cold-wall reactor. The precursor temperature was maintained between 72 and 81 °C and silicon (100) samples were used as substrates. The deposition process was surface-reaction-limited at temperatures lower than 390 °C and 0.04 torr reactor pressure and mass-transport limited at higher temperatures. The deposition rate varied with temperature from 0.4 $\mu\text{m/h}$ at 400 °C to 2 $\mu\text{m/h}$ at 620 °C.

Measurements by XRD revealed that the films consisted of β -W; only a few samples also contained a low percentage of the α -W phase. The formation of the β -phase was probably caused by oxygen impurities in the deposits. The deposited tungsten films (α - and β -phase films) contained 5-10 at.% O and 5-15 at.% C. The XPS measurements also showed that surface carbon was present as WC and carbonaceous material and surface oxygen was present as WO_3 . The resistivity varied greatly from 40-600 $\mu\Omega\text{cm}$ with extreme values of 15 and 17 $\mu\Omega\text{cm}$ and 0.01-0.1 Ωcm . As already implied by the wide range of resistivity values, results varied greatly from experiment to experiment and were difficult to reproduce. The authors assumed that this was due to the presence of varying amounts of tungsten oxide in the films.

3.3.2.8 Bis(cyclopentadienyl)dihydridotungsten [$(\eta^5\text{-C}_5\text{H}_5)_2\text{WH}_2$]

The deposition experiments were carried out in a hot-wall, short-path CVD apparatus. All the experiments were operated at atmospheric pressure and H_2 or argon were used as carrier gases. The substrates were Si(100), SiO_2 , and silicon substrates coated with a thick (1-3 μm) platinum film. Experiments were performed at temperatures ranging from 300 to 650 $^\circ\text{C}$ to investigate the deposition behavior of this precursor at different temperatures and to find the optimal deposition conditions for highly pure tungsten films.^{83,155}

In a typical experiment, the precursor is heated to 80-130 $^\circ\text{C}$ under a stream of H_2 (flow rate 20-25 mL/min) and transported to the substrate located in the heating zone. To prevent premature condensation in the apparatus, the feed gas lines were also held at the source temperature of 80-130 $^\circ\text{C}$. On silicon substrates, 145 nm thick, bright, and mirror-like metal films were obtained at 360-380 $^\circ\text{C}$. The growth rates were in the range 0.3-0.9 nm/min (carrier gas: H_2 ; deposition time: 8 hours). The tungsten films showed excellent adhesion and withstood repeated "Scotch-Tape" pull-tests. The tungsten was deposited in amorphous form, but could be converted into a crystalline phase when annealed under hydrogen for 2 hours at 600-650 $^\circ\text{C}$. The XRD-patterns of the annealed films showed the typical powder pattern of metallic tungsten with (110) as the preferred orientation.¹⁵⁶ Auger depth profile analysis revealed that at the interface the silicon substrate surface layers contained equal amounts of oxygen and carbon (5 at.% each). In the beginning of the deposition process, when the tungsten concentration of the deposited layers increased rapidly to 65 at.%, the oxygen concentration went down to almost zero. Throughout further film growth, oxygen kept a concentration of 3.5 at.%. It was assumed that this oxygen contamination came from traces in the H_2 gas and/or was caused by the SiO_2 surface layer of the silicon substrate. The carbon content, on the other hand, increased rapidly in the beginning of the film growth maintaining a concentration of 24-26 at.% throughout the film. Finally, it reached 45 at.% in the surface layers of the completed tungsten deposits. The resistivity

of these tungsten films was 150-250 $\mu\Omega\text{cm}$, much higher than in bulk tungsten (α -phase: 5.65 $\mu\Omega\text{cm}$ at 300 K). The high resistivity of the unannealed films was due to the high carbon content, the amorphous nature of the deposits, and the poor contact between adjacent metal clusters. Scanning electron micrographs revealed that the metal clusters in this amorphous film had a size of 100-500 Å. Annealing converted them into microcrystallites.

No deposition was observed below 325 °C. At temperatures between 330-360 °C, some reaction occurred, but most of the precursor passed the heating zone unchanged. Under such conditions it took 12-18 hours to deposit a 100-200 Å thick film. The best decomposition temperature was 360-380 °C when using hydrogen as carrier gas at atmospheric pressure. Above 380 °C, however, contamination with carbon and oxygen increased with higher temperatures. The tungsten deposited more easily on silicon than on glass (SiO_2). After a six hour deposition period, glass substrates were coated with a very thin, transparent brown layer and consisted mainly of carbon and oxygen and a minor amount of tungsten. Employing argon as a carrier gas led to films with similar W, C, and O contents on Si(100) and no deposition on glass.

A few deposition experiments were carried out on platinum surfaces (1-3 μm thick platinum films on silicon (100) under the same conditions as for the silicon and glass substrates. The XRD patterns of the unannealed deposits showed only platinum. After annealing however, both tungsten and platinum were observed. This means that the tungsten films formed initially were amorphous and were transformed into microcrystallites containing tungsten layers with high-temperature treatment. Analysis by XPS showed significant amounts of platinum not only on the surface but also throughout the whole tungsten film. These W/Pt films did not show significant differences compared to the tungsten films deposited on pure silicon substrates.

An interesting point when using this precursor was the influence of the flow rate of the carrier gas on precursor conversion. If the flow rate was too high, most of the precursor passed the heating zone unchanged and crystallized in the colder parts downstream from the reaction zone. If the flow rate was too low, the deposition rate decreased unacceptably accompanied by the production of poor quality films. A flow rate of 20 mL/min gave the best results for an apparatus with a one inch diameter reactor. These observations can be explained by the relatively high stability of $(\eta^5\text{-C}_5\text{H}_5)_2\text{WH}_2$, the poor heat transfer conditions of the gas atmosphere in the reactor, and feed-rate-limited conditions (see Ch. 9).

3.3.2.9 **Bis(methylcyclopentadienyl)dihydridotungsten** $[(\eta^5\text{-CH}_3\text{C}_5\text{H}_4)_2\text{WH}_2]$

Only a few deposition experiments have been carried out with this precursor.⁸³ The same conditions were employed as for $(\eta^5\text{-C}_5\text{H}_5)_2\text{WH}_2$. The derivative $(\eta^5\text{CH}_3\text{C}_5\text{H}_4)_2\text{WH}_2$ behaves like $(\eta^5\text{-C}_5\text{H}_5)_2\text{WH}_2$. However, the major advantage

over $(\eta^5\text{C}_5\text{H}_5)_2\text{WH}_2$ is a much lower melting point of 94-95 °C and the somewhat higher stability against oxidation, which make it easier to store and handle. Therefore, in the deposition experiments, $(\eta^5\text{-CH}_3\text{C}_5\text{H}_4)_2\text{WH}_2$ is always kept in the liquid state at 95-100 °C. The carrier gas is bubbled through the liquid precursor under conditions that ensure maximum saturation of the tungsten source in the gas stream. The tungsten films obtained from $(\eta^5\text{-CH}_3\text{C}_5\text{H}_4)_2\text{WH}_2$ showed similar properties as films deposited from $(\eta^5\text{-C}_5\text{H}_5)_2\text{WH}_2$. No significant increase in carbon contamination due to the additional methyl group at the cyclopentadiene rings was detected. A lower deposition temperature and a faster film growth with respect to the experiments using $(\eta^5\text{C}_5\text{H}_5)_2\text{WH}_2$ was not observed.

3.3.2.10 Cyclopentadienyhydridotricarbonyltungsten [HW($\eta^5\text{-C}_5\text{H}_5$)(CO)₃]

The precursor HW($\eta^5\text{-C}_5\text{H}_5$)(CO)₃ was used to deposit films on Si(100) wafers in a cold-wall OMCVD reactor with a base pressure of 10⁻⁷ torr.⁸⁴ The precursor was evaporated in a dynamic vacuum at temperatures between 80 and 100 °C. At 540 °C and 7 mtorr, reflective, adherent tungsten-carbon films were deposited at a rate of 40 μm/h. The surfaces of the as-deposited films were carbon-rich (70% C) but incorporated only about 1% oxygen. Depth profiling with AES showed the W:C ratio was nearly 1:1 in the bulk of the films. The C (KLL) lineshape indicated that the surface carbon was primarily graphitic but that the bulk contained a mixture of carbidic and graphitic carbon. SEM images showed very smooth growth surfaces. According to XRD, the as-deposited films were amorphous. The resistivities of the films were very poor, ranging from 0.05-0.1 Ωcm.

3.3.2.11 Cycloheptatrienetricarbonyltungsten [($\eta^6\text{-C}_7\text{H}_8$)W(CO)₃] and 1,5-Cyclooctadienetetracarbonyltungsten [(1,5-COD)W(CO)₄]

Preliminary investigations of ($\eta^6\text{-C}_7\text{H}_8$)W(CO)₃ and (1,5-COD)W(CO)₄ were carried out in a cold-wall ultra-high-vacuum- (UHV) compatible reactor.⁸⁴ Owing to the low vapor pressures of the precursors, deposition experiments were conducted at 1-2 mtorr with the source compounds heated to 100-120 °C. It was possible to deposit reflective, adherent tungsten-carbon films at temperatures between 350 and 700 °C. The surfaces of films deposited at 540 °C contained about 40 at.% tungsten, 60 at.% carbon, and ≤1 at.% oxygen. The resistivities of the films were 300-1500 μΩcm. Films deposited at 350-400 °C were similar in surface composition but contained slightly less carbon and about 3% oxygen.

3.4 In Situ Catalysis of Tungsten Deposition

As shown in the previous section, the major drawback of tungsten CVD using organometallic precursors is contamination of the metal films with carbon and oxygen. However, in the last five years scientists have developed techniques and systems to deposit highly pure films of platinum (Ch. 7), copper (Chs. 4 and 5), and other transition metals (Ch. 8).

Zinn et al.⁸³ and others¹⁵⁷⁻¹⁵⁹ examined Pt CVD processes using $(\eta^5\text{-C}_5\text{H}_5)\text{Pt}(\text{CH}_3)_3$ or $(\eta^5\text{-CH}_3\text{C}_5\text{H}_4)\text{Pt}(\text{CH}_3)_3$ which exhibited autocatalytic behavior in the presence of H_2 ; the deposition rate would increase after some Pt metal had been deposited. This autocatalytic behavior can be explained by the observation that platinum is a Fischer-Tropsch active catalyst. Platinum adsorbs hydrogen at its surface and activates the H_2 molecules enough to react with surface carbon forming CH_4 and other volatile hydrocarbons and with oxygen to yield water. If a metal can adsorb and activate H_2 on its surface, it is able to clean itself from adventitious carbon and oxygen by forming highly volatile hydrocarbons and water. These compounds can desorb easily from the film surface leaving behind highly pure metal layers. Therefore, not only Pt but also Rh and Ir¹⁶⁰ can give clean metal deposits in the presence of hydrogen (see also Ch. 8).

It is important to know whether it would be possible to introduce just enough platinum into the deposition process of non-Fischer-Tropsch metals to serve as a catalyst for the clean CVD of metals under an atmosphere of hydrogen. Kaesz and Niemer^{148,155} investigated the possibility of Pt/W co-deposition with enough platinum to catalyze the hydrogenolysis of the carbon impurities observed in tungsten films formed during the deposition.

Deposition experiments were carried out in a glass reactor tube 1 inch in diameter. The tungsten precursor $(\eta^5\text{-C}_5\text{H}_5)_2\text{WH}_2$ was placed about 2 inches upstream from the substrate and was heated to $120 \pm 20^\circ\text{C}$ by a resistance heater located directly underneath. The vapor pressure of $(\eta^5\text{-C}_5\text{H}_5)_2\text{WH}_2$ at this temperature was about 0.3 torr.^{83,154} The section of the tube containing the substrates, about 1 inch long, was heated to $380 \pm 20^\circ\text{C}$ by heating tape wrapped uniformly around the glass tube. Hydrogen was fed at $8\text{ cm}^3/\text{min}$, and argon was fed at $16\text{ cm}^3/\text{min}$. Before mixing with hydrogen, argon was passed through a glass frit containing $(\eta^5\text{-C}_5\text{H}_5)\text{Pt}(\text{CH}_3)_3$ or $(\eta^5\text{-CH}_3\text{C}_5\text{H}_4)\text{Pt}(\text{CH}_3)_3$ at room temperature and became saturated with 0.045 torr of the organometallic complex. The deposition periods ranged from 6 to 20 h. The tungsten films were deposited on glass and silicon (100) substrates. The tungsten deposited more easily on Si(100) than on glass. After a 6 hour deposition period the glass substrate was coated with a very thin, transparent brown layer of unknown material (probably a

mixture of W, C, and O). By contrast, the silicon was covered with a uniform, highly reflective, metal film. The film thickness was 3050 Å with a growth rate of 1 nm/min. The films showed very good adhesion (Scotch-tape test). After deposition, the W/Pt films were amorphous. Annealing under an atmosphere of hydrogen at 750 °C converted them into a micro-crystalline form. The annealed W/Pt films exhibited only the diffraction pattern of tungsten. The absence of any lines for Pt suggested that the platinum deposited along with the tungsten was dispersed throughout the metal layer even after annealing. This is consistent with tungsten's ability to dissolve up to 5 at.% platinum. Apparently, platinum can not form separate crystallites under the reported conditions.

An Auger depth profile showed a film composition of 89.6% W, 3.3% Pt, 5.3% C, and 1.8% O. The resistivity of the unannealed W/Pt films averaged $52 \pm 4 \mu\Omega\text{cm}$. This value is higher than would be expected from a pure platinum-containing tungsten film with this composition. At 20 °C, pure tungsten and platinum have resistivities of $5.29 \mu\Omega\text{cm}$ and $10.6 \mu\Omega\text{cm}$ respectively. The discrepancy can be explained by assuming that the films contain carbon, oxygen, and the high-resistivity β -tungsten phase ($40 \mu\Omega\text{cm}$ and higher) (see Sect. 3.1). The improved purity of these tungsten films appears to be the result of the catalytic hydrogenolysis of the hydrocarbon ligands by the co-deposited platinum. This work demonstrates the possibility of adding small amounts of (η^5 -C₅H₅)Pt(CH₃)₃ or (η^5 -CH₃C₅H₄)Pt(CH₃)₃ together with other organometallic precursors of non-Fischer-Tropsch metals to improve the purity of transition metal films obtained by OMCVD.

Besides the relatively expensive metals platinum, rhodium, and iridium, other cheaper metals should function in an analogous manner. The first choices may be nickel and cobalt. These metals are also known to be good hydrogenation catalysts and can be deposited easily, with high purity, and at relatively low temperatures from organometallic precursors such as Ni(CO)₄, Ni(η^5 -C₅H₅)₂, Ni(η^5 -CH₃C₅H₄)₂, Co(η^5 -C₅H₅)₂, and Co(η^5 -CH₃C₅H₄)₂.^{55,160} (See also Chs. 5, 7, and 8.) Investigations by Zaera¹⁴³ revealed that nickel might be as good as Pt (see Sect. 3.3.2).

3.5 Laser-Assisted Chemical Vapor Deposition (LCVD)

Besides the widely investigated thermally-induced CVD, two other methods to deposit thin tungsten films have been explored. These are laser-assisted CVD (thermal and photo-chemically induced deposition) and plasma-enhanced CVD (activation by a gas

discharge). The most important advantage of these techniques is the possibility of carrying out the deposition processes at relatively low temperatures (<500 °C);¹² this would protect sensitive microstructures on the substrate. The deposition of tungsten using these two techniques will be reported in the next two sections.

Hexacarbonyltungsten and WF₆ are the only compounds so far that have been employed as tungsten sources in LCVD processes.¹⁶¹ The major drawback of the W(CO)₆ precursor is incorporation of carbon and oxygen impurities in the tungsten films, leading to high resistivity values of the deposited tungsten dots, lines, and films. The tungsten precursor WF₆ does not exhibit this disadvantage. This precursor usually gives good quality films with a low resistivity. Sources such as excimer,^{38,162,163} CO₂,^{164,165} and Ar⁺ or Kr⁺ ion¹⁶⁶⁻¹⁷⁶ lasers were employed to deposit tungsten from W(CO)₆ and WF₆. Hydrogen is usually used to reduce WF₆, but SiH₄ has also been used recently as a reducing agent.¹⁷⁴ Silicon, usually covered with a thin native SiO₂ layer is the most common substrate. However, processing in silicon and GaAs microelectronics requires deposition of tungsten lines over much thicker passivation layers. This is the case for circuit repair and modifications. Therefore, selective deposition of tungsten on SiO₂, Si₃N₄, SiO_xN_y, TiN, GaAs, and InP was investigated by a number of groups. The most significant and important results are discussed below.

3.5.1 Hexacarbonyl Tungsten [W(CO)₆]

3.5.1.1 Mechanistic Findings

In the photolytic deposition process, excitation of dissociative metal-ligand charge-transfer states $^1A_{1g} \rightarrow ^1T_{1u}^{(1)}$ and $^1A_{1g} \rightarrow ^1T_{1u}^{(2)}$ takes place. The main absorption bands are relatively broad with maxima near 285 and 225 nm.^{177,178} The dissociation energy ΔH° to break the first metal-CO bond is 192.5 kJ/mol. For the complete dissociation of W(CO)₆, ΔH° was 1071 kJ/mol. This gives an average of 180 kJ/mol for the dissociation of each ligand.^{179,180} Information on the nascent product distribution in the gas phase was obtained by using transient infrared absorption spectroscopy of the CO and W(CO)_x products¹⁸¹⁻¹⁸⁶ and UV laser-induced fluorescence of the CO products.^{187,188} To avoid secondary photolytic reactions, PF₃ was added as a scavenger¹⁸⁹⁻¹⁹¹ and the laser intensity was kept so low that only one photon was absorbed per reactant molecule. After absorption of one 248 nm photon in a collisionless molecular beam, two or three CO ligands were eliminated. The formation of pure atomic tungsten occurred only after the absorption of three such photons.^{186,192} However, the laser intensities used in LCVD experiments for tungsten deposition were usually not high enough to meet this requirement. Especially in continuous wave (CW)

laser photolysis, the intensities were so low that only one photon could be absorbed by a precursor molecule. This was not enough to remove all the CO ligands¹⁹³ and explains the heteroatom impurities in most of the experiments. For instance, experiments using a 257 nm CW laser resulted in tungsten coatings containing 30-40 at.% oxygen and 10-30 at.% carbon. Further studies on the photo-dissociation of $W(CO)_6$, which was adsorbed on Si or Ni surfaces and cleaned in UHV, also showed incomplete decomposition.^{143,194} Similar studies have been performed on excimer laser photo-deposition of tungsten using 248 nm (KrF laser) and 308 nm (XeCl laser) and revealed the same results.^{195,196} Besides incomplete photolysis, an additional source for impurities was dissociative chemisorption of CO. This process became a major problem under high coverage conditions and during fast film growth (embedding of CO molecules in the films before desorption was possible).^{197,198}

3.5.1.2 Deposition Experiments

Table 3-11 summarizes LCVD using $W(CO)_6$ as a precursor. Highly contaminated tungsten films were reported by Jackson and Tyndall^{180,199} and Gluck et al.¹⁹⁷ using the metal carbonyl precursor. The deposits were typically grown at ambient temperature accompanied by surface heating when pulsed lasers (257 nm) were used. The complex gas mixture generally consisted of the metal carbonyl (vapor pressure under these conditions 0.01-0.1 torr), a buffer gas (>1 torr), and background gases such as water vapor or oxygen with a partial pressure of about 10^{-4} torr. The films contained ~25-55 at.% tungsten, 27-40 at.% oxygen, and 10-37 at.% carbon. Similar experiments carried out more recently by Solanki et al.^{200,201} revealed much cleaner films. In the experiments a pulsed laser was used to illuminate large substrate (Si and SiO_2) areas (>5 cm²) and the effect of four different wavelengths was studied (157/193/248/308 nm). The films were deposited at a rate of 170 nm/min. They showed good adherence (>9400 PSI), and contained more than 92 at.% tungsten, some carbon (0.9 at.%), and less than 7 at.% oxygen. The resistivity was in the range of 105-120 $\mu\Omega$ cm.

To assure a deposition environment which allows only photochemical reaction pathways, Singmaster et al.²⁰² used a laser setup (Ar^+ ion laser, 257 nm, 4 mW, 7 μ m spot radiation area) which avoids heating the substrate to a temperature where pyrolysis of the precursor could be initiated. The tungsten films grown in HV (10^{-4} torr) and UHV (10^{-9} torr) revealed deep ripples 110-130 nm wide on the surface and high carbon (12-40 at.%) and oxygen (12-30 at.%) contamination even after sputtering.

Similar work was performed by several other groups.^{177,203-208} The results varied significantly. However, purer films were obtained when the laser beam heated the substrate locally to temperatures of 700 °C and higher. This is supported by the work of Singmaster and Houle^{209,210} who were able to deposit highly pure (100% W) tungsten dots (10 μ m in diameter) by heating the substrate with a laser (CW: 514 nm) to about

Table 3-11. Comparison of LCVD conditions and film properties using $W(CO)_6$ as precursor.

Laser, Wavelength (nm), Power	Deposition Rate ($\mu\text{m}/\text{h}$)	Deposition Temperature ($^{\circ}\text{C}$)	Carrier Gas	Reactor Pressure (torr)	Substrate	Film Properties	Ref.
pulsed, 257	---	surface heating	carbonyl buffer gas	0.01-0.1 >1	Si, SiO_2	22-55% W 27-40% O	180,197,199
excimer pulsed 157, 193, 248, 308	10	25, 150	H_2O or O_2 He	10^{-4} ---	Si, SiO_2	10-37% C 7% O, 1% C good adherence	200,201
Ar^+ ion, 257 70-3000W/cm 2	3.6-108	---	HV, UHV	10^{-4} , 10^{-9}	Si(111) Si(100)	12-40% C 12-30% C	202
cw Ar^+ , 514, 2MW/cm 2	2250	800	---	LV, HV, UHV	Si(100)	100% W	209,210

800 °C under UHV conditions (10^{-8} - 10^{-9} torr); experiments using a much poorer base pressure (10^{-3} - 10^{-4} torr) still gave very pure deposits. The growth rates of 200-600 nm/sec are among the highest ever observed. They concluded that only at elevated temperatures (above 500 °C) obtained by using a high power laser is it possible to achieve highly pure tungsten coatings. This method might be useful for integrated circuit repair.

Direct writing of tungsten from $W(CO)_6$ has been demonstrated by using a focused CW laser.^{180,197,199,200,211-214} Large-area deposition of tungsten using the metal carbonyl precursor has been carried out by excimer laser deposition.^{177,201} The excimer laser either impinged upon the surface, which induced a combination of photolysis and pyrolysis of gas-phase or surface-adsorbed molecules, or was adjusted parallel to the substrate surface to afford mainly photolytic gas phase reactions. The former experimental setup gave much cleaner metal films. They showed ≤ 7 at.% oxygen and ~ 1 at.% carbon impurities.²⁰¹

3.5.2 Tungsten Hexafluoride (WF_6)

The use of WF_6 as tungsten source for LCVD does not, in general, exhibit the problem of major heteroatom impurities in the deposited metal coatings. This precursor usually gives good quality films with low resistivities (see Table 3-12). The three main reducing agents H_2 , Si, and SiH_4 used in thermal CVD experiments are also used for LCVD processes.

3.5.2.1 Mechanistic and Kinetic Observations

The WF_6/H_2 System

Lin and Allen^{172,215} studied the kinetics of local laser deposition of tungsten on silicon substrates for the WF_6/H_2 system with respect to native oxide layers. The reaction order was 1/6 for WF_6 and 1/2 for H_2 ; the growth rate followed the equation:

$$\text{growth rate [nm / sec]} = k_0 e^{-E/RT} P_{(H_2)}^{1/2} P_{(WF_6)}^{1/6} \quad (3.28)$$

where k_0 = pre-exponential factor ($\text{nm s}^{-1} \text{Pa}^{-0.67}$); P = partial pressure in Pa; E = apparent activation energy of reaction (J/mol); T = temperature (K); R = universal gas constant ($8.314 \text{ J mol}^{-1} \text{K}^{-1}$). This suggested, from the analysis in Section 3.3.1, that the rate-limiting step for laser deposition is desorption of HF from the substrate surface.^{110,172,215} The analogous thermal deposition process, where H_2 dissociation is

Table 3-12. Comparison of LCVD conditions and film properties using WF₆ as precursor.

Laser, Wavelength (nm), Power	Deposition Rate (μm/h)	Deposition Temperature (°C)	Carrier Gas (ratio)	Reactor Pressure (torr)	Substrate	Film Properties	Ref.
Ar ⁺ ion, focused cw	writing speed 1.8/3.6x10 ⁴	—	H ₂	100	SiO _x N _y , GaAs	100% W, good adhesion	208
Ga _{1-x} Al _x As diode 820, 100 mW	writing speed 1.8/3.6x10 ⁴	—	WF ₆	1	TiN	WSi _{0.7-0.9}	208
ArF	—	200-450	SiH ₄	3		no other impurities	38
ArF	—	250-500	LV	8	Si, SiO ₂	β-W, 17 μΩcm	162
			H ₂ , UHV, UHV	10-8	Si, SiO ₂	% C, % O varies, good adhesion	222
Ar ⁺ focused cw 514, 450 mW/cm ²	scan speed 21.6-72x10 ⁴	600	WF ₆ :H ₂ 1:10-1:40	425	Si, BN	purity varies	223
Ar ⁺ focused cw 514, 1.5 W/cm ²	scan speed 9x10 ⁵	—	WF ₆ :H ₂ 1:10	20-200	Al ₂ O ₃	13-20 μΩcm	175
UV, 253, 12 mW/cm ²	2-2.4	230-300	Ar	1	Si(100)	100-300 μΩcm no encroachment	37
ArF focused	3.6-21.6	25-450	H ₂ :Ar (40:100)	4	Si(100)	8 μΩcm	170
Ar with He-Ne probe	—	>600	WF ₆ Ar	50-100 760	Si	W and WSi ₂	174
Ar ⁺ , 488, 30-60 mW	—	150-175	(WF ₆ :SiH ₄ / Si ₂ H ₆ :Ar)	380-700	polyimide, Si	100% α-W, 12 μΩcm	226
Ar ⁺ , 488, 0.4-0.6 W	—	320-475	WF ₆ :Ar	0.625	Si	100% W	163
ArF excimer, 193, 160 mJ, 0-50 Hz	—	400	H ₂ /N ₂	0.1-1	Si(100)	α-W, 10-20 μΩcm excellent adhesion	

the rate-limiting factor, shows a reaction order of 0 and 1/2 respectively. The reason for this difference is still not fully understood. For the local laser direct writing process using the WF_6/H_2 system, the activation energy is 40.6 kJ/mol³⁸ (or 34.3 kJ/mol²¹⁶). This is much lower than the activation energy of the respective thermal process, 67.0 kJ/mol, and indicates that surface chemistry is important in photo-deposition. The substrate temperature also plays a significant role in the deposition process. Therefore, the photolytic process is a combination of photolysis and pyrolysis. For the pure photolytic laser deposition process the reaction order is 1/2 for WF_6 and 1 for H_2 .¹⁶² That is very different from the thermal process (see Sect. 3.3.1). The growth rate for the photolytic process follows the Equation:

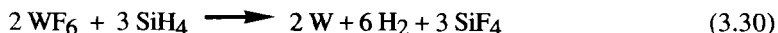
$$\text{growth rate [nm / sec]} = k_0 e^{-E/RT} P_{(H_2)}^1 P_{(WF_6)}^{1/2} \quad (3.29)$$

where k_0 = pre-exponential factor ($\text{nm s}^{-1} \text{Pa}^{-1.5}$); P = partial pressure in Pa; E = apparent activation energy of the reaction (J/mol); T = temperature in K; R = universal gas constant ($8.314 \text{ J mol}^{-1} \text{K}^{-1}$).

No satisfactory reaction model has been found to explain the kinetic behavior for this kind of laser-assisted deposition.

The WF_6/SiH_4 System

More recently, scientists started to use SiH_4 or a SiH_4/H_2 gas mixture as a reducing environment^{88,101-105} in thermal CVD to avoid the problems encountered when WF_6 is reduced with Si or H_2 . Only a few groups tried to transfer this process to LCVD.^{174,208} It can be assumed that the overall reaction, which was exothermic ($\Delta H = -96.23 \text{ kJ/mol}$)⁸⁸ in the case of thermal deposition, is also valid for the LCVD process:



This reaction takes place at relatively low temperatures ($\leq 300^\circ \text{C}$), which is common for laser deposition experiments. No HF formation could be detected below 600°C (see also Section 3.3.1).

3.5.2.2 Deposition Experiments

The WF_6/H_2 System

Laser direct writing of tungsten was carried out by a number of groups (see Table 3-12) using the H_2/WF_6 system and heating the substrate locally with a focused argon ion

or CO₂ laser.^{172,216,217-223} Meunier et al.²⁰⁸ were able to lay down highly pure tungsten lines with widths as narrow as 2.5 μm and resistivities of 13-25 $\mu\Omega\text{cm}$. Attempts to deposit lines on GaAs substrates failed. The authors suspected that a spontaneous reaction between WF₆ and GaAs, involving instantaneous tungsten reduction and formation of GaF₃, takes place and might prevent any tungsten deposition.²⁰⁸

Other groups^{38,162,216} used this system to coat large areas. Deutsch and Rathman³⁸ carried out their deposition experiments under vacuum (8 torr) using an ArF laser beam (193 nm) parallel to the heated substrate (200-440 °C). At temperatures below 350 °C β -tungsten was obtained with high resistivity (100-300 μWcm). These films were converted into an α -tungsten layer by annealing at elevated temperatures. After this treatment they showed significantly reduced resistivity values. Film resistivities as low as 17 $\mu\Omega\text{cm}$ could be achieved only at deposition temperatures above 440 °C. In contrast to these observations, Tsuzuku et al.²²⁴ found no indication of β -tungsten formation using the same reaction conditions.

Laser-induced thermal deposition of pure tungsten lines on boron nitride (BN) or polyimide was achieved by Grossman and Karnezos.²²² A 514.5 nm laser beam was focused to a 2.5 μm spot to locally heat the substrate under an atmosphere of WF₆/H₂ in the ratio 1:10 to 1:40 with a total pressure of 425 torr. Using a scan speed of 60-200 $\mu\text{m/sec}$ and a laser power density of 25-300 mW/cm^2 , pure tungsten lines (10% W) 0.1-1 μm thick and with a line width of 0.5-1 μm were generated on BN or polyimide substrates. Increasing the laser power increased the thickness and width of the tungsten lines. No data on the resistivity were given. Tungsten lines on alumina were deposited by Gottleben and Stuke²²³ using the same laser with a power density of 1.5 W/cm^2 and a scanning speed of 250 $\mu\text{m/sec}$. The experiments were carried out at 30-300 mbar with a 1:10 mixture of WF₆/H₂. The resistivity of the tungsten averaged only 13-20 $\mu\Omega\text{cm}$.²²³

Selective LCVD of tungsten films by direct photo-excitation of WF₆ on Si(100) was studied by Fang et al.¹⁷⁵ The UV light source array generated UV light with peak intensity at 253.7 nm (4.886 eV) and a power density of 12 mW/cm^2 . A constant pressure of 1 torr was maintained during all the experiments. The obtained films were amorphous (XRD) and contained only small amounts of carbon and oxygen. They showed a resistivity of 100-130 $\mu\Omega\text{cm}$. Annealing at 800 °C for 30 min under an atmosphere of argon led to polycrystalline films with a resistivity as low as 18 $\mu\Omega\text{cm}$. The deposition rate increased with higher temperatures. At 230 °C a value of 2 $\mu\text{m/h}$ was determined and at 300 °C the deposition rate was 40 nm/min. Selective deposition on silicon was maintained for 40 min at 230 °C and for 30 min at 300 °C. Above 400 °C selectivity was totally lost. No encroachment problems and no self-limiting of the deposition process were observed during the growth of a 2.25 μm thick film. The tungsten functioned as an excellent diffusion barrier in Al/Si contacts up to 450 °C. Sheet resistivity and barrier height of the tested Al/W/Si samples were constant up to

this temperature. Above 500 °C, both values increased quickly with increasing temperature. Therefore, the reported method seems suitable to manufacture diffusion barriers for Al and Si contacts for electronic devices.

Shintani et al.¹⁶² observed good step coverage in experiments using an ArF excimer laser with 0.2 J/pulse, 0.0004 Pa background pressure and the WF₆/H₂ system at temperatures between 200 and 500 °C. Severe encroachment problems, especially at higher temperature and higher partial pressure of WF₆, were overcome by using a 5:1 H₂/WF₆ gas mixture. Only with such a reactant ratio was good adherence achieved above 500 °C. The resistivity of the tungsten films ranged from 8-11 μΩcm and was consistent with the occurrence of the low resistivity α-tungsten phase only. At 400 °C the preferred orientation in the deposits was the (200) phase. Below 300 °C, however, the XRD pattern showed (200) and (110) orientations. With an increase in the H₂/WF₆ ratio, the dominant crystal orientation shifted from (200) to (100).

In contrast to these results, Mogyrosi and Carlsson³⁷ found formation of the high resistivity β-tungsten phase at temperatures below 350 °C. Values as high as 160-260 μΩcm were found for pure β-tungsten phases formed below 250 °C. At higher temperatures formation of α-tungsten increased until the pure phase was formed above 400 °C with a resistivity of 8 μΩcm. The experiments were carried out using an ArF laser parallel to the silicon substrate and a WF₆/H₂/Ar mixture with a 1:40:100 ratio. This mixture was more dilute than that used by Shintani¹⁶² who obtained excellent results. Below 250 °C the growth rate was 10 nm/sec for a pure photolytic reaction and 60 nm/sec at 450 °C when deposition was a combination of photolysis and thermolysis. The contribution of photolysis and thermolysis apparently cause the increase in growth rate. The results obtained with a focused laser beam were slightly better than with an un-focused laser beam. This was probably due to a lower power density causing lower deposition temperatures.

The WF₆/Si System

Fewer studies have been carried out for the WF₆/Si system.^{170,225,226} As mentioned earlier, this process is self-limiting to a maximum film thickness of 50-100 nm because silicon and WF₆ have to diffuse through the already deposited tungsten film to react with each other and to allow further film growth.^{170,225-230} Nevertheless, these films turn out to have good morphology and are pure.

Liu et al.¹⁷⁰ deposited tungsten on silicon by local heating with a focused argon ion laser directed perpendicular to the substrate. The line width which was obtained from a 20 μm beam spot could be as small as 3 μm and was controlled by the scan speed and the laser power. In small enough reacting areas, gas-phase diffusion can become three dimensional. The product gases can diffuse away not only vertically, but also to the sides of the deposition zone, allowing more rapid diffusive transport away from the deposition spot than in large-scale deposition processes, where only one dimensional

diffusive transport vertical to the substrate can take place. This leads to much higher deposition rates of up to 7 $\mu\text{m}/\text{sec}$ for the laser-induced process. The deposition was selective for silicon in the presence of SiO_2 . Analysis of these tungsten lines showed that they contain a high percentage of WSi_2 which indicates processing temperatures (local heating of the substrate) higher than 600 $^\circ\text{C}$.

The WF_6/SiH_4 System

Direct writing of tungsten lines using a WF_6/SiH_4 gas mixture with a fast scanning speed has been demonstrated by Black et al.¹⁷⁴ The low activation temperature of 150 $^\circ\text{C}$ is sufficient to trigger this highly exothermic reaction. A high WF_6 to SiH_4 ratio in the gas phase generates very pure tungsten deposits; a high concentration of SiH_4 , on the other hand, leads to the formation of WSi_2 which is useful for gate formation, interconnects, and adhesion layers.³ By controlling the process parameters, it is possible to control the composition of the deposited thin films. A major processing difficulty is the violent reaction of WF_6 with SiH_4 which can lead to tremendous explosions. This can be avoided by using a low total pressure, low partial pressure of silane, and a fast flow rate in the deposition experiments.

Meunier et al.²⁰⁸ explored laser direct writing on substrates such as SiO_xN_y , TiN , and GaAs . Diode laser processing ($\text{Ga}_{1-x}\text{Al}_x\text{As}$ substrate, 200 mW, 820 nm) on TiN from a WF_6/SiH_4 gas mixture at low pressure (≈ 4 torr) yielded $\text{WSi}_{0.7-0.9}$ lines having a width of 4 μm and no impurities. In most cases the writing speed was 5 or 10 $\mu\text{m}/\text{sec}$. For the lower writing speed the deposition threshold with respect to the laser power was approximately 100 mW. Lines deposited at a laser power above 400 mW were irregular and showed poor adherence to the substrate.

Despite the corrosiveness of WF_6 and its decomposition products, this tungsten source has proven to be the best precursor to deposit high-quality, pure tungsten films by laser deposition technologies. Other potential tungsten sources for LCVD are the hexachloride and hexabromide. The disadvantage of a much lower vapor pressure compared to WF_6 might be compensated by the more favorable processing properties such as non-corrosive deposition conditions or non-self-limiting selective deposition.

3.6 Plasma-Enhanced Chemical Vapor Deposition (PECVD)

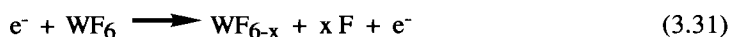
Plasma-enhanced CVD is the preferred commercial technique for low-temperature (<400 $^\circ\text{C}$) deposition of silicon nitride and oxide films, and it shows great promise for the deposition of amorphous and crystalline semiconductor films. Currently, new techniques are being explored (e.g., remote PECVD), and new types of reactors are

emerging to improve the quality of the deposited thin metal films (low heteroatom impurities and low-resistivity metal deposits).^{228,229} Relatively few studies have been carried out to obtain highly pure metal films by PECVD,^{3,228,229} and in comparison with other deposition techniques, production rate and yield are low. The major drawback of this method lies in the difficulties of controlling deposition conditions and results. Because of these complexities, this process is currently of minor interest. A summary on the formation of tungsten coatings using PECVD follows.

Several research groups^{224,230-236} have employed PECVD to achieve highly pure tungsten films at low temperatures. Currently, two different methods are used in PECVD to create a plasma.

The Parallel Plate, Radial Flow Reactor

The parallel plate, radial flow reactor generates a plasma by applying a RF or DC discharge. In this case the application of a pure WF_6 atmosphere causes etching of tungsten according to the gas-phase reaction



and generates atomic fluorine which subsequently etches already deposited tungsten by forming volatile tungsten subfluorides. This can be avoided with the presence of hydrogen gas during the deposition. Under such conditions Chu et al.²³⁷ obtained smooth and pinhole free tungsten films with a growth rate of 4 nm/min and a resistivity between 45 and 200 $\mu\Omega\text{cm}$. Typical reaction conditions were 350 °C substrate temperature, 0.2 torr pressure, 0.06 W/cm² power density (4.5 MHz RF), and a H_2/WF_6 ratio in the gas stream of 3:1. Annealing at 950-1100 °C lowered the resistivity to 7-8 $\mu\Omega\text{cm}$. The films were contaminated with silicon, oxygen, and fluorine (1.1-1.5 at.%). The silicon impurities were believed to come from impurities in the WF_6 source. Only 0.5 at.% fluorine remained after annealing above 650 °C. The film resistivity was very sensitive to the H_2/WF_6 ratio. A low partial pressure of WF_6 and high deposition temperatures generated tungsten films with resistivities close to bulk tungsten. The increase of the RF power is similar to the decrease of RF frequency and higher vacuum. It is assumed that higher hydrogen concentration more effectively scavenges the fluorine in the gas phase, thus lowering the fluorine contamination in the films. The high resistivity values are probably caused by large grains with poor connectivity and/or lower defect concentrations. Tang et al.^{35,238} determined in further experiments that the high resistivity is caused by the formation of the meta-stable β -tungsten phase. The main disadvantage of ion-bombardment-enhanced reactions as used in this method is that it causes poor step coverage in small features. This is caused by the shielding effect of the microstructure on the ion flux and deposited films will be less dense at the side

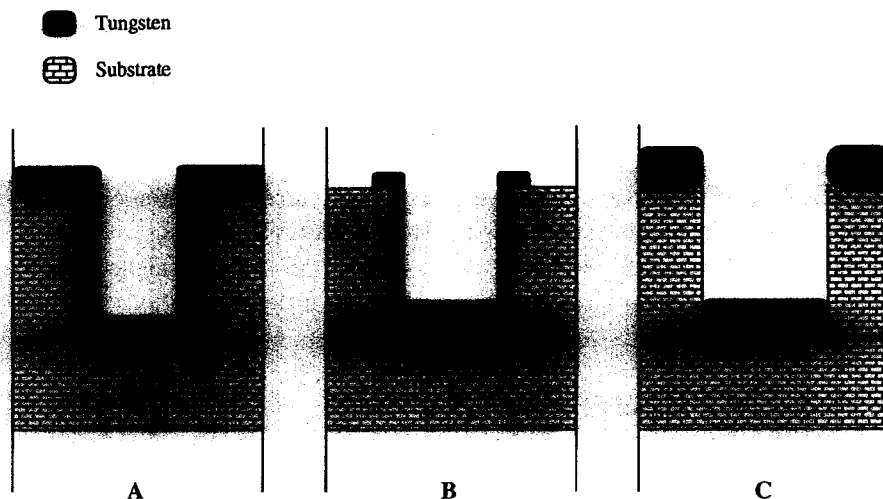


Figure 3-3. Effects of different deposition methods on the coverage of microstructures: (A) conformal coverage achieved with CVD, (B) creep-up effect during via filling (e.g., silane chemistry), (C) poor step coverage caused by shielding of ion flux during PECVD.

walls in holes and vias (see Fig. 3-3).²³⁹ However, this disadvantage might turn into an advantage for certain applications where deposition on sidewalls of small features or patterns on the substrate is not desired. This is sometimes the case for selective via and plug filling where "creep up" is highly undesirable.

The Remote Microwave Plasma Reactor

Another PECVD technique involves the excitation of one of the reactants by a remote microwave plasma which produces, for instance, atomic hydrogen and removes the need of a catalytic surface to activate the molecular hydrogen. The extremely reactive atomic hydrogen can diffuse to the substrate surface and react with the precursor (activation energy for the reaction with WF_6 : 39 kJ/mol). In this way tungsten coatings with a resistivity of 8-12 $\mu\Omega\text{cm}$ can be deposited.^{224,239} The advantage of this technique is that it avoids ion-bombardment of the substrate and fluorine generation in the gas phase as mentioned above. Both of these factors are characteristic of the parallel plate discharge PECVD setup (method 1) and are assumed to cause the formation of the high resistivity β -tungsten phase.²³⁹

The use of WF_6 in PECVD was studied by Mahowald and Ianno.²³⁰ The deposition was carried out in a parallel-plate reactor at 13.56 MHz using a 6:1 and 10:1 ratio of

H₂/WF₆ and maintaining a total pressure of 0.5 torr. The resulting metal films contained mainly carbon impurities in the range of 10-25 at.% and oxygen impurities of about 3-10 at.%. The resistivity of samples as deposited lay in the range of 1.45-14.3 Ω/square and between 0.07-1.74 Ω/square after annealing. Increasing pressure lowered the contamination with heteroatoms and the deposition rate increased as well. The quality of the tungsten deposits, however, obtained with this precursor was apparently not good enough for fabrication of high-quality microelectronic devices.

3.7 Summary and Outlook

Since its discovery as a precursor for CVD of W in 1960, WF₆ is still the best tungsten source for deposition of highly pure and well adherent tungsten films with resistivities close to bulk α-tungsten. Despite significant disadvantages, several exceptional properties of WF₆ put it ahead of all other precursors investigated so far.

- (1) High vapor pressure (WF₆ is a gas at room temperature).
- (2) Metal films can be 100% pure.
- (3) Selective deposition can be obtained on silicon surfaces.

No other precursor investigated to date fulfills all three of these requirements. In addition, the development of SiH₄ and GeH₄ as reducing agents for WF₆ has led to significantly lower deposition temperatures (270 °C), higher deposition rates, and less encroachment compared to WF₆, SiH₄, and H₂. Also, as techniques have evolved, several difficult problems have been overcome such as tungsten deposition on III/V-semiconductors using WF₆ as a precursor. In early work, the corrosiveness of this process made it impossible to obtain high-quality tungsten films on these substrates. However, it was possible to overcome this problem with the development of RT-CVD.¹²⁹⁻¹³¹

Despite these advantages, the disadvantages observed with CVD using WF₆ still limit the range of applications for this precursor. The microelectronics industry has a need for the deposition of tungsten at lower temperatures and under less corrosive conditions. The industry, therefore, has interest in other tungsten precursors.

Organometallic tungsten compounds are promising, because they often show high vapor pressures and low decomposition temperatures. They can be liquids at temperatures below 100 °C, which facilitates transport processes. However, the two main disadvantages of organometallic precursors are their difficult synthesis and purification compared to the tungsten halides and the high carbon (and oxygen) concentration in the films. The Pt co-deposition process¹⁵⁴ has the potential to

minimize this problem. Tungsten films obtained by W/Pt co-deposition show 5.3% carbon and 1.8% oxygen impurities, which is relatively high purity for decomposition of an organo-tungsten precursor. Two inexpensive and promising alternatives to Pt are Ni and Co. Their organometallic precursors, $\text{Ni}(\eta^5\text{-C}_5\text{H}_5)_2$ and $\text{Co}(\eta^5\text{-C}_5\text{H}_5)_2$, are easy to synthesize, show sufficiently high vapor pressures, and give pure metal films. As good hydrogenation catalysts, they might be even more effective than Pt.

Using organometallic compounds for LCVD gives films with very high impurity levels. Clean tungsten deposits can only be obtained when the substrate is heated above 700 °C. Thermodynamic calculations confirm these experimental results for the precursor $\text{W}(\text{CO})_6$. On the other hand, WF_6 gives high-purity tungsten films with low resistivity by LCVD. An unsolved problem for LCVD is tungsten deposition on III-V semiconductors without damage to the substrate.

Finally PECVD of W shows promising results. Still more research has to be done to optimize this process.

Acknowledgments: I would like to thank the Deutsche Forschungsgemeinschaft for funding my 21 months stay at UCLA. I am especially grateful to Professors Herbert D. Kaesz and Robert F. Hicks who guided me into the exciting field of CVD and for their interesting and fruitful discussions. Furthermore, I would like to thank Professors Toivo T. Kodas and Mark Hampden-Smith who gave me the opportunity to write this chapter and who helped me with important comments and suggestions.

References

1. *Proceedings of the Workshop on Tungsten and Other Refractory Metals, for VLSI Applications I-VI*, Materials Research Society, Pittsburgh, PA **1985-1991**.
2. Pierson, H.O. *Handbook of Chemical Vapor Deposition*, Noyes, Park Ridge, New Jersey, **1992**, p. 148/347.
3. Pierson, H.O. *Handbook of Chemical Vapor Deposition*, Noyes, Park Ridge, New Jersey, **1992**.
4. Miller, N.E., Beinglass, I. *Solid State Technol.* **1980**, 12, 79.
5. Miller, N.E., Beinglass, I. *Solid State Technol.* **1982**, 12, 85.
6. Gargini, P.A. *Ind. Res. Dev.* **1983**, 3, 141.
7. Green, M.L. Levy, R.A. *J. Met.* **1985**, 37, 63.
8. Green, M.L. Levy, R.A. *J. Electrochem Soc.* **1987**, 134, 37C.
9. Williams, J.O. *Angew. Chem. Adv. Mater.* **1989**, 101, 1136.
10. Herndon, T.O. *Proceedings of the Symposium on Electromigration of Metals, First International Symposium on Multilevel Metallization and Packaging*, Electrochemical Society, Pennington, New Jersey, 1983, 87.

11. MacDonald, N.C. Chen, L.Y., Yao, J.J., Zhang, Z.L., McMillan, J.A., Thomas, D.C. *Sensors and Actuators* **1989**, 20, 123.
12. Schmitz, J.K.J. *Chemical Vapor Deposition of Tungsten and Tungsten Silicides*, Noyes, Park Ridge, New Jersey, 1991.
13. Kaesz, H.D., Williams, R.S., Hicks, R.F., Zink, J.I., Müller, H.-J., Chen, Y.-J., Xue, Z., Shuh, D.K., Kim, Y.-K. *New J. Chem.* **1990**, 14, 527.
14. Williams, R.S., Lince, J.R., Tsai, T.C., Pugh, J.H., in *Thin Films - Interfaces and Phenomena*, Mater. Res. Soc. Symp. Proc., **1986**, 54, 335.
15. Saraswat, K.C., Swirhun, S., McVittie, J.P., in *VLSI Science & Technol.*, Bean, K.E., Rozgonyi, (eds.), Electrochem. Soc. Softbound Proc. Series, Pennington, NJ, 1984, 409.
16. Swirhun, S., Saraswat, K.C., Swanson, R.M. *IEEE Electron Device Lett.* **1984**, EDL-5, 209.
17. Vossen, J.L., Kern, W. (eds.), *Thin Film Processes I and II*, Academic, San Diego, New York, 1978 and 1991.
18. Moriya, T., Shima, S., Hazuki, Y., Chiba, M., Kashiwagi, M. *IEDM Tech. Dig.*, Ch. 1973-7/83, 1983, 55.
19. Broadbent, E.K., Ramiller, C.L., *Electrochem. Soc. San Francisco, CA, May 1983*, Extended Abstracts, Electrochem. Soc., 1983, Vol 83, p. 657.
20. Schmitz, J.K.J. *Chemical Vapor Deposition of Tungsten and Tungsten Silicides*, Noyes, Park Ridge, New Jersey, 1991, p.95 and references therein.
21. Thomas, O., Charai, A., D'Heurle, F.M., Finstad, T.G., Joshi, R.V. *Thin Solid Films* **1989**, 171, 343.
22. Krusin-Elbaum, L., Aboelfotoh, M.O., Lin, T., Ahn, K.Y. *Thin Solid Films* **1987**, 153, 348.
23. Donohue, J. *The Structure of the Elements*, Wiley, New York, 1974, 187.
24. Pearson, W.B. *Handbook of Lattice Spacings and Structures of Metals and Alloys*, Pergamon, London, 1958, p. 884, Vol. 2, Oxford, 1967, 1286.
25. Hartmann, H., Ebert, F., Breitschneider, O. *Z. Anorg. Allgem. Chem.* (German) **1931**, 198, 116/140.
26. Smithells, C.J. *Metals Reference Book*, London, **1955**, 195.
27. Morcom, W.R., Worrell, W.L., Sell, H.G., Kaplan, H.I. *Metallurgical Trans.* **1974**, 5, 155.
28. Basaviah, S., Pollack, S.R. *J. Appl. Phys.* **1968**, 39, 5548; *Appl. Phys. Lett.* **1968**, 12, 259.
29. Paine, D.C., Bravman, J.C., Yang, C.Y. *Appl. Phys. Lett.* **1987**, 50, 498.
30. Davazoglou, D., Donnadiou, A. *Thin Solid Films* **1987**, 147, 131.
31. Busta, H.H., Tang, C.H. *J. Electrochem. Soc.* **1986**, 133, 1195.
32. Hagg, G., Schonberg, N. *Acta Crystallogr.* **1954**, 7, 351.
33. Gasgnier, M., Nevot, L., Baillif, P., Bardolle, J. *Phys. Status Solidi* **1983**, A 79, 531.
34. Chopra, K.L., Randlett, M.R., Duff, R.H. *Appl. Phys. Letters* **1966**, 9, 402.

35. Tang, C.C., Hess, D.W. *Appl. Phys. Lett.* **1984**, 45, 633.
36. Ammerlaan, A.M., Boogaard, D.R.M., van der Putte, P.J., Schoonman, J. *Appl. Surf. Sci.* **1991**, 53, 24.
37. Mogyrosi, P., Carlsson, J.-O. *J. Vac. Sci. Technol.* **1992**, A 10, 3131.
38. Deutsch, T.F., Rathman, D.D. *Appl. Phys. Lett.* **1984**, 45, 623.
39. Petroff, P., Sheng, T.T., Sinha, A.K., Rozgonyi, G.A., Alexander, F.B. *J. Appl. Phys.* **1973**, 44, 2545.
40. Wöhler, F., Uslar, *Lieb. Ann.* **1855**, 94, 255.
41. Lander, J.J., Germer, L.H. *Am. Inst. Mining Met. Engrs., Inst. Metals Div., Metals Technol.* **1947**, 14(6), Tech. Publ. 2259; *Metal Ind.*, London, **1947** 71, 487.
42. Lander, J.J., Germer, L.H. *Trans. Met. Soc., Am. Inst. Mining Met. Engrs.* **1948**, 175, 648.
43. Caves, R.M. *Trans. Met. Soc. AIME* **1962**, 224, 267.
44. *Gmelin Handbuch der Anorganischen Chemie, Ergänzungsband A1 (Metall Tech.)* Syst. Nr. 54 (Wolfram), 1979, Section 4.3.2.2, 205.
45. Ohba, T., Inoue, S., Maeda, M. *IEDM* **1987**, 214.
46. Ohba, T., Suzuki, T., Hara, T. *Proceedings of the Workshop on Tungsten and Other Refractory Metals for VLSI Applications IV*, Materials Research Society, Pittsburgh, PA, 1989, 17.
47. Herd, S.R., Ahn, K.Y., Fryer, P.M., Karasinski, J.M. *Proceedings of the Workshop on Tungsten and Other Refractory Metals for VLSI Applications IV*, Materials Research Society, Pittsburgh, PA, 1989, 47.
48. van der Jeugd, C.A., Leusink, G.J., Janssen, G.C.A.M., Radelaar, S. *Appl. Phys. Lett.* **1990**, 57, 354.
49. van der Jeugd, C.A., Janssen, G.C.A.M., Radelaar, S. *J. Appl. Phys.* **1992**, 72, 1583.
50. Stacy, W.T., Broadbent, E.K., Norcott, M.H. *J. Electrochem. Soc.* **1985**, 132, 444.
51. Broadbent, E.K., Morgan, A.E., DeBlasi, J.M., van der Putte, P., Coulman, B., Burrow, B.J., Sadana, D.K. *J. Electrochem. Soc.* **1986**, 133, 1716.
52. van der Putte, P., Sadana, D.K., Broadbent, E.K., Morgan, A.E. *Appl. Phys. Lett.* **1986**, 49, 1723.
53. Ellwanger, R.C., van Dijk, A.J.M., Schmitz, J.E.J., Verhaar, R.D.J. *Proceedings of the Workshop on Tungsten and Other Refractory Metals for VLSI Applications IV*, Materials Research Society, Pittsburgh, PA, 1989, 93.
54. Hårsta, A., Carlsson, J.-O. *Proceedings of Workshop on Tungsten and Other Refractory Metals for VLSI Applications IV*, Materials Research Society, Pittsburgh, PA, 1989, 245.
55. Kruck, T., Lang, W., Engelmann, A. *Angew. Chem.* **1965**, 77, 132
56. Kruck, T. *Angew. Chem.* **1977**, 79, 27.
57. Morabito, J.M., Rand, M.J. *Thin Solid Films* **1974**, 22, 293.
58. Rand, M.J. *J. Electrochem Soc.* **1973**, 120, 686.
59. *Comprehensive Organometallic Chemistry Volume 3*, Wilkinson, G., Stone, F.G.A., Abel, E.W. (eds.), Pergamon, NY, 1982, Chapt. 29.2 and references therein.

60. Patokin, A.P., Sagalovich, V.V., *Zhur. Fiz. Khim.* **1976**, 50(3), 630 (Russ.); *Russ. J. Phys. Chem.* **1976**, 50 (3), 370 (Engl. Transl.).
61. Syrkin, V.G., Uel'skii, A.A. *Zhur. Fiz. Khim.* **1969**, 43(11), 2763 (Russ.); *Russ. J. Phys. Chem.* **1969**, 43 (11), 1554 (Engl. Transl.).
62. Syrkin, V.G. et al. *J. Appl. Chem. USSR* **1972**, 45, 2366.
63. Fischer, E.O., Scherer, F., Stahl, H.O. *Chem. Ber.* **1960**, 93, 2065; Fischer, E.O., Hafner, W. *British Patent* 829 574, **1960**; Closson, R.D. *US Patent*: 3 115 510, **1963**.
64. Cloke, G.N.F., Green, M.L.H., Morris, G.E. *J. Chem. Soc., Dalton Trans.* **1981**, 1938, and references cited therein.
65. Silvon, M.P., Van Dam, E.M., Skell, P.S., *J. Am. Chem. Soc.* **1974**, 96, 1945.
66. Fischer, E.O., Fritz, H.P. *Angew. Chem.* **1961**, 11, 353.
67. Zorin, A.D., Umilin, V.A., Vanchagova, V.K. *Zh. Obshch. Khim.* **1974**, 44, 592 (Russ.); *J. Gen. Chem. USSR* (Engl. Transl.) **1974**, 44, 567.
68. Skell, P.S., Van Dan, E.M., Silvon, M.P. *J. Am. Chem. Soc.* **1974**, 96, 626.
69. Gausing, W., Wilke, G. *Angew. Chem. Int. Ed. Engl.* **1981**, 20, 186.
70. Bogdanovich, B., Bönneman, H., Goddard, R., Startsev, A., Wallis, J.M. *J. Organomet. Chem.* **1986**, 299, 347, and references cited therein.
71. Kirss, R.U., Gordon, D., Kirlin, P.S. *Mat. Res. Soc. Symp. Proc.* **1993**, 282, 275.
72. Cotton, F.A., Pipal, J.R. *J. Am. Chem. Soc.* **1971**, 93, 5441.
73. Benn, R., Brock, T.H., Dias, M.C.F.B., Jolly, P.W., Rufinska, A., Schroth, G., Seevogel, K., Wassmuth, B. *Polyhedron* **1990**, 9, 11.
74. Kirss, R.U., Chen, J. *National Meeting of the American Chemical Society, Atlanta, GA, April 1991, Abstracts*, INOR 385, 1991.
75. Kirss, R.U., Chen, J., Hallock, R.B. *Mat. Res. Soc. Symp. Proc.* **1992**, 250, 303.
76. Wilke, G., Bogdanovic, B., Hardt, P., Heimbach, P., Keim, W., Kröner, M., Oberkirch, W., Tanaka, K., Steinrücke, E., Walter, D., Zimmermann, H. *Angew. Chem.* **1966**, 78(3), 157.
77. King, R.B., Fronzaglia, A. *J. Chem. Soc. Chem. Comm.* **1966**, 9, 274; *Inorg. Chem.* **1966**, 5, 1837.
78. Moriarty, R.E., Ernst, R.D., Bau, R. *J. Chem. Soc. Chem. Comm.* **1972**, 15, 1242.
79. Piper, T.F., Wilkinson, G. *J. Inorg. Nucl. Chem.* **1956**, 3, 104.
80. Green, M.L.H., McCleverty, J.A., Pratt, L., Wilkinson, G. *J. Chem. Soc.* **1961**, 4854; see also: *Organometallic Syntheses*, Eisch, J.J., King, R.B. (eds.), Vol. 1, *Transition Metal Compounds*, King, R.B., (ed.), Academic, New York, **1965**, 79.
81. Green, M.L.H., Knowles, P. J. *J. Chem. Soc. Perkin Trans. I* **1973**, 989.
82. Brauer, G. *Handbuch der präparativen anorganischen Chemie*, Vol. I-III, Ferdinand Enke, Stuttgart, **1975**.
83. Zinn, A.A., Stovall, W.K., Kaesz, H.D., unpublished work; Zinn, A.A., Niemer, B., Kaesz, H.D. *Adv. Mat.* **1992**, 4, 375.

84. Lai, K.K., Lamb, H.H., unpublished work.
85. Morosan, C.-E., Soltuz, V. *Thin Solid Films* **1978**, 52, 181.
86. Broadbent, E.K., Ramiller, C.L. *J. Electrochem. Soc.* **1984**, 131, 1427.
87. Yu, M.L., Eldridge, B.N., Joshi, R.V. *Proceedings of the Workshop on Tungsten and Other Refractory Metals for VLSI Applications III*, Materials Research Society, Pittsburgh, PA, 1988, 75.
88. Yu, M.L., Eldridge, B.N. *J. Vac. Sci. Technol.* **1989**, A 7 (3), 1441.
89. Kuiper, A.E.T., Willemsen, M.F.C., Schmitz, J.E.J. *Applied Surface Science* **1989**, 38, 338.
90. Ahn, K.Y., Lin, T., Angilello, J., *Proceedings of the Workshop on Tungsten and Other Refractory Metals for VLSI Applications III*, Materials Research Society, Pittsburgh, PA, 1988, 25.
91. Kobayashi, N., Suzuki, M., Saitou, M., *IEEE Trans.* **1990**, 37, 577.
92. Wong, M., Kobayashi, N., Browning, R., Paine, D., Saraswat, K.C. *J. Electrochem. Soc.* **1987**, 134, 2339.
93. Green, M.L., Ali, Y.S., Boone, T., Davidson, B.A., Feldman, S.C., Nakahara, S. *J. Electrochem. Soc.* **1987**, 134, 2285.
94. Hitchman, M.L., Jobson, A.D., Kwakman, T. *Applied Surface Science* **1989**, 38, 312.
95. Joshi, R.V., Smith, D.A. *Mat. Res. Soc. Symp. Proc.* **1986**, 71, 309.
96. Tsao, K.Y., Busta, H.H. *J. Electrochem. Soc.* **1984**, 131, 2702.
97. Green, M.L., Levy, R.A. *J. Electrochem. Soc.* **1985**, 132, 1243.
98. Levy, R.A., Green, M.L., Gallagher, P.K., Ali, Y.S. *J. Electrochem. Soc.* **1986**, 133, 1905.
99. DeBlasi, J.M., Sadana, D.K., Norcott, M.H. *Mat. Res. Soc. Symp. Proc.* **1986**, 71, 303.
100. Blewer, R.S., Headley, T.J., Tracey, M.E. *Proceedings of the Workshop on Tungsten and Other Refractory Metals for VLSI Applications III*, Materials Research Society, Pittsburgh, PA, 1988, 115.
101. Rosler, R.S., Rice, M.J., Mendonca, J. *J. Vac. Sci. Technol.* **1988**, B6, 1721.
102. Foster, R.F., Tseng, S., Lane, L., Ahn, K.Y. *Proceedings of the Workshop on Tungsten and Other Refractory Metals for VLSI Applications III*, Materials Research Society, Pittsburgh, PA, 1988, 69.
103. Kusumoto, Y., Takakuwa, K., Hashinokuchi, H., Ikuta, T., Nakayama, I. *Proceedings of the Workshop on Tungsten and Other Refractory Metals for VLSI Applications III*, Materials Research Society, Pittsburgh, PA, 1988, 103.
104. Park, Y.W., Park, C.O., Chun, J.S. *Thin Solid Films* **1991**, 201, 167.
105. van der Jeugd, C.A., Leusink, G.J., Oosterlaken, T.G.M., Aikmade, P.F.A., Nanver, L.K., Goudena, E.J.G., Janssen, G.C.A.M., Radelaar, S. *J. Electrochem. Soc.* **1992**, 139 (12), 3615.
106. Yu, M.L., Ahn, K.Y., Joshi, R.V., *J. Appl. Phys.* **1990**, 67, 1055.

107. Körner, H. *Thin Solid Films* **1989**, 175, 55.
108. McConica, C.M., Krishnamani, K. *J. Electrochem. Soc.* **1986**, 133, 2542
109. Schmitz, J.K.J., *Chemical Vapor Deposition of Tungsten and Tungsten Silicides*, Noyes, Park Ridge, New Jersey, 1991, 59.
110. Bryant, W.A. *J. Electrochem. Soc.* **1978**, 125, 1534.
111. Pauleau, Y., Lami, P. *J. Electrochem. Soc.* **1985**, 132, 2779.
112. Holman, W.R., Huegel, F.J., in *Proceedings of the Conference on Chemical Vapor Deposition of Refractory Metals, Alloys and Compounds*, Schaffhauser, A.C. (ed.), American Nuclear Society, Hinsdale, IL, 1967, 127.
113. Sivaram, S., Rode, E., Shukla, R. *Proceedings of the Workshop on Tungsten and Other Refractory Metals for VLSI Applications V*, Materials Research Society, Pittsburgh, PA, 1990, 47.
114. Schmitz, J.E.J., Buiting, M.J., Ellwanger, R.C. *Proceedings of the Workshop on Tungsten and Other Refractory Metals for VLSI Applications IV*, Materials Research Society, Pittsburgh, PA, 1989, 27.
115. Schmitz, J.E.J., van Dijk, A., Graef, M., *Proc. 10th Int. Conf. on CVD*, Electrochem. Soc., Pennington, New Jersey, 1987, 87-8, 625.
116. Ng, S.L., Rosner, S.J., Laderman, S.S., Kamins, T.I., Breadbury, D.R., Amano, J. *Proceedings of the Workshop on Tungsten and Other Refractory Metals for VLSI Applications II*, Materials Research Society, Pittsburgh, PA, 1987, 93.
117. Smith, G.C., Jucha, R.B. *Proc. 3rd Int. VLSI Multilevel Interconn. Conf.*, IEEE, **1986**, 403.
118. Broadbent, E. K. *J. Vac. Sci. Technol.* **1987**, B5, 1661.
119. Creighton, J.R. *J. Vac. Sci. Technol.* **1989**, 7, 621.
120. Creighton, J.R. *J. Electrochem. Soc.* **1989**, 136, 271.
121. Bradbury, D.R., Kamins, T.I. *J. Electrochem. Soc.* **1989**, 133, 1214.
122. Chow, R., Schmitz, J., Arnold, P., Gasner, J.T., Butler, J.D. *Proceedings of the Workshop on Tungsten and Other Refractory Metals for VLSI Applications VI*, Materials Research Society, Pittsburgh, PA, 1991, 89.
123. Itoh, H., Nakata, R., Kaji, N., Endo, T., Watanabe, T., Okano, H. *Mat. Res. Soc. Symp. Proc. VLSI V*, Materials Research Society, Pittsburgh, PA, 1990, 23.
124. Schmitz, J.K.J. *Chemical Vapor Deposition of Tungsten and Tungsten Silicides*, Noyes, Park Ridge, New Jersey, 1991, 80.
125. Dass, M.L.A., Sivaram, S., Tracy, B. *Mat. Res. Soc. Symp. Proc.* **1990**, 168, 185.
126. Metz, W.A., Mahan, J.E., Malhotra, J.E., Martin, T.L. *Appl. Phys. Lett.* **1984**, 44, 1139.
127. Melliar-Smith, C.M., Adams, A.C., Kaiser, R.H., Kushner, R.A. *J. Electrochem. Soc.* **1974**, 121, 298.
128. Fuhs, C., McInerney, E.J., Watson, L., Zetterquist, N. *Proceedings of the Workshop on Tungsten and Other Refractory Metals for VLSI Applications I*, Materials Research Society, Pittsburgh, PA., 1985, 257.

129. Katz, A., Feingold, A., Nakahara, S., Pearton, S.J., Lane, E. *Appl. Phys. Lett.* **1992**, 61, 525.
130. Katz, A., Feingold, A., El-Roy, A., Pearton, S.J., Lane, E., Nakahara, S., Geva, M. *Semicond. Sci. Technol.* **1992**, 7, 1325.
131. Katz, A., Feingold, A., El-Roy, A., Pearton, S.J., Lane, E., Nakahara, S., Geva, M. *Appl. Phys. Lett.* **1992**, 61, 1522.
132. Powell, C.F., Oxley, J.H., Blocher, J.M. *Vapor Deposition*, Wiley, New York, 1966, 322.
133. Powell, C.F., Campell, I.E., Gonser, B.W. *J. Electrochem Soc.* **1948**, 93, 258.
134. Mehalchick, E.J., MacInnis, M.B. *Electrochem. Technol.* **1968**, 6, 66.
135. Hårsta, A., Carlsson, J.-O. *Thin Solid Films* **1989**, 176, 263.
136. Pring, J.N., Fielding, W. *J. Chem. Soc.* **1909**, 95, 1502.
137. Sirtl, E., (Siemens AG.), *US Patent* 3 619 288, Nov. 9, **1971**.
138. Hieber, K., Von Tomkewitsch, J., Treichel, H., Kruck, T., Spindler, O., (Siemens A.-G.), *Eur. Pat. Appl.*, EP 338,206, 25 Oct. 1989; *DE Appl.* 3,810,025, 24 Mar. 1988.
138. Kaplan, L.H., d'Heurle, F.M. *J. Electrochem. Soc.* **1970**, 117, 693.
140. Diem, M., Fisk, M., Goldman, J. *Thin Solid Films* **1983**, 107, 39.
141. Boyes, E.D. *J. Less-Common Metals* **1971**, 26, 207.
142. Vogt, G.J. *J. Vac. Sci. Technol.* **1982**, 20, 1336.
143. Zaera, F. *J. Phys. Chem.* **1992**, 96, 4609.
144. Karapet'yants, M. Kh., Karapet'yants, M.L. *Thermodynamic Constants of Inorganic and Organic Compounds*, Ann-Arbor-Humphrey Science, Ann Arbor, 1970.
145. Barnes, D.B., Pilcher, G., Pittman, D.A., Skinner, H.A., Todd, D. *J. Less Common Met.* **1974**, 38, 53.
146. Hafner, W., Fischer, E.O., *British Patent* 976 573, Nov. 25, 1964.
147. Whaley, T.P., Norman, V., *US Patent* 3 252 824, May 24, 1966.
148. Kaesz, H.D., Niemer, B., unpublished work.
149. Kirss, R.U., Brown, D.W., Higa, K.T., Gedridge, R.W. Jr. *Organomet.* **1991**, 10, 3589.
150. Gozum, J.E., Pollina, D.A., Jensen, J.A., Girolami, G.S. *J. Am. Chem. Soc.* **1988**, 110, 2688.
151. Klein, R., Kelley, R.D. *J. Phys. Chem.* **1975**, 79, 1780.
152. Korenstein, R., Hoke, W.E., Lemonias, P.J., Higa, K.T., Harris, D.C. *J. Appl. Phys.* **1987**, 62, 4929.
153. Gibson, V.C., Parkin, G. Bercaw, J.E. *Organomet.* **1991**, 10, 220.
154. Spee, C.I.M.A., Verbeek, F., Kraaijkamp, J.G., Linden, J.L., Rutten, T., Delhay, H., van der Zouwen, E.A., McInema, H.A. *Mat. Sci. Eng. B* **1993**, 17, 108.
155. Niemer, B., Zinn, A.A., Stovall, W.K., Gee, P.E., Hicks, R.F., Kaesz, H.D. *Appl. Phys. Lett.* **1992**, 61(15), 1793.
156. Joint Committee on Powder Diffraction Standards, Powder Diffraction File:

- Inorganic Phases (International Center for Diffraction Data, Swarthmore, PA, 1985).
157. Chen, Y.J., Kaesz, H.D., Thridandam, H., Hicks, R.F. *Appl. Phys. Lett.* **1988**, 53, 1591.
 158. Xue, Z., Strouse, J.M., Knobler, C.B., Kaesz, H.D., Williams, R.S., Hicks, R.F., Shuh, D.K. *J. Am. Chem. Soc.* **1989**, 111, 8779.
 159. Xue, Z., Thridandam, H., Kaesz, H.D., Hicks, R.F. *Chem. Mater.* **1992**, 4, 162.
 160. Kaesz, H.D., Williams, R.S., Hicks, R.F., Chen, Y.-J., Xue, Z., Xu, D., Shuh, D.K., Kim, Y.-K., Thridandam, H. *Mater. Res. Soc. Symp. Proc.* **1989**, 131, 395.
 161. Herman, I.P. *Chem. Rev.* **1989**, 89, 1323.
 162. Shintani, A., Tsuzuku, T., Nishitani, E., Nakatani, M. *J. Appl. Phys.* **1987**, 61, 2365.
 163. Van Maaren, A.J.P., Krans, R.L., De Haas, E., Sinke, W.C. *Appl. Surf. Sci.* **1989**, 38, 386.
 164. Allen, S.D., Trigubo, A.B., Jan, R.Y., in *Laser Diagnostics and Photochemical Processing for Semiconductor Devices*, Mat. Res. Soc. Symp. Proc., Osgood, R.M., Brueck, R.J., Schlossberg, H.R. (eds.), Materials Research Society, Pittsburgh, PA, Vol. 17, 207.
 165. Allen, S.D., Trigubo, A.B. *J. Appl. Phys.* **1983**, 54, 1641.
 166. Black, J.G., Ehrlich, D.J., Rothschild, M., Doran, S.P., Sedlacek, J.H.C. *J. Vac. Sci. Technol.* **1987**, B5, 419.
 167. Black, J.G., Doran, S.P., Rothschild, M., Ehrlich, D.J. *Appl. Phys. Lett.* **1987**, 50, 1016.
 168. Chen, C.L., Black, J.G., Doran, S.P., Mahoney, J., Murphy, R.A., Ehrlich, D.J. *J. Electron. Lett.* **1988**, 24, 1369.
 169. Miracky, R.F., in *Tungsten and Other Refractory Metals for VLSI Applications IV*, Mat. Res. Soc. Symp. Proc., Blewer, R.S., McConica, C.M. (eds.), Materials Research Society, Pittsburgh, PA, 1989, 299.
 170. Liu, Y.S., Yakymyshyn, C.P., Phillip, H.R., Cole, H.S., Levinson, L.M. *J. Vac. Sci. Technol.* **1985**, B 3, 1441.
 171. Liu, Y.S., in *Tungsten and Other Refractory Metals for VLSI Applications*, Mat. Res. Soc. Symp. Proc., Blewer, R.S., McConica, C.M. (eds.), Materials Research Society, Pittsburgh, PA, 1986, 43.
 172. Lin, J.Y., Allen, S.D., in *In-situ Patterning: Selective Area Deposition and Etching*, Mat. Res. Soc. Symp. Proc., Bernhardt, A.F., Black, J.G., Rosenberg, R. (eds.), Materials Research Society, Pittsburgh, PA, 1990, Vol. 158, 85.
 173. Auvert, G., Pauleau, Y., Tonneau, D., in *In-situ Patterning: Selective Area Deposition and Etching*, Mat. Res. Soc. Symp. Proc., Bernhardt, A.F., Black, J.G., Rosenberg, R., (eds.), Materials Research Society, Pittsburgh, PA, 1990, Vol. 158, 155.
 174. Black, J.G., Doran, S.P., Rothschild, M., Ehrlich, D.J. *Appl. Phys. Lett.* **1990**, 56, 1072.

175. Fang, Y.K., Hwang, S.B., Sun, C.Y. *J. Electrochem. Soc.* **1991**, 138, 1720.
176. Lecours, A., Meunier, M., Izquierdo, R. *Appl. Surf. Sci.* **1992**, 54, 60.
177. Flynn, D.K., Steinfeld, J.I., Sethi, D.S. *J. Appl. Phys.* **1986**, 59, 3914.
178. Gray, H.B., Beach, N.A. *J. Am. Chem. Soc.* **1963**, 85, 2922.
179. Lewis, K. E., Golden, D. M., Smith, G. P. *J. Am. Chem. Soc.* **1984**, 106, 3905 and references cited therein. See also: Fletcher, T.R., Rosenfeld, R.N. *J. Am. Chem. Soc.* **1988**, 110, 2097.
180. Jackson, R.L., Tyndall, G.W. *J. Appl. Phys.* **1988**, 64, 2092.
181. Seder, T.A., Church, S.P., Weitz, E. *J. Am. Chem. Soc.* **1986**, 108, 4721.
182. Seder, T.A., Ouderkirk, A.J., Weitz, E. *J. Chem. Phys.* **1986**, 85, 1977.
183. Weitz, E. *J. Phys. Chem.* **1987**, 91, 3945.
184. Ganske, J.A., Rosenfeld, R.N. *J. Phys. Chem.* **1989**, 93, 1959.
185. Fletcher, T.R., Rosenfeld, R.N. *J. Am. Chem. Soc.* **1985**, 107, 2203.
186. Holland, J.P., Rosenfeld, R.N. *Chem. Phys. Lett.* **1988**, 145, 481; Holland, J.P., Rosenfeld, R. N. *J. Chem. Phys.* **1988**, 89, 7217.
187. Waller, I.M.; Hepburn, J.W. *J. Chem. Phys.* **1988**, 88, 6658.
188. Waller, I.M., Davis, H.F., Hepburn, J. W. *J. Phys. Chem.* **1987**, 91, 506.
189. Nathanson, G., Gitlin, B., Rosan, A.M., Yardley, J.T. *J. Chem. Phys.* **1981**, 74, 361.
190. Yardley, J.T., Gitlin, B., Nathason, G., Rosan., A.M. *J. Chem. Phys.* **1981**, 74, 370.
191. Tumas, W., Gitlin, B., Rosan, A.M., Yardley, J.T. *J. Am Chem. Soc.* **1982**, 104, 55.
192. Venkataraman, B.K., *Photodissociation Dynamics of Transition Metal Carbonyls*, Ph.D. Dissertation, Columbia University, 1989; Venkataraman, B.K., Hou, H., Zhang, Z., Chen, S., Bandukwalla, G., Vernon, M., unpublished work.
193. Hellner, L., Massanet, J., Vermeil, C. *Chem. Phys. Lett.* **1981**, 83, 474.
194. Zaroni, R., Piancastelli, M.N., Marsi, M., Margaritondo, G. *J. Vac. Sci. Technol.* **1991**, 9A, 931.
195. Swanson, J.R., Friend, C.M. *J. Vac. Sci. Technol.* **1988**, A6, 770
196. Friend, C.M., Swanson, J.R., Flitsch, F.A. *Mater. Res. Soc. Symp. Proc.* **1989**, 131, 461.
197. Gluck, N.S., Wolga, G.J., Bartosch, C.E., Ho, W., Ying, Z. *J. Appl. Phys.* **1987**, 61, 998.
198. Andreoni, W., Varma, C.M. *Phys. Rev. B* **1981**, 23, 437.
199. Jackson, R.L., Tyndall, G.W. *J. Appl. Phys.* **1987**, 62, 315.
200. Solanki, R., Boyer, P.K., Mahan, J.E., Collins, G.J. *Appl. Phys. Lett.* **1981**, 38, 572.
201. Solanki, R., Boyer, P.K., Collins, G.J. *Appl. Phys. Lett.* **1982**, 41, 1048.
202. Singmaster, K.A., Houle, F.A., Wilson, R.J. *J. Phys. Chem.* **1990**, 94, 6864.
203. Xuebiao, L., Jie, Z., Mingxin, Q. *Thin Solid Films* **1991**, 196, 95.
204. Flitsch, F.A., Swanson, J.R., Friend, C.M. *Surf. Sci.* **1991**, 245, 85.
205. Radloff, W., Below, E., Durr, H., Stert, V. *Appl. Phys. A* **1990**, 50, 223.
206. Swanson, J.R., Flitsch, F.A., Friend, C.M. *Surf. Sci.* **1990**, 226, 147.
207. Rager, B., Bachmann, F., in *In-situ Patterning: Selective Area Deposition and*

- Etching*, Mat. Res. Soc. Symp. Proc., Bernhardt, A.F., Black, J.G., Rosenberg, R. (eds.), Materials Research Society, Pittsburgh, PA, 1990, 158, 161.
208. Meunier, M., Izquierdo, R., Desjardins, P., Tabbal, M., Lecours, A., Yelon, A. *Thin Solid Films* **1992**, 218, 137.
 209. Singmaster, K.A., Houle, F.A. *Mat. Res. Soc. Symp. Proc.* **1991**, 201, 159.
 210. Singmaster, K.A., Houle, F.A. *Proc. Electrochem. Soc.* **1992**, 92.
 211. Gilgen, H.H., Cacouris, T., Shaw, P.S., Krchnavek, R.R., Osgood, R.M. *Appl. Phys. B*, **1987**, 42, 55.
 212. Petzold, H.C., Putzar, R. *Mater. Res. Soc. Symp. Proc.* **1988**, 101, 75.
 213. Ehrlich, D.J., Osgood, R.M., Jr., Deutsch, T.F. *J. Electrochem. Soc.* **1981**, 128, 2039.
 214. Chiu, M.S., Tseng, Y.G., Ku, Y.K. *Opt. Lett.* **1985**, 10, 113.
 215. Lin, J.Y., Imen, K., Hsiao, K.C.C., Allen, S.D. *Proc. Electrochem. Soc.* **1991**, 91; *Proc. Int. Symp. Process Phys. Model. Semicond. Technol.*, 2nd, **1990**, 376.
 216. Adams, A.E., Lloyd, M.L., Morgan, S.L., Davis, N.G., in *Laser Processing and Diagnostics. Chemical Physics*, 39, Bäuerle, D. (ed.), Springer, New York, 1984, 269.
 217. McWilliams, B.M., Herman, I.P., Mitlitsky, F., Hyde, R.A., Wood, L.L. *Appl. Phys. Lett.* **1983**, 43, 946.
 218. Allen, S.D., Jan, R.Y., Mazuk, S.M., Vernon, S.D. *J. Appl. Phys.* **1985**, 58, 327.
 219. Allen, S.D., Tringubo, A.B. *J. Appl. Phys.* **1983**, 54, 1641.
 220. Berg, R.S., Mattox, D.M., *Proceedings of the Fourth International Conference on Chemical Vapor Deposition*, Wakefield, G.F., Blocher, J.M., Jr., (eds.), Electrochemical Society, Princeton, NJ, 1973, 196.
 221. Zhang, G.Q., Szörényi, T., Bäuerle, D.J. *J. Appl. Phys.* **1987**, 62, 673.
 222. Grossman, W.M., Karnezos, M. *J. Vac. Sci. Technol.* **1987**, B 5, 843.
 223. Gottleben, O., Stuke, M. *Appl. Phys. Lett.* **1988**, 52, 2230.
 224. Tsuzuku, S., Nishitani, E., Nakatani, M., Shintani, A. *Proc. Electrochem. Soc.* **1987**, 87-4, 24.
 225. Herman, I.P., McWilliams, B.M., Mitlitsky, F., Chin, H.W., Hyde, R.A., Wood, L.L. *Mater. Res. Soc. Symp. Proc.* **1984**, 29, 29.
 226. Black, J.G., Ehrlich, D.J., Sedlacek, J.H.C., Feinerman, A.D., Busta, H.H. *IEEE Electron Dev. Lett.* **1986**, EDL-7, 422.
 227. Boyes, E.D. *J. Less-Common Metals* **1971**, 26, 207.
 228. Deneuille, A., Benyahya, M., Brunel, M., Oberlin, J.C., Torres, J., Bourhila, N., Paleau, J., Canut, B. *Appl. Surface Sci.* **1989**, 38, 139.
 229. Schuegraf, K.K. (ed.), *Handbook of Thin Film Deposition Processes and Technologies*, Noyes, Park Ridge, New Jersey, 1988, 112.
 230. Mahowald, M.A., Ianno, N.J. *Thin Solid Films* **1989**, 170, 91.
 231. Hess, D.W., in *Plasma Processing for VLSI*, 8, 55, Brown, D.M. (ed.), in the series VLSI Electronics: Microstructure Science, Einspruch, N.G., (ed.), Academic, San Diego, New York, 1984.

232. Hess, D.W., in *Reduced Temperature Processing for VLSI*, Reif, R., Srinivasan, G. R., (eds.), p. 3, Electrochemical Society, Pennington, New Jersey, 1986.
233. Hess, D.W., Jensen, K.F., Anderson, T.J. *Rev. Chem. Eng.* **1985**, 3, 1985.
234. Pauleau, Y. *Thin Solid Films* **1984**, 122, 243.
235. Suhr, H., Bald, J., Deutschmann, Etspüler, A., Feurer, E., Grünwald, H., Haag, C., Holzchuh, H., Oehr, C., Reich, S., Schmid, R., Traus, I., Waimer, B., Weber, A., Wendel, H. *J. Phys.* **1989**, 50 (5), C5-739.
236. Suhr, H., *New J. Chem.* **1990**, 14, 523.
237. Chu, J.K., Tang, C.C., Hess, D.W. *Appl. Phys. Lett.* **1982**, 41, 75.
238. Tang, C.C., Chu, J.K., Hess, D.W. *Solid State Technol.* **1983**, 26 (3), 125
239. Schmitz, J.K.J. *Chemical Vapor Deposition of Tungsten and Tungsten Silicides*, Noyes, Park Ridge, New Jersey, 1991, 160.

Chapter 4

CVD Of Copper From Cu(II) Precursors

Gregory L. Griffin^a
Andrew W. Maverick^b

^aDepartment of Chemical Engineering

^bDepartment of Chemistry

Louisiana State University

Baton Rouge, LA 70803

Abstract

We review the current status of Cu CVD processes based on Cu(II) precursor compounds. Topics include: A chronological review of the field, the synthesis and properties of volatile Cu(II) compounds, adsorption studies of these and related compounds, mechanistic considerations, growth rates and reaction conditions, film properties, CVD reactor design considerations, plasma-assisted CVD, and photo-assisted CVD.

Contents

4.1	Introduction	178
4.2	Historical Review	179
4.3	Reactant Chemistry	182
4.3.1	Volatile Cu(II) Compounds	182
4.3.2	Reactant Geometry	185
4.3.3	Synthesis of Cu(II) Precursors	186
4.3.3.1	Cu(hfac) ₂ • nH ₂ O (n = 0, 1, 2)	186
4.3.3.2	Schiff-Base Complexes	187
4.3.4	Volatility	188
4.3.5	Reaction Stoichiometry	190
4.4	Adsorption Studies	191
4.4.1	Adsorption of Cu(II) Compounds	193
4.4.1.1	Molecular Adsorption	193
4.4.1.2	Dissociative Adsorption	193
4.4.1.3	Ligand Geometry	196
4.4.1.4	Reversibility	197
4.4.1.5	Non-Metallic Substrates	198
4.4.2	Adsorption of Cu(I) Compounds	199
4.4.3	Adsorption of H(hfac)	200
4.4.4	Ligand Decomposition	201
4.5	Growth Kinetics	202
4.5.1	Deposition Rates	202
4.5.2	Deposition Temperature	203
4.5.3	Reactant Concentration	204
4.5.4	Carrier Gas Effects	206
4.5.5	Substrate Selectivity	208
4.6	Film Properties	210
4.6.1	Purity	210
4.6.2	Resistivity	211
4.6.3	Microstructure	212
4.6.4	Other Properties	214
4.7	Reaction Mechanism	214
4.8	Rate Expression	216
4.8.1	Response Surface	216
4.8.2	Mechanism Fitting	217
4.9	Reactor Design	219
4.9.1	Transport Effects	220
4.9.2	Reactor Modeling	220
4.10	Plasma-Assisted CVD (PACVD)	222

4.10.1	Operating Variables	224
4.10.1.1	Reactor Configuration	224
4.10.1.2	Substrate Temperature	224
4.10.1.3	Power Density	225
4.10.1.4	Reactant Concentration	225
4.10.1.5	Carrier Gas	226
4.10.2	Reaction Mechanism	226
4.10.3	Film Properties	226
4.10.3.1	Purity	226
4.10.3.2	Resistivity	227
4.10.3.3	Morphology	227
4.10.3.4	Conformality	228
4.11	Laser-Assisted CVD (LCVD)	228
4.11.1	Operating Variables	229
4.11.1.1	Reactants	229
4.11.1.2	Growth Kinetics	229
4.11.1.3	Substrate Temperature	230
4.11.1.4	Laser Intensity	231
4.11.2	Film Properties	231
4.11.2.1	Purity	231
4.11.2.2	Resistivity	231
4.11.2.3	Morphology	231
4.11.3	Reaction Mechanism	232
4.11.3.1	Transport Effects	233
4.12	Summary	233
	Acknowledgments	235
	References	235

4.1 Introduction

Metallization has become the dominant hurdle for yield and reliability in many areas of VLSI (very large scale integration) technology. For example, the total number of processing steps required for four-level metallization in a typical ASIC (application specific integrated circuit) technology exceeds the number of steps used to fabricate the transistors.¹ As device density increases and line widths decrease, the associated increase in current density will lead to greater concern about electromigration and stress-induced void formation in metal interconnect lines.

In light of these concerns, chemical vapor deposition (CVD) of Cu has been proposed as an alternative to Al or CVD-W metallizations for future generations of deep sub-micron integrated circuits. It is being considered for upper level interconnects² and for filling contact and via holes.³ Copper offers several intrinsic property advantages over Al, including lower resistivity ($1.7 \mu\Omega\text{cm}$ for Cu, vs. $2.7 \mu\Omega\text{cm}$ for Al), improved electromigration resistance (up to 4 orders of magnitude greater than Al⁴) and increased resistance to stress-induced voidage (i.e., reflecting its higher melting point vs. Al). There are also reported advantages for Cu related to device performance such as greater speed and reduced cross talk⁵ and smaller RC time constants.⁶

Beginning in 1989, the number of exploratory studies of CVD of Cu reported in the literature expanded rapidly. These studies identified two basic types of reaction chemistry which can be classified according to the oxidation state of the Cu-containing reactant. Processes based on H₂ reduction of volatile Cu(II) complexes originated with the early work of Van Hemert et al.⁷ Potential advantages include greater stability of the reactants and greater flexibility in reactor design because of the ability to adjust the H₂ partial pressure as a control variable. Processes based on the disproportionation of Cu(I) compounds have emerged more recently^{8,9,10} (see Ch. 5) and may offer the advantage of significantly higher deposition rates and the ability to operate without a carrier gas at the possible expense of greater restrictions on process design and control.

In this chapter we review the current status of the Cu(II) CVD processes [Cu(I) processes are reviewed in Ch. 5]. Where appropriate, we will point out similarities and differences including elementary steps in the reaction mechanism that may be common to both processes. Our review of the Cu(II) process will include the synthesis and properties of volatile Cu(II) compounds, adsorption studies of these and related compounds, mechanistic considerations, growth rates and reaction conditions, film properties, reactor design considerations, plasma-assisted CVD, and photo-assisted CVD.

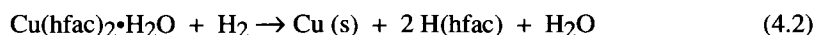
4.2 Historical Review

The first report of Cu CVD using a metal-organic complex was the result of U.S. Air Force research to develop volatile chelates that could be used for gas chromatography of metal cations. Van Hemert and coworkers⁷ described the use of two Cu(II) β -diketonate complexes, Cu(tfac)₂ and Cu(hfac)₂•H₂O (see Table 4-1 for ligand abbreviations). Films

Table 4-1 Ligand Abbreviations (see also list of Chemical Abbreviations)

H(acac)	=	2,4-pentanedione
H(tfac)	=	1,1,1-trifluoro-2,4-pentanedione
H(hfac)	=	1,1,1,5,5,5-hexafluoro-2,4-pentanedione
H(dpm)	=	2,2,6,6-tetramethyl-3,5-heptanedione
H(fod)	=	6,6,7,7,8,8,8-heptafluoro-2,2-dimethyl-3,5-octanedione
H(tdf)	=	1,1,1,2,2,3,3,7,7,8,8,9,9,9-tetradecafluoro-4,6-nonanedione
H(ppm)	=	6,6,7,7,7-pentafluoro-2,2-dimethyl-3,5-heptanedione
H(acim)	=	4-imino-2-pentanone
H ₂ (acen)	=	4,4'-(1,2-ethanediyldinitrilo)bis(2-pentanone)
H(nona-F)	=	1,1,1,5,5,5-hexafluoro-4-[(2,2,2-trifluoroethyl)imino]-2-pentanone
COD	=	1,5-cyclooctadiene
VTMS	=	vinyltrimethylsilane

were deposited on a heated substrate in a warm-wall, horizontal tube reactor using H₂ at atmospheric pressure as the carrier gas and reducing agent:



The two reactants differed in terms of their respective vaporization temperatures; Cu(hfac)₂•H₂O could be evaporated into the carrier gas stream at 90 °C while Cu(tfac)₂ required a temperature of 150 °C. For both compounds, a substrate temperature of 250 °C gave optimum film quality. Moshier et al.¹¹ later reported a deposition rate of 80 nm/min at 300 °C using Cu(hfac)₂•H₂O.

Several of the peripheral observations in this early work foreshadowed issues that have become relevant for present day CVD metallization technology. The authors reported

that an inert carrier gas such as N_2 could be used in place of H_2 . In this case the reaction must proceed by self-reduction of the Cu(II) complex, including partial decomposition of the ligands. Higher deposition temperatures were required, and the films were less pure. Second, although they did not report selective deposition, the authors did note differences in adhesion for films deposited on different substrates. Finally, by trapping and analyzing the reaction products, the authors confirmed that the β -diketonate ligands are regenerated in their protonated form when H_2 is used as the carrier gas. This confirms the stoichiometry of reactions 4.1 and 4.2 and provides some insight to the reaction mechanism.

Charles and Cleary¹² disclosed the use of β -ketoiminato compounds such as $Cu(acim)_2$ and $Cu(acen)$. Both compounds were reduced in H_2 to regenerate the protonated form of the ligand by analogy with reactions 4.1 and 4.2 for β -diketonate complexes. Of the two compounds, $Cu(acen)$ had the lower evaporation temperature, but both required excessively high deposition temperatures. The reaction conditions are summarized in Table 4-2. Later, Fine and associates¹³ showed that a fluorinated β -ketoiminato compound, $Cu(nona-F)_2$, required much lower temperatures for both evaporation and deposition, even below those required for $Cu(hfac)_2$.

Temple and Reisman¹⁴ published the first quantitative study of the influence of reaction conditions on film purity. Studying the thermal decomposition of $Cu(hfac)_2$ in Ar carrier gas at atmospheric pressure, they measured significant formation of C and O impurities at deposition temperatures of 420 °C and above as well as a significant worsening of film resistivity. The impurities were postulated to arise from ligand decomposition that occurred because H_2 was not available to protonate and desorb the β -diketonate ligands from the surface. This suggestion has been supported by later UHV studies of $Cu(hfac)_2$ adsorption and decomposition on metal surfaces (see Section 4.4 below).

In 1990, Kaloyeros et al.¹⁵ published the first report of film resistivities that approach the value of bulk copper. Using the reduction of $Cu(hfac)_2$ in H_2 carrier gas, they obtained resistivities below 2.0 $\mu\Omega cm$ (1.67 $\mu\Omega cm$ for bulk Cu) for films deposited between 300–450 °C. Fine and associates reported values nearly as low (2.1 $\mu\Omega cm$) using H_2 reduction of $Cu(nona-F)_2$.¹³

Awaya and Arita³ reported the first demonstration of selective deposition. Using a patterned substrate, they showed normal and cross-sectional SEM micrographs of selectively filled via holes. Copper films were also deposited selectively on pre-patterned $TiSi_2$, W, Cr, Al, and Zr layers with no nuclei observed on surrounding SiO_2 or Si_3N_4 .

The first quantitative study of the influence of operating conditions on deposition rate was also reported by Fine et al.¹³ They performed a response surface analysis of deposition rate as a function of reactant concentration and temperature for H_2 reduction of $Cu(nona-F)_2$ and reported the reaction order for both $Cu(nona-F)_2$ and H_2 and the apparent activation energy for the reaction.

Table 4-2 Studies of Copper CVD Using Other Cu(II) Compounds

Compound	Evaporation Temperature (°C)	Deposition Rate (nm/min)	Deposition Temperature (°C)	Carrier Gas	Reactor Pressure (torr)	Substrate	Refs.
Cu(tfac) ₂	135-160	---	250-300	H ₂	760	glass, SS	7 11
Cu(acac) ₂	180-200	20	225-250	H ₂ /Ar	760	SiO ₂	37
Cu(dpm) ₂	100	---	400	none	< 10 ⁻²	SiO ₂ (vs. Si)	63
Cu(ppm) ₂	100	---	400	none	< 0.3	SiO ₂ (vs. Si)	63
Cu(fod) ₂	---	---	300-400	H ₂	10 ⁻³ -760	SiO ₂ (vs. Si)	15
Cu(acim) ₂	287	---	400	H ₂	730	quartz	12
Cu(acen)	204	----	450	H ₂	730	quartz	12
Cu(nona-F) ₂	85-105	70	270-350	H ₂	10-70	SiO ₂ , W, TiN	13

Notes:

SS = Stainless steel

Deposition was selective against substrate materials shown in parentheses

Lai et al.¹⁶ developed a rate expression consistent with a proposed reaction mechanism for H₂ reduction of Cu(hfac)₂ at atmospheric pressure. The expression included a Langmuir-Hinshelwood denominator to account for both reactant saturation and product inhibition effects. Awaya and Arita¹⁷ subsequently reported evidence to support the Langmuir-Hinshelwood mechanism at low pressure. Their proposed mechanism includes surface coverage effects for both Cu(hfac)₂ and H₂.

Lecohier et al. demonstrated the importance of H₂O vapor in the reactant stream.¹⁸ Studying the H₂ reduction of Cu(hfac)₂, they showed that adding H₂O vapor to the feed stream eliminated the selectivity toward deposition on Pt that had been observed in the absence of H₂O. Instead, the addition of H₂O activated the neighboring SiO₂ surface for deposition. Awaya and Arita¹⁷ later showed that adding H₂O could enhance the deposition rate of Cu by as much as an order of magnitude before the deposition of Cu gave way to deposition of Cu oxides.

Starting in 1985, several papers appeared dealing with laser-assisted CVD of Cu films. Examples include both laser pyrolysis^{19,20} and photochemical CVD.²¹ Several studies of plasma-assisted CVD have appeared since 1988²²⁻²⁴ which have employed a variety of plasma reactor configurations including parallel plate, microwave ECR (electron cyclotron resonance), and remote plasma generation.

Most recently, several authors have reported adsorption studies of Cu(hfac)₂ on both metal and non-metal surfaces.^{2,25-29} These studies include spectroscopic characterization of adsorbed species and measurements of the desorption and/or surface decomposition reaction kinetics. The studies are generally performed under ultra-high vacuum conditions and therefore may not be directly related to kinetic studies at CVD conditions. Nevertheless, the adsorption studies provide valuable direct information about several adsorbed species, their surface reactions, and their possible roles in the overall deposition mechanism.

4.3 Reactant Chemistry

4.3.1 Volatile Cu(II) Compounds

The choice of reactant for a CVD process is usually determined by an overall balance among several competing factors. The compound must have a high enough vapor pressure to provide a useful rate of transport to the reactor. It must be chemically stable at its vaporization temperature and be able to react cleanly and rapidly at the deposition temperature. Once these intrinsic requirements are satisfied, the compound and its deposition conditions must also meet a variety of process-related requirements such as substrate selectivity, surface conformality, and compatibility with barrier and passivation films.¹⁵

One of the limiting factors to date in developing a technology for CVD Cu has been the difficulty of identifying a suitable reactant. Historically, copper was known to form very few stable, volatile alkyl or carbonyl compounds (some early copper alkyl compounds are described by Jarvis et al. and Miyashita^{30,31}). This was thought to eliminate the two major classes of compounds used in most existing processes for CVD of metals or compound semiconductors.

Copper halides have been used for chemical vapor transport growth of Cu-containing semiconductor crystals (e.g., CuAlSe₂³²). There have been limited reports of their use for depositing Cu metal. Lampe-Onnerud et al.³³ reported growth rates of 5 nm/min at deposition temperatures between 350 and 500 °C, which is only 50 to 100 °C above the temperatures required for several of the Cu(II) compounds described in Section 4.3.2. However, the evaporator temperatures needed for Cu halides are much higher than those needed for metal-organic compounds. Film purity and resistivity were also a problem, possibly reflecting the high reactivity of Si substrates with metal halides.

Attention has focused instead on Cu(II) bis(β -diketonate) and Cu(II) bis(β -ketoiminate) compounds. These compounds were originally studied as a possible method of applying gas chromatography for the analysis of metal cations.^{34,35} Compounds that have been studied as CVD reactants are listed in Tables 4-2 and 4-3. The structural formulas of these compounds are shown in Figure 4-1. Each compound contains a central Cu(II) atom bonded to two singly-charged β -diketonate or β -ketoiminate ligands. Further structural details are given in Section 4.3.2.

For comparison, the Cu(I) compounds described in Chapter 5 typically contain one singly charged ligand (hfac) that is strongly bonded to the central metal atom and a second neutral ligand (a phosphine or an olefin) that is more weakly bonded to the metal atom. The difference in the metal-ligand bond strengths is reflected in the greater stability, higher deposition temperatures, and lower growth rates of the Cu(II) compounds. In contrast, the neutral ligand in the Cu(I) compounds can dissociate immediately upon adsorption giving rise to higher growth rates. Indeed, the ligand may even dissociate in the gas phase²⁹ which may be a concern in selecting the reactor design and operating conditions for the CVD process.

An important characteristic of both Cu(II) and Cu(I) compounds that have been studied as reactants for CVD is the use of heavily fluorinated ligands such as Cu(tfac)₂ and Cu(hfac)₂, vs. Cu(acac)₂. The main effect of fluorine substitution is a significant increase in the volatility of the complex.³⁶ Proposed reasons for the effect include a reduction in the van der Waals forces between molecules and a decrease in the extent of hydrogen-bonding.

It has also been suggested that the high electronegativity of the F atoms may lead to a weakening of the Cu-ligand bonds.¹⁵ Support for this suggestion may come from the large difference in deposition temperatures reported for Cu(nona-F)₂ vs. Cu(acim)₂.^{12,13} On the other hand, Pauleau and Fasasi³⁷ recently reported that films can be deposited

TABLE 4-3 Studies of Copper CVD Using Cu(II)ac/2

Evaporation Temperature (°C)	Deposition Rate (nm/min)	Deposition Temperature (°C)	Carrier Gas	Reactor Pressure (torr)	Substrate	Refs.
80-95	80	250-300	H ₂	760	glass, SS	7 11
120	4 nh	340-390	Ar	760	SiO ₂	14
45-60	10 nh	350	H ₂	7-15	W, Cr, Al, Zr, TiSi ₂ (vs. SiO ₂ , Si ₃ N ₄)	3
30-60	120-180	250-350	H ₂	10 ⁻³ -760	SiO ₂ , TiN, Al ₂ O ₃	15
90-110	10-15	250-275	H ₂	10 ⁻³ -760	glass	16
100	-	400	none	10	SiO ₂ (vs. Si)	63
50-100	20-90	350-390	H ₂ +H ₂ O	15	Ta/Si	17
80-85	10	200	H ₂	760	glass	70
55-90	20-65	310-380	H ₂	2-10	SiO ₂ , TiW, TiSi ₂	58

Notes:

nh = Compound was stated to be in anhydrous state

SS = Stainless steel

Deposition was selective against substrate materials shown in parentheses

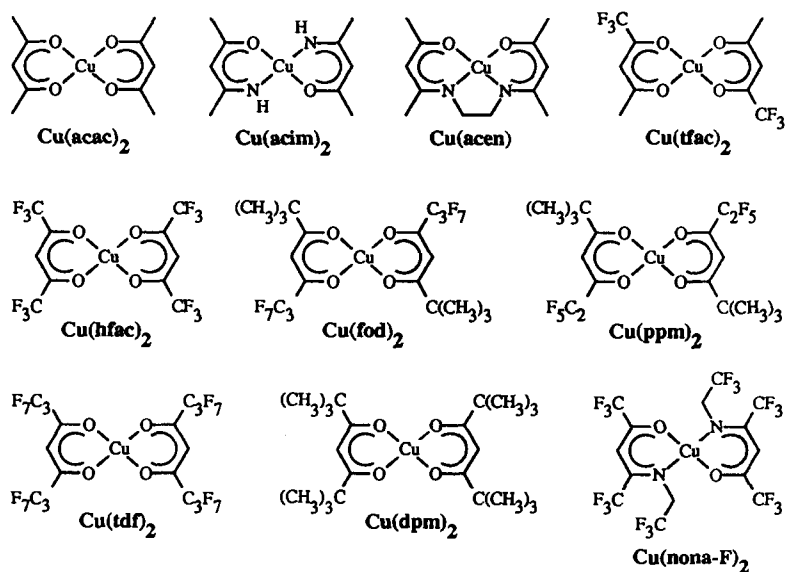


Figure 4-1 Structures of Cu(II) compounds studied as CVD reactants.

using $\text{Cu}(\text{acac})_2$ at 225 to 250 °C, which is similar to or even below the temperature range needed for deposition using $\text{Cu}(\text{hfac})_2$ (see Section 4.).

Another significant factor, at least for $\text{Cu}(\text{hfac})_2$, is the existence of hydrated forms of these complexes.³⁸ The H_2O molecule can datively bond to an open coordination site in the square planar $\text{Cu}(\text{hfac})_2$ complex to form a penta-coordinated Cu atom. A hexa-coordinated dihydrate complex is also known. Exceptions may occur for $\text{Cu}(\text{thd})_2$ and $\text{Cu}(\text{fod})_2$, where the bulky *t*-butyl groups can sterically inhibit H_2O adsorption.³⁵ The partly-tetrahedral geometry of $\text{Cu}(\text{nona-F})_2$ also prevents H_2O coordination in that complex.¹³

In the case of $\text{Cu}(\text{hfac})_2 \cdot \text{H}_2\text{O}$, the hydrated complex is physically distinguishable from the anhydrous complex by differences in color (green vs. purple) and melting point (ca. 133-136 °C vs. 95-98 °C). As described below, the hydrated complex also shows differences in deposition rate and substrate selectivity, which likely reflects a significant difference in its reaction mechanism.

4.3.2 Reactant Geometry

The structures of Cu(II) compounds that have been studied for CVD of Cu are shown in Figure 4-1. The majority of these compounds are β -diketonate complexes, of which

the prototype is $\text{Cu}(\text{acac})_2$.³⁹ Virtually all β -diketonates form simple four-coordinate, square-planar complexes with copper(II).⁴⁰ The Schiff bases, such as $\text{H}(\text{acim})$ and $\text{H}_2(\text{acen})$, also form planar four-coordinate species, except when the N atoms carry bulky substituents.⁴¹ In these cases there can be significant "twisting" away from planar geometry. Of the complexes discussed here, the only one that shows this "tetrahedral" distortion is $\text{Cu}(\text{nona-F})_2$. Here the dihedral angle between the two planes defined by the ligands is about 40 °C.¹³

The most heavily studied of the fluorinated complexes is $\text{Cu}(\text{hfac})_2$. Although the anhydrous, four-coordinate complex can reasonably be assumed to be square-planar, this appears never to have been confirmed by X-ray analysis. Adducts of $\text{Cu}(\text{hfac})_2$ with either one or two additional ligands L [i.e., $\text{Cu}(\text{hfac})_2\text{L}_n$, $n = 1, 2$] have been extensively studied. The five-coordinate species are most often square pyramidal, with basal and apical metal-ligand distances of 1.9-2.0 Å and 2.2-2.3 Å, respectively, and the Cu atom is typically displaced 0.15-0.25 Å out of the basal plane. These are known with L either in the apical⁴² or basal⁴³ position. Most of the six-coordinate complexes ($n = 2$) have the two hfac ligands equatorial (Cu-O 1.9-2.0 Å) and L axial (2.25- 2.55 Å).^{42,44,45}

4.3.3 Synthesis of Cu(II) Precursors

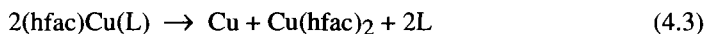
4.3.3.1 $\text{Cu}(\text{hfac})_2 \cdot n\text{H}_2\text{O}$ ($n = 0, 1, 2$)

We discuss this system first because it is by far the most extensively studied of the copper(II) CVD precursors and because it is chemically more complicated than is usually realized. The complex was reported in 1947 by Henne et al.,⁴⁶ who along with Belford et al.⁴⁷ and others, found that the complex precipitates in good yield when aqueous solutions of Cu^{2+} , $\text{H}(\text{hfac})$, and a suitable base are mixed in stoichiometric ratio. The most common method uses hydrated copper(II) acetate, $\text{Cu}_2(\text{OAc})_4 \cdot 2\text{H}_2\text{O}$, as the source of both Cu^{2+} and the base. Alternatively, another Cu salt can be used with sodium acetate added as the base³⁸ or with separately prepared sodium hexafluoroacetylacetonate for direct reaction.³⁶ The approach is successful because the neutral hexafluoroacetylacetonate ligand is somewhat soluble in water. Higher yields are obtained when $\text{Cu}_2(\text{OAc})_4 \cdot 2\text{H}_2\text{O}$ is dissolved in neat $\text{H}(\text{hfac})$.⁴⁷

Bertrand and Kaplan³⁸ were among the earliest to report the preparation of purple anhydrous $\text{Cu}(\text{hfac})_2$. However, several of their conclusions were called into question by Funck and Ortolano⁴⁸ who presented the following now generally accepted scheme. Preparations in aqueous solutions yield the yellow-green dihydrate, $\text{Cu}(\text{hfac})_2 \cdot 2\text{H}_2\text{O}$. This is stable in very humid air or at lower temperatures but slowly loses one molecule of water under typical laboratory conditions to form the "grass-green" monohydrate, $\text{Cu}(\text{hfac})_2 \cdot \text{H}_2\text{O}$. The monohydrate, which is commercially available, can be sublimed

unchanged and melts at 133-136 °C. More vigorous drying over concentrated H₂SO₄ produces the purple anhydrous compound (m.p. 95-98 °C). The purple material is hygroscopic, converting readily into the monohydrate.

Norman⁴⁹ and Shin⁹ observed that Cu CVD via disproportionation of copper(I) complexes (hfac)Cu(L) (L = neutral ligand), according to the reaction



usually yields a *green* copper(II) product, most likely Cu(hfac)₂·H₂O (see Ch. 5). Even small amounts of water adsorbed on the inner surfaces of typical CVD apparatus, which are often made of glass, are sufficient to convert the anticipated anhydrous product into the monohydrate. Scrupulously dried apparatus is required to generate the purple anhydrous material. Thus, CVD studies that utilize "Cu(hfac)₂," even if no water is intentionally added, have almost certainly dealt with the monohydrate.

Other polyfluoro-β-diketonato-Cu(II) complexes are prepared by the methods outlined above for Cu(hfac)₂. Fewer details concerning hydration are available because none of these precursors has been studied as extensively as Cu(hfac)₂.

4.3.3.2 Schiff-base Complexes

Schiff-base complexes include Cu(acim)₂, Cu(acen), and Cu(nona-F)₂. The first two of these can be prepared by mixing Cu(NH₃)₄²⁺(aq) with the pure ligand¹² and by

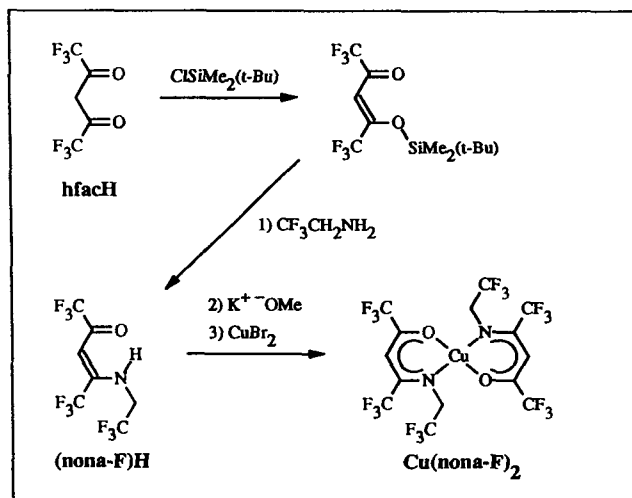


Figure 4-2 Reaction scheme for synthesis of H(nona-F) and Cu(nona-F)₂.⁴⁹

adding freshly prepared solid $\text{Cu}(\text{OH})_2$ to a solution of the ligand in acetone.⁵⁰ Holm has surveyed additional methods for preparing Cu(II) Schiff-base complexes.⁴¹

The synthesis of $\text{Cu}(\text{nona-F})_2$, on the other hand, involved two important developments:⁴⁹ the introduction of the silyl enol ether route to the ligand and its conversion in situ into the desired precursor (reaction scheme shown in Fig. 4-2). The new approach to the ligand was required because, in contrast to non-fluorinated β -diketones, $\text{H}(\text{hfac})$ reacts with amines to produce salts.

4.3.4 Volatility

Most of the available information dealing with the volatility of prospective reactants for Cu CVD concerns kinetics rather than thermodynamics; workers have measured evaporation rates of the compounds rather than their equilibrium vapor pressures. An early illustration of the kinetic approach is the work of Eisentraut and Sievers⁵² who showed the effect of ligand composition on the volatility of complexes for several metals. They applied thermogravimetric analysis to measure the rate of sample loss by evaporation during a linear temperature ramp. For Cr(III) complexes, they showed that the evaporation rate increased in the order $\text{Cr}(\text{acac})_3 < \text{Cr}(\text{tfac})_3 < \text{Cr}(\text{hfac})_3$. The spread in evaporation temperatures was about 120 °C, indicating the significant effect of incorporating fluorinated ligands.

A second approach is to report the evaporation temperature required to volatilize a given amount of compound in reasonable time. This can be done routinely in the course of determining the optimum conditions for CVD experiments and is often the form of volatility information reported in preliminary studies. Typical evaporation temperatures determined in this fashion are included in Table 4-2. While qualitative, these results are sufficient to again demonstrate the important effect of placing fluorinated substituents into the β -diketonate or β -ketoiminate ligands.

There are few direct measurements of the vapor pressure of Cu(II) complexes. Wolf and coworkers⁵³ presented Clausius-Clapeyron plots of vapor pressure as a function of temperature for $\text{Cu}(\text{fod})_2$ and $\text{Cu}(\text{hfac})_2$, along with the fitting parameters:

$$\text{Cu}(\text{fod})_2: \log_{10}[P_{\text{vap}}(\text{torr})] = 9.09 - 3550/T(\text{K}) \quad (4.4)$$

$$\text{Cu}(\text{hfac})_2: \log_{10}[P_{\text{vap}}(\text{torr})] = 9.46 - 3180/T(\text{K}) \quad (4.5)$$

Temple and Reisman¹⁴ determined the vapor pressure of $\text{Cu}(\text{hfac})_2$ over a range of evaporation temperatures using the transpiration technique. This method consists of measuring the weight loss of a sample in the evaporator as a function of time for a series of different carrier gas flow rates and then extrapolating the calculated concentration of

evaporant back to the limit of zero flow rate (where equilibrium conditions would exist in the evaporator). Repeating this procedure for a series of evaporator temperatures, they fitted their results with the expression:

$$\text{Cu(hfac)}_2: \log_{10}[P_{\text{vap}}(\text{torr})] = 9.40 - 3113/T(\text{K}) \quad (4.6)$$

The vapor pressure predicted by Equation 4.6 is about 30% greater than that obtained using Equation 4.5 over the temperature range 95 to 110 °C. The transpiration technique has also been used to study the vapor pressure of Cu(acac)_2 .³⁷

Fine et al.¹³ measured the vapor pressure of Cu(nona-F)_2 directly by measuring the total pressure in a closed, evacuated reactor that contained a sample of the liquid compound:

$$\text{Cu(nona-F)}_2: \log_{10}[P_{\text{vap}}(\text{torr})] = 6.59 - 2091/T(\text{K}) \quad (4.7)$$

Comparing the two compounds over the temperature range 95 to 110 °C (Fig. 4-3), the vapor pressure of Cu(nona-F)_2 as described by Equation 4.7 lies within the bounds of the two equations for Cu(hfac)_2 .

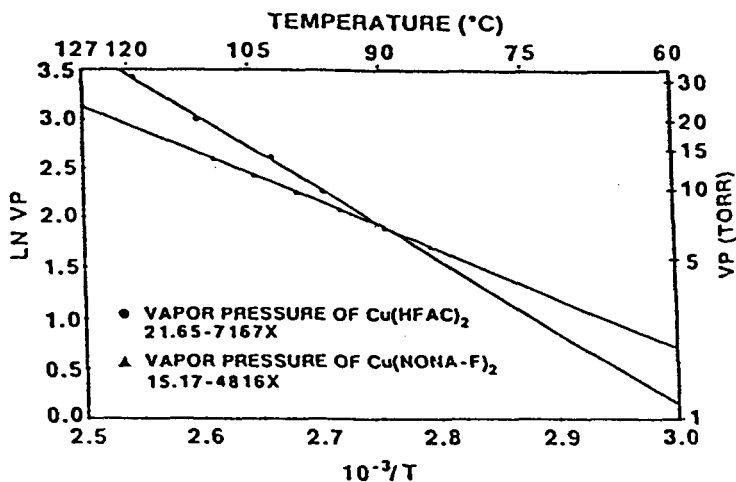


Figure 4-3 Vapor pressure vs. temperature for Cu(nona-F)_2 and Cu(hfac)_2 .¹³

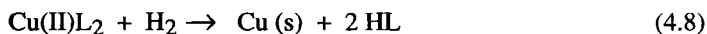
Finally, Lai and associates¹⁶ demonstrated the use of Fourier Transform Infrared Spectroscopy (FTIR) for on-line monitoring of the Cu(hfac)_2 concentration in the feed stream entering the reactor during CVD experiments. The concentration was probed by

measuring the absorbance peak height of the in-plane C-H bending mode at 1117 cm^{-1} . A calibration curve of peak height vs. concentration was obtained by trapping and weighing the amount of Cu(hfac)_2 collected over a given time for each flow rate and evaporator temperature that was tested.

In comparing these methods, it is necessary to distinguish between the equilibrium vapor pressure and the partial pressure (concentration) of reactant that actually leaves the evaporator. The former is an equilibrium quantity that can only be achieved in the limit of low carrier gas flow rate. The latter represents the concentration actually achieved and reflects the possible limiting effects of mass transfer between the evaporant phase and the carrier gas (i.e., the percentage of saturation that is actually achieved). Thus a calibration technique such as transpiration or an on-line monitoring technique such as infrared (IR) spectroscopy is probably more useful for kinetic studies and process control than relying on calculated concentrations based on equilibrium vapor pressure data.

4.3.5 Reaction Stoichiometry

The general features of the reaction stoichiometry of Cu(II) complexes reflect the specific examples given by reactions 4.1 and 4.2 above. For anhydrous Cu(II) compounds, the general form of the H_2 reduction process can be written:



where L^- represents any of the singly charged β -diketonate or β -ketoiminate ligands described above. The regeneration of the ligands in their protonated form has been confirmed by product trapping and analysis. This feature would permit recycling of ligands, if economics warrant.⁷

Reaction 4.8 can be accomplished using reducing agents other than H_2 such as CO or N_2H_4 .¹¹ The reaction stoichiometry has not been clearly demonstrated in these cases, although in the case of CO the reaction is likely to involve at least partial decomposition of the ligands. The stoichiometry of these decomposition reactions is also unclear, but evidence has been reported for a variety of fragments, including acyl groups, ketenylidenes, and methyl or fluoromethyl groups.²⁹ These decomposition products may be incorporated into the film to some degree. For example, the presence of C, O, and F have all been reported in films grown by thermal decomposition of Cu(hfac)_2 in Ar carrier gas.¹⁴

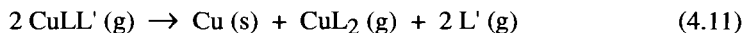
If H_2O is present in the system, an alternate, two-step pathway involving the hydrated complex can be considered:



Reaction 4.9 represents an intramolecular proton transfer between the centrally bound H_2O molecule and the singly charged ligands. This accomplishes the ligand protonation step and allows the protonated ligands to desorb from the surface. The O atom remains coordinated to the Cu atom which may formally retain its +2 oxidation state. Reaction 4.10 represents the elimination of the residual O atom by H_2 reduction. This is expected to be a reasonably facile reaction because of the ease of reducibility of Cu oxides. Taken together, the two steps can be viewed as a process in which the coordinated H_2O molecule acts essentially as a "catalytic carrier" for H atom transfer.

Indirect evidence for the possible importance of reactions 4.9 and 4.10 was given by Sievers,³⁵ who noted difficulties in using the hydrated complexes for gas chromatography at high column temperatures due to alleged hydrolysis and polymerization reactions. More recently, two groups have reported that addition of H_2O vapor to the CVD reactant stream leads to changes in the deposition rate and substrate selectivity.^{17,18}

For comparison, the stoichiometry of the disproportionation reaction using Cu(I) compounds can be written:



where L- represents a singly charged ligand (β -diketonate or β -ketoiminate) and L' represents a neutral ligand (e.g., COD = 1,5-cyclooctadiene, VTMS = vinyltrimethylsilane) (see Ch. 5). No separate reducing agent such as H_2 is needed for this reaction, and the volatile reaction products include one molecule of the Cu(II) compound as well as the two L' neutral ligands.

4.4 Adsorption Studies

Several adsorption studies have appeared since 1990. These are summarized in Table 4-4, which lists the compounds, substrates, and characterization techniques that have been employed. In this Section we organize these results in relation to likely elementary steps in the reaction mechanism. We consider first the molecular and dissociated states of Cu(hfac)_2 , the most commonly studied reactant. We also include relevant results from adsorption studies of Cu(I)(hfac)(L) compounds. This is followed by a discussion of

H(hfac) adsorption studies. Finally, we examine results for the decomposition of adsorbed (hfac) ligands.

Table 4-4 Adsorption Studies of Cu(hfac)₂ and Related Compounds

Adsorbate(s)	Substrate(s)	Techniques	Ref.
Cu(hfac) ₂ , Cu(hfac)(vtms), H(hfac)	Cu(111), Cu(100)	RAIR, HREELS, TPD, IDMS	54
Cu(acac) ₂ , Cu(hfac) ₂ , Cu(hfac)(vtms) H(hfac)	Cu(100), Cu(111)	RAIR, IDMS	29
Cu(hfac) ₂ , Cu(hfac)(COD)	Ag/Si(111)	HREELS, XPS	25
Cu(hfac) ₂ , Cu(hfac)(COD)	Ag, SiO ₂	XPS	26
Cu(hfac) ₂ , Cu(hfac)(vtms)	TiN	XPS, TPD	2
Cu(dpm) ₂	SiO ₂ (powder)	IR	55

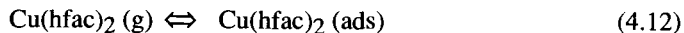
Techniques:

- RAIR = Reflection absorption infrared reflectance spectroscopy
HREELS = High resolution electron energy loss spectroscopy
TPD = Temperature programmed desorption
IDMS = Integrated desorption mass spectroscopy
XPS = X-ray photoelectron spectroscopy
IR = Transmission infrared spectroscopy

4.4.1 Adsorption of Cu(II) Compounds

4.4.1.1 Molecular Adsorption

The precursor $\text{Cu}(\text{hfac})_2$ can be adsorbed in molecular form at low temperatures (ca. 125 K):

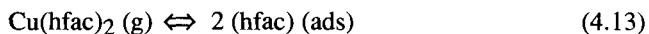


Girolami et al.⁵⁴ studied the adsorption of $\text{Cu}(\text{hfac})_2$ on a $\text{Cu}(100)$ single-crystal surface at 125 K. Using the technique of reflection-absorption infrared (RAIR) spectroscopy, they reported that the spectrum of physically adsorbed $\text{Cu}(\text{hfac})_2$ is essentially identical to that of crystalline $\text{Cu}(\text{hfac})_2$. They concluded that both (hfac) ligands remain coordinated to the central Cu atom at this temperature.

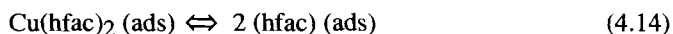
The physically adsorbed layer can be partially desorbed upon warming. Upon heating the sample described above, a small amount of the adsorbed $\text{Cu}(\text{hfac})_2$ desorbed intact below 240 K.⁵⁴ Most of the adsorbed molecules underwent ligand dissociation, as described in Section 4.4.4. This temperature provides an upper limit of approximately 15 kcal/mol for the desorption energy of molecular $\text{Cu}(\text{hfac})_2$. This value is obtained by applying the usual assumptions for analyzing temperature programmed desorption rates (i.e., first order desorption kinetics with a pre-exponential factor of 10^{13}s^{-1}). The low desorption energy suggests that $\text{Cu}(\text{hfac})_2$ will desorb readily at CVD reaction temperatures. This result is also consistent with the fact that $\text{Cu}(\text{hfac})_2$ is desorbed as a reaction product during CVD using Cu(I) disproportionation (see Chapter 5).

4.4.1.2 Dissociative Adsorption

At temperatures above 200 K, $\text{Cu}(\text{hfac})_2$ adsorbs dissociatively on all of the metal surfaces studied to date:²⁹



where the Cu atom is now considered part of the surface. Girolami et al.⁵⁴ also showed that dissociation occurs when a sample prepared by adsorbing $\text{Cu}(\text{hfac})_2$ at 125 K is warmed above 200 K:



As written, Equations 4.13 and 4.14 imply that following the dissociative adsorption process, the (hfac) ligands are no longer strongly co-ordinated to their original Cu atom and instead have migrated onto the neighboring substrate surface to become adsorbed (hfac) ligands. A variety of spectroscopic studies have recently been reported that support this interpretation and provide some direct evidence about the structure and bonding of the adsorbed (hfac) ligands as discussed below.

Girolami et al.⁵⁴ studied the RAIR spectra of molecularly adsorbed Cu(hfac)₂ on Cu(100) as the sample was warmed from 125 K to 225 K. Significant changes were observed in bands near 1200 cm⁻¹ (assigned to CF₃ stretching modes), 1650 cm⁻¹ (C=C stretch), and 1605 cm⁻¹ (C=O stretch). The disappearance of bands associated with molecular Cu(hfac)₂ and the appearance of bands assigned to an isolated (hfac) group oriented perpendicular to the substrate provided evidence that the (hfac) groups had migrated to the surface. The temperature range where these changes occur (225 K) suggests an activation energy of approximately 14 kcal/mol for the ligand dissociation

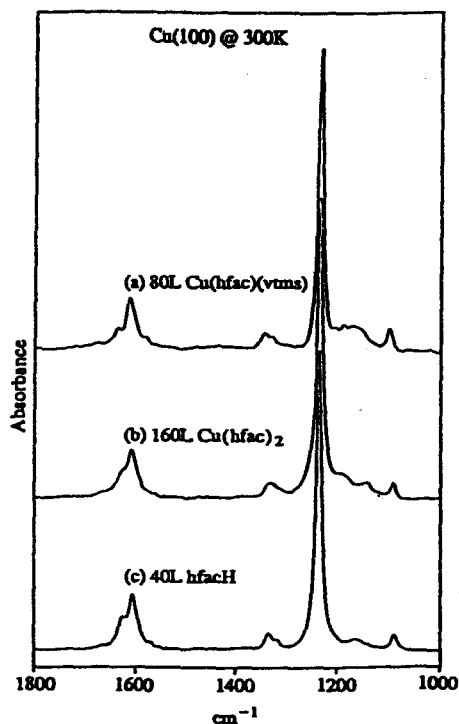


Figure 4-4 Reflection-absorption infrared spectra of a Cu(100) surface exposed to (a) 80 L of Cu(hfac)(vtms), (b) 160 L of Cu(hfac)₂, and (c) 40 L of H(hfac) at 300 K.²⁹

process. This relatively low activation energy suggests that ligand dissociation will occur readily at CVD temperatures.

Dissociative adsorption at room temperature is confirmed by RAIR spectra of $\text{Cu}(\text{hfac})_2$ adsorbed on $\text{Cu}(100)$ surfaces at 300 K (Fig. 4-4).²⁹ These spectra are essentially identical to those obtained after warming a sample prepared by adsorbing $\text{Cu}(\text{hfac})_2$ at 125 K. The same study confirmed that the non-fluorinated analog, $\text{Cu}(\text{acac})_2$, also adsorbs dissociatively at 300 K.

The compound $\text{Cu}(\text{hfac})_2$ also adsorbs dissociatively at room temperature on metal surfaces other than Cu. Cohen and associates²⁵ studied the adsorption of $\text{Cu}(\text{hfac})_2$ on $\text{Ag}/\text{Si}(111)$ films. They concluded that adsorption occurred dissociatively, based on the energy shifts of the Cu $2p$ X-ray Photoelectron Spectroscopy (XPS) and Cu LMM Auger lines in the X-ray photoelectron spectra which suggested that the adsorbed Cu atom was in an oxidation state between Cu(I) and Cu(0) (see Section 4.4.1.3). Gross and Donnelly²

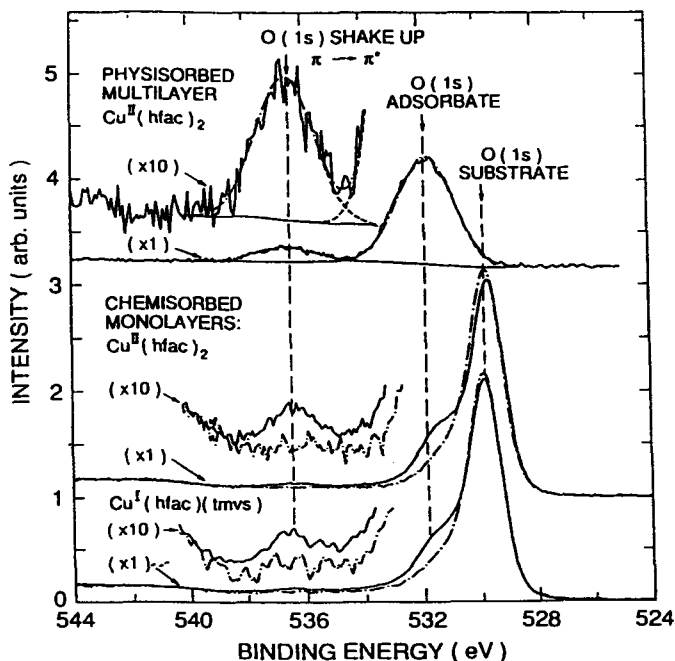


Figure 4-5 O(1s) XPS spectra. (a) Physisorbed $\text{Cu}^{\text{II}}(\text{hfac})_2$ multilayer after dosing at -73°C . (b) Chemisorbed $\text{Cu}^{\text{II}}(\text{hfac})_2$ monolayer after dosing to saturated coverage at room temperature. (c) Chemisorbed $\text{Cu}^{\text{I}}(\text{hfac})(\text{VTMS})$ monolayer after dosing to saturated coverage at room temperature.²

reported that $\text{Cu}(\text{hfac})_2$ adsorbs dissociatively on TiN surfaces based on the shift of the Cu 2p XPS lines.

The adsorption stoichiometry indicated in reaction 4.13 has been verified experimentally. Based on the relative intensity of the C 1s, O 1s, and Cu 2p lines, Cohen and associates²⁵ concluded that adsorption of $\text{Cu}(\text{hfac})_2$ on Ag/SiO_2 resulted in the formation of two adsorbed (hfac) ligands per adsorbed Cu atom. Two groups have also confirmed that a saturation coverage limit exists for $\text{Cu}(\text{hfac})_2$ adsorption at room temperature.^{25,29} The latter point provides justification for developing a Langmuir-Hinshelwood model for the reaction mechanism (see Section 4.7).

Gross and Donnelly reported evidence from adsorption studies on TiN that the (hfac) ligand remains intact following the adsorption step.² This is based on a weak shake-up feature in the O(1s) XPS spectrum (Fig. 4-5) that is assigned to a $\pi^* \leftarrow \pi$ transition in the resonance electronic structure of the $\text{O}=\text{C}(\text{CF}_3)-\text{C}(\text{H})-\text{C}(\text{CF}_3)=\text{O}$ ring of the ligand.

4.4.1.3 Ligand Geometry

Evidence from IR spectroscopy indicates that the (hfac) ligands are oriented perpendicular to the substrate surface. The intensities of the IR absorption peaks are interpreted in terms of the dipole selection rule for absorption at a reflecting surface, which states that only vibrational modes with perpendicular component of motion normal to the surface should be strongly infrared-active. Girolami et al.⁵⁴ observed significant absorbance in peaks assigned to methine C-H, C=O, and C=C stretching modes. Since these modes oscillate within the $\text{C}(\text{CO})\text{CH}(\text{CO})\text{C}$ plane of the adsorbed (hfac) group, the authors concluded that the ligand is oriented perpendicular to the substrate.

There has been conflicting discussion about whether both ligands are dissociated from the initial Cu atom following adsorption of $\text{Cu}(\text{hfac})_2$. Girolami et al.⁵⁴ argued that both ligands are completely dissociated based on the fact that the adsorbed (hfac) ligands produced by adsorbing different compounds [$\text{Cu}(\text{hfac})_2$, $\text{Cu}(\text{hfac})(\text{VTMS})$, or $\text{H}(\text{hfac})$] are all characterized by similar vibrational spectra (Fig. 4-4).

Alternatively, Cohen et al.²⁵ proposed that for $\text{Cu}(\text{hfac})_2$ adsorbed on $\text{Ag}/\text{Si}(111)$, one ligand remains coordinated to the original Cu atom in the form of a Cu-hfac surface intermediate. Their argument was based on the energy shifts of the Cu 2p XPS and Cu LMM Auger lines in the X-ray photoelectron spectra of $\text{Cu}(\text{hfac})_2$ adsorbed on $\text{Ag}/\text{Si}(111)$ films. These shifts indicated that the oxidation state of the Cu atom had changed to a value about halfway between +1 and 0 following the adsorption step. Gross and Donnelly also argued for the existence of a Cu-hfac surface intermediate (Fig. 4-5).² In their XPS study of $\text{Cu}(\text{hfac})_2$ adsorbed on TiN, they interpreted the O(1s) shake-up feature assigned to a $\pi^* \leftarrow \pi$ transition in the ligand ring as evidence that the (hfac) ligand retains bidentate coordination to a Cu(I) atom.

Both of the latter studies were performed using substrates other than Cu, and the results from these studies may be taken as evidence that an adsorbed Cu(hfac) intermediate exists on foreign surfaces, where it may play a role in the initial stages of film nucleation and growth. Direct evidence for a distinguishable Cu(hfac) intermediate on Cu surfaces is lacking (although this does not preclude its possible role in the steady state growth process).

4.4.1.4 Reversibility

There has been considerable discussion about the reversibility of reaction 4.13 [i.e., the desorption of Cu(hfac)₂ from a Cu surface covered by dissociated (hfac) ligands]. That Cu(hfac)₂ is observed as the stoichiometric reaction product during the Cu(I) disproportionation reaction suggests that Cu(hfac)₂ can desorb readily under CVD conditions. This step or a surface disproportionation reaction between two adsorbed Cu(hfac) groups was originally proposed as part of the reaction mechanism for CVD using Cu(I) disproportionation.^{8,9}

Unfortunately, adsorption studies under UHV conditions have not been able to provide conclusive evidence for the surface disproportionation reaction. Girolami and coworkers⁵⁴ reported that they could not observe Cu(hfac)₂ (or any other Cu containing species) in the mass desorption spectrum obtained while heating a saturation monolayer of Cu(hfac)₂ adsorbed on Cu(111). They did, however, observe a variety of other desorbed products over the temperature range from 100 to 400 °C. Based on additional

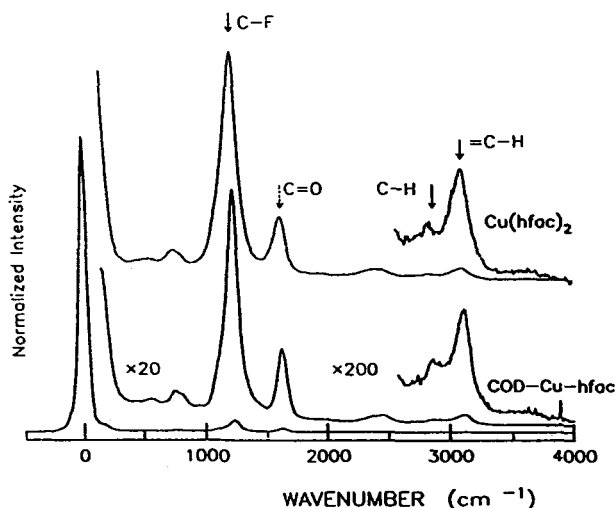


Figure 4-6 HREELS spectra for COD-Cu-(hfac) and Cu(hfac)₂ adsorbed on Ag.²⁵

spectroscopic characterization of surface intermediates, they concluded that adsorbed (hfac) ligands undergo a series of step-wise decomposition reactions (see Section 4.4.2).

Cohen et al.²⁷ studied the behavior of adsorbed (hfac) ligands produced by adsorption of Cu(hfac)(COD) on Cu and Ag surfaces (Fig. 4-6). They reported that the XPS and HREELS (high resolution electron energy loss spectroscopy) signals of these species disappeared upon heating to 200 °C. Cohen et al. proposed that the loss of signal was caused by desorption of Cu(hfac)₂; however, they did not directly observe any of the desorption products. They did note evidence for a small residual C layer in their final XPS spectra. Since 200 °C is within the temperature range of ligand decomposition reactions reported by Girolami et al.,⁵⁴ it is possible that the loss of ligand XPS signal was due to ligand decomposition.

The difficulty of observing Cu(hfac)₂ desorption under UHV conditions arises partly because this process requires a bimolecular surface reaction that involves two adsorbed (hfac) ligands. This reaction will require a high coverage of adsorbed (hfac) ligands to maintain a significant rate. In contrast, ligand decomposition is likely to involve a unimolecular surface reaction. Since decomposition begins at temperatures as low as 100 °C, it is likely that the concentration of adsorbed (hfac) groups will rapidly decrease below the level required to permit significant desorption of Cu(hfac)₂. Under CVD conditions, Cu(hfac)₂ may desorb readily because the surrounding reactant gas can supply fresh reactants to the surface.

4.4.1.5 Non-Metallic Substrates

Several studies have dealt with the adsorption of Cu(hfac)₂ and related compounds on non-metallic substrates. The goal of these studies is generally to understand the factors which affect film nucleation, which in turn provides the basis for understanding selective area deposition. For adsorption on non-metallic surfaces, electron transfer is no longer a facile process. This may affect several of the elementary processes described above (e.g., ligand dissociation).

Cohen et al.²⁶ studied the adsorption of Cu(hfac)₂ and Cu(hfac)(COD) at room temperature on SiO₂. For Cu(hfac)₂, the XPS spectra of the Cu 2*p* lines indicates that Cu remains in the Cu(II) oxidation state. This behavior is in contrast with adsorption on metallic Ag substrates which showed Cu in an intermediate oxidation state between Cu(I) and Cu(0). The authors proposed that Cu(hfac)₂ adsorbs as an intact molecule on SiO₂. They went on to suggest that this barrier to ligand dissociation may account for selectivity against nucleation and growth on SiO₂ surfaces.

Sekine and Kawai⁵⁵ studied a related compound, Cu(dpm)₂, adsorbed on SiO₂ powder. They reported Cu(dpm)₂ adsorbs stoichiometrically at isolated OH groups on SiO₂ surfaces. The transmission IR spectra were interpreted as showing that proton transfer occurs from the OH group to the (dpm) ligand forming a CH₂ band, while the

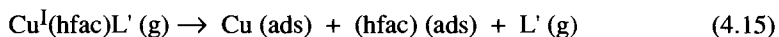
ligand remains coordinated to the Cu atom. They noted a similar reaction between Cu(dpm)_2 and adsorbed H_2O on SrTiO_3 . The adsorbed species reacted with H_2O to produce H(dpm) and CuO .

Gross and Donnelly² reported that Cu(hfac)_2 could be observed in the mass desorption spectrum following adsorption of that compound on TiN. This result is in marked contrast to the general failure to observe Cu(hfac)_2 desorbing from metals, as described above. The authors proposed that Cu(hfac)_2 desorption was the result of disproportionation between two Cu(hfac) intermediates. However, they failed to observe Cu(hfac)_2 desorption following the adsorption of Cu(hfac)(VTMS) , which might also be expected to produce the Cu(hfac) intermediate upon adsorption. The authors suggested that vacant site requirements may permit a single (hfac) ligand to dissociate from Cu(hfac)(VTMS) after the (VTMS) group has desorbed but prevent both ligands from dissociating from Cu(hfac)_2 .

4.4.2 Adsorption of Cu(I) Compounds

The adsorption studies discussed above also include results for several Cu(I) compounds. These compounds are reactants for the disproportionation reaction, and their adsorption behavior is reviewed in more detail in Chapter 5. Here we compare the major conclusions of the Cu(I) adsorption studies with those of Cu(II) compounds.

Several authors have shown the adsorption of Cu(I) compounds occurs dissociatively on clean metal surfaces at or below room temperature.^{25,29} The distinguishing feature for the Cu(I) compounds is the fact that the neutral L' ligand desorbs immediately upon adsorption:



Thus the adsorption of both Cu(I) and Cu(II) compounds results in the formation of surface (hfac) ligands, but with Cu(I) compounds the second ligand does not remain on the surface.

Desorption of the second ligand is consistent with the weak $\text{Cu-L}'$ bond in most of these compounds. For example, Dubois and associates²⁹ reported that the Cu-(VTMS) bond in Cu(hfac)(VTMS) can be cleaved readily by heating the precursor to 500 K in the gas phase. Further evidence cited included the infrared spectrum of the compound, which appeared as merely the sum of the spectra of VTMS and Cu(hfac)_2 with no significant shift in either the frequency or intensity of any of the modes.

Girolami et al.⁵⁴ showed that the second ligand can be retained on the surface at low temperatures. Their RAIR spectra of Cu(hfac)(VTMS) on Cu(100) single-crystal surfaces showed that the (VTMS) ligands remained present following adsorption at 125 K

and then desorbed after warming to 200 K. These results were confirmed by HREELS and Temperature Programmed Desorption (TPD) studies on Cu(111). The observed desorption temperature corresponds to an activation energy of 13-14 kcal/mol for the desorption of (VTMS) from these Cu surfaces.

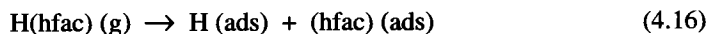
The major result of these Cu(I) adsorption studies in the present context was the conclusion that the surface intermediates produced by their adsorption were similar or identical to those produced by Cu(hfac)₂ adsorption. For example, Girolami⁵⁴ and Dubois²⁹ and their associates studied the adsorption of Cu(hfac)(VTMS) on Cu single-crystal surfaces at higher temperatures (> 200 K). Both RAIR and HREELS results indicated that the same surface species was formed at 300 K upon adsorption of Cu(hfac)(VTMS), Cu(hfac)₂, and H(hfac). Girolami et al.⁵⁴ also confirmed that similar spectra are obtained after warming a sample prepared by adsorption at low temperature (125 K) up to 200 K [to desorb (VTMS)].

Similarly, Cohen et al.²⁵ studied the adsorption of Cu(hfac)(COD) on Ag films using XPS and HREELS (Fig. 4-6). The latter technique showed no evidence of vibrational bands for adsorbed COD groups, implying that these groups had left the surface. The XPS spectrum was similar to that observed for adsorbed Cu(hfac)₂, consistent with the formation of a similar adsorbed Cu(hfac) group. The energy of the Cu *LMM* peak was slightly closer to that of neutral copper, possibly due to the lower surface concentration of adsorbed (hfac) ligands.

The adsorption of Cu(I)LL' compounds also requires vacant sites on the surface. Saturation coverage limits were reported by both groups.^{25,29} The coverage limits are higher than for Cu(II)L₂ compounds, indicating that the area occupied by each molecule is smaller. This is consistent with the loss of the L' ligand from the surface, so that a second adsorption site is not occupied. Cohen and coworkers²⁵ confirmed that the Cu:hfac ratio in the adsorbed layer is close to unity, as expected from the adsorption stoichiometry.

4.4.3 Adsorption of H(hfac)

The adsorption of H(hfac) has also been studied by several groups.^{29,54}



One major result from these studies has been to confirm that the surface (hfac) ligands produced by the adsorption of H(hfac) are similar or identical to those produced by Cu(hfac)₂ adsorption. Studies of H(hfac) adsorption are also of interest because H(hfac) is the gas phase product of Cu CVD via the H₂ reduction of Cu(hfac)₂.⁷ This implies that the reverse reaction (i.e., H(hfac) desorption) must be one of the elementary steps in

the reaction mechanism of the latter process. If these adsorbed ligands are not removed, they will eventually accumulate and block the surface from further reaction. Alternatively, the ligands may decompose, probably resulting in impurity incorporation into the film. Thus under CVD conditions, the surface coverage by (hfac) ligands is likely to affect both the deposition rate through a product inhibition effect in the reaction kinetics and possibly the film purity.

Dubois et al.²⁹ reported that H(hfac) adsorbs dissociatively on a Cu(100) single crystal surface at 300 K. They also confirmed that H(acac) adsorbs dissociatively in analogous fashion. Girolami et al.⁵⁴ reported that molecular H(hfac) is physisorbed at 125 K. Based on RAIR peaks at 1699 cm^{-1} (C=O stretch) and 1634 cm^{-1} (C=C stretch), they concluded that the H(hfac) molecules exist exclusively as the enol tautomer. Upon warming to 150–200 K, part of the H(hfac) molecules desorb intact while the remainder are dehydrogenated to give adsorbed (hfac) ligands. The latter step presumably occurs via H atom migration to the surface, but this was not established directly. The RAIR spectra of the (hfac) ligands produced by either H(hfac) adsorption sequence discussed above are similar to those seen following dissociative adsorption of $\text{Cu}(\text{hfac})_2$ above 200 K.

The reverse reaction, desorption of H(hfac) from the dissociatively adsorbed state, has not been observed under UHV conditions. Dubois and associates²⁹ reported that H(hfac) was not observed in the thermal desorption mass spectra from surfaces prepared by dissociative adsorption of H(hfac). The authors suggest that desorption is not likely to occur under UHV conditions because it requires a bimolecular reaction between surface intermediates. This argument is further supported by the fact that H atoms recombine and desorb as H_2 at 300–350 K on most copper surfaces. Thus the H atom coverage is likely to be quite low as the sample is heated under UHV conditions in the absence of gas phase H_2 to replenish the surface.

4.4.4 Ligand Decomposition

Instead of desorbing as H(hfac), the adsorbed (hfac) ligands undergo a series of sequential decomposition reactions when heated under UHV conditions. These reactions may also be responsible for the formation and incorporation of C, F, and O impurities in films grown under improper CVD conditions.

Dubois et al.²⁹ reported the mass desorption spectra of various species produced while heating samples prepared by adsorption of $\text{Cu}(\text{hfac})(\text{VTMS})$, $\text{Cu}(\text{hfac})_2$, or H(hfac) on Cu(111) to a final temperature of 650 K (also Girolami⁵⁴). Products included F ($m/e=19$), CO (28), CF (31), CO_2 (44), COF (47), CF_2 (50), CF_3 (69), COCF_3 (97), and HOCFCF_3 (117). The F-containing intermediates desorbed in a single, broad peak over the range 500–650 K. In contrast, CO and CO_2 desorbed in three peaks over the range

435-650 K. The rate-limiting step(s) for these peaks were assigned to the sequential fragmentation of adsorbed (hfac) ligands since molecular CO and CO₂ both desorb rapidly from Cu surfaces at these temperatures.

The authors correlated these results with RAIR spectra recorded during the decomposition of (hfac) ligands adsorbed on a Cu(100) surface. In particular, they observed a band at 1205 cm⁻¹ that grew to maximum intensity at 475 K and then decayed. This feature was assigned to adsorbed CF₃ groups, oriented perpendicular to the surface.²⁹

Another band was observed at 2038 cm⁻¹ that grew to maximum intensity at 525 K. This peak was assigned to the C≡O stretch of an adsorbed ketenylidene intermediate (≡C-C≡O). Upon further heating this peak disappeared, CO desorption was observed, and a small amount of residual carbon was observed in the AES spectrum of the surface.²⁹ This evidence suggests that ketenylidene decomposition may be a channel for carbon incorporation in films at high temperature. The authors also noted that the intensity of the ketenylidene intermediate was somewhat lower for surfaces prepared by H(hfac) adsorption [vs. Cu(hfac)₂ or Cu(hfac)(VTMS)]. They suggested that this may be correlated with the presence of residual H atoms on the surface following H(hfac) adsorption.

Welton et al.⁵⁶ studied the adsorption of Cu(hfac)₂ and subsequent decomposition of (hfac) ligands on lightly oxidized W surfaces. Following the adsorption step, reduction to metallic Cu occurred by 323 K. However, evidence of chemical interactions between the (hfac) ligands and the WO_x surface was also observed at this temperature. New phases (e.g., WC) were observed upon heating to 623 K. The authors suggested that the formation of such impurity phases may cause difficulties in growing Cu films on W barrier surfaces.

4.5 Growth Kinetics

Tables 4-2 and 4-3 list the deposition rates and reaction conditions reported by various groups for Cu CVD using Cu(II) compounds. The compounds and evaporation temperatures listed in the first two columns were discussed in Section 4.3. Here we discuss the influence of reaction conditions.

4.5.1 Deposition Rates

There are relatively few reported values of quantitative growth rates. It is interesting to note that most of the values reported to date for H₂ reduction of Cu(hfac)₂ are lower than the value of 80 nm/min originally reported by Moshier and Sievers.¹¹ Exceptions

are the growth rates of 120-180 nm/min reported by Kaloyeros et al.¹⁵ and the rates of 20-90 nm/min reported by Awaya and Arita.¹⁷ Even with these recent improvements, all of the growth rates listed are significantly lower than the rates that are currently being reported for Cu deposition using the disproportionation of Cu(I) compounds. For example, Shin et al.⁵⁷ obtained a growth rate of 900 nm/min at temperatures as low as 200 °C using Cu(hfac)(2-butyne) (see Ch. 5).

In considering the range of growth rates shown in Tables 4-2 and 4-3, it must be remembered that individual values will depend strongly on reaction conditions (substrate temperature, reactant concentration, and carrier gas pressure). The reactor configuration can also have a significant effect on growth rate, especially if the process is being operated at high reactant conversion. Thus a quantitative comparison of the growth rates listed above is of limited value (and is possibly misleading) without additional discussion of the influence of reaction conditions.

4.5.2 Deposition Temperature

Most authors have reported deposition temperatures in the range 250-400 °C. The required temperature is determined partly by the composition of the carrier gas; higher temperatures are needed when H₂ is not present to serve as a reducing agent. Somewhat higher temperatures (~ 50 °C greater) may also be required for CVD at low pressure vs. atmospheric pressure. There is conflicting evidence as to whether higher temperatures are also required for non-fluorinated vs. fluorinated compounds.

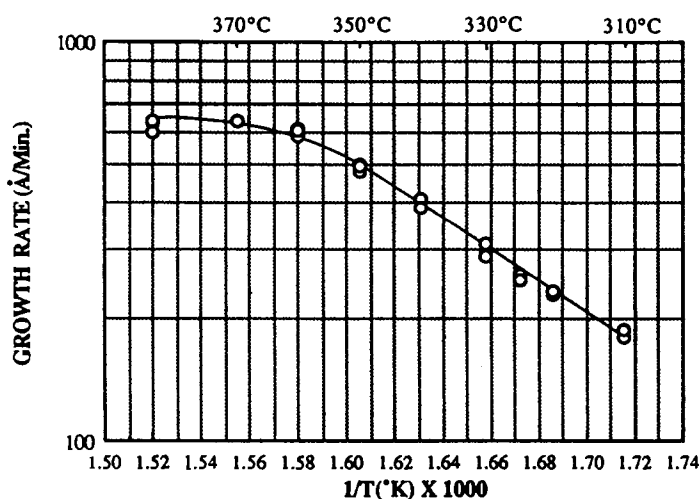


Figure 4-7 Growth rates vs. $1/T(^{\circ}\text{K})$ plot for CVD copper films deposited at 310-385 °C, 0.042 Cu(hfac)₂ mole fraction, and 10 torr total H₂ pressure.⁵⁸

Empirical values of the apparent activation energy (i.e., the temperature dependence of the observed rate) have been determined in a few instances. Fine and associates¹³ have reported an apparent activation energy of 190 ± 40 kJ/mole, using H_2 reduction of $Cu(nona-F)_2$ at 10-70 torr total pressure. Lai et al.⁶ reported a value of 80 kJ/mole, using $Cu(hfac)_2$ in H_2 carrier at atmospheric pressure. Kim and coworkers⁵⁸ reported a similar value of 75 kJ/mole under low pressure conditions (10 torr H_2) and at higher temperature (310-350 °C vs. 250-275 °C) (Fig. 4-7). Interestingly, these values are somewhat lower than the activation energy of 96 kJ/mole reported for the disproportionation process using various Cu(I) compounds containing one (hfac) ligand^{57,59} (see Ch. 5).

4.5.3 Reactant Concentration

There have been few quantitative studies of the influence of reactant concentration on deposition rate. Lai et al.¹⁶ measured growth rates at atmospheric pressure using inlet

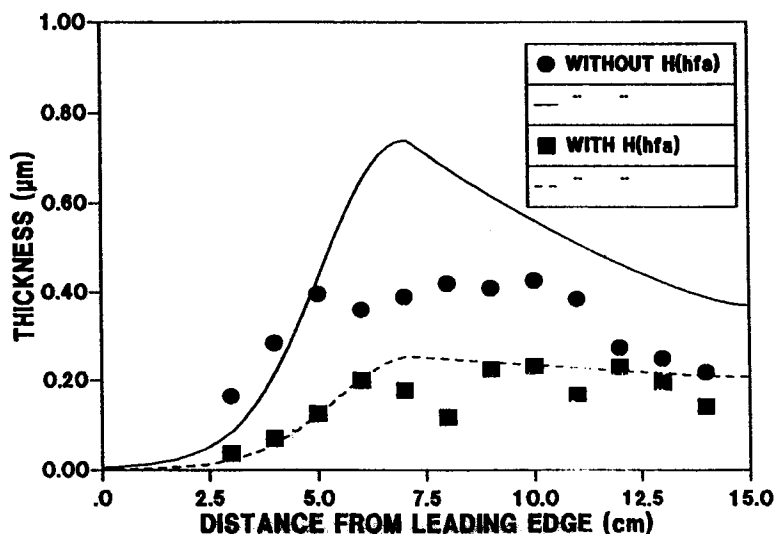


Figure 4-8 Influence of H(hfac) addition on film thickness profile. Upper results: no H(hfac) added; lower results: H(hfac) added.¹⁶

concentrations of $\text{Cu}(\text{hfac})_2$ of 0.08 and $0.4 \mu\text{mol}/\text{cm}^3$. For a reactor temperature of 250°C , the growth rate at the reactor inlet was almost the same for both experiments, despite the five-fold increase in inlet concentration. This apparent zero-order dependence was interpreted in terms of a Langmuir-Hinshelwood (L-H) mechanism involving dissociatively adsorbed $\text{Cu}(\text{hfac})_2$.

The same authors also showed that the addition of comparable amounts of $\text{H}(\text{hfac})$ to the reactant feed caused a decrease in deposition rate (Fig. 4-8). This product inhibition effect was incorporated into the L-H mechanism by including an $\text{H}(\text{hfac})$ adsorption step and proposing that $\text{H}(\text{hfac})$ desorption is the rate-limiting step for the overall reaction.

Awaya and Arita¹⁷ examined the variation in growth rate at low pressure (15 torr) over a wide range of $\text{Cu}(\text{hfac})_2$ concentration and temperature (Fig. 4-9). At 300°C the

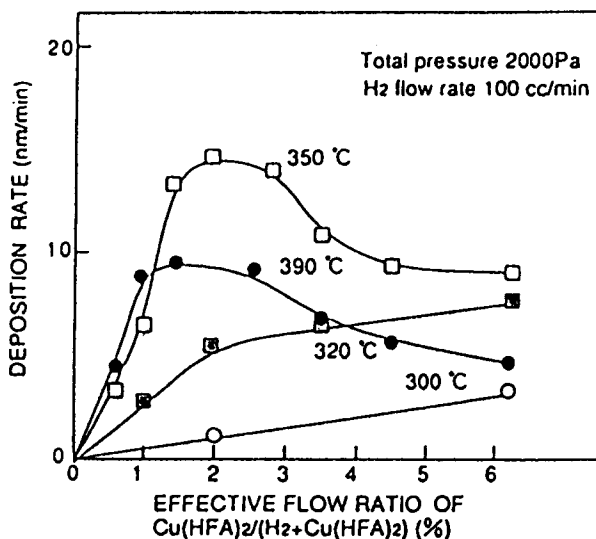


Figure 4-9 Deposition rate vs. source gas concentration: Saturation effects.¹⁷

growth rate varied linearly with concentration. At 320°C the rate began to show evidence of a saturation limit at higher concentration. At 350°C and 390°C the growth rate actually passed through a maximum as a function of $\text{Cu}(\text{hfac})_2$ concentration. To account for their results, the authors proposed a second-order Langmuir-Hinshelwood mechanism involving both adsorbed H and $\text{Cu}(\text{hfac})_2$ intermediates. The decrease in growth rate at high $\text{Cu}(\text{hfac})_2$ observed at the highest temperatures was then attributed to a decrease in available H_2 adsorption sites due to competitive adsorption of $\text{Cu}(\text{hfac})_2$.

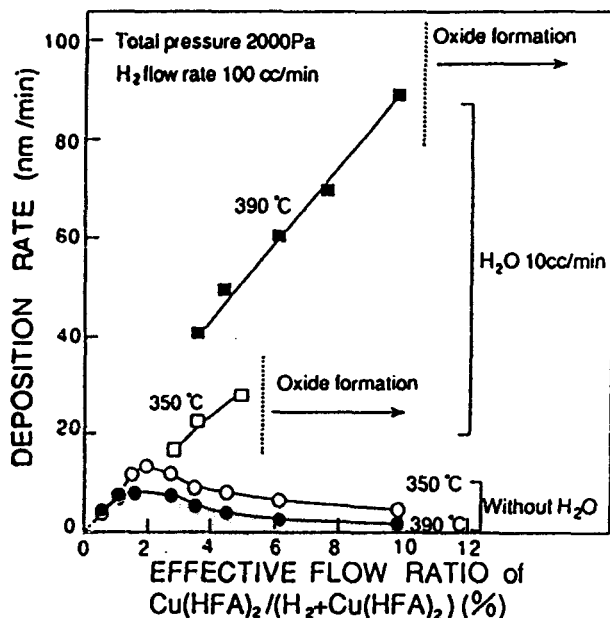


Figure 4-10 Deposition rate vs. source gas concentration: Effect of added H₂O.¹⁷

These authors also showed that the addition of H₂O dramatically increased the growth rate, especially at higher temperatures (Fig. 4-10). The major effect was to eliminate the decrease in growth rate with Cu(hfac)₂ concentration that was observed at 350 °C and 390 °C. Instead, the rate continued to increase linearly with Cu(hfac)₂ concentration up to values approaching 100 nm/min. At this point the formation of Cu oxides became noticeable. The variation of growth rate with H₂O concentration at fixed Cu(hfac)₂ concentration was roughly linear at low H₂O levels with evidence that the effect of H₂O also approached a saturation limit at high concentrations.

4.5.4 Carrier Gas Effects

Numerous studies have compared relative growth rates with and without H₂ in the carrier gas. In general, higher temperatures are needed when an inert carrier is used. Conversely, for a fixed deposition temperature higher growth rates are obtained when H₂ is used. For example, Moshier and colleagues¹¹ reported that temperatures of 350 to 500 °C were required when N₂ was used as the carrier gas vs. temperatures of 250 to

300 °C when H₂ was the carrier. Awaya and Arita¹⁷ showed that the rate at 350 °C could approach 15 nm/min for low pressure CVD using Cu(hfac)₂ with H₂ as the carrier gas compared to a maximum rate of 1 nm/min using Ar as the carrier (Fig. 4-11). Lai et al.¹⁶ had previously demonstrated the same effect for atmospheric pressure CVD by showing that the deposition rate decreased when an H₂/Ar mixture was substituted for pure H₂ as the carrier.

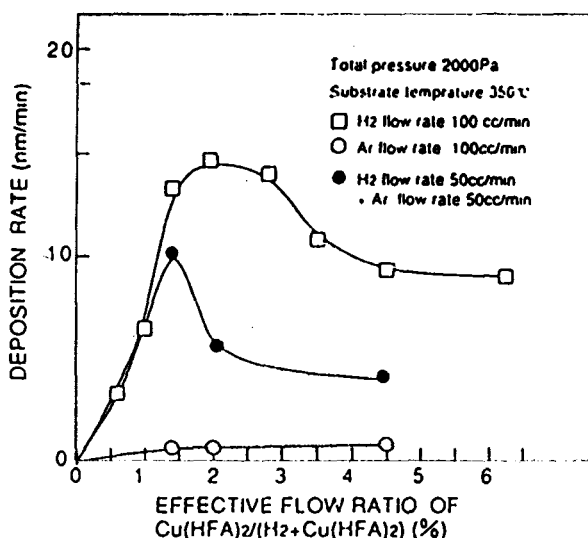


Figure 4-11 Comparison of the deposition rate with various carrier gases.¹⁷

The effects of including gas phase H₂O in the carrier gas mixture were described above. Several groups have also reported evidence that including gas phase alcohols in the carrier gas can have a similar effect. Early on, Jones et al.²¹ reported that gas phase C₂H₅OH had to be present to achieve measureable rates for laser-assisted CVD using Cu(hfac)₂. Pilkington et al.⁶⁰ reported that dissolving Cu(hfac)₂ in ethanol or propanol dramatically increased the deposition rate for conventional CVD. Zeng et al.⁶¹ reported a similar rate enhancement for plasma-assisted CVD using Cu(hfac)₂ dissolved in ethanol.

The reason for this enhancement has not been clearly established. Jones et al. suggested that the effect may be chemical (i.e., intrinsic to the reaction mechanism) with C₂H₅OH serving as a reducing agent for Cu(hfac)₂. The reaction mechanism may therefore be similar to the role suggested for H₂O above. Alternatively, Pilkington et al. noted that measurable deposition rates could be obtained using very low evaporator

temperatures (i.e., 35 °C using Cu(hfac)_2 dissolved in $\text{C}_2\text{H}_5\text{OH}$; 50 °C using $\text{C}_3\text{H}_7\text{OH}$). This suggests that the observed growth rate enhancement may be due to an increased rate of Cu(hfac)_2 transport into the reactor (e.g., possibly via the formation of a more volatile Cu(hfac)_2 :alcohol complex). Further work is needed to resolve this question.

The composition of the carrier gas also has a significant effect on the purity and resistivity of the deposited films. Several authors have reported being unable to obtain pure Cu films with low resistivity ($< 3 \mu\Omega\text{cm}$) when either Ar or dilute H_2/Ar mixtures are used as the carrier gas.^{3, 13, 15}

To date, no one has reported a quantitative study of the effect of total pressure on deposition rates. We are presently investigating this question in our laboratory using pure H_2 as the carrier gas.⁶² Initial results indicate that decreasing the pressure affects both the intrinsic reaction kinetics and the rate of mass transport. The former effect occurs because adsorbed H atoms are required for the desorption of H(hfac) , which is believed to be the rate limiting step in the H_2 reduction mechanism. Thus decreasing the H_2 pressure leads to a decrease in the surface reaction rate.

On the other hand, lower total pressure also causes an increase in the diffusivity of the gas phase reactants (and products) thus increasing the rate of mass transport to and from the substrate. The actual deposition rate reflects the contribution of these two competing effects which combine in series to determine the overall reaction rate. As discussed elsewhere, changes in the relative contribution of the surface reaction rate vs. the gas phase transport rate will define whether deposition occurs under surface reaction limited vs. mass transport limited conditions. This in turn can significantly affect the morphology of the films.

4.5.5 Substrate Selectivity

Even in their early report, Van Hemert et al.⁷ noted differences in the adhesion of Cu films grown on stainless steel vs. glass substrates. To the extent that these differences arise from differences in the morphology of the film/substrate interface, these results may be taken as the first indirect evidence that substrate composition affects the nucleation rate. Similar differences in adhesion were reported between copper and TiN vs. SiO_2 by Kaloyeros et al.¹⁵

The first direct observation of substrate selectivity appears to be the work of Awaya and Arita.³ These authors showed that deposition occurred selectively on several metals and at least one metal silicide but not on SiO_2 or Si_3N_4 . They further noted that selective deposition was maintained using either H_2 or Ar as the carrier gas, although the film resistivity was higher when grown in the absence of H_2 . This was suggested as evidence that film nucleation is controlled more strongly by the reactant adsorption step than by the subsequent reduction step.

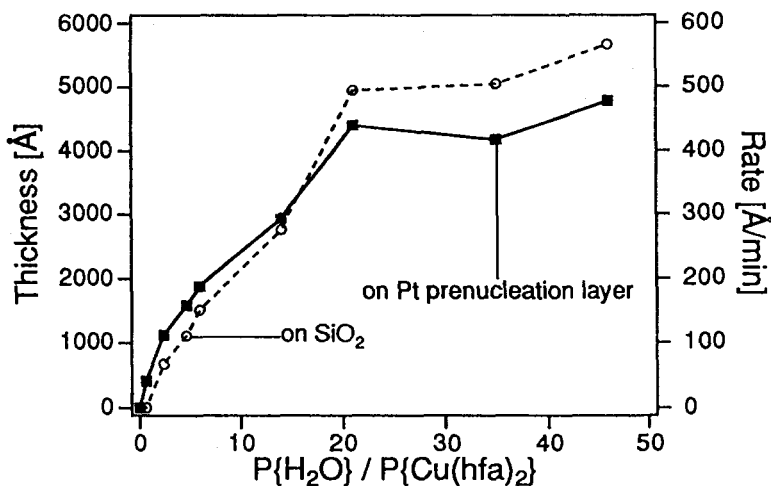


Figure 4-12 Thickness of Cu deposited on a Pt prenucleation layer and on a SiO₂ substrate as a function of the ratio of H₂O and Cu(hfac)₂ in the reactant gas.¹⁸

Lecohier et al.¹⁸ obtained similar results for selective deposition on Pt vs. SiO₂. However, these authors also showed that selectivity could be eliminated by adding H₂O in amounts comparable to or greater than the Cu(hfac)₂ concentration (Fig. 4-12). The effect of adding H₂O was to activate the SiO₂ surface for deposition.

At least two reports of reverse selectivity have also appeared. Studying the pyrolysis of Cu(dpm)₂ in vacuum on patterned substrates, Hazuki et al.⁶³ observed selective deposition on regions of thermally grown SiO₂ but not on neighboring regions of Si that had been exposed by wet chemical etching. Selectivity was restricted to deposition temperatures from 250 to 300 °C; above 300 °C both surfaces became active for growth. These experiments were performed using a stainless steel vacuum chamber with a wall temperature of 250 °C, which is much hotter than the cold-wall reactor temperatures used by most other groups. Analysis of the gas-phase species using quadrupole mass spectrometry revealed a significant concentration of partially decomposed Cu(hfac)₂ fragments, e.g., Cu₄HO₂F₃, Cu₃O₂F₃, and CuC₃HO₂F₃. The authors speculated that these polar fragments might be adsorbed preferentially on the partially ionic SiO₂ surface.

Fine and associates¹³ also reported reverse selectivity in their studies using Cu(nona-F)₂ reduction in H₂ at 10-70 torr. They observed selective deposition on SiO₂ vs. W and TiN, both in experiments using separate, adjacent samples and also in experiments using patterned substrates. Differences between Cu(nona-F)₂ and Cu(hfac)₂ include the partly

tetrahedral geometry of the former compound and also its non-hygroscopic nature. However, the authors did not attempt to correlate these differences with the observed reverse selectivity, nor did they speculate about other possible causes.

4.6 Film Properties

4.6.1 Purity

Temperature and carrier gas composition are the major factors that control film purity. Film composition has usually been measured using Auger electron spectroscopy (AES). This technique is sensitive to the atomic composition of the film and has a lower detection limit of about 1% for most elements. The technique is also surface-sensitive with most of the detected signal originating from the outermost 1-2 nm of the sample. If the sample is exposed to air while being transferred from the CVD reactor to the AES analysis chamber, a layer of Cu oxides and/or other adsorbed species will be formed which will mask the true composition of the CVD material. In this case ion sputtering is used in conjunction with the AES measurements in order to remove this outer layer and expose the deposited film. If sputtering is performed long enough to remove all of the film and expose the substrate, the technique can also be used to estimate the film thickness.

Based on such AES measurements, most authors have concluded that H_2 must be present in the carrier gas to obtain pure films when a Cu(II) compound is the reactant. For example, Kaloyeros et al. obtained films that were 99% Cu when $Cu(hfac)_2$ was reacted in pure H_2 .¹⁵ In contrast, films deposited using a mixture of 10% H_2 in Ar contained significant impurity levels of C (15%), O (10%), and F (5%). Similarly, Fine et al.¹³ needed to use H_2 to obtain pure films using $Cu(nona-F)_2$ as the reactant. Awaya and Arita³ report a still larger fraction of O (~ 30%) for films that were grown at 7-15 torr in pure Ar carrier. Armitage et al.⁶⁴ reported that films produced by decomposition of $Cu(hfac)_2$ in Ar at 1 atm contained a mixture of metallic Cu and Cu_2O .

As implied by the overall reaction stoichiometry (Eq. 4.3), the role of H_2 as a reducing agent is to permit the chelating ligands to desorb cleanly from the surface in their protonated form. In the absence of H_2 , ligand decomposition may occur via alternate pathways, leaving C-, O-, and F-containing fragments which become incorporated into the growing film. Supporting evidence for this hypothesis based on direct observation of such adsorbed fragments has recently been provided by the adsorption studies described above.

A partial exception to this general observation may be the work of Temple and Reisman¹⁴ who showed that pure Cu films (as judged by AES analysis) can be deposited by thermal decomposition of $\text{Cu}(\text{hfac})_2$ in Ar at 1 atm over a narrow temperature range of 340-390 °C. However, the resistivity of these films exceeded the value of bulk Cu which may indicate that impurities are present below the AES detection limit. At 430 °C, the AES measurements confirmed that ligand decomposition resulted in C and O incorporation. At 500 °C and 650 °C, the films were composed entirely of C.

4.6.2 Resistivity

To date, film resistivity has served as the de facto standard for judging the quality of CVD Cu films. In particular, film values are compared to resistivity of bulk copper, $\rho_{\text{Cu}} = 1.7 \mu\Omega\text{cm}$. Kaloyeros et al.¹⁵ were able to obtain values of $1.9 \mu\Omega\text{cm}$ for films grown over a range of temperatures (300-450 °C) using $\text{Cu}(\text{hfac})_2$ with pure H_2 as the carrier gas. Using a film deposited at 300 °C, they went on to demonstrate that the resistivity showed a linear temperature dependence over the range 100-300 K. This was interpreted to indicate that the dominant source of resistivity in this temperature range is phonon scattering which in turn implies that there is a low concentration of structural defects and impurities in the films. Fine et al.¹³ were able to report values that were nearly as low ($2.1 \pm 0.1 \mu\Omega\text{cm}$) for 200 nm thick films grown using H_2 reduction of $\text{Cu}(\text{nona-F})_2$.

In contrast, Temple and Reisman¹⁴ could only obtain resistivities of 3-6 $\mu\Omega\text{cm}$ for films deposited by thermal decomposition of $\text{Cu}(\text{hfac})_2$ in Ar at atmospheric pressure. At substrate temperatures of 340-390 °C, film impurities were not detected by AES analysis. This suggests that the higher resistivity may be caused by film morphology. At higher temperatures the impurity concentration in the film reached measurable levels, and film purity and resistivity both become progressively worse with increasing temperature.

Awaya and Arita³ showed that the film thickness may have to exceed a critical value in order for the film resistivity to approach the bulk value. They were able to obtain resistivities approaching bulk copper only for films thicker than 300 nm. Lecohier et al.⁶⁵ reported a similar value for the critical thickness, while Kim et al. reported a slightly higher value of 500 nm (Fig. 4-13).⁵⁸

Awaya and Arita³ also reported that for films of comparable thickness, lower resistivity was obtained using higher evaporator temperatures [i.e., higher $\text{Cu}(\text{hfac})_2$ inlet concentrations]. This was attributed to the smaller grain size obtained using the higher reactant flux. The authors also reported that film resistivity increased when Ar instead of H_2 was used as the carrier gas.

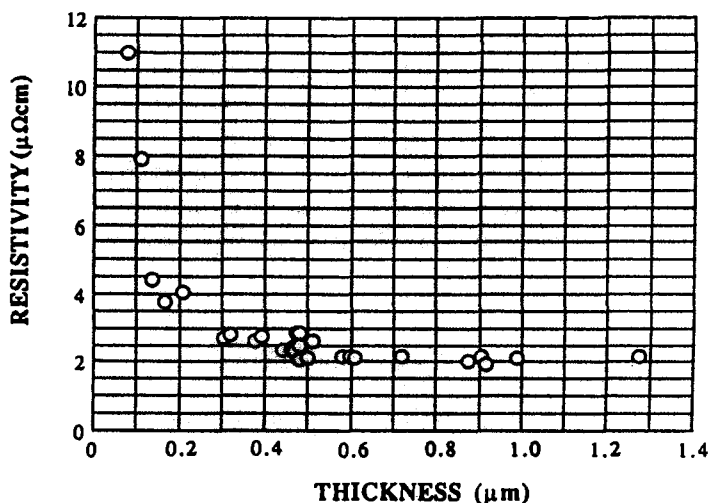


Figure 4-13 Resistivity of deposited copper films as a function of film thickness.⁵⁸

4.6.3 Microstructure

Kaloyeros et al.¹⁵ presented a plane view SEM image that showed a continuous polycrystalline film with uniform sub-micron grain size. Awaya and Arita³ reported plane view images that showed a cauliflower structure. The length scale of the structure decreased when the inlet concentration was raised. This suggests that the nucleation rate for forming new crystallites is higher at higher inlet concentrations, as expected from classical heterogeneous nucleation theory. Kim et al.⁵⁸ reported that grain size increased linearly with increasing thickness for LPCVD films (Fig. 4-14). We have observed similar behavior for APCVD films in our laboratory.⁶²

Fine et al.¹³ presented plane view and fracture cross-section SEM images of films grown at 280 °C and 350 °C. An average grain size of 0.1 μm was observed in the film grown at 280 °C. Grain size was increased by an order of magnitude for the 350 °C film, suggesting that the crystallite growth rate was enhanced more strongly than the nucleation rate. These authors went on to perform a regression analysis of grain size as a function of deposition conditions and showed that a strong correlation exists between grain size and growth rate.

Wang et al.⁶² showed that the morphology is strongly affected by the total pressure. Plane view and cross-sectional images of films grown at atmospheric pressure resembled "rock gardens" with large, well-separated crystallites protruding to various heights from a rough, polycrystalline base layer. Such structures are typical of films grown under mass transport limited conditions.⁶⁶ In contrast, films grown at 40 torr were smooth, well-

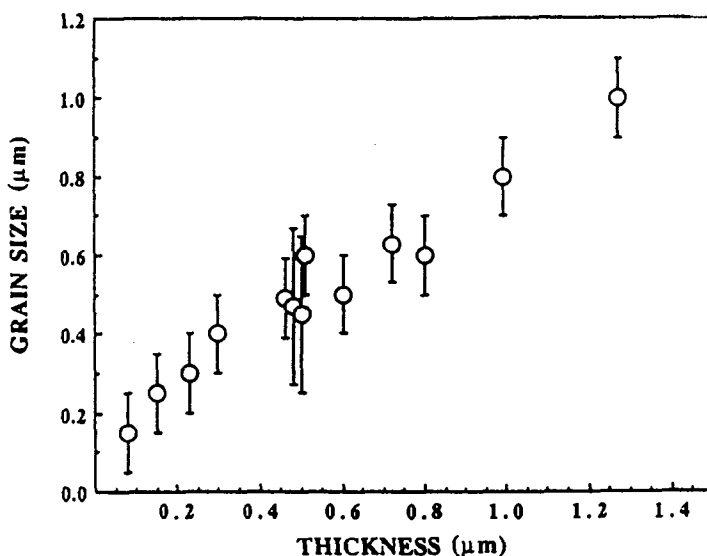


Figure 4-14 Average grain sizes of deposited copper films as a function of film thickness.⁵⁸

connected polycrystalline layers, as expected for growth under surface reaction limited conditions.

For thin films, the major morphological issue becomes film continuity. The fact that a minimum critical film thickness is needed to achieve bulk resistivity values (see above) suggests that thinner films may be discontinuous. Lai et al.¹⁶ reported that films thinner than 0.1 μm consisted of isolated clusters. The lateral dimensions of these clusters (based on SEM images) were comparable to their vertical dimension (based on step profilometry). The discontinuous structure was independent of the conditions that produced the thin film; similar morphology was observed at the inlet of their reactor where the growth rate was limited by low temperature and also at the end of the reactor where the growth rate was limited by low $\text{Cu}(\text{hfac})_2$ concentration.

Awaya and Arita¹⁷ reported that the reflectivity of the film increased, and a smoother surface was obtained when H_2O was added to the reactant stream. Together with their evidence that the addition of H_2O also activated non-selective surfaces for film growth, they provided further evidence that H_2O acts to increase the nucleation rate of new crystallites. This results in smaller grain sizes and smoother films.

Lecohier et al.⁶⁵ demonstrated the influence of pre-nucleation "seed" layers on the morphology of the CVD Cu film. Using different amounts of Pt evaporated onto a SiO_2 substrate, they showed that the grain size of the deposited Cu film decreased significantly

as the Pt concentration was increased. This is consistent with the principles of classical heterogeneous nucleation theory which predicts that a higher concentration of nucleation sites will result in a smaller final cluster size since the total amount of material deposited is distributed among a larger number of clusters.

4.6.4 Other Properties

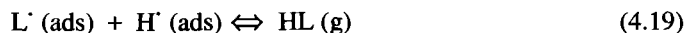
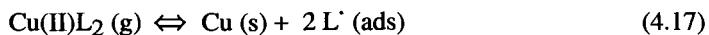
The reported X-ray diffraction spectra of CVD Cu films are relatively straightforward. Sharp patterns are obtained that are indicative of a well-crystallized FCC phase. The relative intensity of the (111) and (200) peaks indicates that the films usually contain some degree of preferential orientation in the (111) direction.³⁷

Arita et al.⁶⁷ have reported a value of 2.7×10^9 dyn/cm² for the internal stress (tensile) of Cu CVD films.

4.7 Reaction Mechanism

Our understanding of the reaction mechanism of Cu CVD using Cu(II) compounds has not reached the level of sophistication achieved for CVD of other electronic materials (Si or III-V compounds, for which the reaction chemistries have been studied much more intensively). The adsorption studies of Cu(II)(hfac)₂, Cu(I)(hfac)L', and H(hfac) described above have provided evidence for several surface intermediates that might be present. In particular, there is considerable evidence that adsorbed (hfac) ligands can be present under reaction conditions and that the fate of these ligands may be the determining factor for film growth kinetics and film properties (notably film purity). The kinetic studies by Lai et al.¹⁶ and Awaya and Arita¹⁷ demonstrated saturation effects in the dependence of growth rate on reactant concentration. This provides kinetic evidence that the rate-limiting step in the overall deposition mechanism takes place on the surface and involves one or more adsorbed species.

Starting from these experimental results, a list of possible steps for Cu CVD via H₂ reduction of Cu(II) compounds would include:

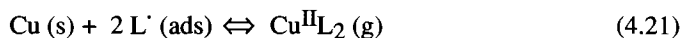
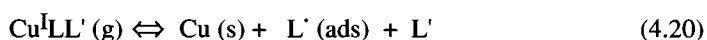


The surface intermediates involved in reactions 4.17 and 4.19 were discussed in the section dealing with adsorption studies. The coverage of these intermediates will likely be different under CVD conditions because of the high concentration of reactant and product molecules in the gas phase that surrounds the substrate.

The H₂ adsorption step (reaction 4.18) was not discussed above as it has been extensively studied.⁶⁸ Dissociative adsorption occurs readily and reversibly at room temperature and above on most metals, including Cu. The equilibrium heat of adsorption is relatively low (~ 10 kcal/mole), which means that the surface is not likely to be blocked by strongly bound H atoms under reaction conditions. There is a significant kinetic barrier for the adsorption step (~ 10-15 kcal/mole).⁶⁸ Depending on the coverage of adsorbed (hfac) ligands and the partial pressure of H₂ in the gas phase, there may be conditions where H₂ adsorption becomes the rate-limiting step for the deposition of pure Cu films.

Efforts to identify these conditions will require further understanding of the nature and extent of competitive adsorption between H₂ and CuL₂. Adsorption of H₂ may require a smaller ensemble of exposed metal atoms than are needed for CuL₂ adsorption. It may be possible for H₂ to adsorb "between" neighboring adsorbed (hfac) ligands, depending on the spacing between the latter groups. In contrast, Awaya and Arita¹⁷ have proposed that competitive adsorption may account for the maximum they observed in the growth rate as a function of Cu(hfac)₂ concentration. They suggested that competitive adsorption of Cu(hfac)₂ at high concentration may block the surface for H₂ adsorption.

The mechanism for reduction of Cu(II) compounds described in reactions 4.17 to 4.19 can be compared with the proposed mechanism for disproportionation of Cu(I) compounds:



Evidence dealing with reaction 4.20 was described briefly in the section dealing with adsorption studies. Reaction 4.21 is simply the reverse of reaction 4.17, the first step in the proposed mechanism for Cu(II) reduction. Both reactions 4.20 and 4.21 may be considered reversible, as indicated by reports that chemical vapor etching of Cu can be performed using the appropriate combination of Cu(II)L₂ and L'.^{8,69}

It is interesting to note that Kumar et al.⁷⁰ reported that H₂ reduction of Cu(I)(hfac)(COD) occurs more rapidly than disproportionation when the deposition reaction is carried out in the presence of H₂ carrier gas. Specifically, a layer of green Cu(hfac)₂ crystals is formed at the exit of the reactor when disproportionation is performed using an inert carrier. This layer is no longer observed when H₂ is used as the

carrier gas and appears to imply that adsorbed (hfac) ligands can react more rapidly with adsorbed H atoms than with neighboring (hfac) groups. This leads to the formation of H(hfac) rather than Cu(hfac)₂ as the major reaction product.

4.8 Rate Expression

The rate expression represents the quantitative relationship between deposition rate and the gas phase concentration near the surface. If information about the temperature dependence is also available, it can be included in the form of an activation energy for one or more of the coefficients in the rate expression. A rate expression may be determined empirically, in which case a power law or similar equation is developed to correlate measured growth rates with concentration (and temperature). Such expressions are generally adequate for reactor design and control over a limited range of operating conditions that do not deviate greatly from the conditions of the original measurements. Alternatively, a rate expression may be derived on the basis of a proposed reaction mechanism. In this case the analytical form of the rate expression is derived from a set of assumptions about the mechanism. As a result, the coefficients are expected to have some physical significance: they should correspond to the rate constants for individual steps in the mechanism.

4.8.1 Response Surface

The former approach is illustrated by a response surface analysis performed by Fine et al.¹³ to describe the temperature and concentration dependence of CVD rates using Cu(nona-F)₂ in H₂ carrier at low pressure (Fig. 4-15). By regression analysis of growth rates as a function of temperature and reactant concentrations, these authors obtained a rate expression of the form:

$$R_S = A \exp(-E_a / RT) [\text{Cu(nona-F)}_2]^X (\text{H}_2)^Y \quad (4.22)$$

where the optimized values of the fitting parameters were $E_a = 45 \pm 10$ kcal/mole, $X = 0.2 \pm 0.5$, and $Y = 2.0 \pm 0.7$. A similar analysis was performed to correlate mean grain size with operating conditions.

The apparent activation energy derived from Equation 4.22 is higher than values reported for other reactants. The H₂ reaction order also seems high while the reaction order for Cu(nona-F)₂ may be consistent with saturation behavior observed using Cu(hfac)₂. Such comparisons must be made cautiously, however, since the response

surface analysis approach does not attempt to include transport effects (see below) or any assumptions about the reaction mechanism.

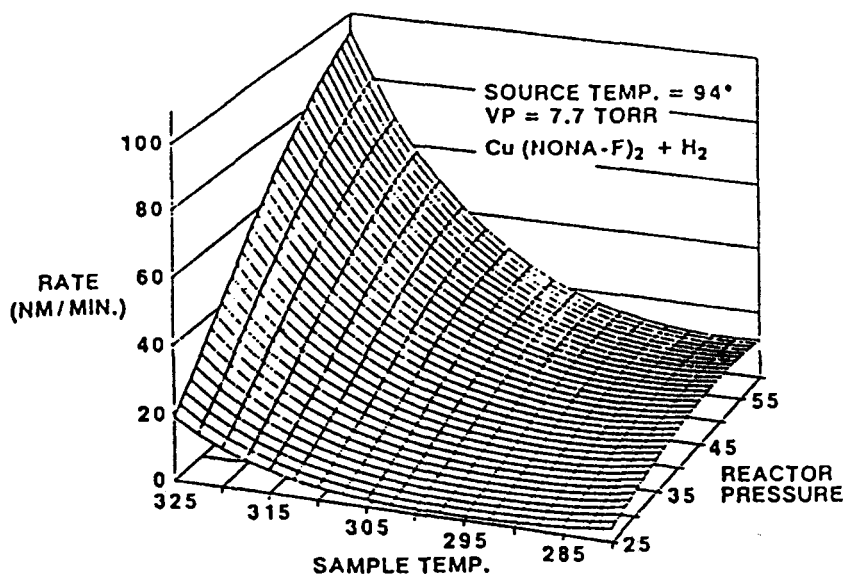


Figure 4-15 Response surface plot for deposition rate vs. process parameters for $\text{Cu}(\text{nona-F})_2$.¹³

4.8.2 Mechanism Fitting

This approach is illustrated by Lai et al.¹⁶ in their analysis of growth rates using $\text{Cu}(\text{hfac})_2$ reduction in H_2 at atmospheric pressure. The analysis began with the three main observations from their experimental results that formed the basis for assumptions about the reaction mechanism:

- (1) The growth rate is nearly independent of $\text{Cu}(\text{hfac})_2$ concentration at the inlet of the reactor. The observation of zero-order reaction kinetics suggests that the reaction proceeds via an adsorbed intermediate and that the surface becomes fully saturated by this intermediate at the inlet conditions of the reactor. Thus, a Langmuir-Hinshelwood rate expression is indicated.
- (2) The growth rate decreases when the mole fraction of H_2 in the inlet reactant stream is decreased. This suggests that H_2 is also involved in the rate-limiting step of the reaction.

- (3) The growth rate decreases when H(hfac) is added to the inlet reactant stream. This suggests that H(hfac) is adsorbed in competition with Cu(hfac)₂, thereby decreasing the number of vacant surface sites available to adsorb the reactant.

These observations are consistent with the mechanism proposed in reactions 4.17 to 4.19 with the regeneration of vacant sites by H(hfac) desorption (reaction 4.19) being the rate-limiting step.

The individual molecular steps are assumed to obey elementary kinetics:

$$\text{Cu(hfac)}_2 \text{ adsorption: } r_1 = k_{\text{ads},1} C_{\text{Cu(hfac)}_2} \Theta_V \quad (4.23)$$

$$\text{H(hfac) adsorption: } r_2 = k_{\text{ads},2} C_{\text{H(hfac)}} \Theta_V \quad (4.24)$$

$$\text{H(hfac) desorption: } r_3 = k_{\text{des}} P_{\text{H}_2} (1 - \Theta_V) \quad (4.25)$$

It is assumed that surface sites are either vacant or occupied by (hfac) ligands. Then Θ_V represents the fraction of sites that are vacant, and $(1 - \Theta_V)$ is the fraction occupied by adsorbed (hfac) ligands. In Equation 4.25 a single, first-order reaction rate is used to represent the combined steps of H₂ adsorption and H(hfac) desorption.

By assuming that the fractional coverage of (hfac) ligands is constant at steady state conditions, these equations are combined to yield the overall rate expression for Cu deposition:

$$R_s = r_1 = \frac{k_{\text{ads}} k_{\text{des}} C_{\text{Cu(hfac)}_2} P_{\text{H}_2}}{[2k_{\text{ads},1} C_{\text{Cu(hfac)}_2} + k_{\text{ads},2} C_{\text{H(hfac)}}] + k_{\text{des}} P_{\text{H}_2}} \quad (4.26)$$

This equation reproduces the major observations listed above. At high Cu(hfac)₂ concentration, the rate becomes zero order with respect to Cu(hfac)₂ and first order with respect to H₂. As the conversion increases, or if H(hfac) is added to the inlet mixture, the rate decreases as the reaction becomes inhibited by H(hfac).

Values for the kinetic parameters in this expression were determined by using Equation 4.18 in conjunction with Equation 4.30, the one-dimensional model for reaction and transport within the reactor (see below). The optimized parameter values were determined by judging the agreement between calculated and measured thickness profiles obtained over the entire range of reactor conditions:

$$k_{\text{des}} = 2.2 \times 10^{23} \exp(-80 \text{ kJ} / RT) \text{ molecule cm}^{-2} \text{ s}^{-1} (\text{atmH}_2)^{-1} \quad (4.27)$$

$$k_{\text{ads},1} = k_{\text{ads},2} = 0.1 \text{ cm s}^{-1} \quad (4.28)$$

The activation energy determined for the (hfac) desorption step agrees fairly well with the apparent activation energy of 75 kJ/mol reported by Kim et al. for low pressure CVD.⁵⁸ They did not, however, report a pre-exponential factor for comparison.

It is important to stress that obtaining agreement between the predictions of a reactor model and experimentally measured growth rates does not constitute verification of a particular rate expression or reaction mechanism. For example, Awaya and Arita¹⁷ recently presented quantitative results for the influence of $\text{Cu}(\text{hfac})_2$ concentration on growth rate over a wider range of conditions than studied by Lai et al.¹⁶ These new results confirmed the saturation behavior but showed that the rate actually passes through a maximum as a function of $\text{Cu}(\text{hfac})_2$ concentration. This supports the assumption of a Langmuir-Hinshelwood mechanism but suggests that a mixed second-order rate expression should be used to account for competitive adsorption between $\text{Cu}(\text{hfac})_2$ and H_2 on the same surface sites.

4.9 Reactor Design

Relatively little reactor modeling work has been done for Cu CVD. Most of the experimental studies with Cu(II) precursors have been performed using a cold-wall, impinging-flow reactor configuration (Fig. 4-16).^{3,7,13,18} Early experiments were generally performed at atmospheric pressure while later studies have focused to a greater extent on low pressure CVD. Other reactor configurations include the cold-wall horizontal flow reactor used by Temple and Reisman¹⁴ and the hot-wall horizontal reactor used by Lai et al.¹⁶ Both horizontal flow reactors were operated at atmospheric pressure. In the latter study, the reactor was operated at integral conversion and non-isothermal conditions, in order to obtain information about activation energy and reaction order in a single experiment.

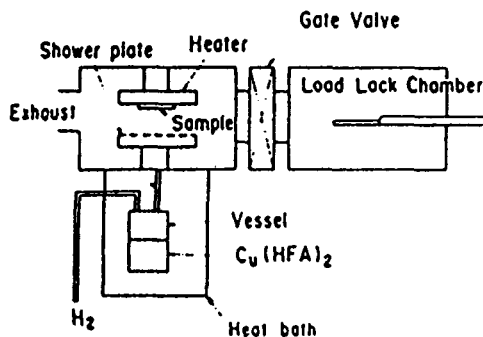


Figure 4-16 Cold wall, impinging flow low pressure CVD reactor configuration.¹⁷

4.9.1 Transport Effects

The influence of transport effects on the deposition rate must be considered whenever there are significant variations in the concentration of reactants (or products) within the reactor (see Ch. 9). The reactant concentration is lower within the main body of the reactor than at the inlet because reactant is being consumed. The magnitude of this effect can be estimated by comparing the overall rate of consumption (which can be estimated as the product of the deposition rate times the area on which deposition is occurring) vs. the rate at which reactant is entering the reactor (i.e., the product of the inlet concentration times the volumetric flow rate). Stated differently, the magnitude of the effect is proportional to the fractional conversion of the limiting reactant.

Concentration gradients may also exist between different locations within the reactor. This will occur if the rate of gas phase reactant transport by diffusion and convection is not fast enough to keep up with the rate of reactant consumption at the substrate. This is generally a more severe problem in atmospheric pressure reactors, although film non-uniformity due to concentration gradients may also occur in LPCVD reactors at high enough deposition rates. The presence of significant internal concentration gradients due to transport effects can be judged qualitatively by evaluating the surface Damköhler number:

$$Da_s = RL/CD \quad (4.29)$$

where R is the deposition rate, L is the characteristic dimension of the reactor, C is the reactant concentration, and D is the diffusivity of the reactant.

For low pressure CVD where the diffusivity is large, the value of Da_s is much less than one (except at the highest deposition rates), and concentration gradients within the reactor will be negligible. At atmospheric pressure, the lower diffusivity means that Da_s can approach or exceed unity, and concentration gradients will be significant. In the limit of very large Da_s values, the concentration gradient needed to maintain equality between the rates of transport and reaction will force the reactant concentration near the surface to approach zero. Under these conditions the deposition rate is determined solely by the rate of diffusive transport, which will completely mask the intrinsic kinetics of the surface reaction.

4.9.2 Reactor Modeling

To describe the deposition rate and spatial uniformity in reactors that are operating at finite levels of reactant conversion, it is necessary to incorporate the effects of both mass transport and surface reaction kinetics in an overall reactor model. The development of such models has reached a high degree of sophistication for several well-established CVD

processes such as epi-Si APCVD, poly-Si LPCVD, CVD of GaAs and other III-V compounds, and CVD W.⁷¹⁻⁷³

Reactor modeling efforts for CVD Cu are still in the early stages of development. In the only example published to date, Lai et al.¹⁶ described a simplified reactor model based on a one-dimensional Cu(hfac)_2 species conservation equation and compared the calculated and observed thickness profiles to obtain estimates of the kinetic parameters. After using the Damköhler criterion to show that gas phase concentration gradients in the vertical direction could be neglected, the species conservation equation for Cu(hfac)_2 was written in the form of the one-dimensional plug flow reactor equation with axial dispersion⁷¹:

$$\frac{d^2 C_{\text{Cu(hfac)}_2}}{d\chi^2} - \frac{UL}{D} \frac{dC_{\text{Cu(hfac)}_2}}{d\chi} - \frac{PL^2 R_s}{AD} = 0 \quad (4.30)$$

where $\chi = x/L$ is the fractional position along the reactor, R_s is the reaction rate, U is the average velocity of the carrier gas, D is the diffusivity of Cu(hfac)_2 , and P and A are the perimeter and cross-sectional area of the reactor, respectively. The use of the plug-flow average velocity, in place of the more accurate parabolic velocity profile, was justified by the neglect of vertical concentration gradients described above.

The boundary conditions at the reactor inlet and exit were those suggested by Danckwerts for the plug flow tubular reactor:⁷⁴

$$\frac{dC_{\text{Cu(hfac)}_2}}{d\chi} - \frac{UL}{D} (C_{\text{Cu(hfac)}_2} - C_{\text{Cu(hfac)}_2, \text{in}}) = 0 \quad \text{at } \chi = 0 \quad (4.31)$$

$$\frac{dC_{\text{Cu(hfac)}_2}}{d\chi} = 0 \quad \text{at } \chi = 1 \quad (4.32)$$

Equation 4.31 accounts for the fact that axial diffusion causes the concentration at the reactor inlet to decrease below the feed stream concentration, $C_{\text{Cu(hfac)}_2, \text{in}}$. Equation 4.32 sets the gradient to zero as the gas leaves the reaction zone.

In these experiments, samples were positioned so that they were partially located within the temperature gradient zone between the inlet and the heated section of the reactor (Fig. 4-17). This provided information about the temperature dependence of the deposition rate from the axial thickness profile measured along the front part of each substrate. In addition, the reactor was deliberately operated under conditions that caused nearly complete conversion of Cu(hfac)_2 . The temperature profile was measured independently and was used when solving Equation 4.30. The equation was solved numerically by the finite difference method using trial estimates of the kinetic parameters

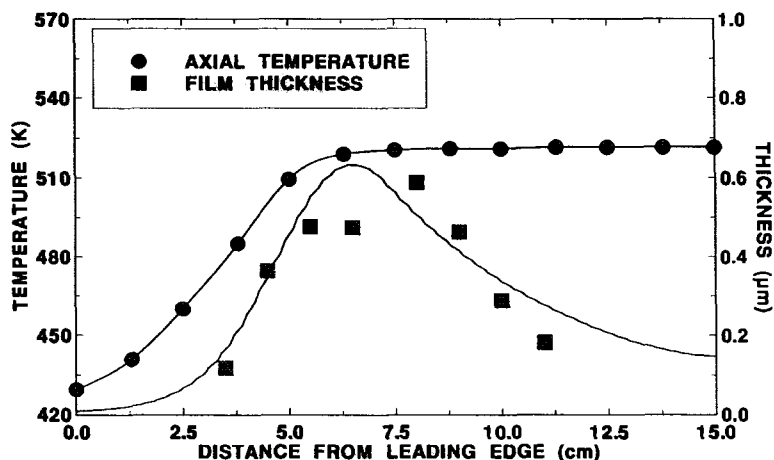


Figure 4-17 Axial reactor temperature profile (upper results) and axial film thickness profile (lower results) for atmospheric pressure CVD in an integral conversion reactor.¹⁶

to evaluate the rate expression. The optimized parameter values (Eqs. 4.27 and 4.28) were determined by judging the agreement between calculated and measured thickness profiles obtained over the entire range of reactor conditions.

4.10 Plasma-Assisted CVD (PACVD)

A number of studies of plasma-assisted Cu CVD have been reported since 1988. The potential advantages of PACVD include higher growth rate and/or lower substrate temperatures, and possibly improved microstructure. Disadvantages may include lack of substrate selectivity, poorer conformality, and possibly plasma-induced substrate damage. Thus Cu PACVD may be suitable for applications requiring blanket growth.

A partial list of Cu PACVD studies is given in Table 4-5. All of these studies have used Cu(II) β -diketonates as the reactant; e.g., Cu(hfac)₂,^{22,24,75} Cu(acac)₂,^{3,76,77} and Cu(tdf)₂.⁶¹ Growth rates up to 100 nm/min using direct plasmas have been reported by Eisenbraun, Awaya, and Zheng.^{3,24,61} Li et al.⁷⁵ reported a slower growth rate of 5-7.5 nm/min using a remote plasma, which may however reduce plasma-induced surface damage to the underlying substrate.

Table 4-5 Studies of Plasma-Assisted Cu CVD

Compound	Reactor Type	Power Density	Deposition Rate (nm/min)	Substrate Temperature (°C)	Carrier Gas	Reactor Pressure (torr)	Refs.
Cu(tfac) ₂	Parallel plate RF	0.05-0.06 W/cm ³	---	150-170	Ar/H ₂	0.2	22
Cu(hfac) ₂	Parallel plate RF	0.1-0.2 W/cm ²	100	160	H ₂	0.5-2.0	24
Cu(acac) ₂	Parallel plate RF	0.02-0.12 W/cm ³	10-100	200-280	H ₂	0.75-7.5	23
Cu(acac) ₂	ECR microwave	---	1-2	---	Ar/H ₂	0.001-0.01	76
Cu(acac) ₂	Remote plasma	---	---	---	He/H ₂	---	77
Cu(hfac) ₂	Remote plasma	1.5-2.2 W/cm ²	5-7.5	150-250	H ₂	0.5-2.0	75

4.10.1 Operating variables

4.10.1.1 Reactor Configuration

Awaya et al.³ used a parallel plate reactor with 20 cm electrode diameter and 5 cm electrode spacing. The substrate was mounted on the bottom electrode, and RF power (13.5 MHz, 20-300 W) was applied to the upper electrode. Eisenbraun et al.²⁴ also used a parallel plate reactor (Fig. 4-18). Oehr et al.²² compared results using two parallel plate reactors with different volumes. The highest film quality (as judged by resistivity) was obtained when the power densities were approximately the same in the two reactors.

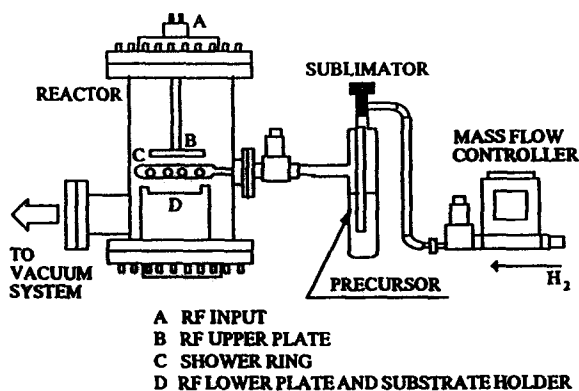


Figure 4-18 Plasma-assisted CVD system.²⁴

Pelletier et al.⁷⁶ used an electron cyclotron resonance (ECR) microwave (2.45 GHz) plasma reactor with an imposed magnetic field of 875 G parallel to the axis of the cylindrical reactor. Wisniewski et al.⁷⁷ and Li et al.⁷⁵ used remote plasma configurations.

4.10.1.2 Substrate Temperature

Values of substrate temperature in the range 150-170 °C have been used.^{22,24,75} Oehr et al.²² reported that temperature had a significant effect on film purity, with higher temperatures leading to decreased carbon content. Temperatures above 150 °C were necessary to obtain metallic Cu films. Awaya and Arita²³ also reported that impure films were obtained at very low temperature (100 °C), and also at very high temperatures (400 °C). At low temperatures, they proposed that the ligand desorption step is too slow to maintain a clean film; at high temperatures ligand decomposition takes place leading to

impurity incorporation. Pelletier et al.⁷⁶ used an unheated substrate which they estimate reached a maximum of 80 °C in their ECR microwave plasma reactor. Zheng et al.⁶¹ studied the temperature dependence of the deposition rate using Cu(tdf)₂ and obtained an apparent activation energy of 5.8 kcal/mole.

4.10.1.3 Power Density

Most authors have provided at least some discussion of the effect of plasma power density on film deposition and properties. Oehr et al.²² studied the influence of power level on resistivity and purity of the PACVD films. The optimum power density was 0.05-0.06 W/cm³; both the impurity level and the resistivity of the film increased at higher or lower power levels. The optimum power density was independent of electrode spacing based on two reactor geometries. The authors did not discuss the effect of power density on deposition rate. They did state that there was no apparent threshold value as deposition occurred continuously down to the lowest power density studied.

Eisenbraun et al.²⁴ employed a substrate power density of 0.1- 0.2 W/cm². The electrode spacing was not specified, but this probably corresponds to a volume power density several times lower than that used by Oehr et al.²² The authors proposed that low power density generates H atoms without disrupting the surface.

Pelletier et al.⁷⁶ did not describe the influence of power density. They operated at 100 W, which was sufficient to produce a saturation ion current density. The ion current at the substrate position was 0.2 mA/cm². They also reported that direct bias voltage had a significant effect on film purity. A negative bias of -50 V on the substrate was necessary to obtain film resistivity in the range 2-3 μΩcm.

Wisniewski et al.⁷⁷ studied decomposition of Cu(hfac)₂ using a remote plasma configuration. They reported that microwave power density can control the composition and stoichiometry of the film (i.e., Cu vs. CuO_x). Awaya and Arita²³ used power densities between 0.02 - 0.12 W/cm³. This corresponds to substrate power densities between 0.10 - 0.6 W/cm². Li et al.³ used a substrate power density of 1.5-2.2 W/cm² in their remote plasma deposition study.

4.10.1.4 Reactant Concentration

The effect of reactant concentration on PACVD kinetics has not been carefully studied. For example, simple reaction order plots have not been reported. Awaya and Arita²³ varied the inlet concentration of Cu(hfac)₂ by changing the evaporator temperature from 150 to 170 °C. The increase in reactant concentration led to smoother films with less island-like appearance. This suggests there may be a higher nucleation rate and/or faster cluster coalescence at the higher reactant concentration. Eisenbraun et al.²⁴ observed that the measured DC bias depended on the inlet concentration which varied with time over the course of their experiments.

4.10.1.5 Carrier Gas

There is also only limited information about the influence of carrier gas pressure on PACVD films. Awaya and Arita²³ reported that H₂ was necessary to reduce C and O contamination in the film and to obtain low-resistivity films. The total pressure was varied between 0.75-7.5 torr. Pelletier et al.⁷⁶ also reported that a H₂-rich carrier gas was needed to reduce C contamination in the films. The optimum composition was reported to be 1:10 Ar:H₂.

Oehr et al.²² reported H₂ had to be present with Ar carrier to obtain metallic films. They varied the Ar/H₂ ratio in the carrier gas from 4:1 to 1:1, with the lowest resistivity being obtained at the highest H₂ concentration. Wisniewski et al.⁷⁷ were able to observe metallic copper using pure He as carrier gas, but Cu₂O and CuO phases were also present. Eisenbraun et al.²⁴ emphasized the role of H₂ for generating H atoms in the plasma.

4.10.2 Reaction Mechanism

Very little quantitative work has been done to elucidate the role of plasma-enhanced processes in the mechanism of Cu CVD. Awaya and Arita²³ do not discuss the role of plasma processes directly; they mainly describe the importance of H₂ and substrate temperature in suppressing carbon impurities. Eisenbraun et al.²⁴ emphasize the role of H atom generation in the plasma as a means of increasing the rate of H(hfac) desorption (i.e., the probable rate-limiting step under thermal CVD conditions).

Oehr et al.²² observed that film purity is correlated with power density. They suggested that at low power density the (hfac) ligands cannot desorb, while at high power density the ligands are decomposed. Pelletier et al.⁷⁶ stressed the absence of oxygen contamination in plasma assisted film deposition. They suggested that H atoms from within ligand fragments can serve as scavengers for O removal. When H₂ is present in the carrier gas, it can eliminate C fragments from the film.

4.10.3 Film Properties

4.10.3.1 Purity

The major issue in plasma-assisted CVD of copper films appears to be film purity. The use of H₂ in the carrier gas is essential to reduce oxygen and carbon incorporation.²³ Film purity is also affected by power density according to Oehr et al.²² who reported that

copper content varied between 80-100 wt % depending on operating conditions. Their results could not define a quantitative trend but did suggest that highest Cu content was achieved at an intermediate power density ($0.05\text{--}0.06\text{ W/cm}^3$) and at substrate temperatures above $130\text{ }^\circ\text{C}$. Their ESCA (electron-spectroscopy for chemical analysis) results suggest that F is incorporated by retention at C atoms.

Awaya and Arita²³ observed C and O impurities by AES (Auger electron spectroscopy) analysis in films deposited below $200\text{ }^\circ\text{C}$ or above $300\text{ }^\circ\text{C}$. More specifically, O (but not C) was detected in the low temperature films, while C (but not O) was found in the high temperature films. Carbon impurities were also observed in films deposited using He as the carrier gas in the absence of H_2 . The authors proposed that at low temperature, the rate of ligand desorption cannot keep up with the film growth rate, and ligand incorporation occurs (although this does not account for the lack of C signals in their AES analysis). At high temperature, or in the absence of H_2 , ligand decomposition occurs with subsequent incorporation of ligand fragments into the film.

Pelletier et al.⁷⁶ reported that carbon atoms were the major impurity (up to 50%). The carbon content and resistivity depended strongly on the direct bias voltage and gas phase composition. Pure films were obtained with a bias voltage of -50 V and a hydrogen-rich carrier gas. They noted that oxygen was not an impurity, even in C-containing films. Eisenbraun et al.²⁴ also claimed to obtain pure films, although no AES results were given. Wisniewski et al.⁷⁷ were able to control the relative deposition of Cu vs. CuO or Cu_2O by controlling the composition of the carrier gas with addition of N_2O or O_2 .

4.10.3.2 Resistivity

Eisenbraun et al.²⁴ reported values as low as $1.7\text{ }\mu\Omega\text{cm}$. Awaya and Arita²³ obtained resistivities of $1.8\text{ }\mu\Omega\text{cm}$. The resistivity depended on substrate temperature, with the lowest value obtained for substrate temperatures from $200\text{--}280\text{ }^\circ\text{C}$. The resistivity was correlated with film purity which was also optimum over this temperature range.

Under optimized conditions, Oehr et al.²² obtained resistivities in the range $1.7\text{--}2.4\text{ }\mu\Omega\text{cm}$. It was necessary to include H_2 in the carrier gas to obtain metallic films. Pelletier et al.⁷⁶ obtained resistivities between $2\text{--}3\text{ }\mu\Omega\text{cm}$. As noted above, resistivity depended strongly on the direct bias voltage and gas phase composition.

4.10.3.3 Morphology

Awaya and Arita²³ showed that smoother films can be deposited using PACVD, compared to thermal CVD. Planar SEM images suggested that the surfaces of PACVD films grown at $280\text{ }^\circ\text{C}$ were fairly continuous in contrast to a strong cluster-like morphology that appeared for films grown by thermal CVD at $400\text{ }^\circ\text{C}$. The morphology of the PACVD film was reported not to depend on the substrate material in contrast to

thermal CVD films which depended considerably on the nature and temperature of the substrate. Li et al.⁷⁵ reported a smooth, uniform, dense surface with grain size of order 1.0 μm .

Pelletier et al.⁷⁶ reported that XRD measurements showed preferential orientation (i.e., $I_{\text{Cu}(111)}/I_{\text{Cu}(200)} = 8:1$ vs. 2:1 for random orientation). The observed line broadening suggested the presence of very small grains of metallic copper embedded in a matrix of an amorphous material.

4.10.3.4 Conformality

Awaya and Arita²³ reported that conformality of PACVD films is superior to films prepared by sputtering methods. For an isolated step, they obtained essentially ideal conformal coverage. For a patterned set of adjacent steps, coverage at the bottom of the trenches degraded somewhat to about 50% of the top surface coverage. Eisenbraun et al.²⁴ reported that trenches and interlevel vias with aspect ratios as high as 3:1 were completely filled by their H_2 plasma assisted CVD process. They suggested that plasma energy was transferred to the nucleating copper atoms on the surface resulting in enhanced surface diffusion rates.

4.11 Laser-Assisted CVD (LCVD)

Several papers have appeared since 1985 that deal with laser-assisted Cu CVD. These techniques are potentially useful for direct writing applications such as mask repair, circuitization, or localized doping. Good general reviews of direct writing are given by Osgood and Gilgen⁷⁸ and Herman.⁷⁹ Houle et al. have prepared a thorough review of laser deposition using acetylacetonate compounds.⁸⁰

Two general methods are available to accomplish LCVD. In *pyrolysis* LCVD, the role of the laser is to heat the substrate and induce pyrolysis of the metal compound.^{19,20} This approach can be implemented using a laser source at any wavelength absorbed by both the substrate and the growing film.

In *photochemical* LCVD, the laser (or other light source) is used to excite a specific electronic excitation in the reactant (or sensitizer) which activates the molecule for a subsequent chemical reaction. In the case of $\text{Cu}(\text{hfac})_2$, excitation has been performed using a strong, broad absorption band at 230–255 nm. This band is assigned to a ligand to metal charge transfer transition with the photoactivated σ_{L} orbital donating an electron into the metal $3d_{xy}$ orbital.⁸⁰ Various light sources have been used, including a Hg arc lamp (low power density), frequency doubled Ar ion laser (medium power), and ArF and KrF excimer lasers (pulsed, high power density).²¹

4.11.1 Operating Variables

4.11.1.1 Reactants

All of the studies reported to date have used Cu(hfac)_2 as the reactant.¹⁹⁻²¹ These studies have generally been performed without using a carrier gas; i.e., the gas phase composition is determined by the vapor pressure of a sample of solid reactant located somewhere within the reactor. One exception is the photochemical LCVD study by Jones et al.²¹ These authors reported that gas phase $\text{C}_2\text{H}_5\text{OH}$ had to be present to achieve measurable LCVD growth rates when a (low power density) Hg arc lamp was used as the excitation source. They proposed that $\text{C}_2\text{H}_5\text{OH}$ played the role of reductant under these conditions. Gas phase $\text{C}_2\text{H}_5\text{OH}$ was not required at higher power density (i.e., when using a frequency doubled Ar ion laser or an excimer laser).

4.11.1.2 Growth Kinetics

Deposition rates for LCVD are reported in several formats which include writing speed (= distance/time) or amount deposited (volume/time). Houle et al. originally reported

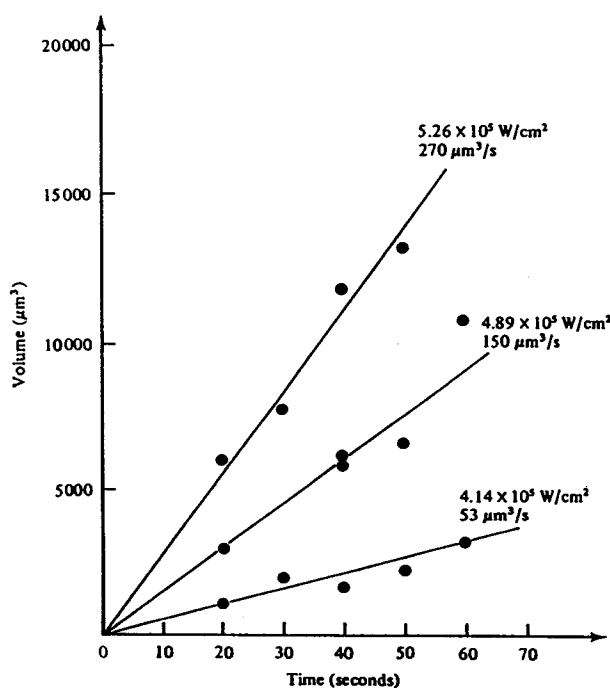


Figure 4-19 Volumes of copper spots obtained by laser pyrolysis CVD as a function of irradiation time for various laser power densities.¹⁹

growth rates in units of volume of Cu deposited vs. time for various light intensities (Fig. 4-19).¹⁹ In later work the group reported being able to produce deposits that were several microns thick at writing speeds on the order of microns per second.⁸⁰ Jones et al. obtained film thicknesses in the range 1-200 Å using an Ar ion laser (power density = $0.2\text{--}2.0 \times 10^4 \text{ W/cm}^2$).²¹ Films were limited to 500 Å when higher intensity pulsed excimer lasers were used, presumably due to ablation effects at higher thickness. Markwalder et al.⁸¹ discussed their results in terms of the height and width of the deposited Cu lines as a function of writing speed (Fig. 4-20).

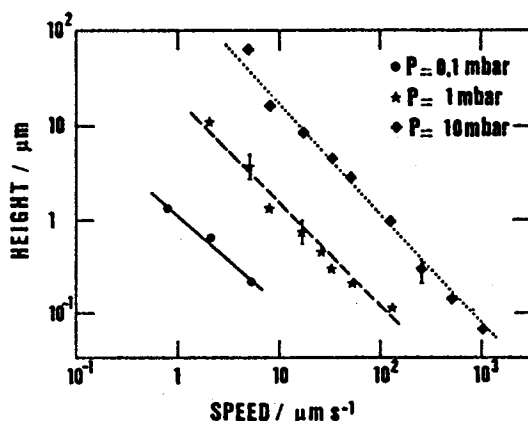


Figure 4-20 Copper stripe height as a function of writing speed for laser pyrolysis CVD at three metalorganic vapor pressures.⁸¹

4.11.1.3 Substrate Temperature

The ambient substrate temperature has not been considered as a major experimental variable in studies to date. This likely reflects the fact that the laser-assisted mechanism is intended to override the effects of ambient thermal processes. For photochemical LCVD, the sample can be kept near room temperature.²¹

For pyrolysis LCVD, the local temperature on the substrate surface must be calculated as a function of laser intensity and spot size.^{19,20} For example, Houle et al. have estimated that the maximum local temperature on a silicon substrate reaches 800 °C at an incident power density of $5 \times 10^5 \text{ W/cm}^2$.¹⁹ The authors also noted that the calculated temperature is much lower on a Cu substrate (~250 °C) because of the higher reflectivity of Cu vs. Si. In at least one instance, Markwalder et al. report that the line width saturates at slow writing speed due to thermal conduction effects.⁸¹ Under these conditions, the authors suggest that the local temperature rise becomes great enough to activate re-evaporation of Cu monomers, thus preventing further film growth.

4.11.1.4 Laser Intensity

Laser intensity generally replaces ambient substrate temperature as the major experimental variable in LCVD processes. Houle et al. have reported a threshold intensity effect.¹⁹ At intensities below $2.5 \times 10^5 \text{ W/cm}^2$, deposition does not occur. Above the threshold intensity, growth rate increases with intensity. Moylan et al. reported that the power level strongly affects the line shape (i.e., whether the profile is Gaussian, flat, or volcano-like).²⁰ Markwalder et al. compared results using laser powers of 0.1, 0.3, and 1 W.⁸¹ They observed that increasing laser power led to higher growth rates. They also noted that increasing the reactant concentration had a greater effect on the growth rate.

4.11.2 Film Properties

4.11.2.1 Purity

Film purity is a major concern for Cu LCVD. For photochemically deposited films, purity may be the limiting factor.⁸⁰ Jones et al. reported C contents of up to 50% for films grown using a Hg arc source with $\text{C}_2\text{H}_5\text{OH}$ as reactant with lower amounts (<10%) of O and F also present.²¹ High C levels were also present using the Ar ion laser, but the O and F levels were reduced to less than 1%. Houle et al. reported that the C impurity decreases as light intensity increases.⁸⁰ They observed that the C/Cu ratio shows a spatial variation which is also correlated with periodic ripples observed in the surface topography (see below).

For laser pyrolysis CVD, metal purities greater than 95% have been achieved.⁸⁰ This suggests that ligands can desorb and/or decompose to volatile products at the higher local substrate temperatures achieved in laser pyrolysis.

4.11.2.2 Resistivity

The resistivity of Cu LCVD films has not been studied comprehensively. This may reflect the problems with film purity noted above. Houle et al. have reported values as low as $3.6 \mu\Omega\text{cm}$.¹⁹ Markwalder et al. studied resistivity as a function of writing speed and reactant concentration.⁸¹ The observed values approached the bulk resistivity to within one order of magnitude. An optimum writing speed was observed at each pressure studied, and the optimum speed increased in direct proportion to the pressure.

4.11.2.3 Morphology

A variety of film morphologies and line width profiles have been observed for Cu LCVD. Houle et al.⁸⁰ (also Moylan²⁰) reported that Gaussian or flat-topped profiles are

produced at low power density, giving way to volcano-like profiles at high intensity. The film morphology consisted of small, domed crystallites at low coverage. As the film coverage increases, these crystallites eventually merge. Renucleation also begins to take place.

Markwalder et al. showed that the film morphology was a function of writing speed.⁸¹ Film roughness increased at high or low speeds, an effect which the authors attributed to thermal conduction effects. They also reported that the mean feature size increases with reactant concentration. Films can also contain a significant degree of porosity, which can be partially eliminated by subsequent annealing.

Houle et al. reported an intriguing rippling effect in films grown by photochemical LCVD.⁸⁰ The length scale of these lateral ripples was of the order of 100 nm, which is much shorter than the gas phase mean free path at deposition conditions. The authors suggested that the rippling may arise from a standing electromagnetic field that is created by interference effects of the incident light reflecting from the metal surface.

4.11.3 Reaction Mechanism

Very little work has been done to quantify the mechanism of Cu LCVD. For pyrolysis LCVD, the mechanism is expected to be the same as conventional CVD. Observed differences in film purity, morphology, etc. may arise because the local substrate temperature during LCVD may be much higher than for conventional CVD; thus the coverage and reaction rates of specific surface intermediates may be different.

For photochemical LCVD, a major difference in the reaction mechanism is the initial photoactivation step, which is not present in conventional CVD. For example, Marinero et al. confirmed that Cu atoms are produced by the photochemical activation of Cu(hfac)₂ using a 249 nm KrF excimer laser.⁸² Based on the time delay (<2ns) observed at 0.1 torr pressure, the authors suggested that the process occurs via a unimolecular photodissociation step.

Houle et al. concluded that a substantial portion of critical dissociation events occur close to the surface.⁸⁰ This was based on the observation that spot size is limited to the width of the laser beam (10^{-3} - 10^{-2} cm), and the deposited film shows surface topography of order 100 nm. Both dimensions are much shorter than gas phase mean free path at deposition conditions.

The same authors also proposed that the principal mechanism for carbon contamination in the films is the secondary photolysis of (hfac) ligands.⁷⁹ As evidence, they cited examples from acetone and H(acac) photochemistry. Depending on the substrate temperature and carrier gas composition, thermal ligand decomposition reactions may also contribute significantly to film impurity levels.

4.11.3.1 Transport Effects

Deposition rates may be controlled either by mass transfer or surface reaction. In the first case (transport limited), all reactant molecules that reach the surface decompose immediately, and the net deposition rate is the rate at which reactants collide and react with the hot surface. In the second case (reaction limited), the rate is determined by the intrinsic surface reaction kinetics which are slow enough that diffusion in the gas phase can prevent significant concentration gradients from developing. A thorough discussion of transport effects in LCVD is given by Kodas and Comita.⁸³

In transport limited cases, the rate will be proportional to the product of the diffusivity and the reactant concentration. If the composition of the reactant mixture is fixed (or if pure reactant is used without a carrier gas), the diffusivity will be inversely proportional to reactant concentration. This leads to the curious situation that the rate will be independent of the reactant pressure. If the total pressure is kept fixed by simultaneously adjusting the carrier gas pressure and the reactant/carrier gas ratio, then the deposition rate becomes directly proportional to reactant concentration.

The latter condition appears to be illustrated by the work of Markwalder et al. who showed that the deposition rate was more strongly affected by reactant concentration than laser power.⁸¹ In contrast, Moylan et al. identified conditions where the rate should be surface reaction limited.²⁰ In this case, they were further able to determine a reactive sticking coefficient of about 0.02 for the incident molecules.

4.12 SUMMARY

Chemical vapor deposition of Cu films using H₂ reduction of volatile Cu(II) precursors is a viable method for preparing Cu metallization layers. It is possible to obtain films that approach bulk resistivity and show good conformality and selective area deposition. Deposition rates obtained to date are significantly lower than rates that have been reported using the disproportionation of Cu(I) precursors. However, the reaction mechanism for the reduction of Cu(II) compounds appears to involve only surface intermediates, which may result in better control of film conformality and selective area deposition, as well as reducing the potential for gas phase particle formation. The reduction of Cu(II) compounds may also provide greater flexibility in the choice of reactor design and operating conditions because the H₂ partial pressure can be adjusted as an additional operating variable.

At the fundamental level, a qualitative outline of the reaction chemistry for Cu(II) reduction has emerged. Adsorption studies under UHV conditions have confirmed the presence of adsorbed (hfac) groups on the surface. These groups are probably present as the major surface intermediate under CVD reaction conditions. The desorption of these

groups as H(hfac) molecules formed via bimolecular surface reaction with adsorbed H atoms appears to be the rate-limiting step in the overall reaction mechanism. Adsorbed (hfac) groups are also proposed as surface intermediates during the disproportionation of Cu(I) compounds. Given this common intermediate, further work is needed to learn why the Cu(II) reduction process has historically shown lower growth rates.

Additional fundamental research is needed in several areas:

Alternate reactants. Quantitative kinetic studies of Cu(II) compounds other than Cu(hfac)₂ (e.g., β -ketoiminates) should be performed to determine whether higher growth rates can be obtained. If promising alternate compounds are found, then additional rate expression studies should be performed to determine whether the kinetics are consistent with the reaction mechanism that has been proposed for the reduction of Cu(hfac)₂. These results can then be combined with separate adsorption studies, and a realistic effort can be made to correlate the differences in CVD reactivity with the structure and chemical properties of the compound(s).

Reaction kinetics. Further quantitative work is needed to determine the role of H₂ partial pressure in the rate expression. In particular, experiments should address whether H₂ adsorption is the rate-limiting step under certain conditions. Experiments are also needed to verify whether the rate expression developed for atmospheric pressure CVD can be applied to LPCVD conditions.

Further work is needed to quantify the role of product inhibition. This information will give additional insight into the magnitude of ligand coverage effects (competitive adsorption) and will be helpful for developing reactor design rules for the maximum allowable conversion of reactant. Combined with further studies of the effect of reactant concentration on growth rates, this should also provide an understanding of the saturation effects reported by several authors.

The effect of H₂O concentration should be examined more carefully, especially with regard to the possible trade-off between increased growth rates vs. increased oxygen content in the film.

Nucleation. Quantitative studies of film nucleation on various substrates are needed in order to better understand the factors which control selective area deposition. These results may also suggest ways to reduce the minimum thickness required to obtain continuous films thereby permitting the resistivity to approach the bulk value. Specific experiments should examine the role of H₂ partial pressure, trace concentrations of H₂O, and the pretreatment conditions used to prepare the substrate (e.g., extent of surface dehydroxylation). Further work is also needed to understand the instances of reverse selectivity that have been reported by a few authors.

Film properties. In view of the current evidence that ligand desorption is the rate-limiting step for the Cu(II) reduction process, a quantitative correlation should be established between film purity (and resistivity) and film growth rates. Film purity is probably also the main concern for both plasma- and laser-assisted CVD processes.

Acknowledgments: The authors' research cited here was supported by a joint research agreement between IBM Corporation and Louisiana State University. Principal coworkers during this period include graduate students W. Gilbert Lai and Reginald Little, and post-doctoral associates Dr. Jue Wang and Dr. Ravi Kumar.

References

1. Panousis, P.T., Favreau, D.P., Merchant, S.M., Ryan, V., Dein, E.A. in *Advanced Metallization for ULSI Applications*, Rana, V.V.S., Joshi, R.V., Ohdomari, I. (eds.), Materials Research Society, Pittsburgh, PA, 1992, 3-12.
2. Gross, M.E., Donnelly, V.M. in *Advanced Metallization for ULSI Applications*, Rana, V.V.S., Joshi, R.V., Ohdomari, I. (eds.), Materials Research Society, Pittsburgh, PA, 1992, 355-66.
3. Awaya, N., Arita, Y. *Digest of Technical Papers* **1989**, Section I2-4, 103-04.
4. Shingubara, S., Nakasaki, Y., Kaneko, H. *Appl. Phys. Lett.* **1991**, 58, 42.
5. Pai, P.-L., Ting, C.H., Chain, C., Wei, C.-S., Fraser, D.B. in *Tungsten and Other Advanced Metals for VLSI/ULSI Applications V*, Wong, S.S., Furukawa, S. (eds.), Materials Research Society, Pittsburgh, PA, 1990, 359-67.
6. Hu, C.-K., Small, M.B., Kaufman, F., Pearson D.J. in *Tungsten and Other Advanced Metals for VLSI/ULSI Applications V*, Wong, S.S., Furukawa, S. (eds.), Materials Research Society, Pittsburgh, PA, 1990, 369-73.
7. Van Hemert, R.L., Spendlove, L.B., Sievers, R.E. *J. Electrochem. Soc.* **1965**, 112, 1123.
8. Norman, J.A.T., Muratore, B.A., Dyer, P.N., Roberts, D.A., Hochberg, A.K. *J. de Phys. IV* **1991**, Coll. C2, 1, 271-78.
9. Shin, H.-K., Chi, K.-M., Hampden-Smith, M.J., Kodas, T.T., Farr, J.D., Paffett, M. *Mater. Res. Soc. Symp. Proc.* **1991**, 204, 421-27.
10. Reynolds, S.K., Smart, C.J., Baran, E.F., Baum, T.H., Larson, C.E., Brock, P.J. *Appl. Phys. Lett.* **1991**, 59(18) 2332-34.
11. Moshier, R.W., Sievers, R.E., Spendlove, L.B. *US Patent* 3 356 527, **1967**.
12. Charles, R.G., Cleary, J.G. *US Patent* 3 594 216, **1971**.
13. Fine, S.M., Dyer, P.N., Norman, J.A.T., Muratore, B.A., Iampietro, R.L. *Mater. Res. Soc. Symp. Proc.* **1990**, 204, 415.
14. Temple, D., Reisman, A. *J. Electrochem. Soc.* **1989**, 136(11), 3525-29.
15. Kaloyeros, A.E., Feng, A., Garhart, J., Brooks, K.C., Ghosh, S.K., Saxena, A.N., Luehersch, F. *J. Electronic Mater.* **1990**, 19, 271.
16. Lai, W.G., Xie, Y., Griffin, G.L. *J. Electrochem. Soc.* **1991**, 138, 3499-3504.
17. Awaya, N., Arita, Y. in *Advanced Metallization for ULSI Applications*, Rana, V.V.S., Joshi, R.V., Ohdomari, I. (eds.), Materials Research Society, Pittsburgh, PA, 1992, 345-54.

18. Lecohier, B., Philippoz, J.-M., Calpini, B., Stumm, T., van den Bergh, H. *J. de Phys. IV* **1991**, Coll. 1, 279-86.
19. Houle, F.A., Jones, C.R., Baum, T., Pico, C., Kovac, C.A. *Appl. Phys. Lett.* **1985**, 46, 204.
20. Moylan, C.R., Baum, T.H., Jones, C.R. *Appl. Phys. A* **1986**, 40, 1-5.
21. Jones, C.R., Houle, F.A., Kovac, C.A., Baum, T.H. *Appl. Phys. Lett.* **1985**, 46, 97.
22. Oehr, C., Suhr, H. *Appl. Phys. A* **1988**, 45, 151-54.
23. Awaya, N., Arita, Y. *Jpn. J. Appl. Phys. Pt. 1* **1991**, 30(8), 1813-17.
24. Eisenbraun, E.T., Zheng, B., Li, H., Wax, A., Kaloyeros, A.E., Dettelbacher, C., Toscano, P.J., Devashrayee, N., Murarka, S.P., Olowolafe, J.F., Pintchovski, F. in *Advanced Metallization for ULSI Applications*, Rana, V.V.S., Joshi, R.V., Ohdomari, I. (eds.), Materials Research Society, Pittsburgh, PA, 1992, 397-401.
25. Cohen, S.L., Liehr, M., Kasi, S. *Appl. Phys. Lett.* **1992**, 60(1), 50-52.
26. Cohen, S.L., Liehr, M., Kasi, S. *Appl. Phys. Lett.* **1992**, 60(13), 1585-87.
27. Cohen, S.L., Liehr, M., Kasi, S. *J. Vac. Sci. Technol.* **1992**, A 10(4), 863-68.
28. Donnelly, V.M., Gross, M.E. *J. Vac. Sci. Technol* **1993**, A 11(1), 66-77.
29. Dubois, L.H., Jeffries, P.M., Girolami, G.S. in *Advanced Metallization for ULSI Applications*, Rana, V.V.S., Joshi, R.V., Ohdomari, I. (eds.), Materials Research Society, Pittsburgh, PA, 1992, 375-81.
30. Jarvis, J.J., Pearce, R., Lappert, M.F. *J. Chem. Soc., Dalton Trans.* **1977**, 999-1003.
31. Miyashita, A., Yamamoto, A. *Bull. Chem. Soc. Jpn.* **1977**, 50, 1102-08.
32. Chichibu, S., Shishikura, M., Ino, J., Matsumoto, S. *J. Appl. Phys.* **1991**, 70, 1648-55.
33. Lampe-Onnerud, C., Harsta, A., Jansson, U. *J. de Phys. IV* **1991**, Coll. C2, 1, 881-888.
34. Moshier, R.W., Sievers, R.E. *Gas Chromatography of Metal Chelates*, Pergamon, Oxford, 1965.
35. Sievers, R.E., Sadlowski, J.E. *Science* **1978**, 201, 217.
36. Sievers, R.E., Ponder, B.W., Morris, M.L., Moshier, R.W. *Inorg. Chem.* **1963**, 2, 693-98.
37. Pauleau, Y., Fasasi, A.Y. *Chem. Mater.* **1991**, 3, 45-50.
38. Bertrand, J.A., Kaplan, R.I. *Inorg. Chem.* **1966**, 5, 489-91.
39. Starikova, Z.A., Shugam, E.A. *J. Struct. Chem.* **1969**, 10, 267-69.
40. Mehrotra, R.C., Bohra, R., Gaur, D.P. *Metal β -Diketonates and Allied Derivatives*, Academic Press, London, 1978 (esp. chapter 2).
41. Holm, R.H., Everett, G.W., Jr., Chakravorty, A. *Prog. Inorg. Chem.* **1966**, 7, 83-214.
42. Belford, R.C.E., Fenton, D.E., Truter, M.R. *J. Chem. Soc., Dalton Trans.* **1974**, 17-24.
43. Kogane, T., Ishii, M., Harada, K., Hirota, R., Nakahara, M. *Bull. Chem. Soc. Jpn.* **1989**, 62, 2524-29.

44. Belford, R.C.E., Fenton, D.E., Truter, M.R. *J. Chem. Soc., Dalton Trans.* **1972**, 2208-13.
45. Kogane, T., Ishii, M., Harada, K., Hirota, R., Nakahara, M. *Bull. Chem. Soc. Jpn.*, **1990**, 63, 1005-09.
46. Henne, A.L., Newman, M.S., Quill, L.L., Staniforth, R.A. *J. Am. Chem. Soc.* **1947**, 69, 1819-20.
47. Belford, R.L., Martell, A.E., Calvin, M. *J. Inorg. Nucl. Chem.* **1956**, 2, 11-31.
48. Funck, L.L., Ortolano, T.R. *Inorg. Chem.* **1968**, 7, 567-73.
49. Norman, J.A.T., Personal communication (1992).
50. McCarthy, P.J., Hovey, R.J., Ueno, K., Martell, A.E. *J. Am. Chem. Soc.* **1955**, 77, 5820-24.
51. Norman, J.A.T. *US Patent* 5 008 415, April 16, **1991**.
52. Eisentraut, K.J., Sievers, R.E. *J. Inorg. Nucl. Chem.* **1967**, 29, 1931-36.
53. Wolf, W.R., Sievers, R.E., Brown, G.H. *Inorg. Chem.* **1972**, 11, 199.
54. Girolami, G.S., Jeffries, P.M., Dubois, L.H. *J. Am. Chem. Soc.* **1993**, 115, 1015-24.
55. Sekine, R., Kawai, M. *Appl. Phys. Lett.* **1990**, 56 (15), 1466-68.
56. Welton, T., Prasad, J., Kelber, J.A., Lujan, R.D., Fleming, J., Blewer, R.S. in *Advanced Metallization for ULSI Applications*, Rana, V.V.S., Joshi, R.V., Ohdomari, I. (eds.), Materials Research Society, Pittsburgh, PA, 1992, 383-88.
57. Shin, H.K., Chi, K.M., Jain, A., Hampden-Smith, M.J., Kodas, T.T., Paffett, M., Farr, J.D. in *Advanced Metallization for ULSI Applications*, Rana, V.V.S., Joshi, R.V., Ohdomari, I. (eds.), Materials Research Society, Pittsburgh, PA, 1992, 403-11.
58. Kim, D.-H., Wentorf, R.H., Gill, W.N. in *Advanced Metallization and Processing for Semiconductor Devices and Circuits - II*, Katz, A., Murarka, S., Nissim, Y.I., Harper, J.M.E. (eds.), Materials Research Society, Pittsburgh, PA, 1992, San Francisco Spring Meeting, 1992, 107-112.
59. Jain, A., Chi, K.-M., Kodas, T.T., Hampden-Smith, M.J., Farr, J.D., Paffett, M.F. *Chem. Mater.* **1991**, 3, 995-97.
60. Pilkington, R.D., Jones, P.A., Ahmed, W., Tomlinson, R.D., Hill, A.E., Smith, J.J., Nutall, R. *J. de Physique IV* **1991**, Coll. C2, 1, 263-270.
61. Zheng, B., Eisenbraun, E.T., Liu, J., Kaloyeros, *Appl. Phys. Lett.* **1992**, 61, 2175.
62. Wang, J., Little, R., Griffin, G.L. unpublished results.
63. Hazuki, Y., Yano, H., Horioka, K., Hayasaka, N., Okano, H. in *Tungsten and Other Advanced Metals for VLSI/ULSI Applications V*, Wong, S.S., Furukawa, S. (eds.), Materials Research Society, Pittsburgh, PA, 1990, 351-57.
64. Armitage, D.N., Dunhill, N.I., West, R.H., Williams, J.O. *J. Crystal Growth* **1991**, 108, 683-87.
65. Lecohier, B., Philippoz, J.-M., van den Bergh, H. *J. Vac. Sci. Technol.* **1992**, B 10 (1) 262-67.
66. van den Brekel, C.H.J., Characterization of Chemical Vapour-Deposition Processes. Part I, *Philips Res. Reports* 32, 118-133, 1977.

67. Arita, Y., Awaya, N., Ohno, K., Sato, M. *IEDM Technical Digest* **1990**, 90-39, p. 3.1.1.
68. Oveson, C.V., Stoltze, P., Norskov, J.K., Campbell, C.T. *J. Catal.* **1992**, *134*, 445-68.
69. Farkas, J., Chi, K.M., Hampden-Smith, M.J., Kodas, T.T., Dubois, L.H. *Mater. Sci. Eng.* **1993**, *B 17* 93-96.
70. Kumar, R., Fronczek, F.R., Maverick, A.W., Lai, W.G., Griffin, G.L. *Chem. Mater.* **1992**, *4* (3), 577-82.
71. Jensen, K.F. in *Microelectronics Processing: Chemical Engineering Aspects*, Hess, D.W., Jensen, K.F. (eds.), ACS Advances in Chemistry Series No. 221, Washington, DC, American Chemical Society, 1989, p 199.
72. Hess, D.W., Jensen, K.F., Anderson, T.J. *Rev. in Chemical Eng.* **1985**, *3*, 97-186.
73. Kleijn, C.R. *Thin Solid Films* **1991**, *206*, 47-53.
74. Danckwerts, P.V. *Chem. Eng. Sci.* **1953**, *2*, 1.
75. Li, H., Eisenbraun, E.T., Kaloyeros, A.E. *J. Vac. Sci. Technol. B*, **1992**, *10*(4), 1337-40.
76. Pelletier, J., Pantel, R., Oberlin, J.C., Pauleau, Y. *J. Appl. Phys.* **1991**, *70* (7), 3862-68.
77. Wisniewski, B., Durand, J., Cot, L. *J. de Phys. IV* **1991**, *Coll.. C2, 1*, 389-95.
78. Osgood, R.M., Gilgen, H.H. *Ann. Rev. Mater. Sci.* **1985**, *15*, 549-76.
79. Herman, I.P. in *Laser Chemical Processing for Microelectronics*, Ibbs, K.G., Osgood, R.M. (eds.), Cambridge Univ., Cambridge, 1989, 61-108.
80. Houle, F.A., Baum, T.H., Moylan, C.R. in *Laser Chemical Processing for Microelectronics*, Ibbs, K.G., Osgood, R.M. (eds.), Cambridge University, Cambridge, 1989, 25-60.
81. Markwalder, B., Widmer, M., Braichotte, D., van den Bergh, H. *J. Appl. Phys.* **1989**, *65* (6) 2470-74.
82. Marinero, E.E., Jones, C.R. *J. Chem. Phys.* **1985**, *82*, 1608-09.
83. Kodas, T.T., Comita, P.B. *Accts. Chem. Res.* **1990**, *23*(6), 188-94.

Chapter 5

Chemical Vapor Deposition of Copper from Cu(I) Compounds

**Mark J. Hampden-Smith^a
Toivo T. Kudas^b**

**Departments of Chemistry^a and Chemical Engineering^b
University of New Mexico
Albuquerque, NM 87131**

Abstract

The chemical vapor deposition of copper using Cu(I) compounds as precursors is addressed in this chapter. The synthesis, characterization, and physical and chemical properties of the Cu(I) precursors are described. The characteristics of Cu CVD are surveyed followed by a discussion of mechanisms. Two pathways for Cu CVD are identified: thermally-induced disproportionation and thermally-induced decomposition (including reaction with H₂). In general, high-purity, bulk-resistivity films have been prepared via the disproportionation of (β -diketonate)CuL, L = triorganophosphine, olefin or alkyne compounds or their reactions with hydrogen. Selective deposition is discussed in terms of factors affecting selectivity and mechanistic information available from surface science experiments. The final topic is copper etching in which recent advances in low-temperature etching at high rates are discussed because of their close relationship to copper CVD processes.

Contents

5.1	Introduction	242
5.2	Precursor Design	244
5.3	Synthesis and Characterization	249
5.4	Physical and Chemical Properties	251
5.4.1	Degree of Oligomerization	251
5.4.2	Vapor Pressures	254
5.5	Chemical Vapor Deposition	255
5.5.1	Reactor Types	255
5.5.2	Deposition Conditions	256
5.5.3	Physical Properties of Films	260
5.6	Reaction Stoichiometry, Kinetics, and Mechanisms	264
5.6.1	Reaction Pathways	264
5.6.1.1	Thermally-Induced Disproportionation	264
5.6.1.2	Thermally-Induced Decomposition	266
5.6.2	Reaction Kinetics	268
5.6.3	Surface Reaction Mechanisms	271
5.7	Selectivity	275
5.7.1	Factors Influencing Selectivity	275
5.7.2	Mechanism of Selectivity	281
5.7.3	Selective Deposition onto Patterned PTFE Substrates	286
5.8	Chemical Vapor Deposition of Copper Alloys	289
5.9	Etching	292
5.9.1	Comproportionation	293
5.9.2	Copper Oxide Formation and Removal	294
5.9.3	Formation of XCuL_2	295
5.10	Summary and Conclusions	295
	Acknowledgments.....	296
	References	296

5.1 Introduction

The semiconductor industry is undergoing rapid technological changes, especially in fabricating submicron integrated circuit (IC) devices. Continually shrinking device feature sizes and a need for increased chip surface area for interconnects has led to the use of multilevel interconnections which utilize the third dimension and promote greater flexibility for designing highly functional devices.¹⁻³ The search for better performance levels has led to consideration of low-resistivity materials such as copper (see Ch. 1). Motivations for using copper as metallization material and the associated problems of integration of copper into silicon-based devices are also discussed in Chapter 1.

In considering methods to deposit copper and other metals, *chemical* vapor deposition (CVD) processes have several advantages over *physical* vapor deposition (PVD) processes including the ability to achieve conformal coverage and the possibility of selective deposition (see Ch. 1).⁴ Currently, a challenging problem is to develop molecularly-tailored metal-organic copper compounds for CVD capable of depositing high-purity metal films at low temperatures and high deposition rates in both selective and blanket modes. It is also important to understand how differences in molecular composition and structure affect thermally-induced decomposition on different surfaces which can lead to selectivity.

An alternate method to selective deposition for forming patterned copper films is blanket deposition followed by etching. Although both dry- and wet-etching processes are common, dry-etching processes are more desirable because of their higher resolution, anisotropy, and reduced waste. For dry-etching of copper, the most critical problem is to develop a rapid, low-temperature, selective, anisotropic process.^{5,6} Some of these potential dry etching processes are closely related to copper CVD processes because they rely on the same types of volatile copper compounds. For this reason copper etching will also be discussed in this chapter.

Although CVD of metals offers many advantages, it has not been adopted as a method for *metal* deposition in the electronics industry (although CVD of Si, SiO₂ and other non-metals is well-accepted), except in the case of tungsten (see Ch. 3).^{7,8} This is partially due to the complexity of CVD processes and the availability of well-established alternative approaches such as PVD. Another reason is that CVD using organometallic compounds can lead to incorporation of impurities such as C or O which are detrimental to metal film properties. These impurities are generally derived from thermal decomposition of the organic ligands and may arise because many decomposition mechanisms rely on rearrangement of liberated organic radicals. For example, CVD of Al from Al(*i*-Bu)₃⁹⁻¹⁵ results in liberation of *i*-Bu radicals. Under optimum conditions (< 350 °C), these radicals can undergo β-hydride elimination to form H₂ and isobutylene leading to complete removal of the organic supporting ligands. However, the isobutyl

groups can also undergo mischievous methyl group migration ($>350\text{ }^{\circ}\text{C}$), which ultimately incorporates carbon into the aluminum film. To alleviate this problem, alternative precursors including Lewis base adducts of alane, $\text{AlH}_3\cdot\text{L}_n$, in which the only carbon-containing moiety is the readily dissociated Lewis base [e.g., $\text{L} = \text{N}(\text{CH}_3)_3$], are currently being evaluated as precursors for aluminum CVD.¹⁶⁻²⁰ These and other approaches to aluminum CVD are discussed in Chapter 2. Similar strategies used to obtain high-purity copper films are discussed in this chapter and in Chapter 4.

To avoid the problem of impurity incorporation, it is necessary to prepare metal-organic precursors designed to deposit copper without ligand decomposition. Alternatively, ligand decomposition must lead to formation of volatile products that are *not* incorporated in the growing film. This may allow deposition of copper films with lower impurity levels, lower resistivities, better film morphologies, and at lower temperatures than can be achieved currently. Furthermore, with suitable molecular design of the copper precursors, the mechanisms of selective deposition onto different substrates may be explored with a view to understanding and controlling selectivity. This chapter discusses this crucial step that must be accomplished before selective copper CVD processes are accepted for microelectronic applications.

Molecules designed as precursors for CVD of any metal should have the attributes of high volatility, thermal lability, and cleanly removed supporting ligands (see Ch. 9). In designing the coordination environment of copper molecules (i.e., the nature of the ligands attached to copper) for CVD precursors, a number of key points must be considered. Based on the concepts of hard/soft, acid/base theory,²¹ the Cu(I) center is likely to be significantly softer (more weakly acidic) than the Cu(II) center.²² As a result, Cu(I) is more likely to form strong bonds with soft ligands (large, easily polarizable, low electronegativity) such as those bases containing P, S, alkene, alkyne, alkyl, Br^- , and I^- functionalities, whereas Cu(II) is more likely to form strong bonds with hard ligands (small, polarizing, high electronegativity) including O, N, F^- , and Cl^- donor functionalities. The electron configuration of Cu(I) (d^{10}) is such that it has no d-orbital imposed preferred ligand geometry because the 3d sub-shell is full and so could be considered analogous to a monovalent main group element cation where ligand geometry is dictated by the occupancy and hybridization of s- and p-orbitals. The electron configuration of Cu(II) (d^9), on the other hand, is subject to Jahn-Teller distortion as a result of the d-orbital occupancy which exerts a *strong* influence on coordination number and geometry according to the nature of the ligands.^{21,23,24} These issues influence the choice of ligands used to support Cu(I) and Cu(II) molecules as CVD precursors.

Although one- and two-coordinate Cu(I) compounds are known,²⁵ three- and four-coordinate Cu(I) compounds are most common and as a result, oligomerization is possible when less than four donor atoms are present.²⁶ Therefore, in designing volatile Cu(I) molecules, steps to prevent aggregation, such as the use of bulky or multi-dentate

chelating ligands, should be taken. When designing reactivity, a dichotomy exists between creating a ligand environment that provides thermal lability in the temperature range 150 - 350 °C to achieve high deposition rates at these low temperatures but which minimizes the reactivity under ambient conditions to improve shelf-life or transport rates. As an example, a number of the early mechanistic studies of β -hydride elimination were carried out²⁷⁻⁴² using alkyl Cu(I) compounds according to Equation 5.1.



This thermal decomposition is rapid even at -25 °C. The barrier to thermal decomposition can be raised by increased substitution of the β -carbon atom (e.g., *t*-BuCH₂CuPPh₃). In contrast, cyclopentadienyl Cu(I) complexes are significantly more thermally stable as a result of the stronger (η^5 -C₅H₅)-Cu interaction and the steric protection of the metal center afforded by the cyclopentadienyl ligand.⁴³

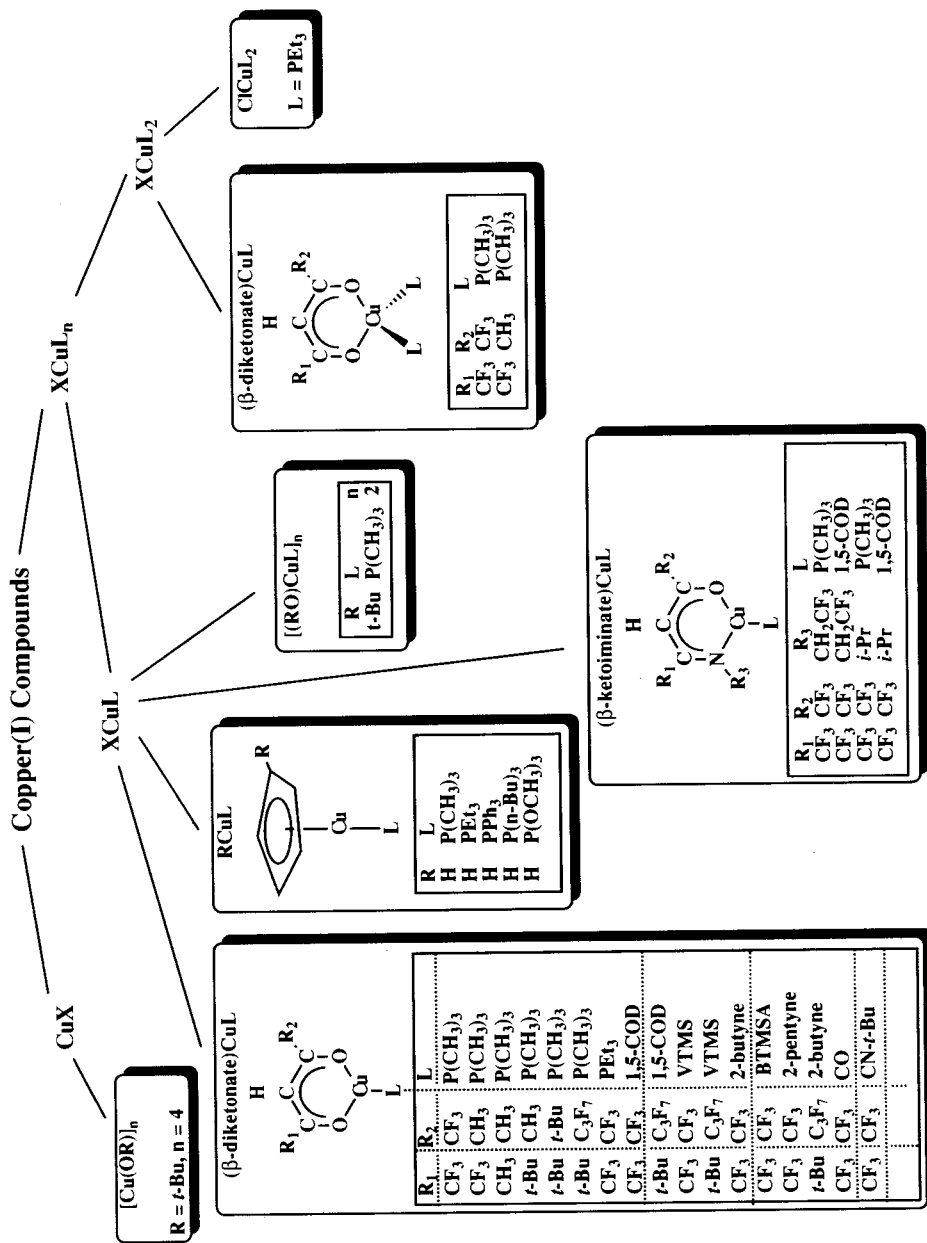
Later in this chapter we examine the relationships between precursor synthesis, precursor properties, and CVD characteristics for Cu(I) compounds. In order to establish these relationships, we will discuss precursor design, synthetic routes, precursor characterization and properties, as well as CVD and UHV studies; the focus will be on purity, morphology, resistivity, kinetics, mechanisms, and selectivity. A brief summary of methods for etching copper will also be discussed due to their intimate relationship to many copper CVD processes.

5.2 Precursor Design

In this section the Cu(I) species used for copper CVD are identified and the rationale for their selection is addressed. A variety of metal-organic precursors have been synthesized for copper CVD and include both Cu(II) and Cu(I) compounds. Copper(II) halides have low volatility and are generally unsuitable for Cu CVD.^{44,45} Compounds of Cu(β -diketonate)₂ have high volatility, deposit pure copper in the presence of hydrogen and have been extensively studied. Studies of copper CVD from Cu(II) compounds⁴⁶⁻⁵⁰ may be found in Chapter 4.

The Cu(I) compounds that have been investigated are described in Table 5-1. These species can be broadly divided into two classes, CuX and XCuL_n, where X is a uninegative ligand and L is a neutral Lewis base electron pair donor. The XCuL_n class can be further subdivided according to the nature of X and L. Many other compounds of these types have been prepared, but their use as precursors for Cu CVD has not been investigated.²⁶

Table 5-1 Copper(I) Precursors Used for CVD.



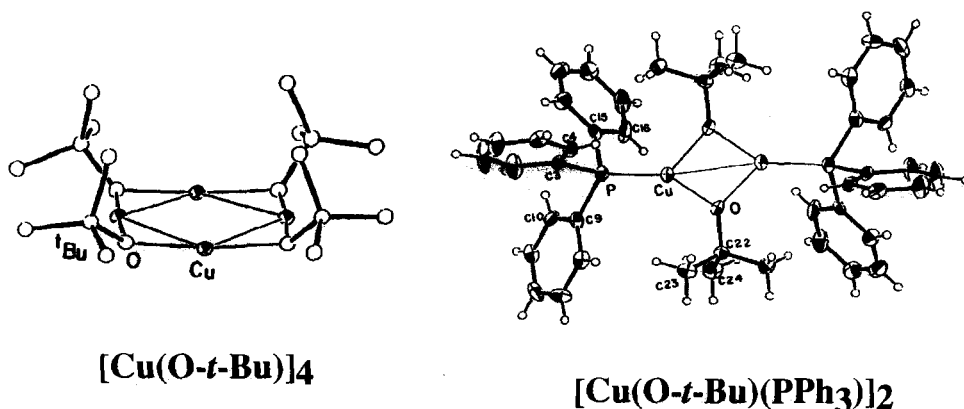


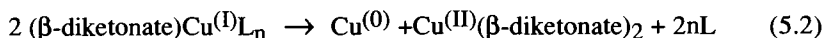
Figure 5-1 Solid-state x-ray diffraction data for $[\text{Cu}(\text{O}-t\text{-Bu})]_4$ and $[(t\text{-BuO})\text{Cu}(\text{PPh}_3)]_2$. (After ⁵³)

Compounds of general formula CuX (e.g., where $\text{X} = \text{O}-t\text{-Bu}$) are likely to be oligomeric resulting in a relatively low vapor pressure.^{51,52} The presence of a neutral donor ligand, L , is likely to reduce the extent of oligomerization compared to CuX by occupying vacant coordination sites. This is the case for $[\text{Cu}(\text{O}-t\text{-Bu})]$ which is tetrameric in the solid-state,⁵² whereas $[(t\text{-BuO})\text{CuPPh}_3]$ is dimeric in the solid-state (see Fig. 5-1).⁵³ Metal alkoxide compounds are expected to undergo thermal decomposition by cleavage of either $\text{M}-\text{O}$ or $\text{O}-\text{C}$ bonds. The homolysis of $\text{O}-\text{C}$ bonds is clearly detrimental to the deposition of metal films.⁵⁴

Organo-copper(I) compounds, RCuL , where $\text{R} = \text{alkyl}$, are thermally unstable, but cyclopentadienyl compounds are likely to be more robust due to the η^5 -bonding of the cyclopentadienyl ligand to the copper center.⁴³ At the same time, the cyclopentadienyl ligand is sterically demanding, occupies three coordination sites at the metal center, and thereby reduces the desire for oligomerization.²⁴ In general, a cyclopentadienyl ligand is a poor choice to support CVD precursors, especially with electropositive metals, because this ligand is unlikely to be labile. However, with late transition metals, clean removal of the cyclopentadienyl ligands may be possible (even in the *absence* of a reducing gas, e.g., H_2).^{55,56} The use of metal-organic cyclopentadienyl derivatives as CVD precursors is addressed more fully in Chapter 8.

Compounds in the family XCuL_2 where X = a halide such as Cl , and L = a triorganophosphine, exhibit relatively high volatility but are thermally stable with respect to formation of copper at low temperatures. These species are therefore suitable as products of etching reactions of copper films (see Section 5.8).

A number of researchers have demonstrated the potential of a series of β -diketonate Cu(I) compounds, $(\beta\text{-diketonate})\text{CuL}_n$, where L = Lewis base, $n = 1$ or 2 , that fulfill most of the criteria outlined for precursor design above.⁵⁷⁻⁶⁷ These species were chosen as copper precursors for the following reasons: (i) They contain the β -diketonate ligand which generally imparts volatility to metal-organic complexes, particularly when fluorinated, as a result of a reduction in hydrogen-bonding in the solid-state. (ii) They are capable of systematic substitution through both the β -diketonate and Lewis base ligands to tailor volatility and reactivity. (iii) Lewis bases such as phosphines, olefins, and alkynes are unlikely to thermally decompose at temperatures where copper deposition occurs. (iv) These precursors can deposit copper via thermally induced disproportionation reactions according to Equation 5.2.



No ligand decomposition is required since the volatile Lewis base and the Cu(II) disproportionation product are transported out of the reactor intact at the disproportionation temperature.^{57-59,66} The Cu(I) compounds are thermodynamically unstable but kinetically trapped. Based on thermodynamic calculations, the equilibrium of Equation 5.3 lies to the right by 10 kcal/mol.



Disproportionation reactions have also been observed for Fe deposition from $(\eta^5\text{-C}_5\text{H}_5)\text{Fe}_2(\text{CO})_4$ where $\text{Fe}(\eta^5\text{-C}_5\text{H}_5)_2$, iron and CO are observed as products⁵⁶ and for AlCl where Al and AlCl_3 are formed.⁶⁸ Disproportionation reactions also play an important role in some Ti CVD routes as discussed in Chapter 8. It is worth noting that cyclopentadienyl Cu(I) and $(\beta\text{-diketonate})\text{Cu(I)}$ compounds are unstable in the absence of a donor ligand, L .

These $(\beta\text{-diketonate})\text{CuL}$ species are capable of systematic substitution via variation of R^1 and R^2 and L and can exhibit relatively high vapor pressures through incorporation of fluorinated substituents. A number of variations on this theme are also possible. For example, one or more carbonyl functionalities can be replaced with isoelectronic imino groups ($=\text{NR}$) to create $(\beta\text{-ketoiminato})$ or $(\beta\text{-diiminato})\text{CuL}$ compounds. Although

this replacement results in an increase in molecular weight, the changes resulting from Cu-N bond lability, the steric and electronic influence of R^3 (see Table 5-1), and the possibility of improving volatility by fluorination of R^3 may be beneficial.

The choice of X and L in CuX and $XCuL$ compounds depends on the reaction pathway that is employed. In most cases it is desirable that the Cu-X bond is homolyzed resulting in reduction of Cu(I) to Cu(0) metal and formation of $X\cdot$. The $X\cdot$ radical liberated can either rearrange {as in the case of O-*t*-Bu \cdot for $[(t\text{-BuO})CuP(CH_3)_3]_2$, see later⁵¹} or react with another radical (e.g., $X\cdot$ or $H\cdot$, see later) to form a neutral, generally less reactive species that can be removed from the deposition system. These ligand reactions are pivotal in determining the purity of the final copper film.

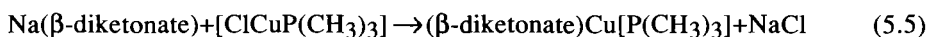
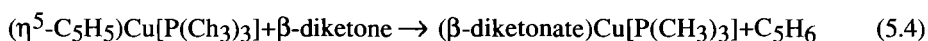
The choice of the neutral donor ligand L is also important in determining the deposition characteristics of Cu(I) compounds as will be demonstrated later. Generally, L must be liberated from the copper coordination sphere intact and removed from the deposition system, and thus should remain thermally stable at the deposition temperature. Many choices for L are available. An example is a triorganophosphine, $L = PR_3$. An attribute of these organophosphine ligands is that during deposition they may act as reducing agents in situ to remove adventitious oxide and form volatile phosphine oxides (OPR_3 , see Eq. 5.8).⁶⁹ However, this aspect has not been investigated in detail. There has been some discussion that organophosphine ligands might poison a metal or metal oxide surface during CVD.⁷⁰ It has been suggested that irreproducibility in the deposition of copper from $(\eta^5\text{-C}_5\text{H}_5)Cu(PEt_3)$ may have arisen as a result of surface poisoning which may be attributed to the liberated organophosphine ligand. Data substantiating this point are unavailable.⁷⁰ However, since phosphorus can dope silicon devices, its liberation as an impurity in copper deposition could be a limitation unless the devices are shielded by appropriate barrier layers (see Ch. 1). The influence of X and L on copper CVD in specific cases will be addressed later.

There is strong motivation to understand the basic relationships between precursor properties and deposition parameters such as CVD reactor operating conditions and film properties to achieve better control over CVD processes. If precursor characteristics could be related to volatility, selectivity, deposition rates, purity, and reactor operating conditions, precursors could be designed on a more rational basis to allow selective deposition on particular surfaces or to produce pure films with bulk properties. Specifically, if this relationship could be determined for Cu precursors, control of Cu CVD characteristics could be demonstrated. Since a large number of Cu(I) precursors are possible depending on the choice of the uninegative ligand (alkyl, alkoxy, β -diketonate, β -ketoiminate, β -diiminate, etc.) and the neutral ligand (phosphine, olefin, alkyne, nitrile, carbonyl, etc.), it should be possible to use copper CVD as a model system to understand the relationships between precursor properties and deposition characteristics. This approach is discussed in more detail in Sections 5.4 to 5.6.

5.3 Synthesis and Characterization

Copper(I) compounds are generally prepared by metathesis reactions with Cu(I) halides, by reduction of Cu(II) compounds, or by reaction of organic acids with Cu(I) oxide. Some examples of these reactions are given in the equations below. The reader is referred to the appropriate citation for experimental details of the synthesis of the following and other copper(I) compounds.

The compounds (β -diketonate)Cu(L), where β -diketonate = hfac, tfac, acac, dpm, and dbm, and L = triorganophosphine, olefin, and alkyne can be prepared by both the metallation reaction (Eq. 5.4) and metathesis reactions (Eqs. 5.5 and 5.6).⁷¹⁻⁷⁵



These reactions generally give the desired products in high yield. In salt elimination (or metathesis) reactions, no complications associated with difficulty in separation of sodium chloride from the final product are encountered, and formation of involatile Cu(I) salts [i.e., "-ate" complexes such as $\text{Na}^+ [(\beta\text{-diketonate})_2\text{CuL}]^-$] is not observed. In the case of (β -diketonate)CuL, separation of the salt is further aided by the high volatility of these species and their essentially quantitative sublimation in all cases except (acac)Cu[P(CH₃)₃] and (dbm)Cu[P(CH₃)₃]. A number of analogous β -diketonate Cu(I) compounds have been prepared previously [e.g., (tfac)Cu(PPh₃)₂]⁷⁶ and (hfac)Cu(CO)]⁷⁷ but with different numbers or types of Lewis base substituents.

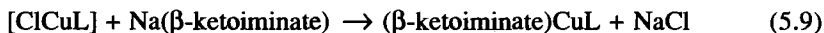
The reaction of β -diketones with Cu(I) oxide in the presence of a Lewis base results in formation of the corresponding (β -diketonate)CuL species (Eq. 5.7).⁷⁷



However, it is difficult to control the stoichiometry of the product and when one equivalent of L is used, substantial amounts of Cu(hfac)₂ are produced.⁷⁸⁻⁸⁰ In some cases more than one copper moiety can coordinate to a single Lewis base. Species that have been prepared by this method and used for Cu CVD include [(hfac)Cu]₂(COT), COT = cyclooctatetraene.⁸¹ The reduction of CuO with an organophosphine in the presence of a β -diketone also results in formation of (β -diketonate)CuL (see Eq. 5.8).⁸²⁻⁸⁵



The β -ketoiminate ligands have been prepared by methods analogous to those reported in the literature for Cu(II) compounds,⁷⁸ and the compounds $(\beta\text{-ketoiminate})\text{CuL}$ have been prepared according to the reaction of Equation 5.9.⁸⁶

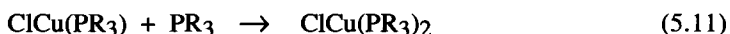


The compounds $(\eta^5\text{-C}_5\text{H}_5)\text{CuL}$ and $(\text{RO})\text{CuL}$ have been prepared by the salt elimination reaction of Equation 5.10 where $\text{MX} = \text{Ti}(\eta^5\text{-C}_5\text{H}_5)$ or NaOR , $\text{L} = \text{PR}_3$, alkyne, CNR.^{43,53,69}

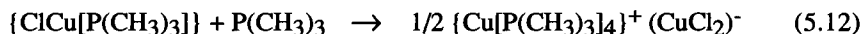


Copper(I) alkoxides are generally prepared by the reaction between Cu(I) chloride and an alkali metal alkoxide. A number of mixed ligand Cu(I) alkoxides have been prepared {e.g., $\text{Cu}(\text{O}-t\text{-Bu})_{0.4}[\text{OC}(\text{CH}_3)_2(\text{CF}_3)_{0.6}]$ } as copper CVD precursors, but detailed synthesis and characterization data were not reported.⁸⁷ The species $[\text{Cu}(\text{OR})]_n$ and $[(\text{RO})\text{CuL}]$ are generally white solids while the species $(\beta\text{-diketonate})\text{CuL}$ are generally pale yellow, volatile solids or liquids at room temperature.

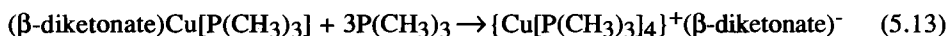
The compounds $\text{ClCu}(\text{PR}_3)_n$ where $(n = 1 \text{ or } 2)$ are generally prepared by reaction of the free triorganophosphine, PR_3 , with $\text{ClCu}(\text{PR}_3)$ according to Equation 5.11.



This generally results in deoligomerization of these starting materials (generally tetramers) to form lower molecular weight species. However, when $\text{R} = \text{CH}_3$, quite different behavior has been observed. Addition of one equivalent of $\text{P}(\text{CH}_3)_3$ to $\{\text{ClCu}[\text{P}(\text{CH}_3)_3]\}$ results in a reaction which is described by Equation 5.12.⁸⁸ An involatile salt, $\{\text{Cu}[\text{P}(\text{CH}_3)_3]_4\}^+ [\text{CuCl}_2]^-$, is formed.



The salt formed when an excess of $\text{P}(\text{CH}_3)_3$ is added to $\beta\text{-diketonate-Cu}[\text{P}(\text{CH}_3)_3]_n$ compounds resulting in displacement of the $\beta\text{-diketonate}$ ligand from the Cu(I) coordination sphere is shown in Equation 5.13.



The small size of $\text{P}(\text{CH}_3)_3$ relative to other triorganophosphines is probably responsible for this anomalous behavior which should be taken into account when designing Cu(I) precursors with $\text{P}(\text{CH}_3)_3$ ligands. Other triorganophosphine ligands do not exhibit this behavior.⁸⁹

The reactions described above illustrate a challenge for synthetic chemists. High-yield syntheses of high-purity (electronic grade) materials are required. Existing routes often rely on the use of Na salts. Sodium, even in trace amounts, cannot be tolerated in integrated circuits (see Ch. 1). Thus, a challenge is to develop synthetic routes that do not involve elements that will degrade device properties.

5.4 Physical and Chemical Properties

5.4.1 Degree of Oligomerization

The volatility of a precursor determines in many cases whether or not it is suitable for CVD. A low-volatility precursor usually results in low deposition rates and difficulties in transporting the precursor into the reactor, making the precursor less useful for CVD, even if the compound deposits pure metal; the volatility is related to the degree of aggregation. Studies of the aggregation of the Cu(I) compounds identified in Table 5-1 have been carried out primarily in the solid-state and liquid phase. There is a paucity of structural data in the gas phase which would determine the degree of oligomerization and absolute gas-phase structure. This information is more relevant to Cu CVD than solid-state data of the same compounds. However, it is *unusual* that a molecular species has a *higher* degree of oligomerization in the gas phase than in solutions of non-polar, non-coordinating solvents (such as benzene or cyclohexane). Cryoscopic molecular weight information is therefore very valuable and the appropriate experiments have been carried out in some cases.

As described above, $[\text{Cu}(\text{O}-i\text{-Bu})]_4$ is tetrameric in the solid-state^{51,52} and in benzene solution, and compounds of the general formula $(\text{RO})\text{CuL}$ are generally dimeric.⁵³ Representative examples of the solid-state structures of these molecules are shown in Figure 5-1. As a result of their aggregation, both these classes of compounds exhibit rather low volatility compared to other monomeric Cu(I) and Cu(II) compounds.

The compounds $(\eta^5\text{-C}_5\text{H}_5)\text{CuL}$ have been structurally characterized and are monomeric in the solid-state as illustrated by a representative example shown in Fig 5-2.^{43,69} As a result, they exhibit reasonably high vapor pressures and provide high deposition rates.

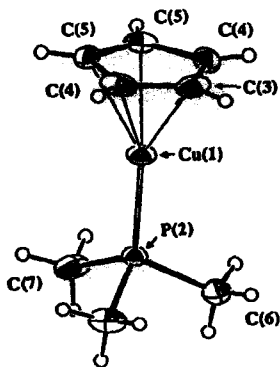


Figure 5-2 Solid-state x-ray diffraction data for $(\eta^5\text{-C}_5\text{H}_5)\text{Cu}[\text{P}(\text{CH}_3)_3]$. (After Ref. 69.)

Structural and spectroscopic characterization of $(\beta\text{-diketonate})\text{CuL}$ species have been carried out in the solid state, liquid phase, and gas phase. In general, these species are monomeric and provide sufficiently high vapor pressures to give adequate deposition rates. A brief discussion of representative examples is given here. The species $(\text{hfac})\text{Cu}[\text{P}(\text{CH}_3)_3]$ and $(\text{tfac})\text{Cu}[\text{P}(\text{CH}_3)_3]$ are monomeric in benzene solution as determined by cryoscopic molecular weight measurement.^{71,72} Single-crystal X-ray diffraction studies revealed that these species are also monomeric in the solid-state. They exhibit the general structural feature of approximately trigonal planar Cu(I) geometry where the β -diketonate ligands are coordinated to the copper center through two oxygen atoms and the remaining coordination site is occupied by the phosphorus atom of the trialkylphosphine ligand. The bis-phosphine derivatives $(\beta\text{-diketonate})\text{Cu}(\text{PR}_3)_2$ are monomeric in the solid-state and probably exhibit a tetrahedral Cu(I) coordination geometry as found for two representative examples.^{76,77,89} The compounds $(\beta\text{-diketonate})\text{Cu}(1,5\text{-COD})$ ^{73,77} are also monomeric. In the solid-state, $(\text{hfac})\text{Cu}(1,5\text{-COD})$ exhibits a "3+1" coordination environment in which the copper center is bonded to the two oxygen atoms of hfac, but is asymmetrically bonded to 1,5-cyclooctadiene.⁷³ This asymmetry is very marked with the two Cu-olefin centroid distances being 1.935 Å and 2.418 Å, respectively. Based on the dynamic behavior observed in solution, it is possible that the 1,5-COD ligand is monodentate in the gas phase. The structure of $(\text{hfac})\text{Cu}(\text{VTMS})$ was recently reported which also exhibited a monomeric structure in the solid-state.⁹⁰

The Cu(I) alkyne complexes, $(\beta\text{-diketonate})\text{Cu}(\text{alkyne})$ may be monomeric or oligomeric in the solid-state due to the ability of the alkyne to act as a two- or four-electron donor.⁷⁷ A number of examples have been structurally characterized, i.e.,

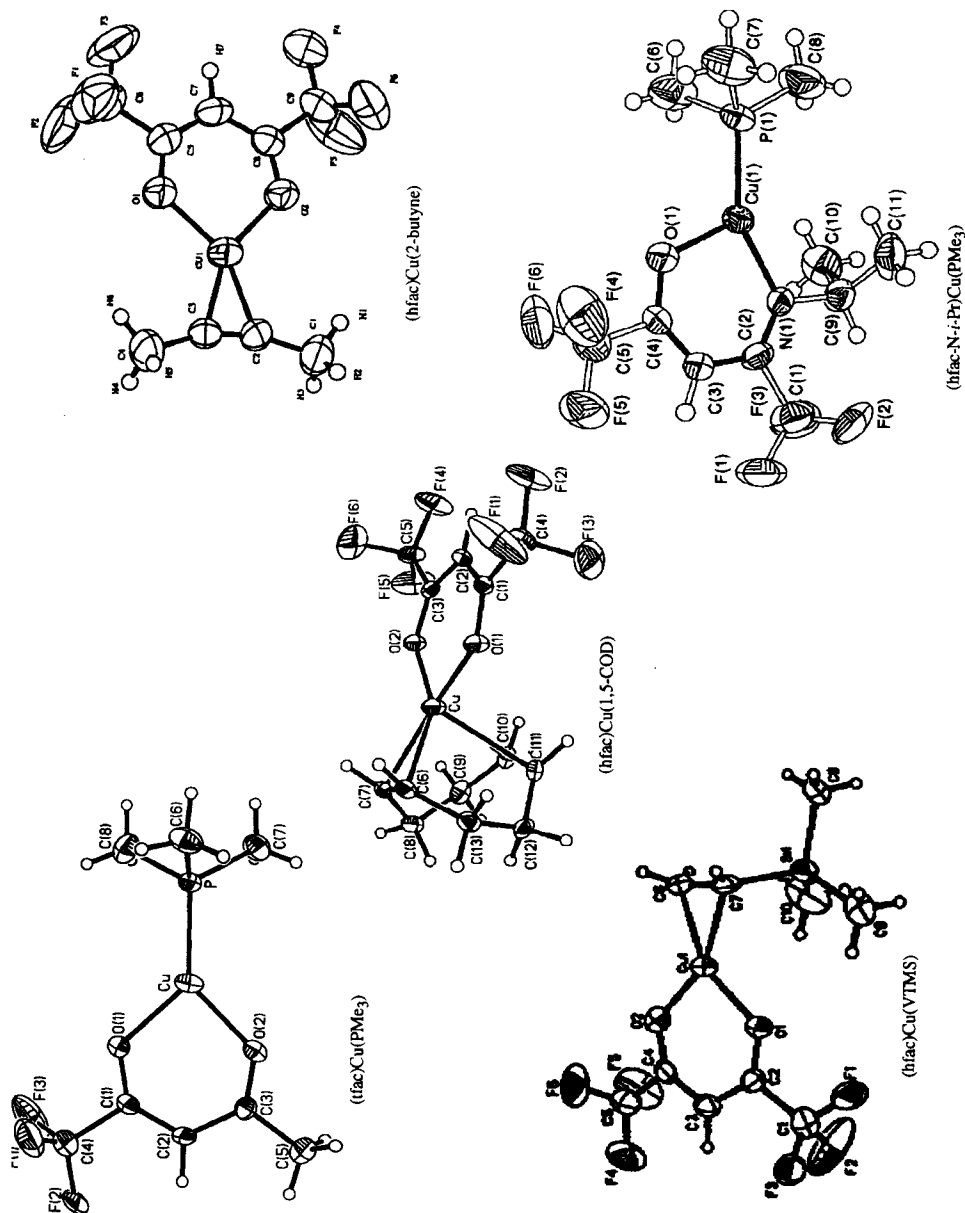


Figure 5-3 Solid-state x-ray diffraction data for copper(I) β -diketonate and β -ketoiminate precursors: (tfac)Cu[P(CH₃)₃], (hfac)Cu(1,5-COD), (hfac)Cu(VTMS), (hfac)Cu(2-butyne), (β -ketoiminate)Cu[P(CH₃)₃]. (After Refs. 71, 73, 74, 86, 90.)

(hfac)CuL, where L = diphenylacetylene,⁷⁴ 2-butyne,⁶⁷ and bis(trimethylsilylacetylene) which are all monomeric in the solid-state.⁹¹ However, under appropriate conditions, dinuclear species have been prepared, e.g., [(hfac)Cu]₂(alkyne),⁹¹ and this is a common feature of the four-electron donor ability⁹² of alkyne ligands.

The (β-ketoiminate)CuL complexes also appear to be monomeric in the solid-state as judged from one example which has been structurally characterized (see Fig 5-3).⁸⁶ These species are interesting when compared to the β-diketonate analogs because the imino nitrogen provides an additional position where reactivity can be tailored. Schematic diagrams showing representative examples of different structural types are presented in Figure 5-3.

The (hfac)CuL species are sufficiently volatile that they can be sublimed in vacuo between room temperature and 60 °C. Their volatility is such that a number of derivatives have been characterized in the gas phase by infrared spectroscopy.⁷² The gas phase IR data are valuable for comparison to IR spectra of these molecules adsorbed on various surfaces under ultra-high vacuum (UHV) conditions (see Section 5.7). Other Cu(I) species described here appear to exhibit lower volatility although quantitative data are sparse.

In solutions of non-polar solvents, (β-diketonate)CuL species undergo various ligand exchange reactions that involve either the Lewis base ligands, the β-diketonate ligands, or both. This dynamic behavior is noteworthy in the present context because it may be relevant to the thermal stability and disproportionation of these compounds.^{71-74,67,88} A comparison of activation parameters for ligand exchange in solution and CVD of copper may provide valuable mechanistic insight into CVD processes by aiding identification of the rate-determining step(s).

5.4.2 Vapor Pressures

The vapor pressures of (hfac)Cu[P(CH₃)₃]⁷² (hfac)Cu(1,5-COD),⁶⁰ and (hfac)Cu(VTMS)⁶² have been measured as a function of temperature and are plotted together with the data for Cu(hfac)₂ for comparison in Fig 5-4. Compared to Cu(hfac)₂ (e.g., 250 mtorr at 60 °C),⁹³ (hfac)Cu[P(CH₃)₃] (100 mtorr at 60 °C),⁷² and (hfac)Cu(1,5-COD) (56 mtorr at 62 °C)⁶⁰ exhibit slightly lower vapor pressures. Some discrepancy in the vapor pressure data exists for (hfac)Cu(VTMS) since vapor pressure measurements were reported at temperatures where thermal decomposition also occurs.⁶² The compound (hfac)Cu[P(CH₃)₃] exhibits excellent thermal stability and is stable at elevated temperatures (80 °C for 4 days).⁷² Vapor pressure data for Cu(II) precursors are given in Chapter 4.

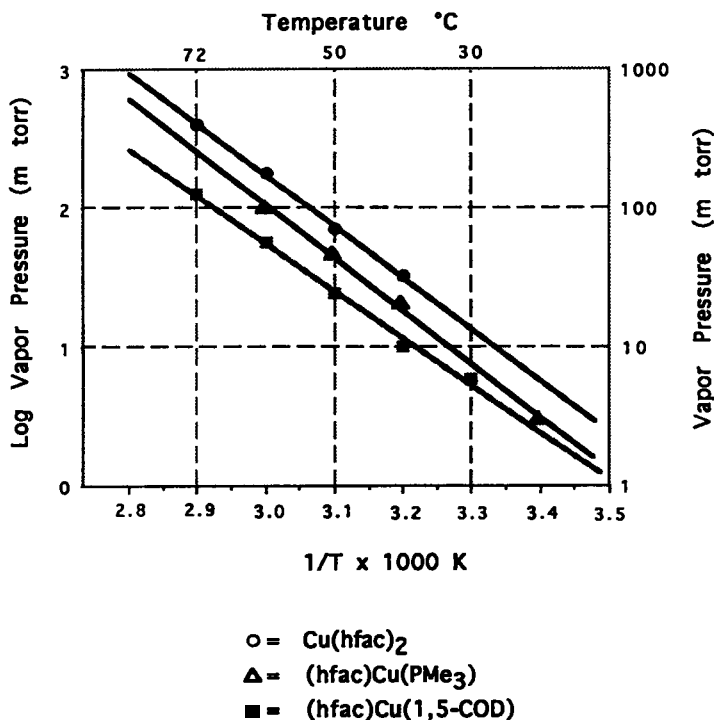


Figure 5-4 Vapor pressures of (hfac)Cu[P(CH₃)₃]₃, (hfac)Cu(1,5-COD), and Cu(hfac)₂. (After Refs. 60, 72.)

5.5 Chemical Vapor Deposition

5.5.1 Reactor Types

Chemical vapor deposition experiments using the precursors described above have been carried out in many types of reactors. These reactors can be categorized into several classes: hot-wall, cold-wall, and plasma-enhanced CVD (PECVD). More detailed descriptions of these systems can be found in Chapters 1 and 9 and the references contained therein. Most of the work with Cu(I) precursors has been carried out in hot-wall and cold-wall reactors as shown by Table 5-2. Little work has been done with PECVD reactors using these precursors. In contrast, more work has been done with PECVD using Cu(II) precursors⁹⁴ and is discussed in Chapter 4.

Each type of reactor has its own advantages and disadvantages which have been exploited for CVD of Cu(I) precursors. Hot-wall reactors have been used because they are simple and can be operated under conditions of relatively high precursor conversion which allows the volatile byproducts to be recovered and analyzed by spectroscopic and analytical techniques.^{4,58} The disadvantage of this type of reactor for copper CVD from Cu(I) and Cu(II) precursors is that deposition can also occur on the walls of the reactor leading to high precursor conversion. For this case, the deposition reaction can be transport- or feed-rate limited, which leads to deposition rates that are relatively low and which often do not reflect the kinetics of the surface reactions.⁴ This is a problem that becomes more severe as the substrate size is increased and a higher precursor supply rate is needed to achieve a given deposition rate. Another problem occurs when studying selective deposition. Deposition may or may not occur on the walls of the reactor depending on the nature of the precursor and the composition of the walls. For example, (hfac)Cu[P(CH₃)₃]₃ deposits selectively on many surfaces in the presence of SiO₂. When the reactor is made of SiO₂, no deposition occurs on the walls.⁵⁷ However, if the reactor is made of other materials or copper deposition is already present from earlier experiments, the precursor may react on the walls. This can lead to difficulty in reproducing results unless great care is taken to clean the reactor after each run.

Cold-wall (or warm-wall) reactors have been used in many cases. The major motivations for their use are higher deposition rates can be obtained, no reaction occurs on the reactor walls, and precursor conversion can be low. For this case, the reactor can approximate a differential reactor^{59,63,66} where reaction product partial pressures are nearly zero and the precursor partial pressure is known and is constant. The rate data obtained from cold-wall CVD reactors operated under these conditions, in the absence of mass transport limitations, reflect the rate of the surface reaction and a plot of log rate versus T^{-1} reveals the activation parameters.^{59,63,66} However, the use of a cold-wall reactor does not guarantee differential reactor operation. A necessary but not sufficient criterion for differential reactor operation is that the feed rate must be higher than the rate at which the precursor may be consumed for a given set of conditions. Feed-rate-limited conditions are manifest by a decrease in the slope of the plot of log rate vs. T^{-1} as the substrate temperature is raised similar to that obtained for transport-limited deposition.^{59,63,66} The disadvantage of this differential mode operation arises from the low extent of reaction of the precursor and the difficulty in identifying reaction products among the unreacted precursor. However, the latter aspect is not important in an industrial setting. Care must also be taken to provide a heated path for the precursor from the source to the substrate to avoid loss of precursor by condensation.

5.5.2 Deposition Conditions

Chemical vapor deposition of Cu(I) compounds has been carried out in various types of reactors under a variety of conditions. The precursors that have been studied most

extensively are (hfac)Cu(VTMS), (hfac)Cu(2-butyne), (hfac)Cu(1,5-COD), (hfac)Cu(PR₃), and (η^5 -C₅H₅)Cu(PR₃). The results are summarized in Table 5-2.

In general, Cu(I) precursors have been used to deposit high-purity copper at rates up to 1 $\mu\text{m}/\text{min}$ ⁶⁶ with typical numbers on the order of 100 nm/min. The highest deposition rates have been reported for (hfac)Cu(2-butyne),⁶⁶ a variety of other (hfac)Cu(alkyne) complexes,¹⁰⁴ (hfac)Cu(1,5-COD), (hfac)Cu(VTMS), and (η^5 -C₅H₅)Cu(PR₃). These high rates were reported in cold-wall reactors where reactant depletion due to reaction on the reactor walls did not occur. Lower deposition rates may be obtained in larger systems where precursor feed-rate limitations become important. These rates were all obtained with precursor source temperatures of 30-100 °C.

Deposition temperatures are generally in the range of 150-400 °C. These temperatures are low enough for deposition onto thermally sensitive polymer substrates such as polyimide¹⁰⁴ and PTFE (see Section 7.3).⁹⁵⁻⁹⁷ To study selectivity, deposition has been investigated for a wide variety of substrates including Si, SiO₂, W, Pt, Al, TiN, Ta, Ag, Au, Cr, TiSi₂, PtSi, PTFE, and polyimide, some in more detail than others. Selective deposition is discussed in Section 5.7.

A major consideration for ease of handling is whether or not a precursor is a liquid. To date, (hfac)Cu(VTMS) is the only liquid-phase precursor at room temperature; it also has one of the highest vapor pressures.⁶² Most other precursors are solids at temperatures used for deposition; however, they can be heated to their melting points (50-100 °C) to form liquids and provide sufficient vapor pressures for deposition at high rates. For example, the highest deposition rates ($\sim 1\mu\text{m}/\text{min}$) reported have been for (hfac)Cu(2-butyne) which is a solid at room temperature but a liquid under typical delivery conditions.

Carrier gases including CO, H₂, N₂, and He have been used. The CO and H₂ can, however, also be considered reactants as they modify the reaction pathways. Carbon monoxide decreases the temperature required for transport of (hfac)Cu(1,5-COD) and lowers the deposition temperature.⁹⁸ Hydrogen modifies the reaction pathway of (β -diketonate)CuL compounds by circumventing the disproportionation reaction to yield Cu, L, and β -diketone as the products.^{61,81} Nitrogen and He have been used primarily for ease of introducing the precursor into the reactor chamber.

The structure of Cu(I) precursors has a strong influence on the minimum deposition temperatures. For (β -diketonate)CuL compounds, in the absence of a carrier gas for example, the minimum deposition temperature varies as a function of both the β -diketonate and Lewis base ligands.⁵⁸ The minimum temperature at which deposition is observed decreases in the order hfac > tfac > acac for a series of compounds with identical Lewis base ligands such as (β -diketonate)Cu[P(CH₃)₃] (see Table 5-2). As the extent of fluorination of the β -diketonate ligand decreases, the strength of the metal β -diketonate bond is expected to decrease. Similarly, the nature of the neutral ligand has a very strong effect on the minimum deposition temperatures (see Table 5-2). The minimum

Table 5-2 Deposition Characteristics for Cu^(I) Compounds.

Process	Precursors	Substrate	T _{Precursor} °C	T _{Substrate} °C	Carrier Gas	Pressure mtorr	Rate Å/min.	Ref.
Hot Wall	(hfac)CuL, L=P(CH ₃) ₃ , PEt ₃ , 1,5-COD, BTMSA, TMSP, 2-butyn	Pt, Cu, W/SiO ₂	45	100-400	none	50	20-200	58
Hot Wall	(hfac)Cu[P(CH ₃) ₃]	Pt/SiO ₂	45-50	150-400	none	1	10-1000	57
Hot Wall	(hfac)Cu[P(CH ₃) ₃]	PTFE	50	200	none	---	---	95-97
Cold Wall	(hfac)Cu[P(CH ₃) ₃]	W/SiO ₂	60	180-210	none	50	400-2000	64
Cold Wall	(hfac)Cu(1,5-COD)	W/SiO ₂ , Pt/SiO ₂ , SiO ₂	70-90	120-250	none	10-50	380-3750	59
Cold Wall	(hfac)Cu(1,5-COD)	Borosilicate glass	35	170-200	CO, H ₂	---	100	98
Cold Wall	(hfac)Cu(1,5-COD); (hfacCu) ₂ (COT); (hfac)Cu(1,3-butadiene); (η ⁵ -C ₅ H ₅)Cu(PR ₃) where R = Et, OCH ₃ , OEt	Si, glass	70-105	200	H ₂	760 × 10 ³	100	98
Cold Wall	(hfac)Cu(1,5-COD)	Ta, Cu, Ag, Au, Cr, SiO ₂ , Si ₃ W ₄ glass, Si	62	150-250	He	70	100-500	60
Hot Wall	(hfac)Cu(1,5-COD) (hfac)Cu(CO)		25-70	200	H ₂	760 × 10 ³	200	98
Cold Wall	(hfac)Cu(2-butyn)	W/SiO ₂	65	150-210	none	50	500-9000	66
Warm Wall	(hfac)Cu(2-butyn)	Cu/Si	60	150-225	He	300	2033	67
Cold Wall	(hfac)Cu(Alkyn)	Cu	60	225	He	300	2033 1751 784 2741 784	104
	2-butyn							
	2-pentyn							
	4,4-dimethyl-2-pentyn							
	2-hexyn							
	4-methyl-2-hexyn							

	3-hexyne 2-heptyne 3-heptyne 6-methyl-3-heptyne 4-octyne TMS-acetylene TMS-propyne bis-TMS-acetylene TF-TMS-propyne							4221 1829 5752 835 1311 2994 1946 351 1282	
Hot Wall	(<i>hfac</i>)Cu(VTMS)	TiN, Si, Cu, SiO ₂	50	160	Ar	---	500	99	
Cold Wall	(<i>hfac</i>)Cu(VTMS)	W, TiN, Ta, Al, PtSi	40-50	120-420	Ar	100	1000	62	
Cold Wall	(<i>hfac</i>)Cu(VTMS)	W/SiO ₂	25	160-190	none	500	2000-5000	63	
Cold Wall	(η^5 -C ₅ H ₅)CuL L=P(CH ₃) ₃ , PEt ₃ , PBu ₃	SiO ₂	70	150-220	none	---	150-2200	100	
Laser- Induced	(C ₅ H ₅)Cu(PMe ₃)	Cr/Cu SiO ₂ /Si polyimide	70	200-300	none	50	2.4×10 ⁴ – 6×10 ⁴	101	
Hot Wall	(η^5 -C ₅ H ₅)Cu[P(CH ₃) ₃] (<i>t</i> -BuO)Cu[P(CH ₃) ₃]	Pt/SiO ₂	40-60 60	260-450 400	none	1 1	6-100	69	
Cold Wall	(η^5 -C ₅ H ₅)Cu(CN- <i>t</i> -Bu) [Cu(O- <i>t</i> -Bu)] ₄	Al, TiN	50	150-450	N ₂	1	---	102	
Hot Wall		glass, Si, KBr, quartz, Al, graphite	100	400	none	10 ⁻²	---	51	
TGA	Cu(O- <i>t</i> -Bu)(OR _F) [R _F = C(CF ₃) ₃ OCH(CF ₃) ₂ , OC(CH ₃) ₂ (CF ₃) Cu(CO)(O- <i>t</i> -Bu) [Cu(OSiPh ₃) ₄ {Cu(OSiPh ₃)[P(CH ₃) ₂ Ph]} ₂	---	---	---	---	---	---	87	
---			---	---	---	---	---	103	

temperature at which deposition occurs for a series of compounds in which only the Lewis base is varied is in the order of $L = P(CH_3)_3 > 1,5\text{-COD} \sim \text{VTMS} \sim 2\text{-butyne}$ for (hfac)CuL compounds.^{58-60,62-64,66,67}

The minimum deposition temperature for other classes of Cu(I) precursors is similar or higher. The compound $(\eta^5\text{-C}_5\text{H}_5)\text{CuL}$ allows deposition at temperatures as low as 150 °C.¹⁰⁰ In these cases, disproportionation does not occur and ligand decomposition is required for film deposition. The minimum reaction temperature for $(\eta^5\text{-C}_5\text{H}_5)\text{CuL}$ depends on the neutral ligand L in the order $L = P(C_6H_5)_3$ (130 °C), $P(C_4H_9)_3$ (100-120 °C), PEt_3 (100-120 °C), $P[O(CH_3)]_3$ (25 °C), $CN(CH_3)$ (25 °C), and CO (-20 °C).¹⁰⁰ This order of stability correlates well with the σ -donor abilities of the two-electron-donor ligand. In all cases, it was proposed that dissociation of the ligand was rate limiting followed by reaction of " $(\eta^5\text{-C}_5\text{H}_5)\text{Cu}$ ".

Deposition temperatures for $(RO)\text{CuL}$ ⁶⁹ and $[(RO)\text{Cu}]_4$ ⁵¹ precursors are higher than for $(\beta\text{-diketonate})\text{CuL}$ and $(\eta^5\text{-C}_5\text{H}_5)\text{CuL}$ precursors and are in the range of 300-500 °C. Again, disproportionation does not occur. Rather, the higher deposition temperature of 400 °C for $[(RO)\text{Cu}]$ was due to cleavage of the Cu-O bonds to produce tert-butoxy radicals which subsequently abstracted hydrogen and desorbed.

5.5.3 Physical Properties of Films

The purity of films deposited using Cu(I) compounds depends strongly on the nature of the uninegative ligand and the neutral ligand. The β -diketonate compounds, $(\beta\text{-diketonate})\text{CuL}$, that deposit copper by disproportionation result in high-purity films under a wide range of temperatures and pressures in both hot- and cold-wall reactors as shown in Table 5-2. This high-purity is due to the removal of the uninegative ligand in the form of $\text{Cu}(\beta\text{-diketonate})_2$ and the desorption of the neutral ligand L into the gas phase as discussed above. In the case of Cu(I) compounds that do not disproportionate, films of varying purity are obtained depending on the nature of the ligands. For example, $(\eta^5\text{-C}_5\text{H}_5)\text{CuL}$ compounds deposit films generally contaminated with C probably as a result of thermal decomposition of the $(\eta^5\text{-C}_5\text{H}_5)$ ligand.^{69,100} Chemical vapor deposition using $\text{Cu}(\text{O}-t\text{-Bu})_4$ resulted in deposition of copper films contaminated with O at elevated temperatures and in Cu(I) oxide films at lower temperatures.⁵¹ The CVD of $\{(t\text{-BuO})\text{Cu}[P(CH_3)_3]\}$ also gave contaminated copper films under all the conditions investigated.⁶⁹

The film resistivities are determined by the purity of the films and by their morphology. Films with resistivities as low as $1.8 \mu\Omega\text{cm}$ (bulk Cu at 20°C has a resistivity of $1.673 \mu\Omega\text{cm}$) have been reported in most cases, but in some cases high-purity films with higher resistivities have also been produced. This variation in resistivity was attributed to poor connectivity between grains in the films.^{58,63} Figure 5-5 shows a film deposited from $(\text{hfac})\text{Cu}[\text{P}(\text{CH}_3)_3]$ with a large grain size which leads to high resistivities. The influence of the nature of the substrate on copper nucleation and its influence on subsequent film morphology and resistivity have not been examined in detail for Cu(I) compounds. The influence of substrate temperature on film morphology and resistivity has been examined for $(\text{hfac})\text{Cu}(\text{VTMS})$ ⁶³ as shown in Figure 5-6. Both morphology and resistivity depended strongly on temperature in a complex manner.

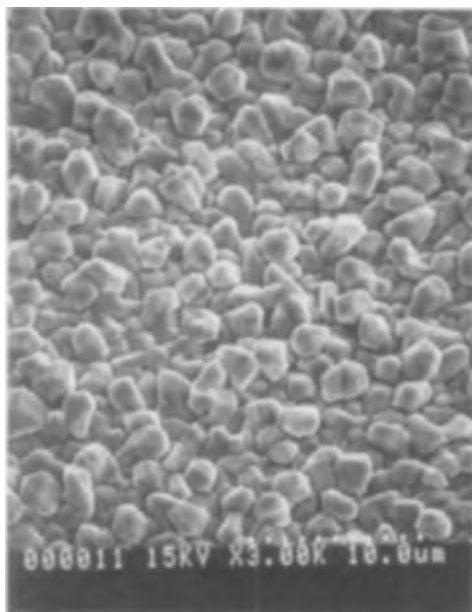


Figure 5-5 Copper film with large grain size and high resistivity deposited from $(\text{hfac})\text{Cu}[\text{P}(\text{CH}_3)_3]$ at 250°C and 50 mtorr. Lower deposition temperatures lead to smaller grain sizes and lower resistivities (see Figure 5-13 for example). (Adapted from Ref. 57.)

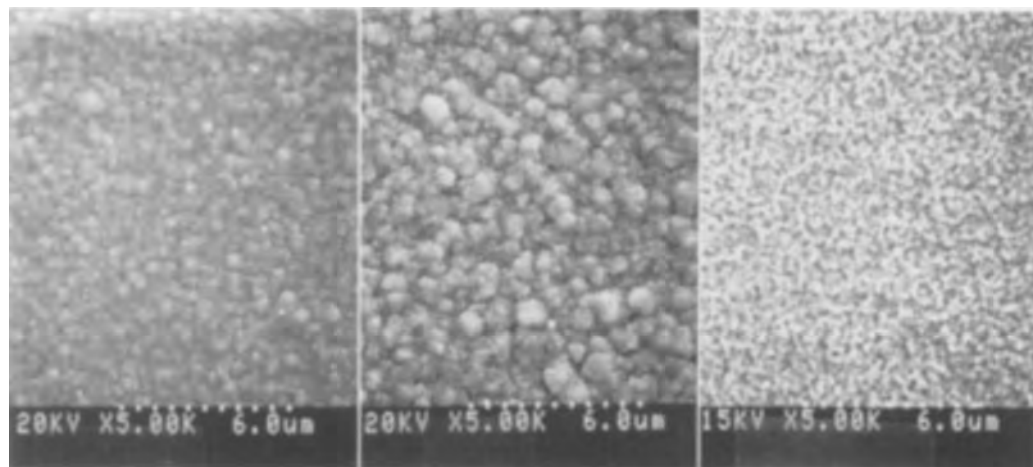


Figure 5-6 Morphology as a function of temperature for films deposited from (hfac)Cu(VTMS). (Adapted from Ref. 63.)

The adhesion of films produced by CVD has not been investigated in detail. However, adherent, smooth, and highly reflective films with thicknesses on the order of 1 μm can be produced easily. Conformal deposition has also been demonstrated for a variety of precursors. A typical example is shown in Figure 5-7.

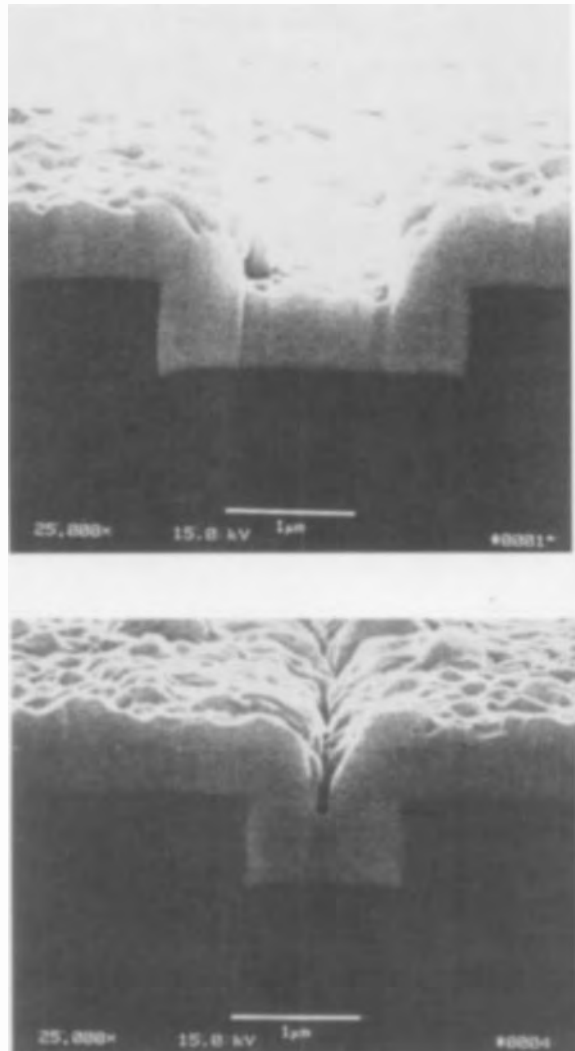


Figure 5-7 Conformal CVD of copper using (hfac)Cu(VTMS). (Adapted from Ref. 121.)

5.6 Reaction Stoichiometries, Kinetics, and Mechanisms

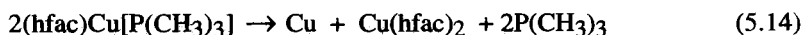
5.6.1 Reaction Pathways

In the case of Cu CVD from Cu(I) compounds, the reactions can be broadly characterized into two types, thermally-induced disproportionation and thermally-induced decomposition. Each category is discussed separately in the next two sections.

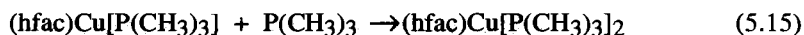
5.6.1.1 Thermally-Induced Disproportionation

The reaction product distribution resulting from CVD using Cu(I) precursors has been explored by a number of groups for a variety of precursors. This is typically achieved by trapping, separating, isolating, and quantifying the volatile byproducts.

For (β -diketonate)Cu[P(CH₃)₃], where β -diketonate = hfac, tfac, and acac, Cu(hfac)₂ and (hfac)Cu[P(CH₃)₃]₂ were isolated on the cold reactor walls and no P(CH₃)₃ was isolated in the liquid-nitrogen cold trap.^{58,64} These results are consistent with a mechanism, shown in Equation 5.14, in which deposition takes place by thermally-induced disproportionation to produce Cu and Cu(hfac)₂.



The liberated phosphine can react with (hfac)Cu[P(CH₃)₃] according to Equation 5.15.



This is consistent with solution experiments where (hfac)Cu[P(CH₃)₃]₂ was formed from the reaction of (hfac)Cu[P(CH₃)₃] with one equivalent of P(CH₃)₃.⁷² In addition, a white solid was often observed in the cold region of the reactor which was identified as the salt {Cu[P(CH₃)₃]₄}⁺[(hfac)]⁻. This species has also been prepared independently by reaction of (hfac)Cu[P(CH₃)₃]_n where n = 1 or 2 with an excess of P(CH₃)₃.⁸⁸

The results for (tfac)Cu[P(CH₃)₃] were qualitatively similar to those for (hfac)Cu[P(CH₃)₃].⁵⁸ At 80 and 100 °C, small amounts of Cu(tfac)₂ were detected. Small amounts of tfacH were also observed along with the reactant and (tfac)Cu[P(CH₃)₃]₂. As the temperature was increased, the relative amounts of Cu(tfac)₂ and (tfac)Cu[P(CH₃)₃]₂ increased. At the highest temperatures, all the reactant was consumed. The species (fod)Cu[P(CH₃)₃] behaved similarly although the low thermal stability of (fod)CuL species made deposition of Cu films difficult.¹⁰⁵

Similar reaction byproducts were observed when a sample of $(\text{acac})\text{Cu}[\text{P}(\text{CH}_3)_3]$ was heated in a closed vessel.⁷² Quantification of the deposition byproducts formed in a closed reactor revealed a product distribution according to the stoichiometry of Equation 5.16.



Thus, the reaction product distributions resulting from CVD using $(\text{hfac})\text{Cu}[\text{P}(\text{CH}_3)_3]$, $(\text{tfac})\text{Cu}[\text{P}(\text{CH}_3)_3]$, and $(\text{acac})\text{Cu}[\text{P}(\text{CH}_3)_3]$ appear to be comparable.

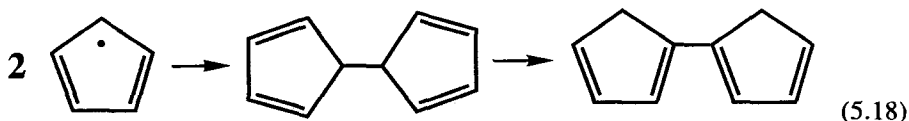
The compounds in the family $(\text{hfac})\text{Cu}(\text{PR}_3)_2$ are much more thermally stable than $(\text{hfac})\text{Cu}(\text{PR}_3)$ which leads to differences in the reaction mechanism. Chemical vapor deposition of $(\text{hfac})\text{Cu}[\text{P}(\text{CH}_3)_3]_2$ does not result in deposition below 300 °C, and in the temperature range 300–400 °C only low deposition rates and small quantities of reaction products are observed.⁵⁸ The major product isolated was unreacted starting material together with a small amount of $\{\text{Cu}[\text{P}(\text{CH}_3)_3]_4\}^+[(\text{hfac})]^-$. No evidence was obtained for the formation of Cu(II) species. Deposition occurred either via thermally-induced decomposition of the ligands or, alternatively, disproportionation occurred, but the Cu(II) species formed thermally decomposed since the substrate temperature was > 300 °C (see Ch. 4). For $(\text{hfac})\text{Cu}(\text{PEt}_3)_2$ no Cu(II) reaction byproducts were observed probably due to the high reactor temperature.⁵⁸ In this case, salt formation was not observed consistent with solution experiments where PEt_3 does not react further with $(\text{hfac})\text{Cu}(\text{PEt}_3)_2$.⁸⁸ The increased thermal stability of the $(\beta\text{-diketonate})\text{Cu}(\text{PR}_3)_2$ compounds over their monophosphine analogues can be explained in two ways: Either the second phosphine is bonded more strongly with the Cu(I) center than a single phosphine ligand, or dissociated phosphine reacts with $(\beta\text{-diketonate})\text{Cu}(\text{PR}_3)$ faster than the second Cu–P bond cleaves. The second explanation seems more likely based on structural data.⁸⁹

Analysis of the by-products from CVD of $(\text{hfac})\text{CuL}$, where $\text{L} = 1,5\text{-COD}$ ⁵⁹ or 2-butyne⁶⁶ over the temperature range 120 °C to 250 °C, is consistent with the disproportionation reaction of Equation 5.2. The Cu(II) product was isolated as large dark green crystals on the cold reactor walls and 1,5-COD was isolated from the liquid nitrogen trap. No evidence for isomerization of 1,5-COD or 2-butyne were observed in contrast to the thermal decomposition of other metal (1,5-COD) complexes.¹⁰⁶ These reactions are virtually quantitative under CVD conditions by mass balance and no evidence for formation of (hfac) thermal decomposition products was observed. This observation is reasonable since the reactor temperature was lower than the thermal decomposition temperature of $\text{Cu}(\text{hfac})_2$ (see Ch. 4).

5.6.1.2 Thermally-Induced Decomposition.

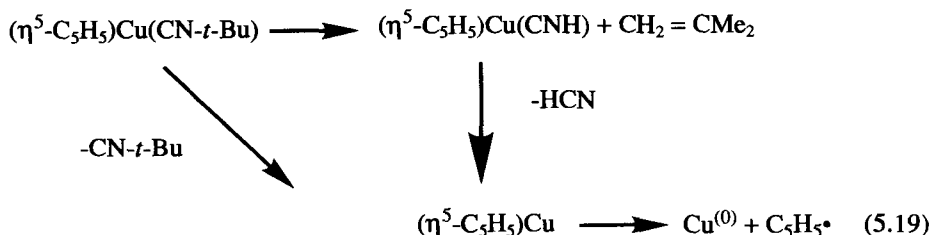
A general feature of the reactions of Cu(I) precursors described above is that they thermally disproportionate, a mechanism likely to be responsible for the high purity of the copper films observed since ligand *decomposition* does not occur. In contrast, other Cu(I) precursors follow reaction pathways which involve other mechanisms such as metal-ligand bond homolysis or metal-mediated rearrangement rather than disproportionation. In some cases this leads to impurities incorporated into the film.

Hot-wall CVD using $(\eta^5\text{-C}_5\text{H}_5)\text{Cu}[\text{P}(\text{CH}_3)_3]$ and $(\eta^5\text{-C}_5\text{H}_5)\text{Cu}(\text{PET}_3)$ resulted in isolation of cyclopentadiene, 9,10-dihydrofulvalene, PR_3 , and OPR_3 .^{69,100} However, based on the literature, the major product derived from the cyclopentadienyl ligand, 9,10-dihydrofulvalene, is unlikely to be the kinetic product of this deposition reaction.¹⁰⁷ The kinetic product is more likely to be $\text{C}_5\text{H}_5^\bullet$, two of which react to form 1,5-dihydrofulvalene with subsequent rearrangement to form 9,10-dihydrofulvalene according to Equations 5.17 and 5.18.



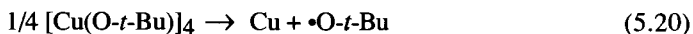
The trace amounts of OPR_3 observed were probably the result of direct oxidation of the phosphine at the CVD reaction temperature by the oxygen present in the reactor.

Analogous observations were made from the byproduct analysis of the CVD of $(\eta^5\text{-C}_5\text{H}_5)\text{Cu}(\text{CN-}t\text{-Bu})$ at 400–450 °C.¹⁰² The byproducts were trapped at liquid-nitrogen temperature and analyzed by mass spectroscopy. While $\text{C}_{10}\text{H}_{10}$, C_5H_6 , $t\text{-BuNC}$, and $(\text{C}_5\text{H}_5)\text{CN}$ were observed, no evidence for isobutylene was reported (see Eq. 5.19).



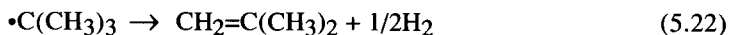
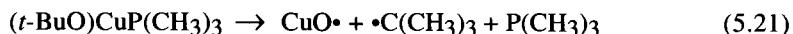
It was proposed that the isocyanide ligand also underwent β -hydride elimination *prior* to dissociation as shown in Equation 5.19 which accounted for the observation of $\text{C}_5\text{H}_5\text{CN}$ as a reaction byproduct through reaction of $\text{C}_5\text{H}_5^\bullet$ with HCN .

Chemical vapor deposition of Cu from $[\text{Cu}(\text{O}-t\text{-Bu})]_4$ resulted in formation of copper films contaminated by O (5%) at 400 °C.⁵¹ Analysis of the volatile byproduct distribution revealed only the presence of tert-butyl alcohol (*t*-BuOH). It was proposed that this was the result of homolytic cleavage of Cu-O bond to form *t*-BuO•, according to Equation 5.20, which abstracted a hydrogen atom from the glass reactor walls. Deposition experiments where the glass reactor walls had been treated with D₂O resulted in formation of *t*-BuO-D, consistent with the proposed mechanism.



It is perhaps surprising that β -hydride elimination was not observed because this is a common decomposition mechanism for metal-organic complexes.^{54,92}

In the hot-wall CVD of $\{(t\text{-BuO})\text{Cu}[\text{P}(\text{CH}_3)_3]\}$, byproduct analysis revealed the presence of *t*-BuOH, isobutylene, $\text{P}(\text{CH}_3)_3$, and $\text{OP}(\text{CH}_3)_3$ together with some unidentified reaction byproducts in small amounts.⁶⁹ The *t*-BuOH and isobutylene are probably derived from homolysis of Cu-O and O-C bonds, respectively. Alternatively, isobutylene may arise via β -hydride elimination (Eqs. 5.21-23).

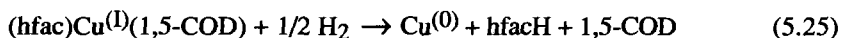


The films, however, were not extensively contaminated with oxygen, but a relatively large amount of $\text{OP}(\text{CH}_3)_3$ was formed {compared to $(\eta^5\text{-C}_5\text{H}_5)\text{Cu}[\text{P}(\text{CH}_3)_3]$ }. This may result from reduction of intermediate “copper oxide” species formed during CVD by the liberated phosphine (Eq. 5.24).



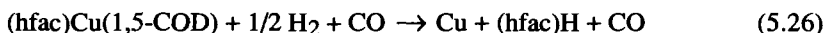
A thermogravimetric study of a number of poorly-defined mixed Cu(I) alkoxide-fluoroalkoxide compounds, essentially derivatives of $\text{Cu}(\text{O}-t\text{-Bu})$, in a 15% H₂/85% N₂ atmosphere showed weight loss consistent with formation of copper metal. However, these data also indicated that these compounds lack the volatility necessary to be suitable CVD precursors.⁸⁷ Sublimation temperatures at 0.1 mtorr were 60-100 °C.

Chemical vapor deposition has also been carried out with (hfac)Cu(1,5-COD), (hfac)Cu(1,3-butadiene) and [(hfac)Cu]₂(COT) in a cold-wall reactor in the presence of added hydrogen.⁶¹ For (hfac)Cu(1,5-COD) and [(hfac)Cu]₂(COT), deposition does not occur by a disproportionation mechanism. Rather, deposition occurs by direct reduction with formation to (hfac)H and Cu as shown in Equation 5.25.



The nature of the Lewis base product in Equation 5.25 was identified as 1,5-COD, and no isomerization or hydrogenation products were reported. The absence of $\text{Cu}(\text{hfac})_2$ in the reaction byproducts is particularly interesting in the case of $[(\text{hfac})\text{Cu}]_2(\text{COT})$ because this species is capable of *intramolecular* disproportionation. In contrast, as a result of the high propensity of $(\text{hfac})\text{Cu}(1,3\text{-butadiene})$ to disproportionate, this species may deposit copper via disproportionation even in the *presence* of H_2 . This approach results in different selectivity and lower deposition temperatures compared to CVD of the same species in the absence of H_2 as carrier gas.

The formation of Cu films using $(\text{hfac})\text{Cu}(1,5\text{-COD})$ with CO and H_2/CO as the carrier gas has been examined.⁹⁸ The reaction in CO without H_2 resulted in films with significant carbon contamination while reaction with H_2/CO resulted in formation of high-purity films with $(\text{hfac})\text{H}$ as a product (Eq. 5.26).



Under these conditions it is proposed that the Cu(I) species is transported as $(\text{hfac})\text{Cu}(\text{CO})$.⁹⁸

5.6.2 Reaction Kinetics

The kinetics of copper deposition from Cu(I) compounds has been studied in some detail in certain cases. Data obtained for surface-reaction-limited conditions in which transport-limited and feed-rate-limited conditions were avoided are only available for $(\beta\text{-diketonate})\text{CuL}$ and $(\eta^5\text{-C}_5\text{H}_5)\text{Cu}(\text{PEt}_3)$ compounds. These data have been obtained using warm-wall reactors. The deposition rates for $(\text{hfac})\text{Cu}[\text{P}(\text{CH}_3)_3]$, $(\text{hfac})\text{Cu}(1,5\text{-COD})$, $(\text{hfac})\text{Cu}(2\text{-butyne})$, and $(\text{hfac})\text{Cu}(\text{VTMS})$ are presented in Figure 5-8.

Activation energies have been measured at different pressures for different precursors. This limited data gives only a partial picture of the behavior of these precursors because of the complex dependence of the rate on precursor partial pressure. For example, CVD with $(\text{hfac})\text{Cu}(\text{VTMS})$ at high pressures gives a zero-order dependence on precursor partial pressure, whereas at low precursor partial pressures, a positive order dependence on reactant partial pressure is observed.⁶³ Activation energies were as follows: $(\text{hfac})\text{CuL}$, $\text{L} = \text{VTMS}$, 43 and 10 kcal/mol at 10 and 500 mtorr;⁶³ 1,5-COD, 26 kcal/mol at 10 mtorr;⁵⁹ 2-butyne, 23 kcal/mol at 50 mtorr;⁶⁶ $\text{P}(\text{CH}_3)_3$, 21 kcal/mol at 50 mtorr.⁶³ The activation energy for $(\text{hfac})\text{Cu}(1,5\text{-COD})$ was also measured by Reynolds et al.⁶⁰ as 29.8 kcal/mol at 18 mtorr which, within the limits of

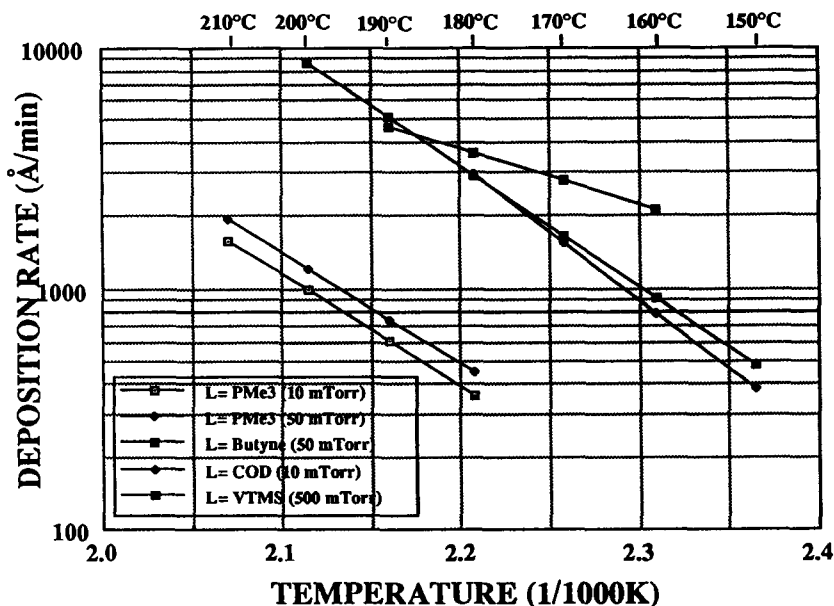


Figure 5-8 Deposition rates as a function of temperature for (hfac)Cu(VTMS), (hfac)Cu[P(CH₃)₃], (hfac)Cu(1,5-COD), (hfac)Cu(2-butyne). (Adapted from Refs. 57, 59, 63, 66.)

error, is the same as the value of 26 kcal/mol reported by Jain et al.⁶³ Beach et al. have reported an activation energy of 18 kcal/mol for CVD of Cu using $(\eta^5\text{-C}_5\text{H}_5)\text{Cu}(\text{PEt}_3)$.¹⁰⁰ Activation energies have not been reported for other Cu(I) precursors.

The variation of deposition rate with temperature had the following general characteristics for most precursors. The logarithm of the deposition rate increased linearly with increasing temperature until a temperature was reached where the deposition rate no longer increased significantly. This temperature corresponded to that at which a feed-rate limitation was reached, where the deposition rate was being limited by the transport of the precursor into the reactor.⁶³ In other cases, this may have been due to diffusive reactant transport limitations.

The dependence of the deposition rate on precursor partial pressure has not been examined in detail for most systems, partially because of the difficulties in dealing with relatively low-vapor-pressure precursors where the flow rate and partial pressure of the precursor are limited to relatively narrow ranges and carrier gases are used. The only data in the literature is for (hfac)Cu(VTMS).⁶³ A positive-order and zero-order

Table 5-3 Kinetics for CVD of Copper by (hfac)CuL Compounds in a Differential Reactor with Negligible Cu(hfac)₂ and L Partial Pressures. (After Ref. 63).

Mechanism	Rate Limiting Reaction Expression	Reaction Rate Order	Apparent Activation Energy (EA)
(hfac)Cu ^(I) L(g) + S <=> (hfac)Cu ^(I) L•S	-R _a = k _a •P _a (K _a)	1st order	k _a
(hfac)Cu ^(I) L•S <=> (hfac)Cu ^(I) L•S + L(g)	-R _{s1} = k _{s1} •K _a •P _a / (K _{s1}) (1+K _a •P _a) ²	LP: 1st order HP: negative order	LP: k _{s1} •K _a HP: k _{s1} •K _a ⁻¹
(hfac)Cu ^(I) •S + (hfac)Cu ^(I) •S <=> Cu ⁽⁰⁾ •S + Cu ^(II) (hfac) ₂ •S (K _{s2})	-R _{s2} = k _{s2}	zero order	k _{s2}
Cu ^(II) (hfac) ₂ •S <=> Cu ^(II) (hfac) ₂ (g) + S (K _d)	-R _d = k _d	zero order	k _d

(L.P. = low precursor partial pressure, H.P. = high precursor partial pressure).

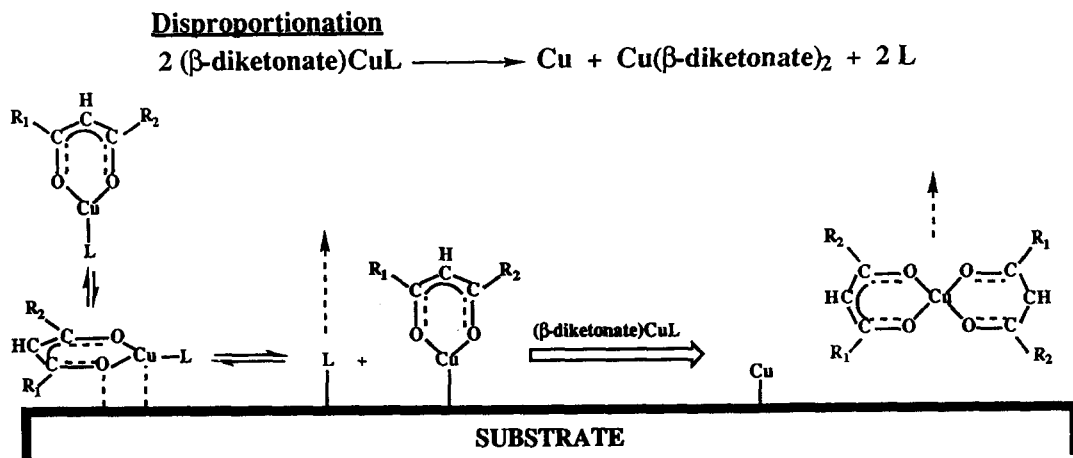


Figure 5-9 Schematic diagram of the disproportionation mechanism.

pressure dependence of the rate were observed at low and high pressures respectively. Different activation energies 43 and 10 kcal (low and high pressures, respectively) were observed within these limits. These results suggest that the deposition rate has a complex dependence on the precursor partial pressure as would be expected from an analysis of possible reaction mechanisms. Table 5-3 shows a possible reaction mechanism based on the reactions shown in Figure 5-9. This mechanism is based on the dissociative adsorption of the precursor to form $\text{Cu}(\text{hfac})$ and L , disproportionation to form $\text{Cu}(\text{hfac})_2$ and Cu , and desorption of $\text{Cu}(\text{hfac})_2$ and L . The mechanism predicts a first order and negative order dependence of the rate on precursor partial pressure. Other schemes are also possible as discussed by Jain et al.⁶³ Another mechanism has been used to describe laser-induced deposition from $(\text{hfac})\text{Cu}(\text{VTMS})$ in which $(\text{hfac})\text{Cu}$ desorption also occurs.¹⁰⁸ This mechanism predicts a second order and zero order dependence on reactant partial pressure.

5.6.3 Surface Reaction Mechanisms

The surface reactions of various $\text{Cu}(\text{I})$ species have been studied under ultra-high vacuum (UHV) conditions using a variety of approaches including Fourier transform infrared spectroscopy (FTIR), high resolution electron energy loss spectroscopy (HREELS), temperature programmed desorption (TPD), X-ray photoelectron

spectroscopy (XPS), and Auger electron spectroscopy (AES).¹⁰⁹⁻¹¹² The precursors examined were Cu(acac)₂, Cu(tfac)₂, Cu(hfac)₂, (hfac)Cu(1,5-COD), (hfac)Cu(VTMS), and [CuO-*t*-Bu]₄, and the substrates studied include Cu(100), Cu(111), Pt(111), Ag, and TiN.

Several observations were common to all of these studies; however, because the disproportionation reaction is bimolecular and the surface coverages present were too low, the experiments carried out under UHV conditions ($< 10^{-6}$ mtorr) did not permit direct observation of the disproportionation reaction. Instead, heating in the absence of hydrogen resulted in deposition of impure copper. Thus, high-purity copper deposition under low pressures must instead depend on the presence of hydrogen for removal of (hfac)H. This suggests that in the absence of hydrogen as a reducing agent, UHV chemical beam approaches using these precursors would lead to low-purity films.

The dissociation of (hfac)Cu(VTMS) and Cu(hfac)₂ on TiN using XPS and TPD was investigated.^{99,111} The TiN substrates were characterized and found to consist of a surface layer of TiO₂ on TiN. The primary difference between dissociation of Cu(hfac)₂ and (hfac)Cu(VTMS) on TiN (actually TiO₂) is that the extra (hfac) unit derived from dissociation of Cu(hfac)₂ on TiN is not associated with Cu but with TiO₂. Dissociation of (hfac)Cu(VTMS) gives only one type of hfac unit associated with Cu(hfac) both on TiN and Cu because only one hfac unit is available per Cu atom. This difference in adsorption behavior results in different product distributions for (hfac)Cu(VTMS) and Cu(hfac)₂ in TPD experiments on TiN (TiO₂). The species CF₄, CO, and CO₂ were produced above 200 °C for both (hfac)Cu(VTMS) and Cu(hfac)₂ and demonstrated that disproportionation did not occur for either precursor. Desorbed copper-containing species were observed during heating between 100-200 °C only for Cu(hfac)₂. Fluorine was observed on the surface from decomposition of the (hfac) ligand for (hfac)Cu(VTMS) and also suggested that disproportionation does not take place under these UHV conditions. A build-up of fluorine was found at the Cu/TiN interface by secondary ionization mass spectroscopy (SIMS) in films deposited at high pressures in a CVD system from (hfac)Cu(VTMS). This suggests that disproportionation may not take place for the first monolayer of deposition on TiN (TiO₂).

Dubois et al.^{109,110} studied the dissociation of (hfac)Cu(VTMS) and Cu(hfac)₂ on Cu(100) and Cu(111) surfaces using infrared spectroscopy (IR), mass spectroscopy (MS), TPD and AES. The VTMS ligand was not observed on the surface above 180 K after dosing with (hfac)Cu(VTMS). Similarly, dosing with the free VTMS ligand showed that the VTMS desorbs at 180 K, suggesting that the VTMS dissociates from the precursor and desorbs rapidly. These results suggest that the high purity of copper films formed from this precursor is partly due to the rapid desorption of VTMS without reaction which could incorporate impurities. When FTIR was employed to study adsorption of (hfac)H, Cu(hfac)₂, and (hfac)Cu(VTMS), the surface species appeared to be identical. The (hfac)-H bond was cleaved at 200 K on both Cu(100) and

Cu(111) surfaces. The identity of the species formed by dosing with (hfac)H, Cu(hfac)₂, and (hfac)Cu(VTMS) and the oxidation state of Cu in this species, however, were not determined. Although the intermediate species formed was the same for these precursors, the overall result is dramatically different. In the case of Cu(I) precursors, disproportionation at sufficiently high surface coverages can lead to removal of two β -diketonate ligands and one (oxidized) Cu atom while the other (reduced) Cu atom remains on the surface and results in film growth. In the case of Cu(II) precursors, comproportionation is thermodynamically disfavored and would not lead to a net deposition of Cu atoms. Disproportionation of two "(hfac)Cu" species formed from surface Cu and Cu(hfac)₂ also would not lead to a net deposition. In all cases, heating of adsorbed layers derived from (hfac)Cu(VTMS), Cu(hfac)₂, and (hfac)H, under UHV conditions, gave fluorine, CO, CO₂, and fluorinated hydrocarbons as products consistent with the results of Donnelly and Gross.^{99,111} Again, this demonstrated disproportionation did not occur under these low-surface-coverage UHV conditions. Another key result was that carbon contamination in the films may be derived from the formation of a copper carbide that is formed from a ketylidene intermediate as shown in Figure 5-10.

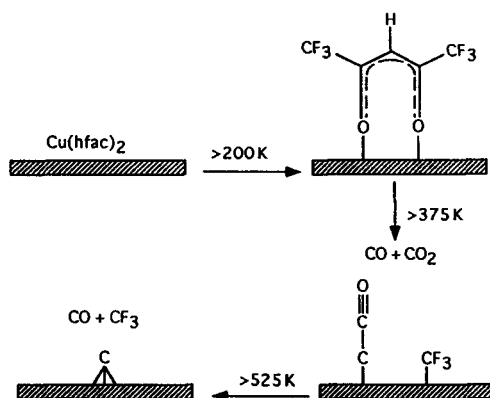


Figure 5-10 Mechanism of formation of ketylidene leading to carbon incorporation. (Adapted from Ref. 110.)

The high purity of films formed from (β -diketonate)CuL species has been partially explained by studies of the interaction of various neutral ligands with copper surfaces by TPD.^{109,110} These results are presented in Figure 5-11 and show that the 2-butyne, VTMS, 1,5-COD, and P(CH₃)₃ desorb from the surface at low temperatures (125, 175, 225, and 450 K respectively). Thus the neutral ligands are liberated and desorb rapidly instead of being incorporated into the films during CVD.

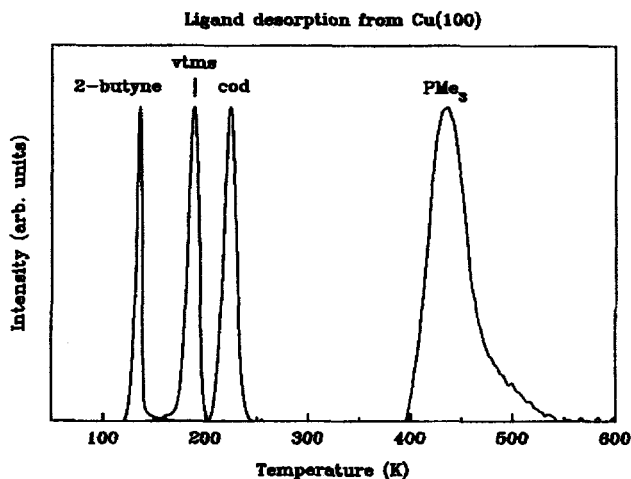


Figure 5-11 Temperature programmed desorption of neutral ligands from Cu(100) surface. (Courtesy of L. DuBois, Ref. 109.)

Cohen et al.¹¹² studied the reactions of $\text{Cu}(\text{hfac})_2$ and $(\text{hfac})\text{Cu}(1,5\text{-COD})$ on Ag. A similar species believed to be " $(\text{hfac})\text{Cu}$ " or " $(\text{hfac})\text{Ag}$ " was observed in both cases. In the case of $\text{Cu}(\text{hfac})_2$, the second hfac was presumably associated with Ag. The 1,5-COD desorbed rapidly at low temperatures and was not detected on the surface consistent with the study by Dubois.^{109,110} The oxidation state of the adsorbed species was determined by XPS to be near unity, but the species was activated by the electron-rich Ag surface.

On Pt(111) surfaces, quite different behavior has been observed.¹¹³ Platinum was chosen as a substrate for UHV studies because it has been used in previous CVD experiments and is likely to be more reactive than copper surfaces. On Pt(111), $\text{Cu}(\text{hfac})_2$ and hfacH reacted to form species that were different, in contrast to the observation for the same precursors on Cu, as determined by FTIR. Furthermore, the adsorbates started to decompose at substantially lower temperatures on Pt relative to Cu resulting in impurities at the interface. High-vacuum CVD of Cu onto Pt(111) using either $(\text{hfac})\text{Cu}(\text{VTMS})$ or $(\text{hfac})\text{Cu}(2\text{-butyne})$ showed that bimolecular disproportionation resulting in formation of high-purity Cu only occurs at pressures greater than 10^{-2} mtorr. Chemical vapor deposition below 10^{-3} mtorr favors unimolecular processes which result primarily in carbon deposition on the Pt surface.

The results of reaction product analysis, UHV surface reaction studies, and reaction kinetics for $(\text{hfac})\text{CuL}$ precursors in the absence of reducing agents such as H_2 are consistent with the reaction mechanism shown in Figure 5-9. Copper deposition

involves dissociative adsorption of the precursor on the substrate to form (hfac)Cu and L on the surface. The neutral ligand desorbs rapidly from the surface, while at the same time, the disproportionation reaction of Cu(hfac) gives copper and Cu(hfac)₂. The quantitative kinetics of the individual steps have not yet been established.

5.7 Selectivity

5.7.1 Factors Influencing Selectivity

Selective deposition of copper (deposition onto one surface, the growth surface, in the presence of another, the non-growth surface) is a complex process which depends on the nature of the precursor, the surface, the reactor type and geometry (hot-wall, cold-wall, plasma, etc.), operating conditions (temperature, pressure, etc.), surface preparation procedure, deposition time, and other factors (see Ch. 9). Thus, deposition parameters from one system cannot always be used in another system unless care is taken to reproduce the conditions.

Selective deposition has been studied in both hot- and cold-wall CVD reactors as a function of the nature of the substrate, the temperature of the substrate, and the nature of the copper substituents. Selectivity has usually been evaluated by using Si substrates on which SiO₂ has been grown and patterned with various metals by either electron-beam deposition, CVD, or sputtering. The results of selective deposition studies are shown in Table 5-4.

Some of these data were obtained under conditions where substrate cleaning was carried out in the same manner, identical substrates were used, the reactor type and operating conditions were kept constant, and the precursor was used from the same source for each experiment.^{58,59,63,64,66} Under these conditions, it is reasonable to compare the selectivity as a function of the copper ligand environment. Nevertheless, the origin of the selectivity and selectivity loss for deposition of copper onto different surfaces from these precursors has not been studied extensively. It is likely that quantitative data to address this point will only come from studies conducted in ultra-high vacuum systems with clean, well-characterized surfaces and from studies with differential reactors. However, a number of qualitative conclusions can be drawn from the data presented in Table 5-4.

Deposition of copper from (hfac)Cu[P(CH₃)₃] onto Pt occurred selectively in the presence of SiO₂ below 300 °C but selectivity was lost above 300 °C. This loss of selectivity above 300 °C may be explained by copper deposition onto SiO₂ from the Cu(hfac)₂ liberated in the disproportionation reaction of Equation 5.2.

Table 5-4 Selectivity Characteristics for Cu(I) Compounds. (After Ref. 120.)

	Precursor	Selectivity	Temp. range	Refs.
I	(β -diketonate)CuL			
	a. (β -diketonate)Cu(PR ₃)			
	(hfac)Cu[P(CH ₃) ₃]	Pt, W, Cu vs SiO ₂	150 - 300 °C	58,64
	(tfac)Cu[P(CH ₃) ₃]	Pt, W, Cu vs SiO ₂	100 - 150 °C	58,64
	(acac)Cu[P(CH ₃) ₃]	Pt, W, Cu vs SiO ₂	<80 °C	58,64
	b. (β -diketonate)Cu(olefin)			
	(hfac)Cu(1,5-COD)	None for Pt, W, Cu vs SiO ₂	120 - 250 °C	59
	(hfac)Cu(1,5-COD)	Certain degree of selectivity for Ta, Cu, Ag, Au, and Cr vs SiO ₂ and Si ₃ N ₄	<200 °C	60
	(hfac)Cu(VTMS)	None for W vs SiO ₂	120 - 250 °C	63,64
	(hfac)Cu(VTMS)	W vs SiO ₂	120 - 420 °C	62
		TiN vs SiO ₂	150 - 180 °C	62
		PtSi vs SiO ₂	150 - 200 °C	62
	(hfac)Cu(VTMS)	None for TiN vs SiO ₂	160 °C	114
		TiN vs SiO ₂	160 C	114
	c. (β -diketonate)Cu(alkyne)			
	(hfac)Cu(BTMSA)	None for Pt, W, Cu vs SiO ₂	120 - 250 °C	64,66
	(hfac)Cu(2-butyne)	None for Pt, W, Cu vs SiO ₂	120 - 250 °C	64,66
	(hfac)Cu(2-butyne)	Some selectivity for Co and Mo vs polyimide and SiO ₂	150 °C	67
	(hfac)Cu(2-butyne)	None for Pt, W, Cu vs SiO ₂	120 - 250 °C	64,66
II	(β -diketonate)Cu(PR ₃) ₂			
	(hfac)Cu(PR ₃) ₂ (R = CH ₃ , Et)	not reported	300 °C	58
III	XCuL			
	[(RO)CuPR ₃] ₂	not reported	not reported	69
	(η^5 -C ₅ H ₅)CuPR ₃	Cr, Cu vs Si and SiO ₂	130 - 200 °C	69,100
IV	(RO)Cu			
	Cu(O- <i>i</i> -Bu) ₄	not reported	not reported	51

The loss of selectivity of copper CVD onto Pt in the presence of SiO_2 as a function of the β -diketonate ligands occurs at successively lower temperatures in the order $(\text{hfac})\text{Cu}[\text{P}(\text{CH}_3)_3] > (\text{tfac})\text{Cu}[\text{P}(\text{CH}_3)_3] > (\text{acac})\text{Cu}[\text{P}(\text{CH}_3)_3]$. Thus, selectivity is influenced by the nature of the β -diketonate ligand substituent in the absence of other changes to the deposition conditions or the copper coordination sphere. However, the mechanism of selectivity loss for $(\text{tfac})\text{Cu}[\text{P}(\text{CH}_3)_3]$ is unlikely to be due to deposition of copper from $\text{Cu}(\text{tfac})_2$ evolved during disproportionation because in control experiments, $\text{Cu}(\text{tfac})_2$ does not significantly thermally decompose below 330°C .

There is some discrepancy in the literature concerning the selective deposition of $(\text{hfac})\text{Cu}(\text{VTMS})$ on W versus SiO_2 (see Table 5-4).^{62,64} These discrepancies probably arise from differences in the preparation of the surfaces involved and reactor operating conditions and geometry. This emphasizes the difficulty in comparing data from different groups where surface preparations, reactor dimensions, and deposition conditions vary.

To illustrate this point, Norman et al. studied selective copper deposition on TiN vs. SiO_2 using SiO_2 surfaces prepared by different methods.¹¹⁴ Only thermally grown SiO_2 reproducibly resisted CVD from $(\text{hfac})\text{Cu}(\text{VTMS})$, while SiO_2 films containing water, especially those derived from PECVD were metallized. The PECVD-derived SiO_2 substrates resisted deposition more effectively after dehydration by thermal annealing in N_2 at 700°C . Similar effects have been reported by other groups.¹¹⁵

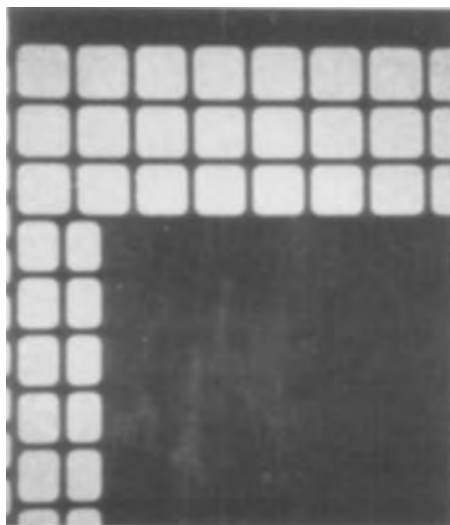


Figure 5-12 Selective deposition of copper onto W in the presence of SiO_2 using $(\text{hfac})\text{Cu}[\text{P}(\text{CH}_3)_3]$. (Adapted from Ref. 57.)

Gas-phase reactions are also likely to be detrimental to selective deposition of Cu and it has been shown that (hfac)Cu(VTMS) can undergo thermally-induced disproportionation in the gas phase.¹¹⁶

An example of selective deposition of copper onto W in the presence of SiO₂ using (hfac)Cu[P(CH₃)₃] is shown in Figure 5-12. An example of blanket deposition of copper onto both W and SiO₂ using (hfac)Cu(1,5-COD) is shown in Figure 5-13.

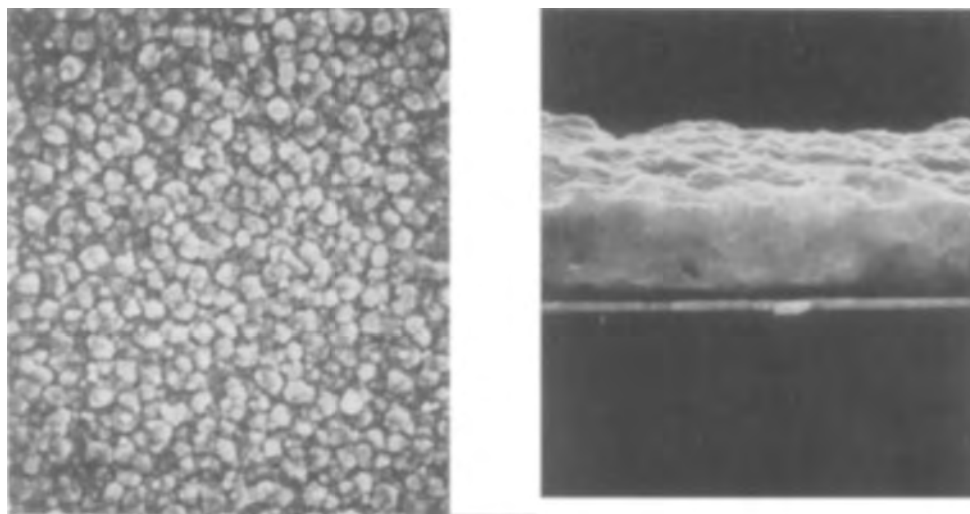


Figure 5-13 Blanket deposition of copper onto W and SiO₂ from (hfac)Cu(1,5-COD). (Adapted from Ref. 66.)

The selectivity for deposition onto metals in the presence of SiO₂ can be intentionally modified by changing the nature and relative surface concentrations of functional groups on the SiO₂ surface. Farkas et al.^{117,118}, Jain et al.¹¹⁹, and Dubois et al.¹²⁰ have shown that hydroxyl groups on SiO₂ surfaces are likely sites for chemisorption of (hfac)CuL precursors. This suggested that eliminating or blocking surface hydroxyl groups could inhibit precursor adsorption and reaction on the SiO₂ surface thereby providing selective deposition onto metals in the presence of SiO₂. This is discussed in more detail in the next section.

Jain et al.¹¹⁹ have shown that the selectivity of CVD of (hfac)CuL, L = P(CH₃)₃, 1,5-COD, VTMS, and 2-butyne, onto W in the presence of SiO₂ can be modified as a function of surface pretreatment. Blanket deposition was obtained for all compounds {except (hfac)Cu[P(CH₃)₃] (Fig. 5-12)} as described above when the substrates were cleaned

with hot aqueous H_2O_2 , rinsed, and dried (Fig. 5-14a). In contrast, reacting the SiO_2 surface with functionalized alkylsilanes such as chlorotrimethylsilane and dimethyldichlorosilane to remove the OH sites eliminated the nucleation of copper on SiO_2 regardless of the nature of L and resulted in selective CVD. Figure 5-14b shows selective deposition obtained by first treating the SiO_2 surface with liquid

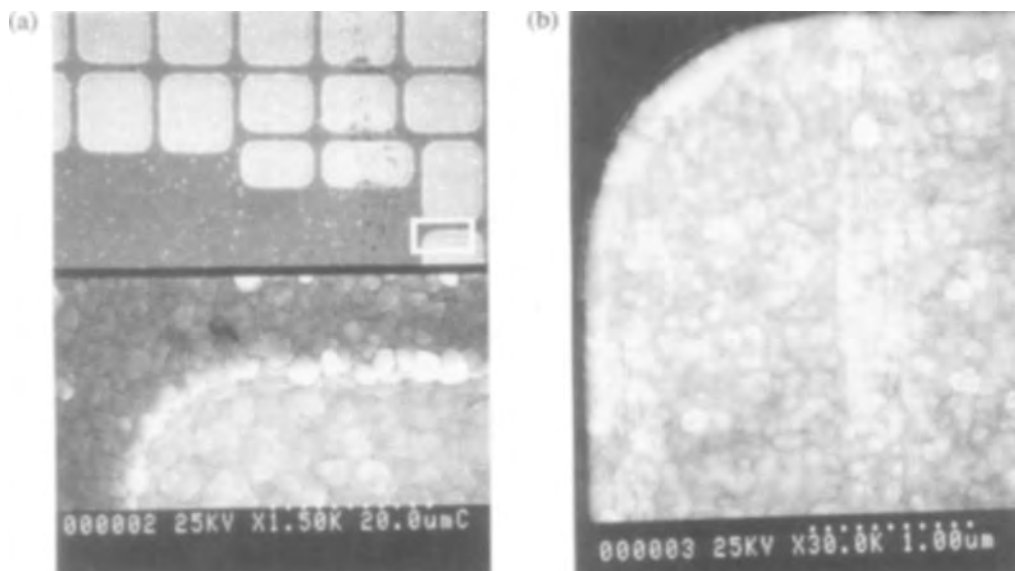
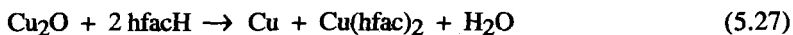


Figure 5-14 (a) Blanket deposition obtained using $(\text{hfac})\text{Cu}(\text{VTMS})$ without pretreating SiO_2 surface with $(\text{CH}_3)_3\text{SiCl}$; (b) Selective deposition obtained under same conditions as (a) after pretreating surface with $(\text{CH}_3)_3\text{SiCl}$. (Adapted from Ref. 119.)

chlorotrimethylsilane. However, selectivity for W in the presence of $(\text{CH}_3)_3\text{SiCl}$ -modified SiO_2 was lost after a few minutes. This was believed to be due to the molecular desorption of $(\text{CH}_3)_3\text{SiCl}$ which re-exposed the surface hydroxyl groups. To combat this problem, Cu CVD was carried out in the presence of an excess of $(\text{CH}_3)_2\text{SiCl}_2$ which reacted with the surface hydroxyl groups in preference to the copper precursor.¹²¹ Other reagents such as $(\text{CH}_3)_3\text{Si}-\text{N}(\text{CH}_3)_2$, $n\text{-Bu}(\text{CH}_3)_2\text{SiN}(\text{CH}_3)_2$ and $[(\text{CH}_3)_3\text{Si}]_2\text{NH}$ provide varying degrees of passivation of SiO_2 with respect to copper metallization.¹²² To date, $(\text{CH}_3)_3\text{SiN}(\text{CH}_3)_2$ has provided the best passivation of SiO_2 against Cu metallization.¹²³

A number of other reagents exhibit a strong effect on the rate of CVD of copper from both copper(I) and copper(II) compounds on different surfaces. These observations are likely to have strong implications for the selective deposition of Cu. The influence of water and alcohols has been studied in some detail. The introduction of water during CVD of Cu from (hfac)Cu(VTMS) onto Si wafers coated with 1000 Å of sputtered TiN increased the deposition rate and reduced the nucleation delay without degrading the film resistivity (2.3 $\mu\Omega\text{cm}$) at low water concentration.¹²⁴ However, at higher water concentrations, a substantial increase in the resistivity of the films occurred and oxygen incorporation was observed by Auger electron spectroscopy. It was proposed that "copper oxide" may be formed at higher water concentrations. Under the correct conditions, the formation of either copper(I) or copper(II) oxides may not be detrimental because hfacH, a probable reaction byproduct, can react with either oxide to produce a pure copper film, see Eqs 5.27 and 5.31.¹²⁵



The role of water at low water concentration was proposed to be either catalytic cleavage of the Cu-VTMS bond or reaction with (hfac)Cu(VTMS) in the gas phase to form a more reactive intermediate.¹²⁴

In a related study, Chiang et al.¹²⁶ studied the interaction of various solvents, including methanol, ethanol, isopropanol, acetone, THF, toluene and water with (hfac)Cu[P(CH₃)₃] and Cu(hfac)₂. While alcohols did not react directly with either (hfac)Cu[P(CH₃)₃] or Cu(hfac)₂ in solution at room temperature, water partially reduced Cu(hfac)₂ and partially oxidized (hfac)Cu[P(CH₃)₃]. The extent of oxidation of the copper(I) species was not quantified and is likely to be small because the technique used to assess the presence of oxidation (nuclear magnetic resonance spectroscopy) is quite sensitive to paramagnetic impurities, such as copper(II) species. Furthermore, copper(I) compounds can be made in high yields (>90%) in the presence of water as a reaction by-product (see Eq. 5.7). The more important issue is the role of water during CVD. Water can react with adsorbed hfac ligands, a common intermediate in the reaction of both (hfac)CuL and Cu(hfac)₂ compounds with Cu surfaces.¹²⁶ As a result, the addition of water can cause the loss of hfac ligands at lower temperatures and can decrease the hfac ligand coverage on copper surfaces compared to the absence of water. This provides a method for the removal of potential contamination sources from the substrate which is particularly an issue in CVD of Cu from Cu(hfac)₂. The presence of water also increases the initial sticking probability of Cu on SiO₂ surfaces¹²⁷ which suggests water can promote nucleation on the SiO₂ surface. These observations are consistent with CVD results for Cu(hfac)₂ in the presence of water which gave rise to high-purity films,¹²⁸⁻¹³⁰ even in the absence of H₂.¹³⁰

Using water, alcohols, and other reagents to increase the deposition rate while retaining selective deposition must be performed with care, especially where the non-growth surface is a metal oxide such as SiO_2 .^{131,132} Water and alcohols modify the SiO_2 surface by interacting or by reacting with the surface hydroxyl groups and strained siloxane rings that occur on SiO_2 substrates. These surface reactions can lead to a complete loss of selectivity or to a shorter time over which selectivity may be obtained. However, methods for selective CVD have been demonstrated that take advantage of the enhancement of the deposition rate in the presence of water while retaining good control over selective deposition using surface passivation strategies in which the surface is modified by reaction of hydroxyl groups with *silylating* agents.¹³³

5.7.2 Mechanism of Selectivity

A number of groups have studied the origin of selectivity for CVD of (β -diketonate)CuL compounds. The adsorption of representative examples of (β -diketonate)CuL where L = phosphine, olefin and alkyne compounds onto silica has been studied by transmission FTIR.¹¹⁷⁻¹²⁰ The FTIR technique is a sensitive method to detect physisorbed water and surface reactive sites such as strained siloxane rings and hydroxyl groups, which significantly influence the surface chemistry of the silica. It is an established technique to characterize surface sites and their reactions with adsorbates on high-surface-area silica.¹³⁴ High-surface-area fumed and porous silica were used to increase the amount of precursor adsorbed per unit area. The (β -diketonate)CuL precursors were chosen because the phosphine compounds deposit selectively on metals (Cu, W, Pt) in the presence of SiO_2 whereas the olefin and alkyne adducts do not exhibit the same selectivity under identical deposition conditions on the same substrate.^{58,119} The substrate studied was high-surface-area silica [Cab-O-Sil (grade M5, 200 m^2/g)]. Depending upon the thermal treatment, this surface exhibits well-defined combinations of hydrogen-bonded surface hydroxyl groups, isolated hydroxyl groups, and (Si-O)₂ four membered rings.

The compounds studied were (hfac)Cu(VTMS), (hfac)Cu[P(CH₃)₃], (hfac)Cu(1,5-COD) and (hfac)Cu(2-butyne) along with the corresponding free ligands.¹¹⁷⁻¹²⁰ Individually, the free ligands, VTMS, P(CH₃)₃, 1,5-COD, and 2-butyne were adsorbed onto Cab-O-Sil at -140 °C; changes in the position and peak width of the isolated surface hydroxyl group were immediately apparent. When heated, 1,5-COD and 2-butyne completely desorbed intact by -25 °C, but P(CH₃)₃ was still present on the surface (intact) even on heating to 200 °C (see Fig. 5-15a). This suggests that if reaction of (hfac)Cu[P(CH₃)₃] occurs on SiO_2 , the P(CH₃)₃ should remain on the surface and could be detected by FTIR.

On adsorption of $(\text{hfac})\text{Cu}[\text{P}(\text{CH}_3)_3]$ below -50°C , the isolated surface hydroxyl band was shifted and broadened, and the bands assigned to the hfac ligand ($1485 - 1672\text{ cm}^{-1}$) were significantly changed compared to the gas-phase spectrum. However, on heating to -25°C , the isolated surface hydroxyl groups were restored and all the bands attributed to $(\text{hfac})\text{Cu}[\text{P}(\text{CH}_3)_3]$ disappeared. Since no bands remained at -25°C , it seems likely that $(\text{hfac})\text{Cu}[\text{P}(\text{CH}_3)_3]$ desorbed molecularly (see Fig. 5-15b). On the other hand, when both $(\text{hfac})\text{Cu}(1,5\text{-COD})$ and $(\text{hfac})\text{Cu}(2\text{-butyne})$ were adsorbed below -50°C and were heated, evidence for both the neutral ligands (i.e., 1,5-COD and 2-butyne) and hfac was observed even after heating to 50°C . This showed these compounds were more strongly bonded to the surface than $(\text{hfac})\text{Cu}[\text{P}(\text{CH}_3)_3]$.

This behavior is consistent with the selectivity observed in CVD experiments. The compound $(\text{hfac})\text{Cu}[\text{P}(\text{CH}_3)_3]$ does not deposit copper onto SiO_2 below 350°C and does not adsorb on Cab-O-Sil above -25°C . The compounds $(\text{hfac})\text{Cu}(1,5\text{-COD})$ and $(\text{hfac})\text{Cu}(2\text{-butyne})$ do deposit copper onto silica at 120°C , and interact (or react) with Cab-O-Sil on heating to 200°C . These correlations should be made with care as different substrate cleaning methods can produce different surface derivatization such as the extent of hydroxylation of silica surfaces.

More detailed studies of the reactions of $(\text{hfac})\text{Cu}(2\text{-butyne})$ and free 2-butyne on high-surface area SiO_2 with three combinations of reactive surface sites (highly

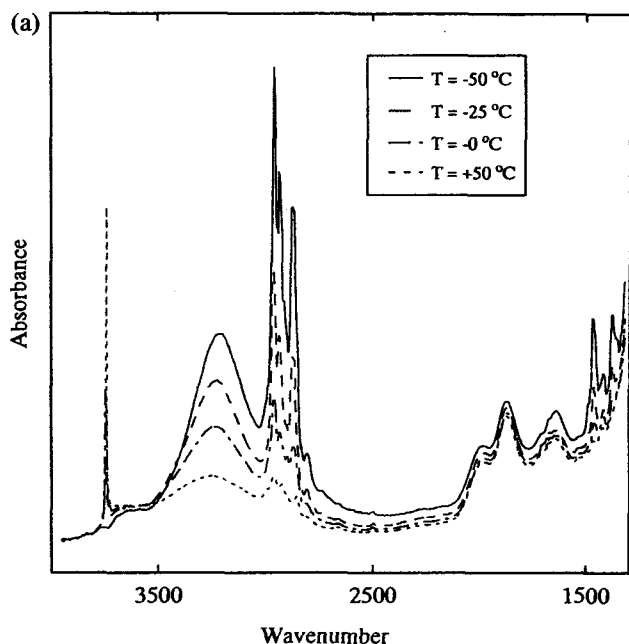


Figure 5-15a

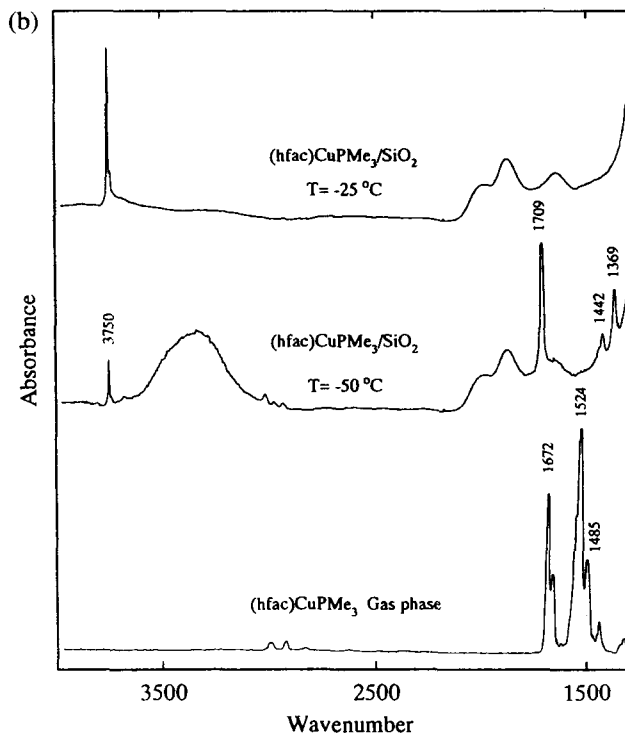


Figure 5-15 FTIR data showing adsorption behavior of (a) P(CH₃)₃ and (b) (hfac)Cu[P(CH₃)₃] on Cab-O-Sil as a function of temperature. The gas-phase FTIR spectrum of (hfac)Cu[P(CH₃)₃] is shown for comparison. (Adapted from Ref. 117.)

dehydroxylated, partially dehydroxylated, and as loaded) have been carried out with transmission FTIR spectroscopy.¹¹⁸ The pressure-dependent, gas-phase spectra showed that the bands of the 2-butyne ligand contribute only weakly to the (hfac)Cu(2-butyne) spectra (about 50 times less than the β -diketonate part of the molecule). The 2-butyne interacted weakly with the SiO₂ surface. Similar adsorption/desorption behavior was observed for (hfac)Cu(2-butyne) in both low- and high-temperature (-130 °C and 25 °C, respectively) studies on all three surfaces. The precursor condensed on the SiO₂ surfaces at -130 °C with no observable interaction with the surface hydroxyl groups or with the Si-O-Si defect bands. On heating the substrate, a change in the ν (C-H) stretching and bending modes was observed around -50 °C and the adsorbate almost completely desorbed from the surface at 25 °C. Dosing the substrate at 25 °C gave no, or significantly weaker, ν (C-H) stretching modes originating from the 2-butyne ligand for

all three surfaces. Interactions with both isolated, hydrogen-bonded surface hydroxyl groups and the Si-O-Si defect bands were detected. The substrate had to be heated to about 400 °C for complete removal of the adsorbate. The observed change in the spectra for the low-temperature desorption experiments around -50 °C, and the lack of the $\nu(\text{C-H})$ stretching modes after room-temperature dosing were consistent with disproportionation of the compound. The similar adsorption/desorption behavior of the compound on all three surfaces and the similar increase in the integrated area of the hydrogen-bonded hydroxyl group bands during desorption suggest that the reactive sites on the SiO_2 surface are the hydrogen-bonded hydroxyl groups and strained siloxanes. Since one or the other of these groups is present on most SiO_2 surfaces, these data are

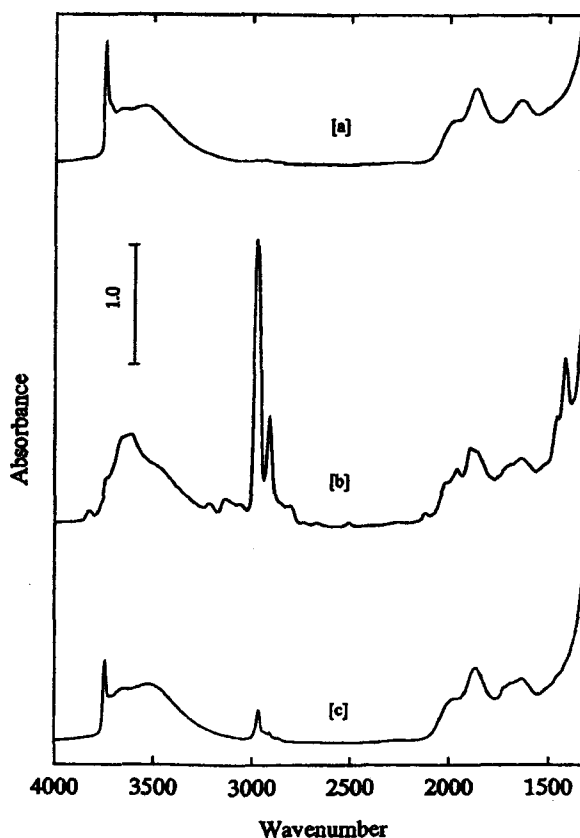


Figure 5-16 FTIR data of (a) an as-prepared Cab-O-Sil surface with isolated and hydrogen-bonded hydroxyl groups, but with adsorbed water removed, (b) after treatment with 150 mtorr of chlorotrimethylsilane for 15 min. at 330 K and (c) after evacuation of the sample chamber.

consistent with CVD results where this compound showed nonselective behavior on SiO_2 versus different metals.

Two groups have examined adsorption of $(\text{hfac})\text{Cu}(\text{VTMS})$ onto dehydroxylated SiO_2 using the approach described above.^{120,133} In one study, no deposition was observed on clean silica (Cab-O-Sil) which had only isolated OH groups present, and the strained Si-O-Si sites played no role in the adsorption and dissociation of the precursor.¹²⁰ Both of these observations are in contrast with the results for $(\text{hfac})\text{Cu}(\text{2-butyne})$ mentioned above. However, in the presence of adsorbed H_2O , reaction,

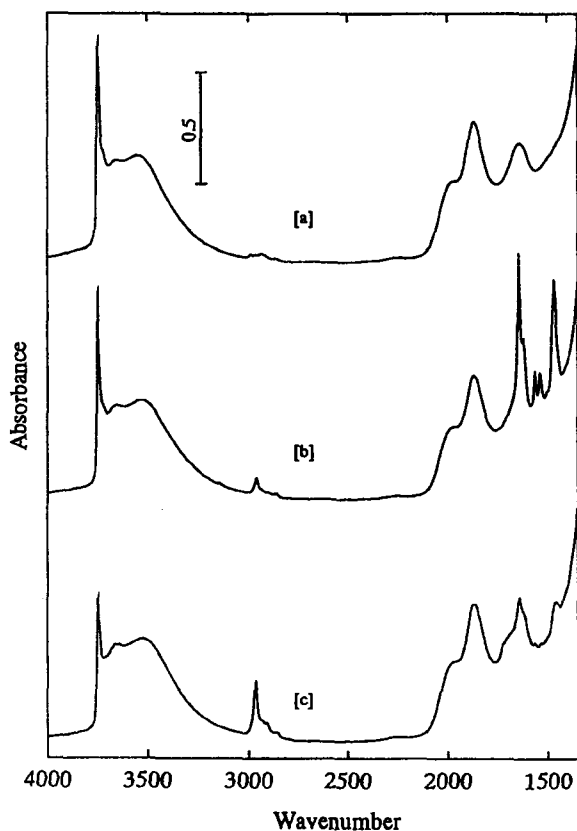


Figure 5-17 A comparison between the FTIR spectra for (a) the Cab-O-Sil surface (as prepared in Figure 5-16a), (b) the Cab-O-Sil surface dosed with $(\text{hfac})\text{Cu}(\text{VTMS})$ (1 mtorr, 10 min, 300 K), and (c) the Cab-O-Sil surface dosed with chlorotrimethylsilane (150 mtorr, 30 min, 330 K) followed by $(\text{hfac})\text{Cu}(\text{VTMS})$ (1 mtorr, 10 min, 300 K).

nucleation, and loss of selectivity occurred for (hfac)Cu(VTMS). The water was extremely difficult to remove from the surface and always required high-temperature treatment. In the other study,¹³³ it was demonstrated that (hfac)Cu(VTMS) molecularly adsorbed on some silica surfaces at room temperature, and that reaction with the surface occurred only on heating above 50 °C.

Further evidence that the surface hydroxyl groups were the active sites at which (hfac)Cu(VTMS) adsorbed came from experiments in which the surface hydroxyl groups were removed by reaction with functionalized alkylsilanes such as (CH₃)₃SiCl.¹¹⁹ In a series of control experiments, Cab-O-Sil was reacted with (CH₃)₃SiCl and the interaction with the surface hydroxyl groups was demonstrated, see Figure 5-16. Then a comparison of the uptake of (hfac)Cu(VTMS) was made on the untreated and (CH₃)₃Si-Cl-treated Cab-O-Sil surface. The FTIR data obtained (Figs. 5-16 and 5-17) showed that negligible amounts of (hfac)Cu(VTMS) were adsorbed on the (CH₃)₃SiCl-treated surface compared to the untreated surface.

As a result of these observations, differences in the selectivity were interpreted in terms of the strength of the Cu-L bond versus the strength of interaction of the (hfac)CuL molecule with surface reactive sites, primarily hydroxyl groups, surface-bound water and strained Si-O-Si bonds. Compounds such as (hfac)Cu[P(CH₃)₃] with stronger Cu-L bonds dissociate at higher temperatures on SiO₂ and therefore provide selectivity over a broader range of conditions. In contrast, compounds such as (hfac)Cu(2-butyne) with much weaker Cu-L bonds dissociate more rapidly on SiO₂ and result in loss of selectivity. Compounds with intermediate strength Cu-L bonds such as Cu-VTMS and Cu-1,5-COD provide selectivity under some conditions, but not under others. However, selective deposition can be controlled by removing adsorption sites from the SiO₂, by treatment with (CH₃)₃SiCl¹¹⁸ or (CH₃)₂SiCl₂,¹²¹ or other functionalized alkylsilanes.^{122,123}

5.7.3 Selective Deposition onto Patterned PTFE Substrates

The deposition of copper onto organic polymer substrates is important since these substrates have low dielectric constants and may act as diffusion barriers.¹³⁵ The combination of the low dielectric constant of fluoropolymers such as poly(tetrafluoroethylene) (PTFE) and the high conductivity of metals such as copper have led to use of this combination of materials in the printed wiring board industry. However, the chemical and physical inertness of PTFE makes it difficult to metallize. For this reason copper films on PTFE are currently prepared for the printed wiring board industry by mechanically rolling copper foils onto PTFE substrates with subsequent patterning using photoresist and wet chemical etching techniques. Using

these methods, it is difficult to make high resolution, sub-micron, or even micron-sized patterns. In order to improve the resolution of the patterning process, a variety of alternative methods to form patterned copper films based on selective CVD have been explored.

In order to metallize the PTFE surface by CVD methods, the surface of the polymer must be rendered reactive towards the precursors and must be patterned with a technique capable of higher resolution than existing processes. There are a number of variations by which this may be achieved, two of which are shown in Figure 5-18. In both variations, sodium naphthalenide is used to render the PTFE surface reactive while pattern definition is achieved either by X-rays, electron beams, or laser irradiation.

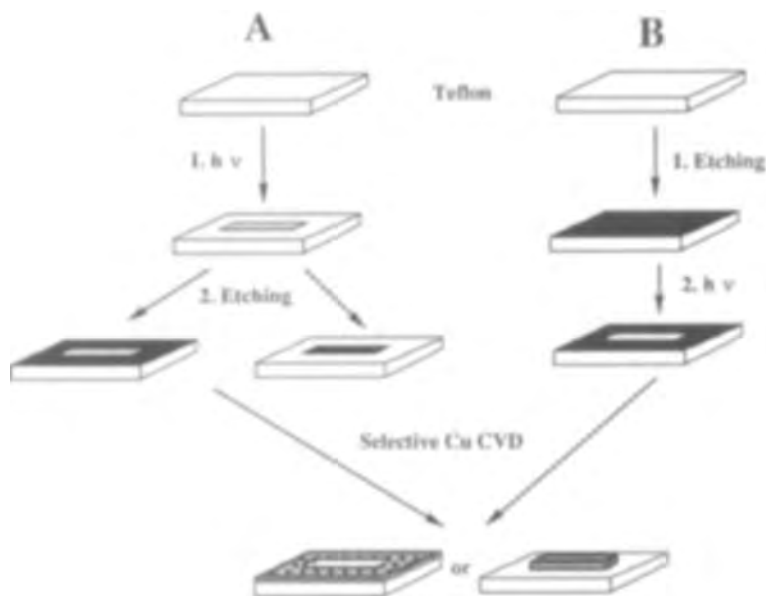


Figure 5-18 Methods for generation of patterned copper films on PTFE. (Adapted from Ref. 151.)

In variation (A), a PTFE substrate is first irradiated with either X-rays or electrons to produce a pattern. This step can be accomplished either by direct writing in the case of electron beams, or through a mask in the case of X-rays. This process has been studied in some detail and is thought to cross-link and chemically reduce the PTFE surface; however, no change is observed with the naked eye.⁹⁵⁻⁹⁷ In the second step, the whole PTFE substrate is immersed in commercially available solutions containing the reducing agent sodium naphthalenide (or sodium naphthalenide/THF solution). The

sodium naphthalenide solution does not significantly affect the irradiated areas of the PTFE surface, but reacts significantly with the unmodified PTFE surface. This is manifest in the observation that after this treatment, the irradiated areas are white, but the unirradiated areas are dark brown or black. Therefore, this step “develops” the pattern. After washing and drying, the patterned sample was placed in a hot-wall CVD reactor where copper was deposited using $(\text{hfac})\text{Cu}[\text{P}(\text{CH}_3)_3]$ as a precursor. This resulted in selective copper deposition onto the areas of the substrate that had been affected by chemical etching but not on the areas that had been subjected to irradiation with X-rays or electrons in the first step. This process is illustrated schematically in Figure 5-19.

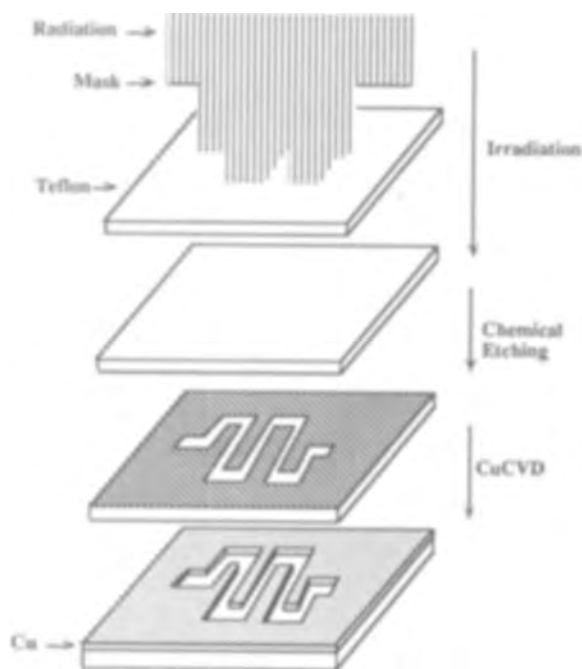


Figure 5-19 Generation of patterned copper film on PTFE by patterned X-ray irradiation, etching, and selective CVD. (Adapted from Ref. 97.)

In variation (B),¹³⁶ the substrate is first reacted with sodium naphthalenide as described above. A pulsed or CW laser is then used to selectively remove portions of the black surface leaving clean (white) PTFE exposed. This patterned surface is then used as a substrate for selective CVD onto the remaining dark, reactive areas. This process is illustrated schematically in Figure 5-20.

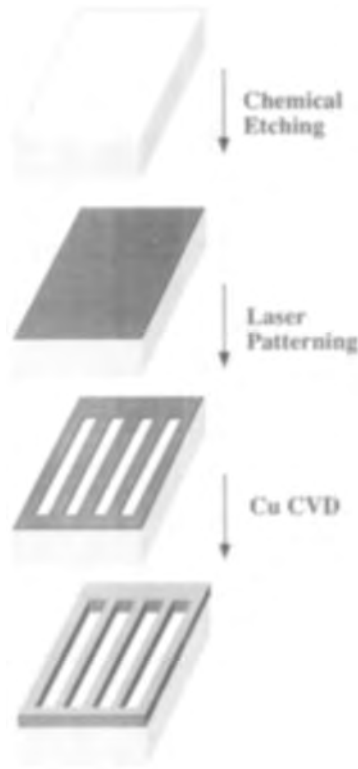


Figure 5-20 Generation of patterned copper film on PTFE by etching laser patterning and selective CVD. (Adapted from Ref. 96.)

In both variations, irradiation of the substrate with either X-rays, electrons, or laser photons produces the pattern by modifying the surface structure. The chemical modification step using sodium naphthalenide plays two important roles: It renders the surface *reactive* towards Cu(I) molecules and makes it rough resulting in good *adhesion* of the vapor deposited metal film. Copper films deposited by both methods exhibit good adhesion strength and resistivities close to that of bulk copper. In contrast, the adhesion strength of copper on virgin or irradiated PTFE is very low.

5.8 Chemical Vapor Deposition of Copper Alloys

There is technological and scientific interest in the deposition of several Cu alloys. Specifically, aluminum/copper alloys have become the metallization materials of choice for VLSI circuits, as they offer some of the lowest resistances of usable interconnect

materials. A typical Al/Cu alloy composition does not normally exceed 5 wt% Cu. These alloys are currently deposited by PVD techniques, but CVD-derived films have the potential for improved conformal coatings of high-aspect ratio vias, better step coverage, and selective deposition. Another motivation for investigating the CVD of copper alloys is derived from problems anticipated in Cu metallization schemes (see Ch. 1). The use of copper alloys may help avoid problems caused by electromigration, corrosion, and poor adhesion to dielectric substrates.

The CVD of copper alloys has been achieved by using copper(I) and copper(II) compounds as precursors, see Table 5-5. In one study,¹³⁷ a comparison was made of the CVD of Al/Cu alloy using three different copper compounds, $\text{Cu}(\text{hfac})_2$, $(\text{hfac})\text{Cu}(\text{P}(\text{CH}_3)_3)_3$, and $(\eta^5\text{-C}_5\text{H}_5)\text{Cu}(\text{PEt}_3)$, each co-deposited with trimethylamine alane (TMAA) on Si, SiO_2 , and TiN substrates in a vertical low-pressure cold-wall reactor. The copper content in the films (up to 5 wt%) was controlled by varying the temperature of the copper precursor. The copper(II) source exhibited a "massive parasitic reaction" during the deposition experiment which hampered control over the composition. This parasitic reaction was thought to be the result of abstraction of $\text{N}(\text{CH}_3)_3$ from TMAA with concomitant precipitation of polymeric alane. The copper(I) compounds did not show such a propensity for this reaction and the films exhibited optimal smoothness at 350 °C. Characterization by microscopy techniques and SIMS revealed that the films derived from the copper(I) precursors were homogeneous on the micron scale. The nanostructures of the films containing approximately 2 wt% Cu were comparable to analogous films deposited by PVD techniques. The purity, resistivity, and adhesion were of a quality suitable for microelectronics applications.

Simultaneous co-deposition has also been studied using other combinations of Cu and Al precursors. Films composed of Al-(0.7-1.4 wt%) Cu were deposited from $[(\text{CH}_3)_2\text{AlH}]_3$ and $(\eta^5\text{-C}_5\text{H}_5)\text{Cu}(\text{PEt}_3)$ in a cold-wall reactor on TiN substrates at 260 °C with a deposition rate of approximately 300 Å/min.¹³⁸ Auger electron spectroscopy depth profiling showed a uniform distribution of Cu in the films and no contamination by either C or P. Precipitates with composition CuAl_2 were identified in the film by transmission electron microscopy and electron diffraction providing evidence that true alloys rather than a mixture of individual Al and Cu grains were formed. The co-deposition of Al/Cu alloys was attempted using TMAA and $(\text{hfac})\text{Cu}(\text{VTMS})$, but porous and filamentary films were formed and subsequent analysis was not pursued.¹³⁹ However, consecutive deposition of these reagents was more successful in deposition of Cu and Al films. In one study¹³⁹ using a high-speed rotating-disk reactor, Cu and Al films were sequentially deposited on Si and TiW substrates by depositing Cu followed by Al or by depositing Al followed by Cu. A high oxygen concentration at the TiW/metal interface, probably derived from exposure of the TiW substrate to air prior to CVD, was observed. Auger electron spectroscopy

Table 5-5 Chemical Vapor Deposition of Copper Alloys.

Precursors	Substrate	T _{Precurs} °C	T _{Substrat} °C	Carrier Gas	Pressure	Rate nm/min	Ref.
TMAA	Si, SiO ₂	50-120	100-400	none	0.5-10 torr	100	137
Cu(hfac) ₂	or TiN	"					
(hfac)Cu[P(CH ₃) ₃] ₃		"					
(η ⁵ -C ₅ H ₅)CuPEt ₃		"					
DMAH	TiN	50	100	none	2 torr	---	138
(η ⁵ -C ₅ H ₅)CuPEt ₃			260				
TMAA	TiW	25	100-700	none	30 torr	166	139
(hfac)Cu(VTMS)	or Si	43					
TMAA	SiO ₂ /Cu	25	110-185	H ₂ or He	0-1 torr	81-583	140
(hfac)Cu(VTMS)	SiO ₂ /TiN	40-120		or Ar			
(hfac)Cu(1,5-COD)	SiO ₂ /W	"					
(hfac)Cu(1,5-dimethyl-1,5-COD)	Cu	0-25	165-180	H ₂ or He	1-5 torr	---	141
Co ₂ (CO) ₈		"					
Te(η ¹ -allyl) ₂		"					

revealed that the O contamination was better confined to the TiW/metal interface when Cu rather than Al was deposited first. At deposition temperatures of 125 °C for Al and 250 °C for Cu, little interdiffusion of the films was observed.

Selective, consecutive Cu and Al deposition has also been achieved using either (hfac)Cu(VTMS) or (hfac)Cu(1,5-COD) for Cu and TMAA for Al.¹⁴⁰ Copper was selectively deposited onto W or TiN at 150 °C followed by selective CVD of Al on Cu in the range 100-120 °C. Under these conditions only a small amount of Cu diffuses into Al, but complete diffusion could be achieved by rapid thermal annealing. Alloys formed by this method were 10-30 % copper.

The formation of Cu-Co and Cu-Te alloys was recently reported by Smart et al. using (hfac)Cu(1,5-dimethyl-1,5-COD) as a copper source, Co₂(CO)₈ as a Co source and Te(η^1 -allyl)₂ as a tellurium source.¹⁴¹ Considerable difficulty in controlling the amount of Co in the film was observed probably as a result of the thermal lability of the Co precursor; however, low resistivity (3 $\mu\Omega$ cm) Cu-Co films were formed. In contrast the Cu:Te ratio was easier to control through the temperature of the source bubbler and conformal films were deposited.

These results illustrate the potential of metal-organic precursors for the deposition of binary alloy materials. The deposition experiments can be carried out at low temperatures, at relatively high rates, and with control over the composition of the film. The deposition of binary phases from individual and single-source precursors is discussed further in Chapter 8.

5.9 Etching

The mechanisms of several chemical approaches to etching of copper are closely related to CVD of copper. In addition, methods for removal of copper from surfaces can be used to clean CVD reactors. Finally, the successful integration of copper will require patterned copper films which can be produced by either chemical-mechanical polishing, selective deposition, or by etching of blanket copper films. Selective deposition was discussed above. Chemical-mechanical polishing is a promising approach and involves conformal CVD of copper into trenches followed by removal of copper from outside of the trenches.¹⁴² However, this approach cannot be used in all applications, and methods for etching copper must also be developed. For these reasons, this section will discuss several approaches for removal of copper from surfaces.

Existing copper etching technologies rely mainly on the formation of copper chloride via oxidation of copper with molecular or atomic chlorine often generated from molecules such as carbon tetrachloride in plasmas. The rate of reaction of chlorine with copper surfaces is extremely fast.¹⁴³⁻¹⁴⁵ However, the vapor pressure of the copper chloride is extremely low at typical etching temperatures which severely limits the

etch rate to values that are not useful for industrial applications.¹⁴⁶ To some extent, this problem can be overcome by using reactive ion etching at elevated temperatures.^{5,147-149} This solution, however, does not allow use of standard polymeric mask materials.

Alternative approaches attempt to generate more volatile copper species. Three such methods related to CVD of copper that rely on generation of high-vapor-pressure copper species on the surface have been reported. These approaches are shown schematically in Figure 5-21.

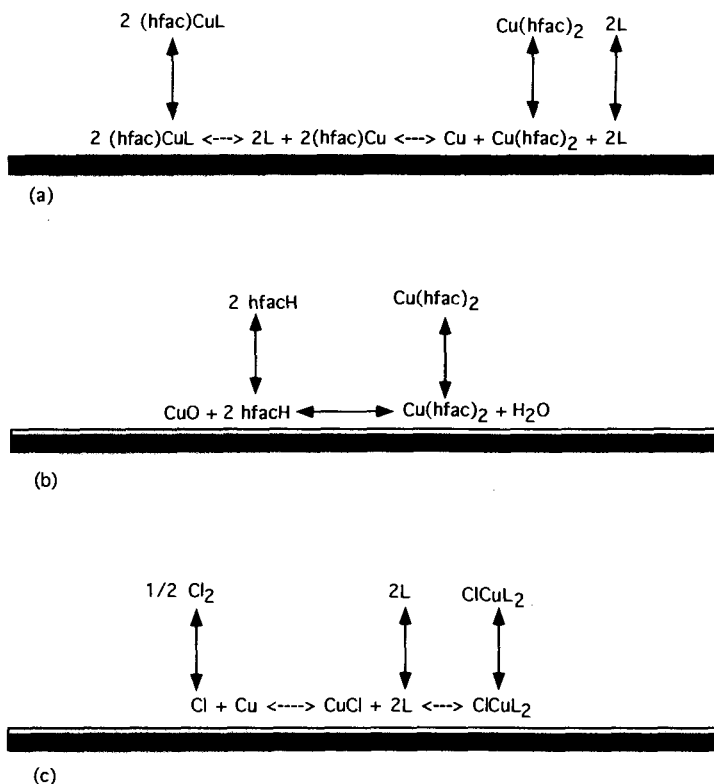
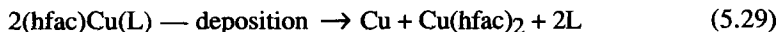
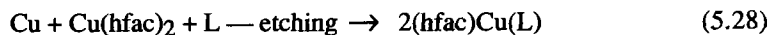


Figure 5-21 Various new chemical approaches for copper etching: (a) comproportionation; (b) copper-oxide formation and removal; (c) formation of XCuL_2 .

5.9.1 Comproportionation

One approach, identified in Equation 5.28, involves the reverse of the disproportionation CVD reactions noted above.^{62,150}



Examination of these reactions suggests that high concentrations of Lewis base and Cu(II) compounds will favor etching even though the reaction is thermodynamically disfavored by ~ 10 kcal/mol. In addition, temperature plays a major role in influencing the etch rate because this process is reversible. Thus, Cu(I) species, $(\text{hfac})\text{Cu}(\text{I})\text{L}$, that have *high* thermal barriers to disproportionation are the most suitable products for the etching reaction. An optimum temperature exists for etching for which the reaction rate to form $(\text{hfac})\text{CuL}$ and desorption are sufficiently fast, but for which the product is sufficiently stable to allow etching. At higher temperatures the disproportionation of the Cu(I) product may lead to a reduction in the net etching rate.

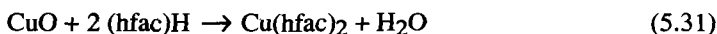
Copper has been etched at $50 \text{ \AA}/\text{min}$ at 140°C using $\text{Cu}(\text{hfac})_2$ and VTMS.⁶² In other reports, different ligands have been used including 2-butyne, pentyne and bis(trimethylsilylacetylene) (BTMSA).¹⁵⁰ The highest etching rate was obtained for the most thermally stable Cu(I) compound, $(\text{hfac})\text{Cu}(\text{I})(\text{BTMSA})$. The etch rate exhibited a maximum with increasing temperature as expected. Also, the temperature corresponding to the maximum etch rate decreased with decreasing Cu(I) product stability. Etch rates of $500 \text{ \AA}/\text{min}$ at 120°C and $100 \text{ \AA}/\text{min}$ at 80°C using BTMSA were obtained. In contrast, the pentyne ligand provided almost negligible etch rates under similar conditions. Chemical vapor deposition experiments using $(\text{hfac})\text{Cu}(\text{BTMSA})$ in a hot-wall reactor revealed that this precursor did not thermally decompose below 200°C .

5.9.2 Copper Oxide Formation and Removal

Another approach for removing Cu from surfaces involves oxidation of copper to form CuO followed by etching of CuO via reaction with $(\text{hfac})\text{H}$ (see Eq. 5.30).



The reaction of Equation 5.31 has been used to etch CuO films at rates up to $1 \mu\text{m}/\text{min}$ at 200°C in a cold-wall system.^{125,151} The CuO films were produced by pulsed laser deposition. The $(\text{hfac})\text{H}$ partial pressure was 1000 mtorr.



The $(\text{hfac})\text{H}$ was passed over the film of copper oxide resulting in formation of $\text{Cu}(\text{hfac})_2$. This process has not been exploited for etching of copper, but can potentially be used if the copper is oxidized first followed by reaction with $(\text{hfac})\text{H}$.

5.9.3 Formation of XCuL_2

This approach involves the formation of volatile Lewis base adducts of copper halides where oligomerization of the halide is prevented by reaction of the copper halide with a tertiary phosphine (L) according to the stoichiometry of Equations 5.32 and 5.33.⁸⁸



Copper films have been reacted with either Cl_2 and PET_3 simultaneously or have been chlorinated first followed by reaction with PET_3 . Similar results were obtained in both cases because of the rapid reaction of the Cl_2 with the Cu. Etch rates up to $1 \mu\text{m}/\text{min}$ at 100°C were obtained for 10 torr of 3.5% Cl_2 in He carrier gas and 500 mtorr PET_3 . This reaction formed a volatile copper-containing product which was trapped and shown to be $\text{ClCu}(\text{PET}_3)_2$.¹⁵¹ This species was prepared independently on a laboratory scale by the reaction of Equation 5.11. Vapor pressure data for this species revealed a value of 900 mtorr at 90°C , the highest reported for a Cu(I) compound.⁸⁸ Again the thermal stability of this species under etching conditions is an important issue. It was demonstrated that $\text{ClCu}(\text{PET}_3)_2$ was sufficiently stable not to deposit copper onto metals or SiO_2 below 250°C . Ultra-high-vacuum studies using RAIR (reflection-absorption infra-red), AES, TPD, and reactive scattering showed that $\text{ClCu}(\text{PET}_3)_2$ was formed by the reaction of PET_3 with chlorinated copper surfaces and desorbed at low temperatures (320 K).¹⁵²⁻¹⁵³

5.10 Summary and Conclusions

The CVD of copper from Cu(I) compounds has become well-established as a method for producing high-purity copper films at low temperatures ($< 200^\circ\text{C}$) and high rates ($0.1\text{--}1 \mu\text{m}/\text{min}$). Many precursors have been developed, and they provide a range of physical and chemical properties such as vapor pressure and reactivity. Precursors that are liquids [(*hfac*)Cu(VTMS)] or high-vapor-pressure solids at typical operating temperatures are available. Chemical vapor deposition from copper(I) β -diketonate precursors has been carried out under conditions where either thermally-induced disproportionation (Eq. 5.25) or reduction with H_2 are the dominant mechanisms. Both methods give rise to high-purity copper films with resistivities close to that of the bulk metal. High-quality copper films have also been deposited from cyclopentadienyl copper^(I) derivatives, however, other copper(I) precursors tend to deposit poorer quality

films. Copper has been deposited in blanket and selective modes on a variety of substrates including metals, metal oxides, metal nitrides, and organic polymers. Precursors and operating conditions have been investigated that provide reproducible selective deposition. The precursor (hfac)Cu[P(CH₃)₃] deposits copper selectively onto many metals over a wide temperature range. Other precursors such as (hfac)Cu(VTMS), (hfac)Cu(2-butyne), and (hfac)Cu(1,5-COD) provide selective CVD when the SiO₂ surface is passivated by reaction with various functionalized alkylsilanes [(CH₃)₃SiCl, (CH₃)₂SiCl₂]. Other reagents such as water and alcohol have various effects on the nucleation, deposition rate, morphology, and quality of the film deposited. Advances in copper CVD have also led to new methods for etching of copper. These approaches involve the reverse of the disproportionation reaction, the formation of XCuL₂ species such as ClCu(PEt₃)₂, and the reaction of β-diketones with CuO and Cu₂O to form Cu(hfac)₂.

Acknowledgments: The authors thank the National Science Foundation for support of studies of copper CVD which have provided much of the results discussed in this chapter. We are deeply indebted to Dr. W. S. Rees, Jr. whose extensive and specific suggestions have helped clarify the manuscript for newcomers to the field. We also thank Dr. Kai-Ming Chi, Dr. Janos Farkas, Dr. Hyun Shin, Mr. Ajay Jain, and Mr. Tom Corbitt for their motivation and enthusiasm in this area. We acknowledge Ms. Judith Binder, whose patience and dedication enabled us to carry out innumerable modifications and additions to the manuscript.

References

1. Pai, P.L., Ting, C.H., Chiang, C., Wei, C.-S., Fraser, D.B. *Mat. Res. Soc. Symp. Proc. VLSI* **1990**, V, 359.
2. Berry, A.D., Holm, R.T., Fatemi, M., Gaskill, D.K. *J. Mater. Res.* **1990**, 5, 1109.
3. Awaya, N., Arita, Y. *J. Electronic Materials* **1992**, 21, 959.
4. Hess, D.W., Jensen, K.F. *Microelectronics Processing*, American Chemical Society, Washington, DC, 1989.
5. Schwartz, G.C., Schaible, P.M. *J. Electrochem. Soc.* **1983**, 130, 1777.
6. Howard, B.J., Steinbruchel, C. *Appl. Phys. Lett.* **1991**, 59, 914.
7. Green, M.L., Levy, R.A., Nuzzo, R.G., Coleman, E. *Thin Solid Films* **1984**, 114, 367.
8. *Advanced Metallization for ULSI Applications*, Rana, V.S., Joshi, R.V. (eds.), Materials Research Society, Pittsburgh, 1991.

9. Cheung, K.P., Case, C.J., Liu, R., Schutz, R.J., Wagner, R.S., Kwakman, L.F.Tz., Huibergtse, D., Piekaar, H.W., Granneman, E.H.A. *Proc. 7th IEEE VLSI Multilevel Interconnect Conference*, 1990.
10. Kwakman, L.F.Tz., Huibergtse, D., Piekaar, H.W., Granneman, E.H.A., Cheung, K.P., Case, C.J., Liu, R., Schutz, R.J., Wagner, R.S. *Proc. 7th IEEE VLSI Multilevel Interconnect Conference*, 1990.
11. Tsubouchi, K., Masu, N., Shigeeda, N., Matano, T., Hiura, Y., Mikoshiba, N. *Appl. Phys. Lett.* **1990**, 57, 1221.
12. Bent, B.E., Nuzzo, R. G., Dubois, L.H. *J. Am. Chem. Soc.* **1989**, 111, 1634.
13. Bent, B.E., Nuzzo, R. G., Dubois, L.H. *J. Sci. Technol.* **1988**, A 6, 1920.
14. Bent, B.E., Nuzzo, R. G., Dubois, L.H. *Mat. Res. Soc. Symp. Proc.* **1988**, 101, 177.
15. Bent, B.E., Dubois, L.H., Nuzzo, R. G. *Mat. Res. Soc. Symp. Proc.* **1989**, 131, 327.
16. Gladfelter, W.L., Boyd, D.C., Jensen, K.F. *Chem. Mater.* **1989**, 1, 339.
17. Gross, M.E., Cheung, K.P., Fleming, C.G., Kovalchick, J., Heimbrook, L.A. *J. Vac. Sci. Technol.* **1991**, A 9, 57.
18. Gross, M.E., Fleming, C.G., Cheung, K.P., Heimbrook, L.A. *J. Appl. Phys.* **1991**, 69, 2589.
19. Beach, D.B., Blum, S.E., LeGoues, F.K. *J. Vac. Sci. Technol.* **1989**, A 7, 3117.
20. Dubois, L.H., Zegarski, B.R., Kao, C.-T. Nuzzo, R.G. *Surf. Sci.* **1990**, 7, 236.
21. Shriver, D.F., Atkins, P.W., Langford, C.H. *Inorganic Chemistry*, W.H. Freeman and Co., New York, 1990.
22. March, J. *Advanced Organic Chemistry*, 3rd Ed., Wiley-Interscience, New York, 1985.
23. Greenwood, N.N., Earnshaw, A. *Chemistry of the Elements*, Pergamon, Oxford, 1984.
24. Cotton, F.A., Wilkinson, G. *Advanced Inorganic Chemistry*, Wiley-Interscience, New York, 1988.
25. Lingnau, R., Strähle, J. *Angew. Chem. Int. Ed. Engl.* **1988**, 27, 436.
26. Caulton, K.G., Davies, G., Holt, E.M. *Polyhedron* **1990**, 9, 2319.
27. Ten Hoedt, R.W.M., Van Koten, G., Noltes, J.G. *J. Organomet. Chem.* **1980**, 111, 1634.
28. Cairncross, A., Sheppard, W.A. *J. Am. Chem. Soc.* **1971**, 93, 248.
29. Cairncross, A., Sheppard, W.A. *J. Am. Chem. Soc.* **1971**, 93, 247.
30. Whitesides, G.M., Panek, E.J., Stedronsky, E.R. *J. Am. Chem. Soc.* **1972**, 94, 232.
31. Tamura, M., Kochi, J. *J. Organomet. Chem.* **1972**, 42, 205.
32. Clinton, N., Kochi, J. *J. Organomet. Chem.* **1972**, 42, 229.
33. Wada, K., Tamura, M., Kochi, J. *J. Am. Chem. Soc.* **1970**, 92, 6656.
34. Whitesides, G., Stedronsky, E.R., Casey, C.P., San Filippo, J. *J. Am. Chem. Soc.* **1970**, 91, 1426.
35. Whitesides, G.M., San Filippo, J., Stedronsky, E.R., Casey, C.P. *J. Am. Chem. Soc.* **1969**, 91, 6542.

36. Ikariya, T., Yamamoto, A. *J. Organomet. Chem.* **1974**, 72, 145.
37. Miyashita, A., Yamamoto, T., Yamamoto, A. *Bull. Chem. Soc. Jpn.* **1977**, 50, 1109.
38. Miyashita, A., Yamamoto, A. *Bull. Chem. Soc. Jpn.* **1977**, 50, 1102.
39. Cotton, F.A., Marks, T.J. *J. Am. Chem. Soc.* **1970**, 92, 5114.
40. Whitesides, G., Bergbrieter, D.E., Kendall, P.E. *J. Am. Chem. Soc.* **1974**, 96, 2806.
41. Whitesides, G.M., Casey, C.P., Krieger, J.K. *J. Am. Chem. Soc.* **1971**, 93, 1379.
42. Whitesides, G.M., Panek, E.J., Stedronsky, E.R. *J. Am. Chem. Soc.* **1972**, 94, 232.
43. Cotton, F.A., Takats, J. *J. Am. Chem. Soc.* **1970**, 92, 2353.
44. Kuznetsov, G.D., Badad-Zakhryapin, A.A., Giod, F. *Protect. Met.* **1972**, 8, 565.
45. Gillardeau, J., Hasson, R., Oudar, J. *J. Crystal Growth* **1968**, 2, 149.
46. Temple, D., Reisman, A. *J. Electrochem. Soc.* **1989**, 136, 3525.
47. Van Hemert, R.L., Spendlove, L.B., Sievers, R.E. *J. Electrochem. Soc.* **1965**, 112(2), 1123.
48. Arita, Y. *Mat. Res. Soc. Proc., VLSI* **1990**, V, 335.
49. Kaloyeros, A.E., Feng, A., Garhart, J., Brooks, K.C., Gosh, S.K., Saxena, A.N., Luethers, F. *J. Electronic Mater.* **1990**, 19, 271.
50. Lai, W.G., Xie, Y., Griffin, G.L. *J. Electrochem. Soc.* **1991**, 138, 3499.
51. Jeffries, P.M., Girolami, G.S. *Chem. Mater.* **1989**, 1, 8.
52. Grieser, T., Weiss, E. *Chem. Ber.* **1976**, 109, 3142.
53. Lemmen, T.H., Goeder, G.V., Huffman, J.C., Gerts, R.L., Caulton, K.G. *Inorg. Chem.* **1990**, 29, 3680.
54. Nardi, M., Rhubright, D., Sen, A. *Inorg. Chem.* **1990**, 29, 3065.
55. Dryden, N.H., Kumar, R., Ou, E., Rashidi, M., Roy, S., Norton, P., Puddephatt, R.J., Scott, J.D. *Chem. Mater.* **1991**, 3, 677.
56. Steigerwald, M.L. *Chem. Mater.* **1989**, 1, 52.
57. Shin, H.K., Chi, K.M., Hampden-Smith, M.J., Kodas, T.T., Paffett, M.F., Farr, J.D. *Angew. Chem. Advanced Materials* **1991**, 3, 246.
58. Shin, H.K., Chi, K.M., Hampden-Smith, M.J., Kodas, T.T., Paffett, M.F., Farr, J.D. *Chem. Mater.* **1992**, 4, 788.
59. Jain, A., Chi, K.M., Hampden-Smith, M.J., Kodas, T.T., Paffett, M.F., Farr, J.D. *J. Mater. Res.* **1992**, 7, 261.
60. Reynolds, S.K., Smart, C.J., Baran, E.F., Baum, T.H., Larson, C.E., Brock, P.J. *Appl. Phys. Lett.* **1991**, 59, 2332.
61. Kumar, R., Maverick, A.W., Fronczek, F.R., Lai G., Griffin, G.L., Precursors for Chemical Vapor Deposition of Copper, 201st American Chemical Society Meeting, Atlanta, April 1991, Abstract INOR256.
62. Norman, J.A.T., Muratore, B.A., Dyer, P.N., Roberts, D.A., Hochberg, A.K. *J. de Physique* **1991**, IV(1), C2-271.
63. Jain, A., Chi, K.M., Hampden-Smith, M.J., Kodas, T.T., Paffett, M.F., Farr, J.D. *J. Electrochem. Soc.* **1993**, 140, 1434.

64. Jain, A., Chi, K.M., Shin, H.K., Hampden-Smith, M.J., Kodas, T.T., Paffett, M.F., Farr, J.D. Metallization: Performance and Reliability Issues for VLSI and ULSI, *SPIE Conf. Proc.* San Jose, CA 1991, 1596, 23.
65. Gross, M.E., Donnelly, V.M., in *Advanced Metallization for ULSI Applications*, Rana, V.S., Joshi, R.V., (eds.), Materials Research Society, 1991, 355.
66. Jain, A., Chi, K.M., Hampden-Smith, M.J., Kodas, T.T., Paffett, M.F., Farr, J.D. *Chem. Mater.* **1991**, 3, 995.
67. Baum, T.H., Larson, C.E. *Chem. Mater.* **1992**, 4, 365.
68. Levy, R.A., Gallagher, P.K., Contolini, R., Schrey, F. *J. Electrochem. Soc.* **1985**, 132, 457.
69. Hampden-Smith, M.J., Kodas, T.T., Paffett, M.F., Farr, J.D., Shin, H.K. *Chem. Mater.* **1990**, 2, 636.
70. Beach, D.B. *IBM J. Res. Develop.* **1990**, 34, 795.
71. Shin, H.K., Hampden-Smith, M.J., Kodas, T.T., Duesler, E.N. *Polyhedron* **1991**, 6, 645.
72. Shin, H.K., Chi, K.M., Farkas, J., Hampden-Smith, M.J., Kodas, T.T., Duesler, E.N. *Inorg. Chem.* **1992**, 31, 424.
73. Chi, K.M., Shin, H.K., Hampden-Smith, M.J., Kodas, T.T., Duesler, E.N. *Polyhedron* **1991**, 10, 2293.
74. Chi, K.M., Shin, H.K., Hampden-Smith, M.J., Kodas, T.T., Duesler, E.N. *Inorg. Chem.* **1991**, 30, 4293.
75. Baum, T.H., Larson, C.E., May G. *J. Organomet. Chem.* **1992**, 425, 189.
76. Bartlett, M., Palenik, G. *Acta. Cryst. Sec. A* **1969**, 25, 173.
77. Doyle, G., Eriksen, K.A., Van Engen, D. *Organometallics* **1985**, 4, 830.
78. Norman, J.A.T. *US Patent* 4 950 790, **1992**.
79. Norman, J.A.T., Muratore, B.A. *US Patent* 5 035 731, **1992**.
80. Norman, J.A.T., Dyer, P.N. *US Patent* 5 098 516, **1992**.
81. Kumar, R., Fronczek, F.R., Maverick, A.W., Lai, W. G., Griffin, G.L. *Chem. Mater.* **1992**, 4, 577.
82. Anderson, W.A., Carty, A.J., Palenik, G.J., Schreiber, G. *Can. J. Chem.* **1971**, 49, 761.
83. Restivo, R.J., Costin, A., Ferguson, G., Carty, A.J. *Can. J. Chem.* **1975**, 53, 1949.
84. Gibson, D., Johnson, B.F.G., Lewis, J. *J. Chem. Soc. A* **1970**, 367.
85. Cariati, F., Naldini, L. *Gazz. Chim. Ital.* **1965**, 3, 95.
86. Shin, H.K., Hampden-Smith, M.J., Kodas, T.T., Duesler, E.N. *J. Chem. Soc., Chem. Commun.*, **1992**, 217.
87. Gross, M.E. *J. Electrochem. Soc.* **1991**, 138, 2422.
88. Shin, H.K., Farkas, J., Hampden-Smith, M.J., Kodas, T.T., Duesler, E.N. *J. Chem. Soc., Dalton Trans.* **1992**, 1113.
89. Shin, H.-K., Hampden-Smith, M.J., Kodas, T.T., Duesler, E.N. *Can. J. Chem.* **1992**, 70, 2954.

90. Norman, J.A.T., Muratore, B.A., Dyer, P.N., Roberts, D.A., Hochberg, A.K., Dubois, L.H. *Mat. Sci. Eng. B* **1993**, 17, 87.
91. Chi, K.-M., Hampden-Smith, M.J., Kodas, T.T., Duesler, E.N., unpublished work.
92. Collman, J.P., Hegedus, L.S., Norton, J.R., Finke, R.G. *Principles and Applications of Organo-transition Metal Chemistry*, University Science Books, Mill Valley, 1987.
93. Wolf, W.R., Sievers, R.E., Brown, G.H. *Inorg. Chem.* **1972**, 11, 1995.
94. Li, H.W., Eisenbraun, E.T., Kaloyeros, A.E. *J. Vac. Sci. Tech. B. Microelectronics Processing and Phenomena* **1992**, 10, 1337.
95. Rye, R.R., Chi, K.M., Hampden-Smith, M.J., Kodas, T.T. *J. Electrochem Soc.* **1992**, 139, L60.
96. Hampden-Smith, M.J., Kodas, T.T., Rye, R.R. *Adv. Materials* **1992**, 4, 524.
97. Rye, R.R., Knapp, J.A., Chi, K.M., Hampden-Smith, M., Kodas, T. *J. Appl. Phys.* **1993**, 72(12) 5941.
98. Griffin, G.L., Lai, W.G., Maverick, A.W., Kumar, R., Ajmera, P.K. *Conf. Proc. ULSI-VII*, Rana, V.V.S., Joshi, R.V., Ohdomari, I., (eds.), Materials Research Society, 1992, 367.
99. Gross, M.E., Donnelly, V.M. in *Adv. Metallization for ULSI Applications*, Rana, V.S., Joshi, R.V. (eds.), Materials Research Society, Pittsburgh, 1991, 355.
100. Beach, D.B., LeGoues, F.K., Hu, C.K. *Chem. Mater.* **1990**, 2, 216.
101. Dupuy, C.G., Beach, D.B., Hurst, Jr. J.E., Jasinski, J.M. *Chem. Mater.* **1989**, 1, 16.
102. Blessmann, D., Grafe, A., Heinen, R., Jansen, F., Kruck, Th., Terfloth, C. *Mater. Sci. Eng.* **1993**, B17, 104
103. McGeary, M.J., Wedrich, R.C., Coan, P.S., Folting, K., Caulton, K.G. *Polyhedron* **1992**, 11, 2459.
104. Baum, T.H., Larson, C.E. *J. Electrochem. Soc.* **1993**, 140, 154.
105. Chi, K.-M., Corbitt, T.S., Hampden-Smith, M.J., Kodas, T.T., Duesler, E.N. *J. Organomet. Chem.* **1993**, 449, 181.
106. Wark, T.A., Gulliver, E.A., Hampden-Smith, M.J., Rheingold, A.L. *Inorg. Chem.* **1990**, 29, 4360.
107. Macomber, D.W., Rausch, M.D. *J. Am. Chem. Soc.* **1983**, 105, 5325.
108. Han, J., Jensen, K. AIChE Annual meeting, Miami, FL, 1992.
109. Dubois, L.H., Jeffries, P.M., Girolami, G.S., personal correspondence 1992.
110. Jeffries, P.M., Dubois, L.H. Girolami, G.S. *Chem. Mater.* **1992**, 4, 1169.
111. Guinn, K.V., Donnelly, V.M., Gross, M.E., Baiocchi, F.A., Petrov, I., Greene, J.E. *Mat. Res. Soc. Symp. Proc.* **1993**, 282, 379.
112. Cohen, S.L., Liehr, M., Kasi, S. *Appl. Phys. Lett.* **1992**, 60 (1), 50.
113. (a) Parmeter, J.E., Omstead, T.R. *Conf. Proc. ULSI-VIII* **1993**, 135; (b) Parmeter, J.E. *J. Phys. Chem.* **1993**, 97, 11530.
114. Norman, J.A.T., Roberts, D.A., Hochberg, A.K. *Mat. Res. Soc. Symp. Proc.* **1993**, 282, 347.

115. Omstead, T.R., Petersen, G.A., Smith, P.M., Gonzales, M.F. *Conf. Proc. ULSI-VIII* **1993**, 129.
116. Chiang, C.-M., Dubois, L.H. *Mat. Res. Soc. Symp. Proc.* **1993**, 282, 341.
117. Farkas, J., Hardcastle, F.D., Hampden-Smith, M., Kodas, T.T., Omstead, T., Peden, C., Blewer, R. *Advanced Metallization For ULSI Applications*, AT&T Bell Laboratories, Murray Hill, NJ, 413, 1992.
118. Farkas, J., Hampden-Smith, M., Kodas, T. unpublished work.
119. Jain, A., Farkas, J., Chi, K.-M., Hampden-Smith, M.J., Kodas, T.T. *Appl. Phys. Lett.* **1992**, 62, 2662.
120. Dubois, L.H., Zegarski, B.R. *J. Electrochem. Soc.* **1992**, 139, 3295
121. Jain, A., Jaraith, R., Kodas, T.T., Hampden-Smith, M.J. *J. Vac. Sci. Tech. B* **1993**, 11, 2107.
122. Jain, A., Farkas, J., Kodas, T.T. Hampden-Smith, M.J., Gelatos, A.V., Marsh, R., Mogab, C.J. *Mat. Res. Soc. Symp. Proc.* **1993**, 315, 105.
123. Farkas, J., Hampden-Smith, M.J., Kodas, T.T. unpublished work.
124. Gelatos, A.V., Marsh, R., Kottke, M., Mogab, C.J. *Appl. Phys. Lett.* **1993**, 63, 2842.
125. Rousseau, F., Jain, A., Kodas, T.T., Hampden-Smith, M., Farr, J.D., Muenchausen, R. *J. Mater. Chem.* **1992**, 2, 893.
126. Chiang, C.M., Miller, T.M., Dubois, L.H. *J. Phys. Chem.* **1993**, 97, 11781.
127. Xu, X.P., Goodman, D.W. *Appl. Phys. Lett.* **1992**, 61, 1799.
128. Awaya, N., Arita, Y. *Jpn. J. Appl. Phys. Pt. 1* **1993**, 32, 3915.
129. Lecohier, B., Calpini, B., Philippoz, J.M., Vandenberg, H., Laub, D., Buffat, P.A. *J. Electrochem. Soc.* **1993**, 140, 789.
130. Lecohier, B., Calpini, B., Philippoz, J.M., Vandenberg, H. *J. Appl. Phys.* **1992**, 72, 2022.
131. Chiang, C.M., Zegarski, B.R., Dubois, L.H. *J. Phys. Chem.* **1993**, 97, 6948.
132. Dubois, L.H., Zegarski, B.R. *J. Phys. Chem.* **1993**, 97, 1665.
133. Farkas, J., Hampden-Smith, M.J., Kodas, T.T. unpublished work.
134. Kiselev, A.V., Lygin, V.I. *Infrared Spectra of Surface Compounds*, John Wiley & Sons, New York, 1975.
135. *Electronic Materials Handbook, vol. 1, Packaging*, ASM International, Materials Park, OK, 1989.
136. Perry, W., Chi, K.M., Hampden-Smith, M., Kodas, T., Rye, R. *Appl. Surf. Sci.* **1993**, 69, 94.
137. Houlding, V.H., Maxwell, Jr., H., Crochiere, S.M., Farrington, D.L., Rai, R.S., Tartaglia, J.M. *Mat. Res. Soc. Symp. Proc.* **1992**, 260, 119.
138. Katagiri, T., Kondoh, E., Takeyasu, N., Nakano, T., Yamamoto, H., Ohta, T. *Jpn. J. Appl. Phys.* **1993**, 32, L1078.
139. Tompa, G.S., Wolak, E., Stall, R.A., George, M.A., Lippitt, M., Norman, J.A.T. *Mat. Res. Soc. Symp. Proc.* **1993**, 282, 323.

140. Fine, S.M., Dyer, P.N., Norman, J.A.T. *Mat. Res. Soc. Symp. Proc.* **1993**, 282, 329.
141. Smart, C.J., Reynolds, S.K., Stanis, C.L., Patil, A., Kirleis, J.T., *Mat. Res. Soc. Symp. Proc.* **1994**, 282, 229.
142. Broadbent, E.K. *IEEE Trans. Electron Dev.* **1988**, July, 952.
143. Winters, H.F. *J. Vac. Sci. Technol.* **1985**, A3 786.
144. Sesselmann, W., Chuang, T.J. *Surface Sci.* **1986**, 176, 32.
145. Sesselmann, W., Chuang, T.J. *Surface Sci.* **1986**, 176, 67.
146. Broydo, S. *Solid State Technol.* **1983**, 26, 159.
147. Gulde, P., Scholtz, C. *US Patent* 4 838 994, **1989**.
148. Schaible, P.M., Schwartz, G.C. *US Patent* 4 352 716, **1982**.
149. Howard, B.J., Wolterman, S.K., Yoo, W.J., Gittleman, B., Steinbruchel, C.H. *Mater. Res. Soc. Symp. Proc.* **1991**, 201, 129.
150. Farkas, J., Chi, K.M., Kudas, T.T., Hampden-Smith, M. in *Advanced Metallization For ULSI*, AT&T Bell Laboratories, Murray Hill, NJ, 445, 1992.
151. Farkas, J., Chi, K.M., Hampden-Smith, M.J., Kudas, T.T., Dubois, L.H. *Mater. Sci. Eng.* **1993**, B17 93.
152. Farkas, J., Chi, K.-M., Hampden-Smith, M.J., Kudas, T., Dubois, L. *J. Appl. Phys.* **1993**, 73, 1455.
153. Hampden-Smith, M.J., Kudas, T.T. *Mater. Res. Bull. Special Issue on Copper Interconnects*, June, 1993, p. 128.

Chapter 6

Chemical Vapor Deposition of Gold and Silver

Thomas H. Baum
Paul B. Comita

IBM Almaden Research Center
650 Harry Road
San Jose, CA 95120

Abstract

Chemical vapor deposition of thin metallic films of Au and Ag is reviewed. The decomposition chemistry of the metal precursor has a profound effect upon the purity of the deposited film. Recently, great progress has been made in the design and optimization of precursors for the deposition of high-purity metals such as Au and to a lesser extent for Ag. The ability to deposit conducting metal films has enabled specific applications to be addressed. The most promising applications are the laser-induced repair of "open" circuit defects, laser interconnects for customization and the repair of "clear" defects in lithographic masks.

Contents

6.1	Introduction	305
6.2	Precursors for Gold CVD	306
6.2.1	Synthesis	306
6.2.2	Physical Properties	308
6.3	Precursors for Silver CVD	310
6.3.1	Synthesis	310
6.3.2	Physical Properties	313
6.4	Deposition Mechanisms and Surface Reactions During CVD of Gold	314
6.4.1	Thermal CVD	314
6.4.2	Photochemical Deposition	317
6.4.3	Plasma-Enhanced CVD	318
6.4.4	Ion and Eletron Beam Deposition	318
6.4.5	Deposition Rates	319
6.5	Applications for Au and Ag Deposition	321
6.5.1	Laser-Induced Circuit Repair	321
6.5.2	Laser Interconnection	322
6.5.3	Laser-Induced Deposition for Bonding	323
6.5.4	Photochemically Deposited Gold Films	323
6.6	Conclusions	324
	Acknowledgements	324
	References	325

6.1 Introduction

Gold metallization is extensively used in the microelectronics industry because of its low resistivity ($2.46 \mu\Omega\text{cm}$) and inertness to chemical corrosion. As a result of its inherent chemical stability, gold may be used for applications where reliability must be rigorously maintained. In GaAs-based semiconductors, the metal interconnects are made of gold to enhance reliability and performance.¹ Commonly encountered applications for gold range from electrical contacts to integrated circuits and wiring in multi-chip packaging modules.² Other applications include its use as an absorber in X-ray lithographic masks and the repair of defects in thin-film circuits.³

Silver is the most conductive of all the metals ($1.59 \mu\Omega\text{cm}$) and for this reason is potentially useful for high-speed microelectronics applications. However, the rapid diffusion of silver into semiconductor device materials such as Si and SiO_2 and its ability to be easily corroded have limited applications of silver for metallization.⁴ Successful applications will require strict precautions to limit intermetallic diffusion and to guard against corrosive degradation. Nonetheless, some specific microelectronics applications using silver have been reported. For example, silver films have proven useful for forming contacts on and for limiting diffusion of high-temperature superconducting ceramics such as $\text{YBa}_2\text{Cu}_3\text{O}_{7-\delta}$.^{5,6}

As is the case with all chemical vapor deposition (CVD) processes, mass transport, sorption, and surface reactions are the most critical physical and chemical processes occurring during deposition. An understanding of the elementary physical processes and chemical reactions occurring during heterogeneous decomposition of the precursor on the initially uncoated substrate and on the growing metal film is necessary for a complete description of the CVD process. For CVD to be generally useful, stable metal precursors that decompose to form high-purity metals are necessary. The precursor and its molecular properties play a critical role in the CVD process because they determine the vapor pressure, the adsorption/desorption behavior, the decomposition temperature, the chemical reaction pathways, the purity of the deposit, and the deposition rate. Also, the cost, stability, ease of precursor handling, and decomposition efficiency are important considerations if CVD is to be of widespread utility for microelectronics applications. The best precursors for gold and silver CVD will perform well with regard to the criteria mentioned above.

We will describe the precursors which have been reported in the literature to deposit metallic and metal-containing films of gold and silver in Sections 6.2 and 6.3. In addition, volatile, chemically-inert decomposition reaction by-products are necessary for achieving pure metallic deposits. Thus, a basic understanding of decomposition mechanisms for the metallic precursors, especially on activated surfaces, can provide guidelines for the synthesis of precursors which are 'tailored' to produce high-purity metallic films. We will examine, in Section 6.4, the work on dissociation mechanisms

and elementary surface reactions which are important for the deposition of gold and silver. Finally, in Section 6.5, we will briefly examine some of the applications for gold and silver CVD in the microelectronics industry.

6.2 Precursors for Gold CVD

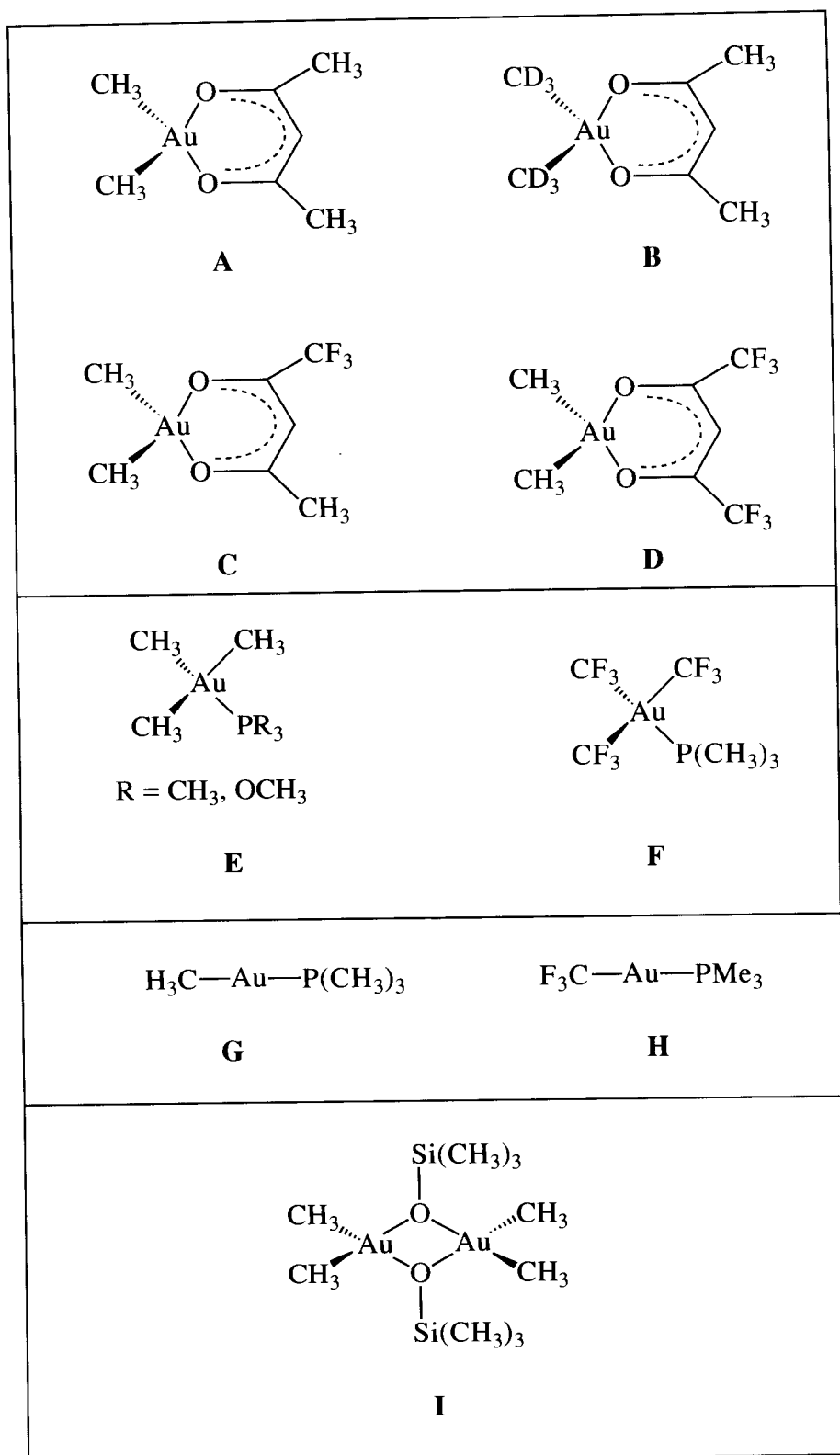
6.2.1 Synthesis

As a result of its widespread applicability, the CVD of gold, via pyrolytic decomposition, has been extensively investigated. A plethora of gold(III) (Scheme 1, A-F) and gold(I) (Scheme 1, G-I) species, which are the most common oxidation states, are known and the inorganic and organometallic chemistry of gold has also been reviewed.^{7,8} In general, the mononuclear gold(I) species are linear in geometry, while the gold(III) species have a preferred square planar geometry as for dimethyl (β -diketonato)gold(III)⁹ as shown in Figure 6-1. Many of the gold halides, including chloroauric acid (HAuCl_4) and trialkylphosphine coordinated halides, are photoactive. Organogold complexes, such as monoalkyl gold(I) or trialkyl gold(III) complexes, often undergo pyrolytic decomposition leading to gold metal films.

In general, the synthesis of organogold complexes is achieved via the reaction of Grignard or alkyl lithium reagents with the appropriate gold halide. For example, the synthesis of gold(III) complexes containing two methyl substituents was first reported using methyl magnesium iodide and gold(III) bromide,¹⁰ and there are other variations. The reaction of methyl lithium with gold(III) halides at -78°C results in the formation of "trimethyl gold(III) dimer"¹¹ which may be used as an intermediate for subsequent reaction or may be chemically trapped. For example, trapping with trialkylphosphines affords the trimethyl(trialkylphosphine)gold(III) complex. Reaction of "trimethyl-gold(III) dimer" with reagents which possess an acidic hydrogen results in the formation of methane gas and the corresponding dimethyl gold(III) analogue. Using this approach, a simplified synthesis for dimethyl(β -diketonato)gold(III) complexes has been reported.¹² This synthetic method enables dialkyl(β -diketonato)gold(III) complexes to be obtained in a single reaction vessel in two steps and in higher yields. This is a dramatic improvement over the synthesis reported originally and lowers the cost of producing larger quantities of these materials.

The synthesis of fluoroalkyl gold complexes has also been reported. The formation of both gold(I) and gold(III) species relies upon the generation of CF_3 radicals via radiolysis¹³ or via fluorinated transfer reagents, such as bis(trifluoromethyl)cadmium(II).¹⁴ Fluorinated alkyl groups may also be introduced by oxidative addition of CF_3I to Au(I) species.¹⁵ The fluoroalkyl analogues of methylgold(I) and trimethylgold(III) complexes display enhanced thermal stability and would be expected to provide increased vapor pressures at elevated temperatures due to the fluorinated substituents.

SCHEME 1



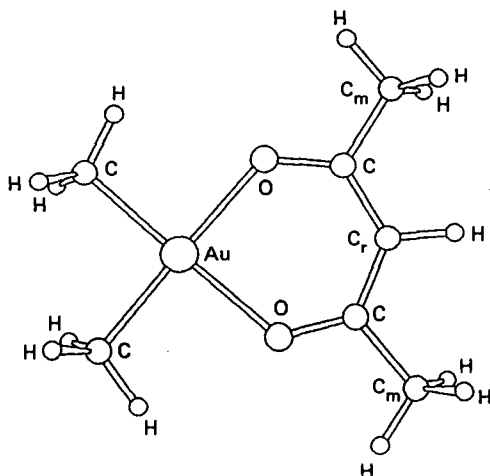


Figure 6-1 The chemical structure of dimethyl(2,4-pentanedionato)gold(III) in the gas-phase as determined by electron diffraction analysis and least-squares fit of the intensities.⁹

6.2.2 Physical Properties

A variety of gold precursors have been used for CVD (Table 6-1). The dimethyl(β -diketonato)gold(III) complexes are outstanding precursors for forming pure, electrically conducting gold films upon pyrolytic decomposition.^{16,17} The ability to alter the β -diketonate ligand affords a facile method for altering the physical state and the partial pressure of the precursor molecule. Fluorine-substituted β -diketones have higher vapor pressures than their non-fluorinated analogues,^{18,19} and a similar trend is observed for the analogous gold complexes.^{20,21} Thus, CF_3 substitution of the acetylacetonate ligand results in an increased vapor pressure of the dimethylgold(III) complex and allows for faster growth rates during pyrolytic decomposition. These precursors have been successfully used for a number of microelectronics applications (see Section 6.5).

Both thermal and photochemical processes have been used for deposition, but the best film purities were obtained via pyrolytic decomposition. Dialkyl(2,4-pentanedionato)gold(III) was first synthesized in 1939 and was reported to be photoactive in ethanol solution upon ultraviolet (UV) exposure.¹⁰ More recent work has demonstrated that gold-containing films can be deposited upon UV irradiation of the gas-phase reactant.²² These films were contaminated with varying amounts of carbon which were dependent upon the wavelength of UV irradiation. In general, the entire class of dimethyl(β -diketonato) gold compounds produce high-purity gold films when thermal processes are

Table 6-1 Reactants for Gold Deposition (NA = not available).

Reactant	Film Composition	Film Resistivity (x bulk)	Deposition Temp Range (°C)	Refs.
Me ₂ Au(hfac)	100% Au, 0% C	1.2x	225-275	78
Me ₂ Au(tfac)	100% Au, 0% C	2x	200-300	77
Me ₂ Au(acac)	95% Au, 5% C	NA	200-300	77
MeAu(PMe ₃)	96% Au, 4% C	NA	200	20
Me ₃ Au(PMe ₃)	95% Au, 5% C	NA	200	20
CF ₃ Au(PMe ₃)	NA	NA	NA	8
(CF ₃) ₃ Au(PMe ₃)	NA	NA	NA	8
((CH ₃) ₂ AuOSiMe ₃) ₂	NA	NA	135	27
MeAu(CNMe)	83% Au, 10% C	NA	200	20

used; the electrical resistance varies from 1.2 to 10 times bulk gold ($2.4 \mu\Omega\text{cm}$) depending upon the method and conditions used during pyrolytic film growth. Similar results have been found with the diethyl compounds.^{23,24} In some cases, the morphology of the deposited gold can vary dramatically²⁵ and thereby alter the electrical properties.^{15,21}

Other gold complexes have proven useful for gold film formation. Methylgold(I) and trimethylgold(III)trimethylphosphine complexes have been used for CVD²⁶ and laser-induced deposition.^{27,28} The reaction chemistry has not been studied in detail for CVD processes. However, the thermal decomposition of trimethylgold(III)trialkylphosphines in solution has been studied in detail. At 120 °C, reductive elimination of the methyl groups occurs with the formation of ethane (57 %) and methylgold(I)trialkylphosphine as the primary reaction products.²⁹ At higher reaction temperatures (170 °C), decomposition of methylgold(I)trialkylphosphine occurs with the formation of free trialkylphosphine, gold metal, and ethane. In the latter reaction, methyl radicals are produced and recombine to form ethane.²⁹ It was later shown that the first step to decomposition was liberation of the trialkylphosphine group.^{30,31}

The pyrolytic decomposition of both methylgold(I) and trimethylgold(III)-trimethylphosphine has been utilized to form gold films of high purity. For the gold(I) complex, a laser deposited gold film displayed a purity of 98 % and a low resistivity ($4.2 \mu\Omega\text{cm}$).²⁷ The laser-induced deposition of gold via decomposition of trimethylgold(III)-trimethylphosphine was achieved using an excimer laser operating at 248 nm.²² In the latter case, the gold(III) complex was condensed onto the desired substrate and irradiated. The high purity obtained is believed to be due to laser heating of the substrate. This is in direct contrast to the poor film purity normally obtained via strictly gas-phase photolytic

dissociation of organometallic precursors.³² Interestingly, fluoroalkylgold(I) and gold(III) trialkylphosphine species have been synthesized,¹⁴ but CVD of gold films has not been reported from these species. The fluorinated complexes display greater thermal stability than the analogous alkyl complexes; these complexes should offer greater volatility at elevated temperatures and thus, faster film growth rates by CVD.

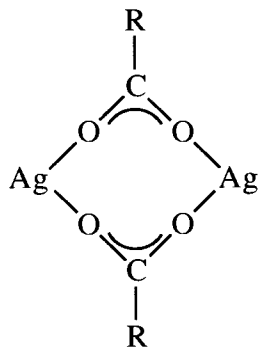
Other gold(I) and gold(III) complexes can also be used for gold CVD. For example, a gold(III) compound which is volatile and thermally decomposes to gold metal is dimethyl (trimethylsiloxy) gold(III) dimer.³³ This complex is a dimer with bridging siloxyl groups, is readily sublimed in vacuum, and decomposes to gold metal at 135 °C. Although this complex displays potential for gold CVD, a rigorous study has not been reported. A series of gold(I) isocyanates has been used to deposit gold films upon pyrolysis.²⁶ An assortment of compounds of this general class was synthesized and displayed varying physico-chemical properties. In general, these materials offer viable alternatives for gold CVD as a result of their volatility and clean decomposition pathways. In some cases, however, chemical substitution with bulky alkyl or aryl groups produce complexes with decreased volatility. In general, these complexes have been used to deposit gold films via pyrolytic decomposition of solid-state precursors.^{34,35} Other gold species, such as gold azide complexes, can be used to photochemically form gold metal via UV irradiation of both solutions and solid films.^{36,37} Upon photolysis, nitrogen is evolved and colloidal gold is deposited. Similarly, gold(I) mercaptide resins can be used to form metal films upon pyrolytic decomposition, but this topic is beyond the scope of this chapter.

6.3 Precursors for Silver CVD

6.3.1 Synthesis

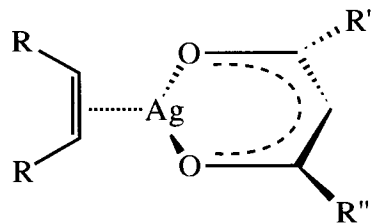
A variety of silver(I) complexes are readily synthesized via reaction of silver oxide (Ag_2O) with acidic reagents; carboxylic acids react to form silver(I) carboxylates and β -diketones react to form silver(I) β -diketonates (see Scheme 2). The silver(I) carboxylates exist as dimeric species in the gas-phase.³⁸ The synthesis of mononuclear silver(I) species can be achieved upon coordination of Lewis bases, which are present during the synthetic reaction. For example, both alkene- and diene- stabilized silver(I) species³⁹ and silver(I)(β -diketonato) complexes have been reported.⁴⁰⁻⁴³ Similarly, trialkylphosphine derivatives of silver(I) carboxylates⁴⁴ and silver(I) (β -diketonates) are known.^{40,45} Other organosilver(I) complexes have been synthesized by reacting silver(I) halides with the appropriate reactants. For example, η^5 -cyclopentadienyl silver(I)⁴⁶ and perfluoro-1-methylpropenyl silver(I)⁴⁷ were formed via reaction of silver(I) halide with lithium

Scheme 2



$R = \text{CH}_3, \text{CF}_3, \text{alkyl (eg. C}_{12}\text{H}_{25})$

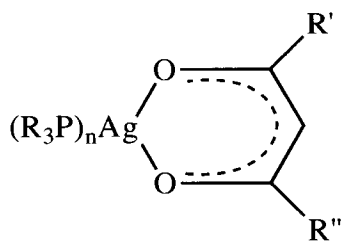
A



$R' = R'' = \text{CH}_3, \text{CF}_3$

$R' = \text{CH}_3, R'' = \text{CF}_3$

B

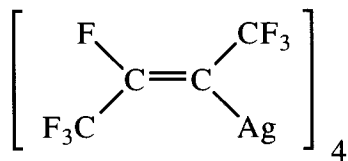


$R = \text{CH}_3, \text{C}_2\text{H}_5, \text{C}_6\text{H}_6$

$R' = R'' = \text{CH}_3, \text{CF}_3$

$R' = \text{CH}_3, R'' = \text{CF}_3$

C



D



Ag

PR_3

$R = \text{CH}_3, \text{C}_2\text{H}_5, \text{C}_6\text{H}_6$

E

cyclopentadiene or perfluoro-2-butyne ($\text{CF}_3\text{C}\equiv\text{CCF}_3$), respectively. Further, organic alkynes have been used to stabilize silver(I)³⁹ and recently alkyne complexes of silver(I) β -diketonates were synthesized.⁴³

The chemistry of silver has been widely investigated as a result of its photoactivity and widespread application in the photographic film industry. A great deal of the information, however, relates to silver halides and other inorganic silver salts. The photoactivity of these species, upon irradiation with visible light, results in the formation of silver metal nuclei and forms the basis for black and white photography. However, most silver halides or inorganic salts are non-volatile and thus are of limited value for gas-phase processing. Nonetheless, several silver(I) halides have been explored for CVD. The solids were heated to elevated temperatures or used in a powder feed method and reacted between 300 and 900 °C.⁴⁸ In the case of silver(I) fluoride, silver deposition on silicon substrates at 600 °C proceeded with etching of the surface.⁴⁹ The mechanism of the overall reaction was postulated to be:



This latter process would be self-limiting based upon the proposed reaction mechanism. However, as has been reported for WF_6 decomposition for forming W films,⁵⁰ SiH_4 or H_2 can be used as a co-reactant to overcome these limitations. All of the silver halide systems require elevated temperatures for volatilization of the precursor and reaction to deposit silver metal. Thus, the utility of these reactants is somewhat limited. Organosilver and silver coordination complexes, on the other hand, are quite common, may exist as mononuclear complexes, decompose at lower temperatures, and offer a wide range of materials which can be explored for CVD.

Silver(I) (β -diketonato) complexes reportedly form silver films upon thermal decomposition.⁴⁸ Although only limited details were given, it is not unexpected that this molecular structure would result in high-purity silver films based upon the large body of knowledge available for metal film formation upon pyrolysis of metal β -diketonates. Lastly, the use of alkene and diene (β -diketonato) silver(I) complexes for silver CVD has recently been achieved.⁴³ Although a great number of organosilver species can be synthesized, relatively few have been used for CVD. This is primarily due to the lack of technological interest in silver metallization and the modest vapor pressures of these complexes. On the other hand, silver complexes are inexpensive and provide economical alternatives to more expensive metal precursors.

Other organosilver complexes have been reported in the patent literature for depositing silver films. For example, the (cyclopentadienyl)silver(I)trialkylphosphine complexes were disclosed.⁵¹ In this case, the cyclopentadienyl ligand is believed to be η^5 -bonded to the metal center,⁴⁶ but no details for forming silver films were given. Similarly, other silver(I) precursors have been utilized for forming silver films via pyrolytic CVD.⁵² Lastly, photochemically induced deposition of silver from silver(I) azide was reported.³⁷

6.3.2 Physical Properties

Many precursors have been used for Ag CVD (Table 6-2), but almost no studies of the decomposition mechanism of organosilver(I) complexes during CVD are reported in the literature. However, the thermal decomposition of neophyl(tri-*n*-butylphosphine) silver(I) has been studied in the liquid phase.⁵³ Thermal decomposition results in free-radical formation based upon the identity of the reaction products and their similarity to neophyl(tri-*n*-butylphosphine)copper(I) decomposition products. Based upon these results, it was determined that both complexes decomposed by a similar mechanism, namely free-radical reaction pathways, in the absence of β -hydrogens. In general, many organosilver(I) complexes will produce free organic radicals upon pyrolytic decomposition as a result of the limited reaction pathways which are available. For example, copper(I) complexes can undergo a disproportionation reaction whereby copper(II) and Cu(0) species are formed (see Ch. 5). This reaction pathway should not be as easily accessed for silver(I) precursor decomposition to silver(0) metal although the disproportionation of silver(I) via silver(III) is known.⁵⁴

Table 6-2 Reactants for Silver Deposition (NA = not available).

Reactant	Film Composition	Film Resistivity (x bulk)	Deposition Temp Range (°C)	Refs.
Ag(trifluoroacetate)	100% Ag, 0% C	NA	600	41
Ag(acetate)	100% Ag, 0% C	100x	380	49
Ag(neodecanoate)	NA	NA	NA	50
Ag(C ₄ F ₇)	99% Ag, 1% C	1.2x	80-120	62
Ag(acac)	NA	NA	NA	41
(alkene)Ag(acac)	95% Ag, 5% O	3x	200-250	6
(C ₅ H ₅)Ag(PR ₃)	NA	NA	NA	45

The laser-induced decomposition of silver(I) carboxylates has been used to deposit silver films. For example, the pyrolytic deposition of silver from silver(I) trifluoroacetate was reported.⁵⁵ In this work, the precursor was heated to 60 °C to provide a suitable concentration of the reactant in the gas-phase and laser-induced pyrolysis enabled silver films to be selectively deposited onto the substrate. Although the purity of the deposited films was not reported, this precursor appears to be useful for forming electrically conductive silver films. More recently, this material was used for the deposition of silver films via conventional CVD.⁴⁸ High-purity silver films were deposited under optimized

conditions consisting of 600 °C substrate temperature and a H₂ flow rate of 1 L/min. Films with good morphology and low resistivity were produced. These deposition temperatures are suitable for copper-oxide based superconducting films, but may be of little value for thermally sensitive microelectronic components.

In related work, the laser-induced pyrolysis of a solid film of silver(I) acetate was reported.⁵⁶ Pure silver films could be selectively deposited onto Mn-Zn ferrite substrates at temperatures in excess of 380 °C in an evacuated atmosphere. However, the resistivities of these pure films were 10⁻³ to 10⁻⁴ Ωcm and probably result from the poor morphology of the films. In a similar fashion, decomposition of a silver(I) neodecanoate film enabled the selective fabrication of metal circuits on a solar cell.⁵⁷ In this latter study, the film was used as a base layer for subsequent copper electroplating. Other silver(I) carboxylates could be useful for forming silver films via pyrolytic decomposition. Also, silver films have proven useful for forming contacts on and for limiting diffusion of high-temperature superconducting YBa₂Cu₃O_{7-δ} films.⁴⁸ Silver incorporation in the bulk of YBa₂Cu₃O_{7-δ} reportedly improves the electrical properties.^{5,6}

6.4 Deposition Mechanisms and Surface Reactions During CVD of Gold

The surface chemical reactions which occur during CVD determine the purity of the deposit and the deposition rate. Both of these characteristics will ultimately determine the usefulness of a particular reactive system for producing metal films. High precursor pressures, on the order of 1 torr, are necessary to achieve the rapid surface reaction rates which are required for many practical applications. Under these conditions, a number of physico-chemical processes can influence the rate of the surface deposition reactions. High surface reaction rates can result in a deposition rate which is limited by the flux of reactant from the gas phase to the heated region of the surface.⁵⁸ A further complication is that reactions can occur both on the substrate surface and in the gas-phase, as may be encountered in photolytic CVD or plasma-enhanced CVD. Therefore, in order to study deposition reactions which occur in the high pressure regime, the influence of gas-phase processes such as diffusion and surface chemical reactions must be understood.

6.4.1 Thermal CVD

The surface chemical reactions occurring during the laser-assisted deposition of gold from dimethyl(hfac)gold(III) have been studied using a diffusive transport relaxation technique.^{59,60} This technique was developed to study laser-induced deposition

processes under standard reactor conditions with moderate vacuum. For these conditions, the biggest problem is detecting the extremely small amounts of product species that are formed when a micron-sized area on a substrate is heated by a laser and differentiating these species from those formed by fragmentation of the reactant in the mass spectrometer. The technique relies on modulation of the laser light intensity which induces a modulation of the surface temperature and surface reaction rate. Modulation of the surface reaction rate produces modulations in the gas-phase reactant and product concentrations but only for the case of high pressures which provide gas-phase transport-limited deposition. The modulations of the reactant and product species concentrations are out of phase because as reactant is consumed, the product is formed. Thus, ionization and fragmentation of the product species can be differentiated from the reactant species due to the phase-sensitive nature of the detection scheme. The species above the surface are sampled by an orifice located at the center of the heated zone and form a molecular beam from the sampling orifice by flowing into a differentially-pumped high-vacuum chamber. The components in the beam are detected with a quadrupole mass spectrometer and a phase-sensitive detector. In the case of surface reaction limited deposition, the concentrations of species in the gas phase are constant and uniform because there is no transport limitation which would lead to concentration gradients. Thus, for these conditions, no information about the identity of reaction products can be obtained.

The laser-induced dissociation pathway for (hfac)AuMe₂ is photothermal with negligible photochemical reaction occurring at 514 nm.¹⁶ This feature eliminates contributions from gas-phase and surface photochemical reactions. Only a single reaction product remains on the surface, metallic gold, which has a purity greater than 95 atom % as measured by standard surface analytical techniques. Thus, the surface reaction is simple and well characterized, an important characteristic since surface species are not measured or observed in real time. Because the deposition process is photothermal, the surface reaction rate depends on the laser intensity only through the temperature rise induced by the laser. Transient signals were observed due to modulation of the laser light for sufficiently high pressures and laser powers [small Kn / α (where $\text{Kn} = \text{Knudsen number based on gas mean-free path and deposit size}$ and α is the fraction of collisions of the reactant with the surface that lead to deposition)] as expected theoretically.⁵⁹ Both reactant and product signals were observed. The most prominent positive ion signals and their molecular fragment assignments for gold deposition from dimethyl(hfac)gold(III) were used to deduce the identity of the desorbed product species formed by the surface chemical reactions. The phase-sensitive detection scheme is important for precursor molecules like dimethyl(hfac)gold(III) because fragments from ionization in the mass spectrometer form species identical or similar to the pyrolytic decomposition products. Comparison of spectra obtained with and without reaction cannot be used to identify reaction products because the amount of product is extremely small relative to the amount of reactant. However, by using this modulation technique the molecular ion signal is out-of-phase with the laser light and product signals due to gas-phase depletion of the reactant

concentration and the increase in product concentration via surface pyrolysis. The high m/e signals with the same phase as the molecular ion are daughter ions of the molecular ion and were assigned by analogy to other metal β -diketonates.⁶⁰

The most unambiguous reaction product signal was for ethane at m/e 30 and its daughter ion m/e 28, both of which were in phase with the laser light (their concentrations increased as the laser light intensity and surface temperature increased indicating they were reaction products). Thus, one reaction channel was the production of ethane via elimination and recombination of two methyl ligands. The remaining signals suggested the presence of two additional reaction products. Strong in-phase signals were observed at m/e 153, 151, 97, and 84. The m/e 153 ($C_5H_4O_2F_3$) may be the base peak in the ligand combination product which has a parent peak of m/e 222. This conclusion is supported by previous work which has shown that fragmentation of fluorinated β -diketonate ligands occurs with cleavage of the $C(O)-CF_3$ bond.⁶¹ Regardless of the precise surface reaction mechanism or ionic fragmentation mechanism, the presence of m/e 153 shows that the methyl ligand is involved in two important dissociation pathways: one channel to form ethane and one channel to form a methylated β -diketone product m/e 153. Evidence for a third reaction channel yielding hexafluoroacetylacetone was also found. To summarize, three species were identified as reaction products derived from the deposition of gold from dimethyl (hfac)gold(III): (1) ethane (m/e 30) which results from elimination and recombination of two methyl ligands; (2) a product which gives rise to a base peak at m/e 153 and results from the combination of a methyl and hfac ligands; and (3) hexafluoroacetylacetone, a combination of the hexafluoroacetylacetone ligand and a hydrogen atom.

In the dimethyl gold(III) β -diketonate complexes, the reductive elimination of the methyl groups provides a means for removing the carbon-containing alkyl ligands during pyrolysis. Reductive elimination indicates that the formal oxidation state and coordination number are reduced by two^{62, 63} without describing the mechanism for elimination. Typically, the *cis*-alkyl groups which are eliminated recombine and provide a method for evaluating the mechanism of reductive elimination. Both solution and gas-phase studies of pyrolytic decomposition of these complexes have found ethane to be a major by-product of the decomposition reaction. In a series of deuterium labeling studies, in which half of the starting gold complex was protonated (d_0) and half was fully deuterated (d_6) at the methyl groups, d_0 -ethane was the predominant recombination product; the d_0 -ethane to d_3 -ethane ratio was 3.6:1.⁶³ A small percentage of the reaction proceeds via free-radical recombination as evidenced by the formation of d_3 -ethane and methane (3% at 50% conversion) products. This study implicates the concerted intramolecular elimination of two *cis*-methyl groups to form ethane as the major reaction pathway and only a minor reaction pathway for methyl radical formation followed by intermolecular recombination. Although some solvent cage effects were noted in this decomposition, similar results were obtained in solvents of widely differing polarity. To date, no rigorous studies of the selective deposition of gold films have been reported.

6.4.2 Photochemical Deposition

The photolysis of dimethyl (hfac)gold(III) adsorbed on quartz substrates was examined with a time-of-flight (TOF) mass spectral technique.⁶⁴ In this work, dimethyl (hfac)gold(III) was adsorbed on a cooled quartz surface and photolyzed using the 222 nm line of a KrCl laser. The same laser pulse was used to desorb the reactants and photolysis products from the cooled surface. As expected, the fragmentation channels for the 222 nm photoexcitation and desorption are more complex than those observed in the thermal decomposition. This is due to the higher energy reaction channels which are available from either the excited electronic states which are accessed or the much higher temperatures which are used in this experimental set-up to desorb the reaction products.

The reactants which were desorbed could be characterized by a Maxwell-Boltzmann temperature distribution of 900 K. The different temperature distributions of the smaller fragment ions allowed the investigators to distinguish the surface reaction products from those resulting from electron impact (EI) fragmentation in the ion source of the mass spectrometer. A dimethyl gold product was observed as well as methyl gold and desorbed or ablated gold atoms. The methyl gold fragment appeared to not arise from dimethyl gold as evidenced by their different TOF temperature distributions. The CF₃-containing fragments appear somewhat more complex to characterize due to contributions to their distributions from the photodesorption of dimethyl(hfac)gold. Interestingly, a photoproduct resulting in *m/e* 153 was formed via photolysis at 222 nm as was found in the thermal decomposition. This indicates that the methyl radical is reacting with the hfac ligand, either in the dimethyl(hfac)gold(III) reactant or as free hfac ligand radical adsorbed on the surface. However, in contrast to the thermal results⁶⁰ and the solution photolysis of the non-fluorinated analogue,⁶³ no evidence for the reductive elimination of ethane was reported. However, extensive fragmentation of the hfac ligand was found, apparently enhanced by the nature of the excitation source. The differing reaction channels upon photolysis may be indicative of the source for carbon and oxygen contamination from these species in comparison to the pyrolytic decomposition pathways. Further, secondary photolysis of the hfac ligand product can result in other reactive carbon-containing species which may be difficult to desorb during film growth. Solution mechanistic studies during photolytic decomposition revealed an increased free radical character as evidenced by the formation of 3-methyl-2,4-pentanedione as a major by-product.⁶³ Further, when 50% of the starting material was d₆-dimethyl(2,4-pentanedionato)gold(III), d₃-ethane was also found as a reaction product. Both of these products are indicative of free methyl radical recombination with 2,4-pentanedione and deuterated methyl radical.

6.4.3 Plasma-Enhanced CVD

Plasma enhanced chemical vapor deposition (PECVD) has been used to deposit pure gold films, gold oxide films, and gold-polymer films.^{65,66} In all cases, dimethyl (2,4-pentanedionato)gold(III) was used as the precursor. For PECVD of gold containing films, a variety of experimental conditions were reported which gave rise to many different film compositions. No work has been reported to date which attempts to define the species and reactions which are important in these processes.

PECVD has also been used for silver film formation.⁶⁷ In these studies, high-purity silver films were deposited with a resistivity of $2 \mu\Omega\text{cm}$ using a silver(I) perfluoro-1-methylpropenyl complex. The film composition varied with substrate temperature, rf power and hydrogen concentration during deposition. Although this complex was useful, growth rates were relatively slow ($8\text{--}55 \text{ \AA}/\text{min}$) owing to the modest vapor pressure of the complex. A cost comparison between this complex and silver(I) trifluoroacetate favored the latter complex for the formation of silver films by pyrolytic CVD.⁴⁸

6.4.4 Ion and Electron Beam Deposition

Ion beam deposition of gold containing films has been accomplished with dimethyl (hfac)gold(III) with energetic argon or gallium ion beams.⁶⁸⁻⁷² Electron beam deposition has also been accomplished^{73,74} as well as deposition with a scanning tunneling microscope tip.^{75,76} Localized deposition with submicron resolution was obtained with Ga^+ ions, but the films contained some Ga metal under all conditions. Even so, some deposited lines exhibited close to bulk conductivity of gold. For energetic Ar^+ beam deposition, the films were typically $> 90 \text{ wt } \%$ Au and contained mainly carbon, at levels of 30-50 at % by Auger electron spectroscopy, as the major impurity. Generally, the yield of gold atoms per incident ion increased with increasing precursor gas pressure and decreasing substrate temperature. This was thought to result from an increase in the adsorption of dimethyl (hfac)gold(III) on the substrate surface. No attempt was made to define the important dissociation pathways during energetic ion bombardment of the precursor.

Focused electron beams have been used to deposit gold-containing films. However, the films incorporated a high percent of carbon.^{73,74} Unfortunately, the mechanism for carbon incorporation in these films has not been investigated. High aspect ratio features are readily deposited and the ability of these films to block X-rays has been demonstrated. Sub-micron, high aspect ratio gold films deposited by focused electron beam CVD are shown in Figure 6-2.

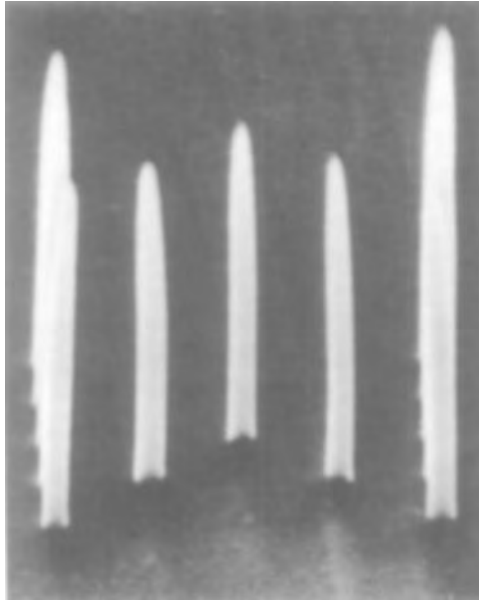


Figure 6-2 Sub-micron, high-aspect ratio gold features deposited using focused electron beam with dimethyl (trifluoro-2,4-pentanedionato)gold(III). Features are roughly $0.2\ \mu\text{m}$ in width.⁷⁴

6.4.5 Deposition Rates

In CVD processes, the overall rate of the reaction can be controlled by the rate of gas-phase or surface reactions, or by the rates of reactant and product transport in the gas phase. In conventional CVD processes, the reaction zone is usually much larger than the gas mean-free path, leading to purely diffusive transport. In contrast to bulk or blanket coating processes, laser, ion or electron beams are generally used to drive chemical reactions in a selected region. For localized reaction zones, the kinetics of deposition can still be influenced by mass transport processes.⁵⁸ The difference in the transport mechanisms between laser-driven and conventional large-area CVD processes leads to the wide differences in rates that can be obtained. For laser-driven reactions, the relative importance of reaction and transport in determining the overall rate is influenced by physical length scales which include the geometry of the deposition apparatus, the size of the reaction zone, and the mean-free path of the gas which surrounds the reaction zone.

Using conventional CVD techniques, blanket films of gold metal have been deposited.^{77,78} The precursor used was dimethyl(hfac)gold(III) because of its liquid

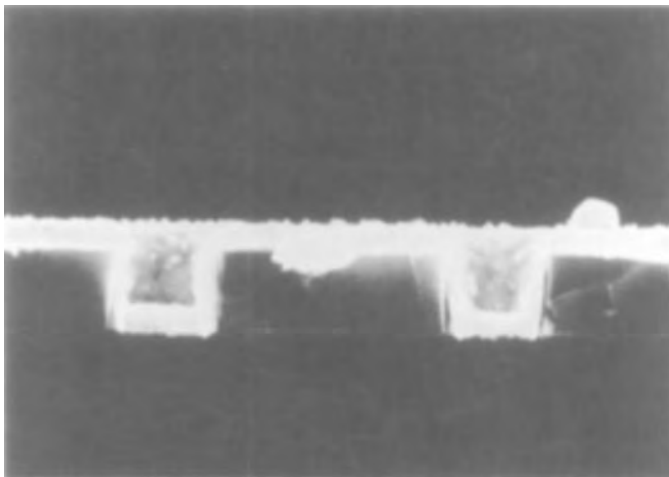


Figure 6-3 Micrograph of a gold film obtained by CVD of dimethyl(hfac)gold(III). Deposited film displays good conformal coverage of the surface features (1.3 μm wide vias).⁷⁸

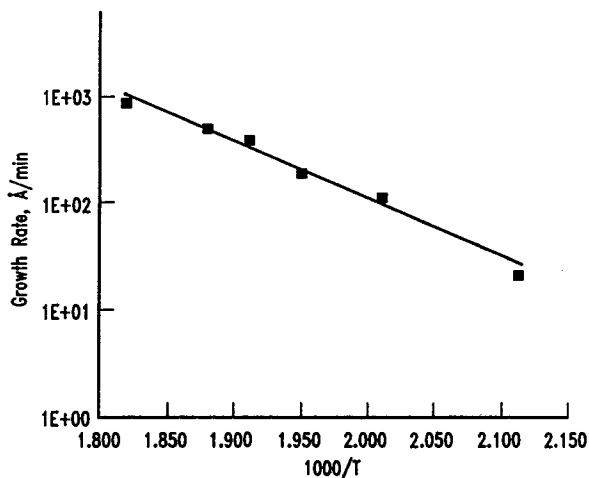


Figure 6-4 Arrhenius plot for growth rate of gold via pyrolytic decomposition of dimethyl(hfac)gold(III) versus inverse of surface temperature during deposition. Activation energy (E_a) was calculated from linear fit and is 25 kcal/mole.⁷⁸

physical state under ambient conditions and increased volatility, compared to the non-fluorinated analogues. The ability to fill high aspect ratio vias and to produce conformal films (Fig. 6-3) was demonstrated.⁷⁸ The morphology of the gold films can be controlled by altering the substrate temperature and buffer gas pressures during deposition. An activation energy of 25 kcal/mole was determined from an Arrhenius plot for CVD from dimethyl(hfac)gold(III) as shown in Figure 6-4.

For pyrolytic gold deposition with a visible laser, vertical growth rates in excess of 3 $\mu\text{m/s}$ were reported from dimethyl(hfac)gold(III).⁷⁹ This work provided the first rigorous comparison of measured and theoretically estimated rates for laser-induced chemical vapor deposition (LCVD), and analytical solutions for all Knudsen numbers were discussed.⁸⁰ For $\text{Kn} \sim 1$, the transition regime between diffusive and ballistic transport, a fit to the experimental vertical growth rate data provided a value for the reaction probability for dimethyl (hfac)gold(III) of approximately 0.6. At high buffer gas pressure, the growth of gold becomes diffusive, and due to the localized heat source of the laser, the deposits can become dendritic.²⁵ The morphology of the deposits can be substantially varied depending on the buffer gas composition, pressure, and laser fluence. In some cases, volcano-like structures can be obtained.^{17,81}

6.5 Applications for Au and Ag Deposition

6.5.1 Laser-Induced Circuit Repair

The laser-induced deposition of gold for the repair of thin-film circuitry has been demonstrated and incorporated into a manufacturing process.^{82,83} The deposition parameters must be maintained to achieve comparable dimensions to the existing metallurgy, to obtain low contact resistances, and to afford repairs which are reliable in post-processing conditions. Further, the repairs must withstand electrical stressing and cycling, exposure to elevated temperature and humidity, and must not electrically degrade with time. Laser-induced CVD of gold meets the above requirements because it provides deposits with high purity, low resistivity, and inertness to chemical decomposition. The thin-film redistribution layers on IBM system 390 multi-chip modules occasionally display open electrical defects. These electrical defects are missing regions of metallurgy (voids) or have a particle imbedded into the polyimide layer and result from particulate contamination either during the lithography or metallization processes. In a typical repair of "open" defects on the multi-chip modules, a low-power laser scan is used to induce gold deposition on the polyimide layer without any surface damage. This is followed by several scans at an intermediate laser power to deposit the desired thickness of gold (roughly 8 μm). Lastly, a high-power laser scan is used at the points of intersection

between the existing metallurgy and the gold metal repair. This ensures good overlap of metal and excellent contact resistance. The ability to repair circuits over surface imperfections such as cracks has been achieved by this technique. Most of the repaired modules have been processed in accordance with the build plan for the completed module; this consists of subsequent polyimide overcoat, polyimide curing cycles, pin-braze, and chip bonding cycles. The electrical integrity of the repaired circuits is excellent, and the circuits are virtually identical to those which were not repaired. An example of a laser-deposited gold repair on a prototype multi-chip module is shown in Figure 6-5.

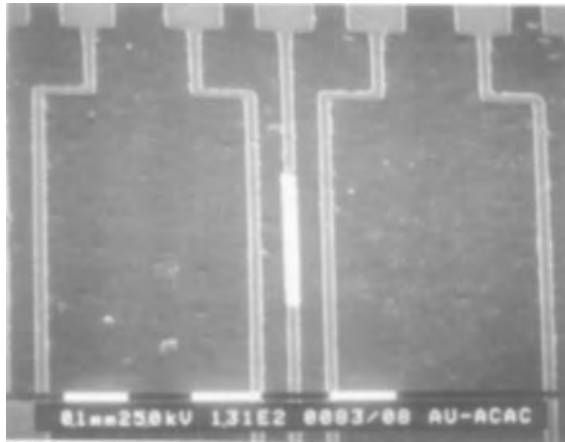


Figure 6-5 Laser-deposited gold used to repair circuit defect (open) on prototype multi-chip module with polyimide dielectric layer. Designed circuits are 15 μm in width and repaired region is in center of micrograph.

6.5.2 Laser Interconnection

In a similar manner to circuit repair, laser CVD can be utilized to interconnect two discrete regions on a module or integrated circuit. This process may be carried out to rewire a defective region of a circuit or to customize the component for a specific design or application. In any application, the laser-deposited metal must meet the electrical requirements of being highly conductive and reliable.

The laser-induced deposition of gold has been used to interconnect features on prototype multi-chip modules. For example the wiring of two large engineering-change (EC) pads has been explored via pyrolytic decomposition of dimethyl(hfac)gold. These connections can be deposited in an analogous manner to that used for circuit repair, but

using shorter processing times (i.e., 30 seconds). The electrical integrity was good and resistances could be minimized by a careful choice of the laser conditions. In general, low resistance connections can be rapidly made on polyimide substrates. Laser "written" interconnects and complete circuitization of low-end components on polyimide was also demonstrated.⁸³ High-purity gold deposits could be formed for interconnection with good electrical properties under specific laser powers and scan velocities.

Laser circuitization and interconnection has been used for solar cell applications.⁵⁶ In this study, laser-induced deposition of silver from Ag neodecanoate thin films was used to define a base layer for the subsequent plating of copper. Fast scan velocities could be utilized and improved contact resistances were obtained. Other solar cell designs require a surface layer of gold and this is a potential application for gold CVD or LCVD.

6.5.3 Laser-Induced Deposition for Bonding

The laser deposition of gold films for bonding applications has been demonstrated.³ Dimethyl(β -diketonato)gold(III) complexes were pyrolyzed using a focused argon ion laser (514 nm). Thin gold films were deposited onto free-standing beams of a thin film carrier or tape automated bond (TAB) style chip carrier. These chip carriers require low-cost methods for forming Au bonding sites; thermocompression bonding is used to connect the integrated circuit (IC) to the inner leads of the carrier circuitization. Therefore, the inner lead fingers require gold films for thermocompression bonding. The ability to laser deposit gold films onto the inner leads avoids repeated lithographic steps and use of plating solutions; it can be rapidly accomplished and can reduce waste of the precious metal by enabling selective gold deposition only onto the bonding sites. Exploratory studies have demonstrated the feasibility for laser depositing gold and for successfully bonding ICs. Preliminary pull-test values are comparable to values obtained by plating techniques.

6.5.4 Photochemically Deposited Gold Films

The photolytic decomposition of dimethyl(β -diketonato)gold(III) produces gold-containing films.²² The ability to pattern the incident irradiation, either from an excimer laser or UV lamp, enables selective patterns to be deposited by this method.⁸⁵ Using an excimer laser which was patterned with a mask and projected onto a substrate, reflective films containing gold metal were deposited, as shown in Figure 6-6. The minimum resolution was 2 μm but later was refined to 1.6 μm resolution.⁸⁶ These films display poor electrical properties but are useful for correcting transparent defects in lithographic

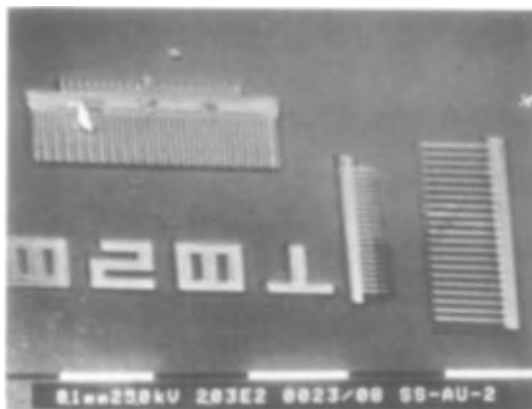


Figure 6-6 Gold pattern photochemically deposited with an excimer laser operating at 248 nm using dimethyl(2,4-pentanedionato) gold(III).⁸⁵

masks⁸⁷ or for the selective catalysis of electroless plating solutions.⁸⁸ Therefore, this technique has the potential for both "direct" and "indirect" selective metallization schemes.

6.6 Conclusions

This chapter presents the state of published work on gold and silver CVD, and shows the variety of precursors available for CVD of these metals to be substantial. However, only a few quantitative studies on deposition kinetics, film properties, film morphology, and the mechanisms of precursor decomposition have been reported to date. Presently, little is known about the quality of the deposited films and how the precursor properties influence both purity and morphology of film growth for the variety of deposition techniques. Even less is currently known about the selectivity of film growth both for gold and silver CVD. Given these facts, substantial detailed research is necessary and it is hoped that the present text will encourage such investigations.

Acknowledgments

The authors would like to thank Stephen Zuhoski, Scott Reynolds, and Karen Holloway for the gold CVD results shown in Figures 6-3 and 6-4 and Kam Lee for the results on electron beam induced gold deposition shown in Figure 6-2. The collaborative efforts of Tom Wassick, Carl Larson, R. Bryan Klassen, Carol Jones, Carol Kovac, Natalie Feilchenfeld, Carolyn Paddock, and Toivo Kodas are gratefully appreciated. We would also like to thank the IBM Corporation and its divisions at East Fishkill, N.Y. and Endicott, N.Y. for their support.

References

1. Oren, M., Masum Choudury, A.N.M. *J. Electrochem Soc.* **1987**, 134(3), 750.
2. See for example *IBM J. Res. Devel.* **1992**, 36(5), 817.
3. Baum, T.H., Comita, P.B. *Thin Solid Films* **1992**, 218, 80.
4. Yang, E.S. *Fundamentals of Semiconductor Devices*, McGraw-Hill, New York, 1978, p. 60.
5. Matsumoto, Y., Abe, T., Tanaka, M., Tazawa, T., Sato, E. *Mater. Res. Bull.* **1988**, 23, 1241.
6. Kuwarbara, M., Kusaka, N. *Japan. J. Appl. Phys.* **1988**, 27, L1504.
7. Puddephatt, R.J. *Topics in Inorganic Chemistry and General Chemistry*, 16, R.J.H. Clark, (ed.), Elsevier, Amsterdam, 1978.
8. Anderson, G.K. *Adv. Organomet. Chem.* **1982**, 20, 39.
9. Shibata, S., Iijima, K., Baum, T.H. *J. Chem. Soc. Dalton Trans.* **1990**, 1519.
10. Brain, F.H., Gibson, C.S. *J. Chem. Soc.* **1939**, 762.
11. Gilman, H., Woods, L.A. *J. Amer. Chem Soc.* **1948**, 70, 550.
12. Baum, T.H., Brock, P.J., Dawson, D. *US Patent* 5 023 060, **1991**.
13. Guerra, M.A., Bierschenk, T.R., Lagow, R.J. *J. Organomet. Chem.* **1986**, 307, C58.
14. Sanner, R.D., Satcher, J.H., Droegge, M.W. *Organometallics*, **1989**, 8, 1498.
15. Johnson, A., Puddephatt, R.J. *J. Chem. Soc., Dalton Trans.* **1976**, 1360.
16. Baum, T.H., Jones, C.R. *Appl. Phys. Lett.* **1985**, 47, 538.
17. Baum, T.H., Jones, C.R. *J. Vac. Sci. Tech.* **1986**, B 4, 1187.
18. Sheppard, W.A., Sharts, C.M. *Organic Fluorine Chemistry*, W. A. Benjamin, Inc., New York, 1969.
19. Moshier, R.W., Sievers, R.E. *Gas Chromatography of Metal Chelates*, Pergamon Press Ltd., Oxford, 1965.
20. Komiya, S., Kochi, J.K. *J. Amer. Chem. Soc.* **1977**, 99, 3695.
21. Baum, T.H. *J. Electrochem. Soc.* **1987**, 134, 2616.
22. Baum, T.H., Marinero, E.E., Jones, C.R. *Appl. Phys. Lett.* **1986**, 49, 1213.
23. Gibson, C.S., Simonsen, J.L. *J. Chem. Soc.* **1930**, 2531.
24. Baum, T.H., unpublished results (1989). Diethyl(hexafluoro-2,4-pentanedionato)-gold(III) is a liquid source for depositing gold metal.
25. Kodas, T.T., Baum, T.H., Comita, P.B. *J. Cryst. Growth* **1988**, 87, 378.
26. Puddephatt, R.J., Treunnicht, I. *J. Organomet. Chem.* **1987**, 319, 129.
27. Jubber, M., Wilson, J.I.B., Davidson, J.L., Fernie, P.A., John, P. *Appl. Surf. Sci.* **1989**, 43, 74.
28. Aylett, M.R. *Chemtronics I* **1986**, 146.
29. Coates, G.E., Parkin, C. *J. Chem. Soc.* **1963**, 421.
30. Tamaki, A., Magennis, S.A., Kochi, J.K. *J. Amer. Chem. Soc.* **1974**, 96, 6140.
31. Komiya, S., Kochi, J.K. *J. Amer. Chem. Soc.* **1976**, 98, 7599.

32. Ehrlich, D.J., Tsao, J.Y. (eds.), *Laser Microfabrication, Thin Film Processes and Lithography*, Acedemic Press, San Diego, CA, 1989.
33. Schmidbaur, H., Bergfeld, M. *Inorg. Chem.* **1966**, 5, 2069.
34. Vaughan, L.G., Sheppard, W.A. *J. Amer. Chem. Soc.* **1969**, 91, 6151.
35. Uson, L., Laguna, A., Vincente, J., Garcia, J., Bergareche, B. *J. Organomet. Chem.* **1979**, 173, 349.
36. Ziolo, R.F., Thich, J.A., Dori, Z. *Inorg. Chem.* **1971**, 11, 626.
37. Volger, A., Quett, C., Kunkley, H. *Ber. Bungsenges.Phys. Chem.* **1988**, 92, 146.
38. Adams, S.K., Edwards, D.A., Richards, R. *Inorg. Chimica. Acta.* **1975**, 12, 163.
39. Hartley, F.R. *Acc. Chem. Res.* **1973**, 73, 163.
40. Partenheimer, W., Johnson, E.H. *Inorg. Chem.* **1972**, 11, 2840.
41. Partenheimer, W., Johnson, E.H. *Inorg. Chem.* **1973**, 12, 1274.
42. Doyle, G., Erickson, K.A., Van Engen, D. *Organomet.* **1985**, 4, 830.
43. Bailey, A., Corbitt, T.S., Hampden-Smith, M.J., Duesler, E.N., Kodas, T.T. *Polyhedron*, **1993**, 12, 1785; Baum, T.H., Larson, C.E., Reynolds, S.K. *US Patent* 5 096 737, **1992**.
44. Edwards, D. A., Longley, M. *J. Inorg. Nucl. Chem.* **1978**, 40, 1599.
45. Gibson, D, Johnson, B.F.G., Lewis, J. *J. Chem. Soc. A* , **1970**, 367.
46. Hofstee, H.K., Boersma, J., van der Kerk, G.J.M. *J. Organometal. Chem.* **1976**, 120, 313.
47. Miller, W.T., Snider, R.H., Hummel, R.J. *Amer. Chem. Soc.* **1969**, 91, 6532.
48. Shapiro, M.J. *Chemical Vapor Deposition of Silver Films for Superconducting Wire Applications*, UMI Diss. Inform. Serv., #9124 543, 1992.
49. Voorhoeve, V.J.H., Merewether, J.W. *J. Electrochem. Soc.* **1972**, 119, 364.
50. Black, J.G., Doran, S.P., Rothschild, M., Ehrlich, D.J. *Appl. Phys. Lett.* **1990**, 56 , 1072.
51. Beach, D.B., Jasinski, J.M. *US Patent* 4 948 623, **1990**.
52. Erbil, A. *US Patent* 4 880 670, **1989**.
53. Whitesides, G.M., Panek, E.J., Stedronsky, E.R. *J. Amer. Chem. Soc.* **1972**, 94, 232.
54. Cotton, F.A., Wilkinson, G. *Advanced Inorganic Chemistry*, 5th ed., Wiley, New York, 1988
55. Anonymous, *Research Disclosure* **1986**, 263, 146.
56. Lu, Y.-F., Takai, M., Nagatomo, S., Kato, K., Namba, S. *Appl. Phys.* **1992**, A 54, 51.
57. Dutta, S., McMullin, P.G., Rai-Choudry, P., Gallagher, B.D. *Mater. Res. Soc. Symp. Proc.* **1984**, EA-70.
58. Kodas, T.T., Comita, P.B. *Acct. Chem. Res.* **1990**, 23 188.
59. Kodas, T.T., Comita, P.B. *J. Appl. Phys.* **1988**, 65, 2413.
60. Comita, P.B., Kodas, T.T. *Appl. Phys. Lett.* **1989**, 51, 2059.
61. Reichert, C., Bancroft, G., Westmore, J. *Can J. Chem.* **1970**, 48, 1364.

62. Kochi, J. K. *Acc. Chem. Res.* **1974**, 7, 351.
63. Klassen, R.B., Baum, T.H. *Organometallics* **1989**, 8, 2477.
64. Dagata, J.A., Villa, E., Lin, M.C. *Appl. Phys.* **1990**, B 51, 443.
65. Feurer, E., Suhr, H. *Appl. Phys.* **1987**, A 44, 171.
66. Suhr, H., Etspuler, A., Feurer, E., Kraus, S. *Plasma Chemistry and Plasma Processing* **1989**, 9, 217.
67. Oehr, C., Suhr, H. *Appl. Phys.* **1989**, A 49, 691.
68. Dubner, A.D., Wagner, A. *J. Appl. Phys.* **1989**, 65, 3636.
69. Shedd, G.M., Lezec, H., Dubner, A.D., Melngailis, J. *J. Appl. Phys.* **1986**, 49, 1584.
70. Blauner, P., Butt, Y., Ro, J., Thompson, C.V, Melngailis, J. *J. Vac. Sci. Tech.* **1989**, B 7, 1816.
71. Kubena, R.L., Stratton, F.P., Mayer, T.M. *J. Vac. Sci. Tech.* **1988**, B 6, 1865.
72. Wagner, A., Levin, L.P., Mauer, J.L., Blauner, P.G., Kirch, S.J., Longo, P. *J. Vac. Sci. Tech.* **1990**, B 8, 1557.
73. Koops, H. W. P., Weile, R., Kern, V., Baum, T. H. *J. Vac. Sci. Tech.* **1988**, B 6, 477.
74. Lee, K.L., Hatzakis, M. *J. Vac. Sci. Tech.* **1989**, B 7, 1941.
75. McCord, M.A., Kern, D.P., Chang, T.H.P. *J. Vac. Sci. Tech.* **1988**, B 6, 1877.
76. Silver, R.M., Ehrichs, E.E., de Lozanne, A.L. *Appl. Phys. Lett.* **1987**, 51, 247.
77. Larson, C.E., Baum, T.H., Jackson, R.L. *J. Electrochem. Soc.* **1987**, 134, 266.
78. Holloway, K., Zuhoski, S.P., Reynolds, S., Matuszewski, C. *Mater. Res. Soc. Symp. Proc.* **1991**, 204, 409.
79. Kodas, T.T., Baum, T.H., Comita, P.B. *J. Appl. Phys.* **1987**, 61, 2749.
80. Kodas, T.T., Baum, T.H., Comita, P.B. *J. Appl. Phys.* **1987**, 62, 281.
81. Comita, P.B. *Advanced Materials (Angewandte Chemie)*, **1990**, 2, 82.
82. Baum, T.H., Comita, P.B., Kodas, T.T. *SPIE Symp. on Lasers in Microelec. Manufac.* **1991**, 1598, 122.
83. Wassick, T.A. *SPIE Symp. on Lasers in Microelec. Manufac.* **1991**, 1598, 141.
84. Metzger, B., Paredes, A., Kruck, Th., Reichel, H. *Microsys. Tech.* Springer, Berlin, 1990, 122.
85. Jackson, R. L. Sather, S. D., Baum, T.H. *unpublished results*, 1988.
86. Rothschild, M., Ehrlich, D.J. *J. Vac. Sci. Tech.* **1989**, B 6 1.
87. Anonymous, *Research Disclosure*, **1987**, 274, 100.
88. Baum, T.H. *J. Electrochem. Soc.* **1990**, 137, 252.

This Page Intentionally Left Blank

Chapter 7

Chemical Vapor Deposition of Platinum, Palladium and Nickel

Alfred A. Zinna^a

Lutz Brandt^a

Herbert D. Kaesz^a

Robert F. Hicks^b

**Departments of Chemistry and Biochemistry^a and
Chemical Engineering^b
University of California
Los Angeles, CA 90024**

Abstract

This chapter reviews the chemical vapor deposition of platinum, palladium, and nickel. A variety of precursors have been developed for use in this process. Precursors such as $\text{Pt}(\text{PF}_3)_4$, $(\text{CH}_3\text{C}_5\text{H}_4)\text{Pt}(\text{CH}_3)_3$, $(\text{C}_5\text{H}_5)\text{Pd}(\text{allyl})$, $\text{Ni}(\text{CO})_4$, and $\text{Ni}(\text{CH}_3\text{C}_4\text{H}_5)_2$ may be used to deposit high-purity metal films at a rapid rate. Direct deposition of metal circuits has been demonstrated by using laser or ion beams to induce the decomposition process. Recently, many advances have been made in understanding the chemistry of the chemical vapor deposition of these metals. The purpose of this review is to examine the chemistry in detail with the aim of revealing fruitful directions for further research.

Contents

7.1	Introduction	331
7.2	Platinum	331
7.3	Palladium	339
7.4	Nickel	340
7.5	Laser-Assisted CVD	342
7.5.1	Platinum	344
7.5.2	Palladium	347
7.5.3	Nickel	348
7.6	Ion-Assisted and Plasma-Assisted CVD	350
7.7	Outlook	351
	Acknowledgments	352
	References	352

7.1 Introduction

Thin films of platinum, palladium, and nickel have a variety of uses, including metal contacts to microelectronic devices,¹⁻⁷ catalysts for electroless metal plating,⁸⁻¹¹ catalysts for pollution control,¹²⁻¹⁶ and protective or decorative coatings.¹⁷ Chemical vapor deposition (CVD) is a low-temperature method for depositing these metals in high purity.¹⁸⁻²⁴ The high purity that can be achieved by CVD was recognized as early as 1890, when Ludwig Mond developed a process for purifying nickel through the decomposition of nickel tetracarbonyl.²⁵ The chemical nature of the CVD process provides an additional advantage of directing deposition to selected areas of a substrate. This is achieved either by confining precursor decomposition to the areas illuminated by a laser or ion beam²⁶⁻²⁸ or by selectively activating regions of a substrate for reaction with the precursor.²⁹ For complicated devices that are made by multistep fabrication procedures, the high purity and selectivity offered by CVD may make this process cost effective over alternative deposition technologies.

In this chapter, we review the chemical vapor deposition of platinum, palladium, and nickel. The three sections provide a comprehensive guide to the precursors, the growth mechanisms and kinetics, and the properties of the films. The fourth and fifth sections discuss laser-, ion-, and plasma-assisted CVD of these metals. Finally, we summarize what has been learned so far and discuss the prospects for future development of the field.

7.2 Platinum

Table 7-1 provides a summary of platinum CVD experiments reported in the literature. The structures of the platinum compounds are shown in Figure 7-1. The earliest example of platinum deposition from a volatile complex is the study by Reerink in 1928.³⁰ He transported $\text{Pt}(\text{CO})_2\text{Cl}_2$ in a stream of carbon monoxide and hydrogen into a hot reaction vessel where the complex decomposed into a bright and reflective metal film. The excess carbon monoxide was needed to prevent decomposition of the $\text{Pt}(\text{CO})_2\text{Cl}_2$ into solid PtCl_2 .³¹ Later, Rand³² examined the deposition of platinum on silicon using this complex. The reaction was carried out in H_2 and CO carrier gas at substrate temperatures between 250 and 500 °C and source temperatures between 120 and 155 °C. In most cases, the platinum films did not adhere to the substrate. Another problem experienced by Rand was the slow decomposition of the $\text{Pt}(\text{CO})_2\text{Cl}_2$ source, which occurred above 125 °C even in 1 atm of CO.

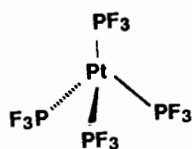
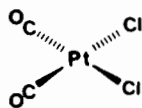
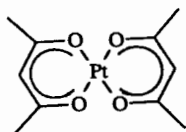
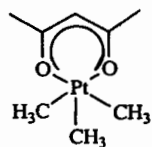
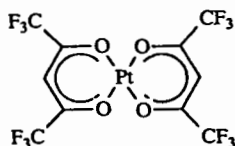
Table 7-1 Prior studies of platinum chemical vapor deposition.

Compound ^a	Evaporation Temperature (°C)	Deposition Rate (μm/h)	Deposition Temperature (°C)	Carrier Gas	Reactor Pressure (torr)	Substrate	Ref.
Pt(CO) ₂ Cl ₂	120-155	0.06-0.6	250-500	H ₂ , C	760	Si, SiO ₂	32
Pt(acac) ₂	150-200	0.06-0.6	500-600	none	<2 × 10 ⁻⁴	Si	32
Pt(PF ₃) ₄	0	0.3-0.6	200-300	H ₂ , N ₂	760	Si, SiO ₂ , Al ₂ O ₃	32
Pt(CH ₃) ₂ [(CH ₃)NC]	30-80	0.5	100-150	H ₂	0.002	Si	36,38
(COD)Pt(CH ₃) ₂	30-80	0.5	100-150	H ₂	0.002	Si	36,38
(COD)Pt(CH ₃)(η ¹ -C ₅ H ₅)	30-80	0.5	100-150	H ₂	0.002	Si	36,38
(COD)Pt(CH ₃)Cl	30-80	0.5	100-150	H ₂	0.002	Si	36,38
(C ₅ H ₅)Pt(CH ₃)(CO)	30-80	0.5	100-150	H ₂	0.002	Si	36,38
(C ₅ H ₅)Pt(allyl)	30-80	0.5	100-150	H ₂	0.002	Si	36,38
(acac)Pt(CH ₃) ₃	30-80	0.5	100-150	H ₂	0.002	Si	36,38
(C ₅ H ₅)Pt(CH ₃) ₃	25	0.05	90-180	H ₂ , He	760	Si, SiO ₂	29,39
(CH ₃ C ₅ H ₄)Pt(CH ₃) ₃	25	0.05	90-180	H ₂ , He	760	Si, SiO ₂	29,39,40

^aacac = acetylacetonate; C₅H₅ = η⁵-cyclopentadienyl; CH₃ = methyl; CH₃C₅H₄ = η⁵-methylcyclopentadienyl; COD = 1,5-cyclooctadiene; η¹-C₅H₅ = η¹-cyclopentadienyl.

Rand also examined the CVD of platinum using $\text{Pt}(\text{acac})_2$ and $\text{Pt}(\text{PF}_3)_4$.³²⁻³⁴ The $\text{Pt}(\text{acac})_2$ was vaporized at 150 to 200 °C in vacuum and allowed to diffuse to the Si substrate where it was decomposed at 500 to 600 °C. The high temperature required for decomposition of the complex is undesirable in many applications. Moreover, films produced from $\text{Pt}(\text{acac})_2$ contain a 50:50 mixture of carbon and platinum. Evidently, the Pt-O bonds in this complex are of comparable strength to the internal C-C bonds of the acetylacetonate so that the ligand decomposes simultaneously with the compound. It is possible that hydrogen in the presence of a platinum film would assist deposition by catalytic hydrogenolysis/hydrogenation of the acetylacetonate ligand. However, if hydrogen is used, it must not contact the $\text{Pt}(\text{acac})_2$ source for it will rapidly decompose to Pt metal.³²

The complex $\text{Pt}(\text{PF}_3)_4$ is a reasonably good precursor for CVD of platinum. It is a volatile liquid with a vapor pressure of ~15 torr at 0 °C and 760 torr at 86 °C.³⁵ It is stable in dry air up to 130 °C but will decompose to the metal at lower temperatures if moisture is present. Rand deposited platinum from $\text{Pt}(\text{PF}_3)_4$ in H_2 carrier gas at

 $\text{Pt}(\text{PF}_3)_4$  $\text{Pt}(\text{CO})_2\text{Cl}_2$  $\text{Pt}(\text{acac})_2$  $(\text{acac})\text{PtMe}_3$  $\text{Pt}(\text{hfac})_2$

continued on p. 334

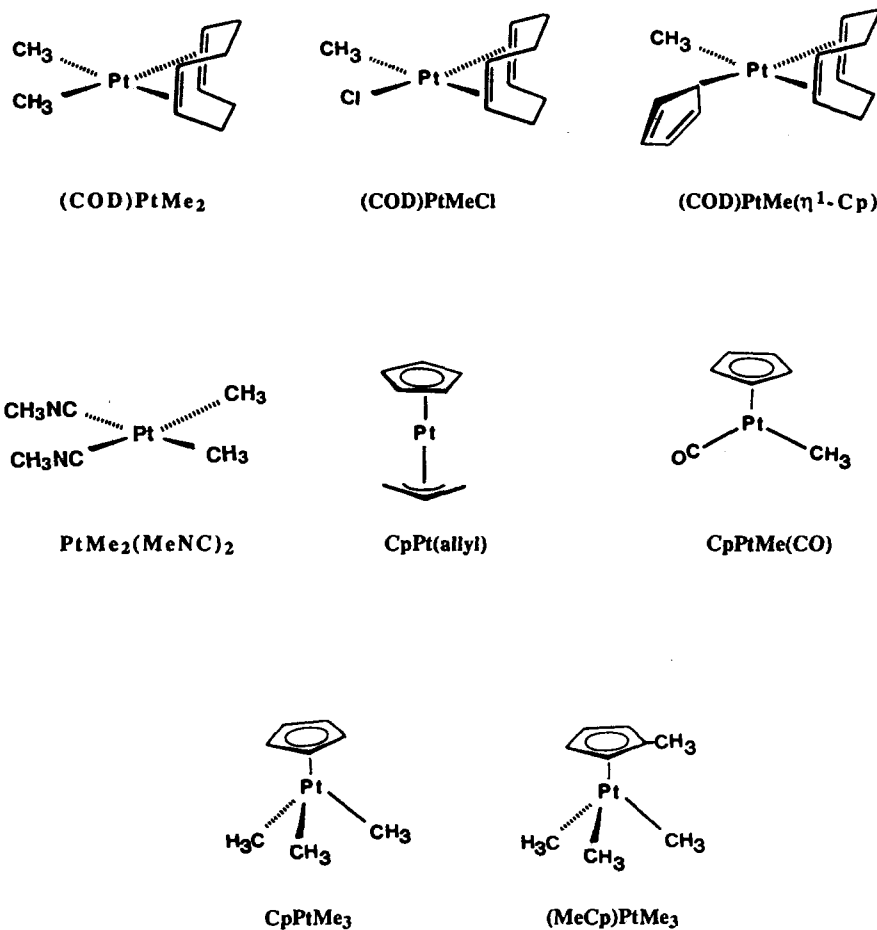


Figure 7-1 Structures of the platinum complexes used for CVD.

substrate temperatures between 200 and 300 °C and a source temperature of 0 °C. Bright and adherent metal films were deposited at rates near 0.5 $\mu\text{m/h}$. The resistivity of the films was 18 $\mu\Omega\text{cm}$ as compared to 10 $\mu\Omega\text{cm}$ for bulk platinum. The only problem encountered with this process was that the films contained ~1 at% phosphorus at the Pt/Si interface. The phosphorus contamination is most likely due to the oxidation of the silicon surface by the trifluorophosphine ligand according to Equation 7.1.²⁹



The equilibrium for Equation 7.1 lies far to the right. With regard to metal contacts, phosphorus contamination is unacceptable because it is an electrically active dopant in silicon.³³

Puddephatt and coworkers³⁶⁻³⁸ have examined the CVD of platinum from $\text{Pt}(\text{CH}_3)\text{RL}_2$ complexes, where R is a methyl, allyl, vinyl, or tertiarybutynyl group and L_2 is two methylisocyanide (CH_3NC) groups or 1,5-cyclooctadiene (COD). The synthesis of these precursors has been discussed.³⁸ The main drawback of these precursors is their low volatility. For example, the vapor pressure of $\text{Pt}(\text{CH}_3)_2(\text{CH}_3\text{NC})_2$ is 3.3×10^{-6} torr at 25 °C and 0.76 torr at 140 °C.³⁸ The complex decomposes at 180 °C. Platinum deposition from the $\text{Pt}(\text{CH}_3)\text{RL}_2$ complexes was carried out at 0.002 torr with a background of H_2 at 100 to 150 °C or without H_2 at 200 to 250 °C. The sources were held at 30 to 80 °C, and growth rates were in the range of 0.5 $\mu\text{m/h}$. Hydrogen reduced the level of carbon and oxygen in the films in agreement with an earlier study of platinum CVD by Chen et al.³⁹ Provided the flow of H_2 is sufficient, essentially pure metal is deposited from $\text{Pt}(\text{CH}_3)_2(\text{CH}_3\text{NC})_2$.

Kinetic studies of the decomposition of $\text{Pt}(\text{CH}_3)_2(\text{CH}_3\text{NC})_2$ revealed that the products of this reaction are platinum, methane, and an oily polymer derived from the isocyanide ligands.^{37,38} In the presence of hydrogen, methane is produced by hydrogenolysis of the methyl group. Also, the free CH_3NC strongly retards decomposition of the complex. These data suggest that the reaction proceeds in two steps:



where $* \text{Pt}(\text{CH}_3)_2$ is either a reactive species in the gas phase, or more likely, an adsorbed species on the platinum surface. Equations 7.2 and 7.3 are each the summation of several elementary reactions. The extent to which these reactions are homogeneous or heterogeneous remains to be resolved.

Kaeszi and Hicks^{22,23,28,29,39,40} and Girolami⁴¹ have investigated the use of $(\text{C}_5\text{H}_5)\text{Pt}(\text{CH}_3)_3$ and $(\text{CH}_3\text{C}_5\text{H}_4)\text{Pt}(\text{CH}_3)_3$ for CVD of platinum. These precursors are stable in air for short periods of time and are relatively volatile. Their preparation is described in other references.^{40,42} Other $(\text{C}_5\text{H}_5)\text{Pt}(\text{alkyl})_3$ precursors may be prepared⁴³ and used as sources for Pt CVD although they will be less volatile and less stable than the complexes with the methyl ligands. Clausius-Clapeyron relationships for $(\text{C}_5\text{H}_4)\text{Pt}(\text{CH}_3)_3$ and $(\text{CH}_3\text{C}_5\text{H}_4)\text{Pt}(\text{CH}_3)_3$, measured from -10 to 25 °C, are:²⁹

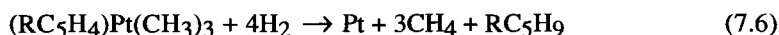
$$\ln(P^{\text{vap}}(\text{torr})) = 25.9 - 8.59 \times 10^3/(T(\text{K})) \quad (7.4)$$

$$\ln(P^{\text{vap}}(\text{torr})) = 26.1 - 8.60 \times 10^3/(T(\text{K})) \quad (7.5)$$

At 25 °C, the vapor pressure of $(C_5H_5)Pt(CH_3)_3$ is 0.055 torr. The advantage of the $CH_3C_5H_4$ precursor for CVD is that it is a liquid above 30 °C. The vapor pressure of liquid $(CH_3C_5H_4)Pt(CH_3)_3$ is 0.4 and 3.5 torr at 50 and 100 °C, respectively.²⁹ The $(C_5H_5)Pt(CH_3)_3$ and $(CH_3C_5H_4)Pt(CH_3)_3$ complexes decompose above 150 °C.^{42,44}

The CVD of platinum from $(C_5H_5)Pt(CH_3)_3$ and $(CH_3C_5H_4)Pt(CH_3)_3$ was carried out in a 50:50 mixture of hydrogen and helium at 1 atm, 90 to 180 °C substrate temperatures, and 14 °C source temperature.^{29,39,40} To prevent premature decomposition, the complexes were sublimed in helium and then mixed with hydrogen just upstream of the deposition zone. In addition, the complexes were not allowed to come in contact with metal surfaces. Bright, adherent, polycrystalline metal films were obtained at growth rates of about 0.05 $\mu m/h$. Analysis of lightly sputtered films by X-ray photoelectron spectroscopy revealed that they were essentially free of impurities. The resistivity of the films was $27 \pm 2 \mu\Omega cm$.

Recently, the kinetics of the decomposition of $(C_5H_5)Pt(CH_3)_3$ in hydrogen has been examined.²⁹ The ligands on the organometallic complexes undergo quantitative hydrogenolysis according to Equation 7.6.



where R is H or CH_3 . On glass and silicon substrates, the deposition rate is initially slow then rapidly accelerates due to autocatalysis by the platinum film. This behavior is shown in Figure 7-2. The rate observed after the induction period is limited only by the

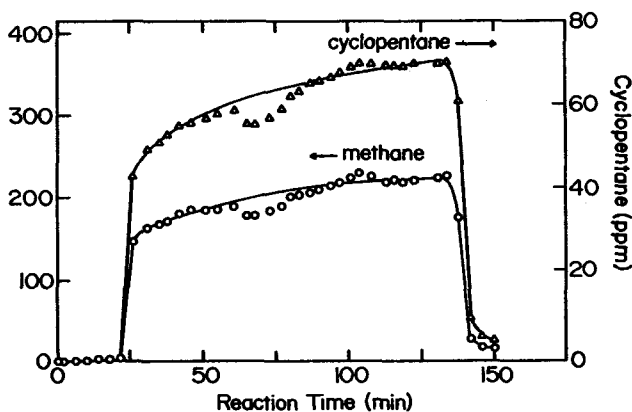
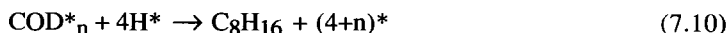
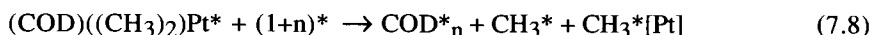
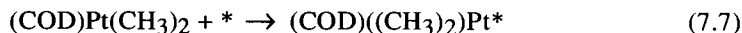


Figure 7-2 Dependence of the methane and cyclopentane concentrations on reaction time for decomposition of $(C_5H_5)Pt(CH_3)_3$ on glass at 95 °C.²⁹

rate at which the organometallic complex is fed to the reactor. When a platinum film is present initially, no induction period is observed even at 25 °C.

These results indicate that the low growth rates obtained in this study (0.05 $\mu\text{m/h}$) are due to an inadequate supply of the precursor to the reactor. The $(\text{C}_5\text{H}_5)\text{Pt}(\text{CH}_3)_3$ complex was sublimed at 14 °C to a vapor pressure of 0.018 torr in 760 torr of helium and then diluted by half with the addition of hydrogen. By heating the source to 50 °C and reducing the pressure to 2 torr, the mass-transfer limited growth rate should increase to about 150 $\mu\text{m/h}$.

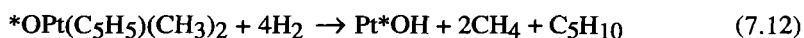
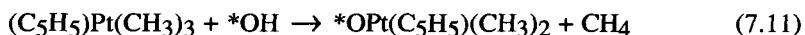
A system analogous to platinum CVD using $(\text{C}_5\text{H}_5)\text{Pt}(\text{CH}_3)_3$ and hydrogen is the hydrogenolysis of (diolefin)dialkylplatinum(II) $[(\text{OL})\text{PtR}_2]$ complexes on platinum black in solution. Whitesides et al.⁴⁵⁻⁴⁸ have studied the mechanism of this reaction in detail. These complexes rapidly convert to platinum metal and the corresponding alkanes. Two different kinetic regimes are observed depending on the reaction conditions: at 40 °C and 0.2 atm H_2 , the rate is controlled by mass transfer of hydrogen to the platinum surface, while at -20 °C and 2.4 atm H_2 , the rate is controlled by a surface reaction. The rate of the surface reaction equals $0.014 \times S_{\text{Pt}}^{1.2} P_{\text{H}_2}^{0.4} C_{\text{OM}}^{0.0}$ [$\mu\text{mol}/(\text{s} \times \text{atm}^{0.4})$], where S_{Pt} is the platinum surface area, P_{H_2} is the partial pressure of hydrogen, and C_{OM} is the concentration of the $(\text{OL})\text{PtR}_2$ complex in solution. Deuterium-labeling experiments revealed that the complex initially coordinates to the metal surface through the Pt center. These authors proposed the following decomposition mechanism:



where $*$ is a single adsorption site on the platinum catalyst, and $*_n$ is one or more of these sites defined before. In Equations 7.7 and 7.8, the complex dissociatively chemisorbs onto the metal surface. The platinum atom from the complex cannot be distinguished from other platinum surface atoms after dissociation. In Equations 7.9 and 7.10, the adsorbed hydrocarbons undergo sequential hydrogenation with regeneration of the metal surface for further reaction. Equation 7.10 is the sum of several elementary steps. The kinetic data suggest that the rate-limiting step is hydrogenation of the adsorbed hydrocarbons, most likely the olefin in Equation 7.10.

The induction period observed during platinum CVD with $(\text{C}_5\text{H}_5)\text{Pt}(\text{CH}_3)_3$ (Fig. 7-2) is the time required for a critical number of Pt nuclei to form to catalyze deposition.

This requires that the reaction rate on Pt surfaces be much higher than the rate on the bare substrate. Xue et al.²⁹ found that the length of the induction period depends on the substrate composition, glass or PTFE, and on the substrate treatment prior to growth. Evidently, the complex initially decomposes via a heterogeneous reaction. A likely mechanism for this reaction is electrophilic attack of $(C_5H_5)Pt(CH_3)_3$ by hydroxyl groups on the glass and PTFE surface.⁴⁹



When the hydroxyl groups are passivated by silylation with $ClSi(CH_3)_3$, deposition does not occur below 150 °C.⁴⁴ This is similar to the situation for CVD of copper onto SiO_2 surfaces using $(\beta\text{-diketonate})CuL$ compounds as discussed in Chapter 5. This chemistry may be used to deposit platinum selectively on a substrate. Shown in Figure 7-3 is a photomicrograph of platinum wires deposited on sapphire. The pattern was

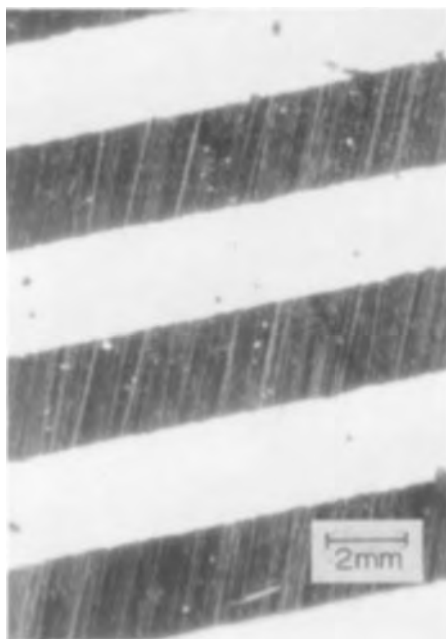


Figure 7-3 A photomicrograph of platinum wires selectively deposited on sapphire. The magnification is 8x.

established by photolithography. After the resist was laid down, the substrate was heated to 200 °C to create reactive hydroxyl groups on the alumina. The sample was then exposed to $(C_5H_5)Pt(CH_3)_3$ and H_2 at 100 °C, and platinum was deposited on the alumina but not on the resist.

7.3 Palladium

Although palladium is used more extensively than platinum in electronic materials,² few studies have been published on the CVD of palladium by thermal means.^{21,41,50} Girolami and coworkers⁴¹ have examined the use of $Pd(allyl)_2$, $Pd(CH_3allyl)_2$, and $(C_5H_5)Pd(allyl)$ for palladium CVD. Their results are summarized in Table 7-2, and the structures of the complexes are shown in Figure 7-4. The main drawbacks of using these precursors for CVD are their low stability, especially in air, and their low volatility (~ 0.02 torr at 25 °C⁵¹).

In Girolami's experiments, the palladium compounds were placed together with glass, steel, copper, and aluminum substrates in a closed vessel. The vessel was then heated under vacuum to 250 °C, resulting in the production of visually bright and reflective metal films. The resistivity of the palladium deposits was $15 \pm 5 \mu\Omega cm$, which is close to the bulk value of $11 \mu\Omega cm$. Auger electron spectroscopy of lightly sputtered films revealed that those deposited from $Pd(allyl)_2$ and $Pd(CH_3allyl)_2$ contained <1 at% carbon and oxygen, whereas those deposited from $(C_5H_5)Pd(allyl)$ contained $\sim 5\%$ carbon and no oxygen. The hydrocarbon products from the decomposition of $Pd(allyl)_2$ were propene (59%) and hexadiene (30%), which is consistent with simple homolysis of the Pd-C bonds. Since palladium is an active hydrogenation catalyst,¹² addition of hydrogen should lead to the removal of any residual carbon in the films.

Table 7-2 Prior studies of palladium and nickel chemical vapor deposition.

Compound	Evaporation Temperature (°C)	Deposition Rate ($\mu m/h$)	Deposition Temperature (°C)	Carrier Gas	Reactor Pressure (torr)	Substrate	Ref
$Pd(allyl)_2$	250	-	250	none	10^{-4}	SiO_2 , Fe, Cu, Al	41
$Pd(CH_3allyl)_2$	250	-	250	none	10^{-4}	SiO_2 , Fe, Cu, Al	41
$(C_5H_5)Pd(allyl)$	250	-	250	none	10^{-4}	Al	41
$Ni(CO)_4^a$	25	15-800	100-200	none	20-200	Fe, Ni	54
$Ni(C_5H_5)_2$	$\sim 100-150$	0.2-0.8	190-230	H_2 , N_2	50-525	ceramic tube	50
$Ni(CH_3C_5H_4)_2$	35	0.05	280	H_2 , He	760	SiO_2 , Si	22

^aHigh pressure gas at 25 °C.

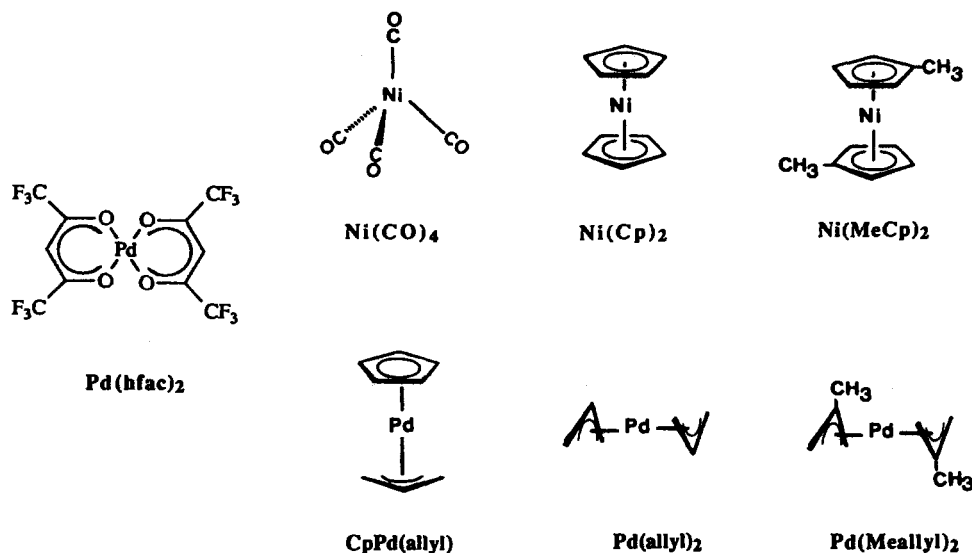


Figure 7-4 Structures of the palladium and nickel complexes used for CVD.

An alternative precursor for palladium deposition is $\text{Pd}(\text{hfac})_2$ (see Fig. 7-4). This precursor has been used for laser-assisted CVD (LCVD) of palladium but so far has not been tried in the conventional process. The hexafluoroacetylacetonate complex is stable in air to 230 °C and has a vapor pressure of 0.1 torr at 60 °C.²⁰ Heating it to between 100 and 150 °C should yield vapor pressures of several torr. One potential disadvantage of $\text{Pd}(\text{hfac})_2$ is that it may decompose in an unfavorable way, i.e., to deposit a palladium-carbon mixture. For example, platinum CVD with $\text{Pt}(\text{acac})_2$ yields a 50:50 mixture of platinum and carbon.³² This problem might be minimized by carrying out the reaction in hydrogen. A study of palladium CVD with $\text{Pd}(\text{hfac})_2$ should be undertaken to evaluate the potential of this precursor.

7.4 Nickel

The earliest example of nickel CVD is the decomposition of $\text{Ni}(\text{CO})_4$ by the Mond process.²⁵ This process produces pure nickel and is used commercially to refine the ore.⁵² However, a major drawback of using $\text{Ni}(\text{CO})_4$ is the extreme toxicity of the compound. The kinetics of nickel tetracarbonyl decomposition was first studied by

Chan and McIntosh at temperatures between 35 and 80 °C.⁵³ The reaction is initially homogeneous then becomes heterogeneous as a nickel film develops on the vessel surface. Carlton and Oxley⁵⁴ measured the steady-state kinetics of nickel CVD from Ni(CO)₄ over a wide range of conditions. Below 175 °C, Ni deposition is controlled by the rate of a surface reaction, whereas above 175 °C, it is controlled by mass transfer of Ni(CO)₄ to the metal surface. In the kinetically controlled regime, the growth rate exhibits the following dependence on the partial pressures of Ni(CO)₄ and CO:

$$R_g = \frac{a P_{\text{Ni(CO)}_4}^2}{\left(1 + b P_{\text{Ni(CO)}_4} + c P_{\text{CO}}\right)^2} \quad (7.13)$$

where a, b, and c are constants. This expression is consistent with the rate-limiting step being the decomposition of dissociatively adsorbed Ni(CO)₄. Carbon monoxide inhibits the reaction by blocking sites for adsorption of the nickel complex. Carlton and Oxley measured an activation energy for the surface reaction of 22 kcal/mol.

The CVD of nickel from Ni(C₅H₅)₂ and Ni(CH₃C₅H₄)₂ has been studied by several groups.^{22,55-57} These precursors are much less toxic than Ni(CO)₄ and exhibit high vapor pressures. The Clausius-Clapeyron relationship for Ni(C₅H₅)₂, valid from 80 to 147 °C, is⁵⁸

$$\ln[P^{\text{vap}}(\text{torr})] = 22.4 - 7.89 \times 10^3/[T(\text{K})] \quad (7.14)$$

Since Ni(C₅H₅)₂ begins to decompose at 175 °C, the highest source temperature that can be used for CVD is approximately 150 °C, yielding a maximum vapor pressure of 43 torr. This vapor pressure is high enough to give deposition rates comparable to those achieved with Ni(CO)₄.

The kinetics of nickel CVD from Ni(C₅H₅)₂ were studied by van den Brekel et al.⁵⁶ Their results are listed in Table 7-2. The growth rate is limited by mass transfer of the reactant to the substrate surface at temperatures ranging from 190 to 230 °C. At Ni(C₅H₅)₂ concentrations of 0.3 to 1.5 mol%, the growth rate varies from 0.2 to 0.8 μm/h. Kaplin et al.⁵⁵ determined the products of the decomposition of Ni(C₅H₅)₂ in hydrogen in a hot-wall reactor at temperatures from 200 to 350 °C. The metal films contained approximately 90 wt% nickel, the remainder being mostly carbon. The C₅H₅

ligands were converted into a mixture of cyclopentadiene, cyclopentene, and cyclopentane. The concentrations of these three products increased, remained constant, and decreased, respectively, with increasing reactor temperature. These results follow from the observation that olefin hydrogenation is thermodynamically more favored at low temperature. Hydrogen is essential for obtaining pure nickel films from $\text{Ni}(\text{C}_5\text{H}_5)_2$. If it is omitted, the films are heavily contaminated with carbon.⁵⁹ Kaesz et al.²² have deposited nickel from $\text{Ni}(\text{CH}_3\text{C}_5\text{H}_4)_2$ in a 50:50 mixture of hydrogen and helium at 280 °C. The nickel films contained no detectable carbon and only 2 at% oxygen. It was speculated that the higher purity achieved with $\text{Ni}(\text{CH}_3\text{C}_5\text{H}_4)_2$ is due to the easier hydrogenolysis of the $\text{CH}_3\text{C}_5\text{H}_4$ ligand.

7.5 Laser-Assisted CVD

Laser-assisted CVD (LCVD) of platinum, palladium, and nickel has been examined by several research groups.^{27,51,60-86} Most of this work is summarized in Table 7-3. This process is usually carried out as follows: the precursor is introduced to an evacuated cell containing the substrate; then the substrate is illuminated with a focused laser beam resulting in deposition of the metal film. When ultraviolet light, 250-350 nm, is used, the precursor undergoes photolysis in the gas phase and on the substrate surface. When visible light, 475-525 nm, or infrared light, 10.6 μm , is used, the substrate is locally heated to a temperature sufficient to pyrolyze the precursor. A unique feature of pyrolytic LCVD is that deposition rates can exceed 1 $\mu\text{m/s}$ within the 1-10 μm spot illuminated on the substrate. This rate is much faster than can be achieved by conventional CVD and is a consequence of confining the reaction to a small region. In conventional CVD the transport limited deposition rate scales inversely with reactor size. Therefore, large reactors give low transport-limited deposition rates. In contrast, for laser CVD, the transport-limited deposition rate depends inversely on laser spot size which is orders of magnitude smaller than the size of typical CVD reactors. Therefore, LCVD deposition rates can be extremely high. Pyrolytic LCVD can be used to write metal lines directly on a substrate by sweeping the focused laser beam across the surface.^{63,81,82,85} An important application of this technique is the repair of integrated circuits.⁶⁹ (See Chapter 6 for a detailed discussion of other applications.)

Table 7-3 Prior studies of laser-assisted chemical vapor deposition of platinum, palladium, and nickel.

Compound	Source Pressure (torr)	Deposition Rate ($\mu\text{m/s}$)	Laser Wavelength (nm)	Laser Power (mW)	Substrate Temperature ($^{\circ}\text{C}$)	Substrate	Ref.
$\text{Pt}(\text{hfac})_2^{\text{a}}$	0.008-0.8	0.01-5.0	458, 514	10-1000	---	SiO_2	63
$\text{Pt}(\text{hfac})_2$	0.002	10^{-5} - 10^{-2}	351-363	0.001-100	50-500	SiO_2	64,65
$\text{Pt}(\text{PF}_3)_4$	0.6	10^{-4} - 10^{-3} b	248	10-100 b	25-150	Si, Al, C, SiO_2 , Cu	66,67
$(\text{C}_5\text{H}_5)\text{Pt}(\text{CH}_3)_3$	0.4	2×10^{-4}	308, 351, 364	10-30	50	SiO_2 , Al_2O_3 , GaAs	68
$(\text{C}_5\text{H}_5)\text{Pd}(\text{allyl})$	<0.001	2×10^{-4}	337	5	25-50	Ni/Si	70
$\text{Ni}(\text{C}_5\text{H}_5)_2$	<0.001	8×10^{-6}	337	5	25-50	Si	70
$\text{Ni}(\text{CO})_4$	40	1-17	10600	500-5000	140-1100	SiO_2	76,77
$\text{Ni}(\text{CO})_4$	300	1-20	476, 531, 647	5-200	---	Si, SiO_2 , Ni	81,82
$\text{Ni}(\text{CO})_4$	0.1-10	0.02-4.0	418-514, 10600	200-3000	220-410	Ni/Si/ SiO_2	83,84

^ahfac = 1,1,1,5,5,5-hexafluoroacetylacetonate.

^bEstimated from data presented in publication.

7.5.1 Platinum

A thorough study of the LCVD of platinum with $\text{Pt}(\text{hfac})_2$ has been made by van den Bergh.⁶⁰⁻⁶⁵ A glass substrate was suspended in a cell in which the platinum compound was vaporized to a known pressure. Then the substrate was irradiated with a focused beam of photons at 257, 351-363, 458 or 514 nm from an argon ion laser. The diameter of the spot illuminated on the substrate was 5 μm . Platinum lines could be deposited by translating the cell along an xy stage. The results of this study are summarized in the first two entries in Table 7-3. Deposition rates as high as 5 $\mu\text{m/s}$ were achieved by pyrolytic decomposition of the precursor with 458 or 514 nm photons. This is similar to the rates obtained during LCVD of gold from $(\text{hfac})\text{Au}(\text{CH}_3)_2$ which is discussed in Chapter 6. By contrast, photolytic decomposition of the precursor with 257 or 350 nm photons yields growth rates of less than 0.01 $\mu\text{m/s}$. Braichotte and van den Bergh⁶² observed that under the right conditions, both pyrolytic and photolytic decomposition produce films with greater than 90% platinum, the remainder being carbon and oxygen.

In the pyrolytic LCVD process, platinum stripes were deposited at scan speeds of 0.5 to 100 $\mu\text{m/s}$. These speeds kept the residence time at a given position below 10 s thereby insuring that the glass substrate did not melt during illumination. Under these transient conditions, the deposition rate is limited only by reaction of the $\text{Pt}(\text{hfac})_2$ on the heated surface. Braichotte and van den Bergh⁶³ found that the height of the platinum stripe increases linearly with increasing $\text{Pt}(\text{hfac})_2$ vapor pressure and laser power and decreasing scan speed. On the other hand, the width of the platinum stripe increases with

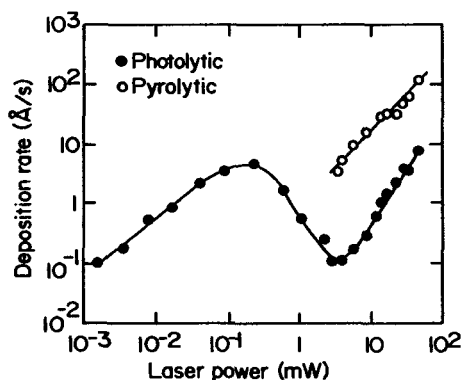


Figure 7-5 The dependence of the platinum deposition rate on the laser power for irradiating a 3 μm spot with 351-363 nm photons at a $\text{Pt}(\text{hfac})_2$ vapor pressure of 0.002 torr and a substrate temperature of 42 °C.⁶⁵

laser power but is not dependent on the $\text{Pt}(\text{hfac})_2$ partial pressure. The stripe width is approximately constant at 45 μm for scan speeds between 0.1 and 2.0 $\mu\text{m/s}$ and then falls to an asymptotic value of 10 μm as the speed increases from 2 to 100 $\mu\text{m/s}$. These authors also measured the dependence of the film resistivity on the LCVD conditions. Minimum values of 1.5 times bulk platinum were obtained at 0.04-0.5 torr $\text{Pt}(\text{hfac})_2$, 10-200 mW laser power, and 5-20 $\mu\text{m/s}$ scan speeds.

Braichotte and van den Bergh^{64,65} measured the rate of platinum LCVD with 351-363 nm photons over a broad range of illumination intensities. Their results are shown in Figure 7-5. The growth rates were monitored by following the change in light transmission through the glass during the first 30 s of reaction. Three growth regimes are evident: with increasing laser power, the deposition rate increases, decreases, then increases again. In the first regime between 10^{-3} and 10^{-1} mW power, deposition is driven by photolysis of $\text{Pt}(\text{hfac})_2$ adsorbed on the glass surface. The rate of deposition can be expressed as follows^{64,87,88}

$$R_g = \frac{P\sigma_s C_s}{h\nu(\pi r^2)} \left(\frac{M_{wt}}{\rho} \right) \quad (7.15)$$

where P is the laser power (W), σ_s is the molecular absorption coefficient of the adsorbed precursor ($\text{cm}^2/\text{molecule}$), C_s is the concentration of the adsorbed precursor (mol/cm^2), h is Plank's constant, ν is the frequency of the light (s^{-1}), r is the radius of the illuminated spot (cm), and M_{wt} and ρ are the molecular weight (g/mol) and density (g/cm^3) of the platinum film. Consistent with Equation 7.15, the growth rate was proportional to P/r^2 in this regime. In addition, the growth rate fell upon heating the substrate because this lowered the concentration of adsorbed precursor. In the second regime between 10^{-1} and 5 mW power, deposition is also driven by photolysis of the adsorbed precursor. However, the glass substrate is heated somewhat by the laser beam. As the laser power increases, the surface temperature rises causing the adsorbate concentration and, in turn, the growth rate to fall.

In the third regime between 5 and 100 mW power, deposition is initiated by photolysis of $\text{Pt}(\text{hfac})_2$ in the gas, then subsequently is driven by pyrolysis of the $\text{Pt}(\text{hfac})_2$ on the surface. The transition from photolysis to pyrolysis is evident as an abrupt change in the rate of decrease of transmitted light during illumination.⁶⁴ The rate of film growth by gas-phase photolysis is given by Equation 7.16^{87,88}

$$R_g = \frac{P\sigma_g C_g}{h\nu(\pi r^2)} \left(\frac{V}{A} \right) \left(\frac{M_{wt}}{\rho} \right) \quad (7.16)$$

where σ_g and C_g are the molecular absorption coefficient ($\text{cm}^2/\text{molecule}$) and the concentration (mol/cm^3) of the precursor in the gas, and V/A is the ratio of the gas volume contributing to deposition to the area of deposition. The V/A ratio can be approximated as the radius of the spot, r .⁸⁷ With this assumption, Equation 7.16 predicts that the growth rate is proportional to P/r . This is precisely the dependence observed by Braichotte and van den Bergh at high laser powers.⁶⁴ Once the platinum film has deposited to a thickness sufficient to absorb all the incident light, the surface temperature rises and pyrolysis takes over. It was calculated that a surface temperature rise of 500 °C occurs in 5 s at 15 mW laser power.

Schröder et al.^{66,67} have investigated platinum deposition by photolysis of $\text{Pt}(\text{PF}_3)_4$ with 248 nm photons from a KrF excimer laser. The laser illuminated a $50 \times 4 \text{ mm}^2$ area of the substrate at fluences ranging from 10 to 200 mJ/cm^2 . The source pressure was 0.6 torr. The rate of platinum deposition was sensitive to the substrate used, decreasing in the following order: $\text{Si} > \text{Al} > \text{C} > \text{SiO}_2 > \text{Cu}$. The authors speculated that irradiation of the substrate with the excimer laser generates "hot" electrons which are captured by the adsorbed metal complex and induce its dissociation. At 200 mJ/cm^2 with an aluminum substrate, 0.6 monolayers are deposited per pulse. Assuming a monolayer thickness of 1.5 Å and a pulse rate of 10 Hz, this yields a growth rate of 3.2 $\mu\text{m}/\text{h}$. The properties of the platinum films were not assessed in this study.

The LCVD of platinum from $(\text{C}_5\text{H}_5)\text{Pt}(\text{CH}_3)_3$ has been examined by Koplitz et al.⁶⁸ They transported the complex in a mixture of argon and hydrogen into a reactor where the substrate was illuminated with 308 nm photons from an XeCl excimer laser and with 351 and 364 nm photons from an argon ion laser. The excimer laser irradiated a circle 1 mm in radius at a power of 2.6 mJ/pulse with a 10 Hz repetition rate. The argon ion laser was operated at 4.5 mW/mm^2 . In the presence of hydrogen, shiny metal deposits approximately 1000 Å thick were deposited in 10 min. Auger electron spectroscopy of sputtered films revealed that they were free of carbon and oxygen. If hydrogen was omitted during deposition, the deposits were black and contained roughly 20 at% carbon. Their results indicate that the $(\text{C}_5\text{H}_5)\text{Pt}(\text{CH}_3)_3$ complex is photodissociated in the gas and possibly on the surface by the 308, 351 and 364 nm photons. The reactive intermediates generated by this process diffuse to the substrate, adsorb and decompose to deposit the film. When hydrogen is present, the adsorbed hydrocarbon fragments are catalytically hydrogenated leaving a pure platinum film.

Recently, Shaver et al.⁶⁹ demonstrated that LCVD of platinum can be used to modify and repair integrated circuits. Laser writing was performed in a static cell containing the circuit to be repaired and 5 torr of $\text{Pt}(\text{PF}_3)_4$. A 1 μm spot on the circuit was irradiated with an argon ion laser operating at 488 nm and 50 mW power at the focal point. Platinum lines 5 μm wide by 1 μm thick were deposited at a rate of about 250 $\mu\text{m}/\text{s}$. The authors claim that writing rates as high as 5 mm/s are achievable on

polyimide substrates. Platinum lines deposited by this technique exhibit a resistivity equal to bulk Pt, 10-11 $\mu\Omega\text{cm}$. In addition, good step coverage is achieved, and the oxide and underlying layers of the integrated circuit are not damaged.

7.5.2 Palladium

Thomas and Park⁵¹ have studied the photolytic deposition of palladium by illumination of $(\text{C}_5\text{H}_5)\text{Pd}(\text{allyl})$ with 254 nm photons from a mercury lamp at $\sim 1.5 \text{ mW/cm}^2$. The complex was sublimed into an evacuated vessel to its equilibrium vapor pressure of about 0.02 torr at 25 °C. The substrate was then illuminated through a mask and deposited a thin film. The films consisted of palladium crystallites about 1000 Å in diameter suspended in an organic polymer matrix. The polymer probably forms by radical polymerization of the photodissociated C_5H_5 and allyl ligands. Thomas and Park found that these films are effective catalysts for electroless copper plating.⁵¹

The laser-assisted CVD of palladium and nickel composites using $(\text{C}_5\text{H}_5)\text{Pd}(\text{allyl})$ and $\text{Ni}(\text{C}_5\text{H}_5)_2$ sources have been studied by Stauff and Dowben.^{70,71} Their results are summarized in Table 7-3. The organometallic compounds were vaporized into an evacuated vessel to a pressure of less than 0.001 torr. Deposition was initiated by irradiating a 1.26 mm² spot on a silicon wafer with 337 nm photons from an N_2 laser. For laser operation at 0.4 W/cm^2 and 10 Hz repetition rate, the nickel deposited on the silicon substrate at 300 Å/h, then the palladium deposited on the nickel film at 8000 Å/h. A depth profile using Auger electron spectroscopy revealed that the Pd/Ni composite contained 5-10 at% carbon and no detectable oxygen. Palladium stripes deposited on polyimide films by this technique are of similar purity.⁷² However, the resistivity of these stripes are approximately 1000 times higher than the value for bulk Pd, indicating that the palladium deposits are porous. Based on an analysis of the gas-phase decomposition of $(\text{C}_5\text{H}_5)\text{Pd}(\text{allyl})$, Stauff and coworkers⁷³ concluded that their LCVD process must be heterogeneous, i.e., the precursor is photolyzed by the 337 nm light after it adsorbs on the Pd film surface.

The deposition of palladium stripes by LCVD of $\text{Pd}(\text{hfac})_2$ was attempted by Cole et al.⁷⁴ A polyimide substrate was mounted in a vessel containing 0.5 torr of the complex. Then a 5- μm -wide stripe on the substrate was irradiated with 351 nm photons from an argon ion laser. Following deposition of a palladium seed layer, the sample was immersed in an electroless copper solution to plate a copper film on the Pd. The laser powers needed to decompose the $\text{Pd}(\text{hfac})_2$ were sufficient to also decompose the polyimide.

The above process competes with an alternative procedure for selective deposition of palladium in which a palladium acetate solution is spun onto a substrate. This solution

is then decomposed to a thin metal film by irradiating it with an ultraviolet excimer laser through a mask.⁸⁹⁻⁹⁵ This process does not involve CVD so it will not be examined here.

7.5.3 Nickel

The first work on LCVD of nickel was undertaken by Allen.⁷⁵⁻⁸⁰ She illuminated a small spot on a quartz substrate with 10.6 μm photons from a pulsed and cw CO_2 laser. The radiation from the laser heated the surface to a temperature sufficient to decompose the $\text{Ni}(\text{CO})_4$ into a nickel film and carbon monoxide gas. At 10.6 μm , the $\text{Ni}(\text{CO})_4$ in the gas absorbed less than 1% of the incident photons. Nickel deposition rates varied from 1 to 17 $\mu\text{m/s}$ at 40 torr of $\text{Ni}(\text{CO})_4$, 140 $^\circ\text{C}$ substrate temperature, and laser powers of 0.5 to 5.0 W. Allen found that nickel films can be deposited up to a maximum thickness of 550 \AA . Thicker films could not be deposited because the metal surface reflected the incident light and did not get hot enough to decompose the $\text{Ni}(\text{CO})_4$. Nickel films deposited by this technique are strongly adherent and exhibit a resistivity of 40 $\mu\Omega\text{cm}$, or 5 times that of the bulk metal.

Bäuerle^{81,82} has examined the LCVD of nickel using $\text{Ni}(\text{CO})_4$ and a cw krypton ion laser at 476, 531 and 647 nm. The beam was focused onto different substrates held in a chamber containing 300 torr of $\text{Ni}(\text{CO})_4$. The nickel films were deposited as stripes along the substrate surface or as rods perpendicular to the substrate. The results of these experiments are summarized in the second to last entry in Table 7-3. No effect of the laser wavelength on the deposition process was observed confirming that the reaction is thermally driven. For a constant scan speed, the height and width of the nickel stripes increases linearly with the laser power. This result is similar to that observed by Braichotte and van den Bergh for LCVD of platinum with $\text{Pt}(\text{hfac})_2$.⁶³ Bäuerle also found that the height and width of the stripes are sensitive to the nature of the substrate. For the same reaction conditions, the deposition rate is more than ten times greater on glass than on 4000 \AA of SiO_2 on silicon. Bäuerle attributed this rate difference to the much higher thermal conductivity of the latter material.^{81,82} The resistivity of the nickel stripes deposited in this study was 2.8 times greater than that of bulk nickel.

Auvert and coworkers^{27,83,84} have made a thorough investigation of the kinetics of nickel LCVD from $\text{Ni}(\text{CO})_4$. An argon ion laser at 488-514 nm and a CO_2 laser at 10.6 μm were used to heat small spots on quartz substrates, 200-300 μm in diameter, to the deposition temperature. In most cases, the quartz substrates were coated with a 1 μm Si film and a 300 nm Ni film in order to achieve more reproducible kinetics. At $\text{Ni}(\text{CO})_4$ pressures below 10 torr, polycrystalline nickel dots which contained 0.5 at% carbon and no oxygen were deposited. Auvert observed two different kinetic regimes depending on the growth conditions: (1) at $\text{Ni}(\text{CO})_4$ pressures below 0.3 torr and laser powers above

1 W, adsorption of the precursor from the gas determined the growth rate, (2) at $\text{Ni}(\text{CO})_4$ pressures above 0.4 torr and laser powers between 0.2 and 1.0 W, a surface reaction controlled the growth rate.

Figure 7-6 shows the effects of $\text{Ni}(\text{CO})_4$ pressure and surface temperature as observed in experiments of Auvert. A thermal energy balance was used to calculate the surface

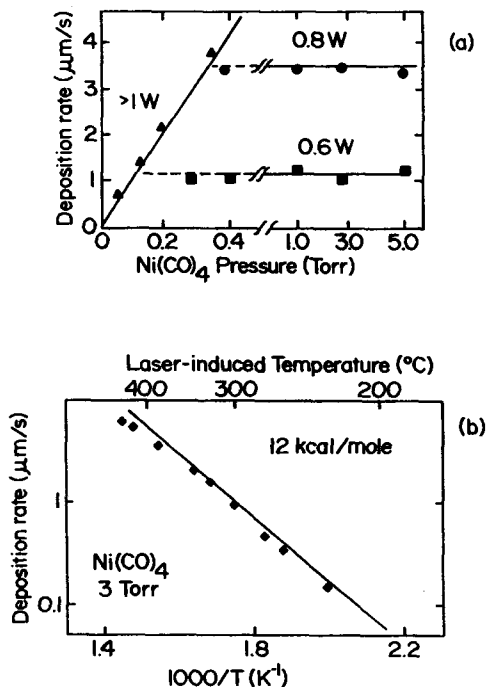


Figure 7-6 The dependence of the nickel deposition rate on (a) $\text{Ni}(\text{CO})_4$ pressure and (b) surface temperature for LCVD with an argon ion laser at 488-514 nm.²⁷

temperature from the incident laser power. The precursor adsorption-limited regime is characterized by the production of flat-topped nickel dots and a growth rate which increases linearly with precursor pressure but is independent of temperature. Conversely, the surface reaction-limited regime is characterized by nickel dots with Gaussian shapes and a growth rate which is independent of precursor pressure but increases with the surface temperature. An activation energy of 12 kcal/mol is measured in the latter regime. These same trends are obtained by illuminating either the front or

back side of the substrate. Since photolytic reactions are rigorously excluded by back-side illumination, this proved that nickel deposition by irradiation with 488-514 nm or 10.6 μm photons is thermally driven.

The activation energy of 12 kcal/mol observed for the laser-induced decomposition of $\text{Ni}(\text{CO})_4$ is considerably lower than the barrier of 22 kcal/mol measured by Carlton and Oxley⁵⁴ for thermal decomposition of $\text{Ni}(\text{CO})_4$. It may be that different steps in the surface reaction are controlling in these two cases. Auvert claims that in his experiment, desorption of carbon monoxide is most likely the rate-determining step, whereas Carlton and Oxley suggest that for their case, a step involving the surface decomposition of $\text{Ni}(\text{CO})_4$ is rate-determining. Another explanation for this discrepancy is that Auvert may have incorrectly calculated the surface temperature induced by the laser irradiation. Further experiments involving spectroscopic characterization of surface intermediates are needed to resolve the decomposition mechanisms of $\text{Ni}(\text{CO})_4$ during thermal and laser-induced CVD.

7.6 Ion-Assisted and Plasma-Assisted CVD

Tao et al.²⁸ have recently evaluated the use of a focused ion beam to induce deposition of platinum lines. The precursor, $(\text{C}_5\text{H}_5)\text{Pt}(\text{CH}_3)_3$, was sprayed through a nozzle onto a substrate mounted in a vacuum chamber at 6×10^{-10} torr. Then, a beam of gallium ions at an energy of 30-40 keV and a current of 20 to 222 pA was scanned across the surface causing the adsorbed organometallic compound to decompose into a solid film. The best results were obtained at the highest beam currents. Under these conditions, the platinum deposits were amorphous and exhibited an atomic composition of 46% Pt, 28% Ga, 24% C, and 2% O. The resistivity of the film was 70 $\mu\Omega\text{cm}$. The main advantage of this approach is the ability to deposit very narrow lines with high precision. In this study, a minimum line width of 0.3 μm was achieved. Thinner lines should be possible with improved ion-beam optics.

A few studies have been made of the plasma-enhanced CVD (PECVD) of group VIII transition metals. Feurer and Suhr^{96,97} deposited palladium and platinum films by decomposing $(\text{C}_5\text{H}_5)\text{Pd}(\text{allyl})$ and $(\text{C}_5\text{H}_5)\text{Pt}(\text{CH}_3)_3$ in a parallel-plate reactor. The precursors were fed at 0.1-2.0 mg/min in an argon flow of 2 to 100 cm^3/min . The reactor was operated with the upper plate at 400 V dc, at power levels of 0.1-0.5 W/cm^2 and a total pressure of 0.15 torr. The films were deposited on glass, polyimide, and alumina. The growth rate and carbon content of the films decreased with increasing substrate temperature. For example, in the case of palladium CVD, the growth rate falls from 12

to $6 \mu\text{g}/(\text{cm}^2\text{min})$, and the film composition changes from 30% C and 70% Pd by weight to 100% Pd, as the substrate temperature increases from 30 to 150°C . Assuming a palladium density of $12.0 \text{ g}/\text{cm}^3$, the lower growth rate equals $0.3 \mu\text{m}/\text{h}$. The lowest recorded resistivities of the metal films were $20 \mu\Omega\text{cm}$ for Pd and $46 \mu\Omega\text{cm}$ for Pt.

Jervis^{98,99} has explored the PECVD of Ni from $\text{Ni}(\text{CO})_4$. He used $10.6 \mu\text{m}$ photons from a pulsed, high-pressure CO_2 laser to create an argon plasma above the surface of the substrate. The $\text{Ni}(\text{CO})_4$ was present in the reactor at a concentration of 1 to 3 mol% in 10 to 20 torr of argon. The carbonyl complex decomposed within the plasma zone resulting in nickel deposition. The films grew at 5 to 15 \AA per pulse, or at 1 to $3 \mu\text{m}/\text{h}$ for a laser repetition rate of 0.5 Hz. Auger electron spectroscopy depth profiling indicated that the atomic composition of the films was 90% Ni, 9% C, and 1% O. However, the average resistivity of the nickel films was $5000 \mu\Omega\text{cm}$, which is 740 times higher than bulk Ni.

7.7 Outlook

A lot of progress has been made in developing viable technologies for CVD of platinum, palladium, and nickel. For the CVD of platinum, two excellent precursors are available, $\text{Pt}(\text{PF}_3)_4$ and $(\text{CH}_3\text{C}_5\text{H}_4)\text{Pt}(\text{CH}_3)_3$. The trifluorophosphine complex is a stable liquid with high vapor pressure, ~ 15 torr at 0°C , that decomposes at $200\text{--}300^\circ\text{C}$ to yield pure platinum films. The main drawback of using this compound is that the PF_3 product is a strong oxidant that reacts with silicon and quartz substrates and deposits phosphorus. The hydrocarbon complex, $(\text{CH}_3\text{C}_5\text{H}_4)\text{Pt}(\text{CH}_3)_3$, is a liquid with good stability but with lower vapor pressure from 0.4 to 3.5 torr at 50 to 100°C . However, by operating at reduced pressures this precursor should provide growth rates between 1 and $150 \mu\text{m}/\text{h}$. The advantage of this compound is that it generates exceptionally pure platinum films in H_2 at low temperature, between 100 and 150°C .

Two excellent precursors are also available for nickel CVD: $\text{Ni}(\text{CO})_4$ and $\text{Ni}(\text{CH}_3\text{C}_5\text{H}_4)_2$. Nickel tetracarbonyl is a relatively stable gas at 25°C . It decomposes at temperatures between 100 and 200°C with deposition of pure nickel films at rates of 10 to $1000 \mu\text{m}/\text{h}$. The only problem with using this compound is its high toxicity. The $\text{Ni}(\text{CH}_3\text{C}_5\text{H}_4)_2$ complex is a liquid above 40°C which can be vaporized at 100 to 150°C to yield source pressures of 4 to 40 torr. This complex deposits pure nickel films in hydrogen at substrate temperatures between 200 and 300°C .

In the case of palladium CVD, suitable precursors appear to be $\text{Pd}(\text{allyl})_2$ and $(\text{C}_5\text{H}_5)\text{Pd}(\text{allyl})_2$. These compounds deposit pure palladium films in hydrogen at low temperature. However, the allyl complexes are air sensitive, thermally unstable, and

exhibit low volatility. Further work needs to be undertaken to test the suitability of other palladium precursors for CVD, such as $\text{Pd}(\text{hfac})_2$, and to better establish the optimal conditions for depositing Pd films from the allyl complexes.

Applications for platinum, palladium, and nickel CVD are just starting to be explored. This process can be used to deposit metal coatings on unusually shaped objects and on materials such as polymers which cannot be heated to high temperatures. Alternatively, these metals may be used as additives in other CVD processes, for example, to deposit aluminum or tungsten, to generate alloys with improved properties, or to catalyze the removal of impurities.¹⁰⁰

Laser-assisted CVD shows promise for direct deposition of metal circuitry without the need for photolithography. The laser can be used to direct-write circuits by scanning a focused beam across the substrate, or it can be used to develop a pattern by illuminating the substrate through a mask. Argon ion lasers emitting photons at ~ 500 nm are well suited for the former application. The visible light selectively heats a $1\text{--}5\text{ }\mu\text{m}$ spot on the substrate, causing pyrolysis of the precursor within the heated region. Exceptionally high deposition rates are achieved with pyrolytic LCVD, on the order of $10\text{ }\mu\text{m/s}$. This enables micron-thick metal lines to be deposited at scan speeds up to 1 mm/s .⁸⁵ In addition, the films can be deposited with high purity and resistivity close to the bulk value. New commercial applications of LCVD have recently been developed,¹⁰¹ and more are expected in the future.

Acknowledgments: We gratefully acknowledge the support of the Deutsche Forschungsgemeinschaft (Germany) for post-doctoral fellowships to A. A. Zinn and L. Brandt; the Department of Chemistry and Biochemistry at UCLA for H. D. Kaesz; and Hughes, Rockwell and the University of California MICRO program for R. F. Hicks.

References

1. Sze, S.M. *Semiconductor Devices, Physics and Technology*, Wiley, New York, NY, 1985.
2. Gurney, P.D., Seymour, R.J. *Chemistry of the Platinum Group Metals; Studies in Inorganic Chemistry 11*, Chpt. 17, Elsevier, New York, 594, 1991.
3. Ghate, P.B. *Proc. Mat. Res. Soc.* **1981**, 10, 371.
4. Eizenberg, M. *Proc. 2nd Intl. Symp. on VLSI Sci. and Technol.* **1984**, 84-7, 348.
5. Green, M.L., Levy, R.A. *J. Met.* **1985**, 37, 63.
6. Gould, H.J. *US Patent* 4 206 540, **1980**.
7. Miller, R.J. *US Patent* 4 322 453, **1982**.
8. Groshart, E. *Met. Finish.* **1972**, August, 49.

9. Bindra, P., Roldan, J. *J. Electrochem. Soc.* **1985**, 132, 2581.
10. Brummett, C.R., Shaak, R.N., Andrews, D.M. *US Patent* 4 006 047, **1977**.
11. Okubi, K., Nogami, T., Takakura, M. *US Patent* 4 830 880, **1989**.
12. Gates, B.C. *Catalytic Chemistry*, Wiley, New York, NY, 1992.
13. Yao, Y.F.Y. *Ind. Eng. Chem. Prod. Res. Dev.* **1980**, 19, 293.
14. Cooper, B.J., Evans, W.D.J., Harrison, B., *Stud. Surf. Sci. Catal.* **1987**, 30, 117.
15. Ghandhi, H.S., Shelef, M. *Stud. Surf. Sci. Catal.* **1987**, 30, 199.
16. Taylor, K.C. *Chemtech* **1990**, September, 551.
17. Locke, R.S. *AESAR Catalog*, Johnson Matthey, Seabrook, NH, 1991.
18. Powell, C.F., Oxley, J.H., Blocher, J.M. *Vapor Deposition*, Wiley, New York, NY 1966.
19. Sherman, A. *Chemical Vapor Deposition for Microelectronics*, Noyes Publ., Park Ridge, NJ, 1987.
20. *Gmelin Handbook of Inorganic Chemistry, Pt Suppl. A1*, Springer-Verlag, New York, NY, 43, 1986.
21. Rubezhov, A.Z. *Nauka (Sci.) Moscow* **1986**, 95.
22. Kaesz, H.D., Williams, R.S., Hicks, R.F., Chen, Y.J., Xue, Z., Xu, D., Shuh, D.K., Thridandam, H. *Mater. Res. Soc. Symp. Proc.* **1989**, 131, 395.
23. Kaesz, H.D., Williams, R.S., Hicks, R.F., Zink, J.I., Chen, Y.-J., Müller, H.-J., Xue, Z., Shuh, D.K., Kim, Y.-K. *New J. Chem.* **1990**, 24, 527.
24. Girolami, G.S., Gozum, J.E. *Mater. Res. Soc. Symp. Proc.* **1990**, 168, 319.
25. Mond, L. *J. Chem. Soc.* **1890**, 57, 749.
26. Gross, M.E., Appelbaum, A., Gallagher, P.K. *J. Appl. Phys.* **1987**, 61, 1628.
27. Auvert, G. *Appl. Surf. Sci.* **1989**, 43, 47.
28. Tao, T., Ro, J.S., Melngailis, J., Xue, Z., Kaesz, H.D. *J. Vac. Sci. Technol.* **1990**, B 8, 1826.
29. Xue, Z., Thridandam, H., Kaesz H.D., Hicks, R.F. *Chem. Mater.* **1992**, 4, 162.
30. Reerink, E.H. *Z. Anorg. Allgem. Chem.* **1928**, 173, 45.
31. Lutton, J.M., Parry, R.W. *J. Amer. Chem. Soc.* **1954**, 76, 4271.
32. Rand, M.J. *J. Electrochem. Soc.* **1973**, 120, 686.
33. Morabito, J.M., Rand, M.J. *Thin Solid Films* **1974**, 22, 293.
34. Rand, M.J. *J. Electrochem. Soc.* **1975**, 122, 811.
35. Kruck, V.Th., Baur, K.Z. *Anorg. Allgem. Chem.* **1969**, 364, 192.
36. Kumar, R., Roy, S., Rashidi, M., Puddephatt, R.J. *Polyhedron* **1989**, 8, 551.
37. Nixon, B., Norton, P.R., Ou, E.C., Puddephatt, R.J., Roy, S., Young, P.A. *Chem. Mater.* **1991**, 3, 222.
38. Dryden, N.H., Kumar, R., Ou, E.C., Rashidi, M., Sujit, R., Norton, P.R., Puddephatt, R.J., Scott, J.D. *Chem. Mater.* **1991**, 3, 677.
39. Chen, Y.J., Kaesz, H.D., Thridandam, H., Hicks, R.F. *Appl. Phys. Lett.* **1988**, 53, 1591.

40. Xue, Z., Strouse, M.J., Shuh, D.K., Knobler, C.B., Kaesz, H.D., Hicks, R.F., Williams, R.S. *J. Am. Chem. Soc.* **1989**, *111*, 8779.
41. Gozum, J.E., Pollina, D.M., Jensen, J.A., Girolami, G.S. *J. Am. Chem. Soc.* **1988**, *110*, 2688.
42. Egger, K.W. *J. Organomet. Chem.* **1970**, *24*, 501.
43. Shaver, A. *Can. J. Chem.* **1978**, *56*, 2281.
44. Zinn, A.A., Brandt, L., Kaesz, H.D., unpublished results.
45. Miller, T.M., Izumi, A.N., Shih, Y.S., Whitesides, G.M. *J. Am. Chem. Soc.* **1988**, *110*, 3146.
46. Miller, T.M., McCarthy, T.J., Whitesides, G.M. *J. Am. Chem. Soc.* **1988**, *110*, 3156.
47. Miller, T.M., Whitesides, G.M. *J. Am. Chem. Soc.* **1988**, *110*, 3164.
48. Lee, T.R., Whitesides, G.M. *Accts. Chem. Res.* **1992**, *25*, 266.
49. Yermakov, Y.I. *Catal. Rev.-Sci. Eng.* **1976**, *13*, 77.
50. Viguié, J.C., Spitz, J. *J. Electrochem. Soc.* **1975**, *122*, 585.
51. Thomas, R.R., Park, J.M. *J. Electrochem. Soc.* **1989**, *136*, 1661.
52. Mond, R. *Chem. Ind.* **1930**, 49T, 371.
53. Chan, R.K., McIntosh, R. *Can. J. Chem.* **1962**, *40*, 845.
54. Carlton, H.E., Oxley, J.H. *AIChE J.* **1967**, *13*, 86.
55. Kaplin, Y.A., Belysheva, G.V., Zhil'tsov, S.F., Domrachev, G.A., Chernyshova, L.S. *Zh. Obsch. Khim.* **1980**, *50*, 118.
56. van den Brekel, C.H.J., Fonville, R.M.M., van der Straten, P.J.M., Verspui, G. *Proc. 8th Intl. Conf. on CVD* **1981**, 142.
57. Stauff, G.T., Driscoll, D.C., Dowben, P.A., Barfuss, S., Grade, M. *Thin Solid Films* **1987**, *153*, 421.
58. *Gmelin Handbook of Inorganic Chemistry, Ni Suppl. 2*, Springer-Verlag, New York, NY, 193, 1974.
59. Dyagileva, L.M., Druzhkov, O.N., Andrianov, Yu.A. *Zh. Obsch. Khim.* **1977**, *47*, 82.
60. Braichotte, D., van den Bergh, H. *Proc. Intl. Conf. Laser Process. and Diagnos., Springer Ser. Chem. Phys.*, **1984**, *39*, 183.
61. Qui, M., Monot, R., van den Bergh, H. *Scientia Sinica A* **1984**, *27*, 531.
62. Braichotte, D., van den Bergh, H. *Proc. Intl. Conf. Laser* **1985**, 688.
63. Braichotte, D., van den Bergh, H. *Appl. Phys. A* **1987**, *44*, 353.
64. Braichotte, D., van den Bergh, H. *Appl. Phys. A* **1988**, *45*, 337.
65. Braichotte, D., van den Bergh, H. *Appl. Phys. A* **1989**, *49*, 189.
66. Schröder, H., Gianinoni, I., Masci, D., Kompa, K.L. *Proc. Intl. Conf. Laser Process. and Diagnos., Springer Ser. Chem. Phys.*, **1984**, *39*, 257.
67. Schröder, H., Kompa, K.L., Masci, D., Gianinoni, I. *Appl. Phys. A* **1985**, *38*, 227.
68. Koplit, L.V., Shuh, D.K., Chen, Y.J., Williams, R.S., Zink, J.I. *Appl. Phys. Lett.* **1988**, *53*, 1705.

69. Shaver, D.C., Doran, S.P., Rothschild, M., Sedlacek, J.H.C. *Proc. Int. Soc. Optical Engr.* **1991** 1596, 46.
70. Stauf, G.T., Dowben, P.A. *Thin Solid Films* **1988**, 156, L31.
71. Emrich, K.H., Stauf, G.T., Hirschwald, W., Barfuss, S., Dowben, P.A., Birge, R.R., Boag, N.M. *Mater. Res. Soc. Symp. Proc.* **1989**, 131, 401.
72. Kim, Y.-G., Bialy, S., Stauf, G.T., Miller, R.W., Spencer, J.T., Dowben, P.A., Datta, S. *J. Micromech. Microeng.* **1991**, 1, 42.
73. Stauf, G.T., Dowben, P.A., Emrich, K., Barfuss, S., Hirschwald, W., Boag, N.M. *J. Phys. Chem.* **1989**, 93, 749.
74. Cole, H.S., Liu, Y.S., Guida, R., Levinson, L.M., Philipp, H.R. *Proc. Electrochem. Soc.* **1988**, 88-10, 187.
75. Allen, S.D., Bass, M. *J. Vac. Sci. Technol.* **1979**, 16, 431.
76. Allen, S.D., Trigubo, A.B., Liu, Y.C. *Proc. 8th Intl. Conf. on CVD* **1981**, 267.
77. Allen, S.D. *J. Appl. Phys.* **1981**, 52, 6501.
78. Allen, S.D., Jan, R.Y., Mazuk, S.M., Shin, K.J., Vernon, S.D. *Mat. Res. Soc. Symp. Proc.* **1984**, 19, 1.
79. Allen, S.D., Jan, R.Y., Mazuk, S.M., Vernon, S.D. *J. Appl. Phys.* **1985**, 58, 327.
80. Allen, S.D., Goldstone, J.A., Stone, J.P., Jan, R.Y. *J. Appl. Phys.* **1986**, 59, 1653.
81. Bäuerle, D. *Mat. Res. Soc. Symp. Proc.* **1983**, 17, 1.
82. Kräuter, W., Bäuerle, D., Fimberger, F. *Appl. Phys. A* **1983**, 31, 13.
83. Tonneau, D., Auvert, G., Pauleau, Y. *J. Appl. Phys.* **1988**, 64, 5189.
84. Tonneau, D., Auvert, G., Pauleau, Y. *J. Appl. Phys.* **1988**, 66, 165.
85. Herman, I.P., Hyde, R.A., McWilliams, B.M., Weisberg, A.H., Wood, L.L. *Mat. Res. Soc. Symp. Proc.* **1983**, 17, 1.
86. Armstrong, J.V., Burk, A.A., Jr., Coey, J.M.D., Moorjani, K. *Appl. Phys. Lett.* **1987**, 50, 1231.
87. Wood, T.H., White, J.C., Thacker, B.A. *Appl. Phys. Lett.* **1983**, 42, 408.
88. Liu, B., Hicks, R.F., Zinck, J.J. *J. Crystal Growth* **1992**, 123, 500.
89. Liu, Y.S., Cole, H.S. *Mat. Res. Soc. Symp. Proc.* **1989**, 129, 1.
90. Liu, Y.S., Cole, H.S. *Mat. Res. Soc. Symp. Proc.* **1989**, 154, 1.
91. Esrom, H., Wahl, G., Stuke, M. *Mat. Res. Soc. Symp. Proc.* **1989**, 131, 581.
92. Esrom, H., Demny, J., Kogelschatz, U. *Chemtronics* **1989**, 4, 202.
93. Esrom, H., Wahl, G. *Chemtronics* **1989**, 4, 216.
94. Zhang, Y., Stuke, M. *Appl. Surf. Sci.* **1990**, 46, 153.
95. Esrom, H., Kogelschatz, U. *Appl. Surf. Sci.* **1990**, 46, 158.
96. Feurer, E., Suhr, H. *Thin Solid Films* **1988**, 157, 81.
97. Feurer, E., Kraus, S., Suhr, H. *J. Vac. Sci. Technol.* **1989**, A 7, 2799.
98. Jervis, T.R. *J. Appl. Phys.* **1985**, 58, 1400.
99. Jervis, T.R., Newkirk, L.R. *J. Mater. Res.* **1986**, 1, 420.
100. Niemer, B., Zinn, A.A., Stovall, W.K., Gee, P.E., Hicks, R.F., Kaesz, H.D. *Appl. Phys. Lett.* **1992**, 61, 1793.
101. Baum, T.H., Comita, P.B., Kodas, T.T. *SPIE Proc.: Lasers in Microelectronic Manufacturing* **1991**, 1598, 122.

This Page Intentionally Left Blank

Chapter 8

Chemical Vapor Deposition of Assorted Metals

Mark J. Hampden-Smith^a
Toivo T. Kodas^b

Departments of Chemistry^a and Chemical Engineering^b
University of New Mexico
Albuquerque, NM 87131

Abstract

The CVD of Ti, Zr, Hf, V, Nb, Ta, Cr, Mo, Mn, Tc, Re, Fe, Ru, Os, Co, Rh, Ir, Zn, Cd, Sn, and Pb is discussed. Precursors are grouped as metal-halide, alkyl, alkene, alkyne, allyl, cyclopentadienyl, arene, carbonyl, phosphine, β -diketonate, and alkoxide complexes for discussions of their characteristics, reaction mechanisms, and kinetics. In most cases, these metals have been studied to a limited extent, with the most comprehensive results being available for Nb, Ta, Cr, Mo, Fe, Ru, Co, Rh, and Ir. The precursors most extensively studied are metal halides, cyclopentadienyls, and carbonyls. Much less attention has been paid to developing organometallic precursors for deposition of high-purity films at low temperatures and high rates. Selective CVD has been studied for Mo but rarely for other systems.

Contents

8.1	Introduction	360
8.2	Chemical and Physical Properties	367
8.2.1	Introduction	367
8.2.2	Precursor Characteristics	369
8.2.2.1	Metal Halides	369
8.2.2.2	Metal Alkyls	372
8.2.2.3	Complexes with Unsaturated Organic Ligands: Alkenes, Alkynes, Allyls, η^5 -Cyclopentadienyls, η^6 -Arenes and Related Complexes	374
8.2.2.4	Metal Carbonyls	378
8.2.2.5	Metal Trifluorophosphines	380
8.2.2.6	Metal β -diketonates	381
8.2.2.7	Metal Alkoxides	383
8.2.3	Vapor Pressures	383
8.3	Syntheses	385
8.4	Chemical Vapor Deposition	385
8.4.1	Deposition Characteristics	385
8.4.1.1	Introduction	385
8.4.1.2	Titanium	386
8.4.1.3	Zirconium	386
8.4.1.4	Hafnium	386
8.4.1.5	Vanadium	386
8.4.1.6	Niobium	387
8.4.1.7	Tantalum	388
8.4.1.8	Chromium	388
8.4.1.9	Molybdenum	390
8.4.1.10	Manganese	392
8.4.1.11	Technetium	392
8.4.1.12	Rhenium	392
8.4.1.13	Iron	393
8.4.1.14	Ruthenium	394
8.4.1.15	Osmium	395
8.4.1.16	Cobalt	395
8.4.1.17	Rhodium	397
8.4.1.18	Iridium	398
8.4.1.19	Zinc	400
8.4.1.20	Cadmium	400
8.4.1.21	Tin	400
8.4.1.22	Lead	400

8.4.1.23	Heterometallic Systems	401
8.4.2	Kinetics and Mechanisms	402
8.4.2.1	Metal Halides	402
8.4.2.2	Metal Alkyls	405
8.4.2.3	Complexes with Unsaturated Organic Ligands: Olefins, Alkynes, Allyls, Metallocenes, and Related Complexes	407
8.4.2.4	Metal Carbonyls	411
8.4.2.5	Trifluorophosphines	413
8.4.2.6	Metal β -diketonates	413
8.4.2.7	Bi- and Multi-Nuclear Complexes	414
8.4.2.8	Heteronuclear Complexes	414
8.4.3	Selectivity	415
8.5	Summary and Conclusions	416
Acknowledgments		417
References		417

8.1 Introduction

In this Chapter we review the chemical vapor deposition (CVD) of several metals used for electronics and other applications. We include metals of Groups 4-9, 12, and the remaining elements of Group 14 (Sn, Pb) which are illustrated schematically in Figure 8-1. Not relevant to the present discussion include Group 1 alkali metal ions, which are extremely detrimental to the performance of electronic devices,¹ Group 2 alkaline earth, and Group 3 metals, all of which are seldom deposited by themselves. Also outside the scope of this discussion are metals used to form "13-15" or "III-V" materials,²⁻⁵ the remaining metals of Groups 13 and 15, silicon, and germanium which have been reviewed in numerous articles and books elsewhere.⁶⁻²² Earlier chapters focused on the metals that have been studied more extensively.

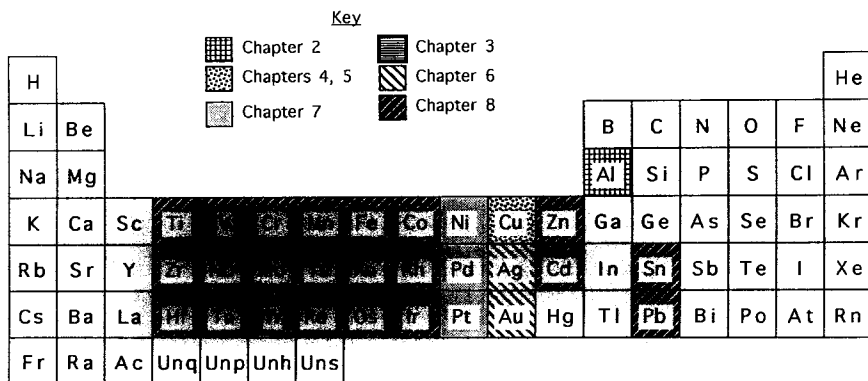


Figure 8-1 Schematic representation of metals reviewed in this and other chapters.

The properties of the metals we discuss, together with the corresponding data for the metals described in the other chapters, are presented in Table 8-1. For microelectronics applications, the resistivity and work function are probably the most important physical properties of the metal. However, melting point is important for high-temperature applications. Other properties important for a variety of applications include density, thermal expansion coefficient, thermal conductivity, oxidation resistance, and corrosion resistance.

There are many applications for these metals (see Table 8-2), and they can be grouped almost entirely by their properties, i.e., corrosion and oxidation protection, dopants in semiconductors, and electronic applications where the metal is used in elemental form or as a metal nitride, silicide, or oxide. Most applications are found in electronics where the

metals we discuss are interesting because of their potential use as contact, gate electrode, diffusion barrier, or interconnect materials in integrated circuits and packaging applications (see Ch. 1). In microelectronics applications, the ability to deposit pure, continuous, dense films with near-bulk physical properties is a critical aspect of CVD, and this aspect will be addressed in the following sections.

Table 8-1 Relevant Properties of Metals for Metallization Applications

Metal	Melting point (°C)	Resistivity ($\mu\Omega\text{cm}$)	Work Function (V)	Density (g/cm^3)
Al	660	2.65	4.08	2.7
Ti	1820	42.0	4.33	4.5
Zr	1750	40.0	4.21	6.5
Hf	2230	35.1	3.53	5.9
V	1915	25	4.30	6.1
Nb	2415	12.5	4.01	8.8
Ta	2996	12.5	4.19	16.6
Cr	1900	12.9	4.60	7.2
Mo	2625	5.2	4.20	10.2
W	3410	5.7	4.52 [‡]	19.3
Mn	1244	185.0	3.83	7.4
Re	3170	19.3	5.1	20
Fe	1535	9.71	4.04	7.9
Ru	2282	7.6 [†]	4.71	12.4
Os	3045	9.5	4.55	22.6
Co	1495	6.24	4.40	8.9
Rh	1960	4.51	4.8	12.4
Ir	2443	5.3	5.27	22.7
Ni	1455	6.84	5.02	8.2
Pd	1552	10.8	4.98	12.0
Pt	1769	10.6	5.34	21.4
Cu	1083	1.67	4.65	9.0
Ag	961	1.59	4.73	10.5
Au	1064	2.35	4.82	19.3

[‡] (001) face

[†] at 0 °C

Table 8-2 Applications of Metals

Ti	Adhesion layers, metal foils, corrosion resistant coatings, titanium aluminides, contacts in ICs, Ti:LiNbO ₃ waveguides, TiN diffusion barriers, TiSi ₂ contact layers
V	V-Si diodes, nitride diffusion barriers
Nb	Nuclear fuel particle coating, cladding for metal tubes, component of Nb ₃ Ge and Nb ₃ Ga superconductors, NbN diffusion barriers, metal alloy diffusion barriers, metal silicide contact layers
Ta	Capacitors, resistors, corrosion-resistant coatings, TaN and Ta-Si-N diffusion barriers, tantalum silicide contact layers
Cr	Corrosion protection, oxidation protection, possible contact metallization, CrN diffusion barriers, silicide contact layers
Mo	IC contact and gate metallization, MoSi ₂ for microelectronics, Schottky contact metallization, wear resistant coatings, infrared reflector, laser mirror coating
Re	Heaters for furnaces, free standing shapes, contact layers, diffusion barriers, thermocouples, W:Re alloys
Fe	GaAs devices, FeN diffusion barriers, metal alloy and metal silicide diffusion barriers
Ru	Electrical contacts, diffusion barriers
Os	Thermionic diodes
Co	CoSi ₂ for microelectronics, catalyst for electroless plating, possible interconnect in specialized applications
Rh	Electrical contacts, diffusion barriers
Ir	Corrosion protection, oxidation protection, thermionic cathodes, silicide diffusion barriers
Zn	Dopant in GaAs materials
Cd	Photoresist and mask repair
Sn	Dopant in GaAs and other materials, metal nitride diffusion barriers
Pb	Solder

Certain criteria can be established for the use of metals as conductors in integrated circuits, packaging applications, adhesion layers, and circuit boards. The metal films should have low resistivity, high melting points, be easy to etch, be stable in oxidizing environments, and at the same time be capable of oxidation. They should also have good mechanical stability, good adhesion characteristics, low stress, be stable to other processing steps, not contaminate devices, and not react with other materials. Unfortunately, most metals do not satisfy all or even many of these requirements as

indicated in previous chapters. For example, while silver has the lowest resistivity of all metals, it is unstable on most surfaces with respect to oxidation, adhesion, and diffusion (see Ch. 6). Copper has low resistivity but a high diffusion rate into Si and SiO₂ necessitating the use of diffusion barrier layers if it is to be used in interconnect applications (see Ch.s 1, 4, and 5). Copper, like a number of noble metals, is also difficult to etch. Gold has low resistivity but forms a low melting (370 °C) alloy with silicon (see Ch. 6). For this reason, copper and gold are used in packaging applications where contact with silicon is not necessary.²¹ With existing metallization schemes, aluminum is the metal with which industry has the most experience and which satisfies most of the requirements for integrated circuits (see Ch.s 1 and 2). The major drawbacks of aluminum, however, include its low electromigration resistance which limits critical current densities and its low melting point which is circumvented by deposition towards the end of the metallization scheme after the highest temperature step. Most of the other metals have resistivities which are too high for metallization applications but have certain unique combinations of properties that make them useful for other applications or make them attractive as components of other materials such as metal nitrides, silicides, and oxides.

A number of properties of metals have been identified that make them undesirable as conductors for very-large-scale integration (VLSI) and ultra-large-scale integration (ULSI) applications (Table 8-3). Many metals suffer from poor thermal or chemical stability, and this has inspired investigations of alloy materials which have significantly improved properties when compared to the individual elements. Molybdenum disilicide, MoSi₂, is a classic example, and according to Galasso, it exhibits good electrical conductivity (100 μΩcm), has a high melting point, and is stable against chemical attack and oxidation even at elevated temperatures; cobalt disilicide, CoSi₂, is another example.²² The CVD of silicides, borides, and nitrides has been discussed in detail elsewhere.²²

Purity levels of metals and other materials containing metal atoms may be impaired by several species used in electronics applications. In particular, the presence of alkali metal ions, generally sodium and potassium and radioactive isotopes, cause problems. Alkali metal ions present in the gate insulator are mobile and migrate to the silicon-insulator interface under the influence of an electric field; carrier mobilities are then diminished and the devices are then also unreliable.²³ The source of these impurities, apart from mishandling, is generally metals and reagents used in the fabrication process. The purity of sputtering targets is a concern for physically deposited films; the choice of reagents and the precursor purification processes are also important for CVD-derived metal films. Radioactive isotopes, particularly alpha-particle emitters such as uranium and thorium, are undesirable because they can lead to soft errors such as the accidental switching of transistors. Although there are no current specifications for tolerable levels of impurities, it is desirable to keep their concentration in the low ppb range.

Table 8-3 Undesirable Properties of Metals for Metallization Applications

Undesirable Property	Metal
Low melting point	Al Mg
Low eutectic temperature ($<800^{\circ}\text{C}$)	Au Pd Al Mg
Medium eutectic temperature ($800^{\circ}\text{C} - 1100^{\circ}\text{C}$)	Ni Pt Ag Cu
High diffusivity into Si	all
Interaction with SiO_2	Hf Zr Ti Ta Nb V Mg Al
High oxidation rate or poor oxidation stability	Refractory metals Rare earth metals Mg Fe Cu Ag
Poor chemical stability (especially in etching solutions)	Refractory metals Fe Co Ni Cu Mg Al
Poor etchability (i.e. good chemical stability)	Pt Pd Ni Co Au Cu
Poor electromigration resistance	Al

Some metals, other than those discussed in Chapters 2 through 7, may function quite well in future generations of integrated circuits. Where short distances are involved (e.g., first level metallization) higher resistivities can be tolerated. In these devices, the formation of patterned metal films will be necessary, and CVD is likely to remain an attractive method for metal-film deposition due to low deposition temperatures, conformal coverage, high purity, lack of radiation damage, and the possibility that selective deposition may be achieved.²⁴ The development of etching processes to achieve selective and anisotropic etching is also important. For example, Mo is a suitable metallization material because it has relatively low resistivity, is inert, has high-temperature stability, has a low thermal expansion coefficient, and can be etched.²⁵

These properties make Mo suitable for incorporation into metallization schemes using existing fabrication techniques.

Other than for use as conductors, there are many applications of these metals for which CVD processes are suitable and a number of cases for which they have been used (Table 8-2). Titanium has been used extensively as an adhesion layer between a metal contact such as Pt and a metal oxide surface such as SiO_2 .²⁶ It is also used as an adhesion layer between metal oxides and metals in packaging applications. Many metals have been deposited on reactive substrates to impart corrosion or oxidation resistance. Metals which have good corrosion resistance include Cr, Mo, W, Nb, Ta, and Ti.²⁷ Many metals are hard and are used as abrasion resistant coatings. For example, Rh has a higher melting point and is harder than Cu or Au. The noble metals tend to be inert with respect to oxidation.²⁴

A number of metals have been deposited on substrates with the intention of inducing reactions with the substrate to form new phases which have specific beneficial properties. Applications of this approach exist for both the coatings and the microelectronics industries. For example, the deposition of Nb,²⁸ Zr, Ir and Mo²⁹ onto graphite substrates at high temperatures via CVD routes often results in formation of metal carbides and generally improves the high-temperature oxidation resistance of the substrate. Many metals, including Mo, Co,³⁰⁻³² and Ti,³³ when deposited on bare silicon substrates form metal disilicides at elevated temperatures. Laser CVD routes have also been used to deposit nuclei of various metals for subsequent electroless deposition processes.³⁴

Many metal films have desirable optical properties. For example, Mo films have high infrared (IR) reflectivity (~97%) and are used in mirrors and other optical applications. In some cases, CVD methods produce films superior to those deposited by more conventional methods (e.g., Rh, electrochemically). In addition, metal nitrides and oxides incorporating metals have useful optoelectronic properties.

A number of metals exhibit properties that result in unique applications. For example, ruthenium films are mechanically strong and chemically inert and can exhibit oxidation resistance at temperatures up to 900 °C.³⁵ However, in the event of adventitious oxidation, RuO_2 , the most stable oxide formed, exhibits a resistivity close to that of the metal and is generally not detrimental to the process. For this reason ruthenium may be applied as a contact material or diffusion barrier (see Ch. 1). Iron- and cobalt-containing films have been used for applications in high-speed, high-power semiconductor lasers due to their properties as semi-insulating confinement layers.^{36,37} Iron-doped semi-insulating InP layers formed by the CVD of Fe, sometimes epitaxially, onto InP substrates have high resistivity and act as blocking layers in long wavelength lasers.³⁶ Rhenium forms high-strength alloys with tungsten and osmium, has a high melting point (3,000 °C), is exceptionally hard, and has a large work function.²⁴ Applications include high-temperature abrasion resistant coatings.

There are many studies of the catalytic behavior of these metals,³⁸ and in many cases, this interest has brought about a need to understand the interaction of metal-organic

molecules with metal surfaces.^{39,40} Molecular information and mechanistic understanding is necessary for insight into ligand-design criteria for metal-organic CVD precursors. There is also extensive interest in the preparation of small metal particles by various techniques, including vapor-phase routes using volatile metal-organic precursors.⁴¹ This interest is often driven by the desire to understand quantum confinement effects in these materials;⁴²⁻⁴⁴ many physical and chemical properties such as electrical conductivity, optical properties, mechanical strength, melting point, catalytic reactivity and catalytic selectivity are size-dependent in the range 1-100 nm.^{45,46} Chemical vapor deposition makes it possible to create thin films and fine particles with dimensions in this range. Furthermore, CVD offers the opportunity to co-deposit more than one metal, either from individual precursors or from a single multimetallic molecule, to prepare alloy films.^{47,48} The reasons for developing CVD methods for the formation of metal films are addressed in Chapters 1 and 9.

It is important to pursue CVD routes as opposed to PVD (physical vapor deposition) or liquid-phase routes to attain conformal coverage, minimize interfacial reactions, avoid changes in stoichiometry during deposition, and reduce dopant redistribution and defects. It will become apparent in subsequent sections that there are many opportunities for the rational design of precursor molecules used to prepare films of these metals. In some cases, existing species are suitable as for $\text{Fe}(\text{CO})_5$; however, only in a few examples have the precursors been designed specifically for the deposition of pure films. The greatest problem, again, is to develop precursors that will deposit high-purity material at low temperatures and high rates for thermally sensitive substrates.

In the following sections we will discuss the physical properties and structures of precursors. The CVD of these metals is summarized to include deposition parameters, kinetic data, selectivity where known, and physical properties of the films deposited. This is followed by a discussion of the kinetics and mechanisms of metal deposition from the different classes of precursors. Many precursors are photo-labile, especially metal carbonyls. Photochemically induced deposition of these metals, particularly using lasers, has been reviewed elsewhere^{34,49-51} and is not discussed here. The CVD of other metals, Be,⁵² U,⁵³ Pu,⁵³ B,^{54,55} and Th⁵⁶ not discussed here, has been covered briefly in the literature.

8.2 Chemical and Physical Properties

8.2.1 Introduction

The following sections are organized according to the position of the metal in the Periodic Table (see Fig. 8-1). The metal-organic derivatives that have been used for CVD are shown in Tables 8-4 and 8-5 and are discussed below. The order of discussion is halides, followed by compounds with metal-carbon bonds, M-R where R = alkyl or aryl, metal-carbon π -complexes such as allyls, cyclopentadienyls and other arene complexes, metal carbonyls, metal trifluorophosphines, and derivatives with M-O bonds, e.g., β -diketonates and alkoxides. Representative examples of the structures of each type of precursor are provided in most sections. These figures are intended to give the reader an appreciation of the metal coordination environment and ligand-bonding mode. These data are generally based on single-crystal X-ray diffraction structures obtained in the solid state and may not be an accurate representation of the structure in the gas phase. In general, there is a paucity of gas-phase structural information for CVD precursors.

Table 8-4 Precursors Used for Deposition of Various Metals

Metal	Derivative	Commercial Availability
Ti	TiI ₄ , TiBr ₄ , (η^5 -C ₅ H ₅) ₂ TiCl ₂	Yes
	"Ti(η^5 -C ₅ H ₅) ₂ "	No
Zr	ZrI ₄ , ZrBr ₄	Yes
	Zr(CH ₂ - <i>t</i> -Bu) ₄	No
Hf	HfI ₄	Yes
V	VI ₂ , VCl ₄ , (η^5 -C ₅ H ₅)V(CO) ₄	Yes
Nb	NbCl ₅ , NbBr ₅	Yes
Ta	TaCl ₅ , TaF ₅ , Ta(CO) ₅	Yes
Cr	CrF ₂ , CrCl ₂ , Cr(CO) ₆ , [η^5 -C ₅ H ₅)Cr(CO) ₃] ₂	Yes
	(η^7 -C ₇ H ₈)Cr(CO) ₃ , Cr(η^6 -C ₆ H ₆) ₂	Yes
	Cr(η^6 -C ₆ H ₅ - <i>i</i> -Pr) ₂ , Cr(cumene) ₂	No
	Cr(CH ₂ - <i>t</i> -Bu) ₄ , Cr(N- <i>i</i> -Pr) ₃	No
Mo	MoF ₅ , MoCl ₅ , Mo(CO) ₆	Yes
	[(η^5 -C ₅ H ₅)Mo(CO) ₃] ₂	Yes

continued

Table 8-4 (continued)

Metal	Derivative	Commercial Availability
	$\text{Mo}(\eta^3\text{-allyl})_4$	No
Mn	$\text{Mn}_2(\text{CO})_{10}$	Yes
Re	ReF_6 , ReCl_5 , $\text{Re}_2(\text{CO})_{10}$, ReOCl_5 , ReOCl_4	Yes
	$\text{HRe}(\text{CO})_5$	No
Fe	FeF_3 , $\text{Fe}(\text{CO})_5$, $\text{Fe}(\eta^5\text{-C}_5\text{H}_5)_2$	Yes
	$[(\eta^5\text{-C}_5\text{H}_5)\text{Fe}(\text{CO})_2]_2$	Yes
Ru	$\text{Ru}_3(\text{CO})_{12}$, $\text{Ru}(\eta^5\text{-C}_5\text{H}_5)_2$, $\text{Ru}(\text{acac})_2$	Yes
	$\text{Ru}(\text{hfb})(\text{CO})_4$	No
Os	OsCl_4	Yes
Co	CoCl_2 , $\text{Co}_2(\text{CO})_8$, $\text{Co}_4(\text{CO})_{12}$	Yes
	$\text{Co}(\text{CO})_3(\text{NO})$, $\text{HCo}(\text{CO})_4$	No
	$\text{CF}_3\text{Co}(\text{CO})_4$, $(\eta^5\text{-C}_5\text{H}_5)\text{Co}(\text{CO})_2$	No
	$\text{Co}(\text{acac})_2$, $\text{Co}(\eta^5\text{-C}_5\text{H}_5)_2$	Yes
Rh	RhCl_3 , $\text{Rh}(\eta^3\text{-allyl})_3$, $\text{Rh}(\text{tfac})_3$	Yes
	$[(\text{PF}_3)_2\text{RhCl}]_2$, $(\text{acac})\text{Rh}(\text{CO})_2$	No
	$\text{Rh}_2\text{Cl}_2(\text{CO})_4$, $\text{Rh}(\eta^3\text{-allyl})(\text{CO})_2$	No
	$\text{Rh}(\eta^5\text{-C}_5\text{H}_5)(\text{CO})_2$	No
	$\text{Rh}(\eta^5\text{-C}_5\text{H}_5)(1,5\text{-COD})$	No
	$(\eta^5\text{-C}_5\text{H}_5)\text{Rh}(\eta^2\text{-C}_2\text{H}_4)_2$	No
Ir	IrF_6 , IrCl_3 , IrBr_3 , $\text{Ir}(\eta^3\text{-allyl})_3$	Yes
	$(\text{acac})\text{Ir}(1,5\text{-COD})$	Yes
	$\{[(\text{CH}_3\text{O})\text{Ir}(1,5\text{-COD})]_2\}$, $\text{Ir}(\text{acac})_3$	No
	$(\eta^5\text{-C}_5\text{H}_5)\text{Ir}(1,5\text{-COD})$, $(1,5\text{-COD})\text{Ir}(\mu\text{-OAc})_2$	No
	$(\eta^5\text{-C}_5\text{H}_4\text{CH}_3)\text{Ir}(1,5\text{-COD})$	No
Zn	$\text{Zn}(\text{CH}_3)_2$, ZnEt_2	Yes
Cd	$\text{Cd}(\text{CH}_3)_2$, CdEt_2	Yes
Sn	SnCl_4 , SnCl_2 , $\text{Sn}(\text{CH}_3)_4$, SnEt_4	Yes
	$\text{Sn}(-n\text{-Bu})_4$, $\text{Sn}(-n\text{-Bu})_2\text{Cl}_2$	Yes
Pb	PbEt_4 , PbPh_4	Yes

Source of data: Chem Sources - USA, Directors Publishing Company, Clemson, South Carolina 29633-1824, 1992.

Table 8-5 Heterometallic Precursors
Used for Deposition of Various Metals*

Metals	Derivative
Mn/Ge	$\text{CH}_2\text{CR}=\text{CRCH}_2\text{Ge}$ $[\text{Mn}(\text{CO})_5]_2$
Mn/Si	$\text{H}_3\text{SiMn}(\text{CO})_5$
Fe/Si	$(\text{H}_3\text{Si})_2\text{Fe}(\text{CO})_4$
Fe/Co	$(\eta^5\text{-C}_5\text{H}_5)\text{FeCo}(\text{CO})_6$ $\text{HFeCo}_3(\text{CO})_{12}$ $(\eta^5\text{-C}_5\text{H}_5)\text{Fe}_2\text{Co}(\text{CO})_9$
Fe/Ni	$(\eta^5\text{-C}_5\text{H}_5)_2\text{FeNi}(\text{CO})_3$
Co/Si	$(\text{H}_3\text{Si})\text{Co}(\text{CO})_4$
Co/Ga	$(\text{CO})_4\text{CoGaCl}_2(\text{THF})$
M/E	$\text{L}(\text{CO})_n\text{M-ER}^1\text{R}^2(\text{D})$ where $\text{L} = \text{CO}, (\eta^5\text{-C}_5\text{H}_5)$ $n = 1\text{-}4$ $\text{M} = \text{Mn, Fe, Co, Ni}$ $\text{E} = \text{Al, Ga, In}$ $\text{R} = \text{H, alkyl}$ $\text{D} = \text{O or N donor ligand.}$

* Not commercially available

8.2.2 Precursor Characteristics

There are several rationales for the choice of ligands that have been used to satisfy the metal coordination environment and electroneutrality in CVD precursors. In many cases, commercial availability has been the major criterion. In fewer cases, the ligands have been chosen to provide suitable precursor deposition characteristics. Some comments on the suitability of the species identified in Tables 8-4 and 8-5 that have been used for CVD or, in many cases, the attempted CVD of metals are warranted. In most sections, a table is given to provide information about properties.

8.2.2.1 Metal Halides

Metal halides are generally unsuitable for CVD for three reasons: (i) generally, they do not thermally decompose below 500 °C, (ii) they can give halide-contaminated films,

and (iii) they often have low volatility (see also Ch. 3). The temperature of thermal decomposition and the purity of the film can be improved in many cases by the addition of a reducing agent during the deposition. Typical reducing agents include H_2 and SiH_4 . Changing to a halide substituent lower in Group 17 (e.g., Br or I as opposed to F or Cl) will tend to lower the thermal decomposition temperature due to a weakening of the M-X bond as a result of the lower electronegativity of the Group 17 element upon descending the group and the larger size of the halide relative to the size of M.⁵⁷⁻⁶⁰ Table 8-6 gives some relevant properties of metal halides, most of which are available commercially.

Table 8-6 Properties of Selected Metal Halides

Halides	Melting Point °C	Boiling Point °C
$SiCl_4$	-70	58
VCl_4	-28	149
$TiCl_4$	-25	136
MoF_6	18	35
ReF_6	19	48
$MoCl_5$	194	268
$NbCl_5$	205	254
$TaCl_5$	216	242
$TaBr_5$	265	349
$HfCl_4$	319	319(s)
$ZrCl_4$	437	331(s)
$ZrBr_4$	450	357(s)
HfI_4	---	400(s)
$CrCl_2$	824	1300(s)

(s) = sublimes

Low volatility is a major problem because it makes transport of the precursor to the CVD reactor difficult and leads to low deposition rates (see Ch. 1). The reason for the general lack of volatility is that in many cases the preferred coordination number of the ion exceeds its oxidation state. This frequently results in oligomerization where the halide ligands bridge metal centers by using one or more of their available lone pairs. One solution to this problem is to use fluoride ligands, because, although they are small and might be expected to facilitate a higher coordination number at the metal center compared to other halides, they are less inclined to form bridges, and as a result, they impart volatility to the metal center. In addition, fluorine tends to stabilize higher

oxidation state precursors better than other members of Group 17 due to its higher electronegativity. This is advantageous because it decreases the tendency for oligomerization by approaching the limit of coordination number = oxidation state which increases the vapor pressure.

A classic example is the case of WF_6 where the coordination sphere of W^{VI} is satisfied by six fluoride ligands resulting in the formation of a highly volatile complex. The halides SnCl_4 and TiCl_4 are other examples where the metal coordination number and oxidation state are satisfied with the result that oligomerization is unnecessary and these species exist as volatile liquids at room temperature and pressure (Fig. 8-2).⁶¹ (It should be noted, however, that higher coordination numbers for Sn^{IV} and Ti^{IV} are common.) In contrast, SnCl_2 is an infinite polymer in the solid state because the number of ligands is lower than the preferred coordination number and makes SnCl_2 unstable with respect to oligomerization (Fig. 8-2).⁶²⁻⁶⁴ However, SnCl_2 can be thermally de-oligomerized to form a monomeric species in the gas phase.⁶⁵ The drawback to this approach is that the use of complexes with a formally high oxidation state may require more forcing conditions (i.e., higher substrate temperature or presence of a reducing agent) to reduce the complex and to form the metal compared to lower oxidation state analogs.

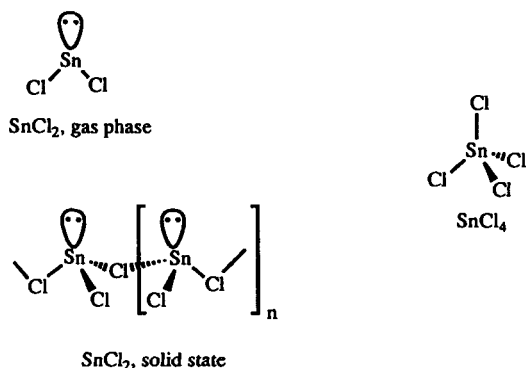


Figure 8-2 Structures of SnCl_4 and SnCl_2 illustrating relationship between preferred coordination number and oxidation state.

The halides of Ti, Zr, Hf, V, Nb, Ta, Cr, Mo, Re, Fe, Os, Co, Ir, and Sn have been used as precursors for CVD experiments at elevated temperatures where thermally sensitive substrates were not used and low substrate temperatures were not necessary.^{31,66-68} A typical reaction is shown in Equation 8.1.



8.2.2.2 Metal Alkyls

Similar trends in coordination number and oxidation state are broadly true for ligand environments other than halides. Where the coordination number of the metal is not satisfied, oligomerization generally occurs resulting in lowering of the volatility when compared to monomeric complexes. Homoleptic (possessing only one type of ligand) metal alkyl, and aryl derivatives of the transition elements are often thermally unstable at room temperature.⁵⁷ For example $W(CH_3)_6$ is a volatile solid that is capable of detonation because the alkyl substituents are insufficiently electronegative to stabilize the high oxidation state (VI) of W. Table 8-7 gives some properties of metal alkyls. In general, most metal alkyls have low melting and boiling points and high vapor pressures. The primary reason they have not been used for CVD of many elements is that carbon-contaminated films are produced. Also, they are often pyrophoric, explode on contact with water, and are toxic.

Table 8-7 Properties of Selected Metal Alkyls

Compound	Formula	MP (°C)	BP (°C)	Vapor Pressure mm Hg
Diethyl beryllium	$(C_2H_5)_2Be$	12	194	---
Dimethyl cadmium	$(CH_3)_2Cd$	4	105	28/20 °C
Tetraethyl tin	$(C_2H_5)_4Sn$	-112	181	---
Tetramethyl tin	$(CH_3)_4Sn$	-54	75	---
Dimethyl zinc	$(CH_3)_2Zn$	-42	46	124/0 °C
Diethyl zinc	$(C_2H_5)_2Zn$	-28	118	6.4/20 °C

Transition metal alkyl complexes have not been studied extensively as precursors for the CVD of metal films. In the absence of a reducing atmosphere such as H_2 , metal carbides are normally formed as in the case of $Ti(CH_2-t-Bu)_4$.⁶⁹ However, metal alkyl derivatives of the relevant main group metals, Sn and Pb, and the pseudo-main group metals, Zn^{II} and Cd^{II} (both d^{10}) have been used for metal deposition. This is probably because these derivatives exhibit sufficient thermal stability that they can be handled at room temperature, they are generally monomeric (see Fig. 8-3), exhibit suitable vapor pressures, and generally thermally decompose at elevated temperatures to liberate the corresponding metal. Some metal alkyl complexes contain bridging alkyl groups or agostic interactions which may be detrimental to their use as precursors for CVD of metals.⁷⁰

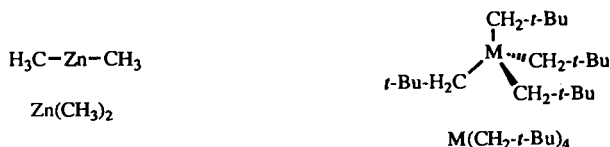


Figure 8-3 Structure of typical metal alkyl precursors, $\text{Zn}(\text{CH}_3)_2$ and $\text{M}(\text{CH}_2-t\text{-Bu})_4$, $\text{M} = \text{Ti}, \text{Zr}$.

Thermal decomposition of metal alkyls to form pure metal may occur by any of three methods, (a) β -hydride elimination (well known in Al CVD; see Ch. 2), (b) α -C-H abstraction, or (c) M-C bond homolysis (Fig. 8-4).⁷⁰ In many cases β -hydrogens are not present in the precursors (i.e., methyl derivatives) and preclude the β -hydride elimination mechanism. Metals at the lower end of a given group in the periodic table tend to have weaker M-C bonds, and as a result, are more likely to undergo M-C bond homolysis compared to those at the higher end. This is particularly the case for lead(IV) alkyl compounds. While some examples of volatile lower oxidation state alkyls of tin (Sn^{II}) and lead (Pb^{II}) are known,⁷¹ they have not been used in CVD experiments.

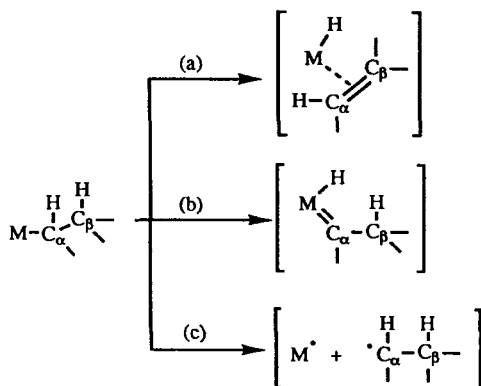


Figure 8-4 Diagrammatic representation of (a) β -hydride elimination, (b) α -hydrogen-abstraction, and (c) M-C bond homolysis pathways which can occur on thermal decomposition of metal alkyl compounds.

8.2.2.3 Complexes with Unsaturated Organic Ligands: Alkenes, Alkynes, Allyls, η^5 -Cyclopentadienyls, η^6 -Arenes, and Related Complexes

This section includes discussion of derivatives such as olefin and alkyne complexes, metal allyls, complexes with aromatic cyclic ligands such as cyclopentadienyl or cycloheptatrienyl and metallocenes [i.e., $M(\eta^5\text{-C}_5\text{H}_5)_2$, e.g., ferrocene], and arene complexes. Examples of each of these compounds are known for most transition elements. A number of metallocene and arene derivatives of the main group metals are known, but they are not common (due to their full underlying d-shells) and have not been reported as precursors for CVD experiments. A note of distinction is necessary to avoid confusion: Metallocene and other cyclopentadienyl or cycloheptatrienyl complexes and metal allyls contain π -bonded ligands which are negatively charged, whereas olefin, alkyne, and arene ligands are neutral (i.e., $\eta^6\text{-C}_6\text{H}_6$ ligands). Examples are $\text{Cr}(\eta^6\text{-C}_6\text{H}_6)_2$ in which the Cr is formally zero-valent and $\text{Fe}(\eta^5\text{-C}_5\text{H}_5)_2$ where Fe is formally divalent.

Alkene and Alkyne Adducts: Alkene adducts of various transition metals have been used to deposit metal films. Depending on the nature of the metal center and its oxidation state, alkene adducts can exist in bonding modes that vary anywhere between the two extremes of $M^{n+}(\text{CH}_2=\text{CH}_2)_n$ (π -bonded olefin) and $M^{(n+2)+}(\text{CH}_2\text{-CH}_2)_n$ (metallacyclopropane), where alkene = ethylene as shown in Figure 8-5.⁷⁰ A similar situation holds for alkyne adducts. These different coordination modes are likely to significantly affect the strength of the metal-olefin and metal-alkyne bonds and change the CVD behavior of the precursor. Insufficient data are available to tabulate the properties of alkene and alkyne complexes that have been used as precursors for CVD by metals.

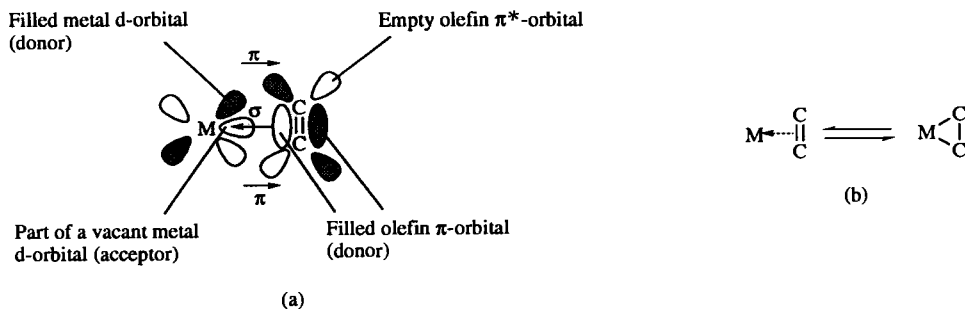


Figure 8-5 (a) Nature of orbital interaction between a transition metal and an alkene ligand. Arrows indicate direction of electron donation. (b) Two canonical form extremes result from extent of overlap between orbitals shown in (a).

It is difficult to generalize about the suitability of such species as precursors for the deposition of pure metal films. However, olefin adducts of the noble metals are likely to be suitable because under a hydrogen atmosphere they are likely to catalyze hydrogenation of the olefin or alkyne rendering it less reactive and allowing it to cleanly desorb from the surface. Examples that have been studied include $[(\text{CH}_3\text{O})\text{Ir}(1,5\text{-COD})]_2$, $[(\text{AcO})\text{Ir}(1,5\text{-COD})]_2$, $(\eta^5\text{-C}_5\text{H}_5)\text{Ir}(1,5\text{-COD})_2$, and $\text{Ru}(\text{hfb})(\text{CO})_4$ and will be discussed in their appropriate sections. The structure of a typical olefin adduct that has been used in CVD experiments is shown in Figure 8-6.

Metal Allyls: Metal allyl (or propenyl) complexes are known for a variety of transition and main group elements, and a number of these derivatives have been used for CVD experiments. In general these species are less labile compared to alkyl compounds because the allyl ligand often acts as a four electron donor and can also act as a π -acceptor (assuming an η^3 -coordination mode). These interactions strengthen the metal allyl bond compared to the metal alkyl bond. In addition the η^3 -allyl ligand occupies two coordination sites at the metal center and as a result stable monomeric metal allyl complexes are formed where the oxidation state is less than the preferred coordination number. To continue the analogy with $\text{W}(\text{CH}_3)_6$ above, $\text{M}(\text{allyl})_4$, $\text{M} = \text{Mo}$ and W , are monomeric complexes where oligomerization is prevented by the steric protection of the metal center afforded by the four allyl groups as shown in Figure 8-7.^{72,73} Insufficient data are available to tabulate the properties of metal allyl compounds that have been used as precursors for CVD of metals.

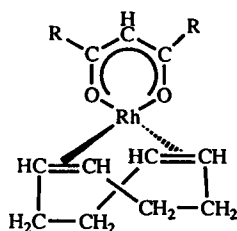


Figure 8-6 Structure of metal olefin adduct: $(\text{hfac})\text{Rh}(1,5\text{-COD})$.

Homoleptic allyl compounds of Rh ,⁷⁴ Ir ,⁷⁴ Mo ,⁷⁵ W ,⁷⁵ and Pd ⁷⁶ have been studied as precursors in CVD experiments. The noble metals^{74,76} give rise to films with relatively low carbon, whereas the more electropositive metals (Mo , W) result in formation of carbides and/or incorporation of graphitic carbon in the growing film.⁷⁴

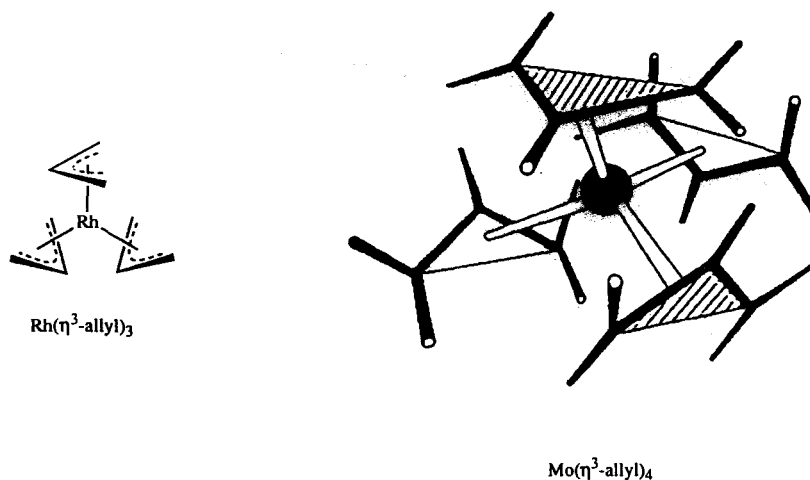


Figure 8-7 Structures of homolytic metal η^3 -allyl complexes; $\text{Rh}(\eta^3\text{-allyl})_2$ and proposed structure of $\text{Mo}(\eta^3\text{-allyl})_4$.

η^5 -Cyclopentadienyl and Related Complexes: Complexes containing cyclopentadienyl ligands generally exhibit higher stability compared to alkyl complexes because these ligands occupy more of the metal coordination sphere and form stronger bonds to the metal center. For example, ferrocene can be considered a six-coordinate complex of Fe^{II} , where each cyclopentadienyl ligand occupies three coordination sites at the metal center (see Fig. 8-8). This results in reasonable volatility for these complexes, but the lower lability of π -bonded ligands generally results in carbon incorporation into the final film, especially for the more electropositive metals. Ferrocene, for example, is unusually thermally stable and in the absence of H_2 does not decompose below 500°C . Similar properties are expected for other π -bonded anionic ligands such as η^7 -cycloheptatrienyl. Chemical vapor deposition using individual metallocene complexes of Fe, Ru, and Co has been studied. A number of other mixed-ligand cyclopentadienyl and cycloheptatrienyl carbonyl complexes, including $[(\eta^5\text{-C}_5\text{H}_5)\text{Fe}(\text{CO})_2]_2$, $[(\eta^5\text{-C}_5\text{H}_5)\text{Mo}(\text{CO})_3]_2$, $(\eta^7\text{-C}_7\text{H}_7)\text{Cr}(\text{CO})_3$, and $(\eta^5\text{-C}_5\text{H}_5)\text{Co}(\text{CO})_2$, have also been studied. As for the metallocene derivatives, the π -bonded $(\eta^5\text{-C}_5\text{H}_5)$ and $(\eta^7\text{-C}_7\text{H}_7)$ ligands are expected to be strongly bonded to these metal centers. For later transition elements, and those lower in a group, these bonds are likely to be weaker and clean removal of the ligand is more likely as for $(\eta^5\text{-C}_5\text{H}_5)\text{Rh}(\text{C}_2\text{H}_4)_2$, $(\eta^5\text{-C}_5\text{H}_5)\text{Ir}(1,5\text{-COD})$, and $(\eta^5\text{-C}_5\text{H}_4\text{CH}_3)\text{Ir}(1,5\text{-COD})$ (see also Ch. 7).

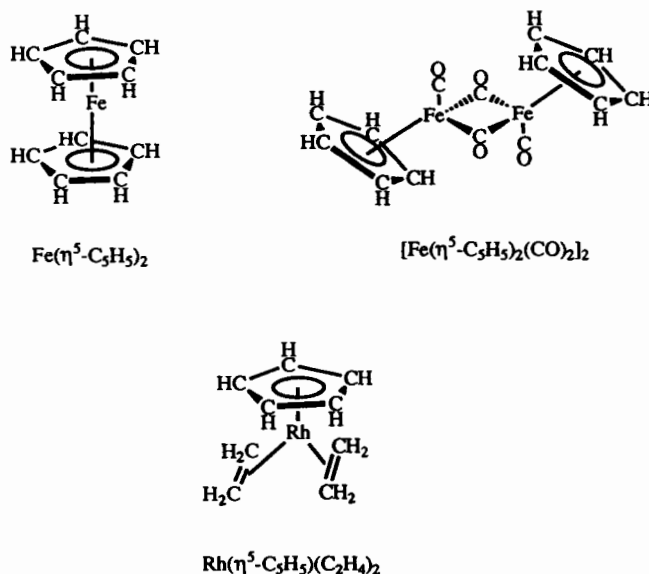


Figure 8-8 Structures of some $\eta^5\text{-C}_5\text{H}_5$ complexes used for CVD, $\text{Fe}(\eta^5\text{-C}_5\text{H}_5)_2$, $[\text{Fe}(\eta^5\text{-C}_5\text{H}_5)_2(\text{CO})_2]_2$, and $\text{Rh}(\eta^5\text{-C}_5\text{H}_5)(\text{C}_2\text{H}_4)_2$.

η^6 -Arene and Related Complexes: Arene complexes are likely to suffer from similar problems as those expected for metallocene and related complexes. Arene ligands coordinated through more than one site, i.e., multihapto ligands, have a high enthalpic and entropic stability against ligand dissociation (see Fig. 8-9). Examples of the compounds that have been studied are $\text{Cr}(\text{cumene})_2$ and $\text{Cr}(\eta^6\text{-C}_6\text{H}_6)_2$. Both gave metal carbides rather than chromium metal.⁷⁷ Insufficient data are available, however, to tabulate the properties of metal arene complexes that have been used as precursors for CVD of metals.

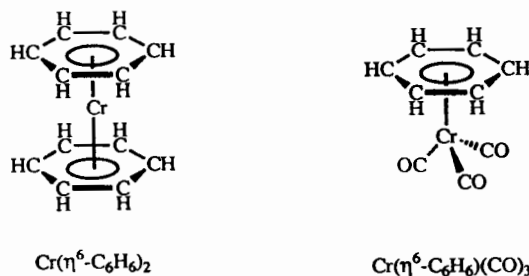


Figure 8-9 Structures of typical η^6 -arene complexes.

8.2.2.4 Metal Carbonyls

Metal carbonyls are commonly thermally stable at room temperature due to the well known σ -donor, π -acceptor bonding of this ligand (see Fig. 8-10).⁷⁰ Their properties are shown in Table 8-8. The results of a solid-state structural study of two archetypal mononuclear metal carbonyls are presented in Figure 8-11.⁷⁸ They are volatile in general but are not used for CVD of many materials because carbon- and oxygen-contaminated films frequently occur. In addition, many carbonyls such as those of Fe are toxic. Related compounds that are suitable for CVD are various substituted metal carbonyls including halides and nitrosyl species such as Co(NO)(CO)_3 ⁷⁹ (see also Ch. 7).

Table 8-8 Properties of Metal Carbonyls and Carbonyl Halides

Compound	MP °C	BP °C	Color / Form	Comments
MONONUCLEAR				
V(CO)_6	65	dec.	Black crystal	Yellow-Orange in solution, volatile, very unstable
Cr(CO)_6	164	dec. 180	White crystal	Volatile
Fe(CO)_5	-20	103	Yellow liquid	Poisonous
Mo(CO)_6	150	dec. 180	White crystal	Volatile
Ru(CO)_5	-22	---	Colorless liquid	Very volatile
Os(CO)_5	-15	---	Colorless liquid	Very volatile
DINUCLEAR				
$\text{Mn}_2(\text{CO})_{12}$	152	---	Yellow	---
$\text{Fe}_2(\text{CO})_9$	80 dec.	---	Yellow crystal	Volatile
$\text{Co}_2(\text{CO})_8$	51	52 dec.	Orange crystal	CO loss

continued

Table 8-8 Continued

Compound	MP °C	BP °C	Color / Form	Comments
$\text{Re}_2(\text{CO})_{10}$	170	250 dec.	Colorless crystal	Volatile
$\text{Ir}_2(\text{CO})_8$	160	---	Yellow crystal	Sublimes in CO at 160 °C
CARBONYL HALIDES				
$\text{Mn}(\text{CO})_5\text{Cl}$	---	---	Yellow	Loses CO at 120 °C in organic solvent
$\text{Re}(\text{CO})_4\text{Cl}_2$	---	250 dec.	White crystal	---
$\text{Ru}(\text{CO})_2\text{I}_2$	---	---	Orange powder	Suitable for CVD
$\text{Os}(\text{CO})_3\text{Cl}_2$	270	280 dec.	Colorless prism	Suitable for CVD
$[\text{Rh}(\text{CO})_2\text{Cl}]_2$	125 sub.	---	Ruby red needle crystal	Suitable for CVD
$[\text{Ir}(\text{CO})_2\text{Cl}]_2$	140	---	Colorless needle crystal	Suitable for CVD

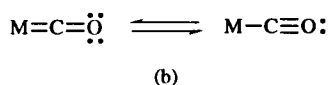
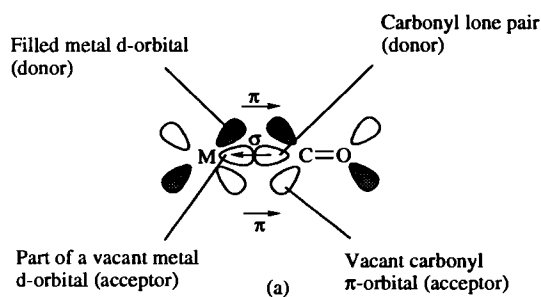


Figure 8-10 (a) Nature of orbital interaction between a transition metal and a carbonyl ligand. Arrows indicate direction of electron donation. (b) Two canonical form extremes result from extent of overlap between orbitals shown in (a).

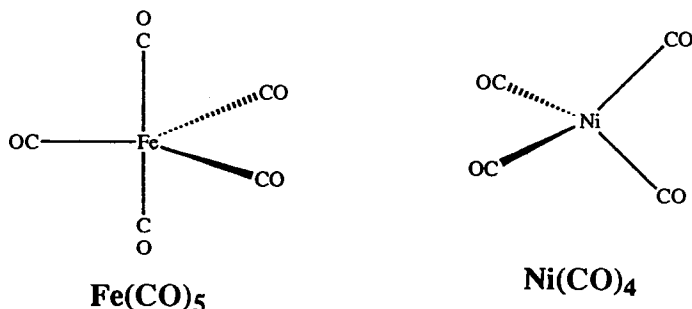


Figure 8-11 Structures of two homoleptic mononuclear metal carbonyl compounds, Fe(CO)_5 and Ni(CO)_4 .

Metal carbonyl derivatives of virtually all the transition elements are known and monomeric derivatives occur for M(CO)_6 ($\text{M} = \text{V}, \text{Cr}, \text{Mo}, \text{W}$), Fe(CO)_5 , and Ni(CO)_4 . Furthermore, the metal is formally in the zero valent oxidation state in a homoleptic metal-carbonyl compound which, in principle, should enable simple dissociation of carbon monoxide to liberate the element itself without the need for a reduction step.



Although many such equations for numerous metal carbonyls have been written for CVD reactions, this simple elimination reaction does not represent the whole picture. In the cases of Co, Fe, and Ni, high-purity deposits can be obtained. Nevertheless, films deposited from other metal carbonyl compounds [Cr(CO)_6 , for example] are invariably contaminated with metal carbides, metal oxides, and graphitic carbon. This is not surprising when the canonical form $\text{M} = \text{C} = \text{O}$ (Fig. 8-10) is considered,⁷⁰ and when it is noted that many of the metals being deposited can catalytically cleave the C-O bond of carbon monoxide (e.g., W) under the deposition conditions employed.⁸⁰

Many examples of homopolynuclear and heteropolynuclear metal carbonyls exist and some of these species have been used for CVD experiments.^{30,81,82}

8.2.2.5 Metal Trifluorophosphines

In some respects, homoleptic metal trifluorophosphine derivatives are analogous to homoleptic metal carbonyl derivatives. The metal is in the zero-valent oxidation state and is coordinated to ligands that on cleavage of the metal-ligand bond release a highly volatile by-product. In principle, the trifluorophosphine derivatives should be more suitable as precursors for metal CVD compared to metal carbonyls since they are volatile,

the PF_3 ligand is a poor σ -donor, PF_3 itself is very volatile (b.p. = -101.8°C), and the PF_3 ligand usually does not dissociate on the metal surface. The synthesis and properties of the trifluorophosphine complexes of Re, Cr, Mo, W, Fe, Ru, Os, Co, Rh, Ir, and Pd are discussed by Kruck.⁸³ These complexes have decomposition temperatures of -20 to 300°C and high vapor pressures. However, PF_3 is known to react with Si substrates under some conditions to form P and liberate SiF_4 (see Ch. 3) which makes these precursors undesirable for some electronics applications.

Complexes with PF_3 have been used to deposit metal films at temperatures between 200 and 300°C . A patent discusses the use of metal trifluorophosphine and trifluorophosphine hydride complexes for CVD at temperatures of 350 – 600°C .⁸⁴ However, CVD using these precursors has not been studied extensively.^{85–87} In other cases, the metal is not zero valent and the complex contains other ligands along with PF_3 . The structure of such a trifluorophosphine complex is shown in Figure 8-12.⁸⁸

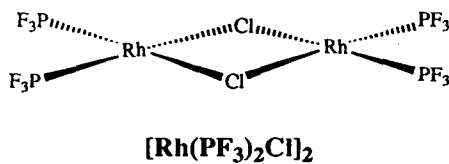


Figure 8-12 Structure of $[(\text{PF}_3)_2\text{RhCl}]_2$.

8.2.2.6 Metal β -diketonates

As precursors for CVD experiments, metal β -diketonates, particularly the fluorinated derivatives, have the advantage that they generally exhibit high vapor pressures but have the disadvantages that they do not generally decompose below 300°C and that the deposit is often contaminated unless a reducing agent such as H_2 is added (Eq. 8.3).



Metal β -diketonates (Table 8-9) show melting points well over 100°C and often near 200°C . All are solids at room temperature and have relatively high vapor pressures as discussed in Section 8.2.3 below. Several review articles and books discuss their synthesis and properties.^{89–99} Graddon discusses Zn, Mn, Cu, Ni, Co, and Fe β -diketonate complexes.⁹³ Their volatility is enhanced because the β -diketonate ligand is bidentate when bonded through the oxygen ligands, although this is not always the case, and generally prefers to chelate rather than bridge. Examples of monomeric β -diketonate complexes can be found in Chapters 4, 5, 6, and 7. To emphasize the possibility of oligomerization, examples of oligomeric, homoleptic metal β -diketonate compounds are

shown in Figure 8-13. In some cases, extra coordination sites have been consumed by coordination of a Lewis base such as in the case of $(\beta\text{-diketonate})\text{CuL}_n$ compounds, described in Chapter 5, which prevents oligomerization. In other cases (e.g., Ni, Co), the $\beta\text{-diketonate}$ is forced to bridge as well as chelate resulting in complex structures (see Fig. 8-13).

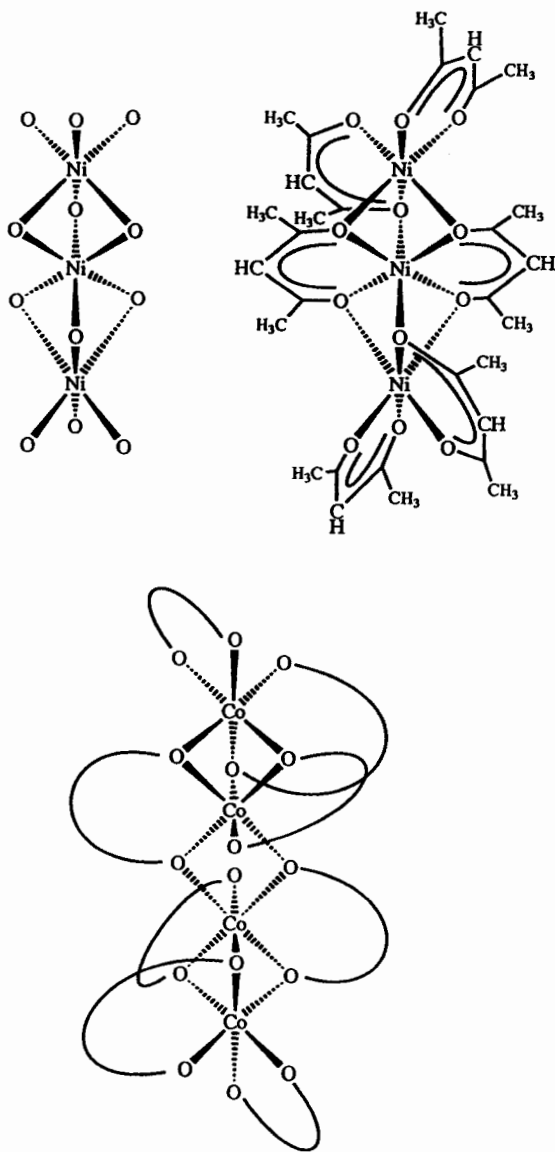


Figure 8-13 Examples of typical homoleptic metal $\beta\text{-diketonate}$ compounds: $[\text{Co}(\text{acac})_2]_4$ and $[\text{Ni}(\text{acac})_2]_3$.

Table 8-9 Properties of Selected Metal β -Diketonates

Metal	Formula	Form	Melting Point °C
Chromium	$\text{Cr}(\text{C}_5\text{H}_7\text{O}_2)_3$	Violet crystal	214
Cobalt	$\text{Co}(\text{C}_5\text{H}_7\text{O}_2)_3$	Green crystal	240
Iron	$\text{Fe}(\text{C}_5\text{H}_7\text{O}_2)_3$	Orange crystal	179
Lead	$\text{Pb}(\text{C}_5\text{H}_7\text{O}_2)_2$	White crystal	---
Manganese	$\text{Mn}(\text{C}_5\text{H}_7\text{O}_2)_2$	Buff crystal	180
Rhodium	$\text{Rh}(\text{C}_5\text{H}_7\text{O}_2)_3$	Yellow crystal	---
Zinc	$\text{Zn}(\text{C}_5\text{H}_7\text{O}_2)_2$	White needles	138
Zirconium	$\text{Zr}(\text{C}_5\text{H}_7\text{O}_2)_4$	White crystal	172

A number of mixed ligand β -diketonate complexes of noble metals including $\text{Rh}(\text{CO})_2(\text{acac})$ and $(\eta^5\text{-C}_5\text{H}_5)_2\text{Ru}(\text{acac})$ have been used for CVD experiments.¹⁰⁰⁻¹⁰⁵

8.2.2.7 Metal Alkoxides

Some metal alkoxide compounds are volatile where the alkoxide ligand is sterically demanding, but they are generally not suitable as precursors for deposition of metals [see Ch. 5, $[\text{Cu}(\text{O}-t\text{-Bu})_4]$]. In most cases metal oxides are deposited, especially when the metal center is electropositive, as in Ti.¹⁰⁶ Occasionally, films of transition metals such as Cu have been deposited from these precursors.¹⁰⁷

8.2.3 Vapor Pressures

Since volatility is only one of the criteria used to select a metal-organic compound for use as a CVD precursor, extensive discussion of these data are not warranted. However, vapor pressure data demonstrate the temperature range over which the precursors are stable as well as the temperature to which they must be heated to carry out CVD. As a rule of thumb, a vapor pressure of at least 100 mtorr is essential for a metal-organic compound to give a sufficiently high deposition rate for most applications using conventional precursor delivery methods. This criterion excludes many potential precursors because they thermally decompose before a sufficiently high vapor pressure is reached.

For comparison, vapor pressure data for representative examples of classes of precursors are presented in Figure 8-14 and Table 8-10. The compounds WF_6 and MoF_6 exhibit relatively high vapor pressures. The compounds SnCl_4 and TiCl_4 exhibit similar

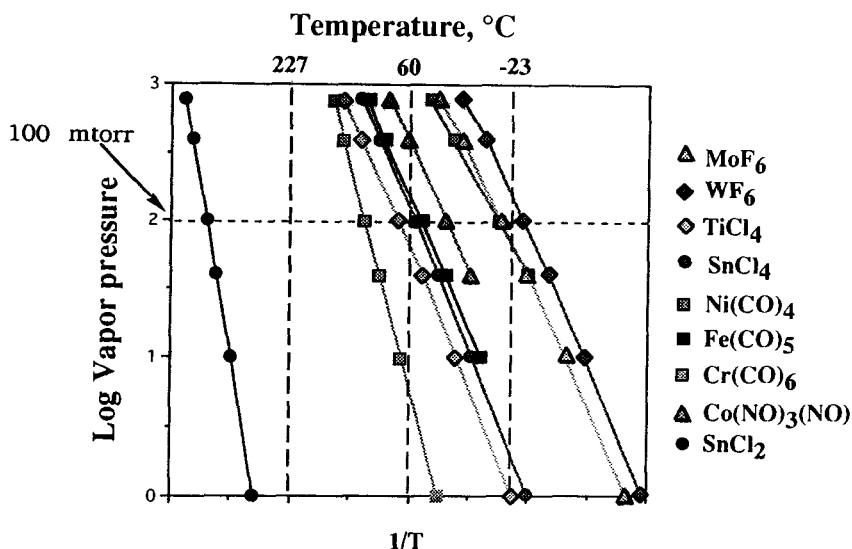


Figure 8-14 Vapor pressures for compounds identified in Table 8-10.

Table 8-10 Temperatures at which Vapor Pressures (mm Hg) are Obtained for Inorganic and Metal-Organic Compounds

Compound	Temperature in °C						m.p.
	1 mm	10 mm	40 mm	100 mm	400 mm	760 mm	
MoF_6	-65.5	-40.8	-22.1	-8.0	17.2	36.0	17.0
WF_6	-71.4	-49.2	-33.0	-20.3	1.2	17.3	-0.5
TiCl_4	-13.9	21.3	48.4	71.0	112.7	136.0	-30.0
SnCl_4	-22.7	10.0	35.2	54.7	92.1	113.0	-30.2
Ni(CO)_4	---	---	-23.0	-6.0	25.8	42.5	-25.0
Fe(CO)_5	---	4.6	30.3	50.3	86.1	105.1	-21.0
Cr(CO)_6	36.0	68.3	91.2	108.0	137.2	151.0	---
$\text{Co(CO)}_3\text{NO}$	---	---	11.0	29.0	62.0	80.0	-11.0
SnCl_2	316.0	391.0	450.0	493.0	577.0	623.0	246.8

vapor pressures but lower than those of the fluorides. For comparison to the structural data presented in Figure 8-2, the vapor pressure data for SnCl_2 are shown and are substantially lower compared to SnCl_4 . The monomeric carbonyl compounds all have similar vapor pressures and are in the range observed for the tetrahalides of Sn and Ti. The vapor pressures of a number of metal β -diketonates (Cr, Rh, Al, Fe, Cu, Pd; hfac and fod) are discussed by Wolf et al.⁹²

8.3 Syntheses

An extensive review of synthetic routes to all the compounds used as CVD precursors is beyond the scope of this book, especially since many of the species studied do not give rise to pure metal films. Many of the compounds used are either commercially available [metal halides, alkyls, allyls, and many of the metal carbonyls, metallocenes, and β -diketonates (see Table 8-4)] or simply prepared in high yield and the reader is directed to standard texts on this subject.^{59,60,70,97} Synthetic routes to the compounds that are not commercially available are generally contained in the papers referenced here or references therein.

8.4 Chemical Vapor Deposition

8.4.1 Deposition Characteristics

8.4.1.1 Introduction

Volatile metal-containing compounds have been used for generation of films by a variety of processes including chemical vapor deposition, large-area photochemically-induced deposition using lamps,¹⁰⁸ focused-laser-induced deposition by photochemical^{34,49-51,108,109} and photothermal routes,^{34,49-51,108-110} atomic layer epitaxy,¹¹¹ chemical beam epitaxy,¹¹² and others. The precursors used for these approaches are primarily the same as those used for CVD. Extensive literature exists for laser-induced deposition of metals^{34,49-51,108-110,113} and will not be covered in this chapter.

This section will discuss metal CVD using the precursors identified in Section 8.2 (see Table 8-1). Emphasis is on the types of precursors used, substrates, temperatures, carrier gases, purities, and rates where known. Section 8.4.2 will focus on kinetics and mechanisms of CVD of these metals where known. In this section each metal is discussed in order of its appearance in the different groups of the Periodic Table.

8.4.1.2 Titanium

Chemical vapor deposition of titanium has not been discussed extensively in the literature, probably due to the difficulty in depositing the pure metal because it is easily oxidized and exposure to oxygen leads to contamination. In the patent literature, however, numerous volatile precursors that provide sources of Ti are claimed, but very little analytical data have been presented to support deposition of high-purity Ti films. A patent by Homer¹¹⁴ reports that " $\text{Ti}(\eta^5\text{-C}_5\text{H}_5)_2$ " can be used to deposit Ti, but no purity data were reported. The species $\text{Ti}(\eta^5\text{-C}_5\text{H}_5)(\eta^7\text{-C}_7\text{H}_7)$ was used as a precursor for CVD of Ti by others.^{115,116} However, even in an H_2 plasma the films were comprised mainly of C. Other titanium alkyl and aryl compounds such as $(\eta^5\text{-C}_5\text{H}_5)_2\text{TiR}_2$, where $\text{R} = \text{CH}_3, \text{C}_6\text{H}_5$, also decompose to form products which contain considerable amounts of carbon.¹¹⁷⁻¹²⁰ Some examples of Ti deposition are from TiCl_4 ¹²¹ and TiBr_4 ¹²² by photochemical reactions or at high temperatures (900 °C) attained by laser heating. The purities reported in these cases were on the order of 90% and the 10% impurities may have been due to exposure to oxygen. Campbell et al. studied the use of TiI_x at 1300-1400 °C for generation of Ti metal but did not examine CVD.¹²³ Chemical vapor deposition of titanium-rich films has also been reported from $\text{Ti}[\text{tris-(2,2'-bi-pyridine)}]$ at temperatures near 600 °C.¹²⁴ The films, however, contained significant amounts of contaminants, up to 35% C, O, N, and H.

8.4.1.3 Zirconium

There have only been a few studies of the CVD of zirconium metal. The "hot-wire" process which involves the thermal decomposition of ZrI_4 has a reaction efficiency of 0.32 at 1152 °C.¹²⁵ The complex $\text{Zr}(\text{CH}_2\text{-}i\text{-Bu})_4$ deposited crystalline ZrC films above 500 °C with a metal:carbon ratio of 1:2. Carbon X-ray photoelectron spectroscopy (XPS) revealed carbidic carbon, graphitic carbon, and a third unidentified type of carbon species.¹²⁶ Thermal decomposition of $(\eta^5\text{-C}_5\text{H}_5)_2\text{ZrR}_2$, where $\text{R} = \text{Me}, \text{C}_6\text{H}_5$, and C_6F_5 , compounds leads to carbon-contaminated products.^{117-120, 127}

8.4.1.4 Hafnium

The decomposition of hafnium iodide was used to form hafnium metal.¹²⁸ The reaction, carried out at 1100 °C, gave hafnium of unknown purity. Apparently, the CVD of hafnium metal from other precursors has not been reported in the literature, although metal-organic hafnium compounds, such as $\text{Hf}(\text{O-}i\text{-Bu})_4$, have been used to deposit Hf-containing films, e.g., HfO_2 .¹²⁹

8.4.1.5 Vanadium

Pure vanadium metal is commercially obtained by thermal decomposition of the halides. Pure vanadium and the vanadium alloys V/Nb, V/Ti, and V/Ti/Nb have been

deposited at temperatures between 850 and 900 °C by thermal decomposition of the halides formed by passing Cl_2 over metal chips.¹³⁰ The films were deposited in the presence of H_2 and He gases. No low-temperature CVD routes exist. The thermal decomposition of a number of organometallic vanadium compounds including $(\eta^5\text{-C}_5\text{H}_5)\text{V}(\text{CO})_4$,²⁴ $(\eta^5\text{-C}_5\text{H}_5)\text{V}(\eta^6\text{-C}_6\text{H}_6)$,¹²⁰ $\text{V}(\eta^5\text{-C}_5\text{H}_5)_2$,¹³¹ $\text{V}(\text{CO})_6$,¹³² and $(\eta^6\text{-C}_6\text{H}_6)_2$ ¹³³ has been reported, but few data are available on the identity of the materials formed.

8.4.1.6 Niobium

Chemical vapor deposition of niobium has been examined primarily in the context of deposition of the superconducting phases Nb_3Ge and Nb_3Ga (Table 8-11). Only the niobium halides have been studied extensively as precursors.^{28,29,134-143} As a result, the lowest deposition temperature obtained is near 700 °C. The films are generally of high-purity. In the case of the superconductors Nb_3Ga and Nb_3Ge , excellent electrical properties have been obtained. Niobium and Nb-containing films have been grown primarily from NbCl_5 in H_2 . Only a few studies have examined NbBr_5 . Niobium films have been deposited at 1200 °C at rates of up to 3,000 nm/min using NbBr_5 .²⁸ The decomposition of $\text{Nb}(\eta^6\text{-C}_6\text{H}_6)_2$ has been reported in the patent literature.¹³³ The CVD of Nb_3Ge ¹⁴¹ and doping of TiO_2 using Nb ethoxide¹⁴⁰ have also been studied. No low-temperature routes to high-purity Nb films exist.

Table 8-11 Niobium Chemical Vapor Deposition Conditions

Precursor	Substrate	$T_{\text{substrate}}$ °C	Carrier Gas	Purity	Rate nm/min	Ref.
NbBr_5	Graphite	1200-1400	none	high	1000-3000	28, 29
NbCl_5	Ruby, Sapphire	850-900	none	---	---	134
NbCl_5^*	Cu	900	Ar H_2	high	---	135
NbCl_5^*	Si	800-1100	Ar H_2	high	1600	137
NbCl_5^*	SiO_2	720	Ar H_2	high	170-340	138
NbCl_5^{**}	Carbon	600-1200	$(\text{CH}_3)\text{N}$, Ar, NH_3 , N_2	high	---	139
NbCl_5^*	SiO_2	700-900	He, H_2	high	170	141

* Deposition of Nb_3Ge or Nb_3Ga .

** Deposition of carbonitride

8.4.1.7 Tantalum

The halide, TaCl_5 , has been the main source for CVD of tantalum (Table 8-12).¹⁴⁴⁻¹⁴⁹ Although high-purity films have been obtained with TaCl_5 at rates of 1,000 nm/min using hydrogen as a reducing agent, the primary problem is the need for temperatures greater than 700 °C. Tantalum deposition has also been attempted from $\text{Ta}(\text{CO})_5$, but the films contained 5-10% impurities.¹⁵⁰ Ugolini, using XPS, studied the surface chemistry of Ta CVD from TaCl_5 .¹⁵¹ This study showed that high-purity Ta could be produced even in the absence of hydrogen. The thermal decomposition of $\text{Ta}(\eta^6\text{-C}_6\text{H}_6)_2$ ¹³³ and $(\eta^5\text{-C}_5\text{H}_5)_2\text{Ta}(\text{C}_6\text{F}_5)_2$ ¹²⁷ has been reported in the patent literature. Tantalum CVD has also been studied by others.¹⁵² No low-temperature CVD routes to Ta films currently exist.

Table 8-12 Tantalum Chemical Vapor Deposition Conditions

Precursor	Substrate	T _{substrate} °C	Carrier Gas	Purity	Rate nm/min	Ref.
TaCl_5	Mo	650-1100	H_2, N_2	high	50-100	144
TaCl_5	Stainless steel	900-1050	H_2	>99%	2000	145
TaCl_5	$\text{SiO}_2, \text{Al}_2\text{O}_3$	800-1500	H_2, N_2	high	30	146
TaCl_5	Al_2O_3	up to 1500	Ar, H_2	high	---	147
TaCl_5	Steel	1000	H_2, N_2	high	2000	148
TaCl_5	Cu, Fe, Ni, Mo	600-1400	H_2, N_2	high	125	149
$\text{Ta}(\text{CO})_5$	Cu	450-600	H_2	90-95%	---	150
TaF_5	Si, SiO_2	250-400	none	high	---	151

8.4.1.8 Chromium

Chromium or Cr-containing films have been deposited from only a few precursors (Table 8-13). The primary problem is the lack of low-temperature routes to the pure metal. Chromium halides deposit pure metal but require deposition temperatures near 1000 °C. For example, CrCl_2 deposits pure Cr at temperatures over 800 °C.^{66,67,154,155} Other precursors have lower deposition temperatures but impure films result. For example, $\text{Cr}(\text{CO})_6$ provides deposition temperatures of 400 °C but the films are contaminated with carbon.

Studies of CVD of Cr using organometallic precursors have been motivated by the lack of other precursors which allow low-temperature deposition of high-purity chromium films. However, in general, no organometallic precursors have been successful in depositing pure Cr films. In a cold-wall reactor, $(\eta^6\text{-C}_7\text{H}_8)\text{Cr}(\text{CO})_3$ deposited carbide and oxide contaminated films above 300 °C.¹⁵⁷ Extensive characterization of the reaction products was performed by gas chromatography and mass spectrometry. Labelling studies showed that most of the carbon was derived from the cycloheptatriene ring with only a minor contribution from the carbonyl ligands (see Section 8.4.2.3).

The precursor $\text{Cr}(\text{cumene})_2$ formed carbide films at 350-520 °C at rates of 4.5-6.5 nm/min in a cold-wall reactor using argon as the carrier gas.⁷⁷ The deposition rate exhibited a maximum at 450 °C, but the origin of this observation was not interpreted. The resistivity of the films was high, decreased with temperature, and remained above 100 $\mu\Omega\text{cm}$ at 550 °C. The films were used to fabricate high-quality Schottky barrier diodes. Similar results were obtained for $\text{Cr}(\eta^6\text{-C}_6\text{H}_6)_2$ and other studies with $\text{Cr}(\text{cumene})_2$ which gave films consisting of Cr and Cr_3C_2 .^{159,160}

Table 8-13 Chromium Chemical Vapor Deposition Conditions

Precursor	Substrate	T _{substrate} °C	Carrier Gas	Purity	Rate nm/min	Ref.
$\text{Cr}(\text{CO})_6$	Fe, Cu, Steel	400-600	H ₂	---	---	153
$\text{Cr}(\text{cumene})_2$	Si, SiO ₂	350-520	Ar	C impurity	4.5-6.5	77
$(\eta^5\text{-C}_5\text{H}_5)\text{Cr}(\text{CO})_3\text{H}$	Si	330-470	none or H ₂	C + O impurity	---	158
$\text{Cr}[\text{CH}_2\text{C}(\text{CH}_3)_3]_4$	Si	330-470	none or H ₂	C + O impurity	---	„
$\text{Cr}(\text{N-}i\text{-Pr})_3$	Si	330-470	none or H ₂	C + N impurity	---	„
$(\eta^6\text{-C}_7\text{H}_8)\text{Cr}(\text{CO})_3$	Glass, Al	300-600	none	28-36% C	---	157
CrCl_2	Steel	750-1000	H ₂	>99% Cr	100-200	67
CrCl_2	Steel	970-1100	H ₂	high purity	---	154
CrCl_2	Ni	950-1050	H ₂	>99% Cr	---	155
CrCl_2	Nb alloy	900	H ₂	>99% Cr	600-5000	66
CrF_2	---	950-1050	H ₂	high purity	---	156

Rutherford et al.¹⁵⁸ used several organometallic precursors in a low-pressure cold-wall reactor to examine the deposition of Cr-containing films. Chromium carbide (Cr_3C_2) films, produced at temperatures as low as 300 °C, were the prime result of CVD using $\text{Cr}(\eta^5\text{-C}_5\text{H}_5)(\text{CO})_3\text{H}$, $\text{Cr}(\text{CH}_2\text{-}i\text{-Bu})_4$, and $\text{Cr}(\text{N-}i\text{-Pr})_3$. In general, higher deposition temperatures led to lower resistivities, and the best of these were in the 200-300 $\mu\Omega\text{cm}$

range. Carrier gas composition (H_2 , Ar, He) had no effect on film properties. Similar behavior was observed for $Cr(t-Bu)_4$ and other tetraalkyl chromium compounds.¹⁶¹⁻¹⁶³ The best source of chromium carbide films was $Cr(N-i-Pr)_3$.

8.4.1.9 Molybdenum

High rates of pure molybdenum film deposition can be obtained at temperatures as low as 200 °C (Table 8-14) using MoF_6 , $Mo(CO)_6$, and $MoCl_5$. All of these precursors allow deposition of clean metal under certain conditions. Deposition temperatures for MoF_6 range from 200-500 °C, for $Mo(CO)_6$ range from 200-600 °C, and for $MoCl_5$ range from 500 to 1100 °C. Because these precursors are widely available, other precursors have not been extensively examined (see Table 8-14). Using $M(allyl)_4$ ($M = Mo$ and W) as

Table 8-14 Molybdenum Chemical Vapor Deposition Conditions

Precursor	Substrate	$T_{\text{substrate}}$ °C	Carrier Gas	Purity	Rate nm/min	Ref.
$MoCl_5$	Ni, Glass	800-1100	H_2	---	8,350	164
$MoCl_5$	---	500-750	H_2	high	---	165
$MoCl_5$	Si	400-1200	H_2	>99%	0.1-40	166
$MoCl_5$	Si	500-750	H_2	>99%	1-20	167
$MoCl_5$	Si	600-1350	H_2	high	---	168
$MoCl_5$	Si	450	H_2	---	---	169
$MoCl_5$	Ni/Fe	850-950	H_2	---	---	146
$MoCl_5$	Si	500-800	H_2	high	8.7-35.0	170
MoF_6	SiO_2	200-400	Ar, H_2	4% O	200	171
$Mo(CO)_6$	SiO_2/Si	100	H_2 , Ar	C+O impurity	---	172
$Mo(CO)_6$	Steel	400	H_2	---	250	27
$Mo(CO)_6$	SiO_2	400-550	H_2 , CO_2 , Ar	>99 %	120-480	173
$Mo(CO)_6$	Graphite	400-600	none	>99 %	1.67-25	29
$Mo(CO)_6$	Ta, Glass	175-250	Ar	C impurity	5-100	174
$Mo(CO)_6$	---	400-750	Ar	C impurity	---	165
$Mo(CO)_6$	Fe, Cu, Steel	350-550	H_2	>99%	10,000	153
$(\eta^6-C_6H_6)Mo(CO)_3$	Cu	250-550	H_2	5-98%	---	150
$[\eta^6-C_6H_3(CH_3)_3]-$ $Mo(CO)_3$	Cu	250-650	H_2	1-100%	---	"
$Mo(\eta^3-allyl)_4$	Pyrex	350-450	H_2 or none	low	0.47-1.8	75, 175

precursors, CVD resulted in the deposition of metal carbides together with amorphous carbon.^{75,175}

Kaplan and d'Heurle examined the deposition of Mo films from $\text{Mo}(\text{CO})_6$ in a cold-wall reactor.¹⁷³ Films with bulk resistivity were grown at 500 °C at a rate of 22 nm/min using 0.001 torr CO and 0.01 torr H_2 . Films deposited at lower temperatures resulted in higher resistivities, presumably due to higher levels of carbon. The lowest deposition temperature was 170 °C but only films deposited above 450 °C had satisfactory properties. Resistivities decreased with increasing temperature until a critical temperature was reached at which the resistivity became independent of temperature. The decrease in resistivity with temperature was dramatic, a factor of 100 for a temperature change of only 50 °C. This effect was explained in terms of the purity of the films which increased with increasing temperature and emphasizes the importance of deposition temperature in determining film properties. Several approaches were investigated to determine the lowest temperature at which high-purity, low-resistivity films could be produced. Production of high-quality films required temperatures of 500 °C or higher.

Molybdenum films can also be obtained by MoF_6 reduction on silicon substrates in the presence of hydrogen (see also Ch. 3).¹⁷¹ Deposition is the result of both the reaction with Si and with H_2 in roughly equal ratios. High deposition rates of 200 nm/min were obtained in the low-pressure, hot-wall reactor and no self-limiting thickness was observed. However, the films were highly porous (30%) due to diffusion of the precursor through the film to the Mo/Si interface where reaction to form Mo occurred. The extensive porosity led to a high surface area which resulted in oxygen contamination (4%) when exposed to air even at room temperature.

As a result of the porosity and oxygen contamination, the resistivities of the films were an order of magnitude higher than bulk. The morphology of films produced by this approach makes this a poor method for Mo film deposition.

The precursor MoCl_5 , in the presence of hydrogen, has been used extensively for deposition of molybdenum films. Sugano et al.¹⁶⁶ have shown that high-purity films with nearly bulk resistivity can be formed between 600 and 800 °C in a cold-wall reactor. The deposition rate was investigated as a function of temperature and exhibited a maximum at 600 °C. The deposition rate was first order in MoCl_5 concentration. The resistivity decreased with increasing temperature until roughly 600 °C where it became constant. Yasuda and Murota¹⁶⁷ studied MoCl_5 reduction by hydrogen in a hot-wall reactor. Diffusion-limited deposition (see Ch. 9) was observed above 600-700 °C. The reaction rate was proportional to the $3/2$ power of the hydrogen partial pressure.

Other investigations of Mo CVD not listed in Table 8-14 include the thermodynamics of selective CVD,¹⁷⁶ the generation of MoS_2 using bromine transport,¹⁷⁷ and CVD using $\text{Mo}(\text{CO})_6$.¹⁷⁸ Wlodek and Wulff¹⁷⁹ have used MoCl_5 to coat surfaces at 900 °C. Molybdenum-silicon Schottky barriers have been prepared by CVD using MoCl_5 .¹⁸⁰ The compound $\text{Mo}(\text{PF}_3)_6$ produced high purity Mo films, analogous to $\text{W}(\text{PF}_3)_6$ ⁸⁴ (see Ch. 3). However, as described earlier, the potential for impurity incorporation exists when PF_3 is liberated.

8.4.1.10 Manganese

The deposition of Mn films, apparently, has not been investigated in any detail, although Mn-Si films have been produced using single-source heterometallic precursors (see Sections 8.4.1.23 and 8.4.2.7). Manganese-containing coatings have been obtained by pyrolysis of $(\eta^5\text{-C}_5\text{H}_5)_2\text{Mn}$ at 460 °C in a glass vessel.¹³¹ The photodissociation of $\text{Mn}_2(\text{CO})_{10}$ at wavelengths of 193-351 nm has been studied suggesting laser-induced deposition is possible.¹⁸¹⁻¹⁸³

8.4.1.11 Technetium

Although technetium is not a naturally occurring element, its chemical attributes are useful for radiopharmaceutical applications. Technetium CVD has not been reported in the open literature.

8.4.1.12 Rhenium

Chemical vapor deposition of rhenium has not been studied extensively (see Table 8-15). The precursors ReF_6 , ReCl_5 , $\text{HRe}(\text{CO})_5$, and $\text{Re}_2(\text{CO})_{10}$ ¹⁸⁴⁻¹⁸⁸ have been used primarily in conjunction with WF_6 to deposit tungsten-rhenium alloys. The purity of the deposited alloy films was high in all cases except for $\text{HRe}(\text{CO})_5$. The compound $\text{Re}_2(\text{CO})_{10}$ deposits films onto substrates heated to temperatures between 400 and 600 °C. A maximum in deposition rate was observed at 500 °C; however, no characterization data were presented so the purity of the films is unknown. No precursors exist for CVD of high-purity Re metal at low-temperatures (< 400 °C), although Re has been deposited by PECVD using $(\text{CH}_3)_3\text{Re}(\text{CO})_5$ and $\text{HRe}(\text{CO})_5$. Several other discussions of rhenium CVD are available.¹⁸⁹⁻¹⁹¹ For example, Aylett et al.¹⁹¹ have used $\text{HRe}(\text{CO})_5$ to deposit Re on porous Si substrates.

Table 8-15 Rhenium Chemical Vapor Deposition Conditions

Precursor	Substrate	T _{substrate} °C	Carrier Gas	Purity	Rate nm/min	Ref.
ReF_6	Mo	500-1000	H_2	high	4,200 to 12,000	184, 185
ReF_6	Al_2O_3	1000-1500	H_2	high	---	186
ReF_6	Cu	200-800	H_2	high	---	187
$\text{HRe}(\text{CO})_5$	SiO_2 , Si	130	H_2 , Ar	30% C + O	---	188

8.4.1.13 Iron

Precursors for CVD of iron allow deposition of high-purity films at temperatures as low as 200 °C at high rates (Table 8-16). The majority of studies used iron pentacarbonyl, $\text{Fe}(\text{CO})_5$, as a precursor. Ferrocene, $\text{Fe}(\eta^5\text{-C}_5\text{H}_5)_2$, has been studied to a lesser extent because it requires higher deposition temperatures near 400 to 500 °C, consistent with its higher thermal stability. Iron halides have been studied to a much lesser extent due to their deposition temperatures of 1000 °C.

Table 8-16 Iron Chemical Vapor Deposition Conditions

Precursor	Substrate	T _{substrate} °C	Carrier Gas	Purity	Rate nm/min	Ref.
FeF_3	---	750-1150	none	>99%	---	192
$\text{Fe}(\eta^5\text{-C}_5\text{H}_5)_2$	Steel rod	550-600	none	---	0.3	193
$\text{Fe}(\eta^5\text{-C}_5\text{H}_5)_2$	Si	400-900	He, H ₂	>99%	---	31
$\text{Fe}(\text{CO})_5$	GaAs	200	none	>99%	0.5	194
$\text{Fe}(\text{CO})_5$	GaAs	150-300	H ₂	>99%	20	195
$\text{Fe}_2(\eta^5\text{-C}_5\text{H}_5)_2(\text{CO})_4$	Si, Glass	260-310	He	3% C + O	8.4	196

Kaplan and Bottka deposited epitaxial films of Fe onto GaAs using $\text{Fe}(\text{CO})_5$ at 200 °C with deposition rates of 0.5 nm/min in an ultra-high-vacuum (UHV) system.¹⁹⁴ Excellent film quality was observed by LEED (low energy electron diffraction) and AES (Auger electron spectroscopy). The films had comparable quality to films grown by MBE (molecular beam epitaxy). Films grown on GaAs proceeded by layer rather than island growth mechanisms. Walsh and Bottka¹⁹⁵ extended this approach to deposition of Fe films onto GaAs using $\text{Fe}(\text{CO})_5$ at substrate temperatures of 150 to 300 °C and deposition rates of 0.3 nm/min in a conventional CVD system using hydrogen as the carrier gas. The optimum temperature for deposition was 200 °C as in the UHV experiments. The films were of high purity, strongly adherent, and showed no indication of tarnishing with time.

Stauf et al. deposited Fe films from $\text{Fe}(\eta^5\text{-C}_5\text{H}_5)_2$ at 500-600 °C at rates of 0.3 nm/min using a low precursor partial pressure (4×10^{-5} torr).¹⁹³ The films were strongly adherent to the steel and nickel substrates. No major impurities were observed, but no analysis for carbon and oxygen was carried out. A more extensive study with $\text{Fe}(\eta^5\text{-C}_5\text{H}_5)_2$ was carried out by Dormans who deposited α -Fe with atmospheric pressure H₂ carrier gas at temperatures of 400 to 900 °C.³¹ Auger electron spectroscopy depth profiles showed no detectable carbon and oxygen. Interestingly, no deposition was

observed in He up to 900 °C for the Si substrates. A similar inhibition was observed for $\text{Co}(\eta^5\text{-C}_5\text{H}_5)_2$ suggesting that the effect was more general and not specific to ferrocene. This type of selectivity has not been studied or exploited for applications.

A binuclear compound, $\text{Fe}_2(\eta^5\text{-C}_5\text{H}_5)_2(\text{CO})_4$, has also been examined (see Fig. 8-8)¹⁹⁶ This precursor was used to deposit films at up to 8.4 nm/min at temperatures of 260-310 °C on a Si(111) substrate and glass plates. The films contained 97% Fe with small amounts of C and O, but the source of the contamination was not identified.

8.4.1.14 Ruthenium

Chemical vapor deposition of Ru has been investigated in only a few cases (Table 8-17). Deposition temperatures as low as 250 °C with adequate rates and high purity have been obtained. The best films have been produced from $\text{Ru}_3(\text{CO})_{12}$ and $\text{Ru}(\text{hfb})(\text{CO})_4$ where hfb = hexafluoro-2-butyne. The volatile $\text{Ru}(\text{CO})_5$ has poor thermal stability which limits its use. Little data are available on film properties obtained using $\text{Ru}(\text{acac})_2$.^{35,199} Ruthenium has been deposited from ruthenocene, $\text{Ru}(\eta^5\text{-C}_5\text{H}_5)_2$, in H_2 above 500 °C.^{35,197} Precursors which allow deposition below approximately 300 °C are not available.

Table 8-17 Ruthenium Chemical Vapor Deposition Conditions

Precursor	Substrate	T _{substrate} °C	Carrier Gas	Purity	Rate nm/min	Ref.
$\text{Ru}(\eta^5\text{-C}_5\text{H}_5)_2$	Vycor	600	H_2	>99%	---	197
$\text{Ru}(\eta^5\text{-C}_5\text{H}_5)_2$	SiO_2	500-800	H_2 , O_2 Vacuum	>80%	---	35
$\text{Ru}_3(\text{CO})_{12}$	SiO_2	250-400	H_2 , O_2 Vacuum	>99%	---	35
$\text{Ru}(\text{acac})_2$	SiO_2	500-600	H_2 , O_2 Vacuum	>99%	---	35
$\text{Ru}(\text{hfb})(\text{CO})_4$	SiO_2	500	none, H_2	>80% >99%	60	198

Deposition of ruthenium films on silicon has been accomplished using $\text{Ru}(\text{hfb})(\text{CO})_4$ in a hot-wall reactor.¹⁹⁸ The high volatility of this precursor (1-2 torr at room temperature) allowed deposition without a carrier gas. High-purity films were deposited which had good adhesion and were smooth and highly reflective.

The precursor $\text{Ru}_3(\text{CO})_{12}$ allowed deposition of high-purity films with resistivities of 17 $\mu\Omega\text{cm}$ at temperatures of 300 °C under vacuum in a hot-wall reactor.³⁵ The films had

excellent adhesion to Si and SiO₂ substrates. The precursor Ru(η^5 -C₅H₅)₂ also allowed high-purity film formation. Interestingly, films could only be deposited from Ru(η^5 -C₅H₅)₂ in oxygen. The same precursor was used to deposit RuO₂ films which have useful properties similar to Ru films. The best RuO₂ film deposited using Ru(η^5 -C₅H₅)₂ in O₂ at 575 °C had a resistivity of 90 $\mu\Omega$ cm. The films were adherent and specular. The precursor Ru(acac)₂ provided films with high resistivities and with high carbon content even in the presence of hydrogen.³⁵

8.4.1.15 Osmium

Very little work has been done with CVD of osmium. The precursor OsCl₄, however, has been used to deposit Os onto Mo and W substrates at temperatures of 1250 °C at pressures of 5×10^{-3} torr.²⁰⁰ The precursor Os(hfb)(CO)₄ has been used to deposit Os films and is analogous to the precursor Ru(hfb)(CO)₄.¹⁹⁸

8.4.1.16 Cobalt

High-purity cobalt films can be deposited at temperatures as low as 200 °C at high rates (Table 8-18). Several precursors, including Co₂(CO)₈, Co(acac)₂, and Co(η^5 -C₅H₅)₂ allow deposition at temperatures near 200-300 °C. Other precursors that have been used to form films containing Co include Co(NO)(CO)₃ for doping InGaAsP,³⁷ CoCl₂ for deposition of CoB and CoSi₂,^{205,206} and Co₄(CO)₁₂ for deposition of cobalt.⁸²

Table 8-18 Cobalt Chemical Vapor Deposition Conditions

Precursor	Substrate	T _{substrate} °C	Carrier Gas	Purity	Rate nm/min	Ref.
Co(η^5 -C ₅ H ₅) ₂	Si	300-700	H ₂ , He	>99%	0.6-60	201
Co(acac) ₂	Glass	324-352	H ₂	high	100	202
Co(acac) ₂	Quartz	275-310	H ₂	>99%	---	100
Co ₂ (CO) ₈	Si	60-450	Ar	>99.5%	10	203, 204
HCo(CO) ₄	Si	60-450	Ar	>99.5%	10	" "
Co ₂ (CO) ₈	Si, SiO ₂	200-400	none	>99%	5.0	30
Co(η^5 -C ₅ H ₅) ₂	Si	200-900	H ₂ , He	>99%	3.6	201
Co ₂ (CO) ₈	Si	150-400	" "	>99%	3	"
(η^5 -C ₅ H ₅)Co(CO) ₂	Si	300-600	" "	>99%	240	"
(CF ₃)Co(CO) ₄	Si	250-750	" "	>99%	0.18	"

Films were deposited from $\text{Co}_2(\text{CO})_8$ at temperatures of 200–400 °C at rates of 3 nm/min in a hot-wall reactor.^{30,203,204} Auger electron spectroscopy analysis of the films deposited at 200 °C showed only surface contamination by carbon, chlorine, and oxygen. Films deposited at higher temperatures had higher impurity concentrations. The films had excellent adhesion, were conformal, and little interdiffusion with the Si substrate was observed by Rutherford Backscattering Spectroscopy (RBS) analysis. The resistivities were 8–20 $\mu\Omega\text{cm}$ which compare well with films produced by other methods. Heating the films resulted in reaction with the silicon substrate to form CoSi_2 . Dormans et al.²⁰¹ observed an upper limit for the deposition temperature using the same precursor which was fixed by the onset of gas phase particle formation in an atmospheric pressure reactor (see Ch. 9).³¹ This problem has been avoided by using low pressures for deposition.³⁰

The compound $\text{Co}(\text{acac})_2$ gave films of Co at temperatures from 275 to 430 °C in a hot-wall reactor.¹⁰⁰ Films deposited in the presence of H_2 had less than 0.5% C and less than 0.2% O. Hydrogen was essential for the reduction to form pure cobalt. The optimum temperature was 275 to 310 °C which was lower than 318 to 350 °C as was suggested by Jablonowski.²⁰² Feed-rate-limited deposition or transport-limited deposition (see Ch. 9) was observed above approximately 250 °C because of the large reaction area. A patent also discusses the use of cobalt β -diketonate compounds.⁸⁹

The precursor $\text{Co}(\eta^5\text{-C}_5\text{H}_5)_2$ gave Co films at temperatures of 400–700 °C in hydrogen carrier gas in a cold-wall reactor.^{31,201} The growth rate was first order in reactant partial pressure and practically independent of temperature, suggesting feed-rate or mass-transport-limited deposition. Deposition rates of 0.6 nm/min were obtained for a precursor partial pressure of 40 mtorr. The films contained no C or O contamination as determined by AES. When the SiO_2 was removed from the Si substrate, no deposition was observed at temperatures up to 900 °C in helium. This illustrates the importance of surface cleaning procedures in providing reproducible selectivity and deposition.

The compounds $(\eta^5\text{-C}_5\text{H}_5)\text{Co}(\text{CO})_2$ and $(\text{CF}_3)\text{Co}(\text{CO})_4$ gave deposition rates of up to 0.18 nm/min in H_2 at temperatures of 300–600 °C in a cold-wall reactor.²⁰¹ The precursors $(\eta^5\text{-C}_5\text{H}_5)\text{Co}(\text{CO})_2$ and $(\text{CF}_3)\text{Co}(\text{CO})_4$ deposited high-purity Co in H_2 as shown by AES. Deposition in He resulted in high carbon content. Experiments with $(\eta^5\text{-C}_5\text{H}_5)\text{Co}(\text{CO})_2$ in helium gave deposition in contrast to results with $\text{Co}(\eta^5\text{-C}_5\text{H}_5)_2$ where no deposition was observed. This demonstrated the role of precursor design in selective deposition. The deposition rates for $(\eta^5\text{-C}_5\text{H}_5)\text{Co}(\text{CO})_2$ and $(\text{CF}_3)\text{Co}(\text{CO})_4$ decreased with increasing temperature due to gas-phase reaction and particle formation as occurred for $\text{Co}_2(\text{CO})_8$. This problem was eliminated by using lower pressures of the hydrogen carrier gas.

A number of other precursors have been studied but in less detail. The precursor $\text{HCo}(\text{CO})_4$ has been used to deposit CoSi_2 by reaction with an Si substrate.²⁰¹

8.4.1.17 Rhodium

Several organometallic precursors have been used to deposit Rh metal at temperatures as low as 100 °C at high rates (Table 8-19). These precursors provide sufficient deposition rates and low enough deposition temperatures for most applications. Although several reports exist in the literature, few in-depth studies are available. Little information exists for deposition rates, resistivities, film morphology, and other properties. The surface chemistry of tris(η^3 -allyl)rhodium^{105,209,210} and (acac)Rh(CO)₂²¹¹ has been studied on TiO₂ mainly in connection with the catalytic behavior of Rh. The CVD of Rh from (hfac)Rh(1,5-COD) has been reported in a patent although few experimental details are available.²¹² A comparison of the CVD of the precursors Rh₂(μ -Cl)₂(CO)₄, Rh(η^5 -C₅H₅)(CO)₂, Rh(η^5 -C₅H₅)(1,5-COD), Rh(η^3 -allyl)(CO)₂, and Rh(η^3 -allyl)₃ under vacuum (10⁻³ torr) and in the presence of H₂ was reported.²¹³ Although films deposited under vacuum were significantly contaminated with C and O, the presence of H₂ gave rise to 90% pure Rh films. The LCVD of Rh from (hfac)Rh(CO)₂ has produced lines with resistivities of 4.5 $\mu\Omega$ cm.²¹⁴

Table 8-19 Rhodium Chemical Vapor Deposition Conditions

Precursor	Substrate	T _{substrate} °C	Carrier Gas	Purity %	Rate nm/min $\mu\text{g}/(\text{cm}^2 \text{ min})$	Ref.
Rh(CO) ₂ (acac)	Glass	20-150	Ar, H ₂	C+O 2-20	0.4-1.1	103
Rh(CO) ₂ (acac)	TiO ₂ /Si	200-500	none	C+O impurity	---	105
(η^5 -C ₅ H ₅)Rh(η^2 -C ₂ H ₄) ₂	Quartz Glass Si	25	He, H ₂	>99	---	207
[(PF ₃) ₂ RhCl ₂] ₂	Pyrex	200	none	Cl	120	208
Rh(tfa) ₃	Glass Steel	250	Ar, H ₂	high	---	101
Rh(η^3 -allyl) ₃	Glass	250	Ar, H ₂	>97 in H ₂ plasma >86 in vacuum	0.3-7.3	74
Rh(η^3 -allyl) ₃	SiO ₂	120	Ar, H ₂	>98	---	188

continued

Table 8-19 continued

Precursor	Substrate	T _{substrate} °C	Carrier Gas	Purity %	Rate nm/min	Ref.
Rh(η^3 -allyl) ₃	SiO ₂	180	none	Rh 86 C 4 O 0	~33	213
	SiO ₂	130	H ₂	Rh 96 C 14 O 0	~33	213
Rh ₂ (Cl) ₂ (CO) ₄	SiO ₂	180	none	Rh 49 C 24 O 27	~33	213
	SiO ₂	180	H ₂	Rh 91 C 7 O 2	~33	213
Rh(η^5 -C ₅ H ₅)(CO) ₂	SiO ₂	180	none	Rh 75 C 20 O 5	~33	213
	SiO ₂	180	H ₂	Rh 89 C 7 O 4	~33	213
Rh(η^5 -C ₅ H ₅)(1,5-COD)	SiO ₂	270	none	Rh 81 C 19 O 0	~33	213
	SiO ₂	230	H ₂	Rh 97 C 3 O 0	~33	213
Rh(η^3 -allyl)(CO) ₂	SiO ₂	180	none	Rh 48 C 40 O 12	~33	213
	SiO ₂	180	H ₂	Rh 94 C 6 O 0	~33	213

8.4.1.18 Iridium

Several metal-organic precursors have been used to deposit Ir at temperatures as low as 100 °C with reasonable rates and high purity (Table 8-20). In addition to the precursors shown in the Table, Ir(acac)₃ has been used for CVD,²¹⁶ and the use of Ir(β -diketonate)₃ precursors has also been discussed in a patent,²¹⁷ but little quantitative information is available about the use of these precursors for CVD.

Table 8-20 Iridium Chemical Vapor Deposition Conditions

Precursor	Substrate	T _{substrate} °C	Carrier Gas	Purity %	Rate nm/min	Ref
IrCl ₃	Graphite	825-975	H ₂ , CO, Ar	high	---	68
IrCl ₄	Graphite	825	H ₂ , CO, Ar	high	---	"
IrBr ₃	Graphite	825	H ₂ , CO, Ar	high	---	"
IrF ₆	Graphite	725-875	H ₂ , CO, Ar	high	200	"
Ir(η^3 -allyl) ₃	SiO ₂	100	H ₂	>98%	---	186
Ir(η^3 -allyl) ₃	Glass	250-450	H ₂ , Ar, vacuum	3-17% C	0.1-3.3	74
Ir(acac)(1,5-COD)	Cu	400-750	H ₂	85-99%	---	150
{(COD)Ir[μ -OCH ₃]} ₂	Cu	600	H ₂	90-95%	---	"
(η^5 -C ₅ H ₄ CH ₃)Ir(1,5-COD)	Quartz	120-680	H ₂ , vacuum	>99%	1.3-1.4	215
(η^5 -C ₅ H ₅)Ir(1,5-COD)	Quartz	"	" "	>99%	"	"
(1,5-COD)Ir(μ -OAc) ₂	Quartz	"	" "	>99%	"	"

Macklin and Withers showed that IrCl₃, IrCl₄, IrBr₃, and IrF₆ allow CVD of high-purity Ir films but at temperatures near 800 °C.⁶⁸ Based on its high deposition rate in the warm-wall reactor system, IrF₆ was the best precursor for film deposition. In addition, IrF₆ is a gas at room temperature which makes introduction into the reactor more reliable and reproducible. Carbon monoxide was important in increasing deposition rates and reducing the temperature required for deposition. The role of CO was probably to coordinate with the iridium halides to form intermediate carbonyl halide species, especially in the cases of IrCl₃, IrCl₄, and IrBr₃.

One of the most complete studies of Ir CVD was carried out by Hoke et al. who examined (η^5 -C₅H₄CH₃)Ir(1,5-COD), (η^5 -C₅H₅)Ir(1,5-COD), and [(1,5-COD)Ir(μ -OAc)]₂ as precursors.²¹⁵ The motivation for this work was that Ir halides, [(1,5-COD)Ir(μ -OCH₃)]₂, Ir(acac)(1,5-COD), and Ir(acac)₃, require deposition temperatures above 500 °C, and in many cases they produce films with measurable impurity levels. In contrast, (η^5 -C₅H₄CH₃)Ir(1,5-COD) and (η^5 -C₅H₅)Ir(1,5-COD) allow deposition of high-purity Ir films at temperatures as low as 120 °C in H₂. The advantage of (η^5 -C₅H₄CH₃)Ir(1,5-COD) is its low melting point, 40 °C, which makes it available as a liquid source. However, deposition in vacuum leads to films heavily contaminated with carbon. This result can be explained by the low oxophilicity of Ir (the oxide is not stable below 550 °C) which allows deposition in the presence of O₂ which serves to oxidize organic species on the surface and convert them into volatile species which can then desorb from the surface.

8.4.1.19 Zinc

The CVD of pure Zn has not been studied in detail. However, a number of studies have examined deposition of zinc as a component of or dopant in materials such as ZnS, InGaAlP, GaAs, and Zn₃P₂.²¹⁸⁻²²⁷ The precursors that have been used most successfully are Zn(CH₃)₂ and ZnEt₂. In addition, the surface reactions of zinc alkyls on Si(100) surfaces have been investigated.²²⁸ The laser-induced CVD of Zn from Zn(CH₂CH₃)₂ has also been achieved.¹¹³

8.4.1.20 Cadmium

The majority of the work on Cd is for deposition of multicomponent materials where Cd is one component such as in CdS and (Cd,Hg)Te, laser deposition, and as a dopant in materials such as InP.^{229,230} The precursors that have been used most extensively are Cd(CH₃)₂ and CdEt₂. Little information exists for CVD of pure Cd.

8.4.1.21 Tin

Chemical vapor deposition of tin has not been studied extensively.²³¹ However, tin has been formed from SnH₄, Sn(CH₃)₄, Sn(*n*-Bu)₄, EtSnH₃, and Br₂Sn(*n*-Bu)₂, and the kinetics of SnH₄ decomposition has been studied in detail (see Section 8.4.2.2). Few data are available for the other species. Most results in the literature are given for laser-induced deposition^{113,232-234} as a component of superconductors (Nb₃Sn),²³⁵ as a component in polymer films,²³⁶ and for incorporation of Sn as a dopant into materials such as In₂O₃,^{237,238} GaAs,^{239,240} and InAs.²⁴¹ Price and Trotman-Dickenson have studied the decomposition of (CH₃)₂SnCl₂ at temperatures between 554 and 688 °C but did not attempt CVD.²⁴² Tin has also been deposited by the pyrolysis of (CH₃)₂SnH₂ or Sn₂Et₆ at 540 °C using CO₂ as a carrier gas.²⁴³ A patent also reports CVD using Sn(CH₃)₄, (CH₃)SnH₃, (CH₃)₂SnH₂, and SnH₄.²⁴⁴ Gonser and Slowter have also studied CVD of Sn.²⁴⁵

8.4.1.22 Lead

Little information exists on CVD of lead. Only a few results are available and these are for photon-induced processes. In these cases, Pb has been deposited primarily from lead alkyls such as PbEt₄. Rigby²⁴⁶ and Chiu et al.²⁴⁷ reported the photodeposition of lead from PbEt₄ at room temperature. Other sources of Pb include PbPh₄²⁴⁸ and Pb(β-diketonate)₂,²⁴⁹ but in these cases the Pb is usually incorporated into other materials such as PbTiO₃ and Pb-Bi-Sr-Ca-Cu-O ceramic superconductors.

8.4.1.23 Heterometallic Systems

The use of heterometallic precursors for CVD of metal films has not been studied extensively, and little information is available about film purity and deposition rates. Much more work has been done for materials such as 13-15 (GaAs), 14-16 (ZnSe), and other semiconductors.²⁵⁰ Table 8-21 shows results for metals. The primary problem with this approach, in addition to the same problems found for simple precursors, is finding precursors with high vapor pressures and deposition rates while maintaining the stoichiometry of the precursor in the film. Existing heterometallic precursors provide low deposition rates and do not always provide controlled stoichiometries in the films.

Liu et al. reported photochemical vapor deposition from $(\eta^5\text{-C}_5\text{H}_5)\text{FeCo}(\text{CO})_6$, $(\eta^5\text{-C}_5\text{H}_5)\text{Fe}_2\text{Co}(\text{CO})_9$, $\text{HFeCo}_3(\text{CO})_{12}$, and $(\eta^5\text{-C}_5\text{H}_5)\text{FeNi}(\text{CO})_3$ which gave Fe-Co and Fe-Ni films.²⁵¹ The precursors $(\eta^5\text{-C}_5\text{H}_5)\text{FeCo}(\text{CO})_6$ and $\text{HFeCo}_3(\text{CO})_{12}$ provided deposition rates of 3.3 and 0.8 nm/min with a substrate temperature of roughly 50 °C and

Table 8-21 Heterometallic Chemical Vapor Deposition Conditions

Precursor	Substrate	T _{substrate} °C	Carrier Gas	Purity	Rate nm/min	Ref.
$(\eta^5\text{-C}_5\text{H}_5)\text{FeCo}(\text{CO})_6$	Al, Si	50	CO	4 % C	3	251
$(\eta^5\text{-C}_5\text{H}_5)\text{Fe}_2\text{Co}(\text{CO})_9$	Al, Si	50	CO	---	---	"
$\text{HFeCo}_3(\text{CO})_{12}$	Al, Si	50	CO	---	0.8	"
$(\eta^5\text{-C}_5\text{H}_5)_2\text{FeNi}(\text{CO})_3$	Al, Si	50	CO	---	---	"
$(\text{H}_3\text{Si})_2\text{Fe}(\text{CO})_4$	---	670-770	He	---	---	252, 253
$(\text{H}_3\text{Si})\text{Co}(\text{CO})_4$	---	670-770	He	---	---	" "
$\text{Mn}(\text{CO})_5(\text{SiH}_3)$	---	670-770	He	---	---	" "
$\text{H}_3\text{SiRe}(\text{CO})_5$	---	670-770	He	---	---	" "
$\text{HFeCo}_3(\text{CO})_{12}$	Glass	300-350	CO	>99%	1.7	254
$(\eta^5\text{-C}_5\text{H}_5)\text{FeCo}(\text{CO})_6$	Glass	300-350	CO	>99%	1.7	"
$(\text{CO})_4\text{CoGaCl}_2(\text{THF})$	Si, glass	500	H ₂	12% C+O+N	---	48, 255
$\text{R}_2\text{GeMn}_2(\text{CO})_{10}$	SiO ₂	250-500	none, H ₂	<20% C or O	50	256
$[\text{Mn}(\text{CO})_5]_2\text{SiH}_2$	Ni	225-500	none	9-24% O, 18-76% C	60	257, 258
$\text{L}(\text{CO})_n\text{M-ER}^1\text{R}^2(\text{D})$	Si	200-400	---	---	<16	259

where

L = CO, $\eta^5\text{-C}_5\text{H}_5$, $\text{P}(\text{CH}_3)_3$; n = 1-4; M = Mn, Fe, Co, Ni; E = Al, Ga, In; R¹ or R² = H or alkyl; D = O or N donor ligand.

were some of the few documented examples of high-purity films. No deposition was observed in the absence of irradiation by the mercury arc lamp. The stoichiometry of the precursor could be maintained in the films.

The precursors $(\eta^5\text{-C}_5\text{H}_5)\text{FeCo}(\text{CO})_6$,²⁵⁴ $(\text{H}_3\text{Si})_2\text{Fe}(\text{CO})_4$, $(\text{H}_3\text{Si})\text{Mn}(\text{CO})_5$, $(\text{H}_3\text{Si})\text{Co}(\text{CO})_4$,^{252,253} $\text{HFeCo}_3(\text{CO})_{12}$,²⁵⁴ and $(\text{CO})_4\text{CoGaCl}_2(\text{THF})$ ^{47,48,255,260,261} have also been examined. Deposition rates were not reported for most of these precursors. For example, $\text{HFeCo}_3(\text{CO})_{12}$ deposited films at temperatures of 300-350 °C with rates of 1.7 - 2.5 nm/min.²⁵⁴

The CVD of manganese germanide and cobalt germanide films from $\text{R}_2\text{GeBr}_x[\text{Mn}(\text{CO})_n]_{2-x}$ ($\text{M} = \text{Mn}, \text{Co}, x = 0,1$) has been examined, and AES data showed that films deposited over the temperature range of 250 to 400 °C retained the Ge:M stoichiometry.²⁵⁶ However, the films were contaminated by carbon.

Fischer²⁵⁹ used several compounds in the family $\text{L}(\text{CO})_n\text{MER}^1\text{R}^2(\text{D})$ (where M and E are metals) to deposit films of CoAl, CoGa, CoIn, NiIn, NiAl, NiGa, MnGa, and MnIn. These precursors are either low-melting solids or liquids with vapor pressures of 10-50 mtorr at room temperature. The metal ratio in the precursor could be retained in the films in some cases, but not in others. Deposition temperatures were 200 to 400 °C and rates of up to 16 nm/min were obtained.

8.4.2 Kinetics and Mechanisms

Determination of the reaction byproduct distribution and the overall stoichiometry is important in understanding the pathways which lead to pure metal deposition. Unfortunately, there is a paucity of information on the identity of the reaction products for most systems. Only a few systems have been studied in sufficient detail to even allow identification of the main reaction products.

This section discusses the different classes of precursors that have been used for metal deposition according to the nature of the ligands and are discussed in the following order: halides, alkyls, alkene and alkyne π -complexes, allyls, metallocenes, carbonyl π -complexes, trifluorophosphine complexes, metal β -diketonates, bi- and multi-nuclear, and heteronuclear precursors. The composition of the product films is also examined because it relates to the reaction pathways and byproduct distributions. These discussions establish a basis for comparison and allow for rational and systematic design of new CVD precursors.

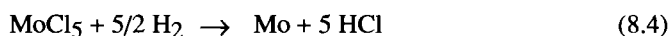
8.4.2.1 Metal Halides

Metal halides in the presence of H_2 or some other reducing agent (which may be the substrate) and without reducing agents at high temperatures allow deposition of pure metals. Deposition has been investigated from virtually all the metal halides. The main

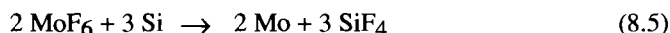
problems with using metal halides as CVD precursors are the low volatility of many of the metal chlorides (see Section 8.2.2.1) and their high thermal decomposition temperatures.

Three deposition mechanisms are possible: (i) reduction by a gas such as H_2 or SiH_4 , (ii) reduction via reaction with the substrate (Si for example) to form the metal and another halide species ($SiCl_4$, for example), and (iii) reaction at high temperatures without a reducing agent to form the metal and the corresponding halogen. These approaches are discussed in detail for W in Chapter 3. Examples of these classes of mechanisms are given below.

An example of the first mechanism is the reaction of $MoCl_5$ with H_2 which has been studied in some detail (Eq. 8.4). The reaction is first order in $MoCl_5$ concentration¹⁶⁶ and 3/2 order in H_2 .¹⁶⁷



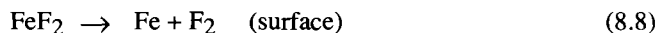
An example of the second mechanism is the reaction of MoF_6 with Si substrates (Eq. 8.5).¹⁶⁸⁻¹⁸⁰



This reaction, if carried out in H_2 carrier gas, can occur simultaneously with the reaction with H_2 (Eq. 8.6) to give two parallel deposition mechanisms.



However, the Si reduction of MoF_6 is much faster than hydrogen reduction (because H_2 must first be dissociated on Mo), and so generally a Mo layer is formed by the reduction of Equation 8.5 followed by steady-state growth according to Equation 8.6. The third mechanism is shown in the reaction of FeF_3 to form Fe. Macheteau¹⁹² has suggested that the reaction of FeF_3 occurs in the gas phase to form FeF_2 (Eq. 8.7), which subsequently reacts on the surface to form high-purity Fe and F_2 , (Eq. 8.8).



Other examples of this third mechanism exist. The energetics of the FeI_2 system have been described.²⁶² Similarly, AgF is known to be easily defluorinated above 500 K to liberate F_2 and Ag metal.²⁶³ Studies of the surface chemistry of TaF_5 on Si and SiO_2 have shown that high-purity Ta can be formed without H_2 .¹⁵¹ Although no evidence was given, Ta deposition probably proceeds with formation of F_2 (Eq. 8.9).



On silicon substrates, the CVD of metal halides can often lead to formation of metal silicides. These reactions are often the basis for selective deposition (see Ch. 9) as in the case of W (see Ch. 3) and can be used for producing metal silicides (see Ch. 1). The reactions of TiCl_4 on Si surfaces have been studied in some detail and the following overall reaction pathways have been proposed (Eqs. 8.10 and 8.11).²⁶⁴



In the absence of H_2 , excessive Si etching has been observed, as expected, based on the stoichiometry of Equation 8.10. This problem can be solved by using TiCl_4 and SiH_4 as source gases to produce either blanket or selective TiSi_2 deposition.²⁶⁴ Thermodynamic calculations reveal that in contrast to the facile reduction of WF_6 by Si to form W at 600 K, the reduction of TiCl_4 to Ti metal by Si is thermodynamically unfavorable (Eq. 8.12).²⁶⁵

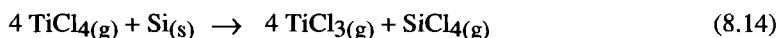


Similar calculations for the reaction of Equation 8.12 to form TiSi_2 reveal it is thermodynamically favorable, $\Delta G^\circ_{298} = -5.4 \text{ kcal/mol}$. However, the reaction of Equation 8.12 is limited by three factors: (i) inhibition by the native oxide layer on Si, (ii) the relatively low thermodynamic driving force and (iii) the necessity for a supply of Si from the substrate to propagate the reaction.²⁶⁵ Unlike WF_6 , TiCl_4 does not react with SiO_2 under normal CVD conditions to give Ti films.

Metal halides also exhibit other deposition mechanisms such as disproportionation. For example, the reduction of TiCl_4 is further complicated by the disproportionation of sub-halides. Thermolysis of TiCl_4 can result in the formation of TiCl_3 and TiCl_2 , observed as purple and brown deposits in CVD reactors. The TiCl_3 can disproportionate to form TiCl_4 and TiCl_2 according to Equation 8.13.



Also, partial reduction of TiCl_4 by Si is possible according to Equation 8.14. These sub-halides can then participate in other complicating reactions leading to a poorly controlled chemistry.



The deposition of Ti metal from heavier halides such as TiBr_4 and TiI_4 has also been investigated. Metal was deposited on stainless steel substrates with 90% purity, and in the case of laser CVD reactions, a simple reduction to give Ti and Br_2 was proposed.¹²² However, an alternative pathway is possible and involves two disproportionation steps according to reactions 8.15 through 8.17 below.



8.4.2.2 Metal Alkyls

A number of metal alkyl compounds have been used as precursors for CVD experiments but often lead to the formation of metal carbides. The metals that have been examined include Sn, Pb, Zn, Cd, Ti, Cr, Zn, and W. In other cases, the metal alkyls are either not stable, not volatile, or react to give impure films.

Tin has been deposited from SnH_4 , $\text{Sn}(\text{CH}_3)_4$, $\text{Sn}(-n\text{-Bu})_4$, and $\text{Br}_2\text{Sn}(-n\text{-Bu})_2$. Although not a metal alkyl compound, studies of stannane are relevant and are described here. Stannane, SnH_4 , has a melting point of -146°C and a boiling point of 52.5°C but is too unstable for most CVD applications.²⁶⁶⁻²⁶⁸ It thermally decomposes even at 298 K to give Sn metal and H_2 . The thermal decomposition can be explosive under certain circumstances. The activation parameters for thermal decomposition of SnH_4 reveal an activation energy of 9.1 kcal/mol with rates that are first order in SnH_4 concentration and independent of H_2 pressure.²⁶⁹ When SnD_4 was decomposed in the presence of H_2 , no HD was observed, but when a mixture of SnH_4 and SnD_4 was used, HD was found. These interpretations are consistent with a lack of chemisorption of H_2 on a tin surface and provide insight into the mechanism of thermal decomposition of organo-tin compounds, especially where β -hydride elimination results in formation of metal hydride intermediates.

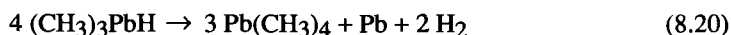
Tin(IV) compounds also undergo facile ligand redistribution reactions which can lead ultimately to the deposition of tin metal.²⁷⁰ Analysis of the byproduct distribution of CVD of EtSnH_3 revealed products associated with homolytic (radical) reaction processes resulting in the well-known ligand redistribution reactions for Sn(IV).



Mechanistic studies of the thermal decomposition of organo-tin compounds during CVD experiments are not widely available, probably because Sn is primarily used as a dopant in other materials. It is possible that a β -hydride elimination mechanism is

operative (where β -hydrogen atoms are available) analogous to the case of Al, but the homogeneous solution chemistry of tin(IV) alkyls is dominated by radical mechanisms. Thermal decomposition of Ph_3SnH in the gas phase reveals products consisting of a small amount of benzene, SnPh_4 , Sn_2Ph_6 , and Sn that are consistent with homolytic processes.²⁷¹

Lead, zinc, and cadmium have been primarily used as dopants in other materials; therefore, the thermal decomposition of these metal alkyls in the absence of other species has not been studied in detail. Lead(IV) alkyl compounds probably undergo thermal decomposition by homolytic mechanisms analogous to the photochemically-induced reactions.²⁴⁶ Alkyl lead hydrides, $\text{R}_{(4-n)}\text{PbH}_n$, undergo thermal and photochemical decomposition below room temperature in the liquid phase by various routes such as those shown in Equation 8.20.²⁷²⁻²⁷⁴ Similar mechanisms may occur in CVD processes.



Zinc and cadmium alkyl compounds also appear to thermally decompose via metal-carbon bond homolysis, although much more attention has been devoted to studies of their photochemically-induced decomposition. The typical temperature for the complete decomposition of $\text{Cd}(\text{CH}_3)_2$ in H_2 is $\sim 380^\circ\text{C}$.²⁷⁵ A study of the adsorption behavior of $\text{Zn}(\text{CH}_3)_2$ and ZnEt_2 on Si(100) surfaces revealed that these species dissociated below 300 K to produce alkyl species and zinc metal.²²⁸ At higher temperatures (400-600 K), Zn desorbed and left the alkyl species on the surface. Dimethyl zinc resulted in formation of surface CH_3 groups which either desorbed as $\text{CH}_3\cdot$ at 825 K or were dehydrogenated to form CH_x , C, and H_2 . Further reaction of these species resulted in formation of acetylene, H_2 , and SiC. Diethyl zinc decomposed to give surface $\text{Et}\cdot$ groups which underwent β -hydride elimination to give both gas-phase and surface ethylene. The physisorbed ethylene either desorbed at 650 K or decomposed to CH_x , C, and H_2 .

Chemical vapor deposition experiments using $\text{Ti}(\text{CH}_2\text{-}i\text{-Bu})_4$ resulted in formation of TiC rather than Ti metal at a substrate temperature as low as 150°C .⁷⁶ Even in the presence of a hydrogen pressure of 10^{-2} torr, TiC was formed. The films were amorphous as deposited and crystallized only on heating above 1100°C . Mechanistic studies revealed a reaction pathway that involved α -hydrogen abstraction to form neopentane and a titanium alkylidene intermediate.

Similar observations were made with $\text{Cr}(\text{CH}_2\text{-}i\text{-Bu})_4$ and $\text{Cr}(\text{N-}i\text{-Pr})_3$ which gave amorphous films with Cr:C ratios of 1.4:1 and 1.9:1 as deposited at 330°C .¹⁵⁸ On annealing at 600°C for 18 hours under vacuum (10^{-3} torr), crystalline Cr_3C_2 was formed. A byproduct analysis of CVD using $\text{Cr}(\text{CH}_2\text{-}i\text{-Bu})_4$ revealed the presence of neopentane, isobutylene, propene, and tetramethylhexene.¹⁵⁸ A mechanism analogous to that proposed for the thermal decomposition of $\text{Ti}(\text{CH}_2\text{-}i\text{-Bu})_4$ was implicated, although binuclear processes were not ruled out.²⁷⁶ Similar results were observed for other early transition metal alkyl compounds including $\text{Zr}(\text{CH}_2\text{-}i\text{-Bu})_4$ which forms ZrC and $(i\text{-Bu-CH}_2)_3\text{W}\equiv\text{CSi}(\text{CH}_3)_3$ which forms WC.²⁷⁷

8.4.2.3 Complexes with Unsaturated Organic Ligands: Alkenes, Alkynes, Allys, Metallocenes, and Related Complexes

Alkene and alkyne complexes: Alkene and alkyne π -complexes of metals have been investigated mainly for the cases of Ir, Ru, and Rh. In general, better results have been obtained in the presence of hydrogen in which case hydrogenation of the unsaturated organic ligand could occur. Few generalizations can be made about reaction pathways because of the wide variety of precursors that have been examined.

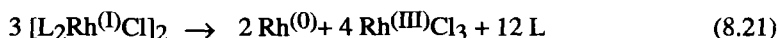
The reactions of $(\eta^5\text{-C}_5\text{H}_5)\text{Ir}(\text{1,5-COD})$ and $(\eta^5\text{-C}_5\text{H}_4\text{CH}_3)\text{Ir}(\text{1,5-COD})$ in hydrogen and low O_2 partial pressure led to formation of high-purity (<1% C) Ir films at 120 °C.²¹⁵ However, when the deposition was carried out in vacuo, 80% C was incorporated. Under an H_2 atmosphere, byproduct analysis revealed the presence of only saturated hydrocarbons, cyclooctane, and presumably methylcyclopentane, although this was not stated clearly. The analysis suggested a simple mechanism in which the organic ligands were hydrogenated to form stable volatile species which desorbed from the surface. The volatile byproducts were not collected in the deposition experiment under an O_2 atmosphere, and the lack of oxidation of the film was consistent with the low oxophilicity of Ir suggesting a mechanism in which the organic substances were oxidized to form volatile species which desorbed from the surface.

The compound $[(\text{1,5-COD})\text{Ir}(\mu\text{-OAc})]_2$ is thermally unstable and decomposed in the precursor reservoir during CVD experiments in vacuo.²¹⁵ Proton NMR spectroscopy revealed the presence of cyclooctadiene, cyclooctene, and cyclooctane in approximately equal amounts and suggested the alkene portion of the precursor was hydrogenated. Thermogravimetric analysis with mass spectroscopy also revealed the presence of CO_2 and ethane, thought to arise from thermal decomposition of the acetate ligands. This suggests a rather complicated reaction mechanism in which ligand hydrogenation and decomposition both occur where the presence of H_2 or O_2 could drastically change the reaction pathways. In other work, the thermal decomposition of $(\text{1,5-COD})\text{Rh}(\text{OR})$ compounds produced 1,5-cyclooctadiene, 1,3-cyclooctadiene, and cyclooctane analogous to the observations for the carboxylate complexes.²⁷⁸

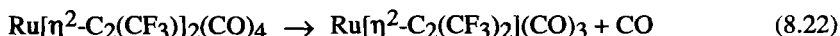
Thermal laser-assisted CVD of $(\eta^5\text{-C}_5\text{H}_5)\text{M}(\eta^2\text{-C}_2\text{H}_4)_2$ ($\text{M} = \text{Rh}$ and Ir) revealed some insight into thermal CVD processes.²⁰⁷ Laser-assisted CVD of these compounds under H_2 resulted in formation of pure Rh and Ir films when the substrate was irradiated in the presence of the precursor for 20 min and then the deposit was further irradiated under H_2 for 20 min in the absence of the precursor. Irradiation of the substrate under H_2 for 20 min without a subsequent annealing step and in the absence of the precursor resulted in deposits that analyzed as $\text{C}:\text{Rh} = 5:1$. Therefore, the authors proposed that irradiation of $(\eta^5\text{-C}_5\text{H}_5)\text{Rh}(\eta^2\text{-C}_2\text{H}_4)$ resulted in loss of the ethylene ligands, probably in the gas phase, with formation of " $\text{Rh}(\eta^5\text{-C}_5\text{H}_5)$." Subsequent annealing with hydrogen resulted in reduction of Rh^{I} to Rh^0 with loss of the hydrogenated cyclopentadienyl ligand. However, under the conditions used, laser-assisted gas-phase reactions seem unlikely

because of the small deposit dimensions and low pressures involved, and loss of the neutral ligand may have occurred during precursor adsorption and reaction.

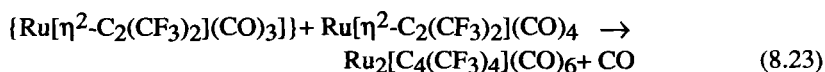
In other work, the lability of a series of Rh^{I} compounds $(\text{L}_2\text{RhCl})_2$ [where $\text{L}_2 = 1,5\text{-COD}$, NBD (norbornadiene) and $(\eta^2\text{-C}_2\text{H}_4)_2$] was studied with respect to formation of Rh under air, nitrogen, and 7% H_2 in N_2 atmospheres.²⁷⁸ The results revealed that the thermal decomposition behavior depended on the nature of the alkene ligand and the composition of the atmosphere. Under 7% H_2 in N_2 atmosphere, the onset of thermal decomposition of these species occurred in the following order: $\text{L}_2 = (\eta^2\text{-C}_2\text{H}_4)_2$, 91 °C; NBD , 143 °C; $1,5\text{-COD}$, 212 °C. Under a nitrogen atmosphere, $(\text{L}_2\text{RhCl})_2$, [$\text{L}_2 = \text{NBD}$ and $(\eta^2\text{-C}_2\text{H}_4)_2$], underwent weight loss consistent with loss of one or more alkene ligands followed by formation of Rh metal at higher temperatures. In contrast, $[(1,5\text{-COD})\text{RhCl}]_2$ formed Rh metal directly. In air, thermal decomposition generally resulted in formation of crystalline Rh metal followed by oxidation above 500 °C to form crystalline Rh_2O_3 , except for $[(\eta^2\text{-C}_2\text{H}_4)_2\text{RhCl}]_2$, which gave Rh_2O_3 directly. The weight loss corresponding to formation of " RhCl " by loss of the neutral ligand was a common feature of these reactions. However, X-ray diffraction studies showed that " RhCl " contained a significant amount of crystalline Rh and was more likely to be the disproportionation products Rh and RhCl_3 , formed according to Equation 8.21. These results imply that while a reducing ambient is desirable to facilitate the reduction of the metal, complexes of noble metals can be thermally reduced in air to form the corresponding crystalline metal.



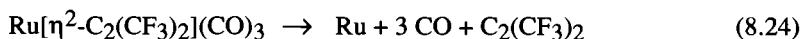
High-purity Ru films were deposited at 500 °C on Si substrates from the ruthenium alkyne complex $\text{Ru}(\text{CO})_4[\eta^2\text{-C}_2(\text{CF}_3)_2]$ under dynamic vacuum.¹⁹⁸ At lower substrate temperature (300 °C), the thickness of the film was noticeably diminished and a yellow crystalline solid was observed. At a substrate temperature of 150 °C, the yellow crystalline solid was formed in sufficient quantity that it could be isolated and characterized as the dimer $\text{Ru}_2[\text{C}_4(\text{CF}_3)_4](\text{CO})_6$, which was also obtained in homogeneous solution on refluxing the starting material in toluene. As a result of this observation, Senzaki et al.¹⁹⁸ proposed that the first step in thermal decomposition of $\text{Ru}(\text{CO})_4[\eta^2\text{-C}_2(\text{CF}_3)_2]$ was carbonyl dissociation in the gas phase (Eq. 8.22).



This product may then react with the starting material to form the dimer according to Equation 8.23.



However, at higher temperatures thermal decomposition of the tricarbonyl intermediate may dominate resulting in Ru deposition (Eq. 8.24).



These byproducts were identified by trapping the volatile decomposition product and analyzing by ^{19}F NMR spectroscopy and GC-MS-FTIR. Evidence for the species C_4F_{14} and C_4F_{12} was obtained. In addition, $\text{Ru}_2[\text{C}_4(\text{CF}_3)_4](\text{CO})_6$ also thermally decomposed to give Ru films. However, whether or not the dimeric species is formed as an intermediate during decomposition was not clear.

Allyls: The allyl (C_3H_5 or propenyl) complexes of Ir and Rh provide routes to the pure metals under certain conditions. The reactions of $\text{Rh}(\eta^3\text{-allyl})_3$ on TiO_2 surfaces have been investigated under UHV conditions.^{74,209} $\text{Tri}(\eta^3\text{-allyl})\text{rhodium}$ reacted with OH groups on the surface to form a diallylrhodium species. Upon reaction with hydrogen at 60–100 °C, an allylrhodium hydride was formed. Further reaction with hydrogen at 120–150 °C resulted in formation of $\text{TiO}_2\text{-RhH}_2$ which reductively eliminated H_2 above 400 °C to yield Rh metal. No direct analysis of reaction products was reported; however, these results suggest that the purity of films can be increased by the presence of hydrogen.

In a comparison of the CVD of $\text{M}(\eta^3\text{-allyl})_3$ ($\text{M} = \text{Rh}$ and Ir) in vacuo, under H_2 , and in the presence of H^\bullet , the metal films were contaminated with C to approximately the same extent in vacuo and under H_2 (13–17 at.% C).⁷⁴ However, introduction of atomic hydrogen increased the purity (2 at.% C) of Ir and Rh films deposited in plasma-assisted experiments. It was proposed that the atomic H^\bullet aids cleavage of the M-allyl bonds with formation of propene and propane. Any carbon incorporated during deposition is then preferentially etched from the growing film by the plasma.⁷⁴

A detailed study of the thermal decomposition pathway of $\text{M}(\eta^3\text{-allyl})_4$ ($\text{M} = \text{Mo}$ and W) has been carried out in both a partial pressure of H_2 and under vacuum.⁷⁵ The volatile byproducts were trapped and analyzed by ^1H NMR spectroscopy. The films deposited from these precursors consisted primarily of the carbides, MC , together with graphitic carbon as determined by XPS, when the deposition was carried out under vacuum. Formation of unidentified metal oxides (due to failure to scrub the H_2 carrier gas) was observed under H_2 . The major volatile byproducts (>95%) identified by ^1H NMR spectroscopy were propene and propane. Minor amounts of benzene, ethylene, and ethane were also observed. No evidence for hexadiene was found, in contrast to the CVD of $\text{Pd}(\eta^3\text{-allyl})_2$ where the product distribution was 67% propene and 33% hexadiene,⁷⁶ $\text{Te}(\eta^1\text{-allyl})_2$ where hexadiene was exclusively observed,¹⁷⁵ and $\text{Se}(\eta^1\text{-allyl})_2$ ²⁷⁹ where a 2 : 1 ratio of propene to hexadiene was observed. The absence of hexadiene in the case of $\text{M}(\eta^3\text{-allyl})_4$ suggests homolytic bond dissociation processes did not occur. A β -hydride elimination mechanism would favor formation of allene or propyne as observed for $[\eta^5\text{-C}_5(\text{CH}_3)_5]_2\text{Ta}(\eta^3\text{-allyl})$ in solution. Reaction pathways involving either α -

hydride elimination or vinyl C-H activation are proposed to be more reasonable for the Mo and W species. These accounted for the observed decomposition products and the resulting increase in the M-C bond order of the intermediate which would favor metal carbide formation. These experiments show the poor characteristics of early transition metal allyl complexes for deposition of pure metal films.

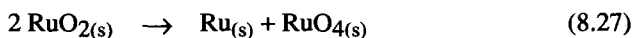
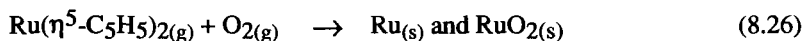
Metalloenes and Related Complexes: Metallocenes, $M(\eta^5\text{-C}_5\text{H}_5)_2$, used in conjunction with H_2 often allow deposition of pure metals. The metallocenes that have been studied in most detail include those of Fe, Cr, Ru, Co, Mo, Ni, and Nb. However, the deposition temperatures tend to be high, often over 500°C . A patent has discussed CVD using Mn, Ti, Mg, and V cyclopentadienyls at temperatures of 500 to 800°C .²⁸⁰ Two classes of reaction pathways are found, one in which the C_5H_5^- ligand reacts to form various volatile and involatile species and one in which it reacts with hydrogen to give C_5H_6 . A problem with the use of many metallocene precursors is that the dissociation of the organic portion of the precursor on the metal surface frequently leads to significant C incorporation. For example, CVD using $\text{Cr}(\eta^6\text{-C}_6\text{H}_6)_2$ and $\text{Cr}(\text{cumene})_2$ leads to formation of Cr and Cr_3C_2 .^{77,159} Similarly, CVD using $\text{Ti}(\eta^6\text{-C}_6\text{H}_6)_2$ leads to TiC.²⁸⁰

Although CVD using $M(\eta^5\text{-C}_5\text{H}_5)_2$ has been studied extensively, detailed studies of mechanistic aspects are quite limited. In the absence of hydrogen the initial product $\text{C}_5\text{H}_5^\bullet$ can react to form dihydrofulvalene or disproportionate heterogeneously to incorporate C in the growing film. Under H_2 , the reaction of Equation 8.25 has been proposed.³¹



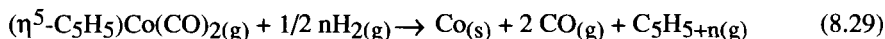
This idea is supported by results in which $\text{Fe}(\eta^5\text{-C}_5\text{H}_5)_2$ gives pure Fe at temperatures ranging from 400 to 900°C , and $\text{Co}(\eta^5\text{-C}_5\text{H}_5)_2$ deposits pure Co between 300 and 700°C . However, $\text{Ni}(\eta^5\text{-C}_5\text{H}_5)_2$ cannot be used under these conditions due to reaction with H_2 at the transport temperature.

Chemical vapor deposition using $\text{Ru}(\eta^5\text{-C}_5\text{H}_5)_2$ has been studied in some detail. In the presence of oxygen, reaction of $\text{Ru}(\eta^5\text{-C}_5\text{H}_5)_2$ leads to formation of Ru and RuO_2 (Eq. 8.26), which can be converted to RuO_4 (Eq. 8.27). This latter species can desorb at higher temperatures (near 900°C) (Eq. 8.28) to provide the pure metal.³⁵ However, this approach is necessarily a high-temperature approach which is incompatible with many substrates.



The reactivity of other unsaturated π -complexes of metals was investigated for Cr, Mo, and Co. The case of $(\eta^6\text{-C}_7\text{H}_8)\text{Cr}(\text{CO})_3$ (C_7H_8 = cycloheptatriene) was investigated in detail¹⁵⁷ and resulted in formation of Cr with high levels of C and small amounts of O. Analysis of the products showed formation of C_7H_8 (unchanged), C_6H_6 (loss of CH_2), cycloheptadiene (reaction with H_2), toluene (rearrangement), and styrene (addition of C). Labelling studies with ^{13}CO showed that the majority of the carbon in the films derived from the C_7H_8 . The cleavage of the C_7H_8 was proposed as the mechanism for carbon incorporation. This study shows the complex reaction chemistry that is possible in some cases.

The reactions of $(\eta^5\text{-C}_5\text{H}_5)\text{Co}(\text{CO})_2$ in hydrogen and helium have been studied, and deposition was observed between 300 and 600 °C. Films without hydrogen contained equal amounts of carbon and cobalt while films deposited in hydrogen had far lower levels of carbon.²⁰¹ Although the byproduct distribution was not studied, Equation 8.29 was proposed to account for the deposition of pure Co under H_2 . This equation again relies on hydrogenation of the organic ligand to form a stable, volatile reaction product.



Chemical vapor deposition of $(\eta^5\text{-C}_5\text{H}_5)\text{Cr}(\text{CO})_3\text{H}$ leads to formation of involatile products and cyclopentadiene, dicyclopentadiene, and cyclopentene suggesting that protonation and $(\eta^5\text{-C}_5\text{H}_5)\text{-Cr}$ bond homolysis also occurred.¹⁵⁸ It was suggested that the carbon was derived from the C_5H_5^- ring and not from the CO based on the results of Truex¹⁵⁷ for $(\eta^6\text{-C}_7\text{H}_8)\text{Cr}(\text{CO})_3$.

8.4.2.4 Metal Carbonyls

Metal carbonyl complexes have been studied extensively as precursors for CVD of Co, Fe, Mo, and Cr. In the cases of Co and Fe, high-purity deposits can be obtained. In contrast, most other metal carbonyls produce films that are contaminated with metal carbides, metal oxides, and graphitic carbon. The reason for this is that CO is dissociatively adsorbed on most metal surfaces and as a result C and O are incorporated into the film.

The most well-studied system is $\text{Fe}(\text{CO})_5$. Ultra-high vacuum studies have shown that reaction on the first monolayer involves dissociation of the CO to form an oxygen overlayer. After the formation of this overlayer, dissociation of the CO no longer occurs and the reaction proceeds by Equation 8.30.

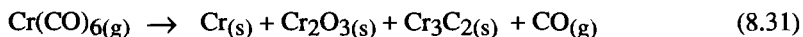


Adsorbing and dissociating $\text{Fe}(\text{CO})_5$ molecules displace the oxygen overlayer as deposition continues. Thus, the only carbon impurities in the film are found at the interface with the substrate.¹⁹⁴

Zaera has also studied the surface chemistry of iron pentacarbonyl using TPD and XPS.²⁸¹ Desorption was molecular and took place in two stages. Most of the adsorbate desorbed near 180-195 K. A small fraction of the adsorbed precursor decomposed as was shown by XPS. The fragmentation took place between 170 and 240 K and resulted in Fe and chemisorbed CO. However, high-purity films could be grown at steady state conditions because the incoming reactant displaced CO from the surface; these results agree with those above.¹⁹⁴ Similar results were obtained by Jackman and Foord²⁸² who also studied the UV photolysis of adsorbed iron pentacarbonyl under UHV conditions.

Syrkin and Kir'yanov studied the thermodynamics of iron CVD using $\text{Fe}(\text{CO})_5$.²⁸³ Analysis of phase diagrams suggested that only Fe, Fe_3C , and Fe_3O_4 can exist at temperatures between 200 and 300 °C. They concluded that small amounts of Fe_3C and Fe_3O_4 could be formed during CVD due to the reaction of Fe with CO.

Reactions of many metal carbonyls lead to formation of metal carbides due to the catalytic dissociation of CO on the metal. One example is the reaction of $\text{Cr}(\text{CO})_6$ (Eq. 8.31).⁸¹

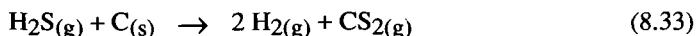


These results suggest that metal carbonyls are good choices as precursors only for those elements which do not allow surface dissociation of CO. In cases where dissociation occurs, it may be possible to remove some of the carbon and oxygen impurities by reaction with added reagents.

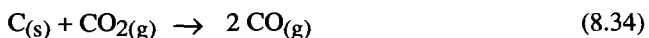
The reactions of $\text{Mo}(\text{CO})_6$ have been studied in some detail and provide an example where film purity can be increased by creating additional reaction pathways.¹⁷³ In certain temperature ranges, the dissociation of CO can be minimized to provide relatively pure Mo. Various strategies for removal of C from the surface were devised to improve the film purity over a wider temperature range. One approach is to add water which can react with carbon in various forms to form hydrogen and CO which then desorb from the surface during film growth (Eq. 8.32).



However, the addition of water can also lead to formation of MoO_3 , so this approach has limited utility. Similarly, addition of H_2S can increase film purity (Eq. 8.33), but again only under certain conditions.



Another approach is to introduce CO_2 which oxidizes C to CO (Eq. 8.34).



Again, this approach was only useful for certain conditions, especially since reaction 8.34 regenerates CO which was responsible for the impurity incorporation in the first place. An analogous approach for removing impurities from surfaces during film growth has been used for tungsten CVD from organometallic precursors (see Ch. 3).

8.4.2.5 Trifluorophosphines

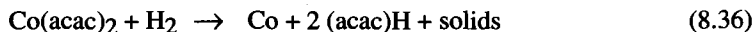
Complexes with PF₃ have been used to deposit metal films at temperatures between 200 and 300 °C. Related complexes include the phosphine complexes of Cu(I) compounds.⁸⁵⁻⁸⁷ The trifluorophosphine complexes of Cr, Mo, Fe, Ru, Co, Rh, and Ir are volatile and suitable for CVD. However, few results are available in the literature for these precursors. A likely reaction pathway for some metals is the reaction of the precursor to give the metal and adsorbed PF₃. The PF₃ can desorb from the surfaces of many metals. For example (see Ch. 5), P(CH₃)₃ cleanly desorbs from copper surfaces to give high-purity copper when precursors incorporating PR₃ ligands are utilized.

The reactions of [(PF₃)₂RhCl]₂ have been investigated in some detail.²⁰⁸ Trapping of reaction products showed formation of PF₃ as the only volatile product. No fluorine was found in the films by XPS and XRD. The films did, however, contain chlorine. X-ray photoelectron spectroscopy also revealed the presence of rhodium in both reduced (Rh⁰) and oxidized (Rh^{III}) states. Crystalline Rh was identified by X-ray powder diffraction. As a result of these observations, the authors suggested that the PF₃ ligand desorbed intact from the surface after reaction of [(PF₃)₂RhCl]₂ leading to formation of Rh and RhCl₃ according to the disproportionation reaction of Eq. (8.35).²⁰⁸



8.4.2.6 Metal β-diketonates

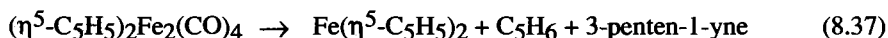
Many metal β-diketonates in the presence of hydrogen allow deposition of high-purity metal. This is similar to the situation for CVD of copper from Cu(β-diketonate)₂ species (Chs. 4 and 5). The major disadvantages are that in some cases the deposition temperature is high and the vapor pressures are relatively low leading to low deposition rates. The metals Co, Cr, Fe, Rh, and Ru have been studied in most detail; however, only a few studies of the reaction byproducts have been reported. More details of the decomposition mechanisms of β-diketonate ligands have recently been obtained from UHV studies of Cu(I) and Cu(II) β-diketonate compounds (see Chs. 4 and 5). These studies suggest that the two major reaction pathways are formation of the β-diketone via reaction with H₂ and decomposition of the β-diketonate ligand to form a variety of products. The latter is undesirable because it can lead to impurities. An example of these two reaction pathways is CVD using Co(acac)₂. No deposition was observed in the absence of hydrogen. In the presence of hydrogen, both (acac)H and other less volatile species were formed (Eq. 8.36).¹⁰⁰



These species were probably formed by the catalytic reactions of the acac ligand on the Co surface (Eq. 8.36).

8.4.2.7 Bi- and Multi-Nuclear Complexes

Several bi- and multi-nuclear complexes have been used for CVD of Mn, Fe, and Co. These complexes include metal carbonyls such as $\text{Ru}_3(\text{CO})_{12}$ and $\text{Co}_2(\text{CO})_8$ and more complex species such as $(\eta^5\text{-C}_5\text{H}_5)_2\text{Fe}_2(\text{CO})_4$ and $\text{Rh}_2(\text{Cl})_2(\text{CO})_4$. However, in only a few cases have the reaction products been examined. The reaction of $(\eta^5\text{-C}_5\text{H}_5)_2\text{Fe}_2(\text{CO})_4$ leads to formation of several products (Equation 8.37).¹⁹⁶



The 3-penten-1-yne was proposed to be derived from a ring opening reaction of the $(\text{C}_5\text{H}_5)^-$ ligand. This ligand decomposition can lead to carbon contamination as observed in other cases such as copper deposition from $(\eta^5\text{-C}_5\text{H}_5)\text{CuL}$ complexes (see Ch. 5).

8.4.2.8 Heteronuclear Complexes

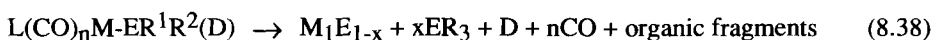
Heteronuclear complexes have been used to deposit films containing numerous metals. One of the main motivations for understanding the reaction pathways is to develop strategies to allow deposition of films with controlled stoichiometry. This requires that after adsorption and reaction of the precursor, both of the desired elements are retained in the film even if two species are formed, each containing one of the metals found in the precursor. Therefore, it is desirable to find reaction pathways that do not result in formation of volatile metal-containing intermediates or that give intermediates that, if formed, react rapidly to give pure metal. Only in a few cases has enough information been obtained to answer these questions.

The reaction of $(\text{CO})_4\text{CoGaCl}_2(\text{THF})$ in hydrogen led to formation of CoGa, CH_4 , THF, CO, acetone, and HCl.⁴⁸ The CO and acetone are presumably formed from THF decomposition on the surface or from the carbonyl. The films had 3% C at 450 °C with lower C content at lower temperatures but with correspondingly higher O content. Deposition in inert gas gave much higher carbon content.⁴⁸ The precursor stoichiometry could be retained in the film.

Films of Fe-Co and Fe-Ni deposited using $(\eta^5\text{-C}_5\text{H}_5)\text{FeCo}(\text{CO})_6$, $(\eta^5\text{-C}_5\text{H}_5)\text{-Fe}_2\text{Co}(\text{CO})_9$, $\text{HFeCo}_3(\text{CO})_{12}$, and $(\eta^5\text{-C}_5\text{H}_5)\text{FeNi}(\text{CO})_3$ contained roughly 4 to 8% C and O.^{251,254} Addition of oxygen during deposition resulted in formation of the metal oxides. The C and O contamination was presumably derived from both the $(\text{C}_5\text{H}_5)^-$ and CO ligands, although no evidence was given. Again, the same stoichiometry was found in both the precursor and film.

Reaction of $\text{H}_3\text{SiCo}(\text{CO})_4$ led to the formation of H_2 , CO , SiH_4 , and CH_4 , which suggests the stoichiometry was not preserved. The CH_4 was proposed to derive from the reaction of CO with H_2 .²⁵³ Stauff et al. studied the deposition of Mn_2Si from $\text{Mn}_2(\text{CO})_{10}(\mu\text{-SiH}_2)$.²⁵⁸ This same stoichiometry was preserved in the film. However, high levels of O and C were observed in films deposited at all temperatures from 300 to 500 °C. The source of the C was thought to be the carbonyl groups which did not fully desorb from the surface.

The reactions of $\text{L}(\text{CO})_n\text{M-ER}^1\text{R}^2(\text{D})$ (see Table 8-21) have been examined via film characterization and volatile byproduct analysis.²⁵⁹ The following reaction was proposed:



where the terms are defined in Table 8-21. In many cases, the metal ratio of the precursor was not necessarily reproduced in the films. For example, during reaction of $(\text{CO})_4\text{CoGa}[\text{CH}_2\text{Si}(\text{CH}_3)_3]_2(\text{THF})$, the formation of $\text{Ga}[\text{CH}_2\text{Si}(\text{CH}_3)_3]_3$ was observed. It was suggested that the stoichiometry could be maintained if the formation of group 13 alkyls is much slower than fragmentation to give involatile intermediates which react to form the metal. In general, complex chemistry was observed for the many systems that were studied.

8.4.3 Selectivity

The selectivity for deposition onto one type of surface in the presence of another has not been studied for the metals discussed in this chapter except in a few cases. A review by Carlsson discusses selective CVD of metals including Mo on patterned substrates.²⁸⁴ In the presence of SiO_2 , MoF_6 can provide selective deposition on Si.¹⁶⁶⁻¹⁷⁰ Selectivity is obtained because the MoF_6 cannot react with SiO_2 while Si can reduce the Mo as shown by Equation 8.39.



The selectivity of $\text{Co}(\eta^5\text{-C}_5\text{H}_5)_2$ has been studied for Si/ SiO_2 .^{31,201} Dicyclopentadienylcobalt is selective for SiO_2 and does not deposit on Si when hydrogen is present. In the absence of hydrogen, no deposition takes place on SiO_2 or Si up to 900 °C. Similarly, $\text{Fe}(\eta^5\text{-C}_5\text{H}_5)_2$ deposits on SiO_2 and not on Si when deposition is carried out in hydrogen.^{31,201} Again, no deposition was observed on either SiO_2 or Si in the absence of hydrogen. In contrast, $\text{Co}_2(\text{CO})_8$ was not selective for Si, reacted on both SiO_2 and Si, and behaved similarly in both He and H_2 .

Tantalum pentachloride is not selective for Si in the presence of SiO₂ in contrast to MoF₆ and WF₆ (see Ch. 3).¹⁵¹ However, UHV studies have shown that TaCl₅ is a good precursor for blanket deposition of Ta.¹⁵¹

In general, few studies have addressed selective CVD using the precursors considered in this chapter. It is likely, however, that many of these precursors would exhibit selectivity if reacted under appropriate conditions and that the surface modification techniques discussed in Chapters 5 and 9 would allow some tailoring of the selectivity. General principles of selective CVD are discussed in Chapter 9.

8.5 Summary and Conclusions

Chemical vapor deposition of the metals discussed in this chapter (Ti, Zr, Hf, V, Nb, Ta, Cr, Mo, Mn, Tc, Re, Fe, Ru, Os, Co, Rh, Ir, Zn, Cd, Sn, and Pb) has been studied to a much lesser extent than CVD of metals such as W, Al, Cu, Au, Ag, Pt, Pd, and Ni. However, several general statements can be made.

- The metal halides, carbonyls, and cyclopentadienyls have been studied most extensively. (Relatively few organometallic precursors have been examined.)
- The major classes of metal-organic and organometallic precursors that have been studied are carbonyls, alkenes, alkynes, allyls, cyclopentadienyls, arenes, and β -diketonates.
- For most of the metals, low-temperature CVD of high-purity metal has not yet been demonstrated. This is a particularly important issue for metals such as Ti which have applications in the microelectronics industry.
- Little is known about the reaction pathways and kinetics of CVD of the metals discussed in this chapter except for Co, Mo, Ta, Cr, and Fe.
- Other than selective Mo CVD which has been examined in detail, there have been only a few studies of the selective deposition onto one type of surface in the presence of another.
- Heteronuclear single-source precursors have only been investigated in a few cases. These precursors may provide alternative routes to more complex materials such as silicides, germanides, and alloy phases and may also allow better control of compositional homogeneity, stoichiometry, and phase purity. However, the benefits have not yet been clearly demonstrated. These precursors have the disadvantage of relatively low vapor pressure, although this problem can be overcome by using alternative precursor delivery methods (see Ch. 9).
- Hydrogen may be added to improve the purity of films produced with precursors containing halide, cyclopentadienyl, β -diketonate, allyl, alkene, and alkyne ligands.

- The addition of oxygen improves film purity in cases where the metal does not form a stable oxide. The oxygen allows oxidation of organic species to form volatile products.

Acknowledgments: The authors thank Judith Binder for her comments and assistance in preparing the manuscript. We also thank Teresa Powers, Dr. Christophe Roger, Dr. Yoshi Senzaki, Steve Drees, and Tom Corbitt for their helpful comments. In addition, we thank Professors Alfred Zinn and William Rees for their useful observations.

References

1. Diesburg, D.E., Castel, E.D. *J. Met.* **1989**, June, 23.
2. O'Brien, P., in *Inorganic Materials*, Bruce, D.W., O'Hare, D. (eds.), John Wiley & Sons, Chichester, 1992.
3. Zanella, P., Rossetto, G., Brainese, N., Ossula, F., Porchia, M., Williams, J.O. *Chem. Mater.* **1981**, 3, 225.
4. Dupuis, R.D. *Science* **1984**, 226, 623.
5. Smith, F.T.J. *Prog. Solid State Chem.* **1989**, 19, 111.
6. Stringfellow, G.B. *Organometallic Vapor-Phase Epitaxy: Theory and Practice*, Academic, New York, 1989.
7. Razeghi, M. *The MOCVD Challenge*, Higer, London, 1989.
8. Stringfellow, G.B., in *Semiconductors and Semimetals, Part A*, Tsang, W.T. (ed.), Academic, London, 1985, 22, 209.
9. Razeghi, M., in *Semiconductors and Semimetals, Part A*, Tsang, W.T. (ed.), Academic, London, 1985, 22, 299.
10. Ludowise, M.J. *J. Appl. Phys.* **1985**, 58, R31.
11. Feist, W.M., Steele, S.R., Readey, D.W., in *Science of Thin Films*, V, Hass, G., Thun, R.E. (eds.), Academic, New York, 1979, 237-322.
12. Dapkus, P.D. *J. Cryst. Growth* **1984**, 68, 345.
13. Hitchman, M.L., Jensen, K.F. (eds.), *Chemical Vapor Deposition: Principles and Applications*, Academic, New York, 1993, 677.
14. Kern, W., Ban, V.S., in *Thin Film Processes*, Vossen, J.L., Kern, W. (eds.), Academic, New York, 1978, Chapter III-2.
15. Maissel, L.I., Glang, R. (eds.), *Handbook of Thin Film Technology*, McGraw Hill, New York, 1970.
16. Sedgewick, T.O., Lydtin, H. (eds.), *Proceedings of the 7th International Conference on CVD*, ECS, Princeton, NJ, 1979.
17. Vossen, J.L., Kern, W. (eds.), *Thin Film Processes*, Academic, New York, 1978.

18. Wakefield, G.F., Blocker, Jr., J.M. (eds.), *Proceedings of the 4th International Conference on CVD*, ECS, Princeton, NJ, 1973.
19. Shaffhauser, A.C. (ed.), *Proceedings of the Conference on CVD of Refractory Metals*, AIME, 1967.
20. Pierson, H.D. *Handbook of Chemical Vapor Deposition*, Noyes, Park Ridge, NJ, 1992.
21. Jensen, K.F., in *Microelectronics Processing*, Hess, D.W., Jensen, K.F. (eds.), American Chemical Society, Washington, D.C., 1989.
22. Galasso, F.S. *Chemical Vapor Deposited Materials*, CRC, Boca Raton, FL, 1991.
23. Snow, E.H., Grove, A.S., Deal, B.E., Sah, C.T. *J. Appl. Phys.* **1965**, 36, 1664.
24. Green, M.L., Levy, R.A. *J. Metals* **1985**, June, 37, 63.
25. Murarka, S.P. Peckarar, M.C., in *Electronic Materials Science and Technology*, Academic, San Diego, 1989.
26. Wolf, S. Tauber, R.N., in *Silicon Processing for VLSI Era, 1: Process Technology*, Lattice, Sunset Beach, CA, 1986.
27. Sheward, J.A., Young, W.J. *Vacuum* **1986**, 36, 37.
28. Miyake, M., Hirooka, Y., Imoto, R., Sano, T. *Thin Solid Films* **1979**, 63, 303.
29. Miyake, M., Hirooka, Y., Imoto, R., Sano, T. *Thin Solid Films* **1981**, 79, 75.
30. Gross, M.E., Schnoes-Kranz, D., Brasen, D., Luftman, H. *J. Vac. Sci. Tech. B* **1988**, 6, 1548.
31. Dormans, G.J.M. *J. Crystal Growth* **1991**, 108, 806.
32. Motojima, S., Kuri, S., Hattori, T. *J. Less Common Metals* **1986**, 124, 193.
33. Murarka, S.P. *Silicides for Very Large Scale Integration Applications*, Academic, New York, 1983.
34. Ehrlich, D.J., Tsao, J. Y. (eds.), *Laser Microfabrication*, Academic, New York, 1989.
35. Green, M.L., Gross, M.E., Papa, L.E., Schnoes, K.J., Brasen, D. *J. Electrochem. Soc.* **1985**, 132, 2677.
36. Macrander, A.T., Long, J.A., Riggs, V.G., Bloemeke, A.F., Johnston, Jr., W.D. *Appl. Phys. Lett.* **1984**, 45, 1297.
37. Cheng, W.H., Pooladdej, J., Huang, S.Y., Buehring, K.D., Applebaum, A., Wolf, D., Renner, D., Hess, K.L., Zehr, S.W. *Appl. Phys. Lett.* **1988**, 53, 1257.
38. Klabunde, K., Li, Y.-X., Tan, B.-J. *Chem. Mater.* **1991**, 3, 30.
39. Gates, B.C., in *Catalyst Design, Progress and Perspectives*, Hegedus, L.L. (ed.), John Wiley and Sons, New York, 1987.
40. Campbell, I.M., in *Catalysis at Surfaces*, Chapman Hall, New York, 1988.
41. Gurav, A., Kodas, T., Pluym, T., Xiong, Y. *Aerosol Sci. Technol.* **1993**, 19, 411.
42. Henglein, A. *Top. Curr. Chem.* **1988**, 113, 156.
43. Marquardt, P., Nimtz, G., Muhlschlegel, B. *Solid State Communications* **1998**, 65, 539.
44. Bawendi, M.C., Steigerwald, M.L., Brus, L.E. *Ann. Rev. Phys. Chem.* **1990**, 41, 477.

45. Che, M., Bennett, C.O., in *Advances in Catalysis*, Eley, D.D., Pines, H., Weisz, P.B. (eds.), Academic, New York, 1989, 36, 55.
46. Glassl, H., Hayek, R., Kramer, R. *J. Catal.* **1981**, 68, 397.
47. Maury, F., Talin, A.A., Kaesz, H.D., Williams, R.S. *Appl Phys. Lett.* **1992**, 61, 1075.
48. Chen, Y.-J., Kaesz, H.D., Kim, Y.-K., Muller, H.-J., Williams, R.S., Xue, Z. *Appl. Phys. Lett.* **1989**, 55, 2760.
49. Ehrlich, D.J., Tsao, J.Y. *J. Vac. Sci. Technol.* **1983**, B, 1, 969.
50. Houle, F. *Appl. Phys. A* **1986**, 41, 315.
51. Bauerle, D. *Chemical Processing with Lasers*, Springer Verlag, New York, 1986.
52. Wood, J.M., Frey, F.W. *Proc. Conf. CVD of Refractory Metals*, Shaffhauser, A.C. (ed.), AIME, 1967, 205.
53. Crisler, L.R., Eggerman, W.G. *US Patent* 3 832 222, Aug. 27, **1974**.
54. Vandenbulcke, L., Vuillard, G. *J. Electrochem. Soc.* **1976**, 123, 278.
55. Pierson, H.O., Mullendore, A.W., in *Proceedings of the 7th International Conference on CVD*, Sedgewick, T.O., Lydtin, H. (eds.), ECS, Princeton, NJ, 1979, 360.
56. Van Arkel, A.E. *Metallwirtschaft* **1934**, 13, 405.
57. Cotton, F.A., Wilkinson, G., *Advanced Inorganic Chemistry*, 5th Ed., John Wiley and Sons, New York, 1988.
58. Greenwood, N.N., Earnshaw, A., *Chemistry of the Elements*, 1st Ed., Pergamon, Oxford, 1984.
59. Huheey, J.E. *Inorganic Chemistry, Principles of Structure and Reactivity*, 3rd Ed., Harper and Row, New York, 1983.
60. Schriver, D.F., Atkins, P.W., Langford, C.H. *Inorganic Chemistry*, W.H. Freeman & Co., New York, 1990.
61. Fujii, H., Kimura, M. *Bull. Chem. Soc. Jpn.* **1970**, 43, 1933.
62. Van Den Berg, J.M. *Acta Cryst.* **1962**, 15, 1051.
63. Rundle, R.E., Olson, D.H. *Inorg. Chem.* **1964**, 3, 596.
64. Wells, A.F. *Structural Inorganic Chemistry*, 5th Ed., Clarendon, Oxford, 1986.
65. Lister, M.W., Sutton, L.E. *Trans. Farad. Soc.* **1941**, 37, 406.
66. Wakefield, G.F. *J. Electrochem. Soc.* **1969**, 116, 5.
67. Hanni, W., Hintermann, H.E. *Thin Solid Films* **1977**, 40, 107.
68. Macklin, B.A., Withers, J.C., in *Proceedings of the Conference on CVD of Refractory Metals*, Shaffhauser, A.C. (ed.), AIME, 1967, 161.
69. Girolami, G.S., Gozum, J.E. *Mat. Res. Soc. Symp. Proc.* **1990**, 168, 319.
70. Collman, J.P., Hegedus, L.S., Norton, J.R., Finke, R.G. *Principles and Applications of Organotransition Metal Chemistry*, University Science Books, California, 1987.
71. Davidson, P.J., Lappert, M.F. *J. Chem. Soc., Chem. Comm.* **1973**, 317.

72. Davis, R., Kane-Maguire, L.A.P., in *Comprehensive Organometallic Chemistry*, Wilkinson, G., Stone, F.G.A., Abel, E.W. (eds.), Pergamon, Oxford, 1982, Ch. 27.2.
73. Wilke, G., Begdanovic, B., Hardt, P., Heimbach, P., Keim, W., Kroner, M., Oberkirch, W., Tanaka, K., Steinrucke, E., Walter, D., Zimmerman, H. *Angew. Chem., Int. Ed. Engl.* **1966**, 5, 151.
74. Smith, D.C., Pattillo, S.G., Elliott, N.E., Zocco, T.G., Burns, C.J., Laia, J.R., Sattelberger, A.P. *Mat. Res. Soc. Symp. Proc.* **1990**, 168, 369.
75. Kirss, R.U., Chen, J., and Hallock, R.B. *Mat. Res. Soc. Symp. Proc.* **1992**, 250, 303.
76. Gozum, J.E., Pollina, D.M., Jensen, J.A., Girolami, G.S. *J. Am. Chem. Soc.* **1988**, 110, 2688.
77. Anantha, N.G., Doo, V.Y., Seto, D.K. *J. Electrochem. Soc.* **1971**, 118, 163.
78. Braga, D., Grepioni, F., Orpen, A.G. *Organometallics* **1993**, 12, 1481.
79. Rayner, D.M., Nazran, A.S., Drouin, M., Hackett, P.A. *J. Phys. Chem.* **1986**, 90, 2882.
80. Shinn, N.D., Madaey, T.E. *J. Chem. Phys.* **1985**, 83, 5928.
81. Owen, B.B., Webber, R.T. *Met. Technol.* **1948**, 15, 230.
82. Psaro, R., Fusi, A., Ugo, R., Basset, J.M., Smith, A.K., Hugues, F. *J. Mol. Catal.* **1980** 7, 511.
83. Kruck, T. *Angew. Chem., Int. Ed. Engl.* **1967**, 6, 53.
84. Sirtl, E. *US Patent* 3 619 288, Nov. 9, **1971**.
85. Rand, M.J. *J. Electrochem. Soc.* **1975**, 122, 811.
86. Morabito, J.M., Rand, M.J. *Thin Solid Films* **1974**, 22, 293.
87. Schroder, H., Gianinoni, I., Masci, P., Kompa, K.L. *Springer Ser. Chem. Phys.* **1984**, 39, 257.
88. Doppelt, P., Ricard, L., Weigel, V. *Inorg. Chem.* **1993**, 32, 1039.
89. Moshier, R.W., Sievers, R.E., Spendlove, L.B. *US Patent* 3 356 527, Dec. 5, **1967**.
90. Sievers, R.E., Sadlowski, J.E. *Science* **1978**, 201, 217.
91. Sieck, R.F., Banks, C.V. *Analytical Chemistry* **1972**, 44, 2307.
92. Wolf, W.R., Sievers, R.E., Brown, G.H. *Inorg. Chem.* **1972**, 11, 1995.
93. Graddon, D.P. *Coord. Chem. Rev.* **1969**, 4, 1.
94. Poston, S., Reisman, A. *J. Electronic Mat.* **1989**, 18, 553.
95. Ivankovitz, J.C., Bohling, D.A., Norman, J.A.T., Roberts, D.A. *US Patent* 5 028 724, Jul. 2, **1991**.
96. Samath, S.A., Raman, N., Jeyasubramanian, K., Ramalingam, S.K. *Polyhedron* **1991**, 10, 1687.
97. Siedle, A.R., in *Comprehensive Coordination Chemistry*, Wilkinson, G., Gillard, R.D., McCleverty, J.A. (eds.), Pergamon, Oxford, 1987, Ch. 15.4.
98. Ismail, H.M. *J. Analytical and Applied Pyrolysis* **1991**, 21, 315.
99. Reichert, C., Bancroft, G.M., Westmore, J.B. *Can. J. Chem.* **1970**, 48, 1364.

100. Charles, R.G., Haverlack, P.G. *J. Inorg. Nucl. Chem.* **1969**, 31, 995.
101. Van Hemert, R.L., Spendlove, L.B., Sievers, R.E. *J. Electrochem. Soc.* **1965**, 112, 1123.
102. Etspuler, A., Suhr, H. *Appl. Phys. A* **1989**, 48, 373.
103. Etspuler, A., Suhr, H. *Appl. Phys. A* **1989**, 49, 1.
104. Flint, E.B., Messelhauser, J., Suhr, H. *Appl. Phys. A* **1991**, 53, 430.
105. Lu, J.-P., Chu, P.W., Raj, R., Gysling, H. *Thin Solid Films* **1992**, 208, 172.
106. Nardi, M., Rhubright, D., Sen, A. *Inorg. Chem.* **1990**, 29, 3065.
107. Jeffries, P.M., Girolami, G.S. *Chem. Mat.* **1989**, 1, 8.
108. McCrary, V.P., Donnelly, V.M., in *Chemical Vapor Deposition: Principles and Applications*, Hitchman, M.L., Jensen, K.F. (eds.), Academic, New York, 1993, 159.
109. Marrs, J.M. *Chem. Eng. Prog.* **1986**, Jan. 31.
110. Kodas, T.T., Comita, P. *Acc. Chem. Res.* **1990**, 23, 188.
111. Santola, T., Antson, J., Pakkala, A., Lindfors, L. *SID 80 Digest* **1980**, 108.
112. Andrews, D.A., Davey, S.T., Tubben, C.G., Wakefield, B., Davies, G.J. *Appl. Phys. Lett.* **1988**, 52, 816.
113. Haigh, J., Aylett, M., in *Laser Microfabrication*, Ehrlich, D.J., Tsao, J.Y. (eds.), Academic, New York, 1989; Aylett, M., Haigh, J., in *Laser Processing and Diagnostics*, Bauerle, D. (ed.), Springer Verlag, New York, 1984, 263.
114. Homer, H.J. *US Patent* 2 887 406, May 19, **1959**.
115. Wyetznes, C., Komarov, S., Freel, C., Jones, M., Hepp, A.F., Fury, M.A., Kaloyeros, A.E. *Fall Mat. Res. Soc. Meeting*, Paper N1.2/Y1.2, Boston, MA, 1993.
116. Charatan, R.M., Gross, M.E. *Fall Mat. Res. Soc. Meeting*, Paper W11.4, Boston, MA, 1993.
117. Boekel, C.P., Teuber, J.H., de Liefde Meijer, M.J. *J. Organomet. Chem.* **1974**, 81, 371.
118. Latyaeva, V.N., Vishinskaya, L.I., Mar'in, V.P. *Zh. Obsheh. Khim.* **1976**, 46, 628.
119. Razuvaev, G.A., Mar'in, V.P., Kosneva, C.P., Vishinskaya, L.I., Cherkasov, V.K., Druzhkov, O.N. *Dokl. Akad. Nauk. SSR* **1976**, 231, 626.
120. Boekel, C.P., Jelsma, A., Teuber, J.H., de Liefde Meijer, M.J. *J. Organomet. Chem.* **1977**, 136, 211.
121. Izquierdo, R., Lavoie, C., Meunier, M. *Mat. Res. Soc. Symp. Proc.* **1990**, 158, 141.
122. Chou, W.B., Azer, M.N., Mazumder, J. *J. Appl. Phys.* **1989**, 66, 191.
123. Campbell, I.E., Jaffee, R.I., Blocher, Jr., J.M., Gurland, J., Gonser, B.W. *J. Electrochem. Soc.* **1948**, 93, 271.
124. Morancho, R., Petit, J., Dabosi, F., Constant, G., in *Proceedings of the 7th International Conference on CVD*, Sedgwick, T.O., Lydtin, H. (eds.), ECS, Princeton, NJ, 1979, 593-603.
125. Holden, R.B., Kopelman, B. *J. Electrochem. Soc.* **1953**, 100, 120.

126. Smith, D.E., Rubiano, R.R., Healy, M.D., Springer, R.W. *Proceedings of the 12th International Conference on CVD* **1993**, 417.
127. Tamborski, C. *US Patent* 3 437 516, Apr. 8, **1969**.
128. Litton, F.B. *J. Electrochem. Soc.* **1951**, 12, 488.
129. Mazdiyasi, K.S., Dolloff, R.T., Smith, II, J.S. *J. Am. Cer. Soc.* **1969**, 52, 523.
130. Miller, K.J., Grieco, M.J., Sze, S.M. *J. Electrochem. Soc.* **1966**, 113, 902.
131. Dyagileva, L.M., Mar'in, V.P., Tsyganova, E.I., Razavaev, G.A. *J. Organomet. Chem.* **1979**, 175, 63.
132. Fillman, L.M., Tang, S.C. *Thermochimica Acta*, **1984**, 75, 71.
133. Hafner, W., Fischer, E.O. *British Patent* 976 573, Nov. 25, **1964**.
134. Korzo, V.F., Lyashchenko, G.A., Kozyrkin, B.I., Rumyantseva, V.P. *Inorg. Mat. USSR* **1971**, 7, 1649.
135. Newkirk, L.R., Valencia, F.A., Wallace, T.C. *J. Electrochem. Soc.* **1976**, 123, 425.
136. Roland, G.W., Braginski, A.I. *Advan. Cryogenic Eng.* **1977**, 22, 347.
137. Weiss, F., Madar, R., Senateur, J.P., Boursier, D., Bernard, C., Fruchart, R. *J. Crystal Growth* **1982**, 56, 423.
138. Madar, R., Weiss, F., Fruchart, R., Bernard, C. *J. Crystal Growth* **1978**, 45, 37.
139. Pike, G.E., Pierson, H.O., Mullendore, A.W., Schirber, J.E. *Appl. Polymer Symp.* **1976**, 29, 71.
140. Kurtz, S.R., Gordon, R.G. *Thin Solid Films* **1987**, 147, 167.
141. Braginski, A.I., Roland, G.W. *Appl. Phys. Lett.* **1974**, 25, 762.
142. Kehr, D.E.R. *High Temperature-High Pressures* **1978**, 10, 477.
143. Kawamura, H., Tachikawa, K. *Physics Letters* **1974**, 50A, 29.
144. Stolz, M., Hieber, K., Wieczorek, C. *Thin Solid Films* **1983**, 100, 209.
145. Hieber, K., Stolz, M., in *Proceedings of the 5th International Conference on CVD*, Blocher, Jr., J.M., Hintermann, H.E., Hall, L.H. (eds.), ECS, Princeton, NJ, 1975, 436.
146. Hieber, K. *Thin Solid Films* **1974**, 24, 157.
147. Vlakhov, E.S., Gesheva, K.A., Kovachev, V.T. *Materials Letters* **1987**, 6, 58.
148. Beguin, C., Horvath, E., Perry, A.J. *Thin Solid Films* **1977**, 46, 209.
149. Powell, C.E., Campbell, I.E., Gonser, B.W. *J. Electrochem. Soc.* **1948**, 85, 258.
150. Papke, J.A., Stevenson, R.D. *Proceedings of the Conference on CVD Refractory Metals*, Shaffhauser, A.C. (ed.), AIME, 1967, 193.
151. Ugolini, D., Kowalczyk, S.P., McFeely, F.R. *J. Appl. Phys.* **1991**, 70, 3899.
152. Spitz, J., Chevallier, J., in *Proceedings of the 5th International Conference on CVD*, Blocher, Jr., J.M., Hintermann, H.E., Hall, L.H. (eds.), ECS, Princeton, NJ, 1975, 204.
153. Lander, J.J., Germer, L.H. *Metals Technology* **1947**, 14, 1. See also: Lander, J.J., *US Patent* 2 690 980, Oct. **1954**; Lander, J.J., Germer, L.H. *AIME Tech. Publ.* 2259 **1947**; Lander, J.J., Germer, L.H. *Metal Ind. London* **1947**, 71, 459; Lander, J.J., Germer, L.H. *Metal Ind. London* **1947**, 71, 487; Lander, J.J., Germer, L.H.,

- Metals Technol.* **1947**, 14, TP2259; Lander, J.J., Germer, L.H. *Trans. Met. Soc. AIME* **1948**, 175, 648.
154. Hoar, T.P., Croom, E.A.G. *J. Iron Steel Inst. (London)* **1951**, 169, 101.
 155. Mazille, H.M.J. *Thin Solid Films* **1980**, 65, 67.
 156. Mazille, H., Andisio, S., Monnier, G. *Corros. Trait. Prot. Finition* **1968**, 16, 346.
 157. Truex, T.J., Saillant, R.B., Monroe, F.M. *J. Electrochem. Soc.* **1975**, 122, 1396.
 158. Rutherford, N.M., Larson, C.E., Jackson, R.L. *Mat. Res. Soc. Symp. Proc.* **1989**, 131, 439.
 159. Nash, B.D., Campbell, T.T., Block, F.E., US Bureau of Mines Report Investigation 7112, Washington, DC, 1968
 160. Tomono, R., Yagi, E., Togashi, Y. *J. Metal Finishing Soc. Jpn.* **1965**, 16, 210.
 161. Maury, F., Ossola, F., Schuster, F., *Surface and Coatings Technology* **1992**, 54, 204.
 162. Maury, F., Ossola, F. *Thin Solid Films* **1992**, 219, 24.
 163. Maury, F., Ossola, F. *Thin Solid Films* **1992**, 207, 82.
 164. Childs, W.J., Cline, J.E., Kisner, W.M., Wulf, J. *Trans. ASM* **1951**, 43, 105.
 165. Carver, G.E. *Thin Solid Films* **1979**, 63, 169.
 166. Sugano, T., Chou, H., Yoshida, M., Nishi, T. *Jpn. J. Appl. Phys.* **1968**, 7, 1028.
 167. Yasuda, K., Murota, J. *Jpn. J. Appl. Phys.* **1983**, 22, L615.
 168. Casey, J.J., Verderber, R.R., Garnache, R.R. *J. Electrochem. Soc.* **1967**, 114, 201.
 169. Simeonov, S.S., Kafedjiiska, E.I., Guerassimov, A.L. *Thin Solid Films* **1984**, 115, 291.
 170. El-Hoshy, A.H. *J. Electrochem. Soc.* **1971**, 118, 2028.
 171. Lifshitz, N., Williams, D.S., Capio, C.D., Brown, J.M. *J. Electrochem. Soc.* **1987**, 134, 2061.
 172. Ianno, N.J., Plaster, J.A. *Thin Solid Films* **1987**, 147, 193.
 173. Kaplan, L.H., d'Heurle, F.M. *J. Electrochem. Soc.* **1970**, 117, 693.
 174. DeRosa, A.I., Dove, D.B., Loehman, R.E. *J. Vac. Sci. Technol.* **1974**, 14, 455.
 175. Kirss, R.U., Brown, D.W., Higa, K.T., Gedridge, R.W. *Organometallics* **1991**, 10, 3589.
 176. Harsta, A., Carlsson, J.-O. *Thin Solid Films* **1990**, 185, 235.
 177. Al-Hilli, A.A., Evans, B.L. *J. Crystal Growth* **1972**, 15, 93.
 178. Hofmann, W.K. *J. Mat. Sci.* **1988**, 23, 3981.
 179. Wlodek, S.T.Y., Wulff, J. *J. Electrochem. Soc.* **1960**, 107, 565.
 180. Kano, G., Inoue, M., Matsuno, J., Takayanagi, S. *J. Appl. Phys.* **1966**, 37, 2985.
 181. Freedman, A., Bersohn, R. *J. Am. Chem. Soc.* **1978**, 100, 4116.
 182. Seder, T.A., Church, S.P., Weitz, E. *J. Am. Chem. Soc.* **1986**, 108, 7518.
 183. Bray, R.G., Seidler, P.F., Gethner, J.S., Woodin, R.L. *J. Am. Chem. Soc.* **1986**, 108, 1312.
 184. Holman, W.R., Huegel, F.J. *Proceedings of the Conference on CVD of Refractory Metals, Alloys and Compounds*, Schaffhauser, A.C. (ed.), Am. Nuc. Soc., Hinsdale, IL, 1967, 427.

185. Holman, W.R., Huegel, F.J. *J. Vac. Sci. Technol.* **1974**, *11*, 701.
186. Federer, J.I., Spruiell J.E. *Proceedings of the Conference on CVD of Refractory Metals, Alloys, and Compounds*, Schaffhauser, A.C. (ed.), Am. Nuc. Soc., Hinsdale, IL, 1967, 443.
187. Donaldson, J.G., Hoertel, F.W., Cochran, A.A. *J. Less-Common Metals* **1968**, *14*, 93.
188. Kaesz, H.D., Williams, R.S., Hicks, R.F., Chen, Y.-J., Xue, Z., Xu, D., Shuh, D.K., Thridandam, H. *Mat. Res. Soc. Symp. Proc.* **1989**, *131*, 395.
189. Syrkin, V.F., Prokhorov, V.N., Romanov, L.N. *J. Appl. Chem. USSR* **1976**, *49*, 1330.
190. Anderson, H.J., Brenner, A. *Proceedings of the 2nd International Conference on CVD*, Blocher, Jr., J.M., Withers, J.C. (eds.), ECS, New York, 1971, 355.
191. Aylett, B.J., Earwaker, L.G., Keen, J.M. *Mat. Res. Soc. Symp. Proc.* **1993**, *282*, 281.
192. Macheteau, Y. *J. Crystal Growth* **1975**, *28*, 93.
193. Stauf, G.T., Driscoll, D.C., Dowben, P.A., Barfuss, S., Grade, M. *Thin Solid Films* **1987**, *153*, 421.
194. Kaplan, R., Bottka, N. *Appl. Phys. Lett.* **1982**, *41*, 972.
195. Walsh, P.J., Bottka, N. *J. Electrochem Soc.* **1984**, *131*, 444.
196. Feurer, E., Larhafi, M., Morencho, R., Calson, R. *Thin Solid Films* **1988**, *167*, 195.
197. Trent, D.E., Paris, B., Krause, H.H. *Inorg. Chem.* **1964**, *3*, 1057.
198. Senzaki, Y., McCormick, F.B., Gladfelter, W.L. *Chem. Mater.* **1992**, *4*, 747.
199. Crosby, J.N., Hanley, R.S. *US Patent* 4 250 210, Jan. 10, **1981**.
200. Lehwald, S., Wagner, H. *Thin Solid Films* **1974**, *21*, S23.
201. Dormans, G.J.M., Meekes, G.J.B.M., Staring, E.G.J. *J. Crystal Growth* **1991**, *114*, 364.
202. Jablonowski, E.J. *Cobalt* **1962**, *14*, 28.
203. West, G.A. Beeson, K.W. *Appl. Phys. Lett.* **1988**, *53*, 740.
204. West, G.A. Beeson, K.W. *Mat. Res. Soc. Symp. Proc.* **1989**, *131*, 389.
205. Motojima, S., Ihama, Y. *J. Crystal Growth* **1986**, *76*, 373.
206. Motojima, S., Kuri, S., Hattori, T. *J. Less-Common Metals* **1986**, *124*, 193.
207. Cohan, J.S., Yuan, H., Williams, R.S., Zink, J.I. *Appl. Phys. Lett.* **1992**, *60*, 1402.
208. Doppelt, P., Weigel, V., Guinot, P. *Mater. Sci. Eng.* **1993**, *817*, 143.
209. Chang, T., Bernasek, S.L., Schwartz, J. *Langmuir* **1991**, *7*, 1413.
210. Smith, P.B., Bernasch, S.L., Schwartz, J., McNulty, G.S. *J. Am. Chem. Soc.* **1986**, *108*, 5654.
211. Smith, P.B., Ph.D. Thesis, Princeton, University, 1986.
212. Baum, T.H., Larson, C.E., Reynolds, S.K. *US Patent* 5 096 737, Mar. 17, **1992**.
213. Kumar, R., Puddephatt, R.J. *Can. J. Chem.* **1991**, *69*, 108.
214. Messelhauser, J., Flint, E.B., Suhr, H. *Adv. Mater.* **1992**, *4*, 347.

215. Hoke, J.B., Stern, E.W., Murray, H.H. *J. Mater. Chem.* **1991**, 1, 551.
216. Harding, J.T., Fry, V.R., Tuffias, R.H., Kaplan, R.B. *AFRPL TR-86-099*, **1987**
217. Kordesch, K.V. *US Patent* 3 364 074, Jan. 16, **1968**
218. Blanconnier, P., Cerclet, M., Heroc, P., Jean-Louis A.M. *Thin Solid Films* **1978**, 55, 375.
219. Chichibu, S., Kushibe, M., Eguchi, K., Funemizu, M., Ohba, Y. *J. Appl. Phys.* **1990**, 68, 859.
220. Kato, Y., Kurita, S., Suda, T. *J. Appl. Phys.* **1987**, 62, 3733.
221. Meehan, K., Dabkowski, F.P., Gavrilovic, P., Williams, J.E., Stutius, W., Hsieh, K.C., Holonyak, Jr., N. *Appl. Phys. Lett.* **1989**, 54, 2136.
222. Hirabayashi, K., Kogure, O. *Jpn. J. Appl. Phys.* **1985**, 24, 1484.
223. Nishikawa, Y., Sugawara, H., Ishikawa, M., Kokubun, Y. *J. Crystal Growth* **1991**, 108, 728.
224. Blaauw, C., Hobbs, L. *Appl. Phys. Lett.* **1991**, 59, 674.
225. Nelson, A.W., Westbrook L.D. *J. Appl. Phys.* **1984**, 55, 3103.
226. Sidorov, Y.G., Vasil'eva, L.F., Sabinina, I.V., Dvoretzky, S.A., Sidorova, A.V. *J. Electrochem. Soc.* **1976**, 123, 698.
227. Nishikawa, Y., Tsuburai, Y., Nozaki, C., Ohba, Y., Kokubun, Y., Kinoshita, H. *Appl. Phys. Lett.* **1988**, 53, 2182.
228. Rueter, M.A., Vohs, J.M. *Mat. Res. Soc. Symp. Proc.* **1991**, 204, 403.
229. Irvine, S.J.C., Mullin, J.B., Giess, J., Gough, J.S., Royle, A., Crimes, G. *J. Crystal Growth* **1988**, 93, 732.
230. Blaauw, C., Emmerstorfer, B., Springthorpe, A.J. *J. Crystal Growth* **1987**, 84, 431.
231. Andosio, S. *J. Electrochem. Soc.* **1980**, 127, 2299.
232. Braginski, A.I., Roland, G.W., Daniel, M.R. *Appl. Polymer Symp.* **1976**, 29, 93.
233. Braichotte, D., van den Bergh, H. *Springer Ser. Chem. Phys.* **1984**, 39, 183.
234. Mingxin, Q., Monot, R., van den Bergh, H. *Scientia Sinica A* **1984**, 27, 531.
235. Hanak, J.J., Strater, K., Cullen, G.W. *RCA Rev.* **1964**, 25, 342.
236. Suhr, H., Etspuler, A., Feurer, E., Oehr, C. *Plasma Chemistry and Plasma Processing* **1988**, 8, 9.
237. Yannopoulos, I.N. *J. Less-Common Metals* **1979**, 63, 111.
238. Kane, J., Schweizer, H.P., Kern, W. *Thin Solid Films* **1975**, 29, 155.
239. Chang, C.Y., Lee, M.K., Su, Y.K., Hsu, W.C. *J. Appl. Phys.* **1983**, 54, 5464.
240. Kowalczyk, S.P., Miller, D.L. *J. Vac. Sci. Technol.* **1985**, B, 3, 1534.
241. Woolley, J.C., Williams, E.W., Gagnon, R. *J. Electrochem. Soc.* **1965**, 112, 1112.
242. Price, S.J.W., Trotman-Dickenson, A.F. *Trans. Farad. Soc.* **1958**, 54, 1630.
243. Sadhir, R.K., Saunders, H.E. *J. Vac. Sci. Technol.* **1985**, A 3, 2093.
244. Homer, H.J., Cummins, O. *US Patent*, 2 916 400, Dec. 8, **1959**.
245. Gonser, B.W., Slowter, E.E. *Tech. Pub. Int. Tin, R & D Devel. Council*, New York, 1938.
246. Rigby, L.J. *Trans. Faraday Soc.* **1969**, 65, 2421.

247. Chiu, M.S., Shen, K.P., Ku, Y.K. *Appl. Phys. B* **1985**, 37, 63.
248. Zhang, J.M., Marcy, H.O., Tonge, L.M., Wessels, B.W., Marks, T.J., Kannewurf, C.R. *Appl. Phys. Lett.* **1989**, 55, 1906.
249. Nakai, T., Tabuchi, T., Sawado, Y., Kobayashi, I., Sugimori, Y. *Jpn. J. Appl. Phys.* **1992**, 32, 2992.
250. Jones, R.A., Cowley, A.H., Ekerdt, J.G. *Mat. Res. Soc. Symp. Proc.* **1991**, 204, 73.
251. Liu, D.K., Lai, A.L., Chin, R.J. *Mater. Lett.* **1991**, 10, 318.
252. Aylett, B.J., Tannahill, A.A. *Vacuum* **1985**, 35, 435.
253. Aylett, B.J., Colquhoun, H.J. *J. Chem. Soc., Dalton Trans.* **1977**, 2058.
254. Czekaj, C.L., Geoffroy, G.L. *Inorg Chem.* **1988**, 27, 8.
255. Kaesz, H.D., Williams, R.S., Hicks, R.F., Zink, J.I., Chen, Y.-J., Muller, H.-J., Xue, Z., Xu, D., Shuh, D.K., Kim, Y.K. *New J. Chem.* **1990**, 14, 527.
256. Hampden-Smith, M.J., Garvey, J.G., manuscript in preparation.
257. Stauf, G.T., LaGraffe, D., Dowben, P.A., Emrich, K., Barfuss, S., Hirschwald, W., Bong, N.M. *Z. Naturforsch.* **1988**, 43a, 758.
258. Stauf, G.T., Dowben, P.A., Boag, N.M., DeLaGarza, L.M., Dowben, S.L. *Thin Solid Films* **1988**, 156, 327.
259. Fischer, R.A. *Mat. Res. Soc. Symp. Proc.* **1993**, 282, 267.
260. Maury, F., Brandt, L., Kaesz, H.D. *J. Organomet. Chem.* **1993**, 449, 159.
261. Maury, F., Talin, A.A., Kaesz, H.D., Williams, R.S. *Chem. Mater.* **1993**, 5, 84.
262. Dowben, P.A., Spencer, J.T., Stauf, G.T. *Mat. Sci. Eng. B* **1989**, 2, 297.
263. Thompson, N.R., in *Comprehensive Inorganic Chemistry*, Bailar, J.C., Emeleus, H.J., Nyholm, R., Trotman-Dickenson, A.F. (eds.), Pergamon, Oxford, 1973, Ch. 28.
264. Chow, T.P., Steckl, A.J., in *VLSI Electronics: Microstructure Science*, Academic, New York, 1985 9.
265. Shaw, J.M., Amick, J.A. *RCA Review* **1970**, 306.
266. Reiferberg, G.H., Conoidine, W.J. *J. Am. Chem. Soc.* **1969**, 91, 2401.
267. Kettle, S.F.A. *J. Chem. Soc.* **1961**, 2569.
268. Moorehouse, R.L., Christiansen, J.J., Gordy, W. *J. Chem. Phys.* **1966**, 45, 1751.
269. Tamaru, K. *J. Am. Chem. Soc.* **1956**, 60, 610.
270. Shin, H.K., Hampden-Smith, M.J., Kudas, T.T. unpublished results.
271. Del Franco, G.J., Remich, P., Dillard, C.R. *J. Organomet. Chem.* **1965**, 4, 57.
272. Duffy, R., Feeney, J., Holliday, A.K. *J. Chem. Soc.* **1962**, 1144.
273. Amberger, E. *Angew. Chem.* **1960**, 72, 494.
274. Beeker, W.E., Cook, S.E. *J. Amer. Chem. Soc.* **1960**, 82, 6264.
275. Irvine, S.J.C., Hill, H., Dosser, O.D., Hails, J.E., Mullin, J.B., Shenaii-Khatkhate, D.V., Cole-Hamilton, D. *Mat. Lett.* **1988**, 7, 25.
276. Davidson, P.J., Lappert, M.F., Pearch, R. *Chem. Rev.* **1976**, 76, 219.
277. Xue, Z., Caulton, K.G., Chisholm, M.H. *Chem. Mater.* **1991**, 3, 384.
278. Duan, Z., Hampden-Smith, M.J. *Organomet. Chem.* **1993**, 449, 173.

- 279. Patnaik, S., Jensen, K.F., Cripis, K.P. *J. Cryst. Growth* **1991**, 197, 390.
- 280. Buloff, J.J. *US Patent* 2 898 235, Aug. 4, **1959**.
- 281. Zaera, F. *J. Vac. Sci. Technol* **1989**, A, 7, 640.
- 282. Jackman, R.B., Foord, J.S. *Surface Science* **1989**, 209, 151.
- 283. Syrkin, V.G., Kir'yanov, Y.G. *J. Appl. Chem. USSR* **1970**, 43, 1068.
- 284. Carlsson, J.-O. *Solid State and Materials Sciences* **1990**, 16, 161.

This Page Intentionally Left Blank

Chapter 9

Overview of Metal CVD

Toivo T. Kodas^a
Mark J. Hampden-Smith^b

**Departments of ^aChemical and Nuclear
Engineering, and ^bChemistry
University of New Mexico
Albuquerque, NM 87131**

Abstract

Chapters 1 through 8 discuss chemical vapor deposition (CVD) of metals using a wide variety of precursors, reactant delivery systems, reactors, and deposition conditions. This chapter brings together the material from previous chapters and summarizes the results. First, the types of precursors used for CVD are categorized, and precursor selection for deposition of a given metal is discussed. In addition, general strategies for achieving selective deposition are summarized. Reactant delivery systems and the best approaches for given sets of precursor properties are presented. The types of reactors and operating conditions that have been used for metal CVD are discussed to provide the perspective needed to interpret results from the literature. The emphasis is on boundary layers, feed-rate-limited deposition, surface-reaction-limited deposition, diffusion-limited deposition, the pressure and temperature dependencies of the deposition rate, and gas-phase particle formation.

Contents

9.1	Introduction	431
9.2	Classification of Precursors	431
9.3	Blanket Deposition: Reaction Pathways	437
9.3.1	Individual Precursors	437
9.3.2	Single-Source Precursors	439
9.4	Selective Deposition	441
9.4.1	Formation of Patterned Films	441
9.4.2	Summary of Selective CVD Methods	446
9.4.2.1	Intrinsic Difference in Reaction Rates	446
9.4.2.2	Sacrificial Solid-State Co-Reactant	447
9.4.2.3	Activation of Growth Surface	449
9.4.2.4	Photochemical Activation of Growth Surface	452
9.4.2.5	Passivation of Non-Growth Surface	453
9.4.2.6	Gettering or Removal of Nucleating Species from Non-Growth Surface	456
9.4.2.7	Physical Nucleation Barrier	456
9.5	Overall Reactor Behavior	458
9.6	Precursor Delivery	460
9.6.1	Bubblers and Direct Vaporization of Precursors	460
9.6.2	Liquid Delivery	461
9.6.3	Aerosol Delivery	463
9.7	Reactor Types: Hot-Wall and Cold-Wall	468
9.8	Boundary Layers; Feed-Rate-, Surface-Reaction-, and Diffusion-Limited Operation; and Temperature and Pressure Dependencies of Rate	469
9.8.1	Boundary Layers of Velocity, Temperature, and Reactant Concentration	470
9.8.2	Feed-Rate-, Surface-Reaction-, and Diffusion-Limited Deposition	475
9.8.2.1	Feed-Rate-Limited CVD	477
9.8.2.2	Diffusion- and Surface-Reaction-Limited CVD	478
9.8.3	Pressure and Temperature Dependencies of Rate	480
9.8.3.1	Reactant Partial Pressure Dependence of Rate	480
9.8.3.2	Temperature Dependence of Rate	481
9.9	Homogeneous Gas-Phase Reactions and Particle Formation	484
9.9.1	Particle Formation During CVD	484
9.9.2	Simultaneous Particle Deposition and CVD	486
9.10	Conclusions and Future Directions	489
	Acknowledgments	490
	References	490

9.1 Introduction

In this chapter, we bring together various topics discussed in previous chapters and in the literature to derive insight into general strategies for chemical vapor deposition (CVD) of metals. Emphasis is placed on the choice of precursor and precursor delivery system, reactor design and operating conditions, and interpretation of data. In addition, an overview of methods to achieve selective deposition is presented.

The first major issue that arises when depositing metals is the choice of precursor. For a given metal, a wide variety of precursors can be used for either blanket or selective CVD. When several precursors are commercially available, we provide general guidelines for choosing the best precursor to obtain blanket deposition of high-purity films and to control selectivity. In cases where existing precursors are inadequate and new ones must be developed, we provide a resource to determine which precursors deposit a given metal and provide guidelines for which ligands to choose.

Once a precursor has been selected, a method for delivering the precursor to the reactor must be chosen, a choice strongly influenced by precursor characteristics. The sophistication of reactant delivery systems varies from simple bubblers to expensive and complex liquid-source delivery systems. We categorize these delivery systems and provide useful guidelines for choosing a particular approach. Given a precursor delivery system, the reactor configuration and operating conditions must be appropriately chosen. We also discuss the types of reactors and operating conditions that have been used for metal CVD. Once a CVD system is operating, a wide variety of physical and chemical phenomena occur which can lead to complex behavior. We identify the overall features that cause specific behavior.

9.2 Classification of Precursors

All the precursors discussed in this book are classified in Tables 9-1 and 9-2 by the identity of the central metal atom and the type of the supporting ligands. The physical and chemical requirements of precursors are found in Chapter 1, and the attributes of various ligands are presented in Chapter 8. The reader is referred to standard references for details of structural inorganic chemistry,¹ metal-organic, and organometallic chemistry.²⁻⁵

The factors which affect the choice of a particular source molecule for CVD of a specific metal are complex and depend on the application being considered. High-purity, dense metal films with smooth surfaces deposited at relatively low temperatures

Table 9-1 Precursors Used for CVD of Metals Listed by Element (in order by chapter).

Element	Derivative	Element	Derivative
Al	AlMe ₃ , AlEt ₃ , Al(<i>i</i> -Bu) ₃ , AlEt ₂ Cl, AlMe ₂ H, AlH ₃ •NMe ₃ , AlH ₃ •NEt ₃ , AlH ₃ •NMe ₂ Et, Al(BH ₃) ₃ •NMe ₃		(<i>hfac</i>)Cu(VTMS), (<i>t</i> -BuO)Cu(PMe ₃), (η^5 -C ₅ H ₅)Cu(CN- <i>t</i> -Bu), [Cu(O- <i>t</i> -Bu)] ₄ ,
W	WF ₆ , WCl ₆ , WBr ₆ , W(PF ₃) ₆ , W(CO) ₆ , W(η^6 -C ₆ H ₆) ₂ , W(η^4 -C ₄ H ₆) ₃ , W(η^3 -allyl) ₄ , W(C ₄ H ₆ O) ₃ , W(η^5 -C ₅ H ₅)(CO) ₃ CH ₃ , W(η^5 -C ₅ H ₅)(CO) ₃ H, (η^5 -C ₅ H ₅) ₂ WH ₂ , (η^5 -C ₅ H ₄ CH ₃) ₂ WH ₂ , (1,5-COD)W(CO) ₄ , (η^6 -C ₇ H ₈)W(CO) ₃		Cu(O- <i>t</i> -Bu)(OR _F), where R _F = C(CF ₃) ₃ , OCH(CF ₃) ₂ , OC(CH ₃) ₂ (CF ₃), [Cu(OSiPh ₃)] ₄ , [Cu(OSiPh ₃)(PMe ₂ Ph)] ₂
Cu	Cu(<i>tfac</i>), Cu(<i>acac</i>) ₂ , Cu(<i>dpm</i>) ₂ , Cu(<i>ppm</i>) ₂ , Cu(<i>fod</i>) ₂ , Cu(<i>acim</i>) ₂ , Cu(<i>acen</i>), Cu(<i>nona-F</i>) ₂ , (β -diketonate)CuL, where L=PMe ₃ , PEt ₃ , COD, BTMSA, TMSP, 2-butyne, (<i>hfac</i> Cu) ₂ cyclooctatetraene, (<i>hfac</i>)Cu(1,3-butadiene), (η^5 -C ₅ H ₅)Cu(PR ₃) where R = Me, Et, Bu, OMe, OEt, (<i>hfac</i>)Cu(CO), (<i>hfac</i>)Cu(alkyne), where alkyne = 2-butyne, 2-pentyne, 4,4-dimethyl-2-pentyne, 2-hexyne, 4-methyl-2-hexyne, 3-hexyne, 2-heptyne, 3-heptyne, 6-methyl-3-heptyne, 4-octyne, TMS-acetylene, TMS-propyne, bis-TMS-acetylene, TF-TMS-propyne,	Au	Me ₂ Au(<i>hfac</i>), Me ₂ Au(<i>tfac</i>), Me ₂ Au(<i>acac</i>), MeAuPMe ₃ , EtAuPMe ₃ , Me ₃ AuPMe ₃ , CF ₃ AuPMe ₃ , (CF ₃) ₃ AuPMe ₃ , [(CF ₃) ₂ Au(OSiMe ₃)] ₂ , MeAuCNMe
		Ag	Ag(trifluoroacetate), Ag(acetate), Ag(neodecanoate), Ag(C ₄ F ₇), Ag(<i>acac</i>), (alkene)Ag(<i>acac</i>), (η^5 -C ₅ H ₅)Ag(PR ₃)
		Pt	Pt(CO) ₂ Cl ₂ , Pt(<i>acac</i>) ₂ , Pt(PF ₃) ₄ , PtMe ₂ (MeNC) ₂ , (1,5-COD)PtMe ₂ , (1,5-COD)PtMe(η^1 -C ₅ H ₅), (1,5-COD)PtMeCl, (η^5 -C ₅ H ₅)PtMe(CO), (η^5 -C ₅ H ₅)Pt(allyl), (<i>acac</i>)PtMe ₃ , (C ₅ H ₅)PtMe ₃ , (C ₅ H ₄ Me)PtMe ₃ , Pt(<i>hfac</i>) ₂
		Pd	Pd(allyl) ₂ , Pd(Meallyl) ₂ , (η^5 -C ₅ H ₅)Pd(allyl)
		Ni	Ni(CO) ₄ , Ni(η^5 -C ₅ H ₅) ₂ , Ni(η^5 -C ₅ H ₄ Me) ₂
		Ti	TiI ₄ , TiBr ₄ , (η^5 -C ₅ H ₅) ₂ TiCl ₂ , "(η^5 -C ₅ H ₅) ₂ Ti",

Table 9-1 (continued)

Element	Derivative	Element	Derivative
	$(\eta^7\text{-C}_7\text{H}_7)\text{Ti}(\eta^5\text{-C}_5\text{H}_5)$		$\text{CF}_3\text{Co}(\text{CO})_4$, $\text{Co}(\text{acac})_2$,
Zr	ZrI_4 , ZrBr_4 , $\text{Zr}(\text{CH}_2\text{-}i\text{-Bu})_4$		$\text{Co}(\eta^5\text{-C}_5\text{H}_5)_2$,
Hf	HfI_4		$(\eta^5\text{-C}_5\text{H}_5)\text{Co}(\text{CO})_2$
V	VI_2 , VCl_4 , $(\eta^5\text{-C}_5\text{H}_5)\text{V}(\text{CO})_4$	Rh	RhCl_3 , $[(\text{PF}_3)_2\text{RhCl}]_2$,
Nb	NbCl_5 , NbBr_5		$\text{Rh}(\eta^3\text{-allyl})_3$, $(\text{acac})\text{Rh}(\text{CO})_2$,
Ta	TaCl_5 , TaF_5 , $\text{Ta}(\text{CO})_5$		$(\eta^5\text{-C}_5\text{H}_5)\text{Rh}(\text{C}_2\text{H}_4)_2$, $\text{Rh}(\text{tfac})_3$
Cr	CrF_2 , CrCl_2 , $\text{Cr}(\text{CO})_6$,	Ir	IrF_6 , IrCl_3 , $\text{Ir}(\text{allyl})_3$,
	$[(\eta^5\text{-C}_5\text{H}_5)\text{Cr}(\text{CO})_3]_2$,		$(\text{acac})\text{Ir}(1,5\text{-COD})$,
	$(\eta^7\text{-C}_7\text{H}_7)\text{Cr}(\text{CO})_2$,		$[(\text{MeO})\text{Ir}(1,5\text{-COD})]_2$,
	$\text{Cr}(\eta^6\text{-C}_6\text{H}_6)_2$,		$\text{Ir}(\text{acac})_3$, IrCl_4 , IrBr_3 ,
	$(\eta^5\text{-C}_5\text{H}_5)\text{Cr}(\text{CO})_3\text{H}$,		$(\eta^5\text{-MeC}_5\text{H}_4)\text{Ir}(1,5\text{-COD})$,
	$\text{Cr}(\text{N-}i\text{-Pr})_2$, $\text{Cr}(\text{CH}_2\text{CMe}_3)_4$,		$(\eta^5\text{-C}_5\text{H}_5)\text{Ir}(1,5\text{-COD})$,
	$\text{Cr}(\eta^6\text{-C}_6\text{H}_5\text{-}i\text{-Pr})_2$, $\text{Cr}(\text{cumene})_2$		$[(1,5\text{-COD})\text{Ir}(\text{OAc})]_2$
Mo	MoF_5 , MoCl_5 , $\text{Mo}(\text{CO})_6$,	Zn	ZnMe_2 , ZnEt_2
	$[(\eta^5\text{-C}_5\text{H}_5)\text{Mo}(\text{CO})_3]_2$,	Cd	CdMe_2
	$(\eta^6\text{-Me}_3\text{C}_6\text{H}_3)\text{Mo}(\text{CO})_3$,	Sn	SnCl_4 , SnCl_2 , SnMe_4 , SnEt_4 ,
	$(\eta^6\text{-C}_6\text{H}_6)\text{Mo}(\text{CO})_3$,		$\text{Sn}(-n\text{-Bu})_4$, $\text{Sn}(-n\text{-Bu})_2\text{Cl}_2$
	$\text{Mo}(\eta^3\text{-allyl})_4$	Pb	PbEt_4 , PbPh_4
Mn	$\text{Mn}_2(\text{CO})_{10}$	Mn/Ge	$(\text{CH}_2\text{CR}=\text{CRCH}_2)$
Re	ReF_6 , ReCl_5 , $\text{Re}_2(\text{CO})_{10}$,		$\text{Ge}[\text{Mn}(\text{CO})_5]_2$
	$\text{HRe}(\text{CO})_5$, ReOCl_5 , ReOCl_4	Mn/Si	$\text{H}_3\text{SiMn}(\text{CO})_5$, $[\text{Mn}(\text{CO})_5]_2\text{SiH}_2$
Fe	FeF_3 , $\text{Fe}(\text{CO})_5$,	Fe/Si	$(\text{H}_3\text{Si})_2\text{Fe}(\text{CO})_4$
	$[(\eta^5\text{-C}_5\text{H}_5)\text{Fe}(\text{CO})_2]_2$,	Fe/Co	$(\eta^5\text{-C}_5\text{H}_5)\text{FeCo}(\text{CO})_6$,
	$\text{Fe}(\eta^5\text{-C}_5\text{H}_5)_2$, $\text{Fe}_2(\eta^5\text{-C}_5\text{H}_5)_2\text{CO}_4$		$\text{HFeCo}_3(\text{CO})_{12}$,
			$(\eta^5\text{-C}_5\text{H}_5)\text{FeCo}(\text{CO})_6$,
Ru	$\text{Ru}_3(\text{CO})_{12}$, $\text{Ru}(\text{hfb})(\text{CO})_4$,		$(\eta^5\text{-C}_5\text{H}_5)\text{FeCo}(\text{CO})_9$
	$\text{Ru}(\text{C}_5\text{H}_5)_2$, $\text{Ru}(\text{acac})_2$	FeNi	$(\eta^5\text{-C}_5\text{H}_5)\text{FeNi}(\text{CO})_3$
Os	OsCl_4	CoSi	$\text{H}_3\text{SiCo}(\text{CO})_4$
Co	CoCl_2 , $\text{Co}_2(\text{CO})_8$, $\text{Co}_4(\text{CO})_{12}$,	GoGa	$(\text{CO})_4\text{CoGaCl}_2(\text{THF})$
	$\text{Co}(\text{CO})_3(\text{NO})$, $\text{HCo}(\text{CO})_4$,		

Table 9-2 Precursors Used for CVD of Metals Listed by Ligand.

Metal	Derivative
Inorganic Precursors	
Metal Halides	TiI ₄ , TiBr ₄ , ZrI ₄ , ZrBr ₄ , HfI ₄ , VI ₂ , VCl ₄ , NbCl ₅ , NbBr ₅ , TaCl ₅ , TaF ₅ , CrF ₂ , CrCl ₂ , MoF ₅ , MoCl ₅ , WF ₆ , WCl ₆ , WBr ₆ , ReF ₆ , ReCl ₅ , FeF ₃ , OsCl ₄ , CoCl ₂ , RhCl ₃ , [(PF ₃) ₂ RhCl] ₂ , IrCl ₄ , IrB ₃ , IrF ₆ , IrCl ₃ , SnCl ₄ , SnCl ₂
Metal Oxyhalides	ReOCl ₅ , ReOCl ₄
Metal-organic Precursors	
Metal β -Diketonates	Ru(acac) ₂ , Co(acac) ₂ , Rh(tfac) ₃ , (acac)Rh(CO) ₂ , (acac)Rh(CO) ₂ , Ir(acac) ₃ , (acac)Ir(1,5-COD), Pt(acac) ₂ , Pt(hfac) ₂ , (acac)PtMe ₃ , Cu(tfac), Cu(acac) ₂ , Cu(dpm) ₂ , Cu(fod) ₂ , Cu(acim) ₂ , Cu(acen), Cu(ppm) ₂ , (hfacCu) ₂ cyclooctatetraene, Ag(acac), (alkene)Ag(acac), Me ₂ Au(hfac), Me ₂ Au(tfac), Me ₂ Au(acac), (β -diketonate)CuPR ₃ where PR ₃ = PMe ₃ , PEt ₃ , (β -diketonate)Cu(olefin) where olefin = 1,5-COD, VTMS, (β -diketonate)Cu(alkyne) where alkyne = 1,3-butadiene, CO, 2-butyne, 2-pentyne, 4,4-dimethyl-2-pentyne, 2-hexyne, 4-methyl-2-hexyne, 3-hexyne, 2-heptyne, 3-heptyne, 6-methyl-3-heptyne, 4-octyne, TMS-acetylene, TMS-propyne, bis-TMS-acetylene, TF-TMS-propyne, BTMSA, TMSP, 2-butyne
Metal β -Ketoiminates	Cu(nona-F) ₂ , (β -ketoiminate)CuL
Metal Hydrides	Trimethylamine alane (TMAA), Triethylamine alane (TEAA), Dimethylethylamine alane (DMEAA), Trimethylamine aluminaborane (TMAAB)
Metal Alkoxides	(<i>t</i> -BuO)Cu(PMe ₃), [Cu(O- <i>t</i> -Bu)] ₄ , Cu(CO)(O- <i>t</i> -Bu), [Cu(OSiPh ₃)] ₄ , [Cu(OSiPh ₃)(PMe ₂ Ph)] ₂ , Cu(O- <i>t</i> -Bu)(OR _F) where R _F = C(CF ₃) ₃ , CH(CF ₃) ₂ , C(CH ₃) ₂ (CF ₃)
Metal Amides	Cr(N- <i>i</i> -Pr ₂) ₃
Metal Carboxylates	[(1,5-COD)Ir(OAc)] ₂ , Ag(trifluoroacetate), Ag(acetate)

Table 9-2 (continued)

Metal	Derivative
Organometallic Precursors	
Metal Alkyls	$\text{Zr}(\text{CH}_2\text{-}i\text{-Bu})_4$, $\text{Cr}(\text{CH}_2\text{CMe}_3)_4$, $\text{Co}(\text{CO})_4$, $\text{CF}_3\text{Co}(\text{CO})_4$, $(1,5\text{-COD})\text{PtMe}_2$, $(1,5\text{-COD})\text{PtMe}(\eta^1\text{-C}_5\text{H}_5)$, $\text{CF}_3\text{AuPMe}_3$, $(\text{CF}_3)_3\text{AuPMe}_3$, $[(\text{CH}_3)_2\text{Au}(\text{OSiMe}_3)]_2$, MeAuCNMe , MeAuPMe_3 , $\text{Me}_3\text{AuPMe}_3$, ZnMe_2 , ZnEt_2 , CdMe_2 , Trimethylaluminum (TMA), Triethylaluminum (TEA), Triisobutylaluminum (TIBA), Diethylaluminum chloride (DEACl), Dimethylaluminum hydride (DMAH), SnEt_4 , $\text{Sn}(-n\text{-Bu})_4$, SnMe_4 , $\text{Sn}(-n\text{-Bu})_2\text{Cl}_2$, PbEt_4 , PbPh_4
Metal Alkenes	$(\text{hfac})\text{Cu}(\text{VTMS})$, $(1,5\text{-COD})\text{W}(\text{CO})_4$, $(\eta^5\text{-C}_5\text{H}_5)\text{Rh}(\text{C}_2\text{H}_4)_2$
Metal Alkyls	$\text{Mo}(\eta^3\text{-allyl})_4$, $\text{W}(\eta^3\text{-allyl})_4$, $\text{Rh}(\eta^3\text{-allyl})_3$, $\text{Ir}(\eta^3\text{-allyl})_3$, $\text{Pd}(\eta^3\text{-allyl})_2$, $\text{Pd}(\eta^3\text{-methylallyl})_2$
Metal Carbonyls	$\text{Ta}(\text{CO})_5$, $\text{Cr}(\text{CO})_6$, $\text{Mo}(\text{CO})_6$, $\text{W}(\text{CO})_6$, $\text{Mn}_2(\text{CO})_{10}$, $\text{Re}_2(\text{CO})_{10}$, $\text{HRe}(\text{CO})_5$, $\text{Fe}(\text{CO})_5$, $\text{Ru}_3(\text{CO})_{12}$, $\text{Ru}(\text{hfb})(\text{CO})_4$, $\text{Co}_2(\text{CO})_8$, $\text{Co}_4(\text{CO})_{12}$, $\text{HCo}(\text{CO})_4$, $\text{CF}_3\text{Co}(\text{CO})_4$, $\text{Ni}(\text{CO})_4$
Metallocenes	$[\text{Ti}(\eta^5\text{-C}_5\text{H}_5)_2]^{+}$, $\text{Cr}(\eta^6\text{-C}_6\text{H}_6)_2$, $\text{Fe}(\eta^5\text{-C}_5\text{H}_5)_2$, $\text{Ru}(\eta^5\text{-C}_5\text{H}_5)_2$, $\text{Co}(\eta^5\text{-C}_5\text{H}_5)_2$, $\text{Ni}(\eta^5\text{-C}_5\text{H}_5)_2$, $\text{Ni}(\eta^5\text{-C}_5\text{H}_4\text{Me})_2$
Metal Cyclopentadienyl Compounds	$(\eta^5\text{-C}_5\text{H}_5)_2\text{TiCl}_2$, $(\eta^5\text{-C}_5\text{H}_5)\text{V}(\text{CO})_4$, $[(\eta^5\text{-C}_5\text{H}_5)\text{Cr}(\text{CO})_3]_2$, $(\eta^5\text{-C}_5\text{H}_5)\text{Cr}(\text{CO})_3\text{H}$, $[(\eta^5\text{-C}_5\text{H}_5)\text{Mo}(\text{CO})_3]_2$, $(\eta^5\text{-C}_5\text{H}_5)\text{W}(\text{CO})_3\text{X}$ where $\text{X} = \text{CH}_3$, H , $(\eta^5\text{-C}_5\text{H}_5)_2\text{WH}_2$, $(\eta^5\text{-C}_5\text{H}_4\text{CH}_3)_2\text{WH}_2$, $[(\eta^5\text{-C}_5\text{H}_5)\text{Fe}(\text{CO})_2]_2$,

Table 9-2 (continued)

Metal	Derivative
	$(\eta^5\text{-C}_5\text{H}_5)\text{Co}(\text{CO})_2$, $(\eta^5\text{-C}_5\text{H}_5)\text{Rh}(\text{C}_2\text{H}_4)_2$, $(\eta^5\text{-MeC}_5\text{H}_4)\text{Ir}(1,5\text{-COD})$, $(\eta^5\text{-C}_5\text{H}_5)\text{Ir}(1,5\text{-COD})$ $(\eta^5\text{-C}_5\text{H}_5)\text{PtMe}(\text{CO})$, $(\eta^5\text{-C}_5\text{H}_5)\text{Pt}(\text{allyl})$, $(\eta^5\text{-C}_5\text{H}_5)\text{PtMe}_3$, $(\eta^5\text{-C}_5\text{H}_4\text{Me})\text{PtMe}_3$, $(\eta^5\text{-C}_5\text{H}_5)\text{Cu}(\text{PMe}_3)$, $(\eta^5\text{-C}_5\text{H}_5)\text{Cu}(\text{CN-}i\text{-Bu})$, $(\eta^5\text{-C}_5\text{H}_5)\text{Cu}(\text{PR}_3)$ where R = Et, OMe, OEt, $(\eta^5\text{-C}_5\text{H}_5)\text{CuL}$ where L = PMe_3 , PEt_3 , PBu_3 , $(\eta^5\text{-C}_5\text{H}_5)\text{Ag}(\text{PR}_3)$
Metal Arenes	$(\eta^7\text{-C}_7\text{H}_7)\text{Cr}(\text{CO})_2$, $\text{Cr}(\eta^6\text{-C}_6\text{H}_5\text{-}i\text{-Pr})_2$, $\text{Cr}(\text{cumene})_2$, $(\eta^6\text{-C}_7\text{H}_8)\text{M}(\text{CO})_3$ where M = Cr, W, $(\eta^6\text{-Me}_3\text{C}_6\text{H}_3)\text{Mo}(\text{CO})_3$, $(\eta^6\text{-C}_6\text{H}_6)\text{Mo}(\text{CO})_3$, $\text{W}(\eta^6\text{-C}_6\text{H}_6)_2$, $[(\text{MeO})\text{Ir}(1,5\text{-COD})]_2$

(<500 °C) and high deposition rates are required for microelectronic applications. Some of these constraints may be relaxed in other coating applications where, for example, high substrate temperatures can be tolerated or impurities are not detrimental.

Precursors for CVD of metals can be broadly classified into three types: inorganic precursors, which do not contain carbon; metal-organic precursors, which contain organic ligands but do not possess metal-carbon bonds; and organometallic precursors, which possess organic ligands and metal-carbon bonds. The reaction pathways for these precursors are summarized below and are followed by a summary of the mechanisms by which selective CVD can be achieved.

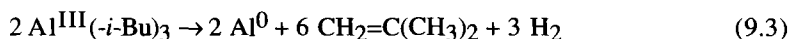
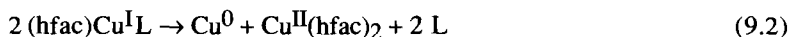
9.3 Blanket Deposition: Reaction Pathways

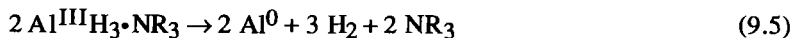
9.3.1 Individual Precursors

Inorganic precursors such as metal halides typically do not produce pure metal films below approximately 600 °C and generally require the presence of a reducing agent such as H₂ or SiH₄ to avoid halide contamination. Furthermore, metal halides (except WF₆, IrF₆, SnCl₄ and TiCl₄) are often solids at the source temperature which makes delivery into the reactor more difficult to control compared to liquid precursors. However, high-purity films can be deposited at high rates, and the precursors are generally inexpensive, easily purified, and commercially available often making metal halides the optimum precursors, as is currently possible with WF₆ (see Eq. 9.1). This is often the case for applications such as wear-resistant and solar coatings where low cost is needed and high deposition temperatures can be tolerated.



In contrast, metal-organic and organometallic precursors offer more advantages than inorganic precursors as they usually have higher vapor pressures, are more often liquids (which can simplify precursor delivery), and often thermally decompose at low temperatures. However, they have the disadvantages that contamination with C, O, F, and P is common and they often require a reagent such as H₂O, a reducing agent such as H₂, or an oxidizing agent such as O₂ to produce pure films. The incorporation of impurities is particularly troublesome for reactive metals such as Cr and Ti for which no good organometallic or metal-organic precursors currently exist.^{6,7} However, there are some examples where high-purity metal films have been deposited from these classes of precursors without co-reactants (such as a reducing agent). This requires a decomposition mechanism where the organic ligands are removed from the reaction chamber intact (see Ch. 5) or where a reaction pathway exists to form volatile products which desorb easily from the surface. Examples of these reactions are the disproportionation of copper(I) compounds (see Ch. 5),⁸⁻¹³ the β -hydride elimination of Al(*i*-Bu)₃ (see Ch. 2),¹⁴ homolysis of Au-C bonds in (CH₃)Au(PMe₃) (see Ch. 6),¹⁵⁻¹⁸ and the use of precursors such as AlH₃•NR₃ which do not contain metal-carbon bonds (see Ch. 2)¹⁹ and are given in Equations 9.2 through 9.5.





The well-known β -hydride elimination is an example of a mechanism which cleaves the metal-carbon bond. However, because this may involve liberation of organic radicals as reactive intermediates (for example, isobutyl radicals on an Al surface), alternate reactions can occur that lead to contamination (e.g., β -methyl group elimination in the case of Al CVD from $\text{Al}(-i\text{-Bu})_3$) (see Ch. 3).¹⁴ Overall, rough guidelines can be derived for choosing the organic portion of the organometallic precursor. As the metal-carbon bond order increases (metal alkene \approx metal alkyne \leq metal alkyl $<$ metal(η^3 -allyl) $<$ metal carbonyl $<$ metal cyclopentadienyl $<$ metal arene) in organometallic compounds, the chances for carbon incorporation are increased due to the increased strength of M-C bonding. For example, CVD of Fe using $\text{Fe}(\text{CO})_5$ (see Eq. 9.6) gives rise to relatively pure films compared to $\text{Fe}(\eta^5\text{-C}_5\text{H}_5)_2$ (in the absence of H_2) (see Ch. 8).²⁰



In general, the more noble the metal (more to the right in a given row) and the lower it is in a given group in the periodic table, the more easily it is reduced, the less stable the M-X bonds, and the less likelihood of C incorporation. For example, $\text{Ni}(\text{CO})_4$ gives rise to purer metal films than transition metal carbonyl compounds from earlier in the first row of the transition metal series in the periodic table (see Ch. 7). Furthermore, films derived from Pd, Pt, Cu, and Ag cyclopentadienyl complexes contain less C than films derived from cyclopentadienyl complexes of metals found earlier in the periodic table. These trends, however, can be modified by the details of the reaction mechanism, which varies depending on the metal and ligands involved.

In the absence of an appropriate reaction pathway, organometallic and metal-organic precursors often give rise to impurity incorporation, particularly C and O, as is apparent from the literature reviewed in Chapter 8. Impurity incorporation can be avoided in certain cases by the addition of a reducing agent or an oxidizing agent to remove the organic ligands. For example, the reduction of metal carbonyl compounds by H_2 produces pure metal films due to Fischer-Tropsch catalysis chemistry.²¹ Metal β -diketonates are popular choices as precursors mainly because the fluorinated derivatives exhibit high vapor pressures and are generally capable of high transport rates. However, the presence of a reducing agent such as H_2 is generally required in order to avoid extensive contamination in the film (see Chs. 4 and 8). For example, the CVD of high-purity copper films has been achieved by reduction of $\text{Cu}(\text{hfac})_2$ with H_2 (see Ch. 4 and Eq. 9.7). Nevertheless, for reactive metals such as Ti, even the use of a hydrogen plasma does not provide sufficiently reducing conditions to form pure metal films from organometallic precursors such as $\text{Ti}(\eta^5\text{-C}_5\text{H}_5)(\eta^7\text{-C}_7\text{H}_7)$.



An example of the use of an oxidizing agent such as oxygen is CVD of Ir from (η^5 -C₅H₅)Ir(1,5-COD)²² and related precursors (see Section 8.4.1.18). The formation of pure metal films in the presence of O₂ is only likely to occur where the metal forms an oxide that is thermodynamically unstable with respect to formation of the metal at the deposition temperature such that only the carbon-containing ligands are oxidized. Reactions catalyzed by the metal surface, such as Wacker-type processes, are likely under these conditions.²¹

9.3.2 Single-Source Precursors

It is sometimes necessary to form films containing more than one element. Metal silicides, M_xSi_y, metal nitrides, M_xN_y, and mixed-metal alloys, M_xM'_y are examples of such materials that are used as contact layers, diffusion barrier layers, and interconnects (see Ch. 1). The most common approach for CVD of these materials is to use two or more separate precursors that react individually on the growing film. Using this strategy, however, makes it difficult to control film stoichiometry. Another approach is to use single-source precursors that contain two or more elements such as two metals or a metal and silicon, germanium, or gallium in the same molecule (Fig. 9-1 and Ch. 8). These precursors often contain metal-metal bonds.

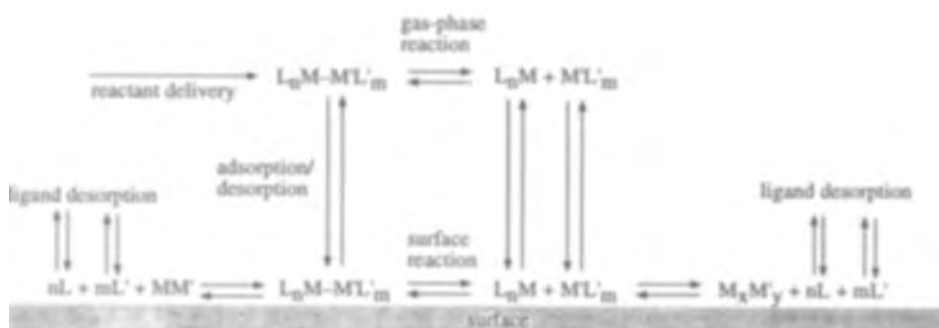


Figure 9-1 Reaction pathways for single-source precursor leading to conservation and loss of precursor stoichiometry.

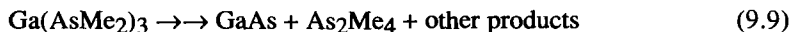
For simplicity, the single-source precursor described contains the two desired elements (M and M') bonded to each other, with several ligands attached to each metal center ($L_nM-M'L'_m$). The desired reaction pathway involves adsorption of the precursor with loss of the supporting organic ligands, L and L', without breaking the M-M' bond. The potential advantages of this approach are: the stoichiometry of the precursor can be retained in the film; the precursor delivery system can be simplified; and better homogeneity can be obtained because the desired elements are effectively premixed at the molecular level. The disadvantages are: single-source precursors often have lower vapor pressures than sources of the individual elements, so that delivery and deposition rates are lower (if special precautions are not taken) (see Section 9.6); the stoichiometry of the precursor is not always retained in the film (depending on the system under consideration); even when the stoichiometry of the precursor is retained in the film, this approach must be modified for materials with non-integral stoichiometry; and finally, single-source precursors are often commercially unavailable.

Figure 9-1 shows how a single-source precursor can form films with non-integral stoichiometry if the M-M' bond breaks either in the gas phase or on the surface to form separate volatile species containing M and M' which desorb at different rates before reacting. This makes it difficult to control film stoichiometry because composition can vary with temperature. Other complications can occur: the stoichiometry of the film may be different from that of the precursor or the desired product stoichiometry may be achieved even though all the M-M' bonds are broken. In such cases, the elements contained in a "single-source" precursor are not necessarily those found in the final material. For example, labeling studies show that in the deposition of TiN from $Ti(NMe_2)_4$ and NH_3 , the N is derived from ammonia rather than the amide ligands ($-NMe_2$).^{23,24} Under these conditions, $Ti(NMe_2)_4$ is only a convenient source of *one* of the constituent elements of the final films (Eq. 9.8).



This reaction occurs by a series of trans-amination steps, but the observation of molecular N_2 , necessary to account for the reduction in oxidation state of Ti^{IV} to Ti^{III} , has yet to be established.²⁵

In other cases, the precursor may not have the desired film stoichiometry, but the loss of one or more metal atoms from the precursor may result in formation of a film with the desired stoichiometry. For example, $Ga(AsMe_2)_3$ thermally decomposes to form GaAs films, presumably with loss of the corresponding diarsine, As_2Me_4 , according to Equation 9.9.²⁶



9.4 Selective Deposition

9.4.1 Formation of Patterned Films

Patterned films are required for many applications primarily in microelectronics where they are used as interconnects, contacts, barriers, vias, plugs, and parts or devices such as transistors, capacitors, and diodes. Patterned metal films can be prepared by blanket deposition followed by selective-area etching, blanket deposition into substrate trenches followed by chemical-mechanical polishing (CMP), or selective CVD.²⁷ Figure 9-2 shows these possibilities schematically. Blanket deposition followed by application and patterning of a photoresist and dry etching is currently the most common approach for forming metal patterns.²⁸ Dry etching is preferable to wet

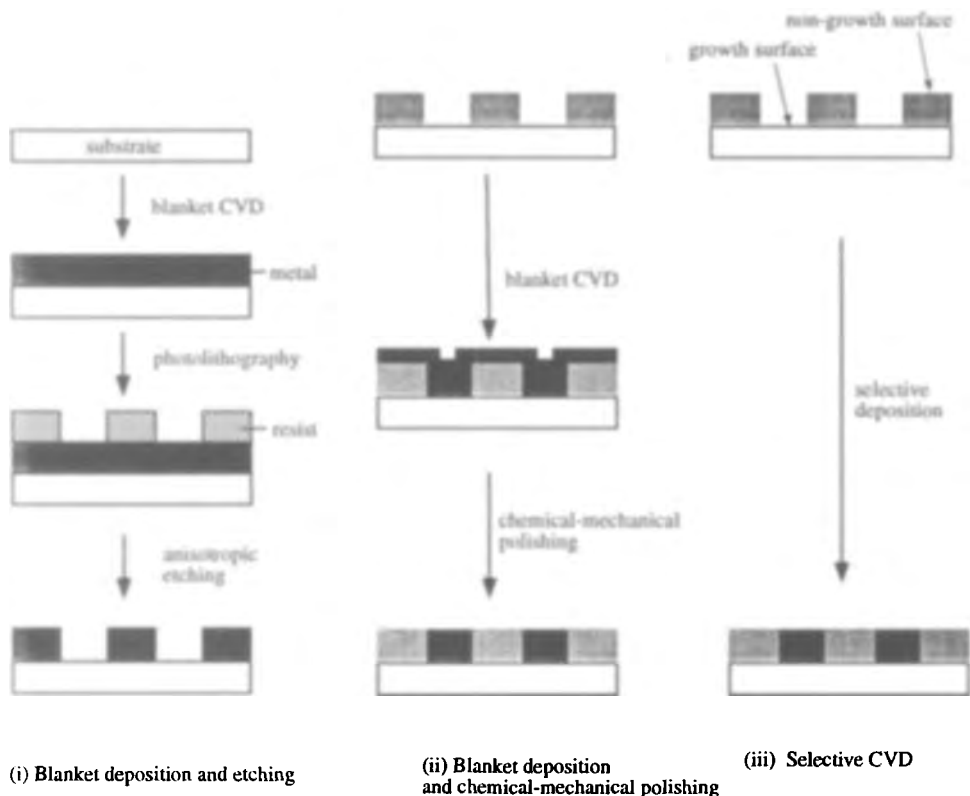


Figure 9-2 Possible methods for formation of patterned metal films.

etching because of the better resolution, the possibility of anisotropic etching, and the smaller amount of waste generated.²⁷ The chemistry of dry etching is often related to the chemistry of CVD of a material, and, as a result, understanding a deposition mechanism also provides insight into the etching process. An emerging technology for the generation of patterned metal films is blanket CVD into trenches followed by CMP to remove metal from outside of the trenches. These patterning approaches are not discussed here because they involve the chemistry of etching or CMP, both of which have been discussed elsewhere.²⁹ Selective CVD is used less often due to problems with repeatability under manufacturing conditions. However, recent advances in methods to control selective deposition are improving the reliability of this approach. Selective CVD is by necessity a chemical approach, therefore, it is summarized here. The chemistry of surface reactions that result in selective film deposition also pertain to blanket CVD.

Selective CVD involves deposition of a material onto one surface (the growth surface) in the presence of another surface (the non-growth surface) as shown in Figure 9-3.¹⁹ For microelectronics applications, the growth surface is typically a metal, semiconductor, or diffusion barrier material (metal silicide, metal nitride, or metal alloy), and the non-growth surface is a dielectric material such as SiO_2 , a metal oxide, or a polymer [polytetrafluoroethylene (PTFE) or polyimide].

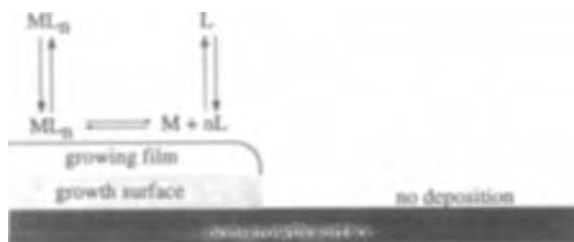


Figure 9-3 General mechanism for selectivity.

There are a variety of mechanisms for selective deposition, and all rely on inhibiting adsorption and reaction of the precursor and nucleation of the metal on the non-growth surface or by promoting these processes on the growth surface. Nucleation processes can be divided into two categories:¹⁹ physical nucleation, where the barrier to the formation of nuclei is the result of the increase in free energy associated with forming a nucleus, and chemical nucleation, where there is no energy barrier for the formation of nuclei but there is a large energy barrier to the chemical reaction. These two categories can be further divided into seven groups, with the first six being chemical nucleation and the seventh physical nucleation:

- (1) The intrinsic reaction rate of the precursor on the non-growth surface is slower than its reaction on the growth surface and on the growing film.
- (2) The growth surface (e.g., Si) acts as a reducing agent and is selectively, sacrificially consumed by a precursor such as WF_6 or MoF_6 .
- (3) Dissociation of a co-reactant (a reducing agent, H_2) occurs on the growth surface (e.g., a metal) but not on the adjacent non-growth surface (SiO_2 , polymer, or metal oxide).
- (4) The rate is increased on the growth surface by photochemically-driven reactions.
- (5) Selective passivation of the non-growth surface prevents adsorption of the precursor on the non-growth surface while adsorption and reaction occur on the growth surface.
- (6) A species is present on the non-growth surface that getters (removes) the nucleating species.
- (7) A free energy barrier exists for the formation of metal nuclei that inhibits nucleation on the non-growth surface while a smaller barrier exists on the initial growth surface that allows physical nucleation to occur.

A process that uses physical nucleation (7 above) is deposition of seed nuclei of a growth material in a pattern on a surface; growth proceeds by CVD on the seed nuclei (nucleation layer) but not on the unseeded, non-growth surface.³⁰ Table 9-3 summarizes the precursors, mechanisms, growth surfaces, and non-growth surfaces discussed in this book.^{8,16,17,30-49}

The first consideration in determining how to achieve selective deposition is understanding the chemical and physical properties of the growth and non-growth surfaces. When the characteristics of these surfaces are dictated by other technological or materials-compatibility considerations (such as the need to have a diffusion barrier for the growth surface and a dielectric layer for the non-growth surface) the intrinsic difference in overall reaction rates on the growth and non-growth surfaces is unlikely to be optimized. In less-constrained situations, either the growth or non-growth surface can be chosen to promote selective deposition. In both cases, it is possible to modify the surface structure to either promote or inhibit surface reactions and nucleation. In the first case, the modification must be carried out on the existing surfaces; in the latter case, the surfaces can be chosen along with the precursor to provide optimum selectivity. In both cases, the bulk of the deposition occurs on the material being deposited, which has properties that are different from those of the initial growth surface.

A wide variety of substrates are common for metal CVD. The most important substrate material is the metal that is being deposited under conditions of steady-state growth. However, selective deposition originates from the reaction of the precursor on the initial growth surface in preference to the non-growth surface (via methods outlined

Table 9-3 Summary of Selective Deposition

Mechanism	Precursor/ Co-reactant	Growth Surface	Non-Growth Surface	Ref.
Intrinsic differences in rates	(hfac)Cu(PMe ₃)	metals	SiO ₂	31,32
	Cu(hfac) ₂	Pt	SiO ₂	30
	Cu(nona-F) ₂	SiO ₂	Si/metals	33
	Co(η^5 -C ₅ H ₅) ₂ /H ₂	SiO ₂	Si	34,35
	Fe(η^5 -C ₅ H ₅) ₂ /H ₂	SiO ₂	Si	34,35
Sacrificial reaction of growth surface	WF ₆ /Si	Si	SiO ₂	36
	MoF ₆ /Si	Si	SiO ₂	37
	Pd(hfac) ₂ /Cu	Cu	Si, SiO ₂ , Al, W, Ni, Co	38
Activation of growth surface	WF ₆ /H ₂	W	SiO ₂	36
	Cu(hfac) ₂ /H ₂	Cu	SiO ₂	30
	Cu(hfac) ₂ /H ₂ /H ₂ O	Pt, W, Pd, Ag, Au	SiO ₂	39,40
	Cu(hfac) ₂ /He/H ₂ O	Pt	SiO ₂	30
	Al alkyls	TiCl ₄ -treated SiO ₂	untreated SiO ₂	41,42
Selective passivation of non- growth surface	(hfac)Cu(2-butyne)	metals	SiO ₂	8
	(hfac)Cu(VTMS)	metals	SiO ₂	43,44
	(hfac)Cu(1,5-COD)	Au	alkanethiol	45,46
	Al(<i>i</i> -Bu) ₃	metals	SiO ₂	47
	(η^5 -C ₅ H ₅)PtMe ₃	PTFE	modified PTFE	48
	WF ₆	W	SiO ₂	36
	RAuPMe ₃	Cr	BF ₃ /Cr	16,17
Gettering	WF ₆ /H ₂	Si	P-doped SiO ₂	49

above). The original growth surfaces themselves can be classified into inorganic and organic materials and have widely varying selective deposition (nucleation) behavior.

Inorganic substrates include conductors, semiconductors such as Si and GaAs, and insulators including oxides (SiO₂, TiO₂, Al₂O₃), some metal silicides, and metal nitrides (Si₃N₄, AlN). In many CVD studies the nature of the surface species was not specified or not known. For example, Si forms a native oxide unless care is taken to first remove it and to passivate the surface. Similarly, TiN can have OH groups on the surface.^{50,51} Many metals readily form oxides when exposed to air, which can result in

the presence of M-OH groups on the surface. Because nucleation and selectivity are heavily influenced by the nature of the surface layer, great care must be taken in characterizing surfaces before deposition if the origin of the selective deposition behavior is to be understood. Selectivity has been observed most often for a metal or semiconductor (such as Si) as the growth surface and SiO₂ as the non-growth surface (see Table 9-3).

A variety of organic polymers, including fluorinated polymers and polyimides, have applications as substrate materials.⁵² However, few studies have examined CVD onto these and related surfaces. Deposition onto these materials must address the problem of adhesion, which is critical for materials such as PTFE. Chemical vapor deposition has been carried out onto modified PTFE,⁵³⁻⁵⁵ but insufficient characterization data are available to define the species present on the initial growth surface.⁵⁶⁻⁵⁸ Selectivity for modified PTFE has been observed for (hfac)CuL species⁵³⁻⁵⁵ (see Ch. 5) and for (η^5 -C₅H₅)PtMe₃ (see Ch. 7).

In general, the surfaces described above have various functional groups, most commonly including -OH and M-O-M.⁵⁹⁻⁶² Depending on their environment and the chemical composition of the substrate, -OH groups will exhibit different pK_a values which, along with variations in their surface concentrations, will lead to different selectivity and nucleation behavior. Even on the same surface a variety of different functional groups (including isolated -OH, hydrogen-bonded -OH, and M-O-M) may be present simultaneously, and each will react in a different manner with the same precursor.⁶³⁻⁶⁷ In addition, the reactive surface sites available (such as -OH groups) influence strategies to optimize selective deposition (such as passivation via removal of the surface OH groups); this difference is only now being exploited.^{34,42-44,68}

The growth surface may vary widely in its reactivity towards the precursor. In most cases, however, the oxidation state of the metal in the precursor must be reduced which requires redox processes. In some cases, this is achieved by sacrificial reduction by the constituent elements of the growth surface (e.g., Si, see Section 9.4.2.2) or by adsorption (dissociation) of a co-reactant such as H₂ (see Section 9.4.2.3).

The second major factor that governs selectivity is the nature of the precursor which can often be varied to promote reaction on the growth surface and to inhibit reaction on the non-growth surface. An example is the reaction of an XCuL species ((hfac)CuL) on metals and SiO₂ where the strength of the Cu-L bond appears to determine whether or not selective deposition occurs (see Ch. 5).

The final major factors that influence selectivity are reactor operating conditions such as pressure, temperature, reactant concentrations, co-reactant concentrations, and reactor type (hot-wall or cold-wall). Often, these can be varied to give selective deposition, as in the case of W deposition from WF₆ or Cu deposition from some (β -diketonate)CuL compounds. Because of these variables, care must be taken when comparing reports of selective deposition from different laboratories. Conditions that promote gas-phase reactions must be avoided because the species formed may be

transported to the non-growth surface where adsorption and reaction can lead to loss of selectivity.

Selectivity is also closely related to the induction time observed before deposition begins on some growth surfaces. Induction time is the time required to nucleate a film on a surface during blanket or selective CVD. Induction time can be a function of reactor operating conditions and substrate surface properties; it can vary widely from run to run, and results may not be reproducible. Therefore, the strategies used to obtain film nucleation and growth for selective CVD are also useful for controlling the induction time for blanket or selective CVD, thereby improving repeatability.

Once film nucleation has occurred, steady-state film growth must proceed. Nucleation plays a key role in the growth of the film. In many cases, only a few nucleation sites are formed on the surface and the reaction rate on the metal nuclei is higher than on the underlying, exposed surface between the nuclei. The incoming reactant then reacts on the surfaces of the nuclei to promote growth of the nuclei to form relatively large crystallites. This is often undesirable because it leads to large, poorly connected crystallites that yield films with high electrical resistivity.

Other film properties of interest include crystallinity, which must be controlled to produce amorphous materials at one extreme and oriented single-crystal films at the other; crystallographic orientation, which is often desired for electromigration resistance; electrical resistivity; and interfacial phenomena that determine adhesion and the extent of interdiffusion. These properties also depend on the nucleation process, the crystallization behavior of the depositing material, and the crystal-lattice match between the film and the substrate. The details of film nucleation and growth have been discussed elsewhere.⁶⁹

9.4.2 Summary of Selective CVD Methods

9.4.2.1 Intrinsic Difference in Reaction Rates

A situation that is often encountered during CVD is the presence of two or more surfaces with different reactivities towards the precursor. If the precursor reacts more slowly on one surface than on another, selective CVD can occur, as illustrated by Figure 9-4. The different reaction rates can result from different rate-determining steps. There are a number of examples: in the presence of H_2 , the precursors $Co(\eta^5-C_5H_5)_2$ and $Fe(\eta^5-C_5H_5)_2$ do not react on Si but do react on SiO_2 surfaces. In the absence of H_2 , no deposition is observed (Ch. 8).^{34,35} Copper CVD using $(hfac)Cu(PMe_3)$ occurs on Cu, Pt, and other metal surfaces, but not on SiO_2 ³¹ and surfaces such as PTFE (Ch. 5).^{55,70} The precursors $Cu(\beta\text{-diketonate})_2$ and $Cu(\text{nona-F})_2$ react with SiO_2 and not on Si in many cases (see Ch. 4).^{33,71} However, in other cases this selectivity is reversed,

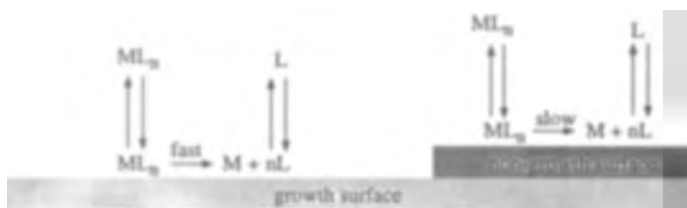


Figure 9-4 Selectivity obtained by difference in intrinsic rates of reaction on growth and non-growth surfaces.

depending on the nature of the Si and SiO₂ surfaces and this emphasizes the importance of controlling the surface chemistry. Although these qualitative features have been identified, no quantitative data exist for the rates of the various reactions on the initial growth and non-growth surfaces.

Differences in reaction rate can be exploited to give selective CVD when seeds of the depositing species are predeposited in a pattern onto a surface.⁷²⁻⁷⁴ Seed particle deposition can be carried out via photo-deposition using an excimer laser with a mask or a continuous-wave laser that is scanned over the surface. The seeds that are deposited serve as reaction (growth) surfaces for the precursor whereas the materials composing the underlying (non-growth) surface do not. The seeds may be the same material as the depositing material. In other cases, the seed nuclei serve to lower or eliminate the physical barrier to nucleation on the initial growth surface (see Section 9.4.2.7).

Selectivity obtained by this approach can be lost for a variety of reasons: contamination of the non-growth surface;⁷⁵ gas-phase reactions producing reactive intermediates or clusters which reach the non-growth surface and form nucleation sites;¹⁹ surface reactions on the growth surface to form reactive species which surface-diffuse or desorb and are then transported in the gas phase to the non-growth surface;^{76,77} high precursor partial pressures leading to reaction pathways which do not occur at lower pressures; and high reaction temperatures leading to reaction pathways which do not occur at lower temperatures on the non-growth surface.¹⁹

9.4.2.2 Sacrificial Solid-State Co-Reactant

Selective deposition can be obtained by the reaction of a volatile CVD precursor with a solid co-reactant that has been formed in a pattern on a surface. The classic example is the reduction of WF₆ (or MoF₆, Ch. 8) by Si to form tungsten metal and SiF₄ (Ch. 3), as shown in Figure 9-5 and Equation 9.10. This approach, however, requires diffusion of atomic species through the solid growing metal layer and as a result can be self-limiting.³⁶

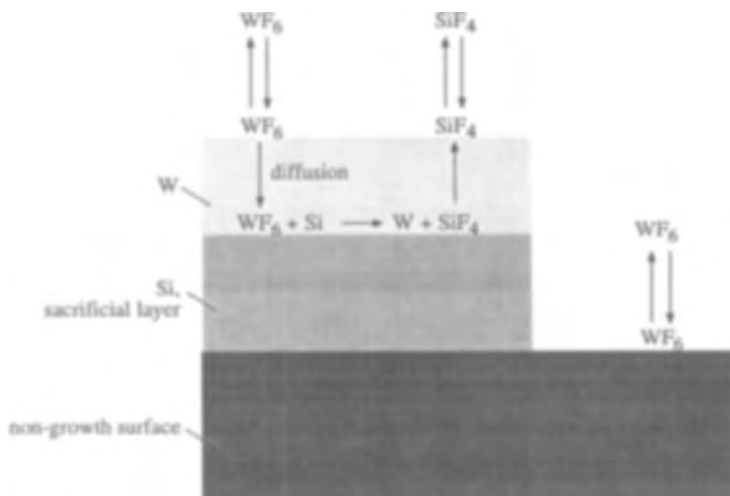
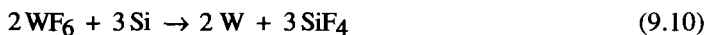
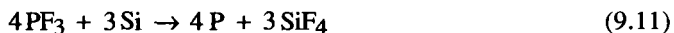


Figure 9-5 Use of sacrificial layer to provide selective CVD.



Porous films can also be produced as in the case of selective Mo CVD from MoF₆ on Si.³⁷ The major limitation of this approach is that it can only be used where there is a thermodynamic driving force for the reaction.⁷⁶ In the case of the WF₆/Si system, this process is rapid, but in other cases this reaction is not thermodynamically favored and does not proceed. Another disadvantage is that the co-reactant must be available on or underneath the growth surface but not on the non-growth surface. Selectivity can be lost for the same reasons listed in Section 9.4.2.1.

This process can be disadvantageous when one of the reaction by-products is also reduced by the sacrificial co-reactant as is the case when PF₃ is used as a supporting ligand in a metal precursor complex; the PF₃ can react with Si to produce P impurities.⁴⁹



Another example of selectivity is the redox transmetallation process in which a metal-organic precursor is reduced by a metallic surface, which is itself oxidized to form a metal-organic complex. For example, Pd(hfac)₂ does not react with Si, SiO₂, Al, W, Ni, or Co substrates in the temperature range 200–425 °C.³⁸ However, reaction occurs readily with copper to give Pd/Cu-alloy films according to the redox reaction of Equation 9.12, as shown in Figure 9-6.

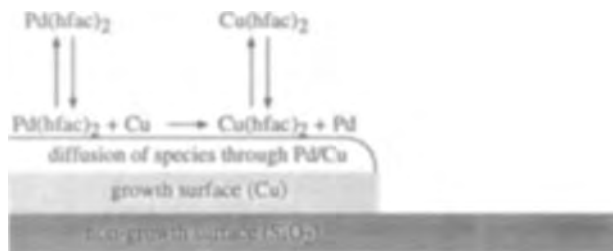


Figure 9-6 Redox transmetalation as mechanism for selective CVD.



The thermodynamics of the redox process dictate whether or not transmetalation occurs. A self-limiting thickness is expected because either the Pd(hfac)_2 and the Cu(hfac)_2 or the Cu must diffuse through the Pd/Cu film in order for the reaction to proceed. Loss of selectivity can be envisioned when the product, Cu(hfac)_2 , reacts with other surfaces present on the substrate or for the reasons listed in Section 9.4.2.1.

9.4.2.3 Activation of Growth Surface

Many CVD reactions require a co-reactant in order to produce pure metal films and to lower the deposition temperature into a range suitable for commercial applications. Examples of co-reactants include H_2 and O_2 . In the case of H_2 , the hydrogen can often act as a reducing agent to reduce the metal contained in the precursor to the zero-valent oxidation state and to react with radicals such as $\text{C}_5\text{H}_5\cdot$ and $\text{C}_3\text{H}_5\cdot$ to form volatile less-reactive species such as C_5H_6 and C_3H_6 , respectively. If the H_2 dissociates on the growth surface but not on the non-growth surface, selective CVD can be obtained as shown in Figure 9-7. An example is CVD of W from WF_6 and H_2 . Atomic hydrogen is not formed on the non-growth surface. As a result, a different reaction pathway must be

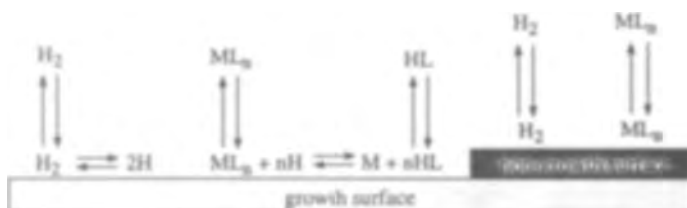


Figure 9-7 Reaction with gaseous co-reactant.

followed for the reaction of the precursor which is slower than the reaction on the growth surface in the presence of atomic H. Thus, this approach to selectivity relies on activation of the growth surface through the availability of a different reaction pathway with a higher rate on the growth surface.

Other reagents have been added to enhance deposition rates (although selective deposition is not necessarily achieved in all cases). Enhancement of the deposition rate of Cu from both Cu^{II} and Cu^{I} precursors has been achieved by the addition of water and alcohols.^{30,77-83} For example, in the CVD of Cu from $\text{Cu}(\text{hfac})_2$, the film growth rate increases with the amount of water vapor in the H_2 or He gas flow. However, deposition of Cu onto a Pt seed layer versus SiO_2 is more selective for Pt when the combination $\text{H}_2\text{O}/\text{He}$ is used rather than $\text{H}_2\text{O}/\text{H}_2$, although the film purity and resistivity are retained.³⁰ Studies of the deposition rate and morphology of metal films deposited in the presence and absence of co-reactants such as water or alcohols indicate that these reagents also serve to promote nucleation on the growth surfaces; for

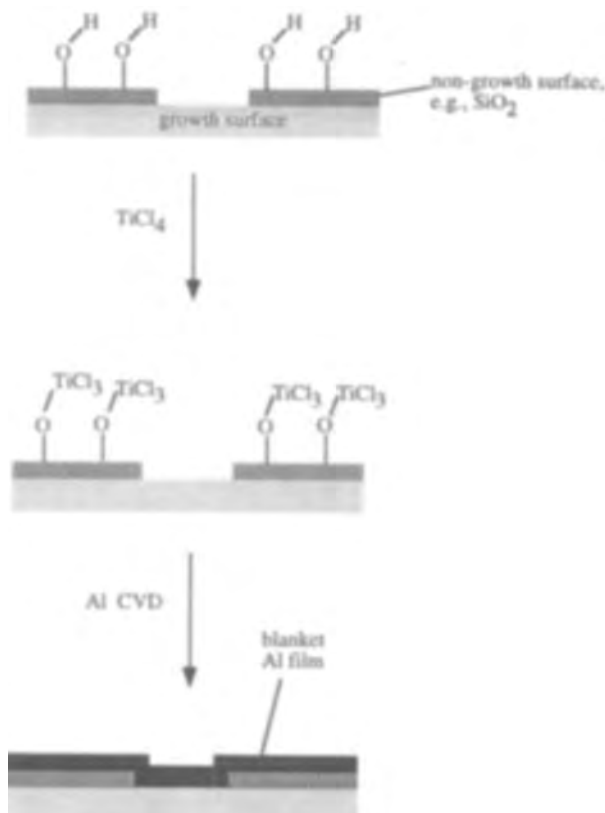


Figure 9-8 Surface activation for deposition of Al.

example, the sticking probability of Cu on SiO_2 is increased by the addition of multilayers of water.⁸⁴ This approach of activating the growth surface can also be used where an existing surface functional group is replaced by a more reactive site. This is the case when TiCl_4 is reacted with SiO_2 surfaces which is believed to result in the formation of chemisorbed TiCl_3 , which subsequently reacts with Al CVD precursors (see Ch. 2 and Fig. 9-8).^{41,42,85-87}

Selective deposition onto organic polymers has been achieved by a variety of patterning methods which often involve activation of the growth surface, as illustrated in Figure 9-9 (see Ch. 5). For example, PTFE surfaces have been activated by chemical etching with a sodium naphthalenide solution⁸⁸ and polyimide surfaces by reaction with potassium hydroxide.

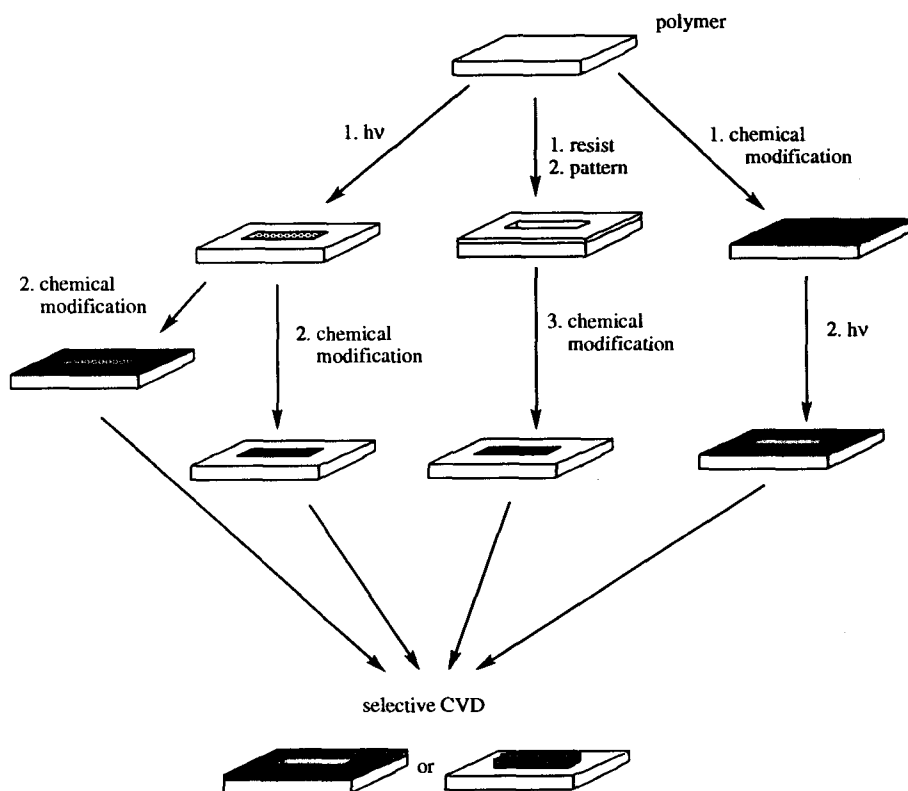


Figure 9-9 Methods for generating patterned films on polymers by surface modification (after Hampden-Smith et al.⁸⁸).

Figure 9-9 shows three approaches to forming metal patterns on PTFE. On the left side of the figure, the surface is exposed to various types of radiation (X-rays, electrons, etc.), which renders it unreactive towards the chemical etchant. Subsequent CVD is then selective for the unexposed regions. In the center of the figure, the substrate is masked before modification, resulting in activation of the exposed regions. On the right side of the figure, the entire substrate is activated, but regions of the activated material are then removed by laser patterning to reveal the original surface. Of these approaches, activation through a patterned resist is probably the most promising, because it relies on conventional patterning techniques with no need for laser, electron, or X-ray scanning of the surface.

Loss of selectivity can occur for the reasons cited in Section 9.4.2.1.

9.4.2.4 Photochemical Activation of Growth Surface

An extensive discussion of photochemical CVD is beyond the scope of this text and can be found elsewhere.⁷²⁻⁷⁴ However, photochemically induced selective deposition is relevant to this discussion. Selectivity can be achieved by a number of different methods which rely on the presence of a chromophore in either the CVD precursor, a reaction intermediate or the growth surface, as shown in Figure 9-10. Selective-area irradiation of a surface using a mask or a laser in the presence of the molecular precursor can give rise to site-specific deposition because reactions occur only on irradiated areas.

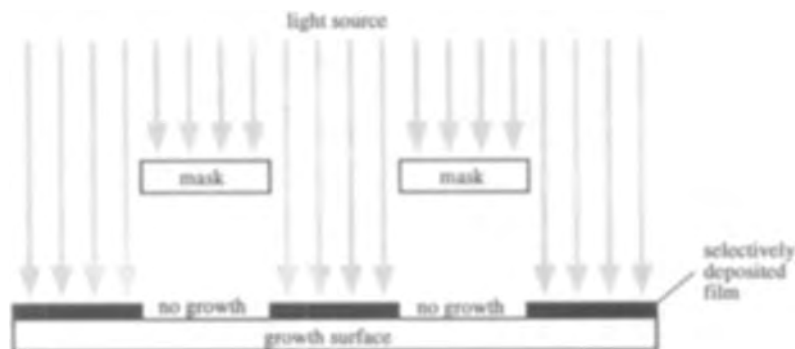


Figure 9-10 Photochemical activation of growth surface.

The primary mechanism by which selectivity is lost is gas-phase reactions which can result in formation of reactive species in the gas phase which are then transported to the non-growth surface where they react to form nucleation sites. Note that structural changes upon adsorption of the precursor onto a surface can change its absorption

wavelength compared to the same species in the gas phase. This can be exploited to favor photochemical reactions on surfaces over those in the gas phase. In addition, surface-bonded reaction intermediates may absorb photons in the wavelength range of interest even though the gaseous or adsorbed precursor does not. Furthermore, the surface can act as a chromophore, which ultimately results in precursor decomposition. This method has been used widely to prepare metal-coated TiO_2 particles in the presence of SiO_2 for catalytic applications.⁸⁹⁻⁹²

9.4.2.5 Passivation of Non-Growth Surface

An approach to selectivity that has been exploited for a variety of systems is to passivate the non-growth surface by reducing its reactivity. This approach relies on modification of the functional groups that are present on the non-growth surface. There are a variety of examples, some of which are examined below.

Chemical vapor deposition of Al from $\text{Al}(-i\text{-Bu})_3$ and related species occurs because $\text{Al}(-i\text{-Bu})_3$ reacts with hydroxyl groups on the SiO_2 surface to form products that do not react further with $\text{Al}(-i\text{-Bu})_3$ (Ch. 2).⁴⁷ This effectively passivates the SiO_2 surface and inhibits further reaction of the precursor on the SiO_2 . In contrast, $\text{Al}(-i\text{-Bu})_3$ rapidly dissociates on the growth (Si, Al) surface, as shown in Figure 9-11.

Passivation of the non-growth surface to obtain selective CVD has also been exploited for Cu CVD (as shown in Fig. 9-12 and reported in Ch. 5). For a number of (β -diketonate) CuL precursors, adsorption and reaction of the precursor occurs with the surface hydroxyl groups on the SiO_2 non-growth surface (left side of Fig. 9-12). Adsorption can be prevented by removing the hydroxyl groups through reaction with various silylating agents such as Me_3SiCl , HMDS, $\text{Me}_3\text{Si}(\text{NMe}_2)$ and $\text{Me}_3\text{CCH}_2(\text{Me}_2)\text{Si}(\text{NMe}_2)$ to form Si-O-SiR_3 ^{43,67,93} which replace the hydroxyl groups and shield the Si-O-Si groups^{94,95} from reaction with the precursor, as shown on the right side of Figure 9-12. As a result, the (hfac) CuL can adsorb and react only on the growth surface resulting in selective CVD. Alternatively, the surface may be dehydroxylated by heating to high temperatures (700 °C) to produce selective deposition,⁴⁴ although this may not be a practical solution because the processing steps used for metallizing integrated circuits cannot be carried out at temperatures exceeding 500 °C.

A similar approach has been used for Pt CVD using $(\eta^5\text{-C}_5\text{H}_5)\text{PtMe}_3$ on PTFE and SiO_2 .⁴⁸ Dosing of the surface with Me_3SiCl prior to reaction increases the induction time before nucleation occurs (see Ch. 7). The reaction removes reactive surface sites from the SiO_2 and PTFE. Methanol has also been used as a passivating agent to remove SiO_2 surface hydroxyl groups during W CVD.⁶⁸

Passivation of a Si surface has been used for selective CVD of Al. A hydrogen-terminated Si surface is patterned by an electron beam which causes desorption of the hydrogen. The exposed Si surface is then passivated by oxidation in air to form SiO_2 . Aluminum is deposited selectively on the H-terminated Si surface using dimethylaluminum hydride (DMAH).⁹⁶

This approach can be generalized to obtain selectivity when two surfaces are present. A common combination is a metallic growth surface and a non-growth surface composed of a metal oxide, nitride, or silicide. The metal oxide, nitride, and silicide surfaces often possess hydroxyl groups^{50,51} which can be removed by the methods described above and replaced with the desired inert functional groups to prevent adsorption and reaction of the precursor.

Another common combination of materials is a metal oxide, nitride, or silicide growth surface (TiN diffusion barrier, for example) and a dielectric non-growth surface such as SiO₂, polyimide or PTFE. These surfaces can possess surface hydroxyl groups which differ in their pK_as, Lewis acidic or basic sites, and/or Brønsted acidic or basic sites. In principle, this difference can be exploited to selectively modify one surface in the presence of another.

Selectivity by this approach can be lost by desorption of the passivating agent from the non-growth surface, incomplete passivation or the reasons described in Section 9.4.2.1.

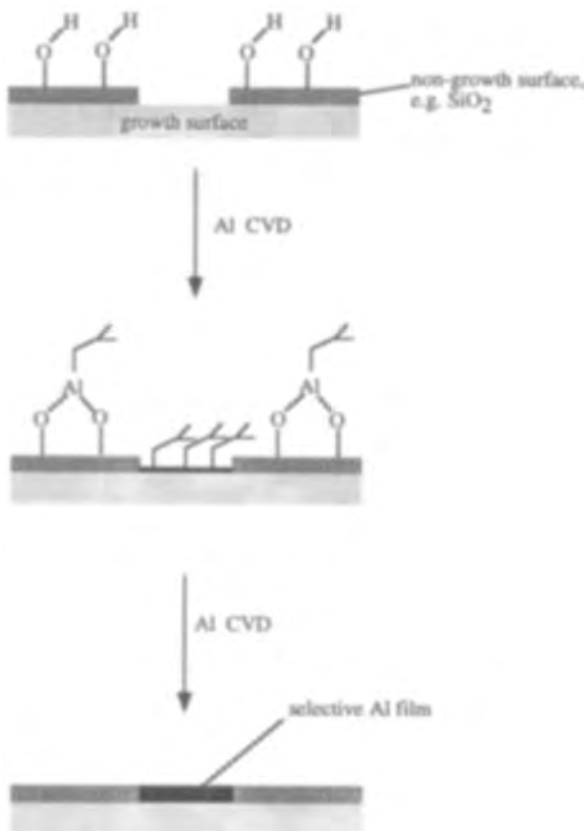


Figure 9-11 Passivation of non-growth surface by reactant leading to selective CVD.

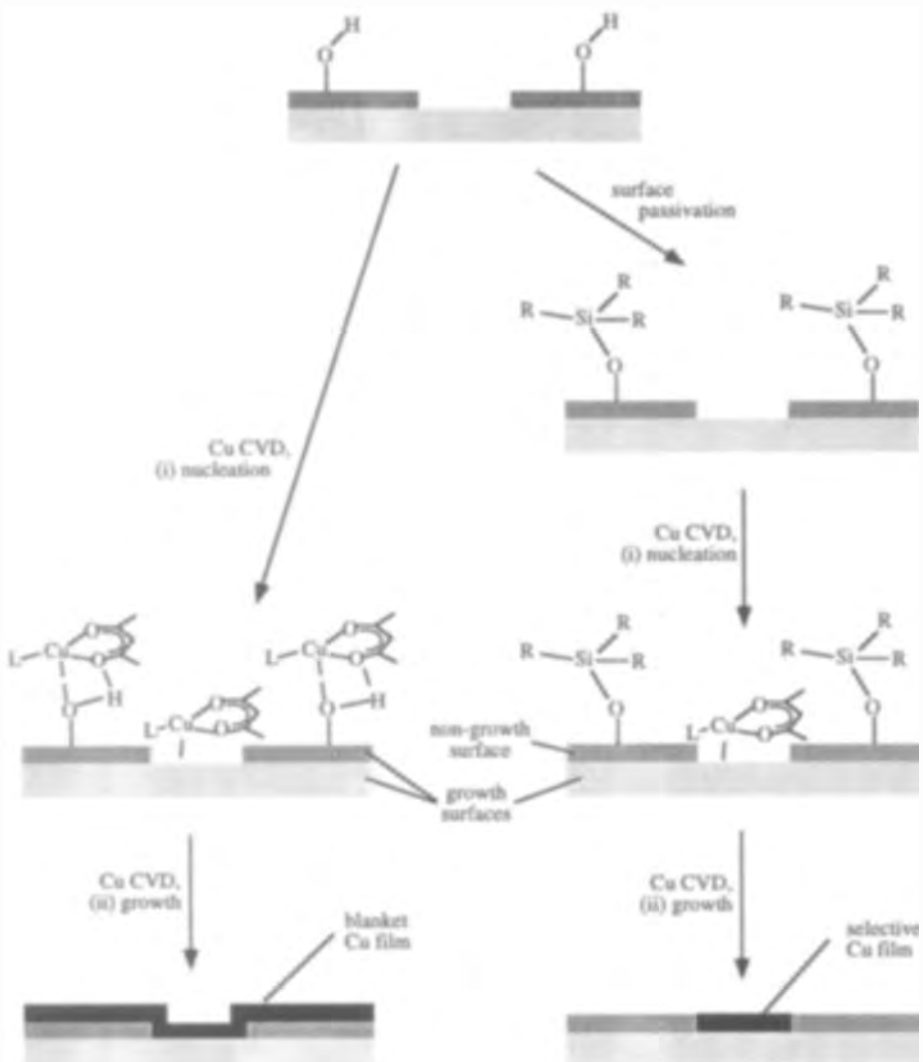


Figure 9-12 Passivation of non-growth surface using silylating agent to achieve selective CVD (after Hampden-Smith and Kodas²⁷).

9.4.2.6 Gettering or Removal of Nucleating Species from Non-Growth Surface

Another method for obtaining selective deposition is to continuously scavenge undesired reaction products from the non-growth surface. This process can be carried out by introducing a reactive (gettering) species onto or into the non-growth surface which reacts with the products from the decomposition of the precursor, as shown in Figure 9-13. A possible example is using P-doped SiO_2 for the gettering (removal) of subfluorides during WF_6 CVD, although the mechanism for this process has not been established conclusively.⁴⁹

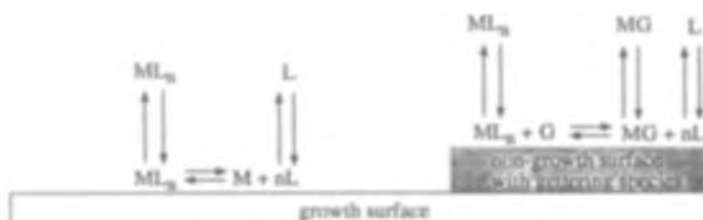


Figure 9-13 Gettering of reactive species by G on non-growth surface.

A related strategy for obtaining selective CVD of W is to periodically etch the depositing species from both the growth and non-growth surfaces to remove nuclei formed on the non-growth surface due to the loss of selectivity.⁴⁹ Etching preferentially removes reactive nuclei from the non-growth surface and minimizes or eliminates deposition.

9.4.2.7 Physical Nucleation Barrier

The physical-nucleation-barrier approach to selectivity can be employed when two surfaces with different surface energies and interfacial energies with the depositing species are used.⁹⁷⁻¹⁰¹ In this physical process, the rate of the CVD reaction is not the barrier to nucleation. Instead, the major concern is the free energies associated with forming nuclei of the metal on the growth and non-growth surfaces. In this situation, atoms of the nucleating materials are either formed on the surface as in CVD processes or are transferred to the surface from the gas phase as in CVD with gas-phase reaction, MBE and related processes, as shown in Figure 9-14. Atoms on the surface can diffuse and collide with other atoms to form clusters, diffuse to existing nuclei to enlarge these nuclei, or desorb from the surface. Each nucleus can grow by addition of atoms or can

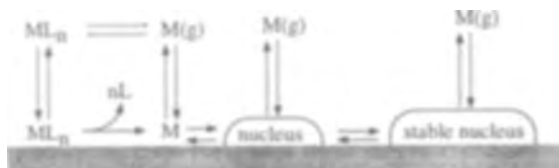


Figure 9-14 Nucleation of metal on surface as the result of surface and gas-phase chemical reactions.

shrink by loss of atoms. The nucleation rate is the rate of formation of thermodynamically stable (critical size) nuclei on the surface. Nucleation is favored by a small critical nucleus size, which occurs for higher concentrations of adatoms, higher binding energy to the surface (roughly, lower vapor pressure of the nucleating species), and lower deposition temperature.

Selective deposition can be obtained by using high-temperature processes with metals that have relatively high vapor pressures, thereby limiting the rate of formation of clusters of critical size on the non-growth surface, as shown in Figure 9-15. The low free energy barrier to the formation of metal nuclei on the growth surface leads to formation of stable nuclei which can grow and eventually coalesce to form a continuous film. The high free-energy barrier on the non-growth surface inhibits the formation of thermodynamically stable nuclei, because nuclei of sub-critical size cannot grow to the critical size, and selective CVD results.



Figure 9-15 Selectivity obtained by differences in physical nucleation rates.

In a number of studies, nucleation has been promoted by addition of co-reactants or surface modification (see Section 9.4.2.5). As described earlier, the deposition of Cu from $Cu(hfac)_2$ in the presence of H_2O/He gas mixtures results in good selectivity for Pt vs. SiO_2 , enhanced deposition rates, shorter induction periods and smoother Cu films, probably as a result of an increase in the nucleation density on the growth surface.³⁰ In

these cases, both the rates of chemical reaction and physical nucleation are influenced by the presence of water. Thus, it is rarely clear whether the enhancement of selectivity is due to chemical or physical processes. Some progress has been made in this direction and a study has shown that added reagents can strongly affect the strength of binding of metal atoms to the substrate surfaces,⁸⁴ although this has not been investigated extensively.

Specific examples of selectivity obtained by exploiting the difference in the nucleation barriers on the growth and non-growth surfaces have not been identified for metal CVD because of the problem with decoupling the effects of surface chemical reactions and nucleation. However, numerous examples exist for semiconductors, such as Si in the presence of SiO₂ where selective Si deposition can be obtained.¹⁰²

The nucleation process shown in Figs. 9-14 and 9-15 can also be limited by the rate of the surface reaction and not by the formation of clusters of critical size. For some low-temperature CVD processes for metals, the critical cluster size is so small that if reaction of the precursor occurs on a surface, even a single atom is stable and nucleation followed by film growth will occur. In this case there is no physical barrier to nucleation and uninhibited nucleation occurs for which the nucleation rate is limited by the rate of the surface reaction which forms the adatoms. Whether or not nucleation occurs on the non-growth surface as well as the growth surface is therefore determined by the relative rates of reaction of the precursor on the two surfaces. In this case, nucleation is indistinguishable from chemical reaction and methods to obtain selectivity must focus on eliminating the reaction of the precursor on the non-growth surface as discussed in Sections 9.4.2.1 - 9.4.2.6.

9.5 Overall Reactor Behavior

A CVD process consists of several key subsystems: the reactant, the reactant delivery system, the reactor, and the substrate. Previous sections have described a number of issues associated with the choice of precursor and the surface chemistry of the substrate as methods for obtaining blanket and selective CVD. Chapter 1 and references therein describe the reactors (see Section 1.4.3) and their operation but provide only a brief introduction. The following sections discuss the overall operation of CVD reactors with an emphasis on the role of precursor delivery, reactor types, boundary layers, limiting steps in the deposition rate and particle formation in the gas phase. Examples from all previous chapters are cited wherever possible.

Figure 9-16 shows the processes involved when a precursor is introduced into a CVD reactor as a vapor, solid particles, or droplets of a liquid precursor or solution. If the precursor is delivered in aerosol form as particles or droplets, the precursor must first

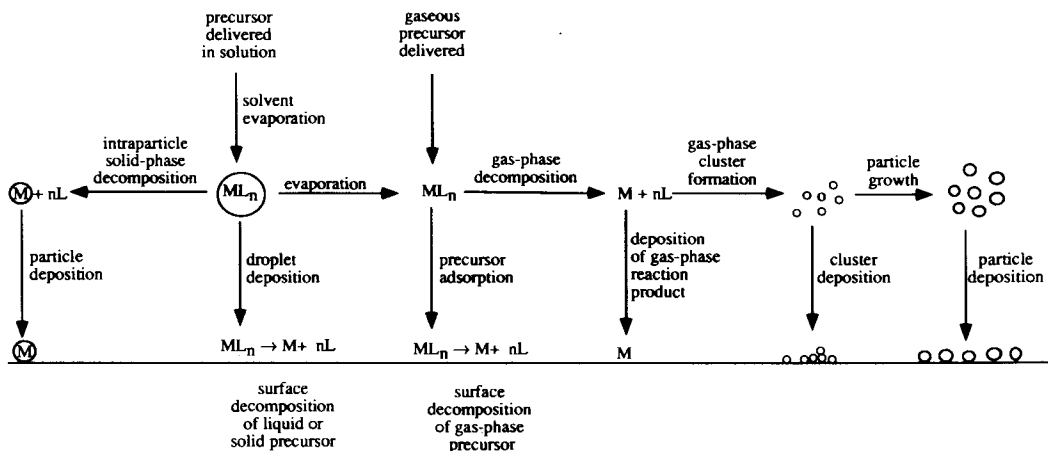


Figure 9-16 Schematic of overall reactor behavior (after Gurav et al.¹⁰³).

evaporate into the gas phase before CVD can occur. This forms the basis for aerosol precursor delivery systems, which are discussed below and have been used for a variety of precursors to several metals, metal oxides, and metal sulfide films. Both CVD and particle formation can occur simultaneously (addressed in Section 9.9). The characteristics of CVD reactors influence all of the processes shown in Figure 9-16. Droplet deposition (generally called spray pyrolysis) can occur and has been used widely with involatile precursors such as metal nitrates to form films.^{103,104} This process is not discussed here because no vapor-phase species are involved during deposition by this method. It is also possible to form particles from the droplets if intra-particle reactions occur to form species with low vapor pressures before the precursor can evaporate. This process has been studied extensively^{103,104} but is not relevant to this discussion.

Once the reactant has evaporated or if the reactant is delivered as a vapor into a given type of reactor, the standard reaction pathways are available to the precursor¹⁰⁵⁻¹⁰⁷ as described in previous chapters (see Fig. 1-11). The precursor can be transported to the surface and react to deposit a film by CVD. The deposition rate, however, can be limited by various steps which are discussed in the sections on boundary layers, rate-limiting steps and the temperature and concentration dependencies of the rate. The precursor can also react in the gas phase to form low-vapor-pressure species which can nucleate to form particles in the gas phase.^{103,104,108} This problem is discussed in Section 9.8.1. The particles can also deposit on the surface by a variety of mechanisms, including thermophoresis, sedimentation, impaction, diffusion, interception and electrophoresis.¹⁰⁹ Particle deposition in most cases leads to poor film properties and is undesirable. In some cases, however, particle formation and deposition are desired because they can increase the deposition rate and lead to composite films. This is discussed in Section 9.9.2.

9.6 Precursor Delivery

Depending on the physical properties of the precursor, delivery methods may vary and play a critical role in CVD of metals because the overall deposition rate can be limited by the rate of precursor delivery into the reactor especially when the precursor has a low vapor pressure (see Tables 2-1, 3-4, 3-5, 8-10; Figs. 5-4, 8-14; and Sections 4.3.4, 7.2, 7.3, 7.4) and is delivered using a carrier gas or by direct evaporation into a vacuum. In the most desirable situation, the precursor is a gas at room temperature, as with IrF_6 (see Section 8.4.1.18) and WF_6 (see Ch. 3). In this case, the precursor can be delivered with conventional mass-flow controllers and, most often, feed-rate limitations do not occur. However, precursors to metals are more often liquids or solids, with relatively low vapor pressures, and are generally introduced through bubblers or by direct vaporization. In some cases, the precursors are also thermally unstable which precludes the possibility of high vapor pressures. For these precursors, conventional delivery methods are either unsuitable or provide delivery rates that are slow and result in feed-rate-limited deposition. Therefore, two categories of delivery systems have been developed: liquid transport with flash vaporization and aerosol delivery with evaporation. These methods are described below.

9.6.1 Bubblers and Direct Vaporization of Precursors

This approach relies on direct evaporation or sublimation of precursors with or without carrier gas. If the vapor pressure of the precursor is high enough to use conventional mass-flow controllers, as with WF_6 (vapor pressure of 1000 torr at 25 °C), the precursor can be used without a carrier gas and feed-rate limitations usually do not occur. In general, vapor pressures above 10 torr are necessary to use commercial mass flow controllers, which is higher than the values for many inorganic, metal-organic or organometallic precursors. For precursors with lower vapor pressures, a carrier gas is passed over the heated solid, through a bed of the heated solid in powder form, or through the heated liquid in a bubbler to introduce the precursor vapor into the carrier gas and then transport the vapor through heated lines to the reactor¹¹⁰ (Fig. 9-17). At sufficiently low carrier gas feed rates the precursor can reach its equilibrium vapor pressure and controlled delivery rates can be obtained when temperatures are carefully controlled in the precursor chamber and delivery lines. This approach is most reliable for liquids, where the carrier gas can be bubbled through the precursor so that constant and known (reproducible) delivery rates can be obtained. Successful applications of this approach include organometallic vapor-phase epitaxy (OMVPE) of

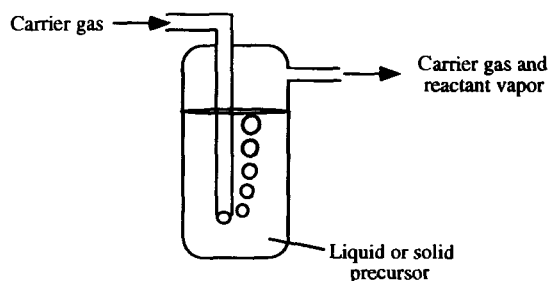


Figure 9-17 Bubbler for precursor delivery.

compound semiconductors from liquid metal alkyls, which often have vapor pressures of less than 10 torr at 25 °C.¹¹¹

Several problems are encountered with this delivery approach. Passing the carrier gas over or through a heated solid powder precursor is undesirable because the decrease in the surface area of the precursor during evaporation produces changes in the overall vaporization rate which can lead to lower precursor partial pressures and a reduced deposition rate. The change in precursor partial pressure may go undetected because the total pressure is nearly equal to the partial pressure of the carrier gas for precursors with low vapor pressures. This approach is also poor when two or more solid precursors are used because the changes in the delivery rates of each precursor can lead to changes in the stoichiometry of the film. A further problem is that bubblers must be heated to high temperatures to obtain useful vapor pressures (see Tables 2-1, 3-4, 3-5, 8-10; Figs. 5-4, 8-14; and Sections 4.3.4, 7.2, 7.3, 7.4). Under these conditions, the precursor often slowly decomposes, leading to a total pressure that is the sum of the precursor partial pressure and the partial pressure of the reaction byproducts. Furthermore, the formation of only small amounts of metal may *catalyze* decomposition of the remaining precursor. An example is (hfac)CuL species, which begin to decompose near 100 °C in the absence of metal, but even lower temperatures in its presence. Since they typically must be heated to over 50 °C to provide sufficient vapor pressures, the thermal window for precursor delivery becomes problematically small (compare Figs. 5-4 and 5-8).^{8,9,12,13,31,32} Condensation in the heated lines can also occur and leads to problems in obtaining constant delivery rates. For these reasons, there is a drive to use alternate delivery systems in which the precursors are not held at elevated temperatures.

9.6.2 Liquid Delivery

Instead of passing a carrier gas over a hot liquid or solid, the precursor can be fed into a vaporizer as a pure liquid or as a solution in a suitable solvent where the precursor is continuously vaporized (Fig. 9-18).¹¹²⁻¹¹⁴ In the approach which utilizes liquid

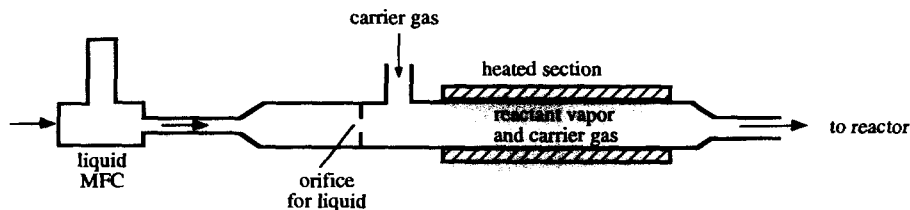


Figure 9-18 Liquid precursor delivery system with evaporation of solvent and precursor by contact with warm surface.

delivery with flash evaporation, the liquid precursor or solution is metered into a chamber where it comes in contact with a warm surface and rapidly evaporates. To provide a constant overall gas flow rate, a carrier gas whose flow rate is controlled by a standard mass-flow controller is usually mixed with the precursor vapor in or near the vaporization region. The precursor vapor in the carrier gas is then passed through heated lines to the reactor.

A liquid delivery system is suitable for liquids and solutions where the precursor is thermally sensitive and would slowly decompose if heated for extended periods of time. It is also a useful method for multicomponent systems where several precursors can be dissolved in the same solution because the relative delivery rates of the precursors do not change with time. A disadvantage is that the precursor contacts a warm surface where chemical reactions can occur over time to give a metal film which can, in some cases, catalyze the decomposition of the precursor. Another disadvantage is that the precursor delivery rate into the reactor is still limited by the vapor pressure of the precursor at the vaporization temperature. This type of delivery system is available commercially.

A variation of liquid delivery is aerosol evaporation within the liquid delivery system (Fig. 9-19).¹¹⁴ For this approach, the liquid precursor or precursor solution is

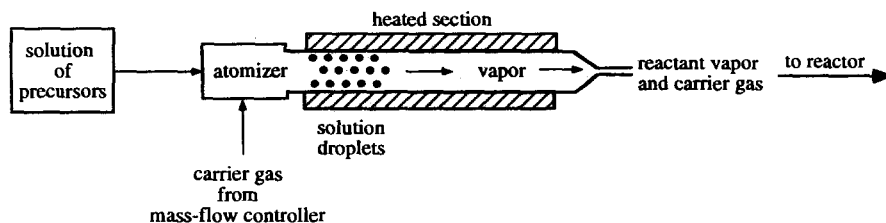


Figure 9-19 Liquid precursor delivery system with aerosol evaporation of solvent and precursor.

atomized into droplets which form a vapor when they come in contact with the hot carrier gas and evaporate. The vapor is then delivered through heated lines to the reactor. This system is similar to the one described above, except that precursor vaporization occurs from droplets in the gas phase and not from a liquid on a warm surface. As a result, heterogeneous reactions are avoided and higher vaporization temperatures can be achieved. However, liquid delivery is hampered by requiring heat-traced lines, something that is avoided with aerosol delivery (discussed below) in which the droplets are introduced directly into the reactor.

9.6.3 Aerosol Delivery

Aerosol delivery is similar to liquid delivery with aerosol evaporation, except that it relies on introducing aerosol droplets directly into the CVD reactor where they evaporate (Fig. 9-20). This technique has been described by numerous names, including Aerosol-Assisted CVD,¹¹⁵ Spray Pyrolysis,¹¹⁶⁻¹²⁵ Pyrosol Process,^{126,127} Spray MOCVD¹²⁸ and others.¹²⁹⁻¹³³ Sometimes the process is simply called CVD without distinguishing from processes with conventional precursor delivery.¹³⁴⁻¹³⁸

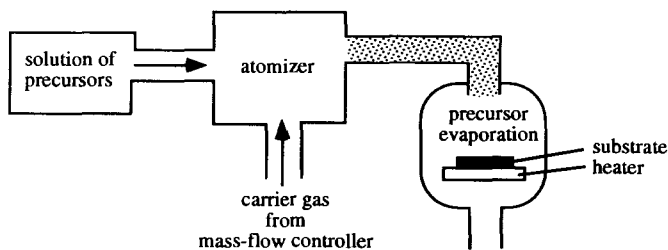


Figure 9-20 Aerosol precursor delivery system with in-situ precursor and solvent evaporation.

Droplets evaporate in the reactor because, at pressures for which the gas mean free path is shorter than the reactor dimensions, the gas above the substrate is heated (see Section 9.7.1). Alternatively, the reactor walls may be warm which also results in gas heating. In both cases, the droplets entering the heated region evaporate, at least partially, before reaching the substrate, after which conventional CVD occurs. In other cases, an evaporation zone, often a tubular heated flow system, is provided to allow the precursor to completely evaporate before reaching the substrate. The major difference from the aerosol approach discussed in the section above is that, in this approach, the

droplet evaporation occurs in the CVD reactor, often immediately above the substrate. This approach has applications in the glass industry for coating large surface areas with metals and metal oxides.^{128,139}

A critical point is that the term "spray pyrolysis" is also used to describe the process in which involatile reactants are dissolved in a solvent which is atomized to form droplets that subsequently impact onto surfaces. Solvent evaporation and reaction of the precursor on the substrate then lead to film formation. The literature in this area is vast and has been reviewed.^{104,140,141} The distinction between processes operating with metals and aerosol CVD and with droplet deposition is often not made in the literature.

Aerosol delivery has not been studied extensively for metal CVD, but has been used extensively for metal oxide CVD, as summarized in Table 9-4. Films of Cu and Ag have been deposited using toluene solutions of (β -diketonate) M_L precursors in a warm-wall reactor with aerosol delivery.¹⁴² A variety of metals, including Al, Cu, Ag, Ni and Pd, have been deposited using metal β -diketonates with supercritical fluid delivery.¹⁴³

Table 9-4 Chemical Vapor Deposition with Aerosol Delivery of Precursors.

Material	Precursor(s)	Notes	Ref.
Cu, Ag	(β -diketonate) Cu_L (β -diketonate) Ag_L	$T_s = 100\text{-}250\text{ }^\circ\text{C}$ conventional spray nozzle	142
Al_2O_3	$Al(acac)_3$	$T_s = 430\text{ }^\circ\text{C}$ ultrasonic atomizer	121
Al_2O_3	$Al(acac)_3$	$T_s = 40\text{-}600\text{ }^\circ\text{C}$ spray nozzle	144
CuO	$Cu(O_2CCH_3)_2$	$T_s = 375\text{ }^\circ\text{C}$ ultrasonic atomizer	120
Cr_2O_3	$Cr(acac)_3$	$T_s = 450\text{ }^\circ\text{C}$ ultrasonic atomizer	125
$\gamma\text{-Fe}_2O_3\text{-Fe}_3O_4$	$Fe(acac)_3$	$T_s = 420\text{-}540\text{ }^\circ\text{C}$ ultrasonic atomizer	116
Fe_2O_3, Fe_3O_4	$Fe(acac)_3$	$T_s = 300\text{-}550\text{ }^\circ\text{C}$	116,145
Fe_2O_3	$Fe(acac)_3$	$T_s = 500\text{ }^\circ\text{C}$ ultrasonic atomizer	124
Nd_2O_3	$Nd(tfac)_3$	$T_s = 600\text{ }^\circ\text{C}$	146
SnO_2	$SnCl_4$	$T_s = 300\text{-}500\text{ }^\circ\text{C}$ ultrasonic atomizer	117
SnO_2	$SnCl_4$	$T_s = 250\text{-}400\text{ }^\circ\text{C}$ conventional spray nozzle	147

Table 9-4 (continued)

Material	Precursor(s)	Notes	Ref.
TiO ₂	Ti(acac) ₄	T _s = 380 °C ultrasonic atomizer	123
ZnO	Zn(O ₂ CCH ₃) ₂	T _s = 300-500 °C	148,149
ZrO ₂	Zr(acac) ₄	T _s = 450 °C ultrasonic atomizer	150
ZrO ₂ (Y)	Y(acac) ₃ , Zr(OBu) ₄	T _s = 500-600 °C	151,152
In ₂ O ₃ , SnO ₂	InCl ₃ , SnCl ₄	T _s = 300-450 °C ultrasonic atomizer	118,119, 153
In ₂ O ₃ , SnO ₂ , Fe ₂ O ₃ , Cr ₂ O ₃ , Al ₂ O ₃ , Y ₂ O ₃ , V ₂ O ₃ , VO ₂ , TiO ₂ , ZrO ₂	Fe, Cr, In, Y, V acetylacetonates, Al(O- <i>i</i> -Pr) ₃ , SnCl ₄ , Zr(OR) ₄ , and Ti(OR) ₄	T _s = 300-650 °C ultrasonic atomizer	126
Fe ₂ O ₃ , SnO ₂ , In ₂ O ₃ , Cr ₂ O ₃ , V ₂ O ₃ , Pd, Ru	Fe, In, Cr, V, Pd, and Ru acetylacetonates, SnCl ₄	T _s = 380-560 °C ultrasonic atomizer	135
Al, Cr, In, Ni, Cu, Pd, Ag, Y, Zr, BPSG, YBa ₂ Cu ₃ O ₇ , CuO, Al ₂ O ₃ , Cr ₂ O ₃ , SiO ₂ ,	β-diketonates of Al, Cr, In, Ni, Cu, Pd, Y, Zr, Ba Si(OEt) ₄ , P(OEt) ₃ , B(OEt) ₃	T _s = 100-800 °C supercritical fluid nozzle delivery	143
Y ₂ O ₃ , La ₂ O ₃ , La ₂ CuO ₄	Y(acac) ₃ , La(acac) ₃ , Cu(acac) ₂	T _s = 400-550 °C ultrasonic atomizer	154
Y ₃ Fe ₅ O ₁₂	Y(acac) ₃ , Fe(acac) ₃	T _s = 520-600 °C	151,152, 155,156
CdIn ₂ O ₄	In(acac) ₃ , Cu(O ₂ CCH ₃) ₂	T _s = 400-480 °C	157
(Ni,Zn)Fe ₂ O ₄	Ni, Zn, Fe acetylacetonates	T _s = 460-500 °C	158
BaTiO ₃	Ba(acac) ₂ Ti(O- <i>i</i> -Pr) ₂ (acac) ₂	T _s = 450-600 °C ultrasonic atomizer	134
LiNbO ₃	LiNb(OEt) ₆	T _s = 463 °C ultrasonic atomizer	159
MgF ₂	Mg(tfac) ₂ , Mg(hfac) ₂	T _s = 400-700 °C ultrasonic atomizer	129

Table 9-4 (continued)

Material	Precursor(s)	Notes	Ref.
ZnS	ZnCl ₂ and CS(NH ₂) ₂	T _s = 500 °C ultrasonic atomizer	130
ZnS	Bis(diethyldithiocarbamato) zinc(II)	T _s = 460-520 °C ultrasonic atomizer	122
In _x Se _y	Me ₂ InSePh, In(SePh) ₃	T _s = 309-477 °C ultrasonic atomizer	160
Y ₁ Ba ₂ Cu ₃ O _{7-δ}	Y, Ba, Cu tmhd	T _s = 430 °C ultrasonic, 10-20 μm droplets	161
Y ₁ Ba ₂ Cu ₃ O _{7-δ}	Y, Ba, Cu tmhd	T _s = 400-5600 °C ultrasonic atomizer	133
Y ₁ Ba ₂ Cu ₃ O _{7-δ}	Y, Ba, Cu tmhd	T _s = 500-970 °C solid particles	137,138
Y ₁ Ba ₂ Cu ₃ O _{7-δ}	Y, Ba, Cu tmhd	T _s = 700 °C ultrasonic atomizer	136
Y ₁ Ba ₂ Cu ₃ O _{7-δ}	Y, Ba, Cu tmhd	T _s = 450 °C ultrasonic atomizer	132,162
Y ₁ Ba ₂ Cu ₃ O _{7-δ}	Y, Ba, Cu tmhd	T _s = 500-900 °C warm wall two-fluid nozzle	115
Y ₁ Ba ₂ Cu ₃ O _{7-δ}	metal nitrates	T _s = 800-900 °C ultrasonic and plasma	163

Most studies have relied on warm-wall or hot-wall reactors for precursor evaporation. High-quality films can be produced by organometallic precursors at substrate temperatures of 300 to 500 °C and at deposition rates of 5 μm/min.¹³⁴⁻¹³⁸ The droplet generator used in most cases is an ultrasonic atomizer although simple two-fluid atomizers have also been used.¹¹⁵ The most commonly used precursors are metal β-diketonates such as metal tetramethylheptanedionates (dipivaloylmethanoates) and acetylacetonates and are listed in Table 9-4.^{115-126,129,130,132-138,142-163}

Aerosol delivery has several advantages over bubblers and liquid delivery systems, mainly for generation of multicomponent films with thermally-sensitive, solid-state precursors with low vapor pressures. Because the precursors are held outside the reactor at room temperature or even reduced temperature, thermal degradation of the precursors does not occur. The precursor delivery rates are constant with time because the ratio and

concentration of precursors in the solution, and the droplet size and delivery rate, do not change with time. This allows the reproducible deposition of multicomponent films with constant composition as a function of deposition time (see papers on Y-Ba-Cu-O in Table 9-4). High deposition rates can be obtained because the amount of precursor per unit volume of gas is dictated by the aerosol generation system and can be orders of magnitude higher than that corresponding to the vapor pressure of the precursor at conventional vaporization temperatures.¹⁴² Precursor vaporization occurs without contact with hot surfaces and can therefore occur at higher temperatures than for all other precursor delivery methods, leading to higher partial pressures and higher deposition rates. As a result, feed rate-limited deposition can be avoided more easily than when using other delivery systems. Finally, heat-traced lines are not necessary.

One of the disadvantages of this approach is that it requires total pressures near atmospheric pressure or high enough that the droplets/particles do not settle in the reactor before evaporating. Heating of the gas to high temperatures and using high pressures favor gas-phase reactions which can result in loss of selectivity, reduced deposition rates and degraded film properties. Another disadvantage is that a solvent is present in many cases and may be incompatible with the precursors or the chemistry of film formation and could lead to contamination. However, this problem can be overcome in most cases by a suitable choice of solvent.¹⁴² Reliable feed systems for delivery of solid precursor particles are not available, making liquid-droplet delivery more desirable. The solvent always contains some impurities which may not be volatile and result in formation of small particles after precursor and solvent evaporation. Fortunately, thermophoretic forces (see Section 9.9.2) drive the particles away from hot surfaces such as the substrate, thereby eliminating or minimizing this problem. This approach is relatively new and commercial systems are not yet available.

A key step in aerosol delivery is evaporation of the solvent and precursor, which must at least partially occur before the droplets or particles reach the surface. Guidelines are available for the time required for droplet evaporation; the time for complete evaporation of liquid droplets or solid particles is given by simple equations which are presented in standard books on aerosol science and engineering.^{109,164} For example, lifetimes for 0.1, 1 and 10 μm diameter droplets of pure water with a vapor pressure of roughly 20 torr are 5×10^{-5} , 2×10^{-3} , and 0.15 seconds, respectively.¹⁰⁹ Lifetimes for pure ethanol droplets of the same sizes at room temperature are 10^{-5} , 3×10^{-4} , and 0.03 seconds, respectively.¹⁰⁹ This suggests that an important requirement for the solvent and precursor is that they have reasonable vapor pressures at the evaporation temperature. Because solvent vapor pressures are typically much higher than precursor vapor pressures, precursor evaporation is usually the rate-limiting step for droplet evaporation.

Droplet diameters of less than 10 μm are obtained by typical droplet generators such as the ultrasonic systems. For droplets of this size, complete evaporation of the precursors can be insured by operating at a temperature that is sufficiently high to

provide a precursor vapor pressure of roughly 1 - 10 torr, which results in precursor droplet or particle lifetimes less than one second.¹⁰⁹ It must be noted, however, that droplet/particle evaporation ceases when the partial pressure of the precursor in the gas phase reaches its vapor pressure. This can result in a situation in which precursor particles are in equilibrium with precursor vapor at the vaporization temperature resulting in incomplete vaporization of the particles. Therefore, the ultimate limit on the precursor partial pressure is still the vapor pressure under the operating conditions.

9.7 Reactor Types: Hot-Wall and Cold-Wall

Chemical Vapor Deposition of metals has been carried out primarily in hot- and cold-wall reactors, and in fewer cases, plasma reactors. In this section, we briefly discuss different reactors and their use for metal CVD to provide a framework for the topics in Sections 9.8 and 9.9. Extended discussions are available in standard books on this subject.¹⁰⁵⁻¹⁰⁷

Hot-wall reactors have been used for laboratory studies of metal CVD, even though most metal CVD in industry is currently carried out in single-wafer, cold-wall systems. The advantages of hot-wall systems are that they are simple to operate, can accommodate several substrates, can be operated under a range of pressures and temperatures, and allow varied orientations of the substrate relative to the gas flow (see Ch. 1). The major problem with hot-wall systems is that deposition can occur on the substrate as well as on the reactor walls. These deposits eventually flake off the walls and can contaminate the substrate. Also, the correspondingly large consumption of the precursor can result in feed-rate-limited deposition (discussed below) at relatively low temperatures compared to cold-wall reactors. Deposition takes place only on the substrate when the reactant does not decompose on the reactor walls.^{31,165} However, reactions usually occur on the walls, and, in most cases, the fraction of the surface area of the reactor covered with deposit can vary and lead to problems when reproducing deposition conditions. In addition, homogeneous gas-phase reactions in the heated gas can occur, which can lead to reduced deposition rates, particle formation and loss of selectivity. For these reasons, hot-wall reactors are used primarily at the laboratory scale to study a given precursor for CVD. They are also used to determine reaction-product distributions because the large heated surface area can consume the precursor completely and provide high yields of the reaction products.^{31,165} They are usually not used for quantitative measurements of reaction kinetics for CVD of metals although some exceptions exist (see, for example, Ch. 4). Hot-wall reactors are, however, used extensively in industry for CVD of semiconductors and oxides.

Cold-wall reactors are used extensively at the laboratory scale and are the industry workhorse for CVD of metals. Cold-wall reactors usually accommodate only a single wafer in various orientations to the flow and allow use of both thermal and plasma deposition. Because the reactor walls are cold, deposition occurs only on the substrate, homogeneous reactions are less favored and higher deposition rates can be obtained than in hot-wall reactors. Cold-wall reactors are also more suitable for studies of selective deposition because deposition does not occur on the reactor walls and gas-phase reactions are less likely. They are also used for measurements of kinetic parameters because surface-reaction-limited kinetics can be achieved⁸⁻¹⁰ and because it is possible to operate in the differential mode where the conversion of the precursor is low enough to minimize the partial pressures of the reaction products.⁸⁻¹⁰ For manufacturing applications, single-wafer cold-wall reactors are preferred because they allow better control of deposition behavior (see Section 1.5).

9.8 Boundary Layers; Feed-Rate-, Surface-Reaction-, and Diffusion-Limited Operation; and Temperature and Pressure Dependencies of Rate

It is important to understand the overall behavior of cold-wall and hot-wall CVD reactors in order to make improvements and control the process (see Section 1.5). There are a variety of measurements available; the simplest and most common are the dependencies of the deposition rate on the substrate temperature and on reactant, product and total pressures and flow rates. Measurements are often made to optimize film characteristics and to maximize the deposition rate, which must often be greater than 0.1 $\mu\text{m}/\text{min}$ (see Section 1.5) for CVD processes used in microelectronics and the large-area coating processes found in the glass industry. The temperature and pressure dependencies of the deposition rate can reflect the kinetics of the surface reaction (but only for surface-reaction-limited deposition as described below). Insight into the surface reaction mechanisms may allow synthesis of new precursors or modification of operating conditions to provide new reaction pathways for improved selectivity and increased deposition rate. In tandem with these measurements, it is also important to know the dependence of film properties such as morphology, purity and resistivity on deposition conditions. This task is usually accomplished by analyzing films once they are deposited, although some in-situ techniques exist.¹⁰⁷ These measurements can also provide insight into the mode of reactor operation.

A problem with the rate measurements described above is that they can give large amounts of complex information which can be difficult to interpret. For example, complex variations of the rate with changes in the temperature and partial pressures of the various species are observed. A classic example is tungsten deposition with SiH_4 as a co-reactant. In this case, positive-, zero-, and negative-order WF_6 pressure dependencies can all be observed depending on the operating regime (see Ch. 3). Similar situations occur for CVD of Cu from Cu^{I} and Cu^{II} precursors (see Chs. 4 and 5). A further complication is that these variations are not necessarily directly related to the reactions occurring on the substrate surface; this is the case for feed-rate-limited or transport-limited deposition. Another complication is that various types of reactors have been used for CVD of metals in industry and in the laboratory for measuring the deposition rate as a function of temperature and partial pressures and for measuring film properties. Because of differences in geometry, reactant introduction, and other factors, inconsistent results are often obtained for the same precursor, making it difficult to compare results.

The following discussion interprets rate measurements from CVD reactors. Our goal is to clarify the data presented in Chs. 2 - 8 which report the results of measurements from a wide variety of reactors, precursors, and operating conditions. Only enough information is given here to introduce the reader to the concepts. Specialized texts on this subject are available for detailed equations, in-depth discussions of these and related concepts, and references to the literature.^{105-107,111,166,167}

9.8.1 Boundary Layers of Velocity, Temperature, and Reactant Concentration

The first step in understanding the qualitative behavior of CVD reactors is to know whether the reactor is operating in the molecular-flow or continuum-flow regime. In the molecular-flow regime [usually encountered during low-pressure CVD (LPCVD)], the gas mean free path is long compared to reactor dimensions, and collisions of molecules and atoms occur primarily with the walls of the reactor and the substrate. An average concentration can be defined based on the pressure, but the transport of the gas through the reactor is not governed by continuum-fluid-mechanics equations. For continuum flow [usually encountered with atmospheric-pressure CVD (APCVD)], the gas mean free path is much less than the reactor size and collisions occur primarily between gaseous species. In this latter case, the gas behaves like a viscous fluid and the variations of gas velocity, temperature, and species concentrations can be obtained from equations based on continuum theory.^{106,107,111,167}

The situation above can be quantified in terms of the Knudsen number (Kn), which is the ratio of the gas mean free path to a characteristic reactor dimension such as diameter. Molecular flow occurs where Knudsen numbers are much greater than unity, and

continuum flow occurs where Knudsen numbers are much less than unity. In terms of pressure, 10^{-3} torr (mean free path $\cong 5$ cm) is roughly the pressure at which the transition from the continuum regime to the molecular flow regime occurs at room temperature. This is also very roughly the dividing point between LPCVD and APCVD processes. Many CVD reactors are operated with $Kn \gg 1$ without carrier gas, while other systems are run at $Kn \ll 1$ with carrier gas or high-vapor-pressure precursors.

The distinction described above is critical because significant variations in reactant concentration, fluid velocity, and temperature cannot occur across the reactor when the Knudsen number is much greater than unity (which occurs at low pressures). In contrast, changes in these variables can occur in the direction transverse to the flow when the Knudsen number is much less than unity and the gas behaves as a continuous fluid. For variation to occur in the reactant concentration in directions transverse to the reactor axis, diffusion limitations must also exist. In cases where large wafers are used and the reactant concentration varies across the wafer, non-uniform deposition can occur (see Figs. 4-8, 4-17). Fortunately, the reactant concentration can be kept roughly constant throughout the reactor if the conversion of precursor to film is low, the rate of the surface reaction is sufficiently low, and the precursor transport rate in the gas is sufficiently high. As a result, it is often desirable to operate at low pressures and low conversions in order to obtain more uniform deposition on the substrate. This situation, however, also results in significant waste of the precursor, which is usually not recycled.

For continuum flow ($Kn \ll 1$), the variations in the species concentrations, gas temperature, and gas velocity are well understood both qualitatively and quantitatively. Figures 9-21, 9-22, and 9-23 show how these quantities can vary with position in a hot-wall tubular flow reactor.

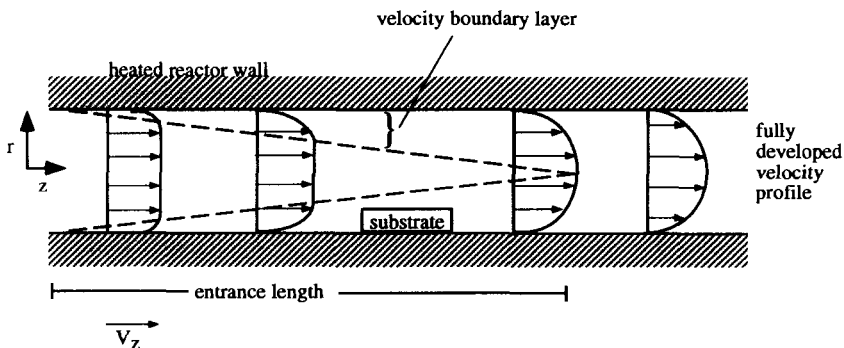


Figure 9-21 Development of velocity profiles along tubular flow reactor (length of arrows represents V_z). Boundary layer is region over which velocity, V_z , varies in radial direction r . After entrance length, velocity profile becomes parabolic and no longer changes along reactor.

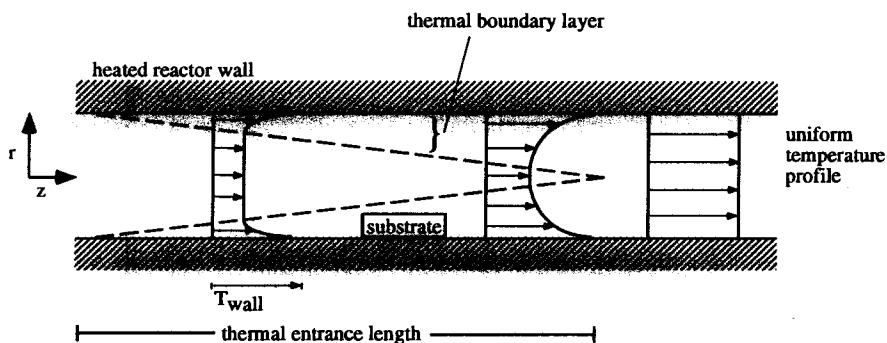


Figure 9-22 Development of temperature profiles along hot-wall tubular reactor (arrows indicate magnitude of temperature at a given axial location). After thermal entrance length, all of the gas has reached the wall temperature and no longer changes along the reactor.

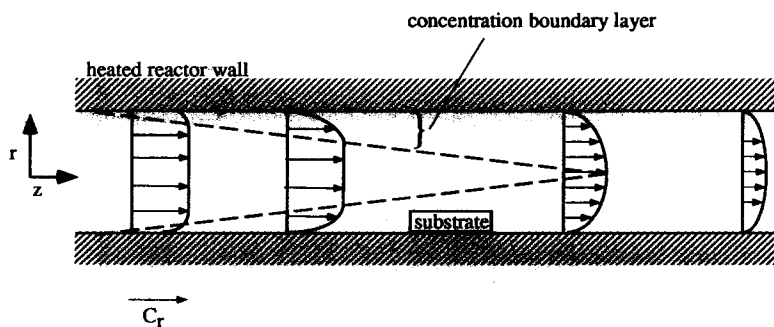


Figure 9-23 Development of reactant concentration, C_r , profiles along hot-wall CVD reactor (length of arrows indicates reactant concentration). For rapid surface reaction at reactor walls, concentration of reactant is zero at walls and reactant diffuses to walls, where it is consumed. For sufficiently long reactors, all reactant is consumed.

For $Kn \ll 1$, the velocity profiles (plots of the velocity vector as a function of position) can change with axial position (z) in the reactor (Fig. 9-21). As a result of its viscosity, the gas immediately adjacent to the surfaces of the reactor clings to the surfaces and does not move (the no-slip condition). Fluid close to the center of the reactor moves at a velocity dictated by the pressure drop through the reactor. This results in a velocity gradient, the so-called "boundary layer for velocity," the region over

which the velocity changes from zero at the walls to the velocity of the free stream. For a sufficiently long reactor, the effects of the walls are felt across the entire reactor cross section, and the gas reaches a velocity profile which does not change with position down the reactor. If complications due to free convection (movement of the gas due to density differences resulting from variations in temperature or species concentrations) are ignored, the velocity profile is parabolic for flow through a tube or between parallel plates (for sufficiently small Reynolds numbers).¹⁶⁸ The velocity profile, to a good approximation, does not depend on the concentrations of the various species in the system. The distance from the reactor entrance required to reach this constant velocity profile depends on gas viscosity, gas flow rate, and reactor diameter and is given by standard equations in fluid mechanics texts.¹⁶⁸

A thermal boundary layer can also be formed as the gas entering the reactor is exposed to hot surfaces for $Kn \ll 1$. Immediately after entering the tube, the gas next to the walls heats up, but not enough time (distance along the reactor) has passed for the gas further away from the walls to heat up, as shown in Figure 9-22. Further down the reactor, the heat has been transferred further into the gas as a result of the hot surfaces and the thermal conductivity of the gas. This results in the "boundary layer for temperature" which is the region near the hot surfaces over which the temperature varies from the inlet temperature to the wall temperature. For a sufficiently long reactor, the entire gas reaches the temperature of the walls and a constant temperature is obtained. The distance required to reach the final temperature (thermal entrance length) depends on the gas flow rate, gas thermal conductivity, and reactor diameter and is given by standard equations.¹⁶⁸

A concentration boundary layer or concentration gradient in the radial direction can also be formed in some cases for $Kn \ll 1$ (see Section 4.9.1). As reactant enters the reactor, the chemical reaction at the wall results in removal of the reactant and formation of reaction products (see Fig. 9-23). If the rate of this reaction is sufficiently rapid and transport from the middle of the reactor to the walls (rather than down the reactor tube) is sufficiently slow, the reactant concentration is nearly zero at the walls and increases with distance away from the walls into the flowing gas stream. As the gas flows down the reactor, more and more of the reactant is consumed by reaction at the heated surface and the distance into the gas over which the reactant concentration has been reduced by the reaction at the walls increases. As a result, the "concentration boundary layer" has a thickness that increases with distance along the reactor. A critical point is that a concentration boundary layer does not exist under all conditions, even for $Kn \ll 1$. If the rate of the reaction is sufficiently slow and transport of the reactant in the radial direction to the surface is sufficiently rapid, then no concentration boundary layer will exist, although the reactant concentration can decrease along the reactor. The distance required to consume all of the reactant for the case of diffusion-limited deposition (rapid reaction) depends on the gas flow rate, reactant/carrier gas diffusion coefficient, and reactor diameter and is given by standard equations.¹⁶⁸

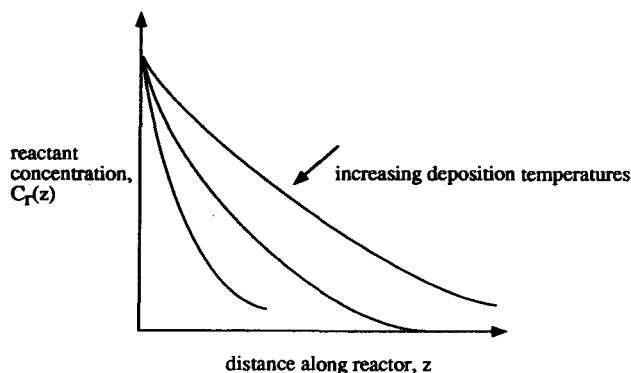


Figure 9-24 Change in reactant concentration along hot-wall reactor.

In the case of a hot-wall reactor where chemical reaction occurs on the walls, the average reactant concentration may decrease along the reactor as shown in Figure 9-24 (see also Figs. 4-8, 4-17). As reactant flows down the reactor, it is consumed by reaction at the walls. This can occur for reaction-limited, diffusion-limited and feed-rate-limited deposition. It can occur at low ($Kn \gg 1$) as well as at high ($Kn \ll 1$) pressures. Figures 9-24, 4-8, and 4-17 illustrate the importance of the position of the substrate in the reactor. Because the reactant concentration (and temperature in the case of temperature gradients along the reactor length) may vary with position, the deposition rate will vary depending on the location of the substrate in the reactor. This is a critical problem with hot-wall reactors when the conversion of the precursor is high and most of the precursor is consumed near the reactor entrance. In applications, the temperature can be increased along the reactor to compensate for the decrease in reactant concentration thereby maintaining a constant deposition rate.

The qualitative outline of the behavior of the temperature, velocity, and reactant concentration presented above shows that different behavior will be observed with different reactors using the same precursors, depending on the geometry of the reactor, the gas flow rate, pressure and other factors. This problem can be mitigated by using well-designed reactor systems. For example, the concentration boundary layer and the reduction in reactant concentration along the reactor can be eliminated by operating at sufficiently low reaction rates and pressures. The temperature and velocity boundary layers can also be eliminated by operating at low pressures, or the reactor can be designed with a sufficiently long region before the deposition zone to allow the temperature and velocity profiles to reach their fully developed, known values. Therefore, it is possible to design hot-wall and cold-wall CVD reactors with well-defined and controlled temperatures, velocities, and reactant concentrations that are suitable for measurements of the kinetics of surface reactions. Lee discusses the design of such CVD reactors for measurement of the intrinsic reaction kinetics.¹⁶⁷

It must be mentioned that, although the discussion above has referred primarily to hot-wall reactors, the same concepts apply to cold-wall reactors with other geometries. Feed-rate-limited, surface-reaction-limited, and diffusion-limited deposition can all occur, as can boundary layers of velocity, temperature and reactant concentration for the cold-wall reactor (Fig. 9-25). The only difference between the hot- and cold-wall reactors is the shapes of the velocity, temperature, and concentration profiles.^{107,168}

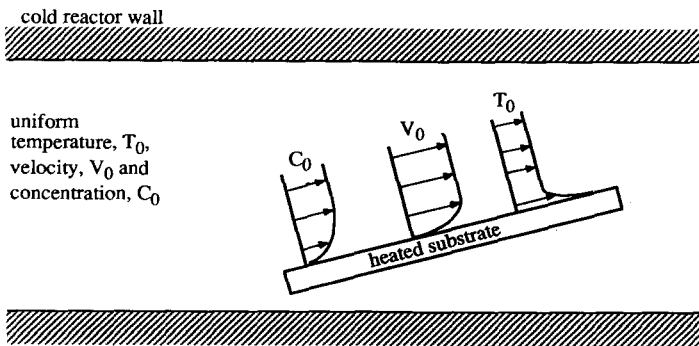


Figure 9-25 Reactant concentration, velocity, and temperature profiles for cold-wall reactor with inclined, heated substrate. Profiles change in direction along substrate in a manner similar to that shown in Figures 9-21 to 9-23. Inlet gas has reactant concentration C_0 , velocity V_0 , and temperature T_0 .

9.8.2 Feed-Rate-, Surface-Reaction-, and Diffusion-Limited Deposition

A major concern for the design and operation of CVD reactors is the dependence of the deposition rate on operating variables (Fig. 9-26). For conventional delivery systems, the deposition process involves a series of three steps: (1) introduction of precursor vapor, (2) transport of precursor to the surface of the substrate, and (3) surface reaction of the precursor. Because these steps are in series, the slowest step will limit the overall rate, and three cases are possible. In this section, this problem is quantified. This problem is also discussed in Chapter 4, Sections 4.5 and 4.9. For aerosol delivery, precursor vaporization occurs after step (2) and can also be rate-limiting.

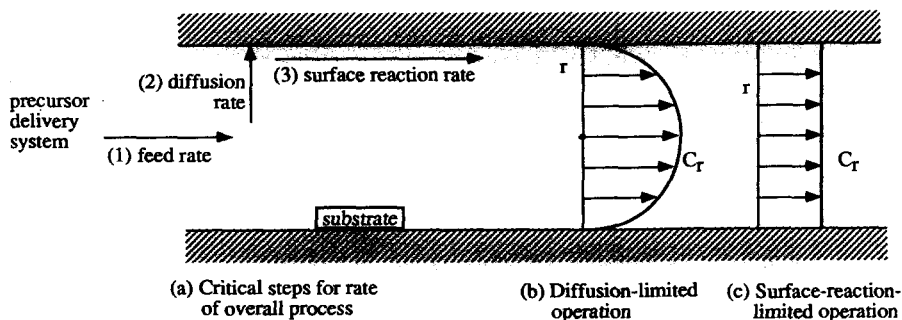


Figure 9-26 Critical steps for deposition which may limit the overall rate. (a) Deposition rate determined by three steps in series, the slowest of which limits the overall rate. (b) For diffusion-limited operation, a concentration (C_r) gradient exists for the reactant in the radial direction r . (c) For surface-reaction-limited operation, reactant concentration is uniform in the radial direction, r .

The maximum deposition rate under any circumstances is given by Equation 9.13.

$$\text{rate} = \frac{\alpha P_s v_m}{\sqrt{2\pi m_r k_B T}} = \frac{\alpha_0 P_s v_m \exp(-E_A / RT)}{\sqrt{2\pi m_r k_B T}} \quad (9.13)$$

where rate = deposition rate, cm/sec

α = fraction of reactant molecules that react after striking surface, dimensionless

P_s = precursor partial pressure immediately above surface, dynes/cm²

v_m = volume of depositing metal atom, cm³

m_r = molecular mass of precursor, g

k_B = Boltzmann's constant, 1.38×10^{-16} ergs/molecule K

T = temperature of gas above substrate, K

α_0 = constant, dimensionless

E_A = activation energy, ergs/mol

R = gas constant, ergs/(mol K)

The quantity $P_s / \sqrt{2\pi m_r k_B T}$ is the flux of reactant to the substrate surface (collisions/(cm²sec)). The quantity v_m converts the flux to units of deposition rate (cm/sec). The parameter α takes into account the details of the adsorption-desorption-reaction phenomena and depends exponentially on temperature. The maximum value of

α is 1 and is achieved when every collision results in reaction. Equation 9.13 predicts that approximately 1 monolayer (roughly 1 Å of metal) can be deposited every second at 10^{-6} torr if $\alpha = 1$. At 10^{-2} torr, 10,000 monolayers per second and at 1 torr, 10^6 monolayers per second can be deposited. In most cases, $\alpha \ll 1$, and the actual deposition rate is much lower than the values mentioned above. The parameter α is also important because values of α near unity result in poor conformality.¹⁶⁷ Conversely, values of α much less than unity provide conformal deposition.

The value of α can be controlled through precursor design. At a given temperature, precursors with lower decomposition temperatures will have higher values of α . Therefore, conformality can be improved by using precursors that are more thermally inert but at the expense of lowering the deposition rate.

For diffusion-limited deposition, the precursor pressure at the surface, P_s , is much lower than the pressure of the precursor in the main gas stream outside the concentration boundary layer (see Fig. 9-23). For this case, the deposition rate is again reduced below the maximum possible value.

9.8.2.1 Feed-Rate-Limited CVD

The case of feed-rate-limited deposition is often encountered for precursors with low vapor pressures under conditions where the reactant conversion is high. In this case, with no diffusion limitation, the local deposition rate is given by Equation 9.13. This is usually observed with low-pressure hot-wall reactors where diffusion is rapid, but the surface area for reaction is large (see Ch. 4). This phenomenon can also occur in cold-wall reactors (see Ch. 5). For a given system and operating conditions, it can be determined whether the deposition rate is feed-rate-limited by estimating the fraction of the precursor consumed by the reaction. This is accomplished by measuring the growth rate and the deposition area to get the total rate of precursor consumption by reaction. It is then compared to the rate at which the precursor is delivered into the reactor. If the fraction (precursor reacted/precursor introduced) is near unity, and little precursor exits the reactor, feed-rate-limited deposition is occurring.

Assuming all of the reactant decomposes on the heated area and assuming only one metal atom is present in each precursor molecule, the deposition rate is given by:

$$\text{rate} = F M_m / (A \rho) \quad (9.14)$$

where rate = deposition rate, cm/sec

F = feed rate of reactant, moles/sec

M_m = atomic weight of depositing metal, g/mole

A = heated area over which deposition takes place, cm^2

ρ = density of depositing metal, g/cm^3

Equation 9.14 suggests that the deposition rate will decrease as the area A , over which deposition occurs, is increased, as long as all other parameters remain constant. This is a problem in hot-wall reactors where a large surface area exists that is heated to the same temperature as the substrate. This is one reason why cold-wall reactors usually provide much higher deposition rates than hot-wall reactors.

Numerous examples of feed-rate-limited deposition are found in Chapters 4 and 5. A key feature is that the deposition rate does not depend on the temperature of the substrate in this operating regime, as discussed in Section 9.8.3.2. The (potential) rate of the surface reaction is much higher than the rate at which precursor is delivered to the reactor. As a result, the delivery rate limits the overall deposition rate. Feed-rate-limited deposition has been reported for LCVD of Au using $\text{Me}_2\text{Au}(\text{hfac})$ ¹⁶⁹ and for UHV CVD of Au from RAuPMe_3 .¹⁵ It has also been reported for CVD of Cu from $(\text{hfac})\text{CuL}$.⁸⁻¹⁰

9.8.2.2 Diffusion- and Surface-Reaction-Limited CVD

The overall deposition rate may be limited by the rate of the surface reaction if the feed rate is sufficiently high that it does not limit the deposition rate and diffusion (transport) limitations do not occur. This situation is obtained with high precursor throughputs at low pressures and low substrate temperatures. Numerous examples of surface-reaction-limited deposition are found in Chapters 2 through 8. At high pressures and temperatures corresponding to high reaction rates and slow transport of the reactant to the surface, transport-limited (diffusion-limited) deposition can occur (Fig. 9-25).

The rate of deposition without limitations imposed by the feed-rate or precursor-droplet vaporization can be quantified.¹⁶⁷ The description below is not adequate to quantitatively describe CVD processes, but it describes the overall qualitative dependence of the rate on the relevant parameters. The analysis assumes a first-order surface reaction written in terms of the gas-phase concentration of the reactant at the surface. It also assumes diffusion through a concentration boundary layer of known thickness. The overall process consists of two steps in series: diffusion to the surface and surface reaction. The rate of diffusion of precursor to the surface in terms of the flux (molecules/cm²sec) is given by:

$$\text{rate of diffusion} = \frac{D}{L} (C_r - C_s) \quad (9.15)$$

The rate of the surface reaction (molecules/cm²sec) is given by:

$$\text{rate of surface reaction} = kC_s \quad (9.16)$$

Equating the two rates, solving for C_s , substituting into the expression for the rate of the surface reaction, and multiplying by the volume of a deposited metal atom (v_m) gives the rate (cm/sec)¹⁶⁷

$$\text{rate} = \frac{C_r v_m}{1/k + L/D} \quad (9.17)$$

$$\text{rate} = kC_r v_m = k_0(P_r/RT)v_m \exp(-E_A/RT) \quad \text{for } k \ll D/L \quad (9.18)$$

$$\text{rate} = \frac{v_m D C_r}{L} = \left(\frac{v_m D_0}{L} \right) \left(\frac{P_0}{P} \right) \left(\frac{T}{T_0} \right)^{\frac{3}{2}} \left(\frac{P_r}{RT} \right) \quad \text{for } k \gg D/L \quad (9.19)$$

where $D = D_0 \left(\frac{P_0}{P} \right) \left(\frac{T}{T_0} \right)^{\frac{3}{2}}$ = diffusion coefficient, cm²/sec

- D_0 = diffusion coefficient at reference conditions, cm²/sec
- L = thickness of the concentration boundary layer, cm
- k = surface reaction rate constant, cm/sec
- C_r = reactant concentration outside concentration boundary layer, molecules/cm³
- C_s = reactant concentration immediately above substrate, molecules/cm³
- k_0 = pre-exponential constant, cm/sec
- T_0 = reference temperature for gas above substrate, K
- P = total pressure, dynes/cm²
- P_0 = total pressure at reference conditions, dynes/cm²
- P_r = reactant partial pressure outside concentration boundary, dynes/cm²

For large k ($k \gg D/L$), the surface reaction is rapid and the rate is given by $v_m D C_r / L$, corresponding to a diffusion-limited process. This expression corresponds to the rate of diffusion of the reactant through the concentration boundary layer discussed above (see Fig. 9-23). For a slow reaction rate ($k \ll D/L$) or rapid diffusion in the gas phase (large D or small L), the rate is $k C_r v_m$, which is simply the rate of the surface reaction corresponding to surface-reaction-limited deposition. Diffusion-limited LCVD of Au has been reported.^{169,170} Photochemical LCVD can also exhibit a diffusion-limited rate.¹⁷¹ Examples of diffusion-limited CVD of Cu are also documented.¹⁷²

Precursor design influences the overall rate through the surface-reaction-rate constant, k , and the reactant concentration, C_r , which can be no higher than the value corresponding to the vapor pressure. Reactor operating conditions influence the overall

rate through D and L , which depend on a variety of parameters which include the temperature of the gas, the total pressure, carrier gas flow rate and properties, and reactor geometry. The sections below discuss the pressure and temperature dependencies of the deposition rate predicted by these expressions.

9.8.3 Pressure and Temperature Dependencies of Rate

9.8.3.1 Reactant Partial Pressure Dependence of Rate

In most cases, as the reactant concentration is increased, the deposition rate increases, as shown in Figure 9-27 (see also Figs. 4-9, 4-10, and 4-11). Above a critical reactant concentration and temperature that depend on the reactivity of the precursor and reactor operating conditions such as total pressure, gas-phase reaction can occur and result in particle formation and reactant depletion leading to a reduced deposition rate.¹⁷³ This has been reported for a wide variety of systems as discussed below (see also Sections 4.5.3 and 4.5.4).

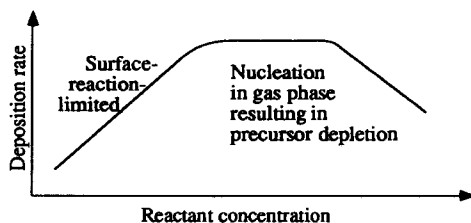


Figure 9-27 Possible dependence of deposition rate on reactant concentration when gas-phase particle formation occurs.

For feed-rate-limited deposition, the rate does not depend on the precursor partial pressure or total pressure at a constant feed rate (Eq. 9.14 and Fig. 9-28). Therefore, increasing the total pressure while keeping the precursor feed rate constant has little effect on the rate. A test for this limit is to increase the feed rate while keeping all other parameters (total pressure, precursor partial pressure, temperature, etc.) constant while avoiding diffusion-limited deposition (which can be influenced by changes in gas flow rate). If the deposition rate increases, then the feed rate is the limiting factor.

For the case of diffusion-limited deposition, the rate is first order in reactant concentration, as shown by Equation 9.19 above. Doubling the pressure of the precursor doubles the rate of the reaction. This effect is sometimes mistakenly interpreted as

surface reaction-rate dependence on the precursor partial pressure to the first power (Eq. 9.18). A first-order dependence can be observed for diffusion-limited deposition regardless of the pressure dependence of the surface reaction as long as the surface reaction is sufficiently rapid. An indicator of diffusion-limited deposition is that increasing the total pressure while keeping the partial pressure of the precursor constant decreases the rate because the diffusion coefficient is inversely proportional to the total pressure, P . Another test for diffusion-limited deposition is to vary the gas flow rate while keeping reactant concentration constant (C_r or P_r). Varying the flow rate can result in variations in L , the thickness of the concentration boundary layer, which leads to changes in the deposition rate. Yet another test is to vary the carrier gas (He, N_2 , Ar), while keeping other conditions fixed (see Eq. 9.17),¹⁶⁸ which varies the diffusion coefficient D through the influence on D_0 . However, one of the best and most conclusive tests is to vary the substrate temperature as discussed below.

The conditions required for diffusion-limited deposition are also those that favor homogeneous reactions in the gas phase which can lead to particle formation. If particles are formed, the rate can decrease as the concentration of the reactant is increased, because the particles formed provide surface area in the gas phase on which CVD can occur to consume the reactant and reduce its concentration (Fig. 9-27 and Section 9.9). This problem is well documented in the literature and is described in Section 9.8.

The case of surface-reaction-limited deposition is the only case for which the kinetics of the surface reaction can be observed (Eq. 9.18). The details of the surface reaction then determine the precursor-pressure dependence of the rate, which can be first order in some cases or can be more complex than the first-order reaction used here as an example. For example, deposition of Cu from (hfac)Cu(VTMS) exhibits a pressure dependence which varies as a function of temperature and precursor partial pressure (Ch. 5).¹⁰ The rate of tungsten deposition from WF_6 also has a complex pressure dependence and can even be negative order in WF_6 partial pressure (Ch. 3).³⁶ In this regime, the partial pressures of reaction products can also influence the rate (see Fig. 4-8), but this effect has not been studied extensively for the precursors discussed in this book. Because a first-order dependence on precursor partial pressure can be observed for both surface-reaction-limited and diffusion-limited deposition, the best test for surface-reaction-limited deposition is to vary the substrate temperature and look for an exponential dependence of the deposition rate on the temperature.

9.8.3.2 Temperature Dependence of Rate

Feed-rate-limited deposition usually provides a rate with a weak temperature dependence (Eq. 9.13 and Figs. 9-28 and 2-5). Increasing the surface temperature does not result in an increase in the rate, which can be no faster than the rate of delivery of the precursor into the reactor.^{10,15} A positive or negative order dependence of the rate on temperature can also occur if the reaction occurs in a hot-wall reactor and deposition

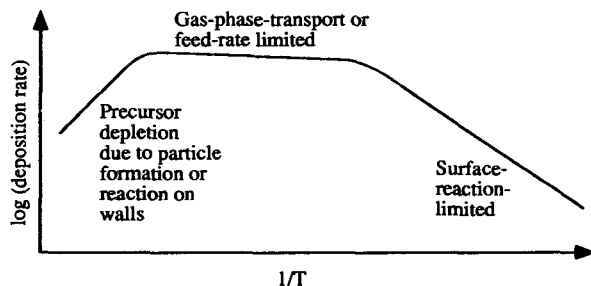


Figure 9-28 Dependence of deposition rate on temperature.

occurs on the walls. In this case, increasing the temperature can result in deposition closer to the reactor inlet. Depending on the location of the substrate, this change may result in more deposition on the substrate if the region of highest deposition rate moves closer to the substrate or less deposition if this region moves away from the substrate.

For diffusion-limited deposition, the rate depends only weakly on the temperature primarily through the temperature dependence of the diffusion coefficient (see Eq. 9.19 above) which is roughly $T^{3/2}$.¹⁶⁸ This dependence¹² is far weaker than the exponential dependence of rate on temperature observed for surface-reaction-limited deposition (see Eq. 9.18 and Chs. 4 and 5) and is nearly flat when plotted on a logarithmic scale. In addition, for diffusion-limited deposition, the precursor concentration at the surface is nearly zero and is not the same as the measured precursor partial pressure. This occurs because the potential rate of the surface reaction is rapid relative to the rate of transport to the surface.

Surface-reaction-limited deposition has a temperature dependence that varies with the details of the surface reaction (see Section 4.5.2). The deposition rate often increases as the substrate temperature is increased at low temperatures and low reactant concentrations, as shown in Figure 9-28 (see Figs. 4-7, 5-8, 6-4, 7-6). In the surface-reaction-limited regime, it is possible to measure the kinetics of the surface reaction and a rate increase as a function of temperature according to the Arrhenius relationship (Eq. 9.18). Also, the reactant concentrations at the substrate surface are often known because they are the same as the overall concentrations in the reactor if precursor conversion is low (Fig. 9-26). However, reactant concentrations can be difficult to measure if the precursor has a low vapor pressure and a carrier gas is used.

Finally, as the substrate temperature is increased, gas-phase particle formation may occur which depletes the reactant concentration in the gas phase and reduces the rate.¹⁰³ Alternatively, the reduction in the rate may be due to the rapid desorption of the precursor from the surface before reaction can occur. This behavior leads to the classical plateau in the deposition rate as a function of temperature, as shown in Figure 9-28.

There are other systems which can provide the same dependence of rate on temperature as that shown in Figure 9-28. Using aerosol delivery of precursors as shown in Figure 9-20, surface-reaction and diffusion-limited deposition have been observed.¹⁴⁷ However, due to thermophoresis, at higher temperatures the rate decreased because droplets did not approach the heated substrate as closely compared to lower temperatures.¹⁷⁴ This led to less vaporization of the precursor in the heated gas near the substrate surface and a lower deposition rate.

When aerosol-assisted CVD is used, it is possible to observe a substrate temperature dependence for the overall deposition rate which corresponds to that for the precursor vaporization (ΔH_{vap}). In this case, the deposition rate is limited by the rate of vaporization of the precursor from the aerosol particles. As the substrate temperature is increased, the gas above the substrate is heated to higher temperatures leading to a higher precursor vapor pressure and a higher vaporization rate. This precursor-vaporization-limited process has been observed for copper CVD with aerosol delivery.¹⁴²

The brief analysis above is an introduction to problems that may occur in CVD reactors. Other problems are discussed in detail elsewhere^{105-107,111,166,167} and are mentioned only briefly here. Loading effects can occur in which the deposition rate depends on the wafer surface area available for reaction; increasing the reaction area can lead to lower deposition rates because less reactant is available per unit area of wafer. This is a key difference between cold-wall or warm-wall reactors with small heated areas and hot-wall reactors with large heated areas. This effect is also important when deposition occurs on the walls of hot-wall reactors and the area covered by the deposit changes with time during a run. A similar effect can also arise when comparing CVD under selective and non-selective (blanket) conditions because the growth area is higher for blanket CVD.

There are a variety of other complications which can arise during CVD. Slow deposition rates are often the result of reactant depletion during transport through hot-wall reactors (see Chs. 4 and 5), gas-phase particle formation which consumes precursor (see section below), transport limitations in the boundary layer above the substrate, feed rate limitations resulting from low precursor vapor pressures, or slow surface reaction rates resulting from high precursor reaction temperatures and low reactor temperatures (discussed in the next sections). Temperature non-uniformities on a substrate can lead to non-uniform film thickness, especially when operating in a surface-reaction-limited regime. This occurs because the deposition rate depends exponentially on temperature in this regime (see Eq. 9.18). This is less of a problem in hot-wall systems, which tend to provide more uniform temperatures than cold-wall reactors. It is also less of a problem when the reactor is operated in a diffusion-limited regime because of the relatively weak temperature dependence of the rate (see Eq. 9.19). However, flow non-uniformity (see Fig. 2-4) can lead to non-uniform deposition especially when precursor depletion along a hot-wall reactor is important.¹⁰⁷ Irreproducible results are often caused by desorption

of precursors and reaction products adsorbed on cold surfaces (such as the inlets and outlets of reactors) and are often a problem in cold-wall systems when the temperature in the reactor is changed. Irreproducible results may also be due to variable precursor delivery rates, changing conditions in the reactor such as the area over which reaction occurs in hot-wall reactors, impurities being generated in the delivery system due to decomposition of the precursor, substrate preparation methods, and varying position and temperature of the substrate from run to run. Other problems include thermodynamic constraints on the conversion of reactants to products.

9.9 Homogeneous Gas-Phase Reactions and Particle Formation

9.9.1 Particle Formation During CVD

Particle formation during CVD has been observed in a wide variety of CVD systems and can lead to decreasing deposition rates as the substrate temperature and reactant concentration are increased (Section 2.6.8 and Figs. 9-27, 9-28). In addition, particle formation can lead to contamination of wafers during integrated circuit manufacture. This has motivated studies of particle formation in CVD reactors.¹⁷⁵⁻¹⁸⁰ Formation of Al particles has been observed (see Ch. 2),^{181,182} and the disproportionation of (hfac)Cu(VTMS) has been observed in the gas phase.¹⁸³ The precursors Co(η^5 -C₅H₅)(CO)₂, Co₂(CO)₈, and Co(CF₃)(CO)₄ all undergo gas-phase reactions at atmospheric pressure, leading to decreases in the deposition rate (Ch. 8).^{34,35} This phenomenon has also been observed repeatedly for CVD of SiO₂,¹⁸⁴⁻¹⁸⁶ Si,¹⁸⁷⁻¹⁹¹ GaAs,¹⁹² metal tellurides,¹⁹³ metal selenides,¹⁹⁴ metal carbides,¹⁹⁵ metal nitrides^{23,196} and other materials.¹⁷³ The problem occurs because the reactants flowing through the CVD reactor are heated by the gas that is itself heated when it contacts the hot reactor walls or substrate (see Fig. 9-22). The high temperature drives gas-phase reactions of the precursors which produce particles. This problem is aggravated when a co-reactant is used which can react with the precursor. Examples are the reactions of WF₆ and SiH₄ (Ch. 3) and Ni(CO)₄ and H₂ (Ch. 8). Plasma reactors are particularly susceptible to particle formation due to the formation of highly reactive intermediates in the gas phase.

Examples of the types of systems and conditions for which particle formation has been observed during CVD are listed in Table 9-5.^{181,182,184-197} These results have shown that particle formation and a corresponding decrease in the deposition rate occur

Table 9-5 Particle Formation During CVD

Material	Precursor(s)	Notes	Ref.
Al	Me ₂ EtNAlH ₃	T _s = 180 °C; trace amounts of CO, H ₂ O, and O ₂ increased particle formation	182
Al ₂ O ₃	AlCl ₃ , H ₂ , CO ₂	Hot-wall reactor	181
TiO ₂	Ti(O- <i>i</i> -Pr) ₄	Increased temperature led to particle formation and decreased rate when particle formation occurred	197
Si	SiCl ₄	HCl depressed particle formation up to rates of 40 μm/min	187
Si	SiH ₄	Particles formed above critical concentration of SiH ₄ when T = 1050 °C	188
Si	SiH ₄	Particles formed above critical SiH ₄ concentration at constant temperature; Low-pressure CVD reactor; T = 1100 °C	189,191
Si	SiH ₄	Particles formed above 725 °C and critical concentration of SiH ₄ ; Low-pressure CVD reactor	190
SiO ₂	N ₂ O-SiH ₄ (He-diluted)	Particle formation at partial pressure of reactants of 130 Pa. T _s = 230 °C; Parallel-plate PECVD reactor	184
SiO ₂	SiH ₄ with O ₂ and Ar	Total pressure below 100 mtorr; Gas-cooled system; T _s = 40 - 50 °C; Post-type rf magnetron PECVD reactor	185
SiO ₂	TEOS (tetraethylortho-silicate)	Particles formed over 740 °C; Amorphous particles formed from 740 - 800°C ; Hot-wall APCVD reactor	186
GaAs	GaMe ₃ , AsH ₃	Particles formed above 750 °C; Deposition rate decreased	192
Cd _x Hg _{1-x} Te	TeEt ₂ , CdEt ₂ , Hg	Particles formed with H ₂ carrier gas; Photo-CVD	193

Table 9-5 (continued)

Material	Precursor(s)	Notes	Ref.
TiC	TiCl ₄ , C ₃ H ₈ , H ₂	Particles formed above 950 °C; Deposition rate decreased	195
BN	B(C ₂ H ₅) ₃ , NH ₃	Particles formed above 1000 °C; Deposition rate decreased	196
ZnSe	ZnMe ₂ + H ₂ Se	Lower pressures eliminated particle formation	194

above a critical temperature and reactant concentration which depend on the total pressure, precursor characteristics, and reactor design. These trends are supported by the theoretical analyses.

In many systems of practical importance, the upper limit on the deposition rate, as shown by theoretical studies,¹⁹⁸⁻²⁰³ can be fixed by the onset of particle formation. Qualitatively, particle formation can be suppressed by using lower pressures, shorter transport distances to the substrate, and lower rates of homogeneous gas-phase reaction of the precursor relative to heterogeneous reaction on the surface. The latter is favored by the use of cold-wall reactors, where the volume of gas heated by the substrate is far lower than in hot-wall reactors. A lower pressure gives a higher rate of transport of the reaction products to the surface, reduces the gas-phase concentration of these species, and reduces the interactions that produce particles. This approach is only feasible when a carrier gas is being used so that the carrier gas partial pressure can be reduced while keeping the precursor partial pressure constant. Under these conditions, higher deposition rates can be achieved before particle formation occurs in the gas phase. A shorter transport distance to the substrate through the heated gas (favored by use of cold-wall reactors in which only the gas above the substrate is heated) results in more rapid removal of the gas-phase reaction products from the surface.¹⁹⁸ This reduces the concentration of these species in the gas phase and reduces the driving force for particle formation. This approach can be used where it is feasible to reduce the dimensions of the system. The last approach involves design of precursors and use of co-reactants that have reaction pathways that are not favorable in the absence of a surface. This approach has been largely empirical, and has not been studied in a systematic manner. Particle formation has also been observed with aerosol delivery of precursors.¹⁷⁴

The intentional formation of particles from CVD precursors has been studied in an effort to understand the conditions required for particle formation. These studies have usually been carried out in hot-wall reactors that are identical to CVD reactors except that no substrate is present. Metal halides such as TaCl₅, MoCl₅, and others have been reacted in the gas phase to give small metal particles.^{103,204} However, the majority of

studies have examined the formation of metal oxides, nitrides, carbides, and borides.^{103,104} Laser-induced metal particle formation has been observed for the reactions of the metal carbonyls of Fe and Mo.²⁰⁵⁻²⁰⁸ Many more cases of laser-induced particle formation have been observed for materials such as Si.²⁰⁹ The results of these studies qualitatively support the generalizations made above in that decreasing total pressure, decreasing reaction rate in the gas, and decreasing the dimensions of the system minimize particle formation.

9.9.2 Simultaneous Particle Deposition and CVD

Particle formation and deposition during CVD has been used as a method for increasing the deposition rate. This approach has not been used for metals but has been used for many other materials. In one approach, the particles deposit by settling due to gravity.²¹⁰ In other cases, the systems are designed to provide a temperature gradient towards the substrate, which drives the particles onto the substrate by thermophoresis.¹⁰⁹ The precursor is introduced near the heated substrate and kept away from the hotter surface, which is used to provide the temperature gradient in the gas phase that drives the particle towards the substrate. This process, particle-precipitation-aided CVD, has been used to form films of TiO₂,²¹¹ AlN,²¹² and TiN²¹³ at rates of 10-1000 $\mu\text{m/hr}$. These rates are much higher than those obtained with conventional CVD processes. Examples of this approach are listed in Table 9-6.²¹⁰⁻²¹⁴

Table 9-6 Simultaneous Particle Deposition and CVD

Material	Precursor(s)	Notes	Ref.
SiC	MeSiCl ₃ + H ₂	T _s = 1550-1620K 10 $\mu\text{m/min}$	210
TiN	TiCl ₄ , H ₂ , NH ₃	T _s = 923-1173 K 10-1000 $\mu\text{m/hr}$	213
AlN, TiO ₂ , ZrO ₂	Zr(C ₈ H ₇ O) ₄ , AlCl ₃ , Ti(O- <i>i</i> -Pr) ₄	T _s = 700-1300 K	212
AlN	AlCl ₃ , NH ₃	T _s = 998-1161 K 100 nm/sec	212
TiO ₂	Ti(O- <i>i</i> -Pr) ₄	T _s = 623 K 30 nm/sec	211
Ag, BaTiO ₃ , YIG, YBa ₂ Cu ₃ O ₇	Assorted metalorganics such as β -diketonates	Flame reactor T _s not specified	214

The theory of particle deposition is well understood.^{109,164} The thermophoretic velocity for ambient conditions with a 100 K/cm gradient is greater than the settling velocity for particles less than 1.0 μm in diameter.¹⁰⁹ Thermophoretic velocity, however, is not a strong function of particle size, so particles of all sizes can be deposited if a sufficient temperature gradient is supplied. The thermophoretic velocity can be much greater than the diffusion velocity, which is usually slow due to the low diffusion coefficients of aerosol particles.¹⁰⁹

Droplets and particles can also deposit onto substrates and hot surfaces by impaction. Particles directed with sufficient initial velocity towards a surface can impact because their inertia does not allow them to follow the gas flow around the substrate.¹⁰⁹ Impaction is only important when a nozzle near the surface is used to direct the aerosol particles at the surface at a high velocity and the particles are sufficiently large. Particles or droplets much smaller than 100 μm cannot easily be deposited by impaction unless small nozzles are used or the pressure is reduced. This problem is important in aerosol delivery of precursors (see Section 9.5.3), where droplets are directed at a substrate and the solvent and precursor must evaporate before reaching the substrate.

Gravitational settling of particles can be an important mechanism for particle deposition and has been used together with CVD to produce films.²¹⁰ The terminal settling velocity of aerosol droplets or particles is given by standard expressions.¹⁰⁹ The settling velocity for a unit-density 10 μm particle is 0.3 cm/sec, which is usually negligible relative to the velocity of the gas stream. However, particles with diameters on the order of 100, 500 and 1000 μm have settling velocities of 25, 200, and 390 cm/sec, respectively. As a result, particles smaller than 1.0 μm move with the gas rather than fall through it, while particles larger than 10 μm have appreciable settling velocities and can strike the surface before leaving the reactor. For example, Allendorf et al.²¹⁰ used solid 30 μm particles with densities many times that of water for gravitational settling with CVD. This phenomenon is again of importance in aerosol delivery where droplet deposition must be avoided.

Diffusion of particles is a mechanism by which only very small particles deposit on surfaces. The reason is that diffusive deposition of particles depends on the value of the diffusion coefficient of particles, and diffusion coefficients of particles larger than roughly 0.01 μm are so small (5×10^{-4} cm^2/sec for 0.01 μm particle) that this mechanism is only effective for very small (< 0.01 μm) particles for most situations. Deposition of small clusters (particles less than 10 Å) by diffusion has been suggested to play an important role in CVD of GaAs.^{200,202,203} However, the role of cluster diffusion in CVD of metals has not yet been identified in the literature.

9.10 Conclusions and Future Directions

We have summarized some general aspects of the CVD of metals. In spite of the large amount of work on CVD of metals, the behavior of many simple precursors has not been examined in detail. The CVD of W, Al, and Cu is the most studied; that of Mo, Pt, Pd, Ni, Ag, Rh, Ir and Au has been studied to a lesser extent. Most of the other metals have only been studied superficially. Several major conclusions can be drawn from the material in this book:

- **Precursor Design**

The most commonly used precursors are metal halides, alkyls, carbonyls, cyclopentadienyls, and β -diketonates, but these are only suitable for some metals. Good precursors are available for CVD of W, Al, Cu, Mo, Rh, Pt, Pd, Ni, Ag, and Au. Many other metals do not have precursors which allow low-temperature deposition of high-purity films at high rates. This is true for Ti, which is important in the microelectronics industry. Single-source precursors have been examined in a few cases, but the benefits of controlled composition and homogeneity have yet to be clearly demonstrated. In most cases, adequate deposition rates have not been obtained.

Precursor design must be carefully matched to a given set of CVD reactor conditions to achieve high-purity films. It is important to measure vapor pressures quantitatively to allow estimates of transport rates.

- **Precursor Delivery**

Improved methods of precursor delivery are necessary to enable the use of low-vapor-pressure precursors and to deliver precursors to substrates under controlled, reproducible conditions. Liquid delivery systems are promising in this regard.

- **Reactor Design and Operation**

Better reporting and characterization of deposition conditions and substrate pretreatment are necessary to compare reports of blanket CVD and selective CVD from different groups of investigators. Quantification of reactor by-product distributions from hot-wall CVD reactors and kinetic data from cold- or warm-wall CVD reactors is necessary. Insufficient information is given in most cases to determine the mode of reactor operation; i.e., surface-reaction-limited, feed-rate-limited, or transport-limited. The understanding of gas-phase chemistry which can lead to particle formation and reduced deposition rates is poor.

- **Film Characterization**

The CVD of high-purity films of a variety of metals has been reported. Deposition rate, thickness, resistivity, and morphology are simple to determine and should be

reported even when film purity cannot be determined for lack of equipment. In many cases it is not possible to evaluate the success of the CVD study because the resulting films are poorly characterized.

- Selective CVD

An understanding of methods to control selectivity is just emerging. Major factors are control of the properties of the growth and non-growth surfaces and tailoring the precursor chemistry where possible. From the data available, it appears that the most reproducible method to obtain selective CVD for a given precursor is to control the functionality of the substrate surface.

- Surface Chemistry

Surface reaction mechanisms and reaction products are only known in a few cases, primarily for precursors to W, Cu and Al films. The measurements of the surface reaction kinetics made for most systems are very limited, and the apparent activation energies for surface reactions are known for only a few precursors and surface compositions. Further work is needed to understand the reaction chemistry involved, which may lead to better strategies for blanket and selective CVD. The extrapolation of chemistry observed under UHV conditions to chemistry proposed under CVD reactor operating conditions should be made with caution.

Acknowledgments: The authors thank Judith Binder for her extensive and careful technical editing of this chapter. We also appreciate the numerous suggestions and useful additions of the following students: Leo Archer, Clive Chandler, James Caruso, Tom Corbitt, Steve Drees, David Gallimore, Adrian Groenendyk, Abhijit Gurav, Ajay Jain, Diptarka Majumdar, May Nyman, Teresa Powers, Yoshi Senzaki, Guihua Shang, Chong-Ying Xu, and Dongshui Zeng.

References

1. Wells, A.F., *Structural Inorganic Chemistry*, 5th ed., Clarendon Press, Oxford, 1986.
2. Cotton, F.A., Wilkinson, G., *Advanced Inorganic Chemistry*, 5th ed., Wiley, New York, 1988.
3. Greenwood, N.N., Earnshaw, E.A., *Chemistry of the Elements*, Pergamon, Oxford, 1984.
4. Huheey, J.E., *Inorganic Chemistry, Principles of Structure and Reactivity*, 3rd ed., Harper and Row, New York, 1983.

5. Shriver, D.F., Atkins, P.W., Langford, C.H., *Inorganic Chemistry*, W.H. Freeman and Company, New York, 1990, 173.
6. Charatan, R.M., Gross, M.E., Talk W11.4, *Mat. Res. Soc. Symp. Proc.*, Boston, Dec., 1993.
7. Wyetzner, C., Komarov, S., Freel, C., Jones, M., Hepp, A.F., Fury, M.A., Kaloyeros, A.E., Talk N1.2/Y1.2, *Mat. Res. Soc. Symp. Proc.*, Boston, Dec., 1993.
8. Jain, A., Chi, K.-M., Hampden-Smith, M.J., Kodas, T.T., Paffett, M.F., Farr, J.D. *Chem. Mat.* **1991**, 3, 995.
9. Jain, A., Chi, K.-M., Hampden-Smith, M.J., Kodas, T.T., Paffett, M.F., Farr, J.D. *J. Mater. Res.* **1992**, 7, 261.
10. Jain, A., Chi, K.-M., Hampden-Smith, M.J., Kodas, T.T., Paffett, M.F., Farr, J.D. *J. Electrochem. Soc.* **1993**, 140, 1434.
11. Baum, T.H., Larson, C.E. *Chem. Mater.* **1992**, 4, 365.
12. Norman, J.A.T., Muratore, B.A., Dyer, P.N., Roberts, D.A., Hochberg, A.K. *J. de Physique* **1992**, IV, 1.
13. Reynolds, S.K., Smart, C.J., Baran, E.F., Baum, T.H., Larson, C.E., Brock, P.J. *Appl. Phys. Lett.* **1991**, 59, 2332.
14. Bent, B.E., Nuzzo, R.G., Dubois, L.H. *J. Am. Chem. Soc.* **1989**, 111, 1634.
15. Seidler, P.F., Kowalczyk, S.P., Banaszak, M.M., Yurkas, J.J., Norcott, M.H., McFeely, F.R. *Mat. Res. Soc. Symp. Proc.* **1993**, 282, 359.
16. Banaszak Holl, M.M., Seidler, P.F., Kowalczyk, S.P., McFeely, F.R. *Inorg. Chem.* **1994**, 33, 510.
17. Paul, A., Bent, B.E., Seidler, P.F. 1993, unpublished work.
18. Banaszak Holl, M.M., Seidler, P.F., Kowalczyk, S.P., McFeely, F.R. *Appl. Phys. Lett.* **1993**, 62, 1475.
19. Gladfelter, W.L. *Chem. Mater.* **1993**, 5, 1372.
20. Kaplan, R., Bottka, N. *Appl. Phys. Lett.* **1982**, 41, 972.
21. Collman, J.P., Hegedus, L.S., Norton, J.R., Finke, R.G., *Principles and Applications of Organotransition Metal Chemistry*, University Science Books, California, 1987.
22. Hoke, J.B., Stern, E.W., Murray, H.H. *J. Mater. Chem.* **1991**, 1, 551.
23. Weiller, B., in *MOCVD of Electronic Materials*, *Mat. Res. Soc. Symp. Proc.*, Boston, 1993, Vol. Y4.4.
24. Weber, A., Nikulski, R., Klages, C.-P., Gross, M.E., Charatan, R.M., Brown, W.L., Dons, E., Talk W11.3, *Mat. Res. Soc. Symp. Proc.*, Boston, 1993.
25. Dubois, L.H., Zegarski, B.R., Girolami, G.S. *J. Electrochem. Soc.* **1992**, 139, 3603.
26. Ekerdt, J.G., Sun, Y.M., Jackson, M.S., Lakhota, V., Pacheco, K.A., Koschmieder, S.V., Cowley, A.H., Jones, R.A. *J. Cryst. Growth* **1992**, 124, 158.
27. Hampden-Smith, M.J., Kodas, T.T. *Mat. Res. Soc. Bulletin* **1993**, XVIII, 39.
28. Wolf, S., Tauber, R.N., *Silicon Processing for the VLSI Era*, Lattice, Sunset Beach, CA, 1987.

29. Broadbent, E.K. *IEEE Trans. Electron Dev.* **1988**, July, 952.
30. Lecohier, B., Calpini, B., Philippoz, J.M., van den Bergh, H. *J. Appl. Phys.* **1992**, 72, 2022.
31. Shin, H.K., Chi, K.-M., Hampden-Smith, M.J., Kodas, T.T., Paffett, M.F., Farr, J.D. *Chem. Mater.* **1992**, 4, 788.
32. Shin, H.K., Chi, K.M., Farkas, J., Hampden-Smith, M.J., Kodas, T.T., Duesler, E.N. *Inorg. Chem.* **1992**, 31, 424.
33. Fine, S.J., Dyer, P.N., Norman, J.A.T., Muratore, B.A., Iampietro, R.L. *Mat. Res. Soc. Symp. Proc.* **1990**, 204, 415.
34. Dormans, G.J.M., Meekes, G.J.B.M., Staring, E.G.J. *J. Cryst. Growth* **1991**, 114, 364.
35. Dormans, G.J.M. *J. Cryst. Growth* **1991**, 108, 806.
36. McConica, C.M., Krishnamani, K. *J. Electrochem. Soc.* **1986**, 133, 2542.
37. Lifshitz, N., Williams, D.S., Capio, C.D., Brown, J.M. *J. Electrochem. Soc.* **1987**, 134, 2061.
38. Girolami, G.S., personal communication.
39. Lecohier, B., Philippoz, J.-M., van den Bergh, H. *J. Vac. Sci. Technol. B.* **1992**, 10, 262.
40. Lecohier, B., Philippoz, J.-M., Calpini, B., Stumm, T., van den Bergh, H. *J. Phys.* **1991**, NC2, 279.
41. Levy, R.A., Green, M.L., Gallagher, P.K. *J. Electrochem. Soc.* **1984**, 131, 2175.
42. Cooke, M.J., Heinecke, R.A., Stern, R.C., Maes, J.W. *Solid State Technol.* **1982**, 25, 62.
43. Jain, A., Farkas, J., Hampden-Smith, M.J., Kodas, T.T. *Appl. Phys. Lett.* **1992**, 62, 2662.
44. Norman, J.A.T., Roberts, D.A., Hochberg, A.K. *Mat. Res. Soc. Symp. Proc.* **1993**, 282, 347.
45. Corbitt, T.S., Crooks, R.M., Ross, C.B., Hampden-Smith, M.J., Schoer, J.K. *Angew. Chem., Adv. Mater.* **1994**, 5, 935.
46. Schoer, J.K., Ross, C.B., Corbitt, T.S., Crooks, R.M., Hampden-Smith, M.J., *Langmuir* **1994**, 10, 615.
47. Mantel, D.A. *Appl. Phys. Lett.* **1988**, 53, 1387.
48. Kaesz, H.D., unpublished work.
49. Creighton, J.R., Parmeter, J.E. *Crit. Rev. Solid State Mat. Sci.* **1993**, 18, 175.
50. Gross, M.E., Donnelly, V.M., in *Advanced Metallization for ULSI Applications*, Rana, V.V.S., Joshi, R.V., Ohdomari, I. (eds.), Materials Research Society, Pittsburgh, 1992, 355.
51. Guinn, K.V., Donnelly, V.M., Gross, M.E., Baiocchi, F.A., Petrov, I., Greene, J.E. *Mat. Res. Soc. Symp. Proc.* **1993**, 282, 379.
52. *Metallized Plastics 3: Fundamental and Applied Aspects*, Mittal, K.L., (ed.), Plenum, New York, 1992.

53. Rye, R.R. *J. Polymer Sci. Polymer Phys.* **1992**, in press.
54. Rye, R.R., Chi, K.M., Hampden-Smith, M.J., Kodas, T.T., in *Advanced Metallization for ULSI Applications*, V. V. S. Rana; R. V. Joshi and I. Ohdomari (ed.), MRS, Pittsburgh, 1992, 421.
55. Rye, R., Knapp, J.A., Chi, K.M., M.J. Hampden-Smith, A.J., Kodas, T.T. *J. Appl. Phys.* **1992**, 72, 5941.
56. Rye, R.R., Arnold, G.W. *Langmuir* **1989**, 5, 1331.
57. Rye, R.R. *Langmuir* **1990**, 6, 338.
58. Rye, R.R., Shinn, N.D. *Langmuir* **1990**, 9, 142.
59. Knoezinger, H., in *Surface Organometallic Chemistry: Molecular Approaches to Surface Catalysis*, Basset, J.-M. (ed.), Kluwer, Dordrecht, the Netherlands, Vol. 231, 35.
60. Hair, M.L., *Infrared Spectroscopy in Surface Chemistry*, Marcel Dekker, New York, 1967.
61. Morrow, B.A., in *Spectroscopic Characterization of Heterogeneous Catalysts. Part 57A: Methods of Surface Analysis*, Fierro, J.L.G. (ed.), Elsevier, Amsterdam, 1990, Vol. 57A.
62. Iler, R.K., *The Chemistry of Silica*, John Wiley and Sons, New York, 1979.
63. Dubois, L.H., Zegarski, B.R., Kao, C.-T., Nuzzo, R.G. *Surf. Sci.* **1990**, 7, 236.
64. Dubois, L.H., Zegarski, B.R., Gross, M.E., Nuzzo, R.G. *Surf. Sci.* **1991**, 1, 1.
65. Dubois, L.H., Jeffries, P.M., Girolami, G.S., in *Advanced Metallization for ULSI Applications*, V. V. S. Rana; R. V. Joshi and I. Ohdomari (ed.), Materials Research Society, 1992, 375.
66. Dubois, L.H. *J. Electrochem. Soc.* **1992**, 139, 3295.
67. Farkas, J., Hampden-Smith, M.J., Kodas, T.T. *J. Phys. Chem.* **1994**, in press.
68. Cheek, R.W., Prasad, J., Kelber, J.A., Blewer, R.S., Fleming, J., Lujan, R.D., in *Advanced Metallization for ULSI Applications*, Rana, V.V.S., Joshi, R.V., Ohdomari, I. (eds.), Materials Research Society, Pittsburgh, 1992, 227.
69. Lewis, B., Anderson, J.C., *Nucleation and Growth of Thin Films*, Academic, New York, 1978.
70. Rye, R., Chi, K.M., Hampden-Smith, M.J., Kodas, T.T. *J. Electrochem. Soc.* **1992**, 139, L60.
71. Awaya, N., Arita, Y. *Digest of Technical Papers* **1989**, Section 12-4, 103.
72. Bauerle, D., *Chemical Processing with Lasers*, Springer-Verlag, New York, 1986.
73. Houle, F. *Appl. Phys. A* **1986**, 41, 315.
74. Ehrlich, D.J., Tsao, J.Y. *J. Vac. Sci. Technol. B* **1983**, 1, 969.
75. Sellers, J.A., Kollke, M., Wilson, S.R., Mattox, R.J. *Mat. Res. Soc. Symp. Proc. VLSI V*, 1990, 227.
76. Harsta, A., Carlsson, J.-O. *Thin Solid Films* **1990**, 185, 235.
77. Awaya, N., Arita, Y., in *Advanced Metallization for ULSI Applications*, Rana, V.V.S., Joshi, R.V., Ohdomari, I. (eds.), Mat. Res. Soc., Pittsburgh, 1992, Vol. V, 231.

78. Awaya, N., Arita, Y. *Jpn. J. Appl. Phys. Pt. 1* **1993**, 32, 3915.
79. Chang, Y. *Mat. Res. Soc. Symp. Proc.*, **1993**, 282, 335.
80. Chiang, C.M., Miller, T.M., Dubois, L.H. *J. Phys. Chem.* **1993**, 97, 11781.
81. Gelatos, A.V., Marsh, R., Kottke, M., Mogab, C.J. *Appl. Phys. Lett.* **1993**, 63, 2842.
82. Jefferies, P.M., Dubois, L.H., Girolami, G.S. *Chem. Mater.* **1992**, 4, 1169.
83. Lecohier, B., Calpini, B., Philippoz, J.M., van den Bergh, H., Laub, D., Buffat, P.A. *J. Electrochem. Soc.* **1993**, 140, 789.
84. Xu, X., Goodman, D.W. *Appl. Phys. Lett.* **1992**, 61, 1799.
85. Kinney, J.B., Staley, R.H. *J. Phys. Chem.* **1983**, 87, 3735.
86. Morrow, B.A., Hardin, A.H. *J. Phys. Chem.* **1979**, 83, 3135.
87. Hair, M.L., Hertl, W. *J. Phys. Chem.* **1973**, 77, 2070.
88. Hampden-Smith, M.J., Kodas, T.T., Rye, R.R. *Adv. Mater.* **1992**, 4, 524.
89. Tanaka, K., Harada, K., Murata, S. *Solar Energy* **1986**, 36, 159.
90. Reiche, H., Dunn, W.W., Bard, A.J. *J. Phys. Chem.* **1979**, 83, 2248.
91. Herrmann, J.M., J.L., M. *J. Catal.* **1990**, 121, 340.
92. Herrmann, J.-M., Disdier, J., Pichat, P. *J. Phys. Chem.* **1986**, 90, 6028.
93. Jain, A., Jaraith, R., Kodas, T.T., Hampden-Smith, M.J. *J. Vac. Sci. Technol. B* **1993**, 11, 2107.
94. Chiang, C.-M., Zegarski, B.R., Dubois, L.H. *J. Phys. Chem.* **1993**, 97, 6948.
95. Dubois, L.H., Zegarski, L.H. *J. Phys. Chem.* **1993**, 97, 1665.
96. Tsubouchi, K., Masu, K. *Thin Solid Films* **1993**, 228, 312.
97. Hirth, J.P. *J. Crystal Growth* **1972**, 17, 63.
98. Halpern, V. *J. Appl. Phys.* **1967**, 18, 163.
99. Lewis, B. *Surf. Sci.* **1970**, 21, 273.
100. Lewis, B. *Surf. Sci.* **1970**, 21, 289.
101. Carlsson, J.-O. *Crit. Rev. Solid State Mat. Sci.* **1990**, 16, 161.
102. Claassen, W.A.P., Bloem, J. *J. Electrochem. Soc.* **1980**, 127, 1836.
103. Gurav, A., Kodas, T., Pluym, T., Xiong, Y. *Aerosol. Sci. Tech.* **1993**, 19, 441.
104. Kodas, T.T. *J. Angew. Chemie, Adv. Mater.* **1989**, 6, 180.
105. Pierson, H.O., *Handbook of Chemical Vapor Deposition*, Noyes, Park Ridge, NJ, 1992.
106. Sherman, A., *Chemical Vapor Deposition for Microelectronics*, Noyes, Park Ridge, NJ, 1987.
107. Hitchman, M.L., Jensen, K.F., *Chemical Vapor Deposition: Principles and Applications*, Academic, San Diego, CA, 1993.
108. Pratsinis, S., Kodas, T.T., in *Handbook of Aerosol Measurement: Principles, Techniques and Applications*, Willeke, K., Baron, P.A. (eds.), Van Nostrand Reinhold, New York, 1993, Ch. 34.
109. Hinds, W.C., *Aerosol Technology*, Wiley, New York, 1982.
110. Meng, G., Zhou, G., Schneider, R.L., Sarma, B.K., Levy, M. *Appl. Phys. Lett.* **1993**, 63, 1981.

111. Stringfellow, G.B., *Organometallic Vapor-Phase Epitaxy: Theory and Practice*, Academic, New York, 1989.
112. Nolet, A.D., Rhine, B.C., Logan, M.A., Wright, L., Monkowski, J.R. *Mat. Res. Soc. Symp. Proc.* **1989**, 131, 319.
113. Kaloyeros, A.E., Feng, A., Garhart, J., Brooks, K.C., Gosh, S.K., Saxena, A.N., Luethrs, F. *J. Electronic Mat.* **1990**, 19, 271.
114. Kodas, T.T., Hampden-Smith, M.J., unpublished work.
115. Salazar, K.V., Ott, K.C., Rye, R.C., Hubbard, K.M., Peterson, E.J., Coulter, J.Y., Kodas, T.T. *Physica C* **1992**, 198, 303.
116. Langlet, M., Labeau, M., Bochu, B., Joubert, J.-C. *IEEE Trans. Mag.* **1986**, 22, 151.
117. Sears, W.M., Gee, M.A. *Thin Solid Films* **1988**, 165, 265.
118. Siefert, W. *Thin Solid Films* **1984**, 120, 267.
119. Siefert, W. *Thin Solid Films* **1984**, 121, 275.
120. DeSisto, W., Sosnowski, M., Smith, F., Deluca, J., Kershaw, R., Dwight, K., Wold, A. *Mat. Res. Bull.* **1989**, 24, 753.
121. DeSisto, W.J., Qian, Y.-T., Hannigan, C., Edwards, J.O., Kershaw, R., Dwight, K., Wold, A. *Mat. Res. Bull.* **1990**, 25, 183.
122. Pike, R.D., Cui, H., Kershaw, R., Dwight, K., Wold, A., Blanton, T.N., Wernberg, A.A., Gysling, H.J. *Thin Solid Films* **1993**, 224, 221.
123. Xu, W.W., Kershaw, R., Dwight, K., Wold, A. *Mat. Res. Bull.* **1990**, 25, 1385.
124. Qian, Y.-T., Niu, C.-M., Hannigan, C., Yang, S., Dwight, K., Wold, A. *J. Solid State Chem.* **1991**, 92, 208.
125. Qian, Y.-T., Kershaw, R., Dwight, K., Wold, A. *Mat. Res. Bull.* **1990**, 25, 1243.
126. Blandenet, G., Court, M., Legard, Y. *Thin Solid Films* **1981**, 77, 81.
127. Langlet, M., Joubert, J.C., in *Chemistry of Advanced Materials*, Rao, C.N.R. (ed.), Blackwell Scientific, Oxford, 1993, 55.
128. Blocher Jr., J.M. *Thin Solid Films* **1981**, 77, 51.
129. Joosten, P.H., Heller, P., Nabben, H.J.P., van Hal, H.A.M., Popma, T.J.A., Haisma, J. *Appl. Optics* **1985**, 24, 2674.
130. Maatman, D., Gruisinga, W., Lambeck, P.V., Popma, T.J.A. *J. Aerosol Sci.* **1988**, 19, 1369.
131. Lambeck, P.V., Hilderink, L., Popma, T.J.A., in *Sensors & Actuators, Proc. S & A Symp. Twente Univ. of Tech.*, Lodder, J.C. (ed.), 1986, 85.
132. Tang, Q., Albers, H., Driessen, A., Hilderink, L.T.H., Lambeck, P.V., Popma, T.J.A., *European Aerosol Conference*, Zurich, 1990.
133. Driessen, A., Tang, Q., Hilderink, L., Popma, T.J.A. *Mat. Res. Soc. Symp. Proc.* **1989**, 169, 601.
134. Lee, C.H., Park, S.J. *J. Mat. Sci.: Mat. Electronics* **1990**, 1, 219.
135. Viguié, J.C., Spitz, J. *J. Electrochem. Soc.* **1975**, 122, 585.
136. Matsuno, S., Uchikawa, F., Utsunomiya, S., Nakabayashi, S. *Appl. Phys. Lett.* **1992**, 60, 2427.

137. Lackey, W.C., Hanigofsky, J.A., Shapiro, M.J., Carter, W.B., Hill, D.N., Barefield, E.K., Judson, E.A., O'Brien, D.F., Chung, Y.S., Moss, T.S., *11th Intern. CVD Conf.*, Seattle, 1990.
138. Lackey, W.J., Carter, W.B., Hanigofsky, J.A., Hill, D.N., Barefield, E.K., Neumeier, G., O'Brien, D.F., Shapiro, M.J., Thompson, J.R., Green, A.J., Moss, T.S., Jake, R.A., Efferson, K.R. *Appl. Phys. Lett.* **1990**, 56, 1175.
139. Parker, D.H., Giacomo, J.P., *US Patent 4 571 350*, Feb. 18, 1986.
140. Tomar, M., Garcia, F. *Prog. Cryst. Growth Charact.* **1981**, 4, 221.
141. Mooney, J., Rodding, S. *Ann. Rev. Mater. Sci.* **1982**, 12, 81.
142. Roger, C., Corbitt, T.S., Hampden-Smith, M.J., Kodas, T.T. *Appl. Phys. Lett.* **1994**, submitted.
143. Hansen, B.N., Hybertson, B.M., Barkley, R.M., Sievers, R.E. *Chem. Mater.* **1992**, 4, 749.
144. Lambeck, P.V., Hilderink, L., Popma, T.J.A., in *Aerosols: Formation and Reactivity, 2nd International Aerosol Conference*, Berlin, 1986, 964.
145. Langlet, M., Labeau, M., Joubert, J.-C. *IEEE Trans. Mag.* **1986**, 22, 600.
146. Langlet, M., Shanon, R.D. *Thin Solid Films* **1990**, 186, L1.
147. Miki-Yoshida, M., Andrade, E. *Thin Solid Films* **1993**, 224, 87.
148. Labeau, M., Rey, P., Langlet, M., Joubert, J.C., *Proceedings International Symposium on Trends and New Applications in Thin Films*, Strasbourg, France, 1987.
149. Rey, P., Labeau, M., Joubert, J.C., Peuzin, J.C., Andre, R., *European Forum of Competitive Technology*, Grenoble, France, 1988.
150. Gao, Y.-M., Wu, P., Kershaw, R., Dwight, K., Wold, A. *Mat. Res. Bull.* **1990**, 25, 871.
151. Deschanvres, J.L., Cellier, F., Delabouglise, G., Labeau, M., Langlet, M., Joubert, J.C., *European CVD 7 Conference*, Perpignan, France, 1989.
152. Deschanvres, J.L., Cellier, F., Delabouglise, G., Labeau, M., Langlet, M., Joubert, J.C. *Phys.* **1989**, 50, C5.
153. Hakim, M.O. *J. Mat. Sci.* **1990**, 25, 1294.
154. Gao, Y.-M., Wu, P., Dwight, K., Wold, A. *J. Solid State Chem.* **1991**, 90, 228.
155. Deschanvres, J.L., Langlet, M., Joubert, J.C., *Proceedings International Symposium on Trends and New Applications in Thin Films*, Regensburg, Germany, 1989.
156. Deschanvres, J.L., Langlet, M., Joubert, J.C. *Thin Solid Films* **1989**, 175, 281.
157. Labeau, M., Reboux, V., Dharhi, D., Joubert, J.C. *Thin Solid Films* **1986**, 136, 257.
158. Lanlet, M., Deschanvres, J.L., Labeau, M., Joubert, J.C., in *Proceedings International Symposium on Trends and New Applications in Thin Films*, Strasbourg, France, 1987, 279.
159. Wernberg, A.A., Gysling, H.J. *Chem. Mater.* **1993**, 5, 1056.
160. Gysling, H.J., Wernberg, A.A. *Chem. Mater.* **1992**, 4, 900.
161. DeSisto, W.J., Henry, R.L., Osofsky, M., Marzik, J.V. *Thin Solid Films* **1991**, 206, 128.

162. Tang, Q., Driessen, A., Hoekstra, P., Hilderink, L.T., Van Silfhout, A., Popma, T.J.A. *J. Less-Comm. Met.* **1990**, 164-165, 1587.
163. Koukitu, A., Hasegawa, Y., Seki, H., Kojimo, H., Tanaka, I., Kamioka, Y. *Jpn. J. Appl. Phys.* **1989**, 28, L1212.
164. Friedlander, S.K., *Smoke, Dust and Haze*, Wiley, New York, 1977.
165. Shin, H.K., Chi, K.-M., Hampden-Smith, M.J., Kodas, T.T., Paffett, M.F., Farr, J.D. *Angew. Chem., Adv. Mat.* **1991**, 3, 246.
166. *Thin Film Processes*, Vossen, J.L., Kern, W., (eds.), Academic, New York, 1978.
167. Lee, H.H., *Fundamentals of Microelectronics Processing*, McGraw Hill, New York, 1990.
168. Bird, R.B., Stewart, W.E., Lightfoot, E.N., *Transport Phenomena*, John Wiley and Sons, New York, 1960.
169. Kodas, T.T., Baum, T.H., Comita, P.B. *J. Appl. Phys.* **1987**, 62, 281.
170. Kodas, T.T., Baum, T.H., Comita, P.B. *J. Crystal Growth* **1988**, 87, 378.
171. Ward, T., Kodas, T.T., Jackson, R.L. *J. Appl. Phys.* **1991**, 69, 1000.
172. Kim, D.H., Wentorf, R.H., Gill, W.N., in *Adv. Metallization and Processing for Semiconductor Devices and Circuits-II*, Katz, A., Murarka, S., Nissim, Y.I., Harper, J.M.E. (eds.), MRS, Pittsburgh, PA, 1992, 107.
173. Bryant, W.A. *J. Mat. Sci.* **1977**, 12, 1285.
174. Chung, G.Y., Kim, H.D., Ahn, B.T., Im, H.B. *Thin Solid Films* **1993**, 232, 28.
175. Borden, P. *Microcontamination* **1991**, March, 39.
176. Stern, J.E., Dopp, D.J., Wu, J.J. *Microcontamination* **1991**, Nov., 17.
177. Borden, P. *Microcontamination* **1991**, Nov., 33.
178. Jairath, R., Anderson, H.M., Wang, R. *Microcontamination* **1991**, Sept., 17.
179. Durham, J.A., Petrucci Jr., J.L., Steinbruchel, C. *Microcontamination* **1990**, Nov., 37.
180. Greenstein, D., Yang, H., Tao, A., Kinney, P., Zhao, J., Gupta, A., Fishkin, B. *Microcontamination* **1991**, Mar., 21.
181. Lux, B., Colombier, C., Altena, H., Stjernberg, K. *Thin Solid Films* **1986**, 138, 49.
182. Simmonds, M.G., Gladfelter, W.L., Li, H., McMurry, P.H. *Mat. Res. Soc. Symp. Proc.* **1993**, 282, 317.
183. Chiang, C.-M., Dubois, L.H. *Mat. Res. Soc. Symp. Proc.* **1993**, 282, 341.
184. Smith, D., Alimonda, A.S. *J. Electrochem. Soc.* **1993**, 140, 1496.
185. Chu, J.H., Lin, I. *J. Appl. Phys.* **1993**, 74, 4741.
186. Adachi, M., Okuyama, K., Tohge, N., Shimada, M., Satoh, J., Muroyama, M. *Jpn. J. Appl. Phys.* **1992**, 31, L1439.
187. Bloem, J. *J. Crystal Growth* **1973**, 18, 70.
188. Eversteijn, F.C. *Philips Res. Rep.* **1971**, 26, 134.
189. Murthy, T.U.M.S., Miyamoto, N., Shimbo, M., Nishizawa, J. *J. Crystal Growth* **1976**, 33, 1.
190. van den Brekel, C.H.J., Bollen, L.J.M. *J. Crystal Growth* **1981**, 54, 310.

191. Sarma, K.R., Rice Jr., M.J. *J. Electrochem. Soc.* **1981**, 128, 2647.
192. Leys, M.R., Veenvliet, H. *J. Crystal Growth* **1981**, 55, 145.
193. Irvine, S.J.C., Giess, J., Mullin, J.B., Blackmore, G.W., Dosser, O.D. *J. Vac. Sci. Technol.* **1985**, B 3, 1450.
194. Stutius, W. *Appl. Phys. Lett.* **1978**, 33, 656.
195. Kim, D.G., Yoo, J.S., Chun, J.S. *J. Vac. Sci. Technol.* **1986**, A 4, 219.
196. Nakamura, K. *J. Electrochem. Soc.* **1986**, 133, 1120.
197. Lee, H.-Y., Kim, H.-G. *Thin Solid Films* **1993**, 229, 187.
198. Pratsinis, S.E., Kodas, T.T., Dudukovic, M.P., Friedlander, S.K. *Ind. Eng. Chem. Proc. Des. Dev.* **1986**, 25, 634.
199. Sladek, K.J. *J. Electrochem. Soc.* **1971**, 118, 654.
200. Okuyama, K., Huang, D.D., Seinfeld, J.H., Takani, N., Matsui, I. *Jpn. J. Appl. Phys* **1992**, 31, 1.
201. Nishizawa, J., Kurobayashi, T. *J. Electrochem. Soc.* **1983**, 130, 413.
202. Frolov, I.A., Tomchinskii, A.M. *J. Crystal Growth* **1985**, 71, 699.
203. Frolov, I.A., Boldyrevskii, P.B., Druz, B.L. *Inorg. Mater.* **1977**, 13, 632.
204. Pluym, T.C., Kodas, T.T., Wang, L.M., Wiedensohler, A., Hansson, H.C., Maximov, I., Samuelson, L. *Mat. Res. Soc. Symp. Proc.* **1993**, 300, 465.
205. Draper, C.W. *Metall. Trans.* **1980**, 11A, 349.
206. Shin, S.M., Draper, C.W., Mochel, M.E., Rigsbee, J.M. *Mater. Lett.* **1985**, 3, 265.
207. Jervis, T.R., Newkirk, L.R. *J. Mater. Res.* **1986**, 1, 420.
208. Jervis, T.R. *J. Appl. Phys.* **1985**, 58, 1400.
209. Kodas, T.T., Comita, P.B. *Acc. Chem. Res.* **1990**, 23, 188.
210. Allendorf, M.D., Hurt, R.H., Yang, N., Reagan, P., Robbins, M. *J. Mater. Res.* **1993**, 8, 1651.
211. Shimogaki, Y., Komiyama, H. *Chem. Lett.* **1986**, 267.
212. Komiyama, H., Osawa, T., Kazi, H., Konno, T., in *High Tech Ceramics*, Vincenzini, P. (ed.), Elsevier, Amsterdam, 1987, 667.
213. Dekker, J.P., van der Put, P.J., Veringa, H.J., Schoonman, J., *Austceram 92 Conf.*, 1992.
214. Hunt, A.T., Carter, W.B., Cochran Jr., J.K. *Appl. Phys. Lett.* **1993**, 63, 266.

Appendix 1: Examples of Chemical Nomenclature^a

Compound	Name
Al(CH ₃) ₃	trimethylaluminum
Al(C ₂ H ₅) ₃	triethylaluminum
Al(C ₂ H ₅)H ₂	ethylaluminumdihydride
Al(C ₂ H ₄) ₂ Cl	diethylaluminumchloride
Al(<i>i</i> -Bu) ₃	triisobutylaluminum
Al(<i>i</i> -Bu) ₂ H	diisobutylaluminumhydride
AlH ₃ (Et ₃ N)	triethylaminealane
WF ₆	tungsten(VI)hexafluoride
W(CO) ₆	hexacarbonyltungsten(0)
W(PF ₃) ₆	hexakis(trifluorophosphine)tungsten(0)
(η^5 -C ₅ H ₅) ₂ WH ₂	bis(cyclopentadienyl)dihydridotungsten
(η^5 -C ₅ H ₄ CH ₃) ₂ WH ₂	bis(methylcyclopentadienyl)dihydridotungsten
Cu(hfac) ₂	bis(1,1,1,5,5,5-hexafluoroacetylacetonato)-copper(II)
Cu(hfac) ₂ •H ₂ O	bis(1,1,1,5,5,5-hexafluoroacetylacetonato)-copper(II) water adduct
(hfac)Cu(1,5-COD)	1,1,1,5,5,5-hexafluoroacetylacetonato(1,5-cyclooctadiene)copper(I)
(hfac)Cu(PMe ₃)	1,1,1,5,5,5-hexafluoroacetylacetonato-(trimethylphosphine)copper(I)
[Cu(O- <i>t</i> -Bu) ₄] ₄	tertiarybutoxycopper(I) tetramer
ClCu(PEt ₃) ₂	chlorobis(triethylphosphine)copper(I)
(hfac)AuMe ₂	dimethyl(1,1,1,5,5,5-hexafluoroacetylacetonato)gold(III)
Ni(η^5 -C ₅ H ₅) ₂	bis(η^5 -cyclopentadienyl)nickel(II), nickelocene
Pd(η^3 -allyl) ₂	bis(η^3 -allyl)palladium(II)
(η^5 -C ₅ H ₅)Pd(η^3 -allyl)	η^5 -cyclopentadienyl- η^3 -allylpalladium(II)
(η^5 -C ₅ H ₅)Pt(CH ₃) ₃	η^5 -cyclopentadienyltrimethylplatinum(IV)
(η^6 -C ₆ H ₆) ₂ Cr	bis(benzene)chromium(0)
(η^6 -C ₇ H ₈)Cr(CO) ₃	η^6 -cycloheptatrienyltricarbonylchromium
Cr(CH ₂ - <i>t</i> -Bu) ₄	tetrakis(neopentyl)chromium(IV)
MoCl ₅	molybdenum(V)pentachloride
Fe(CO) ₅	pentacarbonyliron(0)

^a compounds are arranged according to appearance in this book

Compound	Name
$\text{Fe}(\eta^5\text{-C}_5\text{H}_5)_2$	bis(η^5 -cyclopentadienyl)iron(II), ferrocene
$(\text{H}_3\text{Si})_2\text{Fe}(\text{CO})_4$	bis(silyl)tetracarbonyliron(II)
$\text{Co}(\text{acac})_2$	bis(acetylacetonato)cobalt(II)
$\text{Co}(\eta^5\text{-C}_5\text{H}_5)_2$	bis(η^5 -cyclopentadienyl)cobalt(II), cobaltocene
$\text{Co}(\text{NO})(\text{CO})_3$	tricarbonylnitrosylcobalt(0)
$(\eta^5\text{-C}_5\text{H}_5)\text{Co}(\text{CO})_2$	η^5 -cyclopentadienyldicarbonylcobalt(I)
$\text{Rh}(\eta^3\text{-allyl})_3$	tris(η^3 -allyl)rhodium(III)
$\text{Rh}(\eta^3\text{-allyl})(\text{CO})_2$	η^3 -allyldicarbonylrhodium(I)
$\text{Cd}(\text{CH}_3)_2$	dimethylcadmium
SnCl_4	tin(IV)tetrachloride
$(\text{CH}_3)_2\text{SiCl}_2$	dichlorodimethylsilane
$(\text{CH}_3)_3\text{N}$	trimethylamine
$(\text{CH}_3)_3\text{NBH}_3$	trimethylamineborane
$(\text{CH}_3)_3\text{P}$	trimethylphosphine
$(\text{CH}_3)_2\text{S}$	methylsulfide
MoSi_2	molybdenum disilicide

Appendix 2: Definition of Terms^a

ablation - removal of material from a surface by application of energy, often from a pulsed laser.

abrasion resistance - ability of a material to resist surface wear.

activation energy - minimum energy necessary for a reaction to proceed via an "activated complex" or transition state.

active components - electronic components, such as transistors, diodes, electron tubes, and thyristors that operate on an applied electrical signal to change their basic characteristics, e.g., rectification, amplification, and switching.

additive process - process for obtaining conductive patterns by deposition.

adhesion - ability of a conductor or insulator material to withstand a force attempting to separate it from the substrate.

adsorption - see chemisorb and physisorb

alloy - (a) any of a large number of substances having metallic properties and consisting of two or more usually metallic elements; (b) to make or melt an alloy.

ambient - environment that surrounds and contacts a system or component.

amphoteric - has both acidic and basic properties.

anisotropic - exhibiting different properties when tested along axes in different directions; in magnetics, capable of being magnetized more readily in one direction than in a transverse direction.

anisotropic etching - etching of a material in one direction, generally achieved by accelerating reactive ions towards substrates which results in etching in the direction of the ion velocity with no lateral removal of material.

application-specific integrated circuit - an integrated circuit chip customized for a specific product.

aspect ratio - ratio of vertical dimension to horizontal dimension of a hole diameter.

ballistic transport - transport of a material to a surface from a source without gas-phase collisions.

barrier layers - see diffusion barrier.

base metal - nonprecious metal from which a connector, contact, or other metal accessory is made and on which one or more metals or coatings may be deposited.

bipolar - device in which both majority and minority carriers are present; for integrated circuits, describes a specific type of construction. Bipolar and metal-oxide semiconductor (MOS) are the most common types of integrated circuits (see also metal-oxide semiconductor).

blanket deposition - deposition of a material over the entire surface of a substrate.

^a Adapted from *Electronic Materials Handbook*, Vol. 1. Packaging ASM International, Materials Park, OH 44073, USA.

- bond homolysis** - symmetrical cleavage of a covalent bond.
- Brownian diffusion** - diffusion of atoms or molecules due to a concentration gradient.
- buffer gas** - inert gas added to increase the total pressure.
- bulk resistance** - portion of resistance that is due to the length, cross section, and is characteristic of a material.
- capacitance** - property of a capacitor that determines its ability to store electrical energy when a given voltage is applied; is measured in farads, microfarads, or picofarads.
- capacitive coupling** - electrical interaction between two conductors caused by the capacitance between them.
- capacitor** - device that can store an electrical charge when voltage is applied; its impedance is inversely proportional to the frequency of the voltage impressed; it offers little resistance or impedance to high frequencies, but much to low frequencies.
- ceramic printed board** - printed board made from ceramic dielectric and cermet materials; fulfills same function as traditional organic printed board.
- chemisorb** - chemical binding of a molecule to a surface involving transfer of electrons between the surface and adsorbed molecule.
- chip** - individual circuit or component of a silicon wafer (see also die).
- chip carrier** - integrated circuit package, usually square, with a chip cavity in the center; its connections are usually on all four sides.
- chromophore** - part of an entity (molecule) responsible for light absorption.
- circuit** - interconnection of a number of components in one or more closed paths to perform a desired electrical or electronic function.
- Clausius-Clapeyron relationship** - a thermodynamic equation applying to two-phase equilibrium for a pure substance which relates vapor pressure to temperature.
- complementary metal-oxide semiconductor (CMOS)** - device in which cascaded field-effect transistors of opposite polarity are used to minimize power consumption.
- component** - individual functional part in a physically independent body that cannot be further reduced or divided without destroying its stated function; e.g., a resistor, capacitor, diode, or transistor.
- comproportionation** - reaction between two or more reagents which leads to a species with an oxidation state intermediate between those of the reagents.
- conductance, electrical** - reciprocal of electrical resistance; measure of the ability of any material to conduct an electrical charge; ratio of the current flow to the potential difference.
- conductivity, electrical** - capability of a material to carry an electrical current; i.e., conductance of a unit cube of any material; the reciprocal of resistivity.

conductor - single conductive path in a conductive pattern.

conformal coating - coating that conforms to the configuration of the object coated; often an insulating protective coating applied to completed board assembly or to components.

conformal film - film of uniform thickness that follows the contours of the surface of a substrate.

connector - generally, all devices used to provide rapid connect/disconnect service for electrical cable and wire terminations, board to board.

contact - the part in a connector that makes the actual electrical contact; point of joining in an electrical connection.

contact holes - holes which when filled with a conductor connect the first metal level to the surrounding drain regions of the transistor.

contact layer - thin layer which makes a low-resistance contact with a doped semiconductor for subsequent metallization, usually used in conjunction with diffusion barrier.

contact resistance - electrical resistance due to interface between two different materials.

creep - dimensional change with time of a material under load.

critical nucleus size - size of particle that is thermodynamically stable; particles larger than this size can grow spontaneously, but smaller particles can shrink.

cross-sectional area - area of the cut surface of an object that has been cut at right angles to the long axis of the object.

crosstalk - undesirable interference caused by coupling of energy between signal paths.

degree of aggregation - number of times the empirical formula occurs in the molecular formula of a compound.

delay time - time interval from the point at which the leading edge of the input pulse has reached 10% of its maximum amplitude to the point at which the leading edge of the output pulse has reached 10% of its maximum amplitude.

dendritic growth - branched structures resembling branches of a tree.

deposition - laying down of films of metal or insulators on a substrate.

desorption - reverse process of adsorption.

device - individual electrical part, usually in an independent body, that cannot be further reduced without destroying its stated function; an electronic part consisting of one or more active or passive parts.

die (dies or dice) - individual semiconductor part or integrated circuit after it has been cut or separated out of the processed semiconductor wafer, distinct from a completely packaged or encapsulated integrated circuit with leads attached; a semiconductor chip.

dielectric breakdown - complete failure of a dielectric material characterized by a disruptive electrical discharge through the material due to

deterioration of the material or an excessive sudden increase in voltage.

dielectric constant - also called the relative permittivity ϵ_r , ratio of capacitance of a capacitor with a specified medium (dielectric) between the plates to capacitance of the same capacitor with vacuum between plates.

dielectric loss - electric energy transformed into heat in a dielectric subjected to a changing electric field.

dielectrics - materials that do not conduct electricity; usually materials used as capacitors.

dielectric strength - maximum voltage withstood, under specified conditions, without resulting in a voltage breakdown (usually expressed as volts per unit dimension).

differentially-pumped - situation where several interconnected vacuum chambers are pumped individually.

diffuse reflectance - reflectance of light or species over a range of angles relative to a single incident angle.

diffusion barrier - material that suppresses interdiffusion of underlying and overlying material.

diffusive transport - transport by diffusion, usually Brownian diffusion in gases.

diffusivity - measure of the rate at which molecules diffuse through a substance; also known as diffusion coefficient.

disproportionation - reaction of species which leads to formation of two or more products with higher and lower oxidation states.

dopant - impurity introduced under highly controlled conditions in a very small but accurately known quantity into a silicon slice; dopants modify the electrical characteristics of the silicon material by creating *p* or *n* regions, and hence *pn* junctions.

electric strength - maximum potential gradient that a material can withstand without rupture; function of thickness of material and method and conditions of test; also dielectric strength or disruptive gradient.

electrode - conductor through which a current enters or leaves an electrolytic cell, arc furnace, vacuum tube, gas-discharge tube, or other nonmetallic conductor.

electroless deposition - deposition of metal without an electrode by anodic oxidation of reductant at the surface of the catalytic substrate.

electrolysis - separation of chemical components by the passage of current through an electrolyte.

electrolyte - current-conducting solution (liquid or solid) between two electrodes or plates of a capacitor, at least one of which is covered by a dielectric film.

- electromigration** - in the context of metal wires through which current flows, movement of atoms induced by the flow of electrons.
- electron-beam patterning** - patterning of resist using a narrowly focused electron beam to produce thin lines (as in very-large-scale-integration).
- electronic packaging** - technical discipline of designing a protective enclosure for an electronic circuit so that it will both survive and perform under a variety of environmental conditions.
- electroplating** - deposition of metal thin films from solution on other metals; the deposition surface is one electrode in the bath containing the metal ions so aqua-ions or other complexes, current density, pH, and concentration all have a marked effect on the adhesion and structure of the deposited metal.
- epitaxial** - phenomenon of crystallographically oriented overgrowth of a material on the crystal surface of the same type material, e.g., silicon on silicon.
- etchant** - reagent used to remove, by chemical reaction, the unwanted portion of material from a surface.
- etchback** - process for the controlled removal of materials from surfaces to a specified depth.
- etching** - process by which a printed pattern is formed by either chemical or chemical and electrolytic removal of the unwanted portion of material.
- eutectic** - minimum melting point of a combination of two or more materials; eutectic temperature of a system (if one exists) is always lower than the melting point of any of the individual components of the system; eutectic composition is that particular composition where the eutectic occurs.
- evaporative deposition** - techniques for condensing a thin film of material on a substrate; entire process takes place in a high vacuum; source material may be heated using an electron beam or thermal conduction.
- exothermic** - characterized by the liberation of heat.
- η^x -bond** - nomenclature used to describe the number (x) of ligand atoms from a single ligand bonded to a single metal center.
- failure** - an item that has ceased to perform a required function.
- fatigue** - description of a failure of any structure caused by repeated stress over a period of time.
- feed-rate-limited** - deposition limited by the rate at which reactant is fed into the reactor.
- feed-through** - a connector or terminal block usually having double-ended terminals that permit simple distribution and bussing of electric circuits.
- field-effect transistor** - voltage-controlled transistor analogous to a vacuum tube triode.
- film stress** - compressive or tensile forces appearing in a film, such as internal film stress, which is the intrinsic stress of a film related to its mechanical structure and deposition parameters or induced film stress, which is the

component of film stress related to an external force such as mismatched mechanical properties of the substrate.

Fischer-Tropsch - name given to the reaction between H_2 and CO to form hydrocarbons and H_2O ; catalyzed by transition metals.

flux - number of molecules per unit area per unit time [units: $(cm^{-2} s^{-1})$]; also chemical/physical formulation capable of enabling and promoting the wetting of metals with solder.

gas mean free path - in the gas phase, the mean distance a molecule travels between two successive collisions with other molecules.

gate electrode - electrode in a field-effect transistor to which a bias is applied to modulate the conductivity of the channel.

gettering - process of using a chemical species to remove impurities.

glass transition temperature (T_g) - temperature at which an amorphous polymer (or the amorphous regions in a partially crystalline polymer) changes from a hard and relatively brittle condition to a viscous or rubbery condition. In this temperature region, many physical properties such as hardness, brittleness, thermal expansion, and specific heat undergo significant, rapid changes.

high aspect ratio - aspect ratio much greater than one.

high intrinsic stress - stress that results from the structure of the growing film.

hillock formation - the formation of mounds or piles of material on a feature.

hybrid circuit - circuit that uses two or more fabrication techniques to form the circuit, such as integrated circuit chips attached to a substrate having thin-film devices and conductors.

hysteresis - lag in dielectric response that results from the viscous damping of a variable force impressed upon the dielectric.

impedance - ratio of the effective value of the potential difference between two terminals to the effective value of the current flow produced by that potential difference.

incubation period - time delay before the start of steady-state film growth.

inclusion - foreign particle in a conductive layer, plating, or base material.

ink - synonymous with paste when relating to screenable thick-film materials and with solder mask when referring to screen printing (see also screen printing and thick film circuit).

interconnects - metal lines that connect devices to each other and to external power supplies.

integrated circuit - microcircuit consisting of interconnected parts inseparably associated and formed in situ on or within a single substrate to perform an electronic circuit function.

interface - boundary between two materials.

interlevel vias - see via holes.

intermetallic compound - (a) intermediate phase (a homogeneous phase whose composition range does not include any pure metal) in an alloy system that has a narrow range of composition but has atomic bonding that can be of several types; (b) stoichiometric compound whose strength, brittleness, and hardness differ considerably from those of the metals that make up the compound.

ion implantation - precise method of doping. Ions such as boron or phosphorus are accelerated to high energies and penetrate an integrated circuit wafer target. The energy controls the depth of penetration, and because the amount of energy can be accurately controlled, the doping can be very precise. Areas not to be doped are masked with oxide or aluminum.

junction - (a) in solid-state materials, a region of transition between p- and n-type semiconductor materials as in a transistor or diode. (b) A contact between two dissimilar materials. (c) A connection between two or more conductors or sections of a transmission line.

Knudsen number - ratio of gas mean free path (λ) to a characteristic dimension (d): $Kn = 2\lambda/d$.

laminar flow - viscous fluid flow where stream lines are parallel to each other and there is no intermixing of the fluid.

Langmuir-Hinshelwood kinetics - when the surface reaction proceeds by a dual-site mechanism in which the adsorbed reactant interacts with another site.

large-scale integration (LSI) - usually, monolithic digital integrated circuits with 100 or more gates or gate-equivalent circuits, e.g., metal-oxide semiconductor read-only memories; also hybrid integrated circuits.

leakage (dc) - in capacitors, the stray direct current of relatively small value that flows through the capacitor when voltage is applied across the terminals.

Lewis acid - species that is an electron pair acceptor.

Lewis base - species that is an electron pair donor.

mass-transport-limited deposition - deposition process limited by the rate of mass transport, often by Brownian diffusion, through a stagnant film.

Maxwell-Boltzmann temperature distribution - based on classical statistics, gives the number of molecules in a gas whose total velocity lies within a given range.

metallization - the act of adding metal to a substrate to form interconnect on a chip or to define a place for attachment of bond wires.

metal-oxide semiconductor (MOS) - its method of construction distinguishes this integrated circuit from bipolar integrated circuits. MOS integrated circuits are slower than bipolar integrated circuits but have the advantage of high circuit density and low cost.

metal-oxide semiconductor field effect transistor (MOSFET) - the basic part in MOS ICs; a field effect transistor consists of diffused source and drain

regions on either side of a p- or n-channel region and a gate electrode insulated from the channel by silicon oxide.

metathesis reaction - exchange between substituents of one metal atom and another metal atom in two complexes.

microelectronics - area of electronic technology associated with or applied to electronic systems of extremely small electronic parts, usually with micrometer-sized features.

microstructure - structure of a material at the micrometer level.

microwave - short electrical wave, usually a wavelength < 300 mm or > 1000 Hz.

modules - substrates on which a number of integrated circuits are mounted and interconnected.

moiety (ies) - entity (ies).

mother board - printed board assembly used for interconnecting arrays of plug-in electronic modules.

multichip module - a package capable of supporting several chips on a single package.

multichip packaging - package or substrate on which many integrated circuit chips are mounted.

multi-dentate chelation - complexation of two or more donor atoms with the metal atom to form a cyclic structure.

multilayer printed board - printed circuit or printed wiring configuration consisting of alternate layers of conductive patterns and insulating materials bonded together in two or more layers, includes both flexible and rigid organic multilayer and ceramic multilayer boards.

no-slip boundary condition - when the velocity of the fluid is zero relative to the surface.

nucleation - mechanism of formation of stable clusters called nuclei on a surface or in a gas (or liquid) (see also critical nucleus size).

ohm - unit of electrical resistance, Ω , the resistance being that of a circuit in which a potential difference of one volt produces a current of one ampere.

ohmic contact - contact between two materials across which the voltage drop is the same regardless of the direction of the current flow.

oligomeric - composed of a small number of monomeric units.

open circuit - circuit in which halving the magnitude of the terminating impedance does not produce a change in the parameter being measured.

optoelectronic device - device that detects and/or is responsive to electromagnetic radiation (light) in the visible, infrared, and/or ultraviolet spectral regions; emits or modifies noncoherent or coherent electromagnetic radiation in these same regions; utilizes such electromagnetic radiation for its internal operation.

oxidation state - integral number of charges, usually positive, associated with the metal in a transition metal complex.

- oxidative addition** - addition of an organic moiety to a metal center in a metal complex which leads to an increase in the oxidation state of the metal.
- package** - in microelectronics, an enclosure for a single part, an integrated circuit, or a hybrid circuit. Provides hermetic or nonhermetic protection and serves as the first-level interconnection externally for the device by means of package terminals. Generally consists of a bottom part (case or header) and a top part (cover or lid) sealed into one unit. Passive parts may be enclosed in an encapsulant or a molded package.
- passivation** - formation of an insulating or protective layer directly over the semiconductor surface to protect the surface from contaminants, moisture, or particles. Usually, an oxide of the semiconductor is used; although, other materials are used as well. Alternative usage: ability to render a surface unreactive towards a particular (molecular) substrate, see chapters 5 and 9.
- photo-assisted CVD** - CVD driven by photochemical reactions *and* thermal reactions.
- photochemical CVD** - CVD driven by photochemical reactions on surfaces and/or in a gas.
- photochemical LCVD** - laser assisted CVD driven by photochemical reactions on surfaces and/or in a gas.
- photofragmentation** - fragmentation of a molecular species caused by absorption of one or more photons.
- photolithography** - use of photoresists, patterning using masks, etching, and photoresist removal to form patterned features on surfaces.
- photolysis** - the decomposition or reaction of a substance on exposure to light.
- photolytic CVD** - see photochemical CVD.
- physical vapor deposition by evaporation** - ballistic transport of evaporated material to the substrate surface under a high-vacuum environment.
- physical vapor deposition by sputtering** - sputtering process which results in physical transport of target material to the substrate.
- physisorb** - the weakest form of adsorption which is the result of a physical attraction (van der Waals force) between the adsorbate and surface (see also chemisorption).
- pinhole** - small hole occurring as an imperfection that penetrates a layer of material.
- pitch** - nominal distance from center-to-center of adjacent conductors.
- plasma etching** - action of an electrically conductive gas or plasma (ionized gas or molecules) to remove unwanted portion of conductive or insulative pattern.
- pre-exponential factor** - (k_0 or A) also called frequency factor, is a measure of the frequency of molecular collisions. The Arrhenius relationship $\text{rate} = k_0 \exp(-E/RT)$ implies k_0 is unaffected by temperature; however, there is a weak temperature dependence of k_0 .

- printed board** - a processed printed circuit or printed wiring configuration; includes rigid or flexible boards (organic or ceramic) and single, double, and multilayer printed boards. **Printed wiring board** - board with printed-on point-to-point connections. **Printed circuit board** - board with printed-on components as well as point-to-point connections.
- printed board assembly** - general term for either a printed wiring assembly or a printed circuit assembly.
- printed circuit** - conductive pattern comprising printed components, printed wiring, or a combination thereof, all formed in a predetermined design and intended to be attached to a common base.
- printed circuit assembly** - a printed circuit board on which separately manufactured components and parts have been added.
- pull-test** - method used to quantify adhesion of a film to a surface (see Scotch-tape test).
- pyrolyzed** - material characterized by gaining its final form by the action of heat.
- random access** - type of integrated circuit memory access in which any address can be accessed at random; data retrieval time is relatively fixed.
- rate-limiting step** - any physical or chemical step that limits the overall rate of a process.
- reductive elimination** - removal of an organic fragment from a metal center in a metal complex that results in a reduction of the metal.
- reliability** - collective name for measures of quality that reflect the effect of time in storage or use of a product, as distinct from those measures that show the state of the product at the time of delivery. Generally, an item's ability to perform a required function under stated conditions for a stated period of time.
- resistivity** - resistance of unit length of substance with uniform unit cross-section, also called specific resistance; describes the ability of a material to resist the passage of electric current either through its bulk or on a surface; unit of bulk resistivity is the ohm-centimeter (Ωcm). The unit of surface resistivity or line resistance is the ohm. A convenient way to express the resistivity of film conductors is in sheet resistivity, which is the electrical resistance measured across the opposite sides of a square of deposited film material. Sheet resistivity is expressed in ohms per square.
- resistor** - device that offers resistance to the flow of electric current in accordance with Ohm's law: $R = E/I$, where R is resistance, E is voltage, and I is current.
- roughness** - microscopic peak-to-valley distances of film-surface protrusions and depressions, measured in angstroms.
- salicide formation** - simultaneous formation of a low-contact resistance silicide at the exposed Si areas of source and drain as well as the exposed poly-Si areas of the gate.

- Schottky barrier diodes** - a diode consisting of a metal-semiconductor contact which has rectifying characteristics similar to a p-n junction; differs from a p-n junction diode in that the diode's forward voltage is different (lower for commonly used materials), and there is no charge stored when the diode is forward biased; device can therefore be turned off very rapidly by application of reverse bias, as storage time is negligible.
- "Scotch tape test"** - qualitative test that measures film adhesion; a piece of adhesive tape is pressed to the film, pulled off, and examined for the presence of film.
- screen printing** - transferring an image to a surface by forcing suitable media through a stencil screen (see also ink and thick-film circuit).
- selective CVD** - CVD of a material only on certain areas of a substrate (growth surface) and not on other areas of a substrate (non-growth surface).
- sheet resistance** - electrical resistance of a thin sheet of a material with uniform thickness as measured across opposite sides of a unit square pattern; expressed in ohms per square.
- sheet resistivity** - resistance of a film material with the same length and width (a square); the resistivity of thick-film resistor compositions is expressed in terms of sheet resistivity in ohms per square.
- short circuit** - circuit in which doubling the magnitude of the terminating impedance does not produce a change in the parameter being measured that is greater than the required accuracy of the measurement.
- sinter** - to heat without melting; to cause a metal or refractory dielectric material to become a rigid body free of binders, contaminants.
- slurry** - thick mixture of solids in a liquid suspension.
- solder** - a low melting point alloy, usually of lead-tin that can wet copper, conduct current, and mechanically join conductors.
- solder bumps** - round solder balls bonded to a transistor contact area and used to make connection to a conductor by face-down bonding techniques.
- sputtering** - removal of a material from a solid target into the gas phase by energy transfer due to collisions of ions with the target.
- sticking coefficient** - fraction of incident flux of molecules that stick on a specified surface.
- stress-induced void formation** - void formed in interconnects due to stresses in the underlying and overlying dielectric layers.
- surface-reaction-limited** - deposition rate which is limited by the kinetics of the surface reaction and not by the transport of reactants to the surface or the feed rate of reactants into the reactor; under these conditions, the deposition rate usually increases exponentially with surface temperature.

- susceptor** - plate that holds the wafer for heating.
- tape automated bonding** - a packaging method favored for high lead count (> 200) integrated circuits.
- tape bonding** - utilization of a metal or plastic tape material as a support to and carrier of a microelectronic component in a bonding process.
- tape casting** - thin, tape-like appearance of ceramic slurry when poured after effortless compaction by evaporation of the suspension medium. This method results in two-dimensional, large-size, flat substrates of all shapes, almost devoid of internal stresses, layers for laminated monolithic chip capacitors; also called slip casting.
- temperature coefficient of resistance** - amount of resistance change of a material per degree of temperature rise.
- thermophoresis** - thermal force experienced by particles in the gas phase in the direction of decreasing temperature.
- thick-film circuit** - circuit that is fabricated by the deposition of materials having between 5 and 20 μm (0.2 - 0.8 mil) thickness, such as screen-printed cermet pastes on a ceramic substrate which are fired in a kiln to create permanent conductive patterns (see also ink and screen printing).
- transistor** - an active semiconductor device capable of providing power amplification and having three or more terminals.
- transport-limited deposition** - deposition limited by transport of the reactants to the surface through a boundary layer; the deposition-rate is much less sensitive to surface temperature than in surface-reaction-limited deposition.
- vapor pressure** - equilibrium partial pressure exerted by liquid or solid at a specified temperature.
- velocity field** - vector field created by gradient in velocity.
- via holes** - holes in a substrate which when filled with a conductor connect one interconnect level to another.
- viscosity** - resistance that a gaseous or liquid system offers to flow when it is subjected to a shear stress.
- volatility** - tendency of a material to evaporate (see also vapor pressure).
- Wacker process** - catalytic process using a Pd/Cu redox pair.
- wafer** - usually, a slice of a crystalline semiconductor ingot used as a substrate material. Modified by the addition, as applicable, of impurity diffusion (doping), ion implantation, epitaxy, etc. The active surface is processed into arrays of discrete devices or integrated circuits by metallization, passivation, or other means; metallization of its back side (bottom surface) is optional.
- work function** - energy required to remove an electron from a bulk metal.
- wormhole** - tunnels created in Si during deposition of W by H_2 reduction of WF_6 .

yield - ratio of the number of acceptable items produced in a production run to the total number that were attempted.

yield strength - stress at which a material exhibits a specified strain deviation from purely elastic stress-strain behavior.

This Page Intentionally Left Blank

Index

A		
α -hydride elimination	74, 145, 410	alkene adducts 374
α -hydrogen abstraction	373,406	alkene complexes 407ff
α -tungsten	136, 159	iridium 407
ab initio molecular orbital calculations	66	orbital interaction 374
activation energy	268f	rhodium 407
(hfac)Cu[P(CH ₃) ₃]	268	ruthenium 407
(hfac)Cu(VTMS)	268	alkoxides
(hfac)Cu(1,5-COD)	268	copper(I) 250
(hfac)Cu(2-butyne)	268	alkyne complexes 375, 407ff
Me ₂ Au(hfac)	320	iridium 407
adhesion	50, 180	rhodium 407
surface pretreatment	50	ruthenium 407
adhesion layers	27	allyl complexes 374, 409ff
chromium	27	iridium 409
titanium	27	molybdenum 409
adsorption of Cu(I) compounds	199f	palladium 409
activation energy	200	rhodium 409
Ag	200	selenium 409
Cu(hfac)(COD)	200	tantalum 409
Cu(hfac)(VTMS)	199	tellurium 409
Cu(I)(hfac)(L)	191	tungsten 409
Cu(100)	199	aluminaborane
HREELS	200	aluminum [Al(100), Al(111)] 56, 62, 89
RAIR	199	aluminum 51, 84ff, 363
adsorption of H(hfac)	200	alane precursors 74, 83
Cu(100)	201	selectivity 83
H ₂ reduction of Cu(hfac) ₂	200	aluminum monochloride 91
RAIR	201	aluminum precursors (Table 2-1) 57
adsorption studies	191	chemical vapor deposition 51
Cu(hfac) ₂	191	diethylaluminum chloride (DEACl) 86, 90
(Table 4-4)	192	diisobutylaluminum hydride (DIBAH) 59f
aerosol delivery	463ff, 466, 475,483	dimethylaluminum hydride (DMAH) 74, 88ff
(Table 9-4)	464	heat of association 88
advantages	466	dimethylaluminumhydride trimer
disadvantages	467	[(CH ₃) ₂ AlH] ₃ 290
evaporation of solvent and precursor	467	dimethylethylamine alane
feed-rate-limited deposition	467	(DMEAA) 57, 76, 82ff
multicomponent films	467	particle formation 84
precursors	466	physical vapor deposition 51
solid precursor particles	467	precursors 432
thermal degradation of precursors	466	triethylaluminum (TEA) 86
aerosol-assisted CVD	463, 483	triethylamine alane (TEAA) 75, 81
Ag(acac)	313	triisobutylaluminum (TIBA) 58ff, 62ff
Ag(acetate)	313	trimethylaluminum (TMA) 68ff,89
Ag(C ₄ F ₇)	313	trimethylamine alane (TMAA) 50,75, 77, 290
Ag(trifluoroacetate)	313	tri- <i>n</i> -butylamine alane 75
alane precursors	74, 83	aluminum metallization 18
selectivity	83	

- aluminum, sacrificial diffusion barrier 11
aluminum-silicon contact 9
APCVD, see atmospheric pressure CVD
application specific integrated circuit (ASIC) 5
applications 331, 352, 361ff
 catalysts for electroless metal plating 331
 catalysts for pollution control 331
 chromium 365
 coatings: decorative, protective 331
 cobalt 365
 contact layers 362
 corrosion resistant coatings 362
 diffusion barriers 362ff
 dopants 362
 iridium 365
 metal contacts 331
 molybdenum 365
 nickel 352
 niobium 365
 palladium 352
 platinum 352
 rhenium 365
 ruthenium 365
 ruthenium trioxide 365
 solder 362
 tantalum 365
 titanium 365
 tungsten 365
 zirconium 365
Arrhenius plot, see also activation energy
 gold 482
ASIC, see application specific integrated circuit
atmospheric pressure CVD (APCVD) 470f
atomic layer epitaxy 385
Auger electron spectroscopy 63
autocatalytic deposition 60
- B**
 β -diiminate ligand 247
 β -diketonate ligand 183
 β -diketonatogold(III) complexes 306
 β -hydride elimination 58f, 64ff, 87, 91f, 145, 242, 244, 267, 373, 405, 409, 437f
 β -ketoiminate ligand 183, 247, 250, 254
 β -methyl group elimination 438
 β -tungsten films 136
 β -tungsten phase 115, 147, 151, 159, 161
barrier layers, see also diffusion barrier and
 diffusion barrier layers 248
 copper 25
beryllium 366, 371
bis(acetylacetonato)platinum 333
- bis(arene)tungsten 117, 148
bis(benzene)tungsten 143
bis(cyclopentadienyl)dihydridotungsten 119, 147
 vapor pressure 119
bis(cyclopentadienyl)nickel, Clausius-Clapeyron relationship 342
 kinetics 342
 olefin hydrogenation 343
bis(methylcyclopentadienyl)dihydrido-tungsten 120, 148
blanket deposition 437
 (hfac)Cu(1,5-COD) 278
bonding
 laser-induced deposition 323
boron 366
boundary layers 54, 469f
bubblers 460
- C**
C incorporation 438
C-H activation 410
Cab-O-Sil 281ff
cadmium 400
 dopant 400
carbides 377, 417
 allyl complexes 417
carbon incorporation 69
carbon monoxide 398
 dissociative chemisorption 153
carbonyl halides 379
carrier gas effects 206ff
 ethanol 207
 H₂ 206
 H₂O 207
 N₂ 206
catalysis
 tungsten deposition 150
CF₃Au(PMe₃) 309
chemical and physical properties 367ff
 oligomerization 370f
 precursors 367
 volatility 370f
chemical beam epitaxy 385
chemical vapor deposition (CVD) 30ff
 aluminum 51
 boundary layer 31
 cold-wall 32
 feed-rate limited 32
 hot-wall 31
 mass-transport limited, see also diffusion-limited deposition 31
 reactors 474

- | | | | |
|---|--------------|--|---------------|
| design | 474 | melting point | 185 |
| chemical-mechanical polishing (CMP) | 21, 441ff | precursors | 432 |
| copper | 292 | selective deposition of | 275 |
| chromium | 388 | sticking probability | 280 |
| adhesion layers | 27 | copper compounds | 179ff, 183ff |
| carbide | 389 | (Table 5-1) | 245 |
| metal β -diketonates | 421 | alkyl compounds | 183 |
| metal carbonyl | 419 | β -diketonate ligands | 180 |
| precursors | 433 | β -ketoiminate ligands | 180, 248 |
| Clausius-Clapeyron relationships | 335 | copper halides | 183 |
| clusters | 488 | Cu(acac) ₂ | 186, 195 |
| CMOS, see complimentary metal oxide semiconductor | | Cu(acen) | 180 |
| co-deposition | 163ff | Cu(acim) ₂ | 180 |
| co-reactant | | Cu(fod) ₂ | 185 |
| selective CVD | 443f | Cu(hfac) ₂ | 180 |
| coating large areas | 158 | Cu(hfac) ₂ •H ₂ O | 185ff |
| coatings: decorative, protective | 331 | Cu(nona-F) ₂ | 180, 185ff |
| cobalt | 395 | Cu(thd) ₂ | 185 |
| doping | 396 | copper(I) alkoxides | 250 |
| metal β -diketonates | 421 | copper(I) β -diketonates | 421 |
| metal carbonyl | 419 | structural formulas | 183 |
| selectivity | 415 | structures of | 185 |
| cobalt disilicide | 25, 363, 403 | Cu(acac) ₂ | 186 |
| cold-wall reactors | 468ff | Cu(nona-F) ₂ | 185ff |
| TMAA | 80 | Schiff base | 186ff |
| complimentary metal oxide semiconductor (CMOS) | 8 | vaporization temperatures | 179 |
| concentration boundary layer | 470ff, 481 | volatility | 183 |
| conformal coverage, see also blanket deposition | 262ff | copper CVD | |
| gold | 320 | historical review | 179 |
| conservation of | | copper metallization | 20 |
| energy | 54 | copper precursors | 432 |
| mass | 54 | copper(I) oxide | 249 |
| momentum | 54 | chromium carbide (Cr ₃ C ₂) | 414 |
| contact layers | 8, 14ff | crystallinity | 446 |
| cobalt silicide | 17 | current resistance (IR) | 6 |
| metal silicides | 14 | cycloheptatrienetricarbonyltungsten | 120, 149 |
| molybdenum silicide | 17 | cyclooctadienetetracarbonyltungsten | 120, 149 |
| nickel silicide | 17 | cyclopentadienylhydridotricarbonyltungsten | 120 |
| palladium silicide | 17 | cyclopentadienylmethyltricarbonyl-tungsten | 119, 146, 149 |
| platinum silicide | 16 | vapor pressure | 119 |
| refractory metals | 14 | cyclopentadienyltrimethylplatinum | 335ff |
| titanium silicide | 16 | autocatalysis | 336 |
| contact resistance of W-Si structures | 134 | Clausius-Clapeyron relationships | 335 |
| contamination | | CVD of platinum | 336 |
| particle formation | 484 | induction period | 336f |
| continuum-flow regime | 470 | kinetics | 336 |
| copper | 363 | vapor pressure | 336 |
| alloys | 289ff | | |
| barrier layers | 25 | D | |
| diffusion | 26 | DEACl, see diethylaluminum chloride (aluminum) decomposition | 266 |

- $(\eta^5\text{-C}_5\text{H}_5)\text{Cu}(\text{CN-}i\text{-Bu})$ 266
 $(\eta^5\text{-C}_5\text{H}_5)\text{Cu}[\text{P}(\text{CH}_3)_3]$ 266
 $(\eta^5\text{-C}_5\text{H}_5)\text{Cu}(\text{PEt}_3)$ 266
 deposition mechanism, gold 314
 deposition rate
 copper 288
 maximum 476
 deposition rate of Cu in presence of: acetone,
 alcohols, water, ethanol, isopropanol
 methanol, THF, toluene 280ff
 DIBAH, see diisobutylaluminum hydride
 dichloroplatinumdicarbonyl 331
 dielectric material 442
 diethylaluminum chloride (DEACl) 86, 90
 differential reactor 275
 diffusion 459
 diffusion barrier 9ff, 48, 286, 442
 amorphous 13
 tantalum silicon nitride 13
 passive 12
 metal nitrides 12
 titanium nitride 12
 sacrificial 10f
 aluminum 11
 niobium 11
 titanium 11
 stuffed 11
 titanium-tungsten 12
 diffusion barrier layers for Cu
 tantalum 26
 titanium-tungsten 26
 diffusion coefficient 482
 temperature dependence 482
 diffusion-limited deposition 469, 475, 478, 480f
 concentration boundary layer 478
 rate of diffusion of precursor 478
 diffusivity 364
 diisobutylaluminum hydride (DIBAH) 59f
 dimethyl-2,4-pentanedionatogold(III) 308
 dimethyl(β -diketonato)gold(III)
 photolytic decomposition 323
 dimethyl(hfac)gold(III)
 growth rate 321
 laser-induced deposition 314
 photochemical deposition 317
 dimethyl(trimethylsiloxy)gold(III) 310
 dimethylaluminum hydride (DMAH) 74, 88ff
 heat of association 88
 dimethylaluminumhydride trimer
 $[(\text{CH}_3)_2\text{AlH}]_3$ 290
 dimethylethylamine 75
 dimethylethylamine alane (DMEAA) 57, 76, 82ff
 direct wiring
 tungsten 160
 disilane 61
 disproportionation 91, 247, 254, 257, 260,
 264, 271ff, 277, 284, 404, 408, 411, 437
 aluminum chloride 247
 copper(I) 247
 iron 247
 silver(I) 313
 dissociation (hfac)Cu(VTMS) 272
 Cu(hfac)₂ 272
 dissociation enthalpy 81
 dissociative adsorption 193ff
 Ag/SiO₂ 196
 Cu(hfac)₂ 193
 Cu(100) 194
 TiN (titanium nitride) 196
 DMAH, see dimethylaluminum hydride
 DMEAA, see dimethylethylamine alane
 donor-acceptor 78
 DRAM, see dynamic random access memory
 dry etching 441f
 Dual Damascene 22
 dynamic random access memory
 (DRAM) 5
 E
 effusive molecular beam scattering 63
 electromigration 6, 18, 48, 178
 electron beam deposition
 dimethyl(hfac)gold(III) 318
 electron cyclotron resonance 224
 electronegativity 183
 electrophoresis 459
 epitaxial films 62
 epitaxy aluminum, Al(100), Al(111) 62
 η^6 -arene complexes 377
 etchability 364
 etching 242, 292ff
 comproportionation 293
 copper 292
 dry etching 242
 oxidation of copper 294
 wet etching 242
 evaporation 51
 F
 feed-rate-limited deposition 256, 268, 396,
 467, 469f, 475ff, 480f
 deposition rate 477
 growth rate 477
 reactant conversion 477

(hfac)CuL	478	aluminum	484
Me ₂ Au(hfac)	478	cobalt	484
RAuPMe ₃	478	(hfac)Cu(VTMS)	484
film characterization	489	reactant partial pressure dependence	
film morphology	262ff	of rate	480
film properties	210ff, 231	getter	
Cu(hfac) ₂	210	selective CVD	443f
Cu(nona-F) ₂	210	giga-scale integration (GSI)	22
microstructure, Cu	212	gold	363
morphology	231	activation energy	320
rippling effect	232	Arrhenius plot	320
volcano-like profiles	232	(CF ₃) ₃ Au(PMe ₃)	309
purity, Cu	210	[(CH ₃) ₂ AuOSiMe ₃) ₂	309
purity of Cu in presence of C ₂ H ₅ OH	231	conformal coverage	320
resistivity	231	deposition mechanism	314
resistivity, Cu	211	dimethyl-2,4-pentanedionato gold(III)	308
film stoichiometry	439	dimethyl(β-diketonato)gold(III)	
Fischer-Tropsch catalysis chemistry	438	photolytic decomposition	323
flow non-uniformity	483	dimethyl(hfac)gold(III)	
fluidized-bed reactor	142	growth rate	321
fluoroalkyl gold complexes	306	laser-induced deposition	314
fluoropolymers	286	photochemical deposition	317
flux of reactant to substrate surface	476	dimethyl(trimethylsiloxy) gold(III)	310
focused laser-induced deposition	385	fluoroalkyl gold complexes	306
formation of patterned films		laser-induced deposition	309
chemical-mechanical polishing	441	Me ₂ Au(hfac)	309
dry etching	441	Me ₃ Au(PMe ₃)	309
selective CVD	441	MeAu(CNMe)	309
Fourier transform infrared spectroscopy		MeAu(PMe ₃)	309
(FTIR)	189	metallization	21
free convection	473	precursors	432
free energy barrier		synthesis	306
selective CVD	443f	resistivity	305
FTIR		gold(I)	306
(hfac)Cu[P(CH ₃) ₃]	281	gold(I) isocyanates	310
(hfac)Cu(VTMS)	281	gold(I) mercaptide resins	310
(hfac)Cu(1,5-COD)	281	gold(III)	306
(hfac)Cu(2-butyne)	281	growth kinetics	202f
silica	281	activation energy	204
surface chemistry	281	added H ₂ O	206
functional groups	445	Cu oxides	206
hydrogen bonded -OH	445	Cu(hfac) ₂	202f
isolated -OH	445	Cu(hfac)(2-butyne)	203
M-O-M	445	Cu(nona-F) ₂	204
		deposition rates	202
		deposition temperature	203
		dimethyl (hfac)gold(III)	321
G		GSI (giga-scale integration)	22
gallium arsenide	21, 48		
GaAs(100)	79		
Ga(AsMe ₂) ₃	442		
gas chromatography	179, 183	H	
gas diffusion barriers	49	H bridge	88
gas mean free path	470ff	hafnium	386
gas-phase reactions	468, 480, 484ff	heterometallic precursors (Table 8-5)	369

- | | | | |
|--------------------------------------|--------------------|--|--------------------------------------|
| heterometallic systems | 401 | metal carbonyl | 419 |
| heteronuclear complexes | 414 | selectivity | 415 |
| Co-Ga | 414 | iron carbide (Fe_3C) | 412 |
| Fe-Co | 414 | iron oxide (Fe_3O_4) | 412 |
| Fe-Ni | 414 | | |
| Mn_2Si | 415 | K | |
| SiCo | 415 | kinetic theory of gases | 54 |
| hexacarbonyltungsten | 117, 141ff, 152ff | kinetics, see also growth kinetics | 78, 402ff |
| laser-assisted CVD | 152 | adsorption-limited regime | 348 |
| mechanism | 152 | surface reaction-limited regime | 348 |
| photo-dissociation | 153 | Knudsen number | 315, 321, 470ff |
| photolytic deposition process | 152 | | |
| secondary photolytic reactions | 152 | L | |
| hexakis(trifluorophosphine)tungsten | 115, 141 | laminar flow | 54 |
| phosphorus impurities | 117 | large-scale integration (LSI) | 22 |
| high resolution electron energy loss | | laser direct writing | |
| spectroscopy (HREELS) | 198 | tungsten | 157 |
| hillock formation | 6, 19 | laser interconnection | 322 |
| homolysis | 246, 248, 406, 437 | laser-assisted CVD (LCVD) | 73, 151, 228ff, 342ff, 351, 407, 479 |
| hot-wall reactor | 60, 468ff | argon ion laser | 351 |
| advantages and disadvantages | 468f | bonding | 323 |
| TMAA | 81 | Cu | 228 |
| hydroxyl groups | | $\text{Cu}(\text{hfac})_2$, $\text{C}_2\text{H}_5\text{OH}$ | 229 |
| pK_a values | 445 | dimethyl(hfac)gold(III) | 314 |
| hydrodynamics | 53 | direct deposition | 351 |
| | | direct-write circuits | 351 |
| I | | direct writing | 228 |
| impaction | 459, 488 | electronic excitation | 228 |
| impurity incorporation | 438 | film properties | 231 |
| inorganic precursors | 437, 434, 436ff | morphology | 231 |
| inorganic substrate | 444 | rippling effect | 232 |
| GaAs | 444 | volcano-like profiles | 232 |
| insulators | 444 | purity of Cu in presence of | |
| metal nitrides | 444 | $\text{C}_2\text{H}_5\text{OH}$ | 231 |
| metal silicides | 444 | resistivity | 231 |
| Si | 444 | hexacarbonyltungsten | 152 |
| TiN | 444 | laser intensity | 231 |
| integrated circuits | 4 | nickel | 343ff |
| interception of particles | 459 | operating variables | 229 |
| interconnect | 4ff, 8, 17 | reactants | 229 |
| internal stress, Cu films | 214 | growth kinetics | 229 |
| ion beam deposition | | palladium | 343ff |
| dimethyl(hfac)gold(III) | 318 | photoactivated deposition | 228 |
| ion-assisted CVD | 350 | photochemical deposition | 228 |
| focused ion beam | 350 | platinum | |
| platinum | 350 | integrated circuits - modify, repair | 347 |
| IR (current resistance) | 6 | platinum | 343ff |
| iridium | 398, 407ff | pyrolysis | 228 |
| alkene complexes | 407 | pyrolytic LCVD | 342, 351 |
| alkyne complexes | 407 | reaction mechanism | 232 |
| allyl complexes | 409 | unimolecular | 232 |
| iron | 393 | | |
| metal β -diketonates | 421 | | |

- reflectivity 230
- secondary photolysis 232
- substrate temperature 230
- threshold intensity effect 231
- TMA (trimethylaluminum) 73
- TMAA (trimethylamine alane) 83
- trimethylgold(III)trimethylphosphine 309
- tungsten deposition 151
- tungsten hexafluoride 155, 157
 - deposition experiments 157
 - hydrogen reduction 157
 - mechanism and kinetic observations 157
 - silane reduction 157
- laser-induced circuit repair 321
- laser-induced deposition, see laser-assisted CVD
- lead 400
- Lewis base 74
- ligand decomposition, see also decomposition
 - Cu(hfac)₂ 201
 - Cu(hfac)(VTMS) 201
 - Cu(100) 202
 - H(hfac) 201
 - ketenylidene 202
 - mass desorption spectra 201
- ligand geometry 196
 - Ag/Si(111) 196
 - Cu(hfac)₂ 196
 - Cu(hfac)(VTMS) 196
 - H(hfac) 196
- ligand redistribution 89, 405
- "line-of-sight" deposition 51
- liquid delivery 461f
 - aerosol evaporation 462
 - disadvantages 462
 - flash evaporation 462
 - multicomponent systems 462
 - solution 461
- loading effects 483
- loss of selectivity, see selective CVD
- low-pressure CVD (LPCVD) 470f
- LPCVD, see low-pressure CVD
- LSI (large-scale integration) 22
- M**
- M-C bond homolysis 373
- manganese 392
- manufacturing 34ff
 - cost of consumables 34
 - cost of ownership 33
 - defect density 35
 - DRAM 33
- reactor throughput 36
- scheduled maintenance 36
- scrap cost 35
- tungsten 33
- mask repair 323
- mass transport 54
- mass-transport-limited deposition 56
- mean free path 51
- mechanism 217f, 402ff
 - adsorption
 - Cu(hfac)₂ 218
 - H(hfac) 218
 - Cu(hfac)₂ 217
 - desorption
 - H(hfac) 218
 - Langmuir-Hinshelwood 217
 - one-dimensional model 218
 - rate-limiting step 218
 - transport 218
- melting point 185
- metal alkoxides 383
- metal alkyls 372f, 405
 - homoleptic 372
 - properties 372
 - pyrophoric 372
 - volatility 372
- metal β -diketonates 413
 - chromium 413
 - cobalt 413
 - copper(I) 413
 - iron 413
 - properties 381
 - reducing agent 381
- rhodium 413
- ruthenium 413
- vapor pressure 381
- metal carbides 406
- metal-carbon bond order 438
- metal carbonyls 411ff
 - chromium 411
 - cobalt 411
 - iron 411
 - molybdenum 411
 - properties 378f
 - σ -donor, π -acceptor bonding 379
- metal halides 369, 437
 - reduction 402
- metal nitride passive diffusion barrier 12
- metal-organic precursors 434, 436ff
- metal particles 486f
 - formation 487
 - laser-induced 487
- metal trifluorophosphines 380
- metallation reaction 249

- | | | | |
|---------------------------------------|-------------------|--|----------------------|
| metallization | 4 ff, 27, 178 | cw CO ₂ laser deposition | 348 |
| metallized polymers | 48 | cw krypton ion laser deposition | 348 |
| metallocenes | 410ff | kinetics | 348 |
| chromium | 410 | Mond process | 340 |
| cobalt | 411 | precursors | 432 |
| iron | 410 | silicide | 25 |
| molybdenum | 410 | nickel tetracarbonyl | 340ff, 348 |
| nickel | 410 | activation energy | 341 |
| ruthenium | 410 | growth rate dependence | 341 |
| ruthenium dioxide | 410 | kinetics | 341 |
| titanium | 410 | steady-state kinetics | 341 |
| metathesis reactions | 249 | niobium | 386 |
| methyl radicals | 69 | Nb ₃ Ga | 386 |
| methylcyclopentadienylplatinum | 335ff | Nb ₃ Ge | 386 |
| CVD of platinum | 336 | superconducting phases | 386 |
| vapor pressure | 336 | niobium sacrificial diffusion barrier | 11 |
| microelectronics | 48 | nitrides | 25 |
| interconnects | 48 | no-slip condition | 472 |
| microspheres, coating | 142 | non-metallic substrates, copper CVD on | 198f |
| microstructure, Cu | 212f | Cu(dpm) ₂ | 198 |
| film continuity | 213 | Cu(hfac) ₂ | 198 |
| grain size | 213 | Cu(hfac)(COD) | 198 |
| H ₂ O | 213 | Cu(hfac)(VTMS) | 199 |
| morphology | 213 | H ₂ O | 199 |
| nucleation rate | 213 | SiO ₂ | 198 |
| reflectivity | 213 | SrTiO ₃ | 199 |
| seed layers | 213 | XPS | 198 |
| microwave plasma reactor | 162 | non-uniform deposition | 471 |
| molecular adsorption | 193 | nucleation | 52, 56, 79, 442, 446 |
| Cu(hfac) ₂ | 193 | chemical and physical nucleation | 442 |
| molecular beam epitaxy | 53 | nucleation promoters | |
| molecular beam scattering (Fig. 2-12) | 77ff | titanium(IV) chloride | 61 |
| molecular flow regime | 53, 470 | nucleus | 83 |
| molybdenum | 390, 417 | | |
| allyl complexes | 417 | O | |
| disilicide | 363 | ohmic contacts | 134 |
| metal carbonyl | 419 | olefin complexes | 374 |
| precursors | 433 | oligomerization | 246, 295 |
| selectivity | 414 | volatility | 251 |
| Mond process | 340 | operating variables for PACVD | 224ff |
| multichip modules | 322 | reactor configuration | 224 |
| multicomponent films | 467 | substrate temperature | 224 |
| multihapto ligands | 377 | optical properties | 49f |
| | | absorptivity | 50 |
| N | | reflectivity | 49 |
| nickel | 340ff, 347ff, 351 | organic polymers | 445 |
| applications | 351 | fluorinated polymers | 445 |
| bis(cyclopentadienyl)nickel | 347 | polyimides | 445 |
| Clausius-Clapeyron relationship | 341 | PTFE | 445 |
| kinetics | 341 | organometallic precursors | 435, 436ff |
| olefin hydrogenation | 342 | organometallic tungsten precursors | 115ff, 138 |
| bis(methylcyclopentadienyl)nickel | 340, 351 | deposition conditions (Table 3-9) | 138f |
| CVD experiments (Table 7-2) | 339 | favorable properties | 115 |

film properties (Table 3-10)	140	gravitational settling	488
properties (Table 3-4)	114	impaction	85
synthesis (Table 3-3)	113	laser light scattering	85
organophosphine		settling velocities	488
poisoning, reducing agents	248	passivating agent	
reduction	249	HMDS	453
organosilver(I) complexes	310	$\text{Me}_3\text{CCH}_2(\text{Me}_2)\text{Si}(\text{NMe}_2)$	453
osmium	395	Me_3SiCl	453
overall reactor behavior	458f	$\text{Me}_3\text{Si}(\text{NMe}_2)$	453
oxidation state	196	methanol	453
oxidizing agent	439	passivation	
		$(\text{CH}_3)_3\text{SiCl}$	286
		$(\text{CH}_3)_2\text{SiCl}_2$	286
		chlorotrimethylsilane	279
		dimethyldichlorosilane	279
		functionalized alkylsilanes	279, 286
		selective CVD	443f
P		patterning	
palladium	417	aluminum	66
allyl complexes	417	electron beams	287
applications	339ff, 351	laser irradiation	287
bis(allyl)palladium	351	X-rays	287
bis(hexafluoroacetylacetonate)palladium	347	photo-deposition	447
bis(2-butenyl)palladium	339	photochemical vapor deposition	386, 401, 447
catalysts for electroless copper plating	347	dimethyl(hfac)gold(III)	317
CVD experiments (Table 7-2)	339	selective CVD	443f
cyclopentadienylpalladium	351	photofragmentation	87ff
cyclopentadienylallylpalladium	339, 347	ethyl radical	88
precursors	432	hydrogen radical	88
silicide	25	TEA (triethylaluminum)	87f
spin-on methods	347	photolysis	68
parabolic velocity profile	471	photolytic decomposition	
parallel plate radial flow reactor		dimethyl(β -diketonato)gold(III)	323
tungsten hexafluoride	161	physical entrapment	142
particle deposition	459	physical vapor deposition (PVD)	28, 242
particle-precipitation-aided CVD	487	aluminum	28, 51
thermophoresis	487	evaporation	28
particle formation	459, 481, 484f	sputtering	29
aluminum	84, 484	plasma-assisted aluminum deposition	72
carbides	484	TMA	72
cobalt	484	plasma-assisted CVD (PACVD)	222, 228, 350
contamination	484	(Table 4-5)	223
gallium arsenide	484	Cu	222
(hfac)Cu(VTMS)	484	$\text{Cu}(\text{acac})_2$	222
$\text{Ni}(\text{CO})_4$	484	$\text{Cu}(\text{hfac})_2$	222
nitrides	484	$\text{Cu}(\text{tdf})_2$	222
selenides	484	CVD experiments (Table 7-3)	343
SiH_4	484	dimethyl(2,4-pentanedionato)gold(III)	319
silicon	484	film properties	226f
silicon dioxide	484	conformality	228
suppression	486	Cu vs. CuO or Cu_2O	227
tellurides	484	morphology	227
tungsten hexafluoride	484	N_2O or O_2	227
particle-precipitation-aided CVD	487	purity	226
particles			
diffusion	488		
formation	85		

- | | | | |
|---|-----------------|---|--------------------|
| resistivity | 227 | poisoning | |
| growth rate | 222 | organophosphine | 248 |
| nickel | 351 | polyimide dielectric layer | 322 |
| operating variables | 224f | potassium | 363 |
| carrier gas: H ₂ , Ar/H ₂ | 226 | precursor delivery | 489 |
| DC bias | 225 | flash vaporization | 460 |
| power density | 225 | thermally unstable precursors | 460 |
| reactant concentration | 225 | precursor design | 477, 479, 485, 495 |
| reactor configuration | 224 | precursor vaporization | 483 |
| substrate temperature | 224 | precursors | |
| palladium | 350 | chemical and physical properties | 367 |
| parallel-plate reactor | 350 | classification by element (Table 9-1) | 431ff |
| platinum | 350 | classification by ligand (Table 9-2) | 434ff |
| reaction mechanism | 226 | commercial availability | 367 |
| remote plasma | 160, 222 | pressure dependence of rate | 469 |
| silver(I) perfluoro-1-methylpropenyl | | printed wiring board | 27, 286 |
| complex | 319 | properties | 360, 365, 370 |
| tungsten | 160 | abrasion resistant | 365 |
| tungsten hexafluoride | 160 | adhesion layer | 365 |
| plasma-enhanced CVD, see | | catalytic | 365 |
| plasma-assisted CVD | | corrosion | 365 |
| platinum | 331ff, 351 | diffusion barrier | 365 |
| applications | 351 | infrared reflectivity (IR) | 365 |
| bis(acetylacetonato)platinum | 333 | lasers | 365 |
| bis(hexafluoroacetylacetonate)platinum | 344 | metal halides | 370 |
| CVD experiments (Table 7-1) | 331, 332 | metallization | 365 |
| cyclopentadienyltrimethylplatinum | 335ff, 346 | oxidation resistance | 365 |
| autocatalysis | 336 | pyrosol process | 463 |
| Clausius-Clapeyron relationships | 335 | | |
| CVD of platinum | 336 | R | |
| induction period | 336f | radical chain reactions | 71 |
| kinetics | 336 | radio frequency plasma | 72 |
| vapor pressure | 336 | radioactive isotopes | 363 |
| dichloroplatinumdicarbonyl | 331 | rapid thermal low-pressure CVD | 132 |
| (diolefin)dialkylplatinum(II) complexes | | tungsten deposition on GaAs and InP | 132 |
| decomposition mechanism | 337 | rate expression | 216 |
| reaction mechanism | 337 | Cu(hfac) ₂ | 216 |
| methylcyclopentadienylplatinum | 335ff | Cu(nona-F) ₂ | 216 |
| CVD of platinum | 336 | reactant concentration | 204f |
| vapor pressure | 336 | Langmuir-Hinshelwood | 205 |
| methylcyclopentadienyltrimethyl- | | product inhibition | 205 |
| platinum | 351 | profiles | 472 |
| photolysis | 345 | saturation | 205 |
| photolytic decomposition | 344 | second-order reaction | 205 |
| precursors | 432 | zero-order reaction | 205 |
| pyrolysis | 345 | reactant partial pressure dependence of | |
| pyrolytic decomposition | 344 | rate | 480f |
| tetrakis(trifluorophosphine)platinum | 333ff, 346, 351 | carrier gas | 481 |
| film resistivity | 334 | concentration boundary layer | 481 |
| phosphorus contamination | 334 | diffusion coefficient | 481 |
| platinum laser-assisted CVD | 344ff | diffusion-limited deposition | 480f |
| plutonium | 366 | feed-rate-limited deposition | 480f |
| | | gas-phase particle formation | 480 |

gas-phase reaction	480	resistance capacitance (RC)	6
(hfac)Cu(VTMS)	481	resistivity	360
particle formation	481	gold	305
reactant depletion	480	silver	305
surface-reaction-limited deposition	481	response surface analysis	216
WF ₆	481	Cu(hfac) ₂	216
reaction mechanism	214	Cu(nona-F) ₂	216
competitive adsorption	215	reversibility, Cu precursor adsorption	197
Cu(I)(hfac)(COD)	215	Ag	197
Cu(I)(hfac)L	214	Cu	197
Cu(II)(hfac)	214	Cu(hfac) ₂	197
(diolefin)dialkylplatinum(II)	337	Cu(111)	197
disproportionation	215	disproportionation	197
H(hfac)	214	HREELS	198
H ₂ reduction	214	Reynolds number	473
mass transfer	233	rhodium	
surface reaction	233	tungsten-rhodium alloys	392
transport effects	233	rhodium	397, 407ff
reaction pathways	437	alkene complexes	407
reaction probability	321	alkyne complexes	407
reaction stoichiometry	190ff	allyl complexes	409
catalytic carrier	191	metal β-diketonates	421
H ₂	191	rhodium oxide (Rh ₂ O ₃)	408
H ₂ reduction	190	ruthenium	394, 407ff
reactor	255ff	alkene complexes	407
cold-wall	255ff	alkyne complexes	407
differential	256	metal β-diketonates	421
hot-wall	84, 255f	ruthenium dioxide	399
reactor design	219, 489		
cold-wall	219	S	
reactor modeling	220f	salicide	4, 15f, 24
boundary conditions	221	scanning electron microscopy (SEM)	62
Cu	221	Schiff-base complexes	
Cu(hfac) ₂	221	Cu(acen)	187
Damkohler criterion	221	Cu(acim) ₂	187
LPCVD	221	Cu(nona-F) ₂	187
plug flow reactor	221	Schottky contacts	
reactor operation	489	tungsten hexafluoride	130
recirculation cells	54	sedimentation	459
reducing agents		seed layers	
organophosphine	248	chromium, copper, gold, nickel,	
reduction		titanium nitride	61
(hfac)Cu(1,3-butadiene)	267	seed nuclei	
(hfac)Cu(1,5-COD)	267	selective CVD	443
[(hfac)Cu] ₂ (COT)	267	selective area growth	
organophosphine	248	triisobutylaluminum (TIBA)	66
reductive elimination	309, 316	selective CVD	89, 208f, 257, 281ff, 423, 441ff, 452, 490
gold	316	activation of growth surface	449
molecular hydrogen	92	chromophore	452
reflection-adsorption infrared spectroscopy (RAIR)	193ff	cobalt	423
reflection high energy electron diffraction (RHEED)	62	co-reactant	443, 449
remote plasma-enhanced CVD	160	co-reactant concentrations	445

- | | | | |
|---|--------------------|--|---------------------|
| formation of patterned films | 441 | MoF ₆ | 448 |
| gas-phase reactions | 445 | (Table 9-3) | 444 |
| gettering | 443 | tungsten CVD | 453 |
| growth and non-growth surfaces | 442 | WF ₆ /Si | 448 |
| H ₂ or Ar | 208 | pressure | 445 |
| induction time | 446 | reactant concentrations | 445 |
| iron | 423 | reactor type | 445 |
| loss of selectivity | 125, 447, 449, 452 | silylating agents | 281 |
| proximity effect | 126 | substrate | |
| selective tungsten CVD | 125 | organic polymers | 451 |
| tungsten CVD | 125 | polyimide | 451 |
| tungsten subfluorides | 126 | PTFE | 451 |
| mechanisms | | SiO ₂ or Si ₃ N ₄ | 208 |
| critical cluster size | 458 | TiN vs. SiO ₂ | 208 |
| critical nucleus size | 457 | tantalum | 423 |
| enhancement | 458 | temperature | 445 |
| free energy barrier | 443, 457 | selective CVD of copper | 275ff, 277ff, 286ff |
| gettering or removal of nucleating | | (acac)Cu[P(CH ₃) ₃] | 277 |
| species from non-growth surface | 456 | (hfac)Cu[P(CH ₃) ₃] | 275, 277 |
| hydroxyl groups | 281 | (hfac)Cu(VTMS) | 277 |
| intrinsic differences in reaction rates | 446 | poly(tetrafluoroethylene) | 286 |
| nucleation rate | 457 | SiO ₂ surface | 278 |
| passivation | 443 | (tfac)Cu[P(CH ₃) ₃] | 277 |
| passivation of non-growth surface | 453 | selective LCVD | |
| photochemical activation of | | tungsten films | 158 |
| growth surface | 452 | selective tungsten CVD | 125 |
| photochemically-driven reactions | 443 | selectivity loss | 125ff |
| physical nucleation barrier | 456 | self-limitation mechanism | 121f |
| rate-determining steps | 446 | self-limiting deposition of tungsten | 159 |
| redox reaction | 448 | silane | 60 |
| redox transmetallation | 448 | silane reduction | 124 |
| sacrificial layer | 448 | α-tungsten | 124 |
| sacrificial solid-state co-reactant | 447 | β-tungsten | 124 |
| seed layer | 450 | blanket deposition | 124 |
| seed nuclei | 443 | deposition rate | 125 |
| seed particle | 447 | disilane | 125 |
| self-limiting | 447 | growth rate | 124 |
| self-limiting thickness | 449 | rate law | 124 |
| silylating agent | 281, 453, 455 | reaction mechanism | 125 |
| sodium naphthalenide solution | 451 | reaction pathways | 124 |
| sub-critical nuclei | 457 | selective deposition | 124 |
| surface activation | 450 | surface reactions | 124 |
| molybdenum | 423 | violent reaction | 125 |
| Pd/Cu-alloy films | 448 | silica | |
| porous films | 449 | FTIR | 281 |
| precursors | 445 | surface chemistry | 281 |
| alane precursors | 83 | silicides | 404 |
| Al(<i>i</i> -Bu) ₃ | 453 | silicon dioxide surface | |
| (β-diketonate)CuL precursors | 453 | selective deposition | 278 |
| Cu(dpm) ₂ | 209 | silver | 363 |
| Cu(hfac) ₂ | 209, 450 | Ag(acac) | 313 |
| Cu(nona-F) ₂ | 209 | Ag(acetate) | 313 |
| dimethylaluminum hydride (DMAH) | 453 | Ag(C ₄ F ₇) | 313 |
| (η ⁵ -C ₅ H ₅)PtMe ₃ | 453 | Ag(trifluoroacetate) | 313 |

- | | | | |
|---|------------|--|------------|
| (alkene)Ag(acac) | 313 | surface diffusivity | 53 |
| (cyclopentadienyl)silver(I)trialkyl-phosphine | 312 | surface hydroxyl groups | 278f |
| (η^5 -C ₅ H ₅)Ag(PR ₃) | 313 | surface passivation, see also passivation | |
| precursors | 432 | chlorotrimethylsilane | 279 |
| resistivity | 305 | dimethyldichlorosilane | 279 |
| silver precursors | | functionalized alkylsilanes | 279 |
| synthesis | 310 | surface photolysis | 68 |
| silver(I) β -diketonates | 310 | surface pyrolysis reaction | 68 |
| silver(I) (β -diketonato) complexes | 312 | surface reaction mechanism | 316 |
| silver(I) carboxylates | 310 | TMAA | 77 |
| single-source precursors | 439f | surface reactions | 271ff, 274 |
| advantages and disadvantages | 440 | copper(I) precursors | 271ff |
| metal nitrides | 439 | Cu(hfac) ₂ | 274 |
| metal silicides | 439 | (hfac)Cu(1,5-COD) | 274 |
| mixed metal alloys | 439 | hfacH | 274 |
| non-integral stoichiometry | 440 | surface reactivity | 56 |
| sodium | 251, 363 | surface-reaction-limited deposition | 56, 268f |
| solar cell applications | 323 | 469f, 475, 478, 481f | |
| spray MOCVD | 463 | concentration boundary layer | 478 |
| spray nozzle | | rate of surface reaction | 478 |
| aerosol delivery | 464 | synthesis | 186, 385 |
| spray pyrolysis | 459, 463f | Cu(hfac) ₂ •H ₂ O | 186 |
| sputter deposition | 51 | dihydrate | 186 |
| conventional sputter deposition | 29 | monohydrate | 186 |
| magnetron-based sputter deposition | 29 | gold precursors | 306 |
| titanium | 23 | (hfac)Cu(L) | 187 |
| square planar geometry | 306 | T | |
| stannane | 405 | tantalum | 388, 409 |
| step coverage | 162 | allyl | 409 |
| step-flow mechanism | 79 | selectivity | 416 |
| sticking coefficient | 51 | tantalum silicon nitride amorphous diffusion | |
| sticking probability | 451 | barrier | 13 |
| copper | 280 | tape automated bond | 323 |
| stoichiometry | 180 | TEA, see triethylaluminum | |
| structure zone models | 51 | technetium | 392 |
| substrate | 475 | TED, see transmission electron diffraction | |
| inclined | 475 | tellurium | |
| supercritical fluid delivery | 464 | allyl complexes | 417 |
| aerosol delivery | 464 | temperature boundary layer | 470ff |
| supersaturation | 83 | temperature dependence of rate | |
| surface chemistry | 281ff, 490 | 469, 481f, 482 | |
| (hfac)Cu[P(CH ₃) ₃] | 281 | diffusion-limited deposition | 482 |
| (hfac)Cu(VTMS) | 281 | feed-rate-limited deposition | 481 |
| (hfac)Cu(1,5-COD) | 281 | gas-phase particle formation | 482 |
| (hfac)Cu(2-butyne) | 281 | surface-reaction-limited deposition | 482 |
| surface decomposition mechanism | | temperature non-uniformities / non-uniform | |
| Al(100), Al(111) | 63 | film thickness | 483 |
| surface diffusion | 52f | temperature profiles | 472 |
| bulk diffusion | 53 | tetraallyltungsten | 144 |
| columnar microstructure | 53 | tungsten carbide films | 144 |
| diffusion length | 53 | tetrakis(trifluorophosphine)platinum | 333ff |
| roughness | 53 | film resistivity | 334 |
| surface diffusion length | 53 | phosphorus contamination | 334 |

- | | | | |
|---|----------------|---------------------------------------|-------------------|
| thermal conductivity | 473 | trimethylaluminum (TMA) | 68ff, 89 |
| thermal degradation of precursors | 466 | trimethylamine | 75 |
| thermal desorption spectroscopy | 61 | trimethylamine alane (TMAA) | 50, 75, 77ff, 290 |
| thermal entrance length | 472 | cold-wall reactors | 80 |
| thermophoresis | 459, 483, 487 | hot-wall reactors | 81 |
| thermophoretic velocity | 488 | surface reaction mechanism | 77 |
| thin films | 108 | tris(butadiene)tungsten | 118, 144 |
| tungsten | 108 | tris(methylvinylketone)tungsten | 119, 146 |
| thorium | 366 | tubular flow reactor | 54, 471 |
| TIBA, see triisobutylaluminum | | tungsten | |
| tin | 400 | allyl complexes | 417 |
| dopant | 400 | applications | 108 |
| superconductors | 400 | bis(arene)tungsten | 117, 148 |
| tin(II)chloride (SnCl ₂) | 371 | bis(benzene)tungsten | 143 |
| titanium | 386, 438 | bis(cyclopentadienyl)dihydrido- | |
| adhesion layers | 27 | tungsten | 119, 147 |
| precursors | 432 | vapor pressure | 119 |
| sputter deposition | 23 | bis(methylcyclopentadienyl)dihydrido- | |
| titanium carbide | 406 | tungsten | 120, 148 |
| titanium carbonyl | 411 | cycloheptatrienetetracarbonyltungsten | 120, 149 |
| titanium chloride | 82, 371 | cyclooctadienetetracarbonyltungsten | 120, 149 |
| pretreatment with | 80 | cyclopentadienylhydridotricarbonyl- | |
| titanium nitride | 25, 89 | tungsten | 120 |
| Ti(NMe ₂) ₄ | 440 | cyclopentadienylmethyltricarbonyl- | |
| titanium nitride passive diffusion barrier | 12 | tungsten | 119, 146, 149 |
| titanium sacrificial diffusion barrier | 11 | vapor pressure | 119 |
| titanium silicide | 25 | electromigration resistance | 108 |
| titanium(IV) chloride | 57 | hexacarbonyltungsten | 117, 141ff, 152ff |
| titanium-tungsten stuffed diffusion barrier | 12 | hexakis(trifluorophosphine)tungsten | 115, 141 |
| TMA, see trimethylaluminum | | phosphorus impurities | 117 |
| TMAA, see trimethylamine alane | | historical development | 111 |
| trans-amination | 440 | metal, properties of (Table 3-2) | 111 |
| transition zone in velocity | 54 | precursors | 111 |
| transmission electron diffraction (TED) | 62 | properties and synthesis | 111ff, 432 |
| transport | 321 | properties | 108ff |
| transport effects | 220 | electromigration | 108 |
| concentration gradients | 220 | resistivity | 110 |
| concentration of reactants | 220 | α-tungsten | 110ff |
| convection | 220 | β-tungsten | 110ff |
| Damköhler number | 220 | γ-tungsten | 110ff |
| diffusivity | 220 | tetraallyltungsten | |
| fractional conversion | 220 | tungsten carbide films | 144 |
| transport-limited deposition | 256f, 268, 396 | thin films | 108 |
| transport phenomena | 53 | tris(butadiene)tungsten | 118, 144 |
| tri- <i>n</i> -butylamine alane | 75 | tris(methylvinylketone)tungsten | 119, 146 |
| triethylaluminum (TEA) | 86 | tungsten carbide films | 144 |
| triethylamine | 75 | tetraallyltungsten | 144 |
| triethylamine alane (TEAA) | 75, 81ff | WC | 406 |
| trifluorophosphines | 380, 413 | WC-phase | 108 |
| disproportionation | 413 | tungsten deposition | 150 |
| rhodium | 413 | | |
| triisobutylaluminum (TIBA) | 58ff, 62ff | | |
| trimethylaluminum | | | |
| activation energy | 70 | | |

- | | | | |
|------------------------------------|----------------------|---|---------------------|
| catalysis | 150 | V | |
| contamination of | 150 | vanadium | 386 |
| direct writing | 155 | alloys | 386 |
| laser-assisted CVD | 151 | vapor pressures | 246, 254, 257, 383f |
| tungsten halides | 112ff | Cu(hfac) ₂ | 254 |
| tungsten hexabromide | 112, 138 | (hfac)Cu[P(CH ₃) ₃] | 254 |
| tungsten hexachloride | 112 | (hfac)Cu(VTMS) | 254 |
| corrosive effects | 133 | (hfac)Cu(1,5-COD) | 254 |
| encroachment | 133 | vaporization of precursors | 460f |
| selectivity | 136 | (hfac)CuL | 461 |
| thermodynamic calculations | 135 | liquids | 460 |
| tungsten hexafluoride | 112, 121ff, 163, 371 | problems | 461 |
| critical thickness | 121 | sublimation | 460 |
| deposition conditions (Table 3-6) | 129 | thermal window | 461 |
| deposition experiments | 128, 157 | velocity boundary layer | 470ff |
| deposition rate determinations | 123 | velocity gradient | 472 |
| displacement reaction | 121 | velocity profiles | 471 |
| encroachment | 122 | very-large-scale integration (VLSI) | 22, 60 |
| film properties (Table 3-6) | 129 | viscosity | 472 |
| germane reduction | 132f, 155 | VLSI, see very-large-scale integration | |
| hydrogen reduction | 123 | volatile Cu(II) compounds | 182 |
| reaction kinetics | 123 | volatility | 183, 188ff |
| reaction mechanism | 123 | Clausius-Clapeyron | 188 |
| reaction order | 123 | Cr(acac) ₃ | 188 |
| kinetic observations | 121 | Cr(hfac) ₃ | 188 |
| laser-assisted CVD | 155 | Cr(tfac) ₃ | 188 |
| mechanism | 121 | Cu(fod) ₂ | 188 |
| mechanism and kinetic observations | 155 | Cu(hfac) ₂ | 188 |
| parallel plate reactor | 161 | Cu(nona-F) ₂ | 189 |
| Schottky contacts | 130 | FTIR | 189 |
| selective deposition | 121 | oligomerization | 251 |
| self-limitation mechanism | 121f | on-line monitoring | 189 |
| silane reduction | 157 | transpiration technique | 188 |
| silicon reduction | 121 | | |
| worm-hole formation | 122 | W | |
| tungsten metallization | 19 | Wacker-type processes | 439 |
| tungsten phases | 110 | "Widiametall" | 108 |
| tungsten precursors | 432 | work function | 360 |
| synthesis methods (Table 3-3) | 113 | worm-hole formation | 122 |
| properties (Table 3-4) | 114 | | |
| tungsten properties | | X | |
| diffusion barrier for aluminum | 110 | X-ray diffraction | 246, 252ff |
| tungsten silicide | 25 | [(<i>t</i> -BuO)Cu(PPh ₃) ₂] | 245 |
| tungsten-platinum co-deposition | 150, 164 | (β-diketonate)Cu(alkyne) | 252 |
| | | (β-ketoiminate)Cu[P(CH ₃) ₃] | 254 |
| | | [Cu(O- <i>t</i> -Bu)] ₄ | 246 |
| | | (η ⁵ -C ₅ H ₅)Cu[P(CH ₃) ₃] | 252 |
| | | (Figure 5-3) | 253 |
| | | (hfac)Cu[P(CH ₃) ₃] | 252 |
| | | (hfac)Cu(VTMS) | 252 |
| | | (hfac)Cu(1,5-COD) | 252 |
| | | (hfac)Cu(2-butyne) | 254 |
- U**
- ULSI see ultra-large-scale integration
- ultra-large-scale integration (ULSI) 22
- ultrasonic atomizer 466
- aerosol delivery 464
- ultraviolet laser irradiation 66
- uranium 366

(tfac)Cu[P(CH ₃) ₃]	252	Z	
X-ray diffraction spectra, Cu	214	zinc	
XPS spectra	195	dopant	400
		zirconium	386
		ZrC	387, 406

G. Schmidt (ed.)

Clusters and Colloids

From Theory to Applications

1994. XVI, 555 pages with ca
230 figures, 5 in color, and 41
tables. Hardcover.
DM 248.00.
ISBN 3-527-29043-5

This book offers a comprehensive overview of the rapidly developing field of cluster science. In an interdisciplinary approach, basic concepts as well as recent developments in research and practical applications are authoritatively discussed by leading authors. Topics covered include "naked" metal clusters, clusters stabilized by ligands, clusters in solids, and colloids.

The reader will find answers to questions like:

- How many metal atoms must a particle have to exhibit metallic properties?



- How can the large specific surface of clusters and colloids be employed in catalysts?
- How can metal clusters be introduced into solid hosts?
- Which effects are responsible for the transition from isolated to condensed clusters?

The editor has succeeded in bringing the contributions of various authors together into a homogeneous, readable book, which will be useful for the academic and industrial reader alike.

N. Auner/ E. Weiss (eds.)

Organosilicon Chemistry

From Molecules to Materials

1994. XXII, 549 pages with 78
figures and 31 tables.
DM 128.00.
ISBN 3-527-29061-3

To order please contact your bookseller or:

- VCH, P.O. Box 10 15 47, D-69451 Weinheim, Fax (0) 62 01 - 80 70 81
- VCH, Hardstrasse 10, P.O. Box, CH-4002 Basel
- VCH, 8 Wellington Court, Cambridge CB1 1RZ, UK
- VCH, 305 N.W. 32nd Avenue, Deerfield Beach, FL 33442-1700, USA toll-free: 1-800-367-8249 or fax: 1-800-367-8247
- VCH, Eikestrasse 10, D-69126 Heidelberg, Germany

VCH

Materials for Electronics

Electronic and Magnetic Properties of Metals and Ceramics

edited by K.H.J. Buschow

Volumes 3A/B from the series
Materials Science and Technology edited by R.W. Cahn,
P. Haasen and E. J. Kramer

3A: 1992. XIV, 642 pages with 473 figures and 30 tables. Hardcover.
DM 450.-/Fr. 420.-/US \$310.-.
ISBN 3-527-26816-2

3B: 1994. XVI, 625 pages with 436 figures and 83 tables. Hardcover.
DM 450.-/Fr. 420.-/US \$310.-.
ISBN 3-527-28264-5

3A: Topics included are: - Electronic Structure Calculations - Magneto-Optical Properties of Metals, Alloys and Compounds - Electronic Transport of Normal Metals - Superconductivity - Magnetic Properties of Metallic Systems - Fermi Surfaces in Strongly Correlated Electron Systems.

3B: Topics included are: - Magnetic Properties of Spinel Ferrite - Electronic Properties of Liquid, Amorphous and Quasicrystalline Alloys - Invar Alloys - Magnetic Recording Materials - Hydrogen in Pure Metals and Solid Solution - Ternary Hydrides - Soft Magnetic Metals and Alloys - Permanent Magnet Materials - Magnetostrictive Materials - Magneto-Optical Materials.

Electronic Structure and Properties of Semiconductors

edited by W. Schröter

Volume 4 from the series
Materials Science and Technology edited by R.W. Cahn,
P. Haasen and E. J. Kramer

1991. XIII, 603 pages with 320 figures and 29 tables. Hardcover.
DM 450.-/Fr. 420.-/US \$310.-.
ISBN 3-527-26817-0

This volume spans the field of semiconductor physics, with particular emphasis on concepts relevant to semiconductor technology.

Topics included are: - Band Theory - Optical Properties and Charge Transport - Intrinsic Point Defects - Deep Centers - Equilibria, Nonequilibria, Diffusion, and Precipitation - Dislocations - Grain Boundaries - Interfaces - The Hall Effect in Quantum Wires - Hydrogenated Amorphous - 3d Transition Elements in Silicon.

Processing of Semiconductors

edited by K. A. Jackson

Volume 16 from the series
Materials Science and Technology edited by R.W. Cahn,
P. Haasen and E. J. Kramer

1994. Ca XIII, ca 650 pages with ca 350 figures and 30 tables.
Hardcover. Ca DM 450.-/
ca Fr. 420.-/ca US \$310.-.
ISBN 3-527-26829-4



Materials Science

To order please contact your bookseller or:

VCH, P.O. Box 10 11 81,

D-69451 Weinheim,

Fax: (06201) 60 61 84

VCH, Weinheim 10, P.O. Box,

CH-4000 Basel

VCH, 8 Wallington Court,

Cambridge CB1 1JZ, UK

VCH, 300 N.W. 126 Avenue,

Dearfield Beach, FL 33442-1788,

USA (toll-free: 1-800-367-6340)

VCH, Ekin Building, 10-9 Hong Kong

1 volume, Tokyo 113

Please write for our comprehensive prospectus.

This Page Intentionally Left Blank

This Page Intentionally Left Blank

This Page Intentionally Left Blank

This Page Intentionally Left Blank

Physical Constants^a

Velocity of light	$c = 2.99792458 \times 10^8 \text{ m/s}$
Planck's constant	$h = 6.6260755 \times 10^{-34} \text{ J s}$
	$\hbar = h/2\pi = 1.054573 \times 10^{-34} \text{ J s}$
Boltzmann constant (gas constant per molecule)	$k = 1.380658 \times 10^{-23} \text{ J/K}$
Gas constant	$R = 8.314510 \text{ J/mol K}$
	$= 1.98721 \text{ cal/mol K}$
	$= 8.20578 \times 10^{-2} \text{ L atm/mol K}$
Avogadro's number	$N_A = 6.0221367 \times 10^{23} \text{ /mol}$
Electron charge	$e = 1.602177 \times 10^{-19} \text{ C}$
	$= 4.80320 \times 10^{-10} \text{ esu}$
Faraday	$\mathcal{F} = 9.6485309 \times 10^4 \text{ C/mol}$
Atomic mass unit	$\text{amu} = 1.6605402 \times 10^{-27} \text{ kg}$
Electron rest mass	$m_e = 9.109390 \times 10^{-31} \text{ kg}$
	$= 5.485716 \times 10^{-4} \text{ amu}$
Proton rest mass	$m_p = 1.672623 \times 10^{-27} \text{ kg}$
	$= 1.007261 \text{ amu}$
Neutron rest mass	$m_n = 1.6749286 \times 10^{-27} \text{ kg}$
	$= 1.0086495 \text{ amu}$
Gravitational constant	$G = 6.67259 \times 10^{-11} \text{ m}^3/\text{s}^2 \text{ kg}$
Acceleration of gravity	$g = 9.80665 \text{ m/s}^2$
Rydberg constant	$R = 1.097373153 \times 10^7 \text{ /m}$
Pi	$\pi = 3.1415926536$
Molar volume at NTP	$= 22.414 \times 10^3 \text{ cm}^3 \text{ /mol}$
	$= 22.414 \times 10^{-3} \text{ m}^3 \text{ /mol}$

^a Values from *Quantities, Units, and Symbols in Physical Chemistry*, I. Mills, Ed., Blackwell Scientific, Oxford, 1988, p.81.

Conversion Factors

1 electron. volt	=	1.602×10^{-12} erg	=	1.602×10^{-19} J	
1 electron volt/molecule	=	23.063 kcal/mol	=	96.496 kJ/mol	$\approx 8,065.46 \text{ cm}^{-1}$
10,000 cm^{-1}	=	10 kilokaysers (kK)	\approx	28.6 kcal/mol	= 120 kJ/mol
	=	1000 nanometers (nm)	\approx	1.24 eV/molecule	
20,000 cm^{-1}	=	500 nm			
1 nm	=	10 \AA	=	10^{-9} m	= 1 mp
1 pm	=	10^{-2} \AA			
1 J	=	10^7 erg			
1 cal	=	4.1840 J			
1 dyn	=	1 g cm/sec ²	=	10^{-5} N	
$^{\circ}\text{C}$	=	K - 273.15			
1 L	=	1 dm ³	=	10^3 cm^3	
1 atm	=	760 torr	=	1.01325×10^5 Pa	
1 esu	=	1 dyn ^{1/2} cm			

Multiples of both base and derived units are indicated by one of the following prefixes.

Chemical Numerical Prefixes

SI Prefixes

		Factor	Prefix	Symbol
1	mono	10^{18}	exa	E
2	di (bis)	10^{15}	peta	P
3	tri (tris)	10^{12}	tera	T
4	tetra (tetrakis)	10^9	giga	G
5	penta (pentakis)	10^6	mega	M
6	hexa (hexakis)	10^3	kilo	k
7	hepta (heptakis)	10^2	hecto	h
8	octa (octakis)	10^1	deca	da
9	nona (nonakis)	10^{-1}	deci	d
10	deca (decakis), etc.	10^{-2}	centi	c
11	undeca	10^{-3}	milli	m
12	dodeca	10^{-6}	micro	μ
15	pentadeca	10^{-9}	nano	n
16	hexadeca	10^{-12}	pico	p
20	icosa	10^{-15}	femto	f
30	triaconta	10^{-18}	atto	a
50	pentaconta			
100	hecta			